

# II-VI 2015

## 17th International Conference on II-VI Compounds and Related Materials

PARIS  
13-18 september 2015

### Conference book



---

## 17<sup>th</sup> International Conference on II-VI Compounds and Related Materials

Welcome to the 17<sup>th</sup> International Conference on II-VI Compounds and Related Materials which is held in Paris, France, from september 13<sup>th</sup> to 18<sup>th</sup>, at the *Campus des Cordeliers* located in the historical center of Paris.

II-VI 2015 continues a successful series of biennial conferences which started in Durham (UK) in 1983. Recent conferences were held in Niagara Falls (USA, 2003), Warsaw (Poland, 2005), Jeju (Korea, 2007), Saint Petersburg (Russia, 2009), Mayan (Mexico, 2011), and Nagahama (Japan, 2013).

This conference provides an international forum for scientists, students and industry representatives, to report new developments in basic and applied research on II-VI and related compounds such as oxides and chalcopyrite semiconductors; covering novel synthesis techniques, new physical properties and innovative device development. Since the last conference in Nagahama, the scope has been extended to Related Materials like Photovoltaic materials, novel 2D systems: dichalcogenide and topological insulators.

The scientific program consists of three plenary review lectures, 15 invited talks, 64 contributed talks and about 200 contributed poster presentations. Review lectures are scheduled during sunday 13<sup>th</sup>, talks will be given during the week and are grouped under the following sessions:

Growth and characterization,

ZnO: Nanowires, Plasmonic & optical engineering, Transport & doping, Devices,

Dots & nanowires,

Colloidal systems,

Optical and excitonic properties,

Spin in dots,

Novel 2D systems, topological systems,

Detectors, Photovoltaic.

The local organization of this conference is the result of the commitment of researchers from the *Institut des Nanosciences* in Paris and from the *Groupe d'Etude la Matière Condensée* in Versailles.

Organizing such an important international event is a financial challenge and we want to acknowledge the support from national, international or private institutions.

Paris is a fascinating city and we hope that the situation of the *Campus des Cordeliers* will give the participants the possibility to enjoy its beauty. Furthermore we offer you the possibility on Wednesday afternoon to visit the *Château de Versailles* and its famous garden, and for the banquet, to appreciate the beauty of the center of Paris during a dinner cruise.

We wish you a very nice week and hope that, the conference will be a great success thanks to your participation and will remain in your memory.

Christophe Testelin  
Institut des NanoSciences de Paris

Pierre Galtier  
Groupe d'Etude de la Matière Condensée

II-VI-2015 Conference chair

## Scope and Topics

The II-VI compounds provide a variety of unique optical, electrical and magnetic properties. The Conference will then cover all the aspects of basic and applied research, laying special emphasis on unique physical and material properties of II-VI compounds, related materials and nanostructures. A particular attention will be given to new trends and pioneering directions, as well as to new materials and devices.

The conference will give also the opportunity to review the most important achievements in practical applications of II-VI compounds in mid-infrared, visible and UV range detectors, optoelectronic devices...

It is an international forum aimed at: - reviewing and stimulating the progress in basic and applied research on II-VI semiconductors and related materials, - facilitating the exchange of new ideas and establishing new scientific contacts.

The topics include growth, characterization, structure, physics and devices of II-VI compounds. The evolution of related materials such as oxide and chalcopyrite semiconductors is also included as topics. Typical topical areas in theoretical and experimental research are:

Infrared, visible, and UV materials, structures, and devices

Growth and characterization

ZnO and related oxides

Doping and defects

Magnetic semiconductors

Transparent conductors

Biomaterials

Superlattices and nanostructures

Quantum dots and colloidal nanocrystals

Hybrid organic-inorganic structures

Theory and band structure

Optical and electrical properties

Photonic engineering

Spin-related phenomena

Topological insulators, novel 2D systems (II-A or B-VI), superconductors...

Solar cells

X- and gamma-ray high energy sensors

Magnetic devices

New materials, experimental techniques and devices

## Committees

### International Program Committee

Moungi Bawendi (MIT, USA)  
Lucien Besombes (Institut Néel, France)  
Arnold Burger (Fisk University, USA)  
Irina Buyanova (Linköping University, Sweden)  
Maria Chamarro (P. & M. University, France)  
Christophe Delerue (IEMN, France)  
Jan Franc (Charles University, Czech Republic)  
Marius Grundmann (Leipzig University, Germany)  
Grzegorz Karczewski (Acad. of Science, Poland)  
Akio Kimura (Hiroshima University, Japan)  
Mazakazu Kobayashi (Waseda University, Japan)  
Michal Nawrocki (Warsaw University, Poland)  
Florent Perez (P. & M. University, France)  
Chong-Xin Shan (Changchun Inst. Of Optic, China)  
Alexey Toropov (Ioffe Institute, Russia)  
Ulrike Woggon (Technical University, Germany)  
Gyu-Chui Yi (Seoul National University, Korea)

### International Advisory Committee

Rameshwar Bhargava (Nanocrystals, USA)  
Shizuo Fujita (Kyoto Univ., Japan)  
Jacek K. Furdyna (Univ. Notre Dame, USA)  
Fritz Henneberger (Humboldt Univ., Germany)  
Isaac Hernandez-Caldern (Cinvestav, Mexico)  
Sergey Ivanov (Ioffe Physical -Technical Institute, Russia)  
Tae Won Kang (Dongguk Univ., Korea)  
Piotr Kossacki (Warsaw University, Poland)  
Jacek Kossut (Institute of Physics, PAS, Poland)  
S.J. Lee (Dongguk Univ., Korea)  
Yichun Liu (Northeast Normal University, China)  
Henri Mariette (CNRS, France)  
Maria Tamargo (City Univ. of New York, USA)  
Andreas Waag (Technical Univ. of Braunschweig, Germany)  
Daniel Wolverson (Univ. of Bath, UK)  
Akihiko Yoshikawa (Chiba Univ., Japan)

### Local Committee

#### Conference Chair

Christophe Testelin (INSP,UPMC, Paris)  
Pierre Galtier (GEMAC, UVSQ, Versailles)

#### Scientific Secretary

Florent Perez (INSP,UPMC, Paris)

#### Secretary

Stéphanie Lagarde (INSP,UPMC, Paris)

#### Members

Maria Chamarro (INSP,UPMC, Paris)  
Alain Lusson (GEMAC, UVSQ, Versailles)  
Agnès Maître (INSP,UPMC, Paris)  
Massimiliano Marangolo (INSP,UPMC, Paris)  
Vincent Sallet (GEMAC, UVSQ, Versailles)  
Valia Voliotis (INSP,UPMC, Paris)

#### Communication

Cécile Duflot (INSP,UPMC, Paris)

## Special session

A special session will be devoted to the memory of

### **Prof. Fritz Henneberger**

from Humboldt University, Berlin.



The Humboldt University communicates its sadness and dismay for the sudden death of its colleague. The Institute of Physics he belonged to, will miss an outstanding scientist whose commitment to research, teaching and academic administration promoted the development of the institute significantly.

Fritz Henneberger received his PhD in 1980 from the Humboldt University and was awarded in 1986 with the Heinrich-Hertz Prize from the Physical Society of GDR for his work on optical non-linearity and bistability in II-VI semiconductors. He became full Professor of the Humboldt University in 1993. During the first decade of 21st century, he was director of the Institute of Physics and influenced considerably the structure of the institute. He initiated optics and photonics in structured composite systems involving organic/inorganic semiconductors and oxides (ZnO). For these investigations he became quickly an internationally renowned scientist.

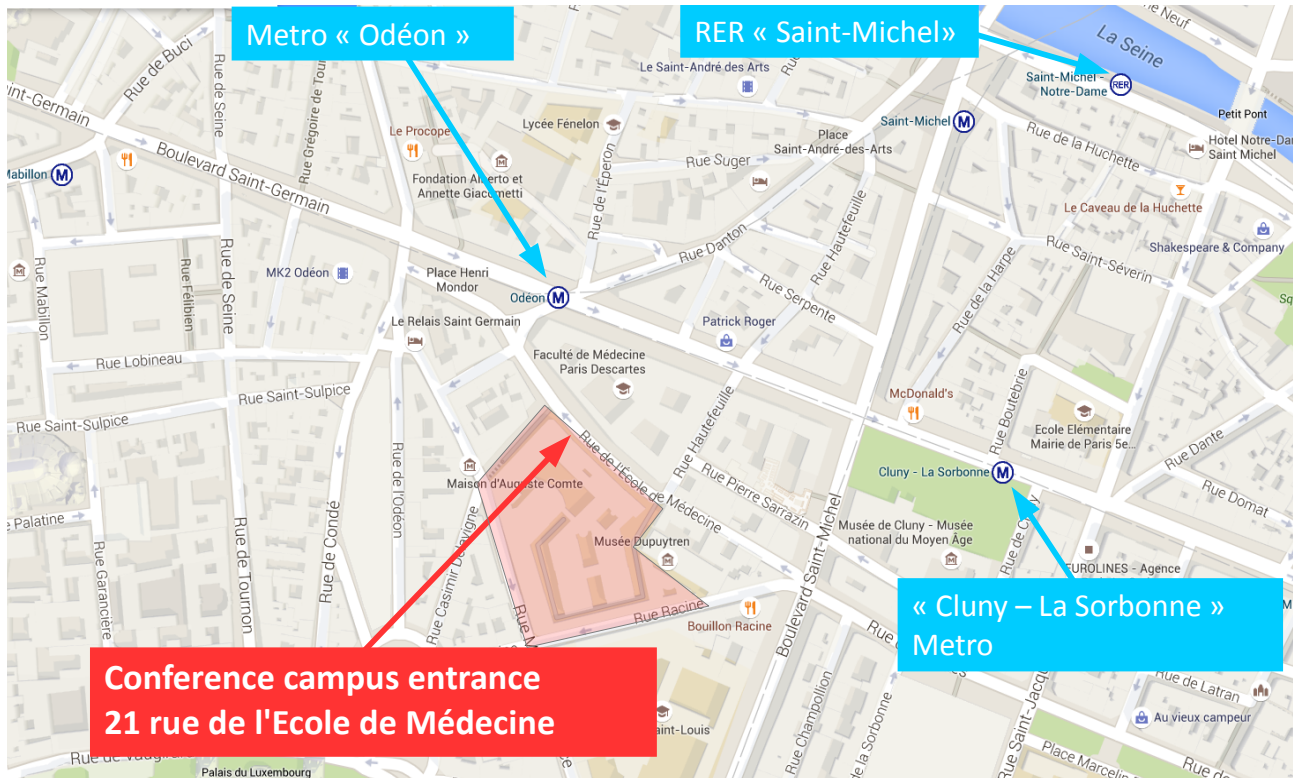
In his memory, Sascha Kalusniak (Humboldt), will give an invited talk on ZnO-based plasmonics .

[Click here for the Institute of Physics communication \(pdf reader only\).](#)

## Venue

II-VI 2015 will be held at the *Campus des Cordeliers* which is located in the geographical center of Paris, in the *Quartier Latin*, and close to Sorbonne University and the Cathedral of Notre-Dame. The campus address is 21 rue de l'École de Médecine, Paris VI.

It is well connected to any part of Paris via the underground ("metro") and local trains ("RER").



The historical site dates back to 1234. It became the Monastery of Cordeliers (Franciscans) until 1571 and also an important educational center in competition with the Sorbonne. During French Revolution the site was the meeting place of one of the popular clubs of this historical period, Club of Cordeliers, founded in 1790 to prevent the abuse of power and human rights violations.

Today it welcomes biomedical research laboratories and hosts the Faculty of Medicine and the Institute of Doctoral Studies of Pierre et Marie Curie University.

## Practical information

The main entrance of the conference campus is 21 rue de l'Ecole de Médecine, Paris VI. It is 2min walk from the closest metro station "Odéon" (Metro lines 4 or 10).

## Presentations

Conferences will take place in the Amphithéâtre Faraboeuf. Poster sessions will be held in the Campus's garden and cloister.

Review lectures are 50 min talk + 10 min of discussion.

Invited talks are 25 min + 5 min discussion.

Contributed talks are 12 min + 3 min discussion.

The maximum poster size is 100cm wide and 150cm high.

## Lunches and coffee breaks

A welcome lunch and evening cocktail will be offered on Sunday, 13<sup>th</sup> in room *Marie Curie* inside the *Campus des Cordeliers*. We also offer lunch for every participants from Monday, 14<sup>th</sup> to Thursday, 17<sup>th</sup>. Coffee breaks will take place in the room *Marie Curie* and cloister.

## Registration

Registration will start from Sunday 13<sup>th</sup>, 11:30 am, inside the *Campus des Cordeliers*.

## Website

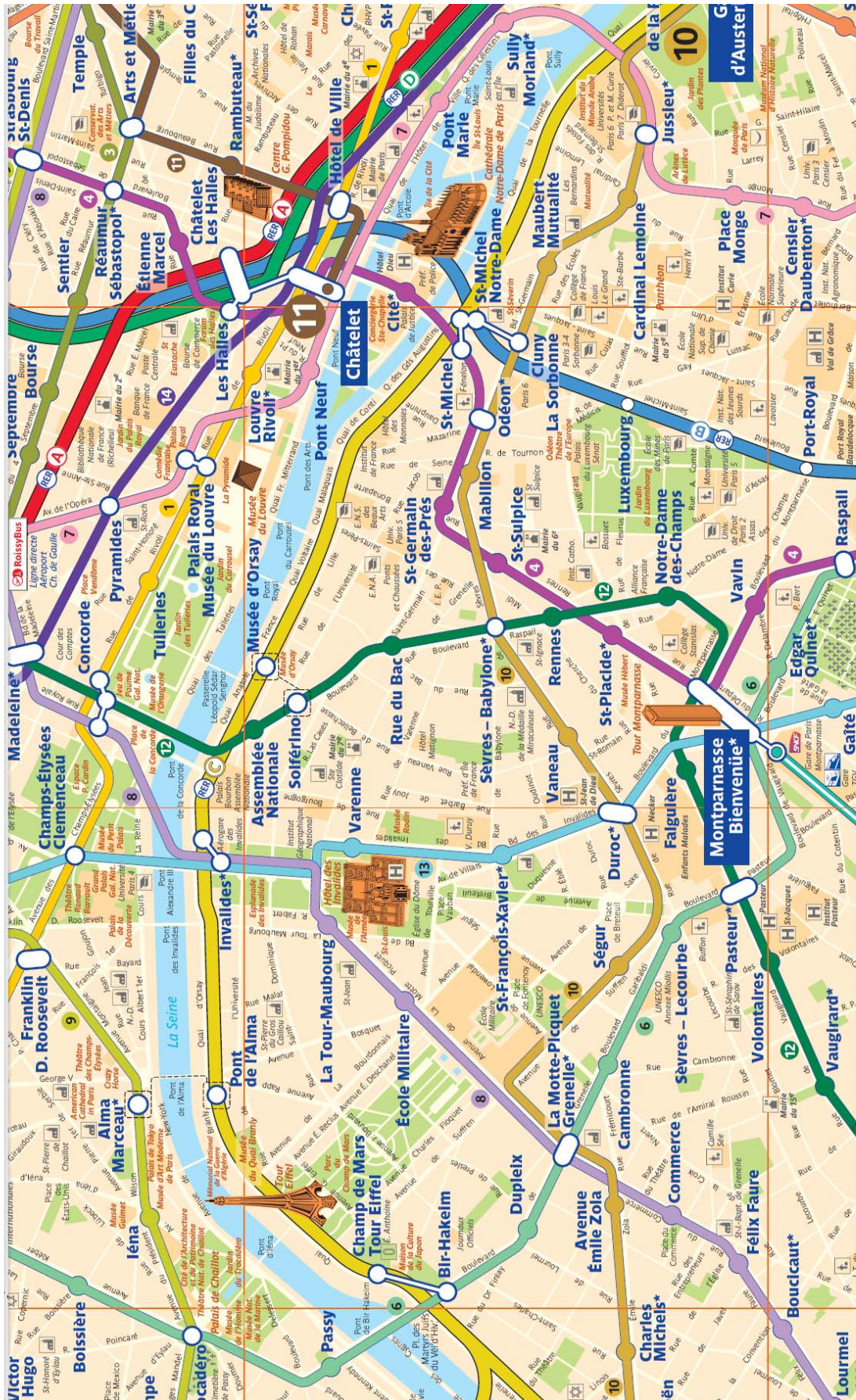
The conference website is:

<http://ii-vi-2015.sciencesconf.org/>

## Contact

Please email us at: [conf26@insp.jussieu.fr](mailto:conf26@insp.jussieu.fr)

# Metro and RER network in the center area



## Social program

We are pleased to invite you for a break at Versailles to visit its famous Palace on Wednesday afternoon.

Departure time is scheduled at 1.30 pm, just after lunch.

Dedicated buses will take you from the Campus des Cordeliers to the Palace of Versailles.

Once on site, the visit is organized by groups of 30 people entering the Palace every 5 minutes, from 2.50 p.m. Everyone will be given an audioguide (11 languages are available).

The visit of the Palace and its most famous places (the Hall of Mirrors, Grand Apartments of the King and of the Queen, King's Bedchamber ...) lasts around 1 hour and a half.

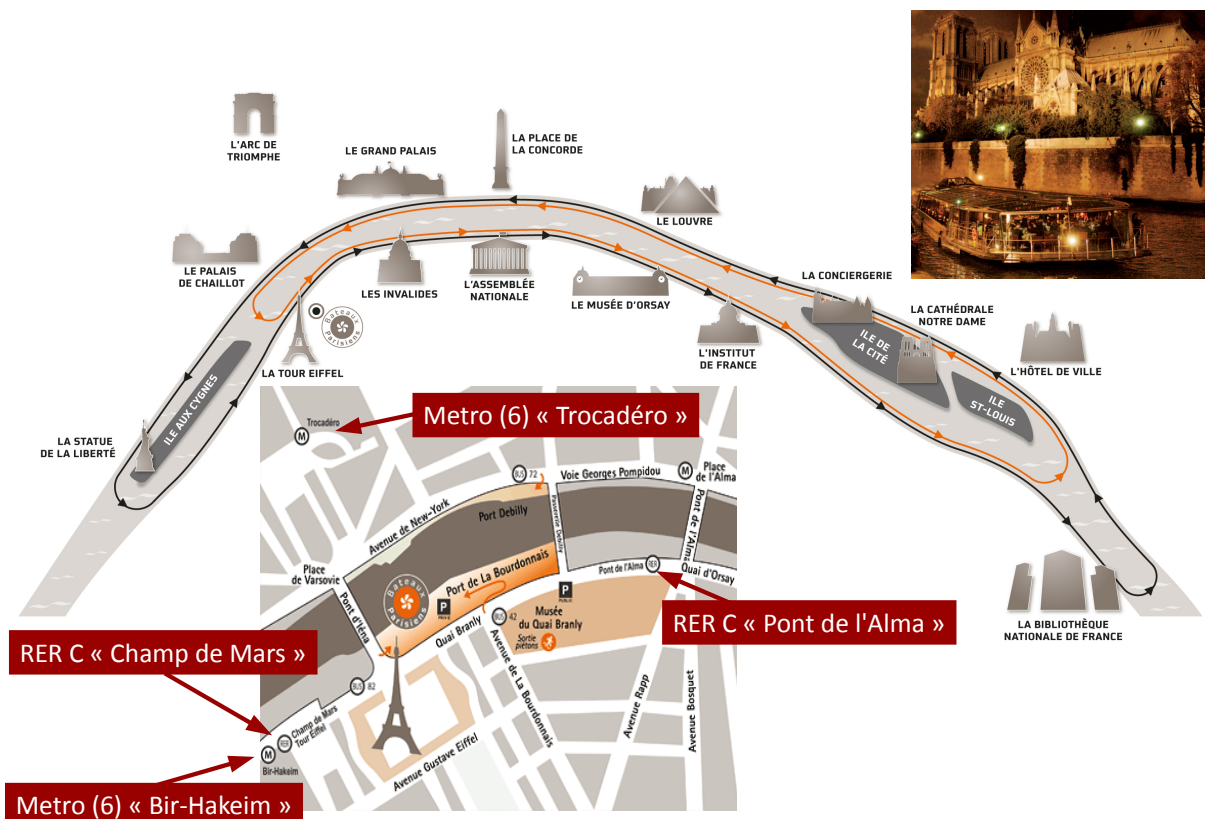
Then, a walk in the gardens will be possible before returning.

The return to Paris by bus is scheduled at 6.00 pm.

## Conference banquet

The conference banquet will be held on board an entirely glass-encased boat. You'll experience a dinner-cruise on the Seine river, at night in the center of Paris, with illuminated historical buildings and monuments. The cuisine is typically french and meticulously presented. Rendez-vous is given on thursday 7:30pm for the boarding, at the dock of the "Bateaux Parisiens" ship company (<http://www.bateauxparisiens.com>). The boat will leave the quay at 8:30pm sharp and return at 11pm. Disembarkation may take 30min.

The map below shows the cruise, the boat and the access to the dock, located at the foot of the Eiffel tower, Port de la Bourdonnais.



## Proceedings

Proceedings of the II-VI 2015 will be published as peer reviewed papers in PHYSICA STATUS SOLIDI (pss) journals. All contributions will be considered as submissions to pss as an international scientific journal. Invited and Contributed Articles may be published as a special issue in pss (c) - current topics in solid state physics.

Selected highlight presentations may be upgraded as Original Papers or Feature Articles in pss (a) - applications and materials science or pss (b) - basic solid state physics, or in selected special cases as Rapid Research Letter or Review@RRL in pss (RRL) - Rapid Research Letters.

The article submitted for publication should be up to 4 printed pages for Contributed (oral and poster) presentations and up to 8-10 printed pages for Invited presentations. Feature Articles (topical review, 8-10 printed pages) contributions are also possible to submit after invitation.

The manuscript should be submitted after the conference, using the journals' online manuscript submission system.

## Manuscript submission

All manuscript must submitted electronically using the online submission system Editorial Manager (link below):

<https://www.editorialmanager.com/pssc-journal/default.aspx>

Please login as an author. First-time users will need to register and enter the requested information. For your paper submission, select "II-VI Paris 2015 conference".

Instructions and guidelines for author are available online (link below):

[http://onlinelibrary.wiley.com/journal/10.1002/\(ISSN\)1610-1642a/homepage/2133\\_authors\\_EM.html](http://onlinelibrary.wiley.com/journal/10.1002/(ISSN)1610-1642a/homepage/2133_authors_EM.html)

## Sponsors



# General planning

	Sunday 13	Monday 14	Tuesday 15	Wednesday 16	Thursday 17	Friday 18
8h30						
8h45		opening session	Liu X.	Akimov	Vanmaekelbergh	Pavlov
9h00		Bougerol	Guziewicz	Cronenberg	Lhuillier	Morhain
9h15		Nakasu	Lorenz	Baboux	Maitre	Klembt
9h30		Dicko	Zuniga-Perez	Puls J.	Pelliser	Rahman
9h45		Aljamani	Wang L.	Debus	Nasifowski	Kochereshko
10h00		Stowe	Coffee break	Komissarova		Kreilkamp
10h15				Coffee break	Coffee break	Coffee break
10h30		Coffee break	Ganichev		Kozuka	Rodina
10h45		Zehani	Shiraiishi	Kalusniak	Lu J.	Artoli
11h00		Gokarna	Wang G.	Sadofev	Przezdziecka	Deligiannakis
11h15		Stehr	Thomas	Aad R.	Jobic	Wojnar
11h30		Bley S.	Wojtowicz	Blumstengel	Ye Z.	Sciesiek
11h45		Yuidashev		Lee S.	Snigurenko	
12h00						
12h15						Closing session
12h30 - 13h30	Welcome Lunch	Lunch	Lunch	Lunch	Lunch	
13h45						
14h00		Pacuski	Klimov		Gloecker	Review 1-3
14h15	Tamargo	Lafuente-Sampietro	Even		Etcheberry	Growth and characterization 1
14h30		Bogucki	Uruno		Tomic	Growth and characterization 2
14h45		Heimbrodt	Suzuki		Sorokin	ZnO, Nanowire
15h00			Srour		Toropov	ZnO, Plasmonic and optical engineering
15h15	Lincot	Coffee break				ZnO, Transport and doping
15h30						ZnO, Device
15h45		Abe T.	Coffee break			Dots & nanowires 1
16h00	Coffee break	De Jesus	Xiong Q.			Dots & nanowires 2
16h15		Okamoto	Hermier			Colloidal systems
16h30		Ivanov	Guyot-sionnest	Social Program		Optical and excitonic properties
16h45		Yakushev	Kulakovskii			Spin in dots
17h00	Buhman	Suzuki K.	Cremel			Novel 2D systems, topological systems
17h15						Spin & Magnetism
17h30						Detectors
17h45						Photovoltaic 1
18h00	Cocktail	Poster Session 1	Poster Session 2			Photovoltaic 2
18h15						
18h30					Poster Session 3	
18h45						
19h00					Conference Banquet	

PROGRAM

**Sunday September, 13**

	12:30-13:30	Welcome Lunch	
<b>SuR</b>	14:00-17:30	<b>Review Lectures</b> Chair: Christophe Testelin, <i>Institut des NanoSciences de Paris (France)</i> Pierre Galtier, <i>Groupe d'Etude de la Matière Condensée, Versailles (France)</i>	<a href="#">36</a>
SuR-1	14:00-15:00	II-VI Semiconductors for Photonic Device Applications: Beyond the Blue Laser <b>Maria Tamargo</b> <i>City University of New York (United States)</i>	<a href="#">37</a>
SuR-2	15:00-16:00	The adventure of copper indium gallium diselenide solar cells : recent developments and future challenges <b>Daniel Lincot</b> <i>Institut de Recherche et Développement sur l'Energie Photovoltaïque, Chatou (France)</i>	<a href="#">38</a>
	16:00-16:30	Coffee break (30min)	
SuR-3	16:30-17:30	Surface-state transport in topological insulators <b>Hartmund Buhman</b> <i>Physikalisches Institut, Universität Würzburg (Germany)</i>	<a href="#">39</a>
	17:30-18:45	Cocktail	

**Monday September, 14**

	08:45-09:00	Opening Session	
<b>MoA</b>	09:00-10:30	<b>Growth and Characterizations 1</b> Chair: Shizuo Fujita, <i>Kyoto University (Japan)</i>	40
MoA-1	09:00-09:30	ZnTe/CdSe type II heterostructures investigated by transmission electron microscopy (HR-STEM) and atom probe tomography (APT) <b>Bougerol Catherine (Invited)</b> <i>Institut Néel, Grenoble (France)</i>	41
MoA-2	09:30-09:45	ZnTe Layers on R- and S-plane Sapphire Substrates <b>Nakasu Taizo</b> <i>Department of Electrical Engineering &amp; Bioscience, Waseda University (Japan)</i>	42
MoA-3	09:45-10:00	Near-forward Raman Study of Zn(Se,S) and (Zn,Be)Se bulk Phonon-polaritons Collapse vs. Reinforcement Regimes of the Intermediary Mixed-bond Branch <b>Dicko Hamadou</b> <i>Laboratoire de Chimie et Physique, Approche Multi-Echelle des milieux complexes, Metz (France)</i>	43
MoA-4	10:00-10:15	Internal Laser Characteristics of Optically Pumped Yellow-Orange Lasers <b>Alyamani Ahmed</b> <i>Stepanov Institute of Physics, National Academy of Science of Belarus (Belarus)</i>	44
MoA-5	10:15-10:30	Growth of $\text{LiIn}_{1-x}\text{Ga}_x\text{Se}_2$ Semi-Insulating Crystals <b>Stowe Ashley</b> <i>Consolidated Nuclear Security Y12 (United States)</i>	46
	10:30-11:00	Coffee break (30min)	
<b>MoB</b>	11:00-12:15	<b>ZnO, Nanowire</b> Chair: Jürgen Gutowski, <i>Institute of Solid State Physics, University of Bremen (Germany)</i>	47
MoB-1	11:00-11:15	On the benefits of annealing ZnO nanowires under zinc pressure <b>Zehani Emir</b> <i>Groupe d'Etude de la Matière Condensée, Université de Versailles (France)</i>	48
MoB-2	11:15-11:30	Large scale well-ordered, periodically patterned multifunctional ZnO <b>Gokarna Anisha</b> <i>Laboratoire de Nanotechnologie et d'Instrumentation Optique, Troyes (France)</i>	49
MoB-3	11:30-11:45	Efficient Nitrogen Incorporation in ZnO Nanowires by Unintentional Doping <b>Stehr Jan Eric</b> <i>Linköping University (Sweden)</i>	50
MoB-4	11:45-12:00	Luminescence dynamics of hybrid ZnO nanowire/CdSe quantum dot structures <b>Bley Stephanie</b> <i>Institute of Solid State Physics, Semiconductor Optics, University of Bremen (Germany)</i>	51

MoB-5	12:00-12:15	Thermal Conductivity of a Single ZnO Nanowire <b>Yuldashev Shavkat</b> <i>Quantum-Functional Semiconductor Research Center, Dongguk University (South Korea)</i>	52
	12:15-13:45	Lunch break (90min)	
<b>MoC</b>	13:45-15:00	<b>Spin in Dots</b> Chair: Sergey Ivanov, <i>Ioffe Physical -Technical Institute (Russia)</i>	53
MoC-1	13:45-14:15	Individual ions of transition metals in II-VI quantum dots and photonic structures <b>Pacuski Wojciech (Invited)</b> <i>Institute of Experimental Physics, Faculty of Physics, University of Warsaw, (Poland)</i>	54
MoC-2	14:15-14:30	Strain controlled coherent dynamics of coupled carriers and Mn spins in a charged Mn-doped quantum dot <b>Lafuente Sampietro Alban</b> <i>Institut Néel, Grenoble (France)</i>	55
MoC-3	14:30-14:45	Spin Relaxation Dynamics of an Individual Co <sup>2+</sup> Ion in a CdTe/ZnTe Quantum Dot <b>Bogucki Aleksander</b> <i>Institute of Experimental Physics, Faculty of Physics, University of Warsaw (Poland)</i>	56
MoC-4	14:45-15:00	Colloidal CdS/ZnS Quantum Dots - Doped with Manganese and Functionalized with Organic Dye Molecules <b>Heimbrodt Wolfram</b> <i>Department of Physics and Material Sciences, Philipps University Marburg (Germany)</i>	57
	15:00-15:30	Coffee break (30min)	
<b>MoD</b>	15:30-17:15	<b>Detectors</b> Chair: Arnold Burger, <i>Fisk University (United States)</i>	58
MoD-1	15:30-16:00	UV-APDs using ZnSe-based organic-inorganic hybrid structure with long lifetime and device integration <b>Abe Tomoki (Invited)</b> <i>Tottori University (Japan)</i>	59
MoD-2	16:00-16:15	II-VI Broadband Quantum Cascade Detectors <b>De Jesus Joel</b> <i>Department of Physics, The Graduate Center and The City College of New York (United States)</i>	60
MoD-3	16:15-16:30	Gamma-Ray Tolerance of CdS/CdTe Photodiodes for Radiation Tolerant Compact Image Sensor with Field Emitter Array <b>Okamoto Tamotsu</b> <i>Department of Electrical and Electronic Engineering, National Institute of Technology, Kisarazu College (Japan)</i>	62

MoD-4	16:30-16:45	High Power II-VI/InGaN Laser Diode Converters Emitting in the Green-Yellow Spectral Region <b>Ivanov Sergey</b> <i>Ioffe Institute, St. Petersburg (Russia)</i>	<a href="#">64</a>
MoD-5	16:45-17:00	HgCdTe p <sup>+</sup> -n structures grown by MBE on Si (013) substrates for high operating temperature MWIR detectors <b>Yakushev Maxim</b> <i>A.V.Rzhanov Institute of semiconductor physics (Russia)</i>	<a href="#">65</a>
MoD-6	17:00-17:15	Electric Field Inhomogeneity in Ohmic Cd(Zn)Te Detectors Measured by Time-of-Flight Technique <b>Suzuki Kazuhiko</b> <i>Hokkaido University of Science (Japan)</i>	<a href="#">66</a>
<b>MoP</b>	17:15-18:45	<b>Poster Session 1 (MoP)</b>	<a href="#">145</a>

## Tuesday September, 15

<b>TuA</b>	08:30-10:00	<b>Growth and Characterizations 2</b> Chair: Maria Tamargo, <i>City University of New York (United States)</i>	67
TuA-1	08:30-09:00	MBE growth of 2D layered chalcogenides <b>Liu Xinyu (Invited)</b> <i>Department of Physics, University of Notre Dame (United States)</i>	68
TuA-2	09:00-09:15	Hydrogen contamination in ZnO films grown at low temperature <b>Guziewicz Elzbieta</b> <i>Institute of Physics, Polish Academy of Sciences, Warsaw (Poland)</i>	69
TuA-3	09:15-09:30	Nearest-neighbour Lattice Distortions in Oxygen-deficient Mn-doped ZnO and MgZnO Thin Films, Probed by Electron Paramagnetic Resonance <b>Lorenz Michael</b> <i>Institut für Experimentelle Physik II, Universität Leipzig (Germany)</i>	70
TuA-4	09:30-09:45	Homoepitaxial nonpolar ZnO/ZnMgO multilayers: fabrication of Distributed Bragg Reflectors and optical microcavities <b>Zuniga-Perez Jesus</b> <i>Centre de recherche sur l'hétéroépitaxie et ses applications, Valbonne (France)</i>	71
TuA-5	09:45-10:00	Characterization of doping by Scanning Capacitance Microscopy and C(V) technique in ZnO nanowires for optoelectronic application <b>Wang Lin</b> <i>Laboratoire de Physique de l'ENS Lyon (France),</i>	72
	10:00-10:30	Coffee break (30min)	
<b>TuB</b>	10:30-12:15	<b>Novel 2D systems, topological systems</b> Chair: Rameshwar Bhargava, <i>Nanocrystals (United States)</i>	74
TuB-11	10:30-11:00	Terahertz Radiation Induced Electric Currents in Topological Insulators <b>Ganichev Sergey (Invited)</b> <i>University of Regensburg (Germany)</i>	75
TuB-2	11:00-11:15	Electrical detection of spin polarization in the surface Dirac states of a 3D topological insulator, BiSeTeSe <b>Shiraishi Masashi</b> <i>Department of Electronic Science and Engineering, Kyoto Univ. (Japan)</i>	76
TuB-3	11:15-11:30	Valley dynamics probed through exciton emission in monolayer Wse <sub>2</sub> , MoSe <sub>2</sub> and MoS <sub>2</sub> <b>Wang Gang</b> <i>Laboratoire de Physique et Chimie des Nano-Objets, Toulouse (France)</i>	77
TuB-4	11:30-11:45	Quantum Transport in HgTe/CdTe Topological Insulator structures. <b>Thomas Candice</b> <i>CEA-LETI, MINATEC, Grenoble (France)</i>	78

TuB-I5	11:45-12:15	Advances and Perspectives in II-VI Telluride Heterostructures <b>Wojtowicz Tomasz (Invited)</b> <i>Institute of Physics, Polish Academy of Sciences, Warsaw (Poland)</i>	79
	12:15-13:45	Lunch break (90min)	
<b>TuC</b>	13:45-15:15	<b>Photovoltaic 1</b> Chair: Alexey Toropov, <i>Ioffe Institute (Russia)</i>	80
TuC-I	13:45-14:15	Semiconductor Quantum Dots and Solar Energy Conversion <b>Klimov Victor (Invited)</b> <i>Chemistry Division, Los Alamos National Laboratory (United States)</i>	81
TuC-2	14:15-14:30	Dielectric Confinement in Layered II-VI Semiconductor Colloidal Nanoplatelets and Hybrid Perovskites <b>Even Jacky</b> <i>Fonctions Optiques pour les Technologies de l'information, Rennes (France)</i>	82
TuC-3	14:30-14:45	Crystallographic and Optical Characterizations of Ag(Ga,Al)Te <sub>2</sub> Layers Grown on c-plane Sapphire Substrates by Closed Space Sublimation <b>Urano Aya</b> <i>Department of Electrical Engineering and Bioscience, Waseda University (Japan)</i>	83
TuC-4	14:45-15:00	Novel Ternary Wurtzite Semiconductor $\beta$ -CuGaO <sub>2</sub> <b>Suzuki Issei</b> <i>Osaka University (Japan)</i>	84
TuC-5	15:00-15:15	Electronic Structure and Relative Stability of Binary (Ga/In)Se and Pseudoternary Cu(In,Ga)Se <sub>2</sub> Semiconductors <b>Sroul Juliana</b> <i>Laboratoire de Chimie et Physique - Approche Multi-échelles des Milieux Complexes, Metz (France),</i>	85
	15:15-15:45	Coffee break (30min)	
<b>TuD</b>	15:45-17:15	<b>Dots and Nanowires 1</b> Chair: Piotr Kossacki, <i>Warsaw University (Poland)</i>	86
TuD-I	15:45-16:15	Laser Cooling of CdS II-VI Semiconductor Nanoribbons: Towards All Solid State Semiconductor Optical Cooler <b>Xiong Qihua (Invited)</b> <i>Nanyang Technological University (Singapore)</i>	87
TuD-2	16:15-16:30	Measurement by Photon-Correlation Fourier Spectroscopy of the spectral diffusion and time-coherence of the trion fluorescence in thick-shell CdSe/CdS nanocrystals <b>Hermier Jean-Pierre</b> <i>Université Versailles Saint-Quentin en Yvelines (France)</i>	88

TuD-3	16:30-16:45	Mid-infrared detection with interband and intraband colloidal quantum dot transitions <b>Guyot-Sionnest Philippe</b> <i>University of Chicago (United States)</i>	89
TuD-4	16:45-17:00	Control of semiconductor quantum dot emission intensity and polarization by metal nanoantennas <b>Kulakovskii Vladimir</b> <i>Institute of Solid State Physics Russian Academy of Sciences (Russia)</i>	90
TuD-5	17:00-17:15	Vertical CdSe/ZnSe nanowire quantum dot and photonic wire for single-photon emission <b>Cremel Thibault</b> <i>Laboratoire Nanophysique des Semiconducteurs, Grenoble (France)</i>	91
<b>TuP</b>	17:15-18:45	<b>Poster Session 2 (TuP)</b>	219

## Wednesday September, 16

<b>WeA</b>	08:30-10:15	<b>Spin and Magnetism</b> Chair: Jacek Kossut, <i>Institute of Physics, Polish Academy of Sciences (Poland)</i>	92
WeA-1	08:30-09:00	Coherent optical spectroscopy in CdTe quantum well structures: Storing light in the electron spin ensemble <b>Akimov Ilya (Invited)</b> <i>TU Dortmund University (Germany)</i>	93
WeA-2	09:00-09:15	Atomic-like spin fluctuations of Manganese atoms in CdTe quantum wells <b>Cronenberger Steeve</b> <i>Laboratoire Charles Coulomb, Montpellier (France)</i>	94
WeA-3	09:15-09:30	Spin-orbit Stiffness of the Spin-polarized Electron Gas <b>Baboux Florent</b> <i>Institut des NanoSciences de Paris (France)</i>	95
WeA-4	09:30-09:45	Charged Carrier Spin Dynamics in ZnO Epilayers and Quantum Wells <b>Puls Joachim</b> <i>Institute of Physics, Humboldt-University, Berlin (Germany)</i>	96
WeA-5	09:45-10:00	Long-range p-d exchange interaction in a ferromagnet-semiconductor hybrid structure <b>Debus Joerg</b> <i>Experimentelle Physik 2, TU Dortmund, Dortmund, Germany (Germany)</i>	97
WeA-6	10:00-10:15	(Al)GaAs:Be/Zn(Mn)Se Heterovalent Quantum Well Heterostructures: Electrical and Structural Properties <b>Komissarova Tatiana</b> <i>Ioffe Institute, St. Petersburg (Russia)</i>	98
	10:15-10:45	Coffee break (30min)	
<b>WeB</b>	10:45-12:15	<b>ZnO, Plasmonic and optical engineering</b> Chair: Joachim Puls, <i>Institute of Physics, Humboldt-University, Berlin (Germany)</i>	99
WeB-1	10:45-11:15	ZnO plasmonic <b>Kalusniak Sascha (Invited)</b> <i>Institut für Physik, Humboldt-Universität zu Berlin (Germany)</i>	100
WeB-2	11:15-11:30	Free-electron concentration and polarity inversion domains in plasmonic (Zn,Ga)O <b>Sadofev Sergey</b> <i>Institut für Physik, Humboldt-Universität zu Berlin (Germany)</i>	101
WeB-3	11:30-11:45	Enhanced luminescence excitation via efficient optical energy transfer <b>Aad Roy</b> <i>Laboratoire de Nanotechnologie et d'Instrumentation Optique, Troyes (France)</i>	102

WeB-4	11:45-12:00	Interface engineering in ZnO/organic hybrid structures for optimized excitonic coupling and charge transfer <b>Blumstengel Sylke</b> <i>Humboldt Universität, Berlin (Germany)</i>	103
WeB-5	12:00-12:15	Colloidal Quantum Dot-Based Excitonic Light-Emitting Devices <b>Lee Seonghoon</b> <i>School of Chemistry, Seoul National University (South Korea)</i>	104
	12:15-13:30	Lunch break (75min)	
	13:30-19:00	Social Program	

**Thursday September, 17**

<b>ThA</b>	08:30-10:00	<b>Colloidal systems</b> Chair: Grzegorz Karczewski, <i>Institute of Physics, Polish Academy of Sciences (Poland)</i>	105
ThA-1	08:30-09:00	Preparation and study of semiconductors with a honeycomb nanogeometry <b>Vanmaekelbergh Daniel (Invited)</b> <i>University of Utrecht (Netherlands)</i>	106
ThA-2	09:00-09:15	Transport properties of 2D colloidal nanoplatelets to achieve enhanced photo-conduction properties <b>Lhuillier Emmanuel</b> <i>Laboratoire de Physique et d'Etude des Matériaux, Paris (France)</i>	107
ThA-3	09:15-09:30	Polarimetric Determination of CdSe/CdS Dipole Orientation <b>Maitre Agnes</b> <i>Institut des Nanosciences de Paris (France)</i>	108
ThA-4	09:30-09:45	Alignment of Rod-Shaped Single-Photon Emitters Driven by Line Defects in Liquid Crystals <b>Pelliser Laurent</b> <i>Institut des Nanosciences de Paris (France)</i>	109
ThA-5	09:45-10:00	Gold Plated and Thick Shell Quantum Dots: Two Examples of Colloidal Quantum Dots with Much Improved Optical Properties <b>Nasilowski Michel</b> <i>Laboratoire de Physique et d'Etude des Matériaux, Paris (France)</i>	110
	10:00-10:30	Coffee break (30min)	
<b>ThB</b>	10:30-12:15	<b>ZnO, Transport and Doping</b> Chair: Chong-Xin Shan, <i>Changchun Institute of Optics, Chinese Academy of Sciences (China)</i>	111
ThB-1	10:30-11:00	Novel Quantum Transport of 2D Electrons in MBE-Grown ZnO Heterostructures <b>Kozuka Yusuke (Invited)</b> <i>University of Tokyo (Japan)</i>	112
ThB-2	11:00-11:15	ZnO-Based Oxide Semiconductors for Transparent Electronics <b>Lu Jianguo</b> <i>School of Materials Science and Engineering, Zhejiang University (China)</i>	113
ThB-3	11:15-11:30	Electrical properties, and Optical properties of p-n and p-i-n heterostructures based on p-ZnO, n-GaN and i-Al <sub>2</sub> O <sub>3</sub> <b>Przedziecka Ewa</b> <i>Institute of Physics Polish Academy of Sciences (Poland)</i>	114
ThB-4	11:30-11:45	Stabilization of p-type N-doped Zn-deficient ZnO Nanoparticles <b>Jobic Stéphane</b> <i>Institut des Matériaux Jean Rouxel, Nantes (France)</i>	115

ThB-5	11:45-12:00	Research on p-type Doping, Bandgap Engineering and Stability of Thin-Film Transistors in ZnO and its Related Oxide <b>Ye Zhizhen</b> <i>School of Materials Science and Engineering, Zhejiang University (China)</i>	116
ThB-6	12:00-12:15	The ZnO:(N, Al)-based homojunction deposited at low temperature <b>Snigurenko Dmytro</b> <i>Institute of Physics, Polish Acad. of Sciences, Warsaw (Poland)</i>	117
	12:15-13:45	Lunch break (90min)	
<b>ThC</b>	13:45-15:15	<b>Photovoltaic 2</b> Chair: Henri Mariette, <i>Institut Néel (France)</i>	118
ThC-1	13:45-14:15	Progress in polycrystalline CdTe PV beyond 21% <b>Gloecker Marcus (Invited)</b> <i>First Solar Inc. (United States)</i>	119
ThC-2	14:15-14:30	Chemical engineering of CdTe and Cd <sub>x</sub> Zn <sub>1-x</sub> Te surfaces in aqueous HBr/Br <sub>2</sub> solutions <b>Etcheberry Arnaud</b> <i>Institut Lavoisier, Université de Versailles (France)</i>	120
ThC-3	14:30-14:45	Valence band offset between CdX and CdCl <sub>2</sub> <b>Tomic Stanko</b> <i>University of Salford (United Kingdom)</i>	121
ThC-4	14:45-15:00	Molecular Beam Epitaxy of Short-Period Zn(S)Se/CdSe/In <sub>0.3</sub> Ga <sub>0.7</sub> As Superlattices with the Effective Bandgap Energy of 2.1-2.2 eV <b>Sorokin Sergey</b> <i>Ioffe Physico-Technical Institute, St. Petersburg (Russia)</i>	122
ThC-5	15:00-15:15	Four-Junction Heterovalent Solar Cells Based on II-VI/III-V/Ge Coherent and Metamorphic Heterostructures <b>Toropov Alexey</b> <i>Ioffe Physico-Technical Institute, St. Petersburg (Russia)</i>	124
	15:15-15:45	Coffee break (30min)	
<b>ThD</b>	15:45-17:15	<b>ZnO, Device</b> Chair: Michael Lorenz, <i>Institut für Experimentelle Physik II, Universität Leipzig (Germany)</i>	125
ThD-1	15:45-16:15	Recent Progress on Electrically Pumped ZnO Lasers <b>Liu Jianlin (Invited)</b> <i>University of California, Riverside (United States)</i>	126

ThD-2	16:15-16:30	10 GHz Operation of Schottky Diodes Based on IGZO <b>Zhang Jiawei</b> <i>School of Electrical Engineering and Electronics, University of Manchester (United Kingdom)</i>	127
ThD-3	16:30-16:45	Resistive-switching Memory and Ultraviolet Light-emitting Diodes Based on ZnO related Materials <b>Liu Yichun</b> <i>Center for Advanced Optoelectronic Functional Materials Research, Northeast Normal University (China)</i>	128
ThD-4	16:45-17:00	ZnO-Based Avalanche Photodetectors <b>Shan Chong-Xin</b> <i>Changchun Institute of Optics, Fine Mechanics and Physics, Chinese Academy of Sciences (China)</i>	129
ThD-5	17:00-17:15	High Performance Indium-Gallium-Zinc-Oxide-Based Schottky Diodes Fabricated at Room Temperature <b>Xin Qian</b> <i>Shandong University (China)</i>	130
<b>ThP</b>	17:15-18:45	<b>Poster Session 3 (ThP)</b>	298
	19:30-23:30	Conference Banquet	

**Friday September, 18**

<b>FrA</b>	08:30-10:00	<b>Optical and Excitonic properties</b> Chair: Irina Buyanova, <i>Linköping University (Sweden)</i>	<a href="#">131</a>
FrA-1	08:30-08:45	Second-Harmonic Generation Spectroscopy of Excitons in ZnO <b>Pavlov Victor</b> <i>Ioffe Physical-Technical Institute, the Russian Academy of Sciences (Russia)</i>	<a href="#">132</a>
FrA-2	08:45-09:00	Spectroscopy of Trion states in non-polar ZnO Quantum Wells and their use to monitor Spin Injection <b>Morhain Christian</b> <i>Centre de recherche sur l'hétéroépitaxie et ses applications, Valbonne (France)</i>	<a href="#">133</a>
FrA-3	09:00-09:15	Exciton-polariton thermodynamics in ZnSe-based microcavities <b>Klembt Sebastian</b> <i>Institut Néel, Grenoble (France)</i>	<a href="#">134</a>
FrA-4	09:15-09:30	Interaction of Tamm plasmons with cavity photons and excitons in ZnSe-based microcavities <b>Rahman Sk. Shaïd-Ur</b> <i>Institute of Solid State Physics, Semiconductor Optics, University of Bremen (Germany)</i>	<a href="#">135</a>
FrA-5	09:30-09:45	Effect of parity in magneto-optical spectra of quantum wells <b>Kochereshko Vladimir</b> <i>Ioffe Physical-Technical Institute, St. Petersburg (Russia)</i>	<a href="#">136</a>
FrA-6	09:45-10:00	Laser Induced Tellurium Formation Detected by Coherent Phonon Excitation in Plasmonic Crystals <b>Kreilkamp Lars Erik</b> <i>Experimentelle Physik 2, Technische Universität Dortmund (Germany)</i>	<a href="#">137</a>
	10:00-10:30	Coffee break (30min)	
<b>FrB</b>	10:30-12:00	<b>Dots and Nanowires 2</b> Chair: Maria Chamarro, <i>Institut des NanoSciences de Paris (France)</i>	<a href="#">138</a>
FrB-1	10:30-11:00	Dangling Bond Magnetic Polaron in CdSe Nanocrystals <b>Rodina Anna (Invited)</b> <i>A.F. Ioffe Physico-Technical Institute of Russian Academy of Sciences (Russia)</i>	<a href="#">139</a>
FrB-2	11:00-11:15	Magnetic Polaron Formation in (Cd,Mn)Te Quantum Dots inserted in ZnTe Nanowires <b>Artioli Alberto</b> <i>Institut Néel, Grenoble (France)</i>	<a href="#">140</a>
FrB-3	11:15-11:30	Magneto-photoluminescence of Tellurium Isoelectronic Bound Excitons in Zn-Se-Te in the Presence of Type-II Submonolayer Quantum Dots <b>Deligiannakis Vasilios</b> <i>The Graduate Center, CUNY, New York, New York 10016 (United States)</i>	<a href="#">141</a>

FrB-4 11:30-11:45 Strain induced energy gap variation and valence band mixing in (Zn,Mn)Te/(Zn,Mg)Te core/shell nanowires 143

**Wojnar Piotr**

*Institute of Physics, Polish Academy of Sciences, Warsaw (Poland)*

FrB-5 11:45-12:00 Cd(Se,Te)/ZnSe Quantum Dots: Beyond the Crossroad of Se and Te Based Systems 144

**Sciesiek Maciej**

*Institute of Experimental Physics, Faculty of Physics, University of Warsaw (Poland)*

12:00-12:30

Closing Session

**Poster Session 1**, Monday September, 14 (17:15-18:45)

<b>MoP-I</b>	<b>Growth and characterization , doping and defects</b>	<b>146</b>
MoP-1	Deuterium diffusion in nitrogen-doped ZnO at room temperature	147
MoP-2	Electronic Band Structure Engineering of $\text{ZnO}_{1-x}\text{S}_x$ and $\text{ZnO}_{1-x}\text{Te}_x$ Highly Mismatched Alloys	148
MoP-3	Quasiamorphous ZnO layers produced by the ALD technique	149
MoP-4	MOCVD growth of ZnO nanowires on Ni-W metallic substrates	150
MoP-5	Influence of ZnO Admixture and $\text{Co}^{2+}$ Doping on the Photolytic Behavior of Nanocrystalline Zinc Sulfide	151
MoP-6	ZnO microstructures Obtained by HFCVD and Its Characterization.	152
MoP-7	High quality ZnO nanotube on conductive substrate by pulsed laser deposition	153
MoP-8	Influence of Substrate Temperature on Crystalline Characteristics and Optical Properties of Tourmaline/ZnO Thin Film	154
MoP-9	Enhanced Photocatalytic Activity of Hierarchical ZnO Nanostructure for Water Purification	155
MoP-10	Chemical and Physical Growth Mechanisms of Zinc Sulfide and Zinc Oxide Thin Films Grown by Mist Chemical Vapor Deposition	156
MoP-11	Energy Harvesting Based on ZnO Nanostructure	157
MoP-12	ZnO Nanostructure Synthesis via Hydrothermal and Electrospinning Methods for Gas Sensor	158
MoP-13	Polarity Effects on the Formation of ZnO Nanowires and Related Heterostructures with CdSe and CdTe	159
MoP-14	Spatially controlled growth of highly crystalline ZnO nanowires by an inkjet-printing catalyst-free vapor-solid method	160
MoP-15	Controlling the structural uniformity of ZnO nanowires grown by chemical bath deposition	161
MoP-16	Structural and optical characterization of hybrid ZnO/polymer core-shell nanowires fabricated by oxidative chemical vapor deposition	162
MoP-17	Transparent Conducting Magnetic V:ZnO	163
MoP-18	Unambiguous defect identification in compound semiconductors by positron annihilation spectroscopy	164
MoP-19	Dependence of the Structural, Chemical and Electrical Properties of GaAs/ZnSe Heterovalent Interface on MBE Growth Mode	165
MoP-20	Significantly improved interface recombination velocity and minority carrier lifetime for CdTe/MgCdTe double heterostructures	166
MoP-21	Influence of Source Transport Rate upon Compositions of Mg and Se in $\text{Zn}_{1-x}\text{Mg}_x\text{Se}_y\text{Te}_{1-y}$ Layers grown by Metalorganic Vapor Phase Epitaxy	168
MoP-22	ZnSTe Lattice-matched to GaP Substrates Grown by Molecular Beam Epitaxy Using ZnS Buffer Layers	170
MoP-23	Low Pressure MOVPE Growth and Characterization of ZnTe Homoepitaxial Layers	171
MoP-24	Diffusion Driven Growth of Nanowires: The case of ZnTe	173
MoP-25	Photoluminescence of High-Resistivity ZnTe Crystals Doped with Gallium and Indium	174
MoP-26	Ultrasonic-Assisted Mist Chemical Vapor Deposition for Oxide and Sulfide Semiconductor Thin Films	175
MoP-27	Percolation-type Multi-phonon Pattern of Zn(Se,S): Ambient/High-pressure Backward/Near-forward Raman Scattering and Ab Initio Calculations	176

MoP-28	Growth and Characterization of $Mg_{1-x}Cd_xO$ Thin Films	177
MoP-29	Electronic spectrum of Bi-related defects in crystalline cadmium telluride	178
MoP-30	Application of the difference spectroscopy for studying of complex acceptors in Cd(Zn)Te	179
MoP-31	Preparation of $Cu_2ZnSnSe_4$ films from selenization of Cu-Zn-Sn spin-coated precursors by dimethyl selenide	180
<b>MoP-II</b>	<b>ZnO , related oxydes and Transparent conductors (devices and physics)</b>	<b>181</b>
MoP-32	Persistent photoconductivity of ZnO nanowires under varying ambient conditions	182
MoP-33	Band Tail Induced Photoluminescence Broadening in Heavily-Doped n-Type ZnO Nanowires	184
MoP-34	Annealing effects on nitrogen-doped ZnO nanowires	185
MoP-35	Enhanced Ultraviolet Luminescence of ZnO Nanorods Treated by High-Pressure Water Vapor Annealing	186
MoP-36	Enhanced ultraviolet emission from Au/Ag-nanoparticles@MgO/ZnO heterostructure light-emitting diodes: A combined effect of exciton- and photon- localized surface plasmon couplings	188
MoP-37	Improvement of thermal stability of p-ZnO:(Al,N) thin films by oxidizing $Zn_3N_2$ :Al thin films	189
MoP-38	Characterization of ZnO Thin Film Grown on Vicinal-Cut Sapphire (0001) Substrates by MOCVD	190
MoP-39	Growth, optical and structural properties of ZnO/ZnMgO core-shell quantum wells	191
MoP-40	MgZnO growth on (0001)sapphire by mist chemical vapor deposition	192
MoP-41	Properties of ZnO/ZnMgO Nanostructures Grown on R-plane $Al_2O_3$ Substrates by MBE	193
MoP-42	Structural, Electrical and Optical Properties of Ga-Doped ZnO Films Grown on Flexible Substrates by Using Plasma-assisted Molecular Beam Deposition	194
MoP-43	ZnO:Tb Films Grown by RF Magnetron Sputtering: the dependence of structural and luminescent properties on the type of the substrate	195
MoP-44	Effects of band anticrossing on the temperature dependence of the band gap of Zn(Cd)TeO	196
MoP-45	Positron lifetime spectroscopy of vacancy-related defects in ZnO	197
MoP-46	Fabrication of Flexible and Freestanding ZnO Few Layers	199
<b>MoP-III</b>	<b>Detectors and new devices: X and gamma high energy sensors , Infrared, visible, and UV materials and devices</b>	<b>200</b>
MoP-47	20 MHz Operation of Organic Nano-Diodes	201
MoP-48	Multi-Band Radiation Detector Based on HgCdTe Heterostructure	202
MoP-49	II-VI Quantum Cascade Emitters in the 6-8 $\mu m$ range	203
MoP-50	Photosensitive MIS Structures with Ultrathin Dielectric Based on $Cd_xHg_{1-x}Te$ ( $x \simeq 0.4$ )	205
MoP-51	Application of Indium Tin Oxide to the p-cladding Layers of Yellow/Green II-VI Compound Semiconductor Laser Diode Structures on InP Substrates	206
MoP-52	Molecular Beam Epitaxy of II-VI/GaAs Laser Heterostructures for Yellow-Orange Spectral Range	208
MoP-53	Terahertz Excitations in HgTe-based Field Effect Transistors	210
MoP-54	Growth and characterization of ZnCdSe/ZnCdMgSe two-color quantum-well infrared photodetectors	211

MoP-55	Mid-infrared light sensitive p-CdZnTe/i-CdTe/n-CdTe diode structures with PbTe nanoinclusions	212
MoP-56	Investigation of Yellow/Green II-VI Compound Semiconductor Laser Diode Structures on InP Substrates	213
MoP-57	Analysis of the diffusion of charge carriers in the photosensing film of photovoltaic n-on-p HgCdTe IR FPA detectors	215
MoP-58	640x512 Focal Plane Assemblies based on HgCdTe heterostructures grown by MBE	217
MoP-59	Investigation of Au/Zn composite electrode on CdZnTe detector	218

**Poster Session 2**, Tuesday September, 15 (17:15-18:45)

<b>TuP-I</b>	<b>Low-dimensional structures and related physics (novel 2D systems, nanostructures, quantum dots, colloidal nanocrystals)</b>	<b>220</b>
TuP-1	Influence of Shell Thickness on the Charge Transfer Dynamics from Photoexcited PbS/CdS Quantum Dots to Metal Oxides	221
TuP-2	Electric field imaging in single ZnO nanowire Schottky diodes	222
TuP-3	Polarization Resolved Photoluminescence Excitation Studies of Individual CdSe Quantum Dots Emitting in Yellow Spectral Range	223
TuP-4	Photoinduced Transformations of Optical Properties of the CdSe and AgInS <sub>2</sub> Quantum Dots Embedded in the Films of Polyvinyl Alcohol	224
TuP-5	Defect composition in acceptor doped ZnO quantum structures	225
TuP-6	Application of DBRs for the Enhancement of CdTe Quantum Dots Photoluminescence in Single Emitter Studies	226
TuP-7	Magneto-Optical Studies of Semimagnetic Cavity Polaritons in a (Cd,Zn,Mg)Te Based Microcavity	227
TuP-8	Collinear Four-Wave Mixing using Laguerre-Gauss modes in CdTe quantum well	228
TuP-9	Comparative studies of CdSe/ZnSe Quantum Dot Structures Epitaxially Grown either with or without a Sub-monolayer CdTe Stressor	229
TuP-10	Direct determination of zero field splitting of a Co <sup>2+</sup> ion in a CdTe/ZnTe QD	230
TuP-11	Coherent spin evolution of acceptor-bound excitons in a CdTe quantum well	232
TuP-12	Spectral selection of excitonic transitions in a dense array of epitaxial CdSe/ZnSe quantum dots	233
TuP-13	Using single CdTe nanocrystals to study excitons from the quantum confined to the bulk regime	234
TuP-14	Mobility of the Two-Dimensional Electron Gas in Modulation Doped CdTe Quantum Well Structures with Gate Controlled Electron Concentration	235
TuP-15	Magneto-optical studies of CdTe and CdSe quantum dots	236
TuP-16	Quantum confined Stark effect of polar and non-polar ZnO/ZnMgO quantum wells grown by MBE	238
TuP-17	Magnetic Ground State of an Individual Fe <sup>2+</sup> Ion in a Strained Semiconductor Quantum Dot	239
TuP-18	Strong excitonic effects dominate linear and nonlinear optical response in monolayer WSe <sub>2</sub> and MoSe <sub>2</sub>	240
TuP-19	Marking of individual CdTe/ZnTe Quantum Dots containing a single Mn <sup>2+</sup> ion using single-color, in situ photolithography technique	241
TuP-20	Synthesis and characterization of opto-magnetic ZnO/MgO core/shell doped copper ions nanoparticles	242
TuP-21	Influence of Phonon Confinement on Optical Phonon-Mediated Carrier Capture into CdSe/ZnS/H <sub>2</sub> O Quantum Dots	243
TuP-22	Tuning the emission energy from CdTe and CdSe quantum dots by copper doping	244
TuP-23	A correlative study of interfacial structure in type II ZnTe/CdSe superlattices	245
TuP-24	Mn-enhanced collective emission of CdMnSe quantum dots	247

<b>TuP-II</b>	<b>Spin related phenomena (topological insulators , magnetic semiconductors , magnetic devices)</b>	<b>248</b>
TuP-25	Growth, Structure, Electronic and Vibrational properties of Epitaxial Bi <sub>2</sub> Se <sub>3</sub> Topological Insulator Films on GaAs(111) Substrates.	249
TuP-26	Rhenium monoselenide: an investigation by density functional theory	250
TuP-27	Sum rule constraints on the surface state conductance of topological insulators	251
TuP-28	Spin Dynamics of Tellurium Isoelectronic Bound Excitons in Zn-Se-Te Nanostructures	252
TuP-29	Peculiarities of Room Temperature Magnetic Properties of single ZnO:Mn Nanowires revealed by Magnetic Force Microscopy	254
TuP-30	Spin dependent energy transfer in II-Mn-VI DMS nanostructures	255
TuP-31	Highly Spin-Polarized Green Electroluminescence Achieved by Spin Filter in Semimagnetic Semiconductor Bicrystals	256
TuP-32	Long Spin-Flip Time and Large Zeeman Splitting of Holes in Type-II ZnTe/ZnSe Submonolayer Quantum Dots	257
TuP-33	Vibrational and Magnetic Properties of Co-doped Hexagonal ZnO	258
TuP-34	Enhanced Conduction- to Valence-Subband Overlap in the HgTe Double Quantum Well	259
TuP-35	Electron Spin Flip Raman Spectroscopy and Magneto-Resistance of the Diluted Magnetic Semiconductor Zn <sub>1-x</sub> Mn <sub>x</sub> Se below the Metal-Insulator Transition	261
TuP-36	Evidence of Exchange Interaction of Localized Carriers and Transition Metals in Diluted II-VI nanostructures: ODMR Study	262
TuP-37	Optical probing of the spin state of a single Cr <sup>2+</sup> ion in a quantum dot	263
TuP-38	EPR Study of Layers Obtained from ZnCrTe Target by PLD Method	264
TuP-39	Optical and magnetic studies on MBE-grown ferromagnetic CrSe and CrS layers in zincblende structure	266
TuP-40	Magnetic Phase Transitions in ZnO Doped by Transition Metals	267
<b>TuP-III</b>	<b>Growth and characterization , doping and defects</b>	<b>268</b>
TuP-41	Spectroscopic and Kinetic Studies of ZnSe and ZnSe:Mn Colloidal Quantum Dots	269
TuP-42	Application of Diffuse X-ray Scattering and Polarization Dependent Photoluminescence for Realistic Modeling of Ultra-thin Quantum Dots	270
TuP-43	Microchip Laser Converter based on InGaN LD and ZnCdSe QDs Heterostructure	272
TuP-44	Cd <sub>x</sub> Zn <sub>1-x</sub> Se quantum dots: Correlation between chemical composition and optical properties	274
TuP-45	Peculiarities of CdS Nanocrystals Formation at Annealing of a Langmuir-Blodgett Matrix	276
TuP-46	Cu <sub>2</sub> ZnSnSe <sub>4</sub> thin film grown by molecular beam epitaxy on GaAs	277
TuP-47	Synthesis and characterization of CuZnSe <sub>2</sub> thin film structures	278
TuP-48	Fabrication of β-CuGaO <sub>2</sub> Thin Films	279
TuP-49	The electrical parameters of Hg <sub>1-x</sub> Cd <sub>x</sub> Te epitaxial films with and without CdTe passivation layers	280
TuP-50	Electrical and optical studies of a tellurium-related defect in molecular-beam epitaxy-grown HgCdTe	281
TuP-51	Acceptor states in HgCdTe films grown by molecular-beam epitaxy on GaAs and Si substrates	282

TuP-52	Admittance of MIS-structures based on graded-gap MBE HgCdTe with Al <sub>2</sub> O <sub>3</sub> insulator	283
TuP-53	Neutronographic characterization of II-VI cubic crystals highly doped by 3d-ions: on possible tendencies to structure rearrangements in the sphalerite crystal lattice.	284
TuP-54	MBE Grown CdTe Absorber Layers on GaAs with In Assisted Thermal Deoxidation	285
TuP-55	Traveling Heater Growth and characterization of (Cd, Mn)Te crystals for radiation detectors	287
TuP-56	Dislocations in MCT heteroepitaxial structures on (013) substrates and possibilities of dislocation density reducing	288
TuP-57	Growth and Characterization of Cd <sub>0.9</sub> Zn <sub>0.1</sub> Te crystal by traveling molten zone method	289
TuP-58	The local electron interaction with crystal defects in wurtzite CdS	290
TuP-59	Vertical Transport of Photoexcited Carriers in a ZnSe/CdSe Superlattice Grown on an In <sub>0.3</sub> Ga <sub>0.7</sub> As Metamorphic Buffer Layer	292
<b>TuP-IV</b>	<b>New materials : Biomaterials, hybrid organic-inorganic structures</b>	<b>294</b>
TuP-60	Study of the effectiveness of CdTe Quantum dots conjugated to Zn(II) tetraethyl-2-pyridil Porphyrin as Photosensitizers in Photodynamic Therapy	295
TuP-61	Morphology and Photoluminescence of Multilayer PbTe/CdTe Heterostructures	296
TuP-62	Interfacial Bonds between CdS Nanoparticles and Polymeric Matrix	297

**Poster Session 3**, Thursday September, 17 (17:15-18:45)

<b>ThP-I</b>	<b>ZnO , related oxydes and Transparent conductors (devices and physics)</b>	<b>299</b>
ThP-1	Homogeneous vertical ZnO nanorod arrays on in-situ conductive Gd nanolayer	300
ThP-2	The Manifestation of Strong d-p - Hybridization in Photoluminescence Spectra of ZnO:Ni and ZnO:Co	301
ThP-3	Electrical properties of ZnO based heterojunctions deposited by Atomic Layer Deposition on 4H-SiC	302
ThP-4	Annealing of Frozen-in Defects in ZnO	303
ThP-5	Identification of Localized Defects in ZnO Nanostructures and Thin Films	304
ThP-6	Defect Related Emission of ZnO and ZnO Cu Nanocrystals Prepared by Electrochemical method	305
ThP-7	Effect of Al and/or Li doping on luminescent properties of highly doped ZnO films	306
ThP-8	Effect of Al doping in Ag layer of MgZnO/Ag/MgZnO dielectric/metal/ dielectric (DMD) UV-visible transparent conductive films	307
ThP-9	Photoconductive properties of non-doped and nitrogen-doped ZnO single crystals in various ambient gases	308
ThP-10	Strain-engineering and Electrical Performance of Aluminium-, Gallium-, and Indium-doped Homoepitaxial ZnO Thin Films	309
ThP-11	Magnetspectroscopy Studies of s, p-d Interaction in Nanocrystalline Zinc Oxide with $Fe_3^+$ Ions	310
ThP-12	Peculiarities of Cu-related and self-activated green emission bands in ZnO and ZnMgO	311
ThP-13	Internal electric fields due to piezoelectric and spontaneous polarizations in ZnO/ZnOS quantum well	312
ThP-14	Anisotropic optical properties of a homoepitaxial (Zn,Mg)O/ZnO quantum wells growth on A plane	313
ThP-15	Luminescence transformation in mixture of ZnO and Carbon nanoparticles at mechanical processing	314
ThP-16	Polariton condensates in ZnO microcavities: propagation Vs localization	315
ThP-17	EPR Investigations on Doped TiO <sub>2</sub> Nanopowders	316
ThP-18	Vertical and Planar ZnO-based Schottky Junctions Obtained by the Atomic Layer Deposition Influence of the Hafnium Dioxide Spacer on Rectifying Properties	317
ThP-19	Effects of the conduction band offset on the efficiency of n-ZnO/p-Si based heterojunctions for photovoltaic applications	318
<b>ThP-II</b>	<b>Optical and electrical properties , photonic engineering</b>	<b>319</b>
ThP-20	Transparent and Flexible AC powder Electroluminescence Device with a Simple Structure of Ag Nanowire/ ZnS:Cu <sup>+</sup> , Mn <sup>2+</sup> /ITO	320
ThP-21	Structural, Optical, and Magnetic Characteristics of II-VI Semiconductor Nanocrystal - Graphene Hybrid Nanostructures	321
ThP-22	Polariton lasing in high-Q fully epitaxial wide-bandgap semiconductor microcavity pillars	322
ThP-23	Enhanced stimulated emission in ZnO thin films by using top-down structuring	323

ThP-24	2D-Localization and Delocalization Effects in Quantum Hall Effect Regime in HgTe Wide Quantum Well	324
ThP-25	Effect of Acoustic Vibrations on Electrical Properties of CdTe Crystals	325
ThP-26	Epitaxial ZnO films implanted with Er and Yb	326
ThP-27	P-D Charge Transfer Excitons in $Zn_{1-x}Ni_xO$ Under Inner Shell Excitation	327
ThP-28	Hopping exciton model of photoluminescence in ZnSeO alloy	328
ThP-29	Excited Electron and Multi-Phonon Coupling in Heavily $Mn^{2+}$ doped ZnS Phosphor	330
ThP-30	RT ZnSe-based Lasers and Laser Arrays Pumped by Low-Energy Electron Beam	331
ThP-31	Influence of the Number of Electronically Coupled CdSe/ZnSe QD Planes on Characteristics of Optically Pumped Green Lasers	332
ThP-32	Innovative approach to the laser mechanoluminescence in II-VI compounds	333
ThP-33	Fabrication of the fully hybrid microcavities based on Zn(S)Se	334
ThP-34	Optical properties of diluted II-VI magnetic semiconductor nanostructures	335
ThP-35	Exciton Spin Hall Effect in Quantum Wells	336
ThP-36	The digital filtration preprocessing of variable magnetic field Hall data before mobility spectrum analysis for p-MCT films	337
ThP-37	MCT Surface Passivation by Atomic Layer Deposition of Thin $Al_2O_3$ Films	338
ThP-38	Optical properties of single wurtzite/zinc-blende ZnSe nanowires grown at low temperature	339
ThP-39	Role of the electron-phonon interaction in the temperature dependence of the phonon mode frequency in the II-VI compound alloys	340
ThP-40	Polariton Lasing and Phase Diagram of a ZnO Microcavity grown on a Patterned Silicon Substrate	341
ThP-41	Study of ZnO exciton-polariton properties by linear and non-linear spectroscopies	342
ThP-42	Electric Field Induced Reversible Photoluminescence Quenching in ZnO Films	343
ThP-43	Electrical Characteristic of ZnO Thin Films Grown on Different p-Si Substrate Elaborated by Sol-Gel Spin-Coating Method	344
ThP-44	Electrical properties of the V-defects of epitaxial HgCdTe	345
ThP-45	Optical properties of II-VI-based Bragg-polariton samples	346
ThP-46	Study on the contact resistivity of Au contacts to (Cd, Mn)Te crystals	347
ThP-47	Light Emitting Properties Dependent on Nitride Stoichiometry of Si-rich-SiN <sub>x</sub> Films Grown by PECVD	348
ThP-48	The stochastic model for ternary and quaternary alloys: Application of the Bernoulli relation to the phonon spectra of mixed crystals	349
<b>ThP-III</b>	<b>Theory and band structure</b>	<b>350</b>
ThP-49	Hall Effect and Negative Energy Gap in HgTe/CdTe Superlattice with Thick Quantum Wells	351
ThP-50	Electronic structure, effective mass and magneto-transport properties in HgTe-CdTe superlattice with large quantum well thickness	353
ThP-51	Donor impurity states in $Ga_xIn_{1-x}As_yP_{1-y}$ stepped quantum well	355
ThP-52	Atomistic Modeling of Zinc Selenide: A molecular Dynamics Study	357
ThP-53	Electron-phonon interaction in anisotropic II-VI quantum wells	358

ThP-54	Full potential calculation of structural, electronic and thermodynamic properties of $Zn_{1-x}Ca_xS$ ternary alloy	359
ThP-55	Structural, electronic and thermodynamic properties of $Sr_xCa_{1-x}S$ : A first-principles study	360
ThP-56	Shape and DMS Doping Effects on the Current and Efficiency of II-VI Quantum Dots Based Solar Cells	361
<b>ThP-IV</b>	<b>Solar cells</b>	<b>362</b>
ThP-57	Preparation and characterization of chemically spray deposited $MoO_3$ thin films and their application as buffer layers in CuPc/C60 based solar cells	363
ThP-58	Application of CdZnS/ZnS Nanocrystals as a Down-converter on the Front Surface of Photovoltaic Cells	364
ThP-59	Monocrystalline ZnTe/CdTe/MgCdTe Double-Heterostructure Solar Cells Grown on InSb Substrates	365
ThP-60	Highly Cr-doped ZnS for intermediate band solar cells	367
ThP-61	Photoresponse Enhancement of $Cu_2O$ Solar Cell with Sulfur-doped ZnO Buffer Layer to Mediate the Interfacial Band Alignment	368
ThP-62	Performance of p+-ZnTe/p-ZnTe:O/n+-GaAs Intermediate Band Solar Cells Grown by Pulsed Laser Deposition	369
ThP-63	Effect of electron correlations on the exciton dynamics of CdTe(Se)/CdTe(Se) core/shell for MEG solar cells	370
ThP-64	Issues with Application of CBD CdS in CdS/i-ZnO/ZnO:Al Window Layer	372

ABSTRACTS

**Sunday September, 13 - SuR**

**14:00-17:30**

**Review Lectures**

Chair: Christophe Testelin, *Institut des NanoSciences de Paris (France)*

Pierre Galtier, *Groupe d'Etude de la Matière Condensée, Versailles (France)*

## **II-VI Semiconductors for Photonic Device Applications: Beyond the Blue Laser**

Maria C. Tamargo  
The City College of New York

Since the rapid development of GaN materials about twenty years ago, the focus of II-VI compound semiconductor research for photonic applications has shifted away from that one time prime goal of development of a blue laser. Several directions emerged, including visible light emitters, vertical cavity surface emitting lasers, intersubband devices, photovoltaics, and others. I will present a brief review of the field with emphasis on some of the most recent activities in this direction.

## The adventure of copper indium gallium diselenide (CIGS) solar cells : recent developments and future challenges

Daniel LINCOT<sup>1,3,4</sup>, Jean François GUILLEMOLES<sup>1,3,5</sup>, Negar NAGHAVI<sup>1,3</sup>, Laurent LOMBEZ<sup>1,3</sup>, Julien VIDAL<sup>2,3</sup>, Myriam PAIRE<sup>2,3</sup>

<sup>1</sup>Centre National de la Recherche Scientifique, Paris, France

<sup>2</sup>Electricité de France, Paris, France

<sup>3</sup> Institut de Recherche et Développement sur l'Energie Photovoltaïque (IRDEP), Unité Mixte de Recherche CNRS-EDF-Chimie Paristech, Chatou, France

<sup>4</sup>Institut Photovoltaïque Ile de France, Antony, France

<sup>5</sup> Next PV, Joint Lab. CNRS-Tokyo University, Tokyo, Japon

Email: daniel.lincot@chimie-paristech.fr

Copper Indium Diselenide  $\text{CuInSe}_2$  (CIS) is belonging to the Cu ternary chalcopyrite semiconductor compounds which appeared in the mid seventies as candidates for non linear optical applications. It was immediately recognized for its photovoltaics properties with heterojunctions between p-type single crystal CIS and n type cadmium sulfide, with efficiencies reaching 12% in 1975. However, the interest for such materials, with high absorption coefficients was mostly driven by the search of light weight and efficient thin film solar cells, especially, at that time, for space applications, as an alternative to wafer based Si technologies. The main explored thin film technologies were cadmium telluride/cadmium sulfide and cuprous sulfide/cadmium sulfide ones, also based on II-VI compounds, with also amorphous silicon as an emerging technology. However cuprous sulfide/CdS solar cells presented important problems of stability and were abandoned at the beginning of the 80's in favor of CIS/CdS cells in thin film form which was taking off from late seventies. As compared to  $\text{Cu}_2\text{S}/\text{CdS}$  solar cells, the striking feature of CIS solar cells was their much better stability, which was explained in the 90's on equilibrium thermodynamic considerations. Then, from the 2% record efficiency in 1975, 30 years of an extraordinary scientific and discovery pathway, have brought this efficiency to 21.7% in 2015, which overpass the record efficiency of polycrystalline silicon (20.8%), representing the highest performance of thin film solar cells, ahead from cadmium telluride which has made also great progress (21,5%) and well beyond silicon thin film solar cells (13.5%).

The progression consists in a succession of discoveries /breakthroughs followed by consolidation phases : the introduction of gallium to tune the band gap, the introduction of sodium by serendipity, the introduction of V shaped Ga/S graded band gap, interface engineering on the back side and the front side of the device with CdS buffer layers and work function controlled Zn(O,S) layers, grain boundaries engineering. Recently, the discovery of the effect of potassium alloying at the surface allowed a new boost in efficiency, which opens the route towards 25 % efficiency in the future. All these improvements are related to specific fundamental properties of CIGS and its interfaces with front and back contacts. An enormous work is presently done to understand these properties by using most advanced characterization and modelling tools, since many of these discoveries have been made without strong preceding knowledge. Fundamental understanding of these complex materials and interfaces is a key challenge for the future [1].

Beside the search for record efficiencies, new directions are explored i.e. : to find higher band gap materials in the (Cu,In,Ga,S,Se) system which could serve for tandem higher efficiency devices (30%), low temperature processes for making technologies on light weigh plastic substrates. Also new architectures are under study like ultrathin CIGS solar cells with light trapping [2] or microcells working under high concentration[3], allowing both an increase of efficiency and indium saving for large scale industrial production.

- [1] M. Paire, S. Delbos, J.Vidal, N. Naghavi, J.F. Guillemoles, Chalcogenide thin film Solar Cells, in Solar Cells Materials, Wiley, 2014
- [2] Z. Li kao, N. Naghavi, F. Erfurth, J.F. Guillemoles, I. Gerard, A. Etcheberry, J.L. Pelouard, S. Collin, G. Voorwinden, D. Lincot, Progress in Photovoltaics, 20(2012)582
- [3] M. Paire, L. Lombez, J.F. Guillemoles, D. Lincot, J. Appl. Phys., 108(2010)034907

# Surface-state transport in topological insulators

H. Buhmann

*Physikalisches Institut, Universität Würzburg, Am Hubland, 97074 Würzburg, Germany*

Topological insulators (TI) are characterized by an insulating bulk and conducting surfaces. The conducting surface states exhibit a characteristic Dirac band dispersion and therefore offer a lot of new and interesting properties, especially with respect to future device applications. In this presentation, I will review the development of transport experiments on topological insulators:

- Summarizing the realization of a 2D TI structure in HgTe quantum wells its potential for spin injection and detection purposes in spintronic applications without any magnetic materials or applied magnetic fields.
- Presenting transport experiments on pure 3D TI surface states which are rare, even though numerous TI materials have been identified and fabricated worldwide.
- And introducing the feasibility of proximity induced superconductivity in the surface of a 3D TI which provides the basis for the formation zero-energy, so-called Majorana bound states.

**Monday September, 14 - Oral Session - MoA**

**09:00-10:30**

**Growth and Characterizations 1**

Chair: Shizuo Fujita, *Kyoto University (Japan)*

## ZnTe/CdSe type II heterostructures investigated by transmission electron microscopy (HR-STEM) and atom probe tomography (APT)

Bastien Bonef<sup>1,2</sup>, Jean-Luc Rouvière<sup>1,2</sup>, Benedikt Haas<sup>1,2</sup>, Adeline Grenier<sup>1,3</sup>,  
 Pierre-Henri Jouneau<sup>1,2</sup>, Edith Bellet-Amalric<sup>1,2</sup>, Henri Mariette<sup>1,4</sup>, Régis André<sup>1,4</sup>,  
Catherine Bougerol<sup>1,4\*</sup>

<sup>1</sup>Univ. Grenoble Alpes, F-38000 Grenoble, France

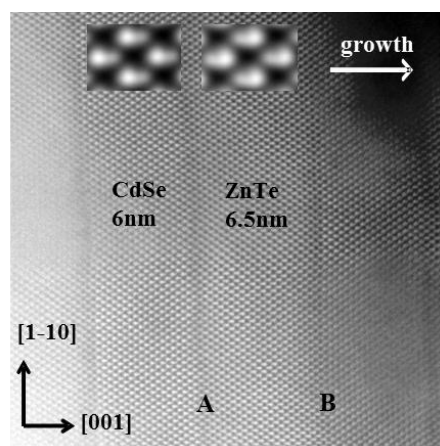
<sup>2</sup>CEA, INAC-SP2M, F- 38054 Grenoble, France

<sup>3</sup>CEA, LETI, MINATEC Campus, F-38054 Grenoble, France.

<sup>4</sup>CNRS, Inst. NEEL, F-38042 Grenoble, France

\*catherine.bougerol@neel.cnrs.fr

II-VI semi-conductors with a wide and direct band gap have attracted considerable interest due to their optical properties and potential applications as photovoltaic devices. Among them, ZnTe and CdSe have a very small lattice parameter mismatch ( $a=0.6103$  nm and  $0.6078$  nm, respectively) in their cubic zinc-blende structure which makes this couple a good candidate to grow almost strain-free super-lattices. Furthermore, ZnTe and CdSe present a staggered band alignment (so-called type-II) allowing a straight forward spatial separation of electrons and holes at their interface. Short period ZnTe/CdSe super-lattices prove to be efficient sun light absorbers and benefit from their type-II band alignment to extracted photo-generated charge carriers at their boundaries. However, even if high-quality super-lattices can be grown by molecular beam epitaxy (MBE), their performances are directly linked to structural properties, and are highly sensitive to details at the interfaces (width of the interfacial area, atomic arrangements,...) when short periods are required. Moreover the ZnTe/CdSe interface is made complex by the simultaneous change of group II and group VI elements and can be ZnSe-like, or CdTe-like or a mixture of ZnTe and CdSe. The atomic scale structure of such ZnTe/CdSe super-lattices grown by MBE has been solved from high resolution scanning transmission electron microscopy (HR-STEM) combined with laser-assisted atom probe tomography (APT). In particular, the presence of ZnSe has been evidenced at both interfaces which may influence the optical properties.



HR-STEM image of a ZnTe/CdSe superlattice

## ZnTe Layers on *R*- and *S*-plane Sapphire Substrates

T. Nakasu<sup>1</sup>, S. Yamashita<sup>1</sup>, T. Aiba<sup>1</sup>, S. Hattori<sup>1</sup>, T. Kizu<sup>1</sup>, W. Sun<sup>1</sup>, K. Taguri<sup>1</sup>, F. Kazami<sup>1</sup>,  
Y. Hashimoto<sup>1</sup>, S. Ozaki<sup>1</sup>, M. Kobayashi<sup>1,2</sup>, and T. Asahi<sup>3</sup>

<sup>1</sup>Dept of Elec. Eng. & Biosci., Waseda University, Tokyo, Japan

<sup>2</sup>Kagami Memorial Res. Inst. for Mater. Sci. & Technol., Waseda University, Tokyo, Japan

<sup>3</sup>Technol. Dev. Center, JX Nippon Mining & Metals Corp., Kitaibaraki, Japan

\*E-mail of the corresponding author: n-taizo.nakasu@asagi.waseda.jp

ZnTe thin films are attractive for electro-optic (EO) devices and terahertz wave devices. Sapphire is an advantageous substrate for the EO device structures because it is a transparent material and simplifies the alignment of the optical path in device applications. It was confirmed that (111)-oriented ZnTe layers with a single domain structure were formed on (0001) *c*-plane sapphire substrates [1], while (211)- and (100)-oriented ZnTe layers were grown on (1-100) *m*-plane sapphire substrates [2]. It is expected that the crystal orientation of ZnTe could be tuned by the surface inclination from the *c*-plane to the *m*-plane. In this study, ZnTe epilayers were grown on (10-11) *S*-plane, and (10-14) *R*-plane sapphire substrates by MBE. The *S*- and *R*-plane of sapphire were inclined from *c*-plane toward the *m*-axis direction about 72 and 38°, respectively. The growth temperature of the ZnTe layer was 340°C, and the film thickness was around 1 μm. The film growth was initiated by the deposition of a thin (a few nanometers) buffer layer of ZnTe at very low temperature, followed by the annealing at 350°C for 5 min prior to the nucleation. The influence of the substrates' orientation on the orientation of the epilayer was studied by means of X-ray diffraction measurements including the  $\theta$ -2 $\theta$  and the wide-range reciprocal space mapping [3]. In particular, X-ray diffraction pole figures were employed and domain structures along with their orientations were extensively investigated. Pole figures of ZnTe 111 and sapphire substrates were mainly analyzed to clarify the relationship of axis between the film and the substrate.

When ZnTe layers were grown on the *S*- and *R*-plane sapphire substrates, (111) ZnTe layers were confirmed by the  $\theta$ -2 $\theta$  measurements. Pole figures of ZnTe 111 indicated that two kinds of (111) domains were formed in layers grown on both kinds of sapphire substrates. After the pole figure measurement, all measured signals were shifted along the  $\chi$  direction by the computer simulation, and the origin of the pole figure was moved to the *m*-plane of the sapphire. The resulting pattern indicated that ZnTe (211)-plane was formed on the sapphire *m*-plane when the *S*-plane sapphire substrate was used. Similarly, ZnTe (100)-plane was formed on the sapphire *m*-plane when the *R*-plane sapphire was used. These results coincided with the domain structures of ZnTe layers grown on the *m*-plane sapphire substrate [2]. The selectivity of the orientation would be related to the interface valency as well as the interfacial bond structure.

This work was supported in part by Waseda Univ. Research Initiatives, "Early Bird" grant for young researcher at Waseda Research Inst. for Sci. & Eng., collaboration between Mitsubishi Mat. Corp. & Faculty of Sci. & Eng., Waseda Univ., JSPS Research Fellowships for Young Scientists, and the Foundation of Ando Laboratory.

[1] T. Nakasu et al., Appl. Phys. Express, **5**, 095502, (2012).

[2] T. Nakasu et al., Phys. Status Solidi, **11**, 1182-1185, (2014).

[3] T. Nakasu et al., J. Cryst. Growth, (2015) in press

## Near-forward Raman Study of Zn(Se,S) and (Zn,Be)Se bulk Phonon-polaritons – Collapse vs. Reinforcement Regimes of the Intermediary Mixed-bond Branch

Dicko H.,<sup>1</sup> Hajj Hussein R.,<sup>1</sup> Pagès O.,<sup>1\*</sup> A.,<sup>2</sup> Firszt F.,<sup>2</sup> Marasek A.,<sup>2</sup> Paszkowicz W.,<sup>3</sup> Maillard A.,<sup>4</sup> Jobard C.<sup>4</sup> and Broch L.<sup>1</sup>

<sup>1</sup>LCP-A2MC / Institut Jean Barriol, Université de Lorraine, Metz, France

<sup>2</sup>Institute of Physics, Nicolaus Copernicus University, Toruń, Poland

<sup>3</sup>Institute of Physics, Polish Academy of Sciences, Warsaw, Poland

<sup>4</sup>LMOPS, Université de Lorraine – Sup'elec, Metz, France

\*Corresponding author: olivier.pages@univ-lorraine.fr

In such a polar material as a zincblende AB crystal, the transverse optic (TO) phonon near the centre of the Brillouin zone ( $\Gamma$ ,  $q=0$ ), is likely to be accompanied by an electric field, i.e. a transverse one, thus identical in nature to that carried by a photon. The ‘frequency ( $\omega$ ) vs.  $q$ ’ dispersion of such mechanical/electrical-coupled TO, currently referred to as a phonon-polariton (PP), was extensively studied in pure AB crystals since the mid-sixties [1], mostly by using near-forward Raman scattering (schematically operating in a ‘transmission’ mode). Due to the quasi vertical dispersion of a photon, a phonon-polariton can exist only close to  $\Gamma$ . Away from  $\Gamma$ , the TO is deprived of electric field; it reduces to a purely mechanical (PM-TO) mode. The strong PP coupling occurs when the quasi vertical photon-like asymptote (electrical aspect) crosses the horizontal PM-TO (mechanical aspect) one in a ‘ $\omega$  vs.  $q$ ’ plot. This gives rise to an anticrossing resulting in two PP’s, i.e. a lower PP<sup>-</sup> that is (PM-TO)-like away from  $\Gamma$  and photon-like near  $\Gamma$ , and an upper PP<sup>+</sup> that is photon-like away from  $\Gamma$  and identifies with the longitudinal optical (LO) mode right at  $\Gamma$ . An interesting question is how such PP picture modifies for a  $A_{1-x}B_xC$  zincblende alloy? Bao and Liang provided a pioneering theoretical insight into the ‘ $\omega$  vs.  $q$ ’ PP-dispersion of various alloys [2]. On the experimental side, we are only aware of our recent near-forward Raman studies of ZnSe-based alloys [3,4]. What emerges is that in a  $A_{1-x}B_xC$  alloy an intermediary (A-C,B-C)-mixed PP (Int-PP) occurs between PP<sup>-</sup> and PP<sup>+</sup>. Int-PP is distinct in nature from the latter two in that it exhibits an overall S-like shape governed by two (horizontal) phonon asymptotes, i.e. the higher PM-TO frequency away from  $\Gamma$ , and the lower LO one near  $\Gamma$ . In this work we report on a near-forward Raman study of the presumed reinforcement of Int-PP when turning LO-like near  $\Gamma$ , following its original collapse when departing from the PM-TO regime away from  $\Gamma$ , as predicted by the linear dielectric response theory of Raman scattering [4]. We study both  $Zn_{1-x}Be_xSe$  ( $x=0.33$ ;  $0.53$ ) and  $ZnSe_{1-y}Se_y$  ( $y=0.22$ ;  $0.32$ ) alloys, corresponding to extreme cases with respect to Int.-PP: ZnBeSe (ZnSeS) exhibits highly contrasted (quasi-identical) bond physical properties (length, stiffness), resulting in a large (narrow) gap between the natural vibration frequencies of the constituent bonds, with concomitant impact on the magnitude of the Int.-PP dispersion. The discussion is supported by a Raman symmetry analysis of the ZnBeSe- and ZnSeS-like Int-PP’s, both in their collapse (PM-TO-like) and reinforcement (LO-like) regimes – depending on the used laser excitation or alloy composition, and by a contour modeling of the multi-PP ZnBeSe and ZnSeS Raman lineshapes in their dependence on the scattering angle within the formalism of the linear dielectric response, based on ellipsometry measurement of the refractive index.

[1] Henry C. H. and Hopfield J. J., Phys. Rev. Lett. **15**, 964 (1965).

[2] Bao J. and Liang X. X., J. Phys. Condens. Matter **18**, 8229 (2006).

[3] Hajj Hussein R., Pagès O., Firszt F., Paszkowicz W. and Maillard A., Appl. Phys. Lett. **103**, 071912 (2013).

[4] Hajj Hussein R., Pagès O., Firszt F., Marasek A., Paszkowicz W., Maillard A. and Broch L., J. Appl. Phys. **116**, 083511 (2014).

## Internal Laser Characteristics of Optically Pumped Yellow-Orange Lasers

A. Alyamani<sup>1</sup>, E.V. Lutsenko<sup>2\*</sup>, A.G. Vainilovich<sup>2</sup>, G.P. Yablonskii<sup>2</sup>, M. Aljoheni<sup>1</sup>,  
A. Aljerwii<sup>1</sup>, S.V. Sorokin<sup>3</sup>, S.V. Gronin<sup>3</sup>, I.V. Sedova<sup>3</sup> and S.V. Ivanov<sup>3</sup>

<sup>1</sup>KACST, National Nanotechnology Center. P.O. BOX 6086, 11442 Riyadh, Saudi Arabia

<sup>2</sup>Stepanov Institute of Physics, National Academy of Science of Belarus,  
220072 Minsk, Nezhaleznyy 68 str., Belarus

<sup>3</sup>Ioffe Physico-Technical Institute, Russian Academy of Science,  
194021, 26 Politekhnicheskaya str., St. Petersburg, Russia

\* e.lutsenko@ifanbel.bas-net.by

The yellow range (560-590 nm) of visible spectrum is of a great importance for medical applications because of the absorption maximum of triple oxygen. The yellow lasers are also demanded for the laser TV and multimedia devices to improve the color rendering. However, the existing DPSS lasers do not allow choosing the lasing wavelength because the wavelength is determined by the laser crystal. The II-VI wide-gap laser heterostructures look perspective to cover the whole yellow spectral range. In part, the microchip laser converters emitting in 565-567 nm were recently demonstrated [1]. This paper reports on the studies of internal laser characteristics of optically pumped CdSe/Zn(Cd)Se quantum dot (QD) laser heterostructures emitting from “true” yellow up to orange ranges. The laser structures have been grown by molecular beam epitaxy (MBE) on GaAs(001) substrates using the double-chamber III-V/II-VI MBE setup (SemiTEq, Russia). The structures consist of top and bottom ZnMgSSe claddings, graded-index waveguide based on Zn(Mg)SSe/ZnSe superlattices (SLs) [2], and 3 nm-ZnSe/2.8 ml-CdSe QDs/(2-3) nm-Zn<sub>1-x</sub>Cd<sub>x</sub>Se/3 nm-ZnSe active layer [3]. The only difference between two structures is the QW thickness and Cd content in Zn<sub>1-x</sub>Cd<sub>x</sub>Se QW: 3 nm-Zn<sub>0.65</sub>Cd<sub>0.35</sub>Se (structure **A**) and 2 nm-Zn<sub>0.5</sub>Cd<sub>0.5</sub>Se (structure **B**), correspondingly. The laser cavities were obtained by cleavage of the heterostructures. The cavity length was varied within 125-730 μm and 120-500 μm ranges for the structures **A** and **B**, respectively. The optical pumping was realized by focusing the emission of N<sub>2</sub> laser into the stripe perpendicular to cavity edge. The lasing wavelength is varied within 555-575 nm and 583-593 nm ranges depending on the cavity length for the structures **A** and **B**. The minimum laser threshold is as low as 1.27kW/cm<sup>2</sup> (L<sub>cav</sub>=734μm) and 2.5kW/cm<sup>2</sup> (L<sub>cav</sub>=500μm) for the structures **A** and **B**, respectively. The threshold increases up to 7.4kW/cm<sup>2</sup> (structure **A**) and 8.8kW/cm<sup>2</sup> (structure **B**) with the cavity length decrease down to ~120μm. The internal laser characteristics were calculated from the experimental dependencies of reciprocal differential quantum efficiency on cavity length and threshold power density on reciprocal cavity length. The details of the calculations could be found in [4]. The characteristic gain is of 51 cm<sup>-1</sup> and 76 cm<sup>-1</sup> for the structures **A** and **B**, respectively. The transparency threshold, internal quantum efficiency and internal losses are 0.6kW/cm<sup>2</sup>, 83%, 4.3cm<sup>-1</sup> (structure **A**), and 1.12kW/cm<sup>2</sup>, 72%, 4.4cm<sup>-1</sup> (structure **B**), respectively. The difference in characteristic gain is likely caused by non-optimum waveguide in structure **A**. Alternatively, the high value of the characteristic gain in structure **B** in comparison with commonly used CdSe/ZnSe QD active region [4] could be explained by localization of non-equilibrium carriers in QD+QW. The increase in the transparency threshold as well as decrease in internal quantum efficiency is likely associated with effects caused by higher Cd content.

[1] E.V. Lutsenko et al., Quantum electronics **43**(5), 418 (2014)

[2] I.V. Sedova et al., Appl. Phys. Lett. **98**, 171103 (2011).

[3] S.V. Gronin et al., Acta Physica Polonica A **126**(5), 1096 (2014)

[4] A.G. Vainilovich et al., Phys. Stat. Sol. (c) **7**(6), 1961 (2010)

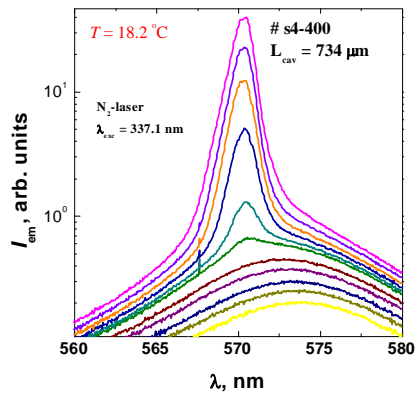


Fig. 1 – Luminescence spectra measured from cavity edge at different excitation levels.

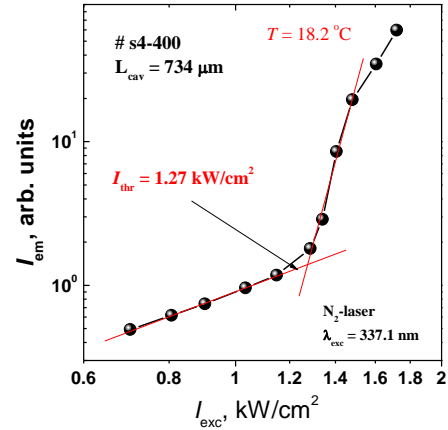


Fig. 2 – Luminescence intensity from cavity edge as a function of excitation level.

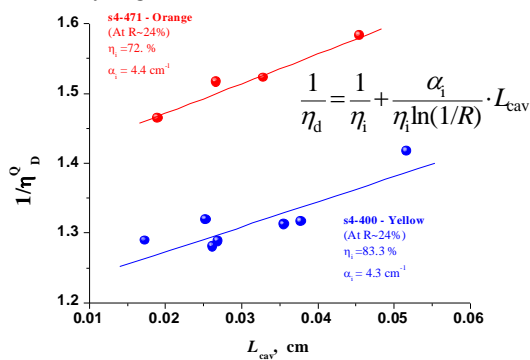


Fig. 3 – Reciprocal differential quantum efficiency as a function of cavity length.

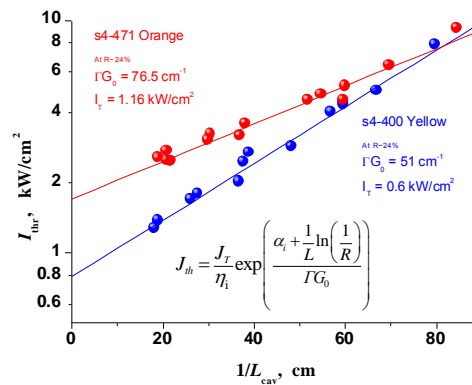


Fig. 4 – Threshold power density as a function of reciprocal cavity length.

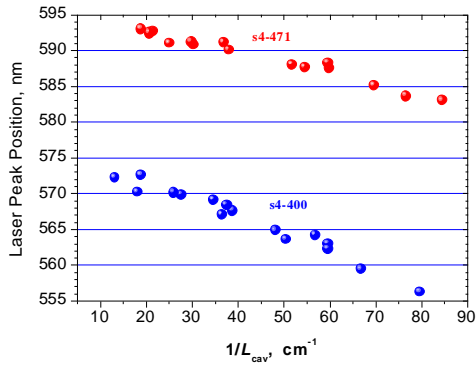


Fig. 5 – Laser spectral peak position as a function of reciprocal cavity length.

## Growth of $\text{LiIn}_{1-x}\text{Ga}_x\text{Se}_2$ Semi-Insulating Crystals

Brenden Wiggins<sup>1,2</sup>, Arnold Burger<sup>2,3</sup>, Keivan Stassun<sup>2,3</sup>, Ashley Stowe<sup>1</sup>

<sup>1</sup>Y-12 National Security Complex, Oak Ridge, TN, USA

<sup>2</sup>Vanderbilt University, Nashville, TN, USA

<sup>3</sup>Fisk University, Nashville, TN, USA

Crystal growth and material engineering have become complementary fields in the development of new materials with versatile optical-electrical properties. Ternary Li-containing chalcogenide single crystals have been intensively investigated over the past fifteen years for non-linear optical applications and more recently detection of ionizing radiation. One such composition in this class,  ${}^6\text{LiInSe}_2$ , respond to radiation both as a semiconductor and as a scintillator with high intrinsic efficiency. One drawback to the  ${}^6\text{LiInSe}_2$  semiconductor is the efficiency lose due to a neutron capture reaction with the indium-115 isotope. In order to improve the overall thermal neutron efficiency and tune the electro-optical properties, gallium has been systematically substituted for indium within the compound.  ${}^6\text{LiInSe}_2$  and  ${}^6\text{LiGaSe}_2$  have been separately synthesized via a two-step synthesis method whereby lithium and either In or Ga are alloyed prior to addition of the chalcogenide. The two ternary compounds are then physically mixed in the appropriate concentration prior to vertical Bridgman growth. Crystallography, electro-optical and radiation response properties will be discussed for the  $\text{LiIn}_{1-x}\text{Ga}_x\text{Se}_2$  single crystals.

**Monday September, 14 - Oral Session - MoB**

**11:00-12:15**

**ZnO, Nanowire**

Chair: Jürgen Gutowski, *Institute of Solid State Physics, University of Bremen (Germany)*

## On the benefits of annealing ZnO nanowires under zinc pressure

E. Zehani\*<sup>1</sup>, S. Hassani<sup>1</sup>, A. Lusson<sup>1</sup>, F. Jomard<sup>1</sup>, J. Vigneron<sup>2</sup>, A. Etcheberry<sup>2</sup>,  
V. Sallet<sup>1</sup> and P. Galtier<sup>1</sup>

<sup>1</sup>Groupe d'Etude de la Matière Condensée (GEMAC), CNRS - Université de Versailles  
St Quentin, 45 avenue des Etats Unis, 78035 Versailles France

<sup>2</sup>Institut Lavoisier Versailles (ILV), CNRS - Université de Versailles St Quentin,  
45 avenue des Etats Unis, 78035 Versailles France

\*corresponding author : emir.zehani@uvsq.fr

ZnO has attracted intensive research effort for its unique properties and versatile applications such as ultraviolet light emitting diodes (LEDs). Nevertheless, the growth of high-quality and stable p-type ZnO material is still a major issue. Several approaches have been investigated to achieve p-type doping in ZnO bulk crystals, layers and nanowires : ion implantation, ex situ diffusion of dopants, or in situ doping during growth. Most of the time, an annealing step under inert gas, air, or oxygen is carried out in an attempt to : i) improve to crystalline and optical quality, and ii) electrically activate the acceptor impurities.

In this work, doped and undoped ZnO nanowires are grown using metal organic chemical vapour deposition (MOCVD) on sapphire substrates. Subsequently, the samples are annealed under zinc pressure in a vacuum-sealed ampoule, at temperatures ranging from 550 to 800°C. The originality, and the main motivation to provide a zinc-rich atmosphere, was to prevent the diffusion of zinc from the nanowires.

Interestingly, photoluminescence experiments performed on nanowires processed in a narrow window of temperature [580-620°C] show a spectacular improvement of the optical quality, as transitions commonly observable in high quality bulk samples are found. In addition, the intensity of the so-called "surface exciton" (SX) is strongly decreased. To accurately investigate the structural modifications of the surface, XPS experiments were carried out, and show that zinc hydroxide species (adsorbed molecules, and/or Zn(OH)<sub>2</sub> sublayer) are removed from the surface. The results suggest that thermal treatment under zinc pressure helps to reconstruction properly the surface of ZnO nanowires, and improves the optical quality of their core.

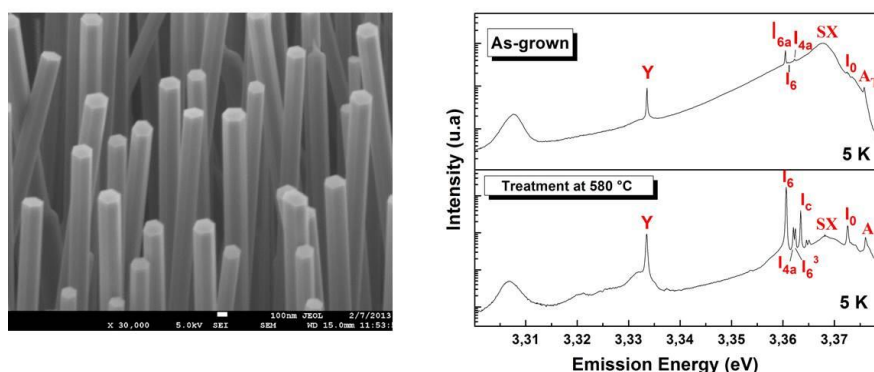


**Figure :** SEM image of as-grown ZnO nanowires (left), and PL spectra measured at 5K for ZnO nanowires samples, as grown and annealed at 580 °C with Zn source (right)

## Large scale well-ordered, periodically patterned multifunctional ZnO

Anisha Gokarna<sup>\*</sup>, Hind Kadiri, Agnieszka Gwiazda, Komla Nomenyo, Roy Aad and Gilles Lerondel<sup>\*</sup>

LNIO, Institut Charles Delaunay, CNRS UMR 6281, University of Technology of Troyes, 12 Rue Marie Curie, CS 42060, 10004 Troyes Cedex, France

<sup>\*</sup>anisha.gokarna@utt.fr, gilles.lerondel@utt.fr

The growth of well-ordered, controlled, periodic two-dimensional (2D) semiconductor nanostructure patterns with enhanced surface morphology and advanced Light-matter Interaction control i.e. absorption and emission enhancement is becoming increasingly important because of the need to understand the fundamental growth mechanism as well as its potential applications in nanoscale electronics, biological sensing and diagnosis, and nanophotonics.

The aim of this work is to demonstrate selective, patterned growth of ZnO using low cost, easy-to-fabricate templates on a large area by the bottom-up and top-down approach. Patterning of silicon substrates was conducted using two methods: top-down and a bottom-up approach. The bottom-up approach involves fabrication of self-organized templates of functionalized polystyrene (PS) beads as masks for patterning silicon. Silicon patterns in the form of small inverted cones is formed by this technique. Earlier Gokarna *et al.* used PS beads as templates for fabrication of urchin-like ZnO structures [1]. In the top-down approach, patterns in silicon are formed using laser interference lithography (LIL) patterning. Different kinds of silicon patterns in the form of inverted cones or pillars can be obtained using two beam LIL technique. This patterning can be performed on a large scale and in a homogeneous manner (Figure 1(a, b)). ZnO nucleation layer is deposited on these patterns using a two-step method prior to the synthesis of ZnO NWs. Chemical bath deposition (CBD) method is used for the growth of the nanowires on these silicon patterns. Formation of highly crystalline, luminescent NWs (of diameter less than 50 nm) is observed to be formed on these silicon patterns as seen in figure 1(b). The structural and optical properties of these patterned ZnO NWs structures will be presented. Combining both these approaches for patterning along with the CBD method allows more access to large-scale uniformly patterned nanostructures at a high-throughput rate and a substantially reduced cost, both in time and in equipment resources, providing an efficient approach for fabricating highly ordered nanostructures at wafer scale without using cleanroom technology.

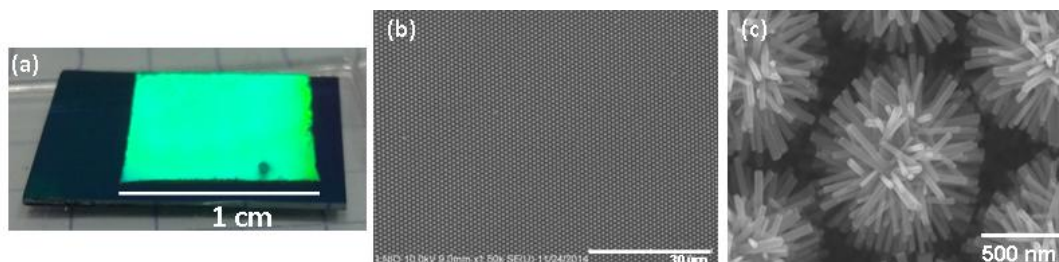


Figure 1: (a) Photograph of the LIL patterned sample, (b) SEM image of homogeneously patterned ZnO on a large scale by LIL (c) zoomed in image of the ZnO nanowires grown on the silicon cone shaped patterns

- [1] A. Gokarna, R. Parize, H. Kadiri, K. Nomenyo, G. Patriarche, P. Miska and G. Lerondel RSC Advances, **4**, 47234 (2014).

## Efficient Nitrogen Incorporation in ZnO Nanowires by Unintentional Doping

Stehr JE<sup>1\*</sup>, Chen WM<sup>1</sup>, Reddy NK<sup>2</sup>, Tu CW<sup>3</sup>, and Buyanova IA<sup>1</sup>

<sup>1</sup>Department of Physics, Chemistry and Biology, Linköping University, 581 83 Linköping, Sweden

<sup>2</sup>Institute of Chemistry, Humboldt University, Berlin, DE 12489, Germany

<sup>3</sup>Department of Electrical and Computer Engineering, University of California, La Jolla, CA 92093, USA

\* Corresponding author: janst@ifm.liu.se

ZnO is a promising electronic material for a wide variety of applications ranging from sensing to light emission. Furthermore, ZnO is a sustainable and cheap material that can be easily synthesized in various nano-scale forms, e.g. tetrapods and nanowires (NWs), which allows one to further enhance its functionality. All these applications, however, require a good understanding and precise control of optical and electrical properties of the material that are known to be largely affected by intrinsic defects and impurities. Thus, chemical identification of these impurities, as well as understanding their local structure and effects on material properties, are the key requirements for advances in nanowire-based device technologies.

In this work we employ magnetic resonance spectroscopy to investigate defect formation processes in nominally undoped ZnO NWs grown by chemical vapor deposition, aiming to single out chemical origin of incorporated contaminants. The EPR spectra of the NWs are found to exhibit three EPR signals. The first signal has an electron spin  $S = 1/2$  and an isotropic  $g$ -value of 2.002 and can be assigned to dangling bonds on the surface of the NWs, which seems to be very likely considering a large surface-to-volume ratio in the NWs. The second signal consists of a single line with  $g_{\parallel} = 1.957$  and  $g_{\perp} = 1.956$  and can be attributed to a shallow donor (SD). And the third signal contains three equally spaced lines implying a resolved hyperfine interaction between an electron with an effective spin  $1/2$  and a nucleus with a nuclear spin 1 with  $g_{\parallel} = 1.995$  and  $g_{\perp} = 1.963$ . This signal is an EPR signature of a nitrogen atom occupying an oxygen lattice site ( $N_O$ ) that acts as a deep acceptor in ZnO. The photo-ionization threshold energy of the  $N_O$  center in the ZnO NWs is lower compared with its value in bulk ZnO, indicating that the defect might be located in proximity to the surface. This assumption is consistent with theoretical predictions of enhanced N incorporation at the ZnO surface [1]. The incorporated nitrogen stems from an unintentional doping from residual  $N_2$  background gas. This doping process is shown to be very efficient leading to a rather high concentration ( $\sim 2\text{-}4 \times 10^{16} \text{ cm}^{-3}$ ) of unintentional N dopants in the NWs. Our finding thus underlines the importance of controlling such background contamination as compensation by the  $N_O$  acceptors may hinder achieving high n-type conductivity in nanostructured ZnO. On the other hand, the lowered formation energy of  $N_O$  in NWs might be beneficial for achieving p-type conducting ZnO nanostructures via nitrogen doping, e.g. due to N-containing defect complexes or nitrogen molecules.

[1] Gutjahr, J, Sakong, S, and Kratzer J, *Nanotechnology*, **25**, 145204, (2014).

## Luminescence dynamics of hybrid ZnO nanowire/CdSe quantum dot structures

Stephanie Bley<sup>1,\*</sup>, Friederike Albrecht<sup>1</sup>, Sebastian Resch<sup>2</sup>, Siegfried R. Waldvogel<sup>2</sup>, Andreas Menzel<sup>3</sup>, Margit Zacharias<sup>3</sup>, Tobias Voss<sup>1,4</sup>, and Jürgen Gutowski<sup>1</sup>

<sup>1</sup>Institute of Solid State Physics, Semiconductor Optics, University of Bremen, 28359 Bremen, Germany

<sup>2</sup>Institute of Organic Chemistry, Johannes Gutenberg University Mainz, 55128 Mainz, Germany

<sup>3</sup>Laboratory of Nanotechnology, IMTEK, TF, Albert Ludwigs University, 79110 Freiburg, Germany

<sup>4</sup>Institute of Semiconductor Technology, Braunschweig University of Technology, 38106 Braunschweig, Germany

\*E-mail of the corresponding author: bley@ifp.uni-bremen.de

Electronic and optical coupling as well as electron transfer across the internal interfaces of hybrid nanostructures opens possibilities to specifically tailor their microscopic transport and luminescence processes by combining specific properties of different organic and inorganic material systems.

In this respect, ZnO nanowires (NWs) functionalized with colloidal quantum dots (QDs) through organic linker molecules allow a detailed coupling investigation of the 3D (NW) and 0D (QD) electronic systems. The tight and selective binding of the QDs to the ZnO NW surface can be achieved through a special design of organic linker molecules, and the interaction between the 3D and 0D electronic systems can be precisely controlled by adjusting the lengths of the linker molecules and their electronic system.

CdSe quantum dots (QDs) with different organic linker molecules are attached to ZnO nanowires (NWs) to study luminescence dynamics and electron tunneling from the QDs to the nanowires in time-resolved photoluminescence (PL) and photoconductivity measurements. The PL transients of the QD luminescence indicate two different recombination channels: the direct recombination inside the QD core and the recombination via QD surface defect states. After linking the QDs to the ZnO NW surface, photo-induced electron tunneling from an excited state of the QD into the conduction band of the nanowire becomes visible by a clear decrease of the PL decay time. By comparing the PL transients of QDs in solution with those of QDs linked to ZnO NWs, the photo-induced electron tunneling (PET) process between excited states of the QD and the nanowire is demonstrated and discussed in the frame of a rate equation model.

Efficient electron tunneling is confirmed by a strong enhancement of the photocurrent through the functionalized nanowires in which the tunneling rate can be controlled by using different organic linker molecules. Desorption and re-adsorption of oxygen molecules from and on the oxide as well as the QD surfaces play an important role for the electron transfer processes between both material systems as shown also in previous studies. Assuming that the linker molecules constitute diffusion barriers for the oxygen molecules, whereby the thickness of the barrier scales with the molecule length we can explain the experimental results based on the typical model<sup>[1]</sup> for photoconductivity in bare or functionalized ZnO nanowire samples.

[1] D. Hou, A. Dev, K. Frank, A. Rosenauer, and T. Voss, *Journal of Physical Chemistry C*, **116**, 19604 (2012)

## Thermal Conductivity of a Single ZnO Nanowire

Sh. U. Yuldashev, V. Sh. Yalishev, H. D. Cho and T. W. Kang

Quantum-Functional Semiconductor Research Center, Dongguk University, 3-26 Pil-dong, Chung-gu, Seoul 100-715, Korea (E-mail: shavkat@dongguk.edu)

Electrical power generation from waste heat, for example, in cars, aircrafts, power plants, and thermo-photovoltaic cells, requires high stability thermoelectric materials with high figures of merit  $ZT$  at temperatures above 600 K, where  $ZT = \alpha^2 \sigma T / k$ ,  $\alpha$  is the Seebeck coefficient,  $\sigma$  is the electrical conductivity,  $k$  is the thermal conductivity, and  $T$  is the absolute temperature. Nontoxic and low-cost oxides such as ZnO are promising for such applications because their excellent charge carrier transport properties are tunable via doping. However, decreasing  $k$  is a major challenge because of the high lattice thermal conductivity  $k_L$  of these materials. Nanostructuring has been shown to be more effective than incorporating dopants and/or alloying elements or nanopores to decrease  $k_L$ . In our recent work [1] we demonstrated the decreasing of the thermal conductivity of ZnO nanowires with different diameters embedded into PMMA matrix compare to the bulk ZnO.

In this work the thermal conductivity of a single ZnO nanowire with diameter of  $\sim 150$  nm was measured using a four-point-probe  $3-\omega$  method over a temperature range of 140-300K.

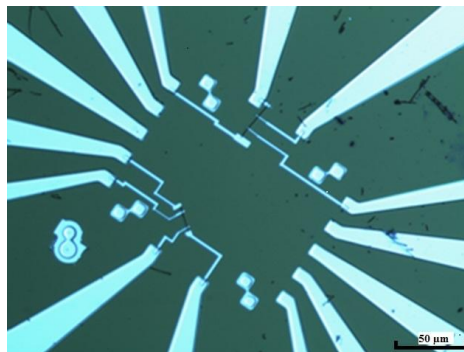


Fig. 1. Optical microscope image of a four-point-probe device for the thermal conductivity measurements.

The measured thermal conductivity of ZnO nanowire is strongly reduced compared to bulk ZnO crystal due to the enhanced phonon-boundary and impurity (isotope) scattering. The maximum of the thermal conductivity is shifted to a higher temperature than that of bulk counterpart. Temperature dependent measurements show that beyond the low-temperature maximum, the thermal conductivity decreases with temperature as  $T^{-1.5}$  indicating strong impurity (isotope) scattering at intermediate and high temperatures.

[1] Kh. T. Igamberdiev, Sh. U. Yuldashev, H. D. Cho, T. W.Kang, and A. G. Shashkov, Appl. Phys. Express **4**, 015001(2011).

**Monday September, 14 - Oral Session - MoC**

**13:45-15:00**

**Spin in Dots**

Chair: Sergey Ivanov, *Ioffe Physical -Technical Institute (Russia)*

## Individual Ions of Transition Metals in II-VI Quantum Dots and Photonic Structures

Wojciech Pacuski

Institute of Experimental Physics, Faculty of Physics, University of Warsaw,  
ul. Pasteura 5, 02-093 Warsaw, Poland

Wojciech.Pacuski@fuw.edu.pl

This work presents molecular beam epitaxy and time-resolved magneto-optical spectroscopy of novel quantum dots (QDs) with individual transition metal ions. We report on the first optical observation of individual cobalt [1] and iron [2] ions in quantum dots. Both CdTe QDs in ZnTe barrier and new (in this context) system - CdSe QDs in ZnSe barrier [1-3] are applied for optical study and spin manipulation of individual magnetic ions: manganese, cobalt and iron. Photoluminescence (PL) study of QDs with single magnetic ions are compared with the measurements of excitonic PL [4,5] of epitaxially grown II-VI diluted magnetic semiconductors (DMS).

One of the most surprising finding is related to the exciton recombination channels. In case of DMS structures with excitonic energy exceeding the intra-ionic transition energy, the excitonic PL is weak due to quenching by magnetic ions. However, for single magnetic ions in QDs, the effect of quenching is found to be negligible. This is proved by the measurements of excitonic PL decay, which revealed no difference in decay dynamics from nonmagnetic QDs and the dots with single magnetic ions [1]. This opens a possibility of exploiting new solotronic systems with reduced sources of decoherence: ions without nuclear spin (such as iron or chromium) and wide gap QDs with weak spin-orbit interaction. Indeed, we observe significant differences in relaxation times of single magnetic ions in various systems [1,6,7].

QDs containing exactly one magnetic ion exhibit characteristic PL spectra modified by the *s,p-d* exchange interaction. As expected [8], the exciton and biexciton emission lines are split by 6 in case of a single  $Mn^{2+}$  in various II-VI QD systems. In case of QDs with individual  $Co^{2+}$ , the exciton and biexciton lines are split by 4 (due to 4 spin projection of  $Co^{2+}$ :  $\pm 3/2$ ,  $\pm 1/2$ ) [1]. The case of  $Fe^{2+}$  ion is more complex:  $Fe^{2+}$  is nonmagnetic (non-degenerate ground state) in bulk, but we find that strain of a QD induces distinctive changes in  $Fe^{2+}$  energy spectrum leading to the magnetic ground state of  $Fe^{2+}$  ion [2]. Consequently, the  $Fe^{2+}$  ion in a QD exhibits a ground state spin projection of  $\pm 2$  [2].

Finally, we present application of lithography techniques for studying individual magnetic ions in microstructures, such as micropillar cavities [9,10].

[1] J. Kobak, T. Smoleński, M. Goryca, M. Papaj, K. Gietka, A. Bogucki, M. Koperski, J.-G. Rousset, J. Suffczyński, E. Janik, M. Nawrocki, A. Golnik, P. Kossacki, W. Pacuski, *Nature Commun.* 5, 3191 (2014).

[2] T. Smoleński, T. Kazimierczuk, J. Kobak, M. Goryca, A. Golnik, P. Kossacki, W. Pacuski, arXiv:1505.06763 (2015); see also related poster at this conference.

[3] T. Smoleński, W. Pacuski, M. Goryca, M. Nawrocki, A. Golnik, P. Kossacki, *Phys. Rev. B* 91, 045306 (2015).

[4] M. Papaj, J. Kobak, J.G. Rousset, E. Janik, M. Nawrocki, P. Kossacki, A. Golnik, W. Pacuski, *J. Cryst. Growth* 401, 644 (2014).

[5] M.J. Grzybowski, A. Golnik, M. Sawicki, W. Pacuski, *Solid State Commun.* 208, 7 (2015).

[6] M. Pilat, M. Goryca, T. Smoleński, W. Pacuski, P. Kossacki, *Acta Phys. Pol. A* 126, 1212 (2014).

[7] M. Goryca, M. Koperski, T. Smoleński, Ł. Cywiński, P. Wojnar, P. Plochocka, M. Potemski, and P. Kossacki, *Phys. Rev. B* 92, 045412 (2015).

[8] L. Besombes, Y. Léger, L. Maingault, D. Ferrand, H. Mariette, J. Cibert, *Phys. Rev. Lett.* 93, 207403 (2004).

[9] W. Pacuski, T. Jakubczyk, C. Kruse, J. Kobak, T. Kazimierczuk, M. Goryca, A. Golnik, P. Kossacki, M. Wiater, P. Wojnar, G. Karczewski, T. Wojtowicz, D. Hommel, *Crystal Growth & Design* 14, 988 (2014).

[10] K. Sawicki, F. K. Malinowski, K. Gałkowski, T. Jakubczyk, P. Kossacki, W. Pacuski and J. Suffczyński, *Appl. Phys. Lett.* 106, 012101 (2015); see also related poster at this conference.

## Strain controlled coherent dynamics of coupled carriers and Mn spins in a charged Mn-doped quantum dot

A. Lafuente-Sampietro<sup>1,2</sup>, H. Boukari<sup>1,2</sup>, L. Besombes<sup>1,2,\*</sup>

<sup>1</sup>Univ. Grenoble Alpes, Grenoble, France

<sup>2</sup>CNRS, Institut Néel, Grenoble, France

\*lucien.besombes@grenoble.cnrs.fr

Semiconductor quantum dots (QDs) allow for the manipulation of single charge and spins in a solid-state system. It has been shown that optical spectroscopy of QDs can be used to access the spin of individual or pairs of magnetic atoms. The spin of a magnetic atom can be prepared, by the injection of spin polarized carriers, and it can be read through the energy and polarization of the photons emitted by the QD. The insertion of a magnetic atom in a QD where the charge and strain states can be controlled offers degrees of freedom to tune the properties of the localized spin. Information processing with individual spins requires a fast coherent control of a single spin and its coherent coupling to neighbour spins. The exchange coupling of the spin of a single carrier with the spin of individual magnetic atoms is an example of system where coherent transfer of information between spins could be realized.

The coherent dynamics of coupled carriers and individual Mn spins is analyzed through resonant photoluminescence (PL) of the positively charged exciton ( $X^+$ ) in a charge tunable CdTe/ZnTe QD [1]. The electron-Mn spin relaxation channels are identified in the energy and polarization of the resonant PL (figure 1a). The auto-correlation of the resonant PL reveals a large photon bunching resulting from the spin fluctuations of the electron-Mn and hole-Mn complexes. The dynamics of the coupled hole-Mn spins is measured in time resolved resonant optical pumping experiments. The coherent dynamics of the coupled electron-Mn spins is directly observed in the time resolved resonant PL: the presence of strain anisotropy at the Mn location induces quantum beats between electron-Mn spin states (figure 1c). The

strain induced coherent coupling can be continuously tuned by an external magnetic field. This complete set of experiments show that a p-doped magnetic QD forms an ensemble of ten optical  $\Lambda$  systems (figure 1 (b)) that could be used for a coherent control of the ferromagnet formed by the coupled hole-Mn spins.

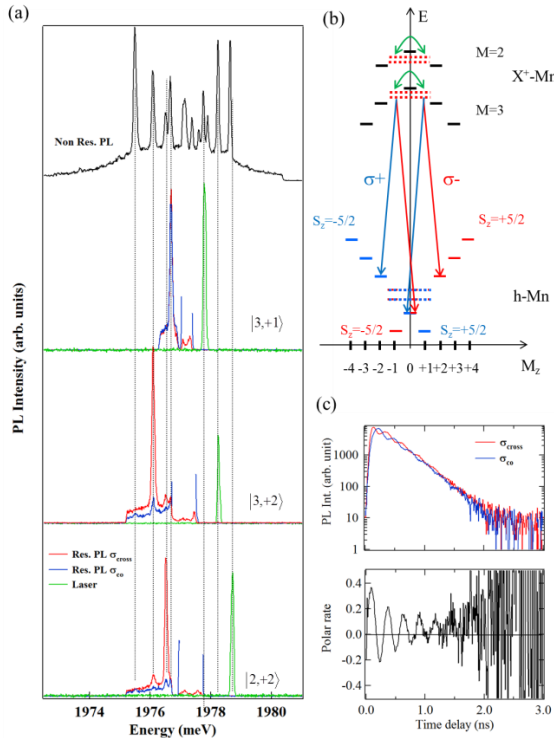


**Figure 1:** (a) PL (black) and resonant PL of  $X^+-\text{Mn}$  in a p-type Mn-doped QD. Resonant spectra are obtained under CW circularly polarized excitation for three different energies of the resonant laser (green). (b) Scheme of the energy levels of  $X^+-\text{Mn}$  and  $h-\text{Mn}$  illustrating the coupling of the  $\Lambda$  levels associated with  $|3,+1\rangle$  and  $|3,-1\rangle$  on one hand and  $|2,+1\rangle$  and  $|2,-1\rangle$  on the other hand by the strain anisotropy term  $E(S_x^2 - S_y^2)$  (green arrows). The states are displayed as a function of their angular momentum  $M_z$ . (c) Time resolved resonant PL for co an cross-circularly polarized excitation-detection of the state  $|3,+1\rangle$  and corresponding time dependence of the circular polarization rate.

[1] B. Varghese, H. Boukari, L. Besombes, Phys. Rev. B 90, 115307 (2014)

## Spin Relaxation Dynamics of an Individual $\text{Co}^{2+}$ Ion in a CdTe/ZnTe Quantum Dot

A. Bogucki\*, M. Goryca, K. Oreszczuk, T. Smoleński, J. Kobak, W. Pacuski, P. Kossacki  
 Institute of Experimental Physics, Faculty of Physics, University of Warsaw,  
 Ul. Pasteura 5, 02-093 Warsaw, Poland  
 \*aleksander.bogucki@fuw.edu.pl

Studies of single dopants in semiconductors constitute one of the research areas of the dynamically developing field of solotronics [1]. The progress of the field is driven by the perspectives of the ultimate miniaturization of information storage and processing devices, as well as by the possibility to investigate interactions between impurities and the host crystal in a single-atom scale. From scientific point of view quantum dots (QDs) containing single magnetic dopants seem to be as a model system to study those interactions. Until recently, only QDs with single manganese ions have been investigated, since other magnetic impurities were believed to quench any photoluminescence (PL) of the dots. However, this turned out not to be true in the case of a single impurity embedded in the dot, as a few new systems of single magnetic ions in semiconductor QDs were presented [2]. Systematic investigations on spin dynamics in those systems are important in the context of future optoelectronic devices.

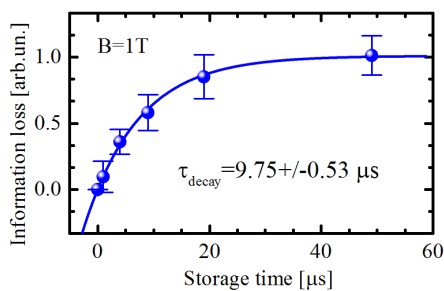


Fig. 1 Spin-relaxation time of the single  $\text{Co}^{2+}$  ion in CdTe/ZnTe QD determined by time-resolved PL under modulated excitation.

In this work we present studies of spin dynamics of a single  $\text{Co}^{2+}$  ion embedded in a CdTe/ZnTe QD. The sample used in the experiment contains a single layer of MBE-grown, self-assembled dots. The presence of a single  $\text{Co}^{2+}$  ion in selected dots was confirmed by observation of characteristic patterns in the excitonic PL spectrum with and without magnetic field [2]. In order to determine spin-relaxation time of the single  $\text{Co}^{2+}$  ion we performed time-resolved measurements of the QD PL under quasi-resonant, modulated excitation (see Fig. 1). It is experimentally simpler than the method previously used for the

$\text{Mn}^{2+}$  ion [3]. The measurements were carried out at various magnetic fields. The obtained values of relaxation time stay in an agreement with the values determined previously under non-resonant excitation [2] and are much shorter than those reported for the  $\text{Mn}^{2+}$  ion [3].

We discuss the impact of the local strain on the spin relaxation. The  $\text{Co}^{2+}$  ion has non-zero orbital momentum, thus it is more sensitive to the local anisotropy of surrounding lattice than the  $\text{Mn}^{2+}$  ion. Analyzing different dots, we show that local distortion has minor influence on the cobalt relaxation time. This new observation can help to determine the spin-lattice relaxation mechanism of a single magnetic ion in a QD.

We also show that similarly to the case of the QDs with  $\text{Mn}^{2+}$  ions [3], quasi-resonant injection of spin polarized excitons leads to the orientation of the  $\text{Co}^{2+}$  spin. The time resolved measurements of this effect reveals that the spin orientation efficiency per one exciton for a  $\text{Co}^{2+}$  ion in a CdTe dot is much larger than for  $\text{Mn}^{2+}$  ion in a similar dot.

- [1] P. M. Koenraad, M. E. Flatté, Nat. Mater. 10, 91–100 (2011)
- [2] J. Kobak, T. Smoleński, et al., Nat. Commun., 5, 3191, (2014)
- [3] M. Goryca, T. Kazimierzczuk, et al., Phys. Rev. Lett. 103, 087401, (2009)

## Colloidal CdS/ZnS Quantum Dots – Doped with Manganese and Functionalized with Organic Dye Molecules

Uwe Kaiser, Mikko Wilhelm, Nadeem Sabir, Carolina Carrillo-Carrion, Wolfgang J. Parak,  
and Wolfram Heimbrodt\*

*Department of Physics and Material Sciences Center, Philipps University Marburg, Germany*

\*wolfram.heimbrodt@physik.uni-marburg.de

Conjugates consisting of semiconductor quantum dots (QDs) and functional dye molecules are widely used for biophysical applications e.g. investigations of cellular processes. The energy transfer between the QDs and these molecules is one of the key aspects in such systems and can be used as a sensitive probe for different properties. Reabsorption as well as fluorescence resonance energy transfer (FRET) lead not only to a change of the optical spectra, but additionally influence the photoluminescence (PL) lifetime of the QDs as well as the attached dye molecules in such conjugates, which lies in the range of several nanoseconds.

In this contribution we present investigations on QD dye conjugates which are additionally doped with Mn atoms. A multistep growth of the ZnS shell around the CdS core preserves the incorporation of the Mn atoms in the shell. The luminescence decay of the QD PL around 440 nm is mainly determined by the interplay between different excitonic states leading to a non-exponential decay in the range of hundreds of nanoseconds. The Mn PL around 580 nm on the other hand shows a rather mono-exponential decay with a decay constant of 6 ms, which is tremendously longer than the QD lifetime.

By coating the doped QDs with an amphiphilic polymer shell we not only obtain water soluble QDs, but we are able to further functionalize these QDs with fluorophores. The attachment of different dye molecules to the polymer shell of the doped QDs introduces another PL band between 600 and 700 nm, depending on the specific molecule. The sophisticated energy transfer pathways in these QD dye conjugates involve a transfer between the QD, the Mn and the dye levels. The interplay of these energetic states is described within a kinetic model leading to a good description of the time resolved measurements of the respective PL bands. Our time resolved investigations reveal the twofold functionality of the Mn ions within the conjugates. On the one hand the Mn states act as energy acceptor for the high energetic CdS states leading to a faster decay of the QD PL. Within the interaction of Mn and dye states the Mn ions in turn act as an energy donor, increasing the lifetime of the dye PL by several orders of magnitude from nanoseconds to milliseconds. The nonradiative energy transfer also leads to a faster luminescence decay of the Mn states. The use of different dye molecules with a variation of the spectral overlap between the Mn emission and the dye absorption even let us control the exact lifetime of the Mn and dye states.

The functionalization of Mn doped QDs with organic dye molecules results in conjugates with a tunable PL lifetime in the range of milliseconds. This time regime opens up several new applications for semiconductor QDs and functional molecules e.g. the use in multiplex sensing applications.

**Monday September, 14 - Oral Session - MoD**

**15:30-17:15**

**Detectors**

Chair: Arnold Burger, *Fisk University (United States)*

## **UV-APDs using ZnSe-based organic-inorganic hybrid structure with long lifetime and device integration**

T. Abe, R. Inoue, T. Fujimoto, K. Tanaka, S. Uchida, H. Kasada, K. Ando, and K. Ichino  
Department of Information and Electronics, Graduate School of Engineering,  
Tottori University, Tottori, Japan  
E-mail: abe@ele.tottori-u.ac.jp

Ultraviolet avalanche photodiodes (UV-APDs) are attractive new optical devices which play a key-role in establishment of medical imaging devices (e.g. positron emission tomography; PET), radiation technology, astronomical applications, and next-generation ultra large capacitive optical storage system. Photomultiplier (PMTs) are commonly used as the UV detectors now for PET system, but they have many disadvantages for using in the PET system. For example, PMTs cannot be integrated due to use of vacuum tubes and operation at high voltage. Therefore, as next-generation alternate devices of PMTs, wide bandgap semiconductor UV photodiodes such as GaN, SiC, ZnO, ZnSe have been developing.

ZnSSe APDs show very low-voltage operation at around reverse bias of  $\sim 30\text{V}$ [1], which is originated from the band structure of ZnSe with very small impact ionization threshold energy. This low APD operation voltage is a very important point for the device full integration. The low voltage operation leads to a low level photosignal cross-talk, so the low-voltage APD operation of ZnSSe is very profitable for integration of UV APDs. Previously, we have developed PEDOT:PSS/ZnSSe organic-inorganic hybrid structure APD with polyimide passivation and sealing the devices into  $\text{N}_2$  atmosphere[2]. The device exhibited lifetime of 25 days. We also demonstrated  $2 \times 6$  integrated APDs operated in PIN photodiode mode.

In this study, we have successfully realized longer lifetimes and lower dark current ( $< 2 \times 10^{-11} \text{ A/mm}^2$ ) of the hybrid APDs by passivation with spin-coated polyimide films and sealing them into  $\text{N}_2$  atmosphere. The device exhibits long lifetimes more than 100 days and over 500 times operation with no detectable device degradation. The present devices also exhibit PIN mode response time of 3 ~ 10 ns (device area;  $0.4 \sim 1.1 \text{ mm}^2$ ), which is the half the decay time of the next-generation scintillator (Pr:LuAG; 20ns) for high-speed PET system. The response times are proportional to device area, which means that response time is limited by CR time constant and can be reduced by reducing device area.

Next, we fabricated an integrated device with three APDs array separated only by window layer spot of PEDOT:PSS without any device isolation process, such as etching, ion implantation, or guard ring structure. We traced the APDs by UV-laser with monitoring photocurrent of each APD in the avalanche region (avalanche gain of  $M = 10 \sim 30$  and responsivity of  $0.75 \sim 2.2 \text{ A/W}$ ). The present APDs array devices show photosignal cross-talk of -50dB under APD operation between the neighboring APDs. These results show that the present PEDOT:PSS/ZnSSe hybrid APD is expected as a new practical integrated UV-APD.

- [1] Y. Inagaki, M. Ebisu, M. Otsuki, N. Ayuni, T. Shimizu, T. Abe, H. Kasada, and K. Ando, *Phys. Status Solidi C* **9**, 1852, (2012).
- [2] T. Abe, N. Ikadatsu, R. Inoue, T. Fujimoto, K. Tanaka, A. Tazue, Y. Inagaki, M. Ebisu, H. Kasada, and K. Ando, *Phys. Status Solidi C* **11**, 1300, (2014).

## II-VI Broadband Quantum Cascade Detectors

Joel De Jesus<sup>1</sup>, Thor A. Garcia<sup>2</sup>, Arvind P. Ravikumar<sup>3</sup>, Claire F. Gmachl<sup>3</sup>, Maria C. Tamargo<sup>2</sup>

<sup>1</sup> Department of Physics, The Graduate Center and The City College of New York (CUNY), New York, NY 10031

<sup>2</sup> Department of Chemistry, The Graduate Center and The City College of New York (CUNY), New York, NY 10031

<sup>3</sup> Department of Electrical Engineering, Princeton University, Princeton, NJ 08544

Quantum cascade (QC) detectors [1] are photo-voltaic intersubband devices that rely on the displacement of charge perpendicular to the growth direction. The electrons in the doped quantum wells (QW) are excited by IR light and are carried away through a series of fast LO phonon transitions, thus creating a photovoltage. The ZnCdMgSe family of II-VI semiconductors offers the possibility of designing such detectors to respond to a wide range of wavelengths due to its large conduction band offset and absence of intervalley scattering.

After demonstrating the first II-VI-based detector [2], which exhibited good device properties, we are now interested in combining two or more active cores designed for response at different wavelengths to achieve broadband detection.

We recently grew a sequentially stacked design [3], where 15 repetition of 3 different cores (8.0  $\mu\text{m}$ , 6.8  $\mu\text{m}$ , 5.0  $\mu\text{m}$ ) are stacked one on top of one another. We obtained better responsivities, but the detector was mostly active in the 5.5  $\mu\text{m}$  region (the top active core). A new design using interleaved active regions (one single active core combining the different wavelength regions) has now been grown and is being tested.

The lattice-matched ZnCdMgSe-based QC structures are grown by molecular beam epitaxy on InP substrates, and characterized by photoluminescence (PL), X-Ray diffraction (XRD), FTIR transmittance, and scanning electron microscope (SEM). The devices are fabricated into rectangular mesas with a 45° wedge configuration using lithography and etching techniques. Top and bottom contacts were made of Ti/Au. The processed devices were mounted on copper sub-mounts and wire bonded for electrical measurements.

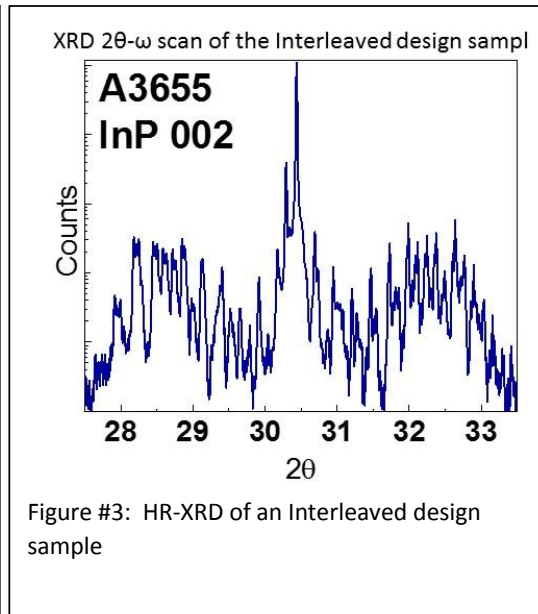
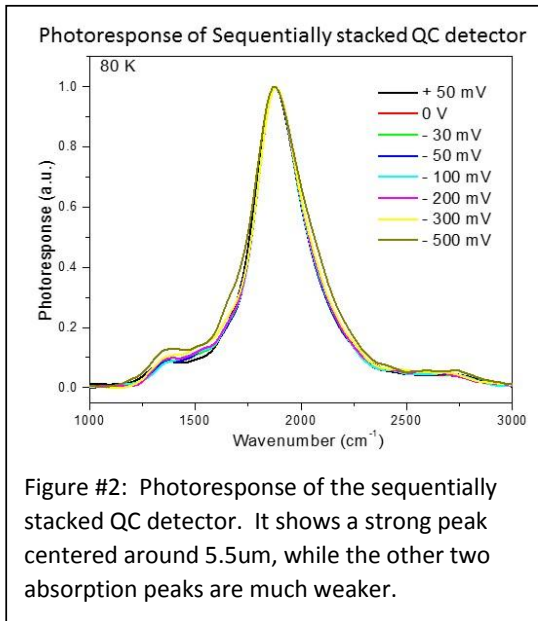
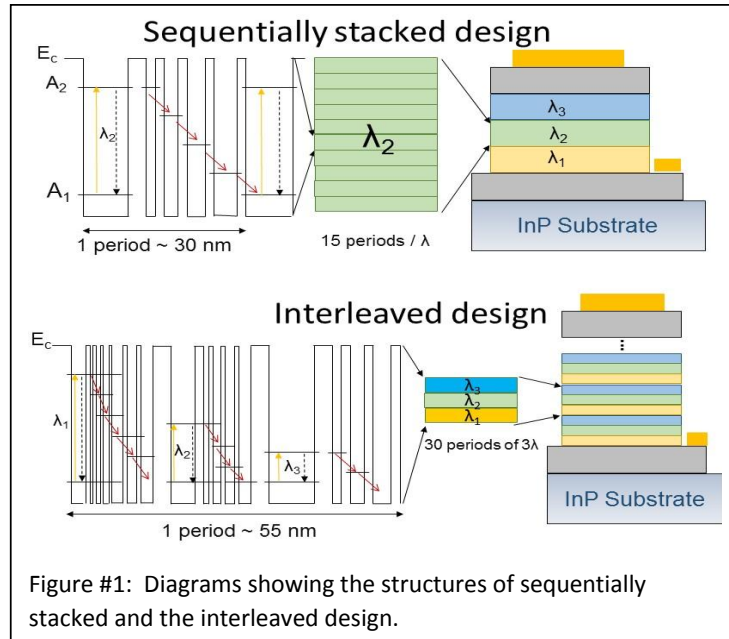
The performance of these novel IR broadband devices will be discussed.

### References:

[1] – F.R. Giorgetta, et al, IEEE J. Quantum Electron. 45 (2009) 1039.  
<http://dx.doi.org/10.1109/JQE.2009.2017929>.

[2] – A.P. Ravikumar, et al, Appl. Phys. Lett. 105 (2014) 061113. <http://dx.doi.org/10.1063/1.4893359>.

[3] – Presented at the 18<sup>th</sup> International MBE Conference, Sept. 2014, at Flagstaff, Arizona, USA



## Gamma-Ray Tolerance of CdS/CdTe Photodiodes for Radiation Tolerant Compact Image Sensor with Field Emitter Array

Okamoto T.<sup>1\*</sup>, Igari T.<sup>1</sup>, Taki M.<sup>1</sup>, Yasuda N.<sup>1</sup>, Takahashi K.<sup>1</sup>, Hosono A.<sup>1</sup>, Ogawa Y.<sup>1</sup>,  
Gotoh Y.<sup>2</sup>, Sato N.<sup>3</sup>, Akiyoshi M.<sup>4</sup>, and Takagi I.<sup>4</sup>

<sup>1</sup> Department of Electrical and Electronic Engineering, National Institute of Technology,  
Kisarazu College, 2-11-1 Kiyomidai-higashi, Kisarazu, Chiba 292-0041, Japan

<sup>2</sup> Department of Electronic Science and Engineering, Kyoto University,  
Kyotodaigaku-Katsura, Nishikyo-ku, Kyoto 615-8510, Japan

<sup>3</sup> Division of Physics and Astronomy, Research Reactor Institute, Kyoto University,  
2, Asashiro-Nishi, Kumatori-cho, Sennan-gun, Osaka 590-0494, Japan

<sup>4</sup> Department of Nuclear Engineering, Kyoto University, Kyotodaigaku-katsura, Nishikyo-ku,  
Kyoto 615-8540, Japan

\*okamoto@e.kisarazu.ac.jp

Since the disaster of the Fukushima nuclear power plant in the Great East Japan Earthquake, image sensors with high-radiation tolerance are strongly required. Until now, we proposed a compact image sensor with a combination of a matrix-driven Spindt-type field emitter array (FEA) and a photoconducting film based on CdTe [1]. In this work, we investigated the influence of gamma-ray irradiation to CdS/CdTe photodiodes as photoconducting films for a compact image sensor with FEA.

First of all, we investigated the gamma-ray irradiation tolerance of the glass/ indium tin oxide (ITO) / n-type CdS / p-type CdTe structure. Corning Eagle XG with thickness of 0.7 mm was used as a glass substrate. The ITO layer was used as a transparent conductive thin film. The CdTe and CdS polycrystalline thin-films were fabricated using close-spaced sublimation (CSS) and chemical vapor deposition (CVD), respectively [2]. The thickness of CdTe and CdS were approximately 5  $\mu\text{m}$  and 60 nm, respectively. In order to evaluate  $I$ - $V$  characteristics and spectral responses, Cu-doped carbon electrode was prepared on the CdTe layer [2]. This structure was the same as the conventional superstrate-type CdTe thin-film solar cells [2]. The gamma-ray irradiation was performed using  $^{60}\text{Co}$  gamma-ray irradiation facility of Kyoto University Research Reactor Institute (KURRI). The dose of gamma-irradiation was approximately 75 kGy. After the gamma-ray irradiation, the glass substrates were colored, and short-circuit current density ( $J_{\text{SC}}$ ) decreased from 23.5 to 21.2  $\text{mA}/\text{cm}^2$  in the  $I$ - $V$  characteristic under the simulated solar light (air mass (AM) 1.5, 100  $\text{mW}/\text{cm}^2$ ). On the other hand, open-circuit voltage ( $V_{\text{OC}}$ ) did not change by the gamma-ray irradiation. The decrease in the  $J_{\text{SC}}$  was probably due to the decrease in the transmittance of glass substrate.

In order to avoid the influence of the coloring of the glass substrate, we fabricated Al-doped ZnO / n-CdS / p-CdTe / graphite structure (substrate-type configuration). The graphite was used as a substrate. The Al-doped ZnO layer was used as a transparent conductive thin film. Little degradation in  $I$ - $V$  characteristic and spectral response was observed after the gamma-ray irradiation. These results suggest that the CdS/CdTe photodiodes have sufficient tolerance against gamma-ray irradiation except the decrease in the transmittance of glass substrate.

A part of this study is the result of "Development of radiation tolerant compact image sensor with a field emitter array", carried out under the Initiatives for Atomic Energy Basic and Generic Strategic Research by the Ministry of Education, Culture, Sports, Science and Technology of Japan.

- [1] Gotoh Y., Tsuji H., Nagao M., Yoshizawa S., Akiyoshi M., and Takagi I., 27th International Vacuum Nanoelectronics Conf., 71-72, (2014).  
[2] Okamoto T., Hayashi R., Ogawa Y., Hosono A., and Doi M., Jpn. J. Appl. Phys., **54**, 04DR01, (2015).

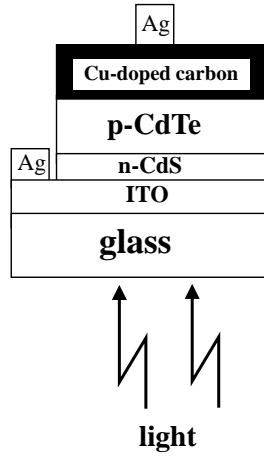


Fig. 1 Cross-sectional structure of the glass / ITO / CdS / CdTe (superstrate-type configuration).

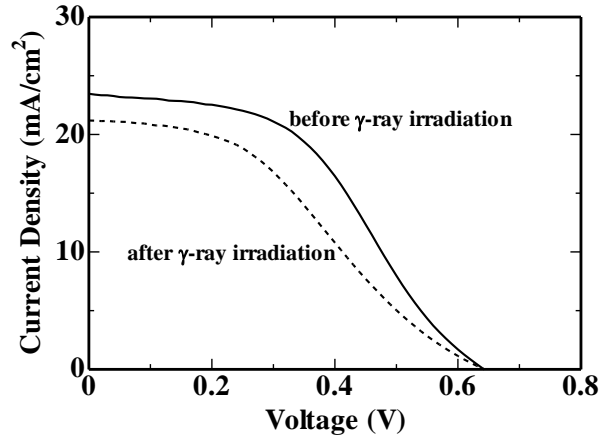


Fig. 2 *I-V* characteristics of the glass / ITO / CdS / CdTe structure under the simulated solar light before and after the gamma-ray irradiation.

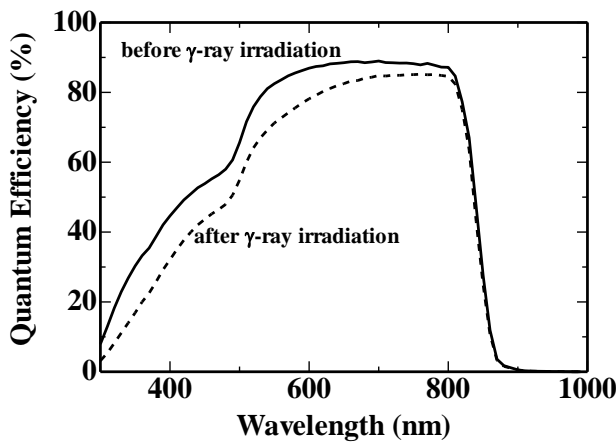


Fig. 3 Spectral responses of the glass / ITO / CdS / CdTe structure before and after the gamma-ray irradiation.

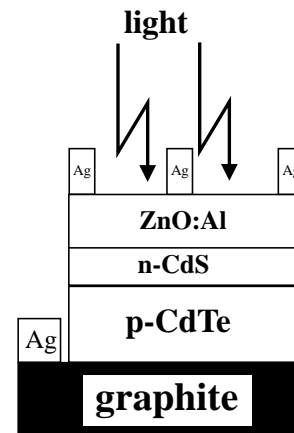


Fig. 4 Cross-sectional structure of the ZnO:Al / CdS / CdTe / graphite substrate (substrate-type configuration).

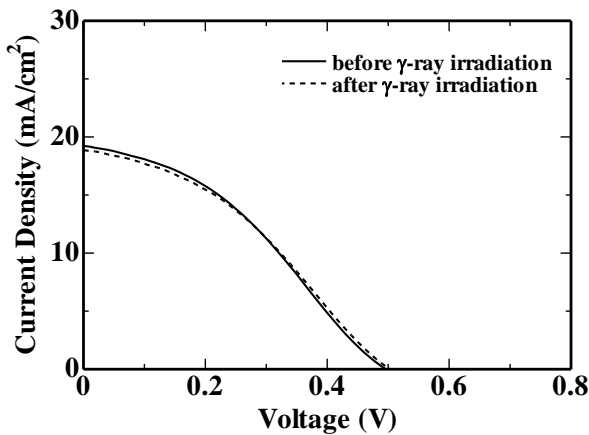


Fig. 5 *I-V* characteristics of the ZnO:Al / CdS / CdTe / graphite structure under the simulated solar light before and after the gamma-ray irradiation.

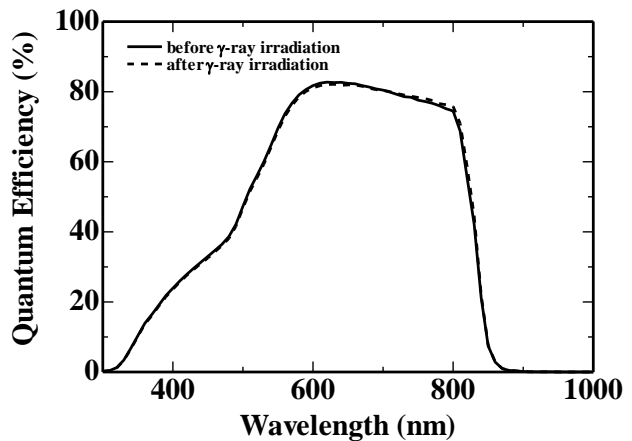


Fig. 6 Spectral responses of the CdTe / CdS / ITO / glass structure before and after the gamma-ray irradiation.

## High Power II-VI/InGaN Laser Diode Converters Emitting in the Green-Yellow Spectral Region

S.V. Ivanov<sup>1\*</sup>, E.V. Lutsenko<sup>2</sup>, A.G. Vainilovich<sup>2</sup>, G.P. Yablonskii<sup>2</sup>, S.V. Sorokin<sup>1</sup>,  
S.V. Gronin<sup>1</sup>, I.V. Sedova<sup>1</sup>, P.S. Kop'ev<sup>1</sup>, M. Aljohenii<sup>3</sup>, A. Aljerwii<sup>3</sup>, A. Alyamani<sup>3</sup>

<sup>1</sup>Ioffe Institute, St.Petersburg 194021, Russia

<sup>2</sup>Stepanov Institute of Physics, NASB, Minsk 220072, Belarus

<sup>3</sup>KACST, National Nanotechnology Center, P.O. BOX 6086, Riyadh 11442, Saudi Arabia

\*ivan@beam.ioffe.ru

The wide-gap II-VI compounds are still the main candidates for fabrication of efficient optoelectronic semiconductor devices emitting in the yellow-green and yellow ranges of visible spectrum. During last two years the significant progress towards the realization of microchip yellow-green ( $\lambda \sim 565$  nm) II-VI/III-N laser converters has been achieved [1]. The optimization of molecular beam epitaxy (MBE) of CdSe/ZnSe quantum dot (QD) based II-VI laser heterostructures with a graded-index waveguide (GIW) has resulted in the decrease of the threshold power density down to  $P_{\text{thr}} \sim 0.8$  kW/cm<sup>2</sup> at T=300K owing to the reduction of the density of non-equilibrium point defects in the active region [2]. The proposed method utilizes the migration enhanced epitaxy growth of ZnSe layers confining the CdSe QD sheet. Furthermore, the proposed the strain-balanced laser structures with the CdSe QDs embedded in a strained Zn<sub>1-x</sub>Cd<sub>x</sub>Se (x < 0.5) quantum well (QW) has resulted in efficient room temperature photoluminescence (PL) up to 590 nm [3]. Recently the GaAs-matched II-VI laser structures emitting in the “true” yellow (570-580 nm) and even orange (590-593nm) spectral ranges have been demonstrated [4].

This paper presents our latest results on II-VI/InGaN LD converters based on the low-threshold II-VI laser heterostructures. The wide spectrum of Cd(Zn)Se/ZnMgSSe QD laser heterostructures grown by MBE pseudomorphically to a GaAs(001) were employed. The general structure design as well as details of MBE growth have been reported earlier [4,5]. The ability to cover the whole green and yellow-green ranges (500-565 nm) with the microchip A<sup>3</sup>N/II-VI converters has been demonstrated, the lasing wavelength being determined mainly by the CdSe QD nominal thickness (2.5-3 MLs). An increase in the output pulsed power of the converters was achieved by optimization of the operation mode of the pulsed InGaN LDs used for the excitation. In particular, the decrease of the pulse time down to 4 ns ( $f=250$  Hz) allowed rising the pumping power of the InGaN LDs from the nominal CW output power  $P_{\text{exc}} \sim 3.5$  W up to the pulse  $P_{\text{exc}} \sim 40-50$  W without catastrophic degradation. This has resulted in the enhancement of the output pulse power and quantum efficiency of the converter based on a single-sheet CdSe/ZnSe QD heterostructure up to 5W and  $\sim 12.5\%$ , respectively. Moreover, the using of other II-VI laser heterostructures with multiple QD sheets and extended waveguide as an active element of the converter allows further enhancement of the converter output pulse power and efficiency owing to the increase in both the absorption efficiency of the pumping LD emission and the internal quantum efficiency. The data on realization of yellow laser converters based on II-VI laser heterostructures with the active region based on two CdSe/ZnSe QD sheets [1] and single CdSe QD sheet embedded in a strained Zn<sub>1-x</sub>Cd<sub>x</sub>Se quantum well [4] will be presented.

[1] E.V. Lutsenko et al., *Quantum Electron.* **43**(5), 418-422 (2013)

[2] S.V. Sorokin et al., *Semiconductors* **49**(3), 331-336 (2015).

[3] S.V. Gronin et al., *Acta Physica Polonica A* **126**(5), 1096-1099 (2014)

[4] S.V. Gronin et al, this conference

[5] S.V. Ivanov, S.V. Sorokin, I.V. Sedova. In: Henini M, editor. *Molecular Beam Epitaxy: From research to mass production.* Elsevier Inc., 2013. pp. 611–630.

## **HgCdTe p<sup>+</sup>-n structures grown by MBE on Si (013) substrates for high operating temperature MWIR detectors**

V.M. Bazovkin, A.A. Guzev, A.P. Kovchavtsev, A.V. Tsarenko, Z.V. Panova,  
M.V. Yakushev\*, V.S. Varavin, V.V. Vasilyev, S.A. Dvoretzky, D.V. Marin,  
 I.V. Sabinina, G.Yu. Sidorov, Yu.G. Sidorov

A.V. Rzhhanov Institute of semiconductor physics, SB RAS, Novosibirsk, Russia  
\*yakushev@isp.nsc.ru

The main trends in the development of 2D focal plane arrays (FPAs) for cooled infrared (IR) detectors include increasing the total number of elements in focal plane arrays and raising the FPA operating temperature over liquid nitrogen temperature. Increasing the FPA operating temperature reduces the weight and power consumption of the detectors through the use of smaller-capacity coolers, improves the performance of the detectors and expands their application range, and reduces the cost of the devices.

HgCdTe (MCT) solid solutions are one of the basic materials in fabrication IR FPA especially as heterostructures on silicon substrates. Such heterostructures are fundamentally solve the problem of matching of the thermal expansion coefficients of IR photosensitive array (PSA) and multiplexer at hybridization.

In using p-n junctions as FPA elements, an increase in the operating temperature can be achieved via reduction of the generation/recombination current density, this density being defined by the density of deep levels in the bandgap of the semiconductor and, hence, by the purity of the semiconductor material.

In the present study, the Cd<sub>x</sub>Hg<sub>1-x</sub>Te heterostructures with graded-gap MCT layers were grown by MBE on Si (013) substrates. The thickness of the Cd<sub>x</sub>Hg<sub>1-x</sub>Te absorber layer ( $x \sim 0.3-0.4$ ) was 4 to 6  $\mu\text{m}$ . During the growth, the MCT layers were doped with In to a concentration of  $(1-5) \cdot 10^{15} \text{ cm}^{-3}$ . The density of morphological V-defects in the layers was about  $500 \text{ cm}^{-2}$ .

The p-n junctions were formed by implantation of arsenic ions into n-type MCT layers followed by annealing-induced activation of arsenic impurities. The diode area in the fabricated focal plane arrays was  $10 \times 10 \mu\text{m}^2$ , and the diode pitch was 30  $\mu\text{m}$ . We measured the temperature dependence of the reverse bias current of diodes at several bias voltages.

A one-dimensional drift-diffusion model was used to calculate the theoretical current-voltage characteristics of the diodes. To this end, we simultaneously solved the Poisson equation for the electric potential as distributed across the MCT photosensing layer with regard for the MCT composition and the continuity equations for the electron and hole concentrations in the allowed bands of the semiconductor. We assumed that the trapping and emission of free charge carriers in the semiconductor proceeded with participation of one type of deep-level traps according to the thermal Shockley-Read-Hall mechanism.

A comparison of experimental curves for dark currents with simulated data was performed to determine the density of deep-level traps in the forbidden gap of the semiconductor, which proved to be  $\sim 5 \cdot 10^{11} \text{ cm}^{-3}$ . Numerical simulations were also performed to determine the optimum position of the metallurgical boundary of the p-n junctions in the contact layer.

Using the designed focal plane arrays,  $320 \times 256$  short-wave IR FPA detectors with long-wave cutoff wavelength  $\lambda_{1/2} \approx 3.0 \mu\text{m}$  at 170 K were fabricated. For NETD and specific detectivity ( $D^*$ ) at  $T=170 \text{ K}$ , values of 40 mK and  $2 \cdot 10^{12} \text{ cm} \cdot \text{Hz}^{1/2} \cdot \text{W}^{-1}$  have been respectively obtained.

This work was supported by the Ministry of Education of the Russian Federation (Grant RFMEFI60414X0134).

## Electric Field Inhomogeneity in Ohmic Cd(Zn)Te Detectors Measured by Time-of-Flight Technique

Kazuhiko Suzuki<sup>1\*</sup>, Takayuki Sawada<sup>1</sup>, and Satoru Seto<sup>2</sup>

<sup>1</sup>Department of Electrical and Electronic Engineering, Hokkaido University of Science, Sapporo 006-8585, Japan

<sup>2</sup>Department of Electrical Engineering, Ishikawa National College of Technology, Ishikawa 929-0392, Japan

\* suzukik@hus.ac.jp

CdTe and Cd<sub>1-x</sub>Zn<sub>x</sub>Te are practically used for X and gamma ray detectors without cooling owing to their high resistivity (typically in the order of 10<sup>9</sup> Ωcm for CdTe and 10<sup>10</sup> Ωcm for Cd<sub>1-x</sub>Zn<sub>x</sub>Te) and good transport properties. Since such high resistivity is attained by electrical compensation induced by intentionally doped donor impurity during growth, there are several deep levels in the band gap of these materials [1]. Space charges resulted from trapping and/or detrapping of charges to these levels may have a possibility to perturb the uniformity of electric field leading to a deterioration of the detection performance. The catastrophic degradation due to the bias induced polarization in Schottky type detectors are well investigated by several authors [2]. While on the other hand, although the effect is less remarkable, an instability of the electric field in Ohmic type detectors is not well understood. We have investigated the internal electric field distribution and its temporal evolution in Ohmic type detectors measured by a time-of-flight (TOF) technique at several different temperatures.

Fig. 1 shows  $\Delta T_L$  dependence of electron transient current waveforms of an Ohmic type CdTe detector at constant bias voltage of 300V. Here,  $\Delta T_L$  is defined as a delay of laser excitation from the onset of pulse bias application. At the shortest  $\Delta T_L$  of 30  $\mu$ s, the current waveform shows a plateau during carrier drift indicative of very long deep trapping time  $\tau^+$  compared with transit time  $T_R$ ,  $\tau^+ \gg T_R$ . While the current waveforms at longer  $\Delta T_L$  show decrease of the current with time which is supposed to be due to a decrease of the electric field from the cathode side to the anode side. Assuming a homogeneous distribution, a positive space charge buildup of  $5 \times 10^{10} \text{ cm}^{-3}$  is estimated at  $\Delta T_L = 4.0 \text{ s}$ . A possible origin for the buildup will be discussed at the conference.

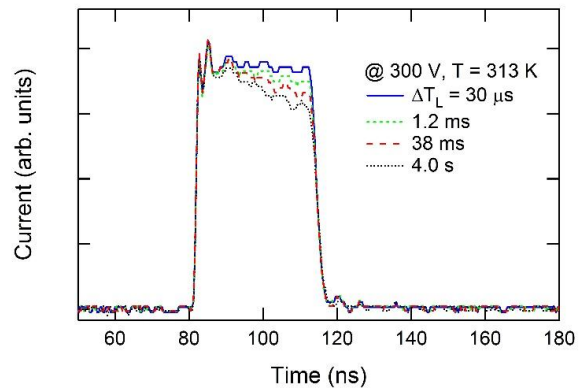


Figure 1. TOF current waveforms for an Ohmic type CdTe detector measured at 313 K with different  $\Delta T_L$  from 30  $\mu$ s to 4.0 s.

[1] M. Fiederle et al., J. Appl. Phys. **84** (1998) 6689-.

[2] See, for example, A. Cola and I. Farella, Appl. Phys. Lett. **94**, (2009) 102113.

**Tuesday September, 15 - Oral Session - TuA**

**08:30-10:00**

**Growth and Characterizations 2**

Chair: Maria Tamargo, *City University of New York (United States)*

## MBE growth of 2D layered chalcogenides (invited)

Xinyu Liu<sup>1\*</sup>, S. Vishwanath<sup>2</sup>, S. Rouvimov<sup>3,4</sup>, D. Jena<sup>2</sup>, H. G. Xing<sup>2</sup>, and J. K. Furdyna<sup>1</sup>

<sup>1</sup>Department of Physics, Univ. of Notre Dame, Notre Dame, IN 46556, USA

<sup>2</sup>School of Electrical and Computer Engineering, Department of Materials Science and Engineering, Cornell University, Ithaca, NY 14853, USA

<sup>3</sup>Department of Electrical Engineering, Univ. of Notre Dame, Notre Dame, IN 46556, USA

<sup>4</sup>Integrated Imaging Facility, Univ. of Notre Dame, Notre Dame, IN 46556, USA

[\\*xliu2@nd.edu](mailto:xliu2@nd.edu)

Intensive research is currently being aimed at understanding both the growth and the physical properties of a wide range of two-dimensional (2D) layered chalcogenides (e.g., Bi<sub>2</sub>Se<sub>3</sub>, MoS<sub>2</sub>, etc.), since this class of materials is expected to lead to entirely new types of devices on the nanoscale. Most of these studies have been performed by exfoliating thin layers from natural or synthetic crystals. However, practical manufacturing will require the production of large-area materials *via* scalable approaches. Molecular beam epitaxy (MBE) is widely used for a variety of materials systems to obtain electronic-grade materials with abrupt interfaces, excellent thickness control and capabilities for precise doping. This technique thus opens the door for precise fabrication of high purity 2D chalcogenide heterostructures over wafer scale that is sufficient for device applications, and for designing experiments aimed at understanding the novel physics of these 2D systems. Here we will address the opportunities and challenges of MBE growth of 2D chalcogenides from three perspectives.

We will first review the MBE growth of typical 2D chalcogenides, such as Bi<sub>2</sub>(SeTe)<sub>3</sub>, Mo(SeTe)<sub>2</sub>, and SnSe<sub>2</sub> on various substrates, including the issue of appropriate substrate preparation. As an illustration of a key step towards achieving high-quality electronic grade 2D chalcogenides, we will present a growth study on one model material, MoSe<sub>2</sub>, on Se-terminated GaAs (111)B, on highly oriented pyrolytic graphite (HOPG), and on CaF<sub>2</sub> (111) substrates, as well as on epitaxial graphene on SiC. Extensive characterizations, such as cross-sectional scanning transmission electron microscopy (STEM), scanning electron microscopy (SEM), X-ray photoelectron spectroscopy (XPS), atomic force microscopy (AFM), Raman spectroscopy, reveal that MoSe<sub>2</sub> grows by van-der-Waals epitaxy on all these substrates with a preferred crystallographic orientation aligning with the underlying substrate. Note that overcoming the observed small grains by promoting mobility of Mo atoms would make MBE a powerful technique to achieve high quality 2D materials and heterostructures.

Stacking of 2D layered materials has been in limelight in this field due to the fact that atomically thin heterostructures can be formed from these materials, thus enabling one to tailor structures for specific nanoscale device requirements. During MBE growth we expect rotational orientation corresponding to thermodynamically stable configuration to be achieved. Importantly, we have been able to fabricate various 2D layered chalcogenides together, such as MoSe<sub>2</sub>/Bi<sub>2</sub>Se<sub>3</sub>; SnSe<sub>2</sub>/Bi<sub>2</sub>Se<sub>3</sub>; and MoTe<sub>2</sub>/MoSe<sub>2</sub>. Here, in the second part of this talk, we will use the MBE growth of MoTe<sub>2</sub>/MoSe<sub>2</sub> superlattice (4 periods) as an illustration of these new structures. Cross-sectional STEM and corresponding energy-dispersive X-ray spectroscopy (EDS) line scan results of the MoTe<sub>2</sub>/MoSe<sub>2</sub> superlattice clearly authenticate the claim that 2D superlattice indeed has been obtained.

Importantly, the introduction of dopants (such as magnetic dopants) into a 2D lattice can bring out new functionalities, providing new opportunities for device applications. In the last part of this talk, we explore this area by introducing Mn ions into the 2D lattice of Bi<sub>2</sub>Se<sub>3</sub> and SnSe<sub>2</sub>. Again, rigorous characterization of the physical properties of these new materials was carried out by a wide range of complementary studies, including XRD, electric transport, magnetometry, Raman spectroscopy, and TEM. Based on these measurements, the Mn distributions in these magnetic 2D materials will be addressed and discussed in some detail.

## Hydrogen contamination in ZnO films grown at low temperature

E. Guziewicz<sup>1\*</sup>, T.A. Krajewski<sup>1</sup>, D. Jarosz<sup>1</sup>, E. Przeddziecka<sup>1</sup>, G. Luka<sup>1</sup>, D. Snigurenko<sup>1</sup>,  
R. Jakiela<sup>1</sup>, K. Kopalko<sup>1</sup>, A. Stonert<sup>2</sup>, R. Ratajczak<sup>2</sup>, W. Lisowski<sup>3</sup>, J.W. Sobczak<sup>3</sup>

<sup>1</sup>Institute of Physics, Polish Academy of Sciences, Warsaw, Poland

<sup>2</sup>National Centre for Nuclear Research, Swierk, Poland

<sup>3</sup>Institute of Physical Chemistry, Polish Academy of Sciences, Warsaw, Poland

\*[guzel@ifpan.edu.pl](mailto:guzel@ifpan.edu.pl)

The origin of the commonly observed high background donor conductivity of zinc oxide has been a subject of extensive research. Theoretical calculations supported by electron paramagnetic resonance experiments show that native point defects alone cannot be responsible for a high electron conductivity, because  $V_o$  is a deep donor while the energy formation of  $Zn_i$  is relatively high [1]. Based on both theoretical and experimental studies hydrogen is widely regarded as a dominant donor in this material [2-3].

However, this model does not work for zinc oxide films deposited at the low temperature range (200°C and below) [4-5]. For such films the scaling of electron concentration with deposition temperature is observed [4-5], i.e. electron concentration in ZnO films deposited at 100°C is at the level of  $10^{16} \text{ cm}^{-3}$  and is 3 orders of magnitude lower than electron concentration observed when the growth temperature achieves 200°C. On the other hand, electron concentration is accompanied by a high hydrogen content as measured by SIMS and both this quantities anti-correlate [4]. Moreover, hydrogen content considerably exceeds electron concentration.

In the presented work we investigated a series of thin ZnO films deposited at temperature between 100 and 200°C by Atomic Layer Deposition with diethylzinc and deionized water precursors. Our detailed X-ray Photoelectron Spectroscopy studies show the increase of the oxygen to zinc ratio when deposition temperature drops from 200 to 100°C. The Rutherford Backscattering (RBS) measurements confirm this result. Rapid Thermal Annealing (RTA) performed in an oxygen atmosphere leads to the slight lowering of the hydrogen content, but it still remains at a very high level of  $10^{20} \text{ cm}^{-3}$ .

In temperature dependent photoluminescence (PL) spectra taken in the range of 10 – 300K we observe a big difference between *as grown* and annealed samples. In both cases the peak related to the donor bound exciton  $D^0X$  at energy 3.367 eV (with FWHM = 8 meV) is observed at 10K. However, the dominant emission appears at 3.322 eV. Phonon repetition have been observed as well. After 3 min. RTA process all PL features become considerable sharper and the intensity of the  $D^0X$  related emission considerably increases. The origin of PL peaks has been analyzed.

The presented data suggest that low deposition temperature provides oxygen-rich conditions in which lower concentration of oxygen vacancies is created. The oxygen vacancies decorated with hydrogen seem to act as shallow donors in this material, while a main part of hydrogen remains electrically inactive.

The Authors EG, SD and KK were supported by the Polish National Science Centre (NCN) Project based on the decision No. DEC-2012/07/B/ST3/03567. The Author EP was supported by the NCN Project based on the decision No. DEC-2013/09/D/ST3/03750.

- [1] A. Janotti and C.G. van der Walle, Phys. Rev B **76**, 165202 (2007).
- [2] A. Janotti and C.G. van der Walle, Rep. Prog. Phys. **72**, 126501 (2009).
- [3] D.M. Hoffman, A. Hofstaetter, F.leiter, H.J. Zhou, et al., Phys. Rev. Lett. **88**, 045504 (2002).
- [4] E. Guziewicz, et al., Semicond. Sc. Techn. **27**, 074011 (2012).
- [5] S.C. Gong, S. Bang, H. Jeon, H.H. Park, Y.C. Chang, H.J. Chang, Metals and Materials Int. **16**, 953 (2010).

## Nearest-neighbour Lattice Distortions in Oxygen-deficient Mn-doped ZnO and MgZnO Thin Films, Probed by Electron Paramagnetic Resonance

Michael Lorenz<sup>1\*</sup>, Andreas Pöpl<sup>1</sup>, Stefan Friedländer<sup>1</sup>, Daniel Spemann<sup>1</sup>, Rolf Böttcher<sup>1</sup> and Marius Grundmann<sup>1</sup>

<sup>1</sup>Institut für Experimentelle Physik II, Universität Leipzig, D-04103 Leipzig, Germany

\*E-mail: mlorenz@physik.uni-leipzig.de

The structure and functional properties of ZnO-based thin films for device applications are largely affected by oxygen vacancies. While the macroscopic relationship between functionality and growth-induced oxygen vacancies is easy to access, the local influence of changing oxygen content on the next-neighbour structure around the incorporated metal ions has been rarely investigated. As a model system, we use 0.02% to 0.05% Mn as a local probe in hetero- and homoepitaxial ZnO and MgZnO thin films for electron paramagnetic resonance (EPR).

Mn is expected to be incorporated as  $\text{Mn}^{2+}$  in the Zn-lattice site of ZnO and MgZnO films. The zero field splitting (ZFS) parameter  $D$  depends on the crystallographic  $c/a$  ratio of ZnO:Mn lattice constants as it measures the trigonal distortion of oxygen tetrahedra at the  $\text{Zn}^{2+}$  site with respect to the  $\text{Mn}^{2+}$  site. The ZFS parameter  $D$  correlates linearly with displacement of  $\text{Mn}^{2+}$  ions along the  $c$ -axis in the  $\text{MnO}_4$  tetrahedra and the corresponding bond lengths between the  $\text{Mn}^{2+}$  ions and the axial oxygen ion [1]. Beginning with 3% Mg content in MgZnO films, there are clear signs of a cubic nearest-neighbour coordination around  $\text{Mn}^{2+}$ , which is expected to be representative also for the  $\text{Zn}^{2+}$  environment [2].

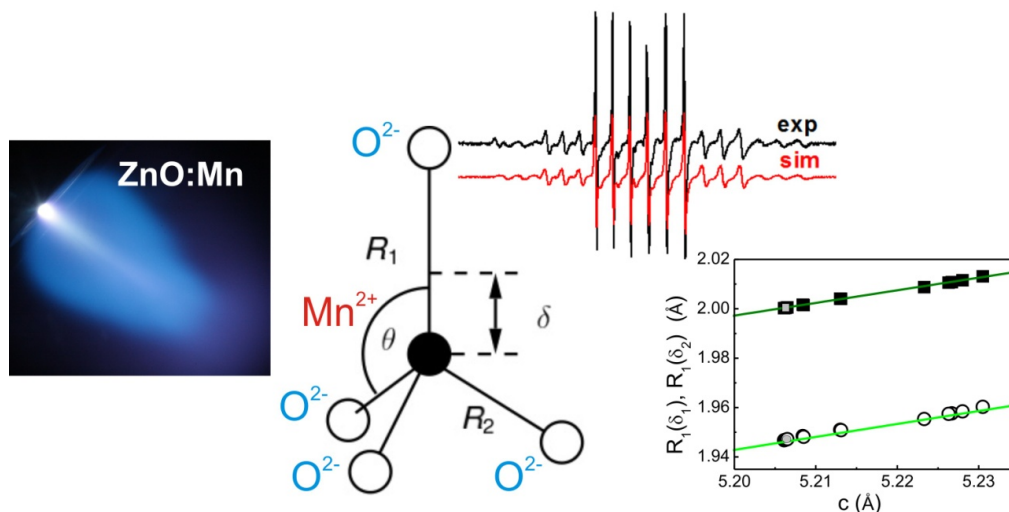


Fig. 1. Electron paramagnetic resonance of PLD-grown oxygen deficient ZnO:Mn thin films provides linear correlation of zero field splitting and displacement of  $\text{Mn}^{2+}$  in the  $\text{MnO}_4$  tetrahedrons, and corresponding bond lengths [1]. Figures adopted from [1].

[1] M. Lorenz, R. Böttcher, A. Pöpl et. al., J. Mater. Chem. C **2**, 4947 (2014)

[2] M. Lorenz, A. Pöpl et al., in preparation (2015)

## Homoepitaxial nonpolar ZnO/ZnMgO multilayers: fabrication of Distributed Bragg Reflectors and optical microcavities

C. Deparis, L. Kappei, and J. Zuniga-Perez\*

*CRHEA-CNRS, Rue Bernard Gregory, 06560 Valbonne, France*

Semiconductor-based microcavities have arisen as a prolific system for studying light-matter interaction between a spatially-confined photonic mode and an excitonic resonance. The quasiparticles resulting from this coupling, namely microcavity-polaritons, have enabled the observation of new lasing regimes, in which no population inversion is required, as well as polariton Bose-Einstein condensates, vortices and lately solitons. In this panorama, ZnO appears as an alternative material to more mature ones, such as GaAs or CdTe, with larger oscillator strengths and enhanced exciton stability. These two properties render ZnO very interesting for studies and applications where large particle densities and/or high temperatures (e.g. 300K) are required. However, the fabrication of ZnO-based planar microcavities is still challenging and it often requires the use of either nitrides [1] or dielectric materials [2] for fabricating Distributed Bragg Reflectors (DBRs). These two approaches have enabled to fabricate state-of-the-art polariton lasers operating at room-temperature [1,2], as well to illustrate ZnO's peculiarities [3], e.g. enhanced phonon-assisted polariton relaxation. Meanwhile, these cavities differ largely from those allowing to study more fundamental polariton physics, mainly based on GaAs-based technology, in which both the active region and DBRs are grown monolithically on GaAs substrates [4].

In this work we will first discuss the advantages and disadvantages of monolithic ZnO-based microcavities as compared to previous approaches (based on nitride and dielectric DBRs). Secondly, to illustrate the feasibility of this monolithic approach ZnO/ZnMgO-based DBRs and microcavities have been grown by molecular beam epitaxy on *m*-plane (10-10) ZnO substrates. The structural and optical properties of the fabricated structures have been characterized by high-resolution X-ray diffraction and reflectivity/photoluminescence measurements. The effect of the total epilayer thickness (i.e. number of DBR pairs) on these properties will be described, outlining the limits and perspectives of the monolithic solution.

[1] J. Zuniga-Perez *et al.*, *Appl. Phys. Lett.* **104** (2014) 241113

[2] Feng Li *et al.*, *Appl. Phys. Lett.* **102** (2013) 191118

[3] Feng Li *et al.*, *Phys. Rev. Lett.* **110** (2013) 196406

[4] E. Wertz *et al.*, *Nature Phys.* **6** (2010) 860

\*Electronic mail: [jzp@crhea.cnrs.fr](mailto:jzp@crhea.cnrs.fr)

## Characterization of doping by Scanning Capacitance Microscopy and C(V) technique in ZnO nanowires for optoelectronic application

L. Wang<sup>1</sup>, J. Laurent<sup>1</sup>, A. Sabac<sup>1</sup>, J.M. Chauveau<sup>3</sup>, V. Sallet<sup>4</sup>, F. Jomard<sup>4</sup>, C.Sartel<sup>4</sup>,  
R. Brenier<sup>5</sup>, G. Brémond<sup>1, 2\*</sup>

<sup>1</sup>Institut des Nanotechnologies de Lyon, UMR-5270, Université de Lyon, INSA Lyon, 7  
avenue Jean Capelle 69621 Villeurbanne, France

<sup>2</sup>Centre Lyonnais de Microscopie, INSA Lyon, 69621 Villeurbanne, France

<sup>3</sup>Centre de Recherche sur l'Hétéro-Epitaxie et ses Applications, CNRS, rue Bernard Grégory,  
06560 Valbonne, France

<sup>4</sup>Groupe d'Etude de la Matière Condensée, UMR-8635, 45 avenue des Etats Unis, 78035  
Versailles, France

<sup>5</sup>Institut Lumière Matière, UMR-5306, Université de Lyon, UCB Lyon 1, 43 boulevard du 11  
novembre 1918, 69622 Villeurbanne, France

\*georges.bremond@insa-lyon.fr

ZnO is a wide band-gap II-VI semiconductor (3.4 eV) very useful for diverse applications such as optoelectronics and sensor devices. The development of its related technology suffers from a lack of p-type doping feasibility. At the same time, with the development of nano-science and technology, semiconductor nanowires open new fields of investigation in fundamental physics and offer opportunities for the future generation of devices. This strongly request methods to quantitatively determine the carrier/dopant profile in such one-dimensional NW structure. In the last two decades, scanning capacitance microscopy (SCM) has been developed as well-recognized techniques for two-dimensional (2D) carrier/dopant profiling in semiconductor materials and devices[1,2]. The objective of our work is to electrically characterize the doping of ZnO nanostructure as NWs by SCM, to detect the local carrier type and determine its concentration.

For SCM measurement on NWs, we have developed a process of NW sample preparation, based on dip-coating filling and polishing of vertical NWs field. The process proved to be viable from the resulted proper topography and the contrast between NWs and SiO<sub>2</sub> matrix under SCM.

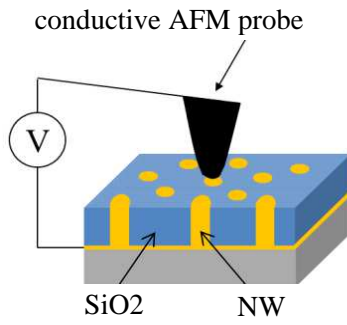
For the purpose of carrier/dopant profiling, calibration methodology is involved. Cross-sectional SCM were performed on Ga-doped MBE grown ZnO multi-layer structures consisting of layers with various Ga concentrations. Good contrasts of SCM signal between the ZnO layers with different Ga densities were obtained. Through comparison with Ga dopant profiles from SIMS measurements, the dynamic range of SCM for dopant profiling in ZnO are identified to be up to 10<sup>19</sup> cm<sup>-3</sup>. Then calibration curves were established and through its combination with the SCM result of NWs, the carrier concentration inside the NW is estimated to be around 5E18 cm<sup>-3</sup>.

Besides nano-characterization with SCM, conventional techniques I(V) and C(V) were employed to investigate the characteristics of the collection of NWs at the macroscale. The results were compared to that from SCM analysis.

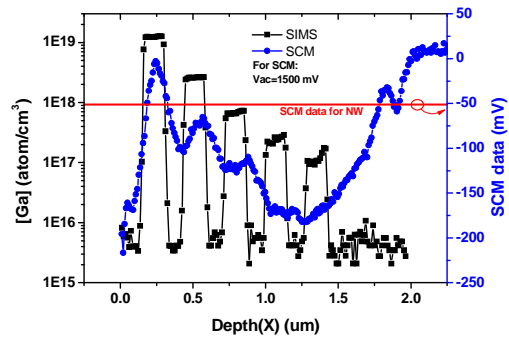
[1] C.C. Williams, Annu. Rev. Mater. Sci. 29, 471 (1999).

[2] R. A Oliver, Reports Prog. Phys. 71, 076501 (2008).

Appendix



Schematic of SCM measurement on NWs structure



SCM profile of multi-layer structure plotted with [Ga] profile and comparison with SCM value for NWs (red straight line)

**Tuesday September, 15 - Oral Session - TuB**

**10:30-12:15**

**Novel 2D systems, topological systems**

Chair: Rameshwar Bhargava, *Nanocrystals (United States)*

## Terahertz Radiation Induced Electric Currents in Topological Insulators

S.D. Ganichev

Terahertz Center, University of Regensburg, Regensburg, 93051 Germany

\*sergey.ganichev@physik.uni-regensburg.de

The paper overviews experimental and theoretical studies of photocurrents excited by polarized terahertz (THz) radiation in  $\text{Bi}_2\text{Te}_3$ ,  $\text{Sb}_2\text{Te}_3$  and  $\text{HgTe}$  based topological insulators (TI). We show that the photocurrents are caused by photogalvanic (PGE) or, in the presence of magnetic field, magneto-photogalvanic (MPGE) effects: nonlinear transport effects yielding a  $dc$  electric current proportional to the square of the  $ac$  electric field [1,2]. We discuss the phenomenological and microscopic theory of these phenomena, present the state-of-the-art of the experiments and show that nonlinear transport excited by THz laser radiation opens up new opportunities for probing of Dirac electrons in 3D TI even in the materials with substantial conductance in the bulk.

The PGE is caused by asymmetric scattering of Dirac fermions driven back and forth by terahertz electric field which results in a  $dc$  electric current [3]. A selective excitation of  $dc$  current in TI surface states becomes possible due to the specific feature of PGE, whose prerequisite is a lack of inversion center. As  $\text{Bi}_2\text{Te}_3$  or  $\text{Sb}_2\text{Te}_3$  crystals, like most of the 3D TI, are centrosymmetric, this requirement is fulfilled for the surface states only. Because of the “symmetry filtration” • the  $dc$  current is generated by the surface electrons only. The photocurrent, being sensitive to the surface symmetry and scattering details, provides a simple method to determine the orientation of the surface domains, to probe high frequency conductivity in TI, and to study details of electron scattering the surface states even at room temperature. Further interesting access to spin transport in TI provide circular PGE solely driven by the light's helicity and yielding photocurrent whose sign reverses upon switching the radiation handedness from left- to right-handed circularly polarized light [4].

Magneto-photogalvanic, in particular cyclotron resonance induced MPGE [5,6], can also be efficiently generated in the topologically protected surface states. We show that the effect belongs to the class of magnetic quantum ratchet effects. It emerges due to the joint orbital action of the  $ac$  electric and static magnetic fields on the 2D Dirac fermions in the system with structure inversion asymmetry. The latter leads to an asymmetric scattering of carriers in the momentum space resulting in a fully spin polarized  $dc$  electric current. Studying CR induced photocurrent in the gated samples enables us to probe the effective masses and the momentum relaxation times of 2D Dirac surface states, when the Fermi energy lies in the bulk energy gap or even in the conduction band [6].

- [1] M.M. Glazov, and S.D. Ganichev, *Physic Reports*, **535**, 101, (2013).
- [2] S. D. Ganichev and W. Prettl, *Intense Terahertz Excitation of Semiconductors* (Oxford University Press, Oxford, UK, 2006).
- [3] P. Olbrich, L.E. Golub, T. Herrmann, S.N. Danilov, H. Plank, V.V. Bel'kov, G. Mussler, Ch. Weyrich, C.M. Schneider, J. Kampmeier, D. Grützmacher, L. Plucinski, M. Eschbach, and S.D. Ganichev, *Phys. Rev. Lett.*, **113**, 096601, (2014).
- [4] J. W. McIver, D. Hsieh, H. Steinberg, P. Jarillo-Herrero, and N. Gedik, *Nature Nanotech.*, **7**, 96, (2012).
- [5] C. Zoth, P. Olbrich, P. Vierling, K.M. Dantscher, V.V. Bel'kov, M.A. Semina, M.M. Glazov, L.E. Golub, D.A. Kozlov, Z.D. Kvon, N. Mikhailov, S.A. Dvoretzky, S.D. Ganichev, *Phys. Rev. B* **90**, 205415, (2014).
- [6] K.-M. Dantscher, D.A. Kozlov, P. Olbrich, C. Zoth, P. Faltermeier, M. Lindner, G.V. Budkin, S.A. Tarasenko, V.V. Belkov, Z.D. Kvon, N.N. Mikhailov, S.A. Dvoretzky, D. Weiss, B. Jenichen, and S.D. Ganichev, arXiv cond-mat 1503.06951 (2015).

## Electrical detection of spin polarization in the surface Dirac states of a 3D topological insulator, BiSeTeSe

Masashi Shiraishi<sup>1</sup>, Yuichiro Ando<sup>1</sup>, Takahiro Hamasaki<sup>1</sup>, Gaku Eguchi<sup>1</sup>,  
Fang Yang<sup>2</sup>, Kouji Segawa<sup>2</sup>, Satoshi Sasaki<sup>2</sup>, Yoichi Ando<sup>2</sup>

1. Department of Electronic Science and Engineering, Kyoto Univ., Kyoto, Japan.

2. Institute of Scientific and Industrial Research, Osaka Univ., Ibaraki, Japan

Topological insulators (TIs) are a new class of solids, where a band gap is formed for a bulk state and a linear Dirac-type band is formed for a surface (or edge) state. More interestingly, the linear band is not spin-degenerated, i.e., 100% spin polarized, which means spin and momentum directions are locked (spin-momentum-locking). Thus, TIs attracts tremendous attention in solid-state physics, especially in spintronics. The first experimental demonstration of detecting the surface spin-polarized state was implemented in a 2-dimensional TI, HgTe [1], and the next challenge is to detect the edge current in 3-dimensional (3D) TIs, because a number of spin channel can be dramatically increased in 3D TIs.

Here, we present the successfully electrical detection of the surface spin polarized state in a 3D TI, BiSbTeSe [2]. BiSbTeSe was known as a bulk insulative 3D TI with the largest bulk band gap [3], until TlBiSe was clarified to have the largest bulk band gap [4]. We introduced a standard non-local spin detection technique, which is widely used in spintronics [5]. The spin signal due to the spin accumulation between a ferromagnetic electrode and BiSbTeSe was detected electrically, and the non-local resistance hysteresis due to the detection of the surface spin polarization was successfully reversed, which provide solid evidence of the detection. The signal was observed up to 150 K.

We will introduce more detail of our results in the presentation.

### References:

- [1] M. Koenig et al., Science 318, 766 (2007).
- [2] Yu. Ando, Yo. Ando, M. Shiraishi et al., Nano Lett. 14, 6226 (2014).
- [3] T. Arakane, Yo. Ando et al., Nature Commun. 3, 636 (2011).
- [4] G. Eguchi, M. Shiraishi et al., Phys. Rev. B90, 201307(R) (2014).
- [5] F.J. Jedema et al., Nature 416, 713 (2002).

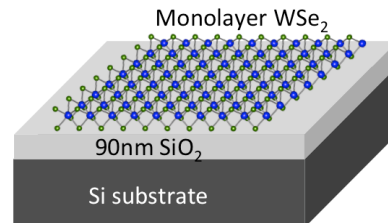
## Valley dynamics probed through exciton emission in monolayer WSe<sub>2</sub>, MoSe<sub>2</sub> and MoS<sub>2</sub>

Gang Wang\*, Louis Bouet, Delphine Lagarde, Andrea Balocchi, Thierry Amand, Xavier Marie and Bernhard Urbaszek

Université de Toulouse, INSA-CNRS-UPS, LPCNO, 135 Avenue de Rangueil, Toulouse, France

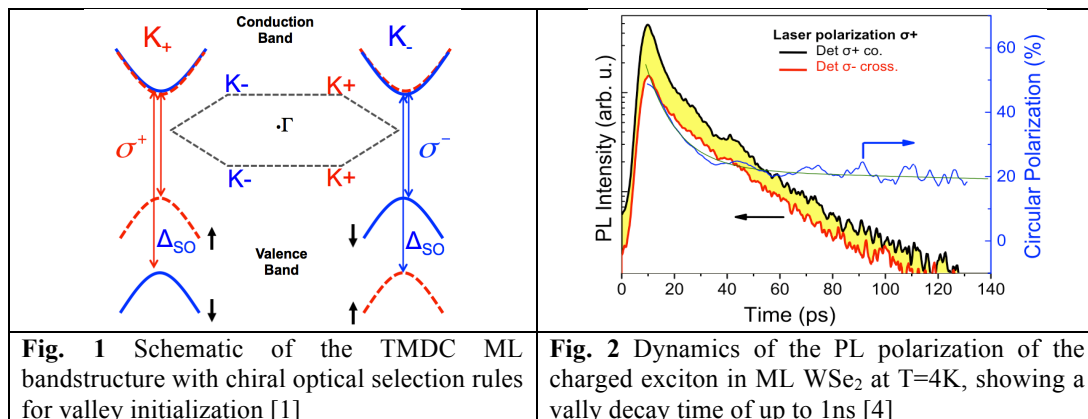
\* g\_wang@insa-toulouse.fr

The physical properties of transition-metal dichalcogenides (TMDCs) MoS<sub>2</sub>, MoSe<sub>2</sub>, WS<sub>2</sub> and WSe<sub>2</sub> change drastically when thinning the bulk material down to one atomic monolayer (ML). TMDCs MLs have a direct optical bandgap in the visible range at the K-point of the Brillouin zone, allowing developing applications such as transistors and LEDs. The absence of an inversion center in the crystal combined with a large spin-orbit



interaction leads to a coupling of carrier spin and k-space valley physics, i.e., the circular polarization ( $\sigma^+$  or  $\sigma^-$ ) of the absorbed or emitted photon can be directly associated with selective carrier excitation in one of the two nonequivalent K valleys (K<sup>+</sup> or K<sup>-</sup>, respectively), see Fig. 1 [1,2]. This provides convenient access to controlling the carrier valley degree of freedom, and makes MLs TMDCs a promising platform for the emerging field of 'Valleytronics'.

Here we probe the valley dynamics in monolayer WSe<sub>2</sub> by monitoring the emission and polarization dynamics of the well-separated neutral excitons (bound electron-hole pairs) and charged excitons (trions) in photoluminescence. The neutral exciton photoluminescence intensity decay time is about 4 ps, whereas the trion emission occurs over several tens of ps, as in the case of ML MoSe<sub>2</sub> [3]. The trion polarization dynamics in ML WSe<sub>2</sub> shows a partial, fast initial decay within tens of ps before reaching a stable polarization of  $\approx 20\%$ , for which a typical valley polarization decay time of the order of 1 ns can be inferred [4]. The limitations of valley index stability of neutral excitons in the presence of strong Coulomb exchange effects are discussed [5].



- [1] D. Xiao et al, Phys. Rev. Lett. **108**, 196802 (2012).
- [2] D. Lagarde et al, Phys. Rev. Lett. **108**, 196802 (2012).
- [3] G. Wang et al, Appl. Phys. Lett. **106**, 112101 (2015)
- [4] G. Wang et al, Phys. Rev. B **90**, 075413 (2014)
- [5] M. Glazov et al, Phys. Rev. B **89**, 201302 (R) (2014)

## Quantum transport in HgTe/CdTe Topological Insulator structures.

C. Thomas<sup>1,\*</sup>, O. Crauste<sup>2</sup>, P. Ballet<sup>1</sup>, T. Meunier<sup>2</sup> and L.P. Lévy<sup>2</sup>

<sup>1</sup>CEA-LETI, MINATEC Campus, 17 rue des Martyrs, F-38054 Grenoble cedex 9, France

<sup>2</sup> Institut Néel, C.N.R.S.- Université Joseph Fourier, BP 166, 38042 Grenoble Cedex 9, France

\*candice.thomas@cea.fr

First predicted in 2005 by Kane and Mele [1] as a new class of matter, topological insulators (TIs) are of main interest in condensed matter physics thanks to their unique electronic and spin properties that arise on their interfaces. TIs gather the graphene-like transport properties with massless Dirac fermions together with the topological protection that prevents backscattering phenomena. These interfaces exhibit spin-momentum locking which polarizes the spin perpendicular to the momentum. Control of the spin and coherent spin transport are then easily achievable in TIs making them very attractive for spintronic applications [2].

Due to its strong spin-orbit interaction, HgTe is a semi-metal with a band inversion around the  $\Gamma$  point and has been identified as a strong TI assuming the opening of a bandgap. Quantum confinement for 2D structures [3] or application of a tensile strain for 3D bulk ones [4] allow to generate this bandgap.

With constant improvement of the growth process by molecular beam epitaxy, HgTe/CdTe structures are now characterized with sharp interfaces having interdiffusion limited to the nanometer scale range [5]. The influence of surface roughness and interface sharpness is clearly seen through low temperature quantum Hall effect measurements. Carrier mobility up to  $440.000 \text{ cm}^2 \cdot \text{V}^{-1} \cdot \text{s}^{-1}$  and density in the range of  $10^{11} \text{ cm}^{-2}$  are measured. Moreover, the topological insulator nature is evidenced as well as quantized conductance in both 2D and 3D structures.

Based on these results, we realized HgTe topological insulator nanostructures. By reducing the dimensions toward 1D and coupling them to superconducting contacts, we aim at studying some of the peculiar spin properties of the TIs. We will present the quantum transport behavior of such nanostructures.

[1] C.L. Kane and E.J. Mele, *Phys. Rev. Lett.* 95, 146802 (2005)

[2] V. Krueckl and K. Richter, *Phys. Rev. Lett.* 107, 086803, (2011)

[3] M. König, S. Wiedmann, C. Brune, A. Roth, H. Buhmann, L.W. Molenkamp, X.L. Qi, and S.C. Zhang, *Science* 318, 766 (2007)

[4] P.Ballet, C.Thomas, X.Baudry, C.Bouvier, O.Crauste, T.Meunier, G.Badano, M.Veillerot, J.P.Barnes, P.H.Jouneau and L.P.Lévy, *Journ.of Elec. Mat.*, 43, 2955-2962, (2014)

[5] C.Thomas, X.Baudry, J.P.Barnes, M.Veillerot, P.H.Jouneau, S.Pouget, O.Crauste, T.Meunier, L.P. Lévy, P.Ballet, *to be published in Journ. Of Crystal Growth*, (2015)

## Advances and Perspectives in II-VI Telluride Heterostructures

T. Wojtowicz<sup>1\*</sup>

<sup>1</sup>Institute of Physics, Polish Academy of Science, Warsaw, Poland

\*wojto@ifpan.edu.pl

The role played by II-VI tellurides in both basic and applied science would be greatly increased if only heterostructures of sufficient quality become available, especially those containing low dimensional electron gas. The great advantage of II-VI telluride nanostructure is that they do not lose their high quality when doped with Mn, which acts as isoelectric impurity carrying localized spin 5/2, as opposite to the case of III-Vs where Mn acts as an acceptor. This is important because incorporation of Mn into II-Te-based heterostructures allows for an effective spin engineering, which provides unique possibilities in the area of spin-based physics and spintronic. Firstly, such nanostructures are characterized by exceedingly high values of the effective Lande g-factor of low-dimensional electrons (reaching +500) which can be manipulated over a wide range (including a change of sign) by choosing appropriate parameters during the growth. Secondly, and even more importantly, the g-factor of electrons in a given structure can be widely tuned by temperature, external magnetic field and voltage applied to electrical gate.

In my talk I will review recent progress in the MBE technology of II-Mn-Te nanostructures containing two dimensional electron gas (2DEG) that led to the first time ever observation of fractional quantum Hall effect in magnetic system (based on CdMnTe) [1]. This, interesting by itself, opens new perspective in the field of spintronics. I will first discuss already demonstrated applications of such high mobility magnetic-2DEG system for: a) THz and microwave radiation induced zero-bias generation of pure spin currents and very efficient magnetic field induced conversion of them into spin polarized electric current [2]; b) clear demonstration of THz radiation from spin-waves excited via efficient Raman generation process [3]; c) experimental demonstration of working principles of a new type of spin transistor based on controlling the spin transmission via tunable Landau-Zener transitions in spatially modulated spin-split bands [4].

I will further discuss the perspective of using magnetic-2DEG for developing of a new system where non-Abelian excitations can not only be created but also manipulated in a two-dimensional plane. The system is based on high mobility CdTe quantum wells with engineered placement of Mn atoms, where sign of the Lande g-factor can be locally controlled by electrostatic gates at high magnetic fields. In a further perspective such a system may allow for building a new platform for topologically protected quantum information processing. I will also discuss our first results where electrostatic control of 2D gas polarization in a quantum Hall regime is demonstrated.

The research was partially supported by National Science Centre (Poland) grant DEC-2012/06/A/ST3/00247, by ONR grant N000141410339, and by the Foundation for Polish Science through International Outgoing Scholarship 2014.

- [1] C. Betthausen *et al.*, Phys. Rev. B **86**, 085310 (2014).
- [2] S. D. Ganichev *et al.*, Phys. Rev. Lett. **102**, 156602 (2009); P. Olbrich *et al.*, Phys. Rev. B **86**, 085310 (2012).
- [3] R. Rungsawang *et al.*, Phys. Rev. Lett. **110**, 177203 (2013).
- [4] C. Betthausen *et al.*, Science **337**, 324 (2012).
- [5] A. Kazakov *et al.*, APS March Meeting 2015, March 2-6, 2015, San Antonio, TX, USA, <http://meetings.aps.org/link/BAPS.2015.MAR.A7.13>

**Tuesday September, 15 - Oral Session - TuC**

**13:45-15:15**

**Photovoltaic 1**

Chair: Alexey Toropov, *Ioffe Institute (Russia)*

## Semiconductor Quantum Dots and Solar Energy Conversion

Victor I. Klimov

Chemistry Division, Los Alamos National Laboratory, Los Alamos, NM 87545, USA  
klimov@lanl.gov

Quantum-confined semiconductor nanocrystals, or “quantum dots,” are promising materials for applications in low-cost solar cells fabricated using solution-based methods. In addition to solution processability, they feature size/shape-tunable optical spectra, as well as a variety of novel physical properties that can enable fundamentally new schemes of solar energy conversion. Specifically, several recent reports have demonstrated the great potential of colloidal nanocrystals for the realization of generation-III photovoltaics by employing concepts such as hot-electron extraction and carrier multiplication, that is, generation of multiple electron-hole pairs by single photons.

This presentation provides an overview of fundamental and applied studies of quantum dots conducted in the context of solar energy conversion. The specific topics will include applications of “Stokes-shift-engineered” quantum dots in luminescent solar concentrators [1], charge transport properties of quantum dot assemblies evaluated via a novel technique of ultrafast photoconductivity, charge transfer at quantum-dot-metal-oxide interfaces [2], and the recent progress in understanding of carrier multiplication in quantum confined materials [3, 4]. The discussion of carrier multiplication will focus on spectroscopic versus photoconductive signatures of photogenerated multiexcitons, the effect of structural parameters such as particle size, shape, and composition on carrier multiplication yields, and recent efforts on increasing multiexciton production by controlling a competing process of intraband cooling.

[1] F. Meinardi, A. Colombo, K.A. Velizhanin, R. Simonutti, M. Lorenzon, L. Beverina, R. Viswanatha, V.I. Klimov, S. Brovelli, *Nature Phot.* **8**, 392 (2014).

[2] H. McDaniel, N. Fuke, N.S. Makarov, J.M. Pietryga, V.I. Klimov, An integrated approach to realizing high-performance liquid-junction quantum dot sensitized solar cells, *Nature Comm.* **4** 2887 (2013).

[3] L.A. Padilha, J.T. Stewart, R.L. Sandberg, W.K. Bae, W.-K. Koh, J.M. Pietryga, V.I. Klimov, *Acc. Chem. Res.* **46** 1261 (2013).

[4] C.M. Cirloganu, L.A. Padilha, Q. Lin, N.S. Makarov, K.A. Velizhanin, H. Luo, I. Robel, J.M. Pietryga, V.I. Klimov, Enhanced carrier multiplication in engineered quasi-type-II quantum dots, *Nature Comm.* **5**, 4148 (2014).

## Dielectric Confinement in Layered II-VI Semiconductor Colloidal Nanoplatelets and Hybrid Perovskites

J. Even<sup>1\*</sup>, L. Pedesseau<sup>1</sup>, M. Kepenekian<sup>2</sup>, D. Saponi<sup>1</sup>, J.-M. Jancu<sup>1</sup>, R. Benchamekh<sup>3</sup>, M. Nestoklon<sup>3,4</sup>, B. Dubertret<sup>5</sup>, P. Voisin<sup>3</sup> and C. Katan<sup>2</sup>

<sup>1</sup>FOTON, Université de Bretagne and CNRS, Rennes, France

<sup>2</sup>ISCR, Université de Rennes 1, Rennes, France.

<sup>3</sup>LPN-CNRS, Marcoussis, France

<sup>4</sup>Ioffe Institute RAS, St Petersburg, Russia

<sup>5</sup>LPEM, ESPCI and CNRS, Paris, France

5

\*jacky.even@insa-rennes.fr

Due to their atomic flatness and strictly quantized thickness distribution, colloidal nanoplatelets (CNP) [1] are ideal objects to test electronic structure theories in a regime of extreme, yet perfectly defined quantum confinement. A first issue is to start with accurate bare single particle states, taking into account native stoichiometry defect (a n-monolayer CdSe CNP consists of n planes of Se and n+1 planes of Cd, with dangling bonds on (001) surfaces saturated with carboxylic ligands). Extended basis spds\* tight-binding model, in connexion with first-principle calculations, is well suited for this purpose, thanks to full-band capability and good transferability of parameters from bulk to nanostructures [2]. However, one must also consider a strong renormalization of bare electron and hole states due to the “dielectric confinement” effect: due to large dielectric constant contrast between CNP and their ligand environment, carriers generate and self-interact with a surface polarization. The same effect substantially increases the exciton binding energy. Band gap renormalization and exciton binding energies become very large (hundred meVs) when thickness reaches the nm scale, but at the same time accurate calculation becomes difficult due to the “atomistic” nature of local charge density and non-abrupt dielectric constant profile. Previous calculations in k.p [3] and TB [2] schemes have provided orders of magnitude, but did not face these difficulties. A method based on first-principle calculations is proposed to compute dielectric constant and self-energy potential profiles in these nanoscale objects, beyond the abrupt dielectric interface model [4]. Understanding of dielectric confinement has also to be gained for 2D layered Hybrid Organic Perovskites (HOP) [5]. The method reveals the real influence of inorganic as well as organic layers, beyond the standard approximation for dielectric constant profiles with abrupt interfaces.

- [1] S. Ithurria, M. D. Tessier, R. P. S. M. Lobo, B. Dubertret and A. L. Efros, *Nat. Mater.*, **10**, 936 (2011).
- [2] R. Benchamekh, N. A. Gippius, J. Even, M. O. Nestoklon, J.-M. Jancu, S. Ithurria, B. Dubertret, A. L. Efros and P. Voisin, *Phys. Rev. B*, **89**, 035307 (2014)
- [3] A. W. Achtstein, A. Schliwa, A. Prudnikau, M. Hardzei, M. V. Artemyev, C. Thomsen and U. Woggon, *Nano Lett.*, **12**, 3151 (2012).
- [4] J. Even, L. Pedesseau, and M. Kepenekian, *Phys. Chem. Chem. Phys.*, **16**, 25182 (2014).
- [5] J. Even, L. Pedesseau, M.-A. Dupertuis, J.-M. Jancu and C. Katan, *Phys. Rev. B*, **86**, 205301 (2012)

## Crystallographic and Optical Characterizations of Ag(Ga,Al)Te<sub>2</sub> Layers Grown on *c*-plane Sapphire Substrates by Closed Space Sublimation

Aya Uruno<sup>1\*</sup>, Yuji Takeda<sup>1</sup>, Tomohiro Inoue<sup>1</sup>, and Masakazu Kobayashi<sup>1,2</sup>

<sup>1</sup>Dept. of Elec. Eng. & Biosci., Waseda Univ., Tokyo, Japan

<sup>2</sup>Kagami Mem. Res. Inst. for Mat. Sci. & Technol., Waseda Univ., Tokyo, Japan

\*a.uruno@fuji.waseda.jp

CdTe is one of the most promising photovoltaic materials available for use in low-cost and high-efficiency solar cells. Ternary I-III-VI<sub>2</sub> group compounds with chalcopyrite structure are also widely used for solar cells. I-III-Te<sub>2</sub> compounds replace Cd in CdTe with group I and III elements, and are hence expected to be another attractive candidate for novel solar cell materials. The bandgap of AgGaTe<sub>2</sub> at room temperature is around 1.3 eV. This value is slightly lower than the optimum value for fabricating solar cells. Formation of solid solutions of AgAlTe<sub>2</sub> (E<sub>g</sub> = 2.2 eV) and AgGaTe<sub>2</sub> is an approach to optimize the bandgap energy. AgGaTe<sub>2</sub> and AgAlTe<sub>2</sub> have been successfully grown on *c*-plane sapphire substrates by the closed space sublimation (CSS) method [1]. The CSS method is widely used in fabrication of CdTe thin film solar cells since it has many advantages for the fabrication of low cost solar cells. In this study, layers of solid solutions were grown on *c*-plane sapphire substrates by the CSS method, and the optical property was studied. The crystallinity and the stoichiometry of grown layers were also studied.

Sources used were powdered AgGaTe<sub>2</sub> and AgAlTe<sub>2</sub> with various mixing ratios. The source temperature and the substrate temperature were 775 °C and 730 °C, respectively. Its crystallographic properties were evaluated by X-ray diffraction (XRD). The transmittance in visible range was measured by an ultraviolet visible spectrophotometry (UV-VIS) and the bandgap of grown layers was evaluated by use of Tauc-plot-type analysis.

Figure 1 shows a transmittance spectrum of a Ag(Ga,Al)Te<sub>2</sub> layer. The source weight ratio of AgGaTe<sub>2</sub>:AgAlTe<sub>2</sub> was 1:5. As shown in Fig. 1, there was a rapid decrease in the transmittance value near absorption edge. Absorption edge of the Ag(Ga,Al)Te<sub>2</sub> layer was appeared about 590 nm. The value of optical bandgap at the room temperature was about 2.1 eV. From this, the growth of the solid solution of AgGaTe<sub>2</sub> and AgAlTe<sub>2</sub> was successfully achieved. Based on the transmittance spectrum, the Ga mole fraction was evaluated, and it was about 18%. The Ga mole fraction was increased when the source weight ratio of Ga to Al was increased. The XRD spectrum of grown layer contained peaks originating from Ag(Ga,Al)Te<sub>2</sub>, and the 112 peak was the dominant peak. From this, the Ag(Ga,Al)Te<sub>2</sub> layer exhibited the strong preference for the (112) orientation. The tuning and lowering of the optical bandgap energy toward the solar cell application is currently ongoing.

This work was supported in part by Waseda Univ. Research Initiatives, Waseda Univ. Grant for Special Research Project, "Early Bird" grant for young researcher at Waseda Research Institute for Science and Engineering and JSPS Research Fellowships for Young Scientists.

[1] A. Uruno, A. Usui, T. Inoue, Y. Takeda, and M. Kobayashi: to be published in J. Electron. Mater.

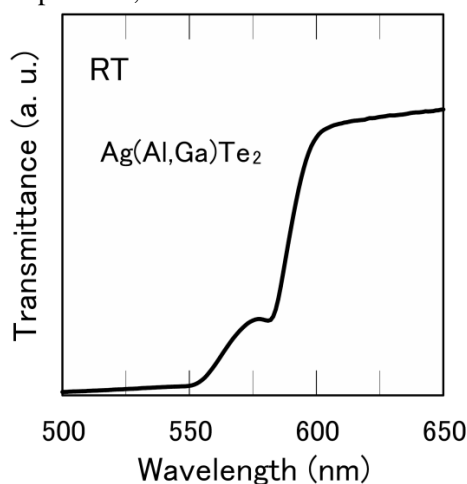


Fig. 1 Transmittance spectrum of Ag(Al,Ga)Te<sub>2</sub>

## Novel Ternary Wurtzite Semiconductor; $\beta$ -CuGaO<sub>2</sub>

I. Suzuki<sup>1</sup>, H. Nagatani<sup>1</sup>, M. Kita<sup>2</sup>, H. Yanagi<sup>3</sup>, N. Ohashi<sup>4</sup>, T. Omata<sup>1,\*</sup>

<sup>1</sup>Graduate School of Engineering, Osaka University, Suita, Japan

<sup>2</sup>Toyama National College of Technology, Toyama, Japan

<sup>3</sup>University of Yamanashi, Kofu, Japan

<sup>4</sup>National Institute for Materials Science (NIMS), Tsukuba, Japan

\* omata@mat.eng.osaka-u.ac.jp

$\beta$ -NaFeO<sub>2</sub> structure is an orthorhombic wurtzite-derived structure, in which divalent zinc ions in wurtzite ZnO are regularly replaced by monovalent sodium and trivalent iron ions similar to the structural relationship between the zincblende and chalcopyrite structures. The oxides with this structure are very attractive materials because of their wide variety of energy band gap, such as  $\beta$ -LiGaO<sub>2</sub> ( $E_g=5.6$  eV),  $\beta$ -AgAlO<sub>2</sub> ( $E_g=2.8$  eV) and  $\beta$ -AgGaO<sub>2</sub> ( $E_g=2.2$ eV). The compounds containing monovalent copper usually shows isostructure with the compounds containing monovalent silver, such as delafossite  $\alpha$ -AgInO<sub>2</sub> and  $\alpha$ -CuInO<sub>2</sub>. However the  $\beta$ -NaFeO<sub>2</sub> type copper oxides had not been reported. Recently, we successfully synthesized the  $\beta$ -NaFeO<sub>2</sub> type  $\beta$ -CuGaO<sub>2</sub> [1]. In the present paper, we report its structural, optical and electrical properties.

$\beta$ -CuGaO<sub>2</sub> was synthesized by the ion-exchange from Na<sup>+</sup> to Cu<sup>+</sup> in the  $\beta$ -NaGaO<sub>2</sub> precursor that possesses  $\beta$ -NaFeO<sub>2</sub> type structure. Rietveld analysis of the obtained powder after the ion-exchange indicated that  $\beta$ -CuGaO<sub>2</sub> with the  $\beta$ -NaFeO<sub>2</sub> structure was successfully obtained. The pseudo-hexagonal wurtzite lattice parameters of  $\beta$ -CuGaO<sub>2</sub>,  $a=3.231$  Å and  $c=5.278$  Å, are very close to those of ZnO,  $a=3.250$  Å and  $c=5.207$  Å; that is, the lattice mismatch between  $\beta$ -CuGaO<sub>2</sub> and ZnO is only 0.6% in the ab-plane and 1.4% along the c-axis. This is an advantage of the  $\beta$ -CuGaO<sub>2</sub> in order to fabricate multilayered thin films with ZnO.

Optical absorption spectrum of  $\beta$ -CuGaO<sub>2</sub> indicated that its energy band gap was 1.47 eV as shown in Fig.1; this is the energy band gap realizable maximum conversion efficiency of the single-junction solar cell. The electrical conductivity at room temperature of the  $\beta$ -CuGaO<sub>2</sub> sinter without intentional doping was very small,  $1 \times 10^{-6}$  Scm<sup>-1</sup>, but the thermoelectromotive force was +400  $\mu$ VK<sup>-1</sup>. This indicates that  $\beta$ -CuGaO<sub>2</sub> exhibits a p-type semiconductor.

The calculated electronic band structure indicated that  $\beta$ -CuGaO<sub>2</sub> is a direct semiconductor and shows intense absorption of light near the band edge. These properties render this new material promising as a solar cell absorber.

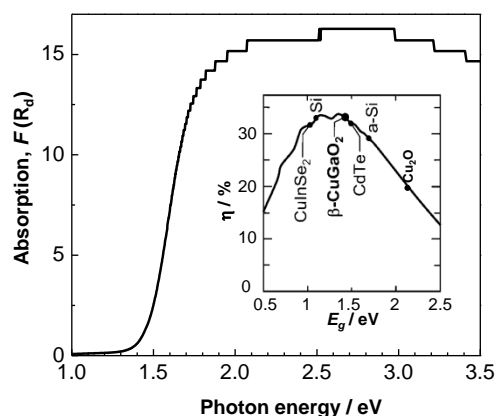


Fig.1 Optical absorption spectrum of powdered  $\beta$ -CuGaO<sub>2</sub>. The inset is conversion efficiency of a single-junction solar cell as a function of the energy band gap based on the Shockley-Queisser theory.

[1] T. Omata, H. Nagatani, I. Suzuki, M. Kita, H. Yanagi, N. Ohashi, J. Am. Chem. Soc. **136**, 3378, (2014)

## Electronic Structure and Relative Stability of Binary (Ga/In)Se and Pseudoternary Cu(In,Ga)Se<sub>2</sub> Semiconductors

Srcour J<sup>1,2</sup>, Postnikov A V<sup>1\*</sup>, and El Haj Hassan F<sup>2</sup>

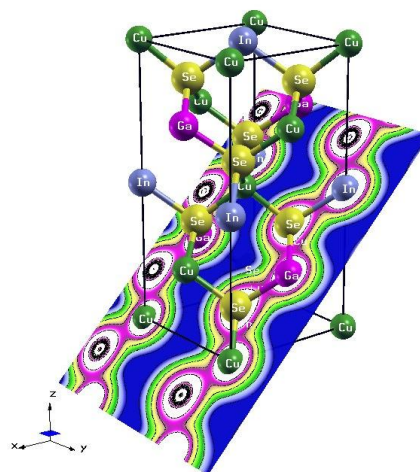
<sup>1</sup>LCP-A2MC, Institut Jean Barriol, Université de Lorraine, Metz, France

<sup>2</sup>Laboratoire de Physique et d'Electronique, Université Libanaise, Beirut, Lebanon

\*andrei.postnikov@univ-lorraine.fr

The GaSe and InSe semiconductors possess cations from column III, that brings about modifications in the crystal structure compared to conventional II-VI compounds: direct cation-cation bondings and weak Se-Se interactions across the van der Waals gap. Still, the bond angles support largely tetrahedral environment, and the optical gap is appreciable. Different stacking of Se-cation-cation-Se layers gives rise to a number of polytypes, whose relative stability seems to differ for GaSe and InSe. An insertion of an anion layer breaking the cation-cation bonds leads to (Ga/In)<sub>2</sub>Se<sub>3</sub> compounds whose structure resembles defected wurtzite. Finally, an addition of copper, a column-I cation, leads to a family of ternary (or pseudoternary, in view of easy Ga-In substitution) semiconductors of mostly chalcopyrite structure, whereby, on the average, the octet rule is maintained as in II-VI systems. These latter pseudoternary alloys are well known in photovoltaic studies, because of high efficiency and stability of properties in this sense [1]. Polycrystalline CuGa<sub>x</sub>In<sub>1-x</sub>Se<sub>2</sub> is since long counted between the best thin-film materials for photovoltaic applications, yielding solar energy conversion efficiencies of up to 18.8% [2]. Note that deviations from nominal chalcopyrite structure are quite common, especially (or, at least) in the surface regions [3].

Interested in the evolution of properties from pure binary to defected binary to ternary etc. structures within the family in question, we offer a thorough analysis of electronic structure and equilibrium crystallographic parameters throughout different phases (of binary systems) and compositions (in the chalcopyrite-structure CuIn<sub>x</sub>Ga<sub>1-x</sub>Se<sub>2</sub>), on the basis of first-principles (density-functional) calculations done with the WIEN2k code [4]. Total energy relations are extracted based on generalised gradient approximation, whereby the band structures and optical properties are moreover systematically analysed with the use of modified Becke-Johnson exchange-correlation potential [5], known for offering a practical way to correct the estimates of the optical gap. Our results systematize, and largely go beyond, a big number of previous studies, done on different systems using methods of variable accuracy.



Calculated charge density in the (102) plane of (ordered) CuIn<sub>0.5</sub>Ga<sub>0.5</sub>Se<sub>2</sub>.

1. Rockett A and Birkmire RW, J.Appl.Phys. 70, R81 (1991).
2. Contreras MA, Egaas B, Ramanathan K, and Hiltner J, Photovolt. Res. Applic. 7, 311 (1999).
3. Kuznetsov MV, Shalaeva EV, Yakushev MV, and Tomlison RD, Surf.Sci.Lett. 50, L297 (2003).
4. <http://www.wien2k.at>
5. Tran F and Blaha P, Phys.Rev.Lett. 102, 226401 (2009).

**Tuesday September, 15 - Oral Session - TuD**

**15:45-17:15**

**Dots and Nanowires 1**

Chair: Piotr Kossacki, *Warsaw University (Poland)*

## **Laser Cooling of CdS II-VI Semiconductor Nanoribbons: Towards All Solid State Semiconductor Optical Cooler**

*Qihua Xiong*

Nanyang Associate Professor and Fellow of Singapore National Research Foundation  
School of Physical and Mathematical Sciences,

Nanyang Technological University

Email Address: [Qihua@ntu.edu.sg](mailto:Qihua@ntu.edu.sg).

Optical irradiation accompanied by spontaneous anti-Stokes emission can lead to cooling of matter, a phenomenon known as laser cooling or optical refrigeration proposed in 1929 by Peter Pringsheim. In solid state materials, the cooling is achieved by annihilation of lattice vibrations (*i.e.*, phonons). Since the first experimental demonstration in rare-earth doped glasses, considerable progress has been made particularly in ytterbium-doped glasses or crystals with a recent record of  $\sim 110$  K cooling from ambient. This has surpassed the thermoelectric Peltier cooler and the cryogenic temperature defined by NIST, reaching the limit imposed by Boltzmann distributions of rare-earth systems. On the other hand, semiconductors exhibit potentially even higher cooling efficiency and lower cooling temperature down to liquid Helium temperature, nevertheless numerous attempts in laser cooling of III-V quantum wells led to very minimum progress in the past decades. Recently, our NTU group discovered that group II-VI semiconductors, such as CdS in nanoribbon morphology, exhibit an exceptionally strong exciton-longitudinal optical phonon coupling, which enables the resonant annihilation of multiple LO phonons during the luminescence upconversion process. We demonstrate a 40 K cooling from room temperature with a cooling efficiency of  $\sim 5.0\%$ , and 15 K cooling from 100 K. Our data also suggest that group II-VI materials exhibit great promise for optical refrigeration, however the challenge is whether we can scale up to achieve laser cooling in bulk crystal or thin film. So in the end of this talk we will discuss our progress in scale up materials for practical applications and all solid state semiconductor cryocoolers.

## Measurement by Photon-Correlation Fourier Spectroscopy of the spectral diffusion and time-coherence of the trion fluorescence in thick-shell CdSe/CdS nanocrystals

L. Biadala<sup>1</sup>, H. Frederich<sup>1</sup>, L. Coolen<sup>2,3</sup>, S. Buil<sup>1</sup>, X. Quélin<sup>1</sup>, C. Javaux<sup>4</sup>, M. Nasilowski<sup>4</sup>, B. Dubertret<sup>4</sup>, and J.-P. Hermier<sup>1,5,\*</sup>

<sup>1</sup>Groupe d'Etude de la Matière Condensée, Université de Versailles Saint-Quentin-en-Yvelines, CNRS UMR8635, 45, avenue des Etats-Unis, F-78035 Versailles, France

<sup>2</sup>Sorbonne Universités, UPMC Univ Paris 06, UMR 7588, Institut de NanoSciences de Paris (INSP), F-75005, Paris, France

<sup>3</sup>CNRS, UMR 7588, Institut de NanoSciences de Paris (INSP), F-75005, Paris, France

<sup>4</sup>Laboratoire de Physique et d'Etude des Matériaux, CNRS UMR8213, ESPCI, 10, rue Vauquelin, F-75231 Paris, France

<sup>5</sup>Institut Universitaire de France, 103, bd Saint-Michel, 75005 Paris, France  
\*jean-pierre.hermier@uvsq.fr

When compared to standard CdSe/ZnS colloidal nanocrystals (NCs), the fluorescence of thick-shell CdSe/CdS NCs exhibit very low blinking at room temperature. At 4K, these emitters are always ionized and Auger recombinations as well as blinking are completely suppressed. The quantum efficiency is perfectly stable and very close to 1. The carriers are also confined in the core of the NC.

Several studies reported that the single CdSe NC emission is characterized by spectral diffusion, i.e the emission wavelength is not constant. It was early shown that the SD dynamic is closely related to the movements of the charges at the surface of the NC. As blinking, SD is due to the interaction between the NC and its very close environment.

The fast dynamics of the SD can be investigated by an original method we developed and that is called photon correlation Fourier spectroscopy (PCFS). Enabling to achieve simultaneously a high resolution in both the temporal and spectral domain [1], it is based on the measurement of the time correlations between the photons collected at the two outputs of a Michelson interferometer.

In this presentation, the SD and time coherence properties of the fluorescence of CdSe/CdS NCs with a very thick shell (greater than 10 nm) are characterized by PCFS. First results are obtained with a standard spectrometer. Several lines (zero phonon line (ZPL), acoustic and longitudinal-optical phonon replicas) are identified. Their linewidth are then measured by PCFS. For the ZPL, the linewidth is equal to 50  $\mu\text{eV}$ . This value is significantly greater than the exciton linewidth observed for standard CdSe/ZnS NCs (6.5  $\mu\text{eV}$ ) [2] and for CdSe/CdS NCs with a 5-nm thick shell (15  $\mu\text{eV}$ ) [3].

To better understand the origin of this enlargement, we studied the dynamic of the SD at a fast time scale reaching 250 ns by PCFS. Above this limit, we show that SD is weak and cannot explain the large ZPL linewidth. We attribute it to the ionization of the NC. The presence of a third charge in the trion (when compared to the exciton) increases the polarizability of the emitting state which is efficiently coupled to the very fast movements of the charges located at the surface of the NC [4]. Even if the crystalline shell is very thick and the charges are confined far from the surface, the trion is not isolated from the environment.

[1] X. Brokmann, M. Bawendi, L. Coolen, and J.-P. Hermier, *Opt. Expr.* **14**, 6333 (2006)

[2] L. Coolen, X. Brokmann, P. Spinicelli, and J.-P. Hermier, *Phys. Rev. Lett.* **100**, 027403 (2008)

[3] A. P. Beyler, L. F. Marshall, J. Cui, X. Brokmann, and M. G. Bawendi, *Phys. Rev. Lett.* **111**, 177401 (2013)

[4] L. Biadala, H. Frederich, L. Coolen, S. Buil, X. Quélin, C. Javaux, M. Nasilowski, B. Dubertret, and J.-P. Hermier, *Phys. Rev B* **91**, 085416 (2015)

## Mid-Infrared Detection with Interband and Intraband Colloidal Quantum Dot Transitions

Philippe Guyot-Sionnest

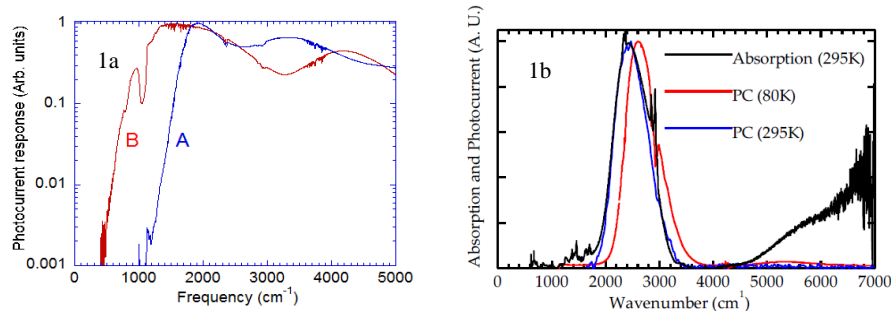
James Franck Institute, The University of Chicago, 929 East 57<sup>th</sup> Street, Chicago, IL 60637, USA

\*pgs@uchicago.edu

HgTe is a II-VI semimetal. Colloidal quantum dots (CQD) of sizes between 10 and 20 nm readily lead to infrared gaps tuning between 3 and 12 microns respectively. Infrared photodetection using dried films of these CQDs has been demonstrated up to 12 microns. Further improvement through device and chemistry will raise the detectivity to the level required to transform thermal infrared detection technology. Figure 1 shows two photocurrent spectra taken with films of HgTe colloidal dots at 80K. The films are drop-cast on a Si/SiO<sub>2</sub> substrate with 50 nm Pd interdigitated electrodes separated by 20 microns. With this low-tech approach and partially absorbing samples (< 10%), the detection is readily obtained with a standard FTIR scanning instrument. The dip at 1100 cm<sup>-1</sup> is due to the absorption of the SiO<sub>2</sub> 1 micron thick layer, and the partial reflection from the Si substrate. The Urbach tail, arising from size distribution and possible gap states, is limited to 10 meV at 80K.<sup>1</sup>

In contrast to HgTe CQDs which tend to be intrinsic, beta-HgS and HgSe CQDs are naturally n-doped, in the first such instance with CQDs. With optimal doping of 2 electrons per CQD, both HgSe and HgS CQDs gave the first CQD photocurrent spectra based on the intraband absorption. This is a breakthrough in the field of colloidal quantum dots where interband transitions had been exclusively used for the past 30 years. Figure 1b shows the photoconductive spectrum with a film of HgSe quantum dots, which differs mostly from HgTe, by the narrower optical response since it is now dominated by the intraband 1Se-1Pe absorption.<sup>2</sup>

Besides optimizing device structures for rapid improvements, two longer term challenges with both interband and intraband infrared CQDs, will be (i) to provide a practical control of the Fermi level and (ii) to reduce the nonradiative recombination, which will improve the detectivity as well as allow to use their infrared luminescence for LEDs and possibly photopumped lasers.



<sup>1</sup> Mercury Telluride Colloidal Quantum Dots: Electronic Structure, Size-Dependent Spectra, and Photocurrent Detection up to 12  $\mu\text{m}$ , SE Keuleyan, P Guyot-Sionnest, C Delerue, G Allan, ACS nano 8 (8), 8676-8682 (2014)

<sup>2</sup> Colloidal Quantum Dots Intraband Photodetectors, Z Deng, KS Jeong, P Guyot-Sionnest, ACS nano 8 (11), 11707-11714 (2014)

## Control of semiconductor quantum dot emission intensity and polarization by metal nanoantennas

V. D. Kulakovskii<sup>1\*</sup>, V. I. Kukushkin<sup>1</sup>, I. M. Mukhametzhano<sup>1</sup>, I. V. Kukushkin<sup>1</sup>,  
I. V. Sedova<sup>2</sup>, S. V. Sorokin<sup>2</sup>, A. A. Toropov<sup>2</sup>, S. V. Ivanov<sup>2</sup>, and A. S. Sobolev<sup>3</sup>

<sup>1</sup>Institute of Solid State Physics, RAS, 142432 Chernogolovka, Moscow district, Russia

<sup>2</sup>Ioffe Physical-Technical Institute, RAS, Polytekhnicheskaya 26, St. Petersburg, Russia

<sup>3</sup>Kotel'nikov Institute of Radio Engineering and Electronics, RAS, 125009, Mokhovaya Street 11/7, Moscow, Russia

\*kulakovs@issp.ac.ru

The emission, detection, and amplification of electromagnetic waves in the radio-frequency range by different antennas have been well studied and detailed in numerous textbooks. However, the emission peculiarities of nano-objects with characteristic sizes close to a nanometer (for instance, emission of a single molecule) and the feasibilities of emission control are still problems of profound importance in modern nano-optics [1,2]. Solutions to these problems would enable us to achieve significant emission amplification coefficients for nano-objects as well as to control their emission directivity. At the low-frequency range metals are nearly perfect mirrors; in contrast, in the visible range they exhibit intensive transmission and absorption of light. Therefore, the ideas on antenna design developed in the radio-frequency range should essentially be revised for application in nano-optics.

We have studied the amplified emission properties of nanoislands with CdSe quantum dots in ZnSe/CdSe/ZnSe heterostructures surrounded

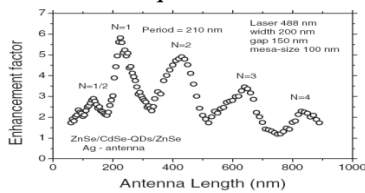


Fig.2 Enhancement factor of the emission of QDs embedded in Ag linear antennas vs its length

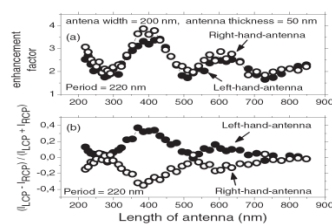


Fig. 3. (a) Enhancement factor and (b) strength of the selective polarization dichroism effect induced by photoexcitation with circular polarization in the emission of QDs embedded in curved antennas as a function of antenna length.

by linear and curved silver nanoantennas as shown in Fig.1.

Variations of the optical antenna length have been found to give rise to periodic amplification of the integral emission intensity (Fig.2) The period of the discovered oscillations is equal to 220 nm, which corresponds to the wavelength  $\lambda_{pp} = \lambda_0 [(\epsilon_1 + \epsilon_D) / \epsilon_1 \epsilon_D]^{1/2} = 207$  nm of the surface plasmon-polariton mode propagating in the metallic antenna. Here  $\lambda_0 = 488$  nm is the light wavelength,  $\epsilon_1 = -9.56$  is the real part of the Ag dielectric constant and  $\epsilon_D = 3.5$  is the effective dielectric constant of the semiconductor structure. The velocity of surface polaritons has been found to depend not only on the parameters of the dielectric constants of the metal and of the semiconductor substrate but also on the width and thickness of the metallic antenna.

The influence of antenna antisymmetry (its helicity) on selective amplification of the degree of circular polarization of photoexcitation is shown in Fig. 3. It shows that plasmon-polaritons induced in curved (S-type, Fig.1) antennas by circularly polarized light, which was used for QD excitation, result in enhanced polarization selectivity of the QD emission. Fig. 3 shows that (i) the sign of polarization is opposite for the left- and right-hand antennas and (ii) the selectivity of the polarization of excitation is a periodic function of its length[3]

[1] Y. W. C. Cao, R. C. Jin, and C. A. Mirkin, *Science* **297**, 1536 (2002).

[2] S. Nie and S. R. Emory, *Science* **275**, 1102 (1997).

[3] V. I. Kukushkin et al, *Phys. Rev. B* **90**, 235313 (2014).

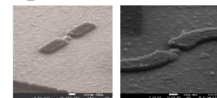


Fig.1 Typical photos

## Vertical CdSe/ZnSe nanowire quantum dot and photonic wire for single-photon emission

**T. Cremel<sup>1,2\*</sup>, E. Bellet-Amalric<sup>1,2</sup>, L. Cagnon<sup>1,3</sup>, N. Gregersen<sup>4</sup>, and K. Kheng<sup>1,2\*</sup>**

<sup>1</sup> Univ. Grenoble Alpes, F-38000 Grenoble, France

<sup>2</sup> CEA, INAC-SP2M, F-38000 Grenoble, France

<sup>3</sup> CNRS, Institut Néel, F-38000 Grenoble, France

<sup>4</sup> Department of Photonics Engineering, DTU Fotonik, Technical University of Denmark, DK-2800 Kongens Lyngby, Denmark

\*[thibault.cremel@cea.fr](mailto:thibault.cremel@cea.fr) and [kkheng@cea.fr](mailto:kkheng@cea.fr)

CdSe/ZnSe nanowire quantum dots (NW-QD) are promising structures for application as single photon sources since they can show single photon emission up to room temperature [1]. By coating such NW-QDs with a shell, it is possible to create photonic wires to extract more efficiently the photons along the photonic wires axis [2]; in this case the control of vertically oriented NWs is compulsory. For this reason, we have first developed the growth of vertically oriented and low density ZnSe NWs by molecular beam epitaxy on a ZnSe(111)B buffer layer, under different II/VI flux ratios. The NWs have a typical diameter of 10 nm and show only weak luminescence. We demonstrate that a ZnMgSe shell passivates the NWs surface and increases the ZnSe near-band-edge luminescence by two orders of magnitude. We also show for the first time luminescence from CdSe insertions in [111] ZnSe NWs covered by a ZnMgSe shell and grown by molecular beam epitaxy. The low NW density we managed to obtain ( $\sim 1$  NW/ $4 \mu\text{m}^2$ ) allows us to study single NWs directly on the as-grown sample. Exciton, biexciton and charged exciton lines are clearly identified.

In a second step, we have created photonic wires by coating the NW-QDs with a thick conformal dielectric coating of  $\text{Al}_2\text{O}_3$  using Atomic Layer Deposition (ALD) [3]. Our calculations show that the emission of the orthogonal dipoles (perpendicular to the NW axis) is strongly inhibited in a 10nm diameter NW, while the dipoles emission can be changed and enhanced with an  $\text{Al}_2\text{O}_3$  coating of 120 nm (NW radius increase). This effect will be presented quantitatively with microphotoluminescence measurements on our CdSe/ZnSe NW-QDs coated with thick  $\text{Al}_2\text{O}_3$  shells.

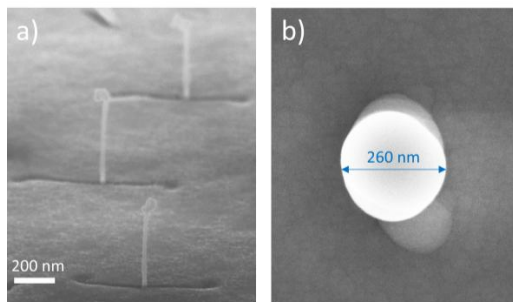


Figure 1. Scanning electron microscope images: a) 65°-tilted image of vertical CdSe/ZnSe NW-QDs with a thin ZnMgSe shell on the as-grown sample b) top view image of a similar NW-QD coated with a 120 nm thick  $\text{Al}_2\text{O}_3$  shell.

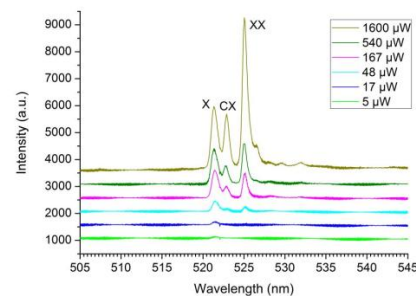


Figure 2. Microphotoluminescence spectrum at 5K of a single CdSe/ZnSe NW-QD (on the as-grown sample) as a function of the 488nm cw laser power.

- [1] S. Bounouar, M. Elouneq-Jamroz, M. den Hertog, C. Marchutt, E. Bellet-Amalric, R. André, C. Bougerol, Y. Genuist, J.-P. Poizat, S. Tatarenko, and K. Kheng, *Nano Lett.* **12**, 2977 (2012).
- [2] J. Claudon, J. Bleuse, N.S. Malik, M. Bazin, P. Jaffrennou, N. Gregersen, C. Sauvan, P. Lalanne, and J.-M. Gérard, *Nat. Photonics* **4**, 174 (2010).
- [3] T. Cremel, M. Elouneq-Jamroz, E. Bellet-Amalric, L. Cagnon, S. Tatarenko, and K. Kheng, *Phys. Status Solidi C* **11**, 1263 (2014).

**Wednesday September, 16 - Oral Session - WeA**

**08:30-10:15**

**Spin and Magnetism**

Chair: Jacek Kossut, *Institute of Physics, Polish Academy of Sciences (Poland)*

## Coherent optical spectroscopy in CdTe quantum well structures: storing light in the electron spin ensemble

Ilya Akimov

Experimentelle Physik 2, Technische Universität Dortmund, D-44221 Dortmund, Germany

\*ilja.akimov@tu-dortmund.de

Coherent optical spectroscopy provides essential information on dynamical properties of charge and spin excitations in semiconductor nanostructures [1]. It delivers rich information on the energy structure and the main mechanisms responsible for the relaxation in the system under study. Here, we present an overview on optical studies in semiconductor (Cd,Mg)Te quantum well structures subject to magnetic field [2,3]. The investigated structures are doped with resident electrons (n-type) which allow optical excitation of both neutral and charge excitons (trions). Use of II-VI structures provides strong oscillator strength of elementary optical excitations and large separation between exciton and trion resonances which is supported by large binding energies. This allows to address solely trion transitions with spectrally broad ultrashort picosecond pulses.

We use spontaneous (two-pulse) and stimulated (three-pulse) photon echoes for studying the coherent evolution of optically excited ensemble of trions which are localized in semiconductor quantum well. Application of transverse magnetic field leads to the Larmor precession of the resident electron spins, which shuffles the coherence between optically accessible and inaccessible states. This results in several spectacular phenomena. First, we demonstrate magnetic field induced oscillations of spontaneous photon echo amplitude [1]. Second, in three-pulse excitation scheme, the extension of photon echo delay time by three orders of magnitude is realized [2]. In this study, short-lived optical excitation, which is created by the first pulse, is coherently transferred into a long-lived electron spin state using the second optical pulse. This coherent spin state of electron ensemble persists much longer ( $\sim 10$  ns) than any optical excitation in the system ( $\sim 100$  ps), preserving phase information on initial optical field, which can be retrieved as a photon echo by means of third optical pulse. Such approach allows to access long-term optical memories in semiconductor nanostructures.

[1] G. Moody et al., *Phys. Rev. Lett.* **112**, 097401 (2014).

[2] L. Langer et al., *Phys. Rev. Lett.* **109**, 157403 (2012).

[3] L. Langer et al., *Nat. Photonics* **8**, 851 (2014).

## Atomic-like Spin Fluctuations of Manganese in CdTe Quantum Wells

S. Cronenberger<sup>1</sup>, D. Scalbert<sup>1\*</sup>, H. Boukari<sup>2</sup>, D. Ferrand<sup>2</sup>, R. André<sup>2</sup> and J. Cibert<sup>2</sup>  
<sup>1</sup>Laboratoire Charles Coulomb, CNRS and Université Montpellier, Montpellier, France  
<sup>2</sup>Institut Néel, CNRS and Université Grenoble-Alpes, Grenoble,  
 \*denis.scalbert@univ-montp2.fr

Spin noise spectroscopy (SNS) is a powerful optical technique, which in atomic vapors revealed detailed information on nuclear magnetism and the hyperfine interaction [1]. In recent years it has been widely used to probe the carrier spin relaxation in various semiconductors and heterostructures [2]. Typically SNS probes spontaneous spin fluctuations by off-resonant Faraday rotation. Spin noise spectra are equivalent to electron spin resonance spectra, by virtue of the fluctuation-dissipation theorem, and are quite interesting for quantum non-demolition measurements of either atomic or electronic spins [3].

We show that atomic-like spin fluctuations of magnetic impurities in semiconductors can also be detected by SNS, with results on bulk and quantum wells of CdTe:Mn. In QWs about  $4 \times 10^6$  Mn spins are detected in the laser spot size of  $\sim 5 \mu\text{m}$ . The spectra exhibit both Zeeman transitions within hyperfine levels with g-factor equal 1, and inter-hyperfine transitions. They also reveal the cubic symmetry of the crystal field and local strain.

To illustrate these findings we show in Figure (1) contour plots of the spin noise spectra for different magnetic field orientations in the (1-10) plane of a bulk  $\text{Cd}_{0.999}\text{Mn}_{0.001}\text{Te}$  sample.  $\theta$  is the angle between the applied field and the [001] crystal axis. The spectra (Fig. 1b) exhibit many of the spectral features predicted by a spin hamiltonian calculation (Fig. 1a). The experimental noise spectra are very well fitted with a single adjustable parameter, the Mn spin coherence time  $T_2=20$  ns. This is close to the expected value for dipolar broadening.

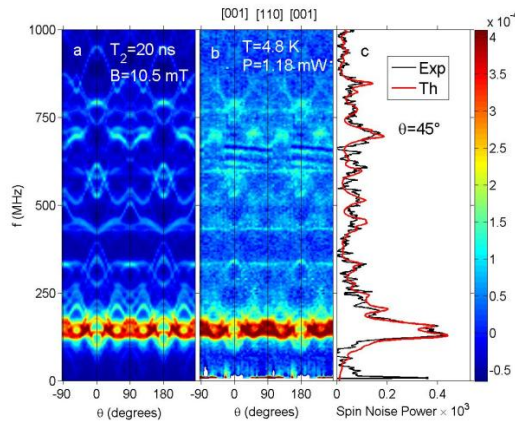


**Figure 1:** Angular resolved Mn spin noise spectra for magnetic field in the (1-10) plane of bulk CdMnTe. **(a)** calculated spectra using spin hamiltonian with cubic crystal field and hyperfine interaction. **(b)** experimental spectra. **(c)** comparison between experimental and theoretical spectra measured at  $\theta=45^\circ$ . The spin noise spectra are normalized to the photon noise.

- [1] S. A. Crooker, D. G. Rickel, A. V. Balatsky, and D. L. Smith, *Nature* **431**, 49 (2004).
- [2] J. Hübner, F. Berski, R. Dahbashi, and M. Oestreich, *Physica Status Solidi (b)*, **251**, 1824 (2014).
- [3] A. Kuzmich, L. Mandel, J. Janis, Y. E. Young, R. Egnisman, N. P. Bigelow, *Phys. Rev. A*, **60**, 2346 (1999).

## Spin-orbit Stiffness of the Spin-polarized Electron Gas

F. Baboux<sup>1#</sup>, F. Perez<sup>1\*</sup>, C. Ullrich<sup>2</sup>, G. Karczewski<sup>3</sup> and T. Wojtowicz<sup>3</sup>

<sup>1</sup>Institut des Nanosciences de Paris, CNRS/Université Paris VI, Paris, France

<sup>2</sup>Department of Physics and Astronomy, University of Missouri, Columbia, Missouri, USA

<sup>3</sup>Institute of Physics, Polish Academy of Sciences, Warsaw, Poland

<sup>#</sup> present : Laboratoire de Photonique et Nanostructures, LPN-CNRS, Marcoussis, France

\*florent.perez@insp.jussieu.fr

In a conducting spin-polarized system, Coulomb interaction couples spin and motion degrees of freedom to build macroscopic oscillation of the spins which propagates as spin-waves. The spin-wave stiffness  $\chi$  quantifies the energy cost to excite a spin-wave with a kinetic disturbance of the electron gas, e.g, in a ferromagnetic metal the spin-wave disperses as  $\hbar\omega_q = \chi\hbar^2q^2 / 2m_b$ , where  $q$  is the transferred momentum and  $m_b$  is the electron band mass. Recently, the spin-orbit (SO) coupling has emerged as an important protagonist for spin-based electronics. It offers new means to manipulate spin-waves with electric fields through the spin-polarization generated by a charge current. Then, an important issue is the cost to excite a spin-wave with a spin-polarization generated by the spin-orbit coupling. We define it as the spin-orbit stiffness. We have investigated the spin-orbit stiffness of a model spin-polarized and conducting electron system. Our model system is a paramagnetic spin-polarized two-dimensional electron gas (SP2DEG) embedded in doped diluted magnetic quantum well of CdMnTe. In past works [1] we investigated the spin-modes of this model SP2DEG and measured the spin-wave dispersion by angle-resolved magneto-Raman scattering. More recently, we investigated the action of spin-orbit fields onto the spin-wave [2]. Here, we calculated by first-principles the SO stiffness of the SP2DEG spin-wave. Surprisingly, the SO stiffness is shown to be  $\chi / \pi$ . We further employed electronic Raman scattering to study the density dependence of the SO stiffness and demonstrate the validity of our theory. We evidenced that the SO stiffness grows with the 2DEG density and decreases with the spin-polarization degree. Recently, spin-waves were excited by SO fields in a spin-wave based transistor. Our findings reveals the importance of the SO stiffness for such a future device.

[1] J. Gomez, F.Perez, E. M. Hankiewicz, B. Jusserand, G. Karczewski, and T. Wojtowicz, [Phys. Rev.B 81, 100403\(R\) \(2010\)](#)

[2] F. Baboux, F. Perez, C. A. Ullrich, I. D'Amico, J. Gomez, and M. Bernard, [Phys. Rev. Lett. 109, 166401 \(2012\)](#); F. Baboux, F. Perez, C. A. Ullrich, I. D'Amico, G. Karczewski, and T.Wojtowicz, [Phys. Rev. B 87, 121303\(R\) \(2013\)](#).

## Charged Carrier Spin Dynamics in ZnO Epilayers and Quantum Wells

Jungtaek Kim, J. Puls\*, and S. Sadofev

Institut für Physik, Humboldt-Universität zu Berlin, D-12489 Berlin, Germany

\*puls@physik.hu-berlin.de

ZnO and related heterostructures are considered as potential materials for spintronics applications. Since the Elliot-Yafet spin relaxation mechanism is dramatically reduced by the extremely small ratio between spin-orbit (SO) coupling and gap energy, only the D'yakonov-Perel mechanism is expected to contribute significantly both in bulk and quantum well structures. For localized electrons, the interaction with magnetic nuclei has to be additionally considered [1]. So far, only studies are known on electron spin coherence [2] and hole spin relaxation [3] on ZnO bulk samples and epilayers. The recent proof of the negatively charged exciton  $X^-$  transitions in ZnO/(Zn,Mg)O quantum wells (QWs) [4] has offered a tool to trace carrier spin dynamic for ZnO in the case of reduced dimensionality, where usually an increased transversal and longitudinal spin relaxation time is expected [1].

Here, an exemplary study on the longitudinal carrier spin dynamic in ZnO related structures will be presented both for QWs and epitaxial layers grown under comparable conditions. The possibility of a reduced SO coupling via increased sub-valence band splitting in ZnO QWs by strain and/or confinement as well as the role of hyperfine interaction in ZnO with extremely diluted magnetic nuclei will be treated. Since  $X^-$  and  $D^0X$  bound exciton in MQW and epilayers, respectively, possess the same spin configuration with paired electron spins, the hole spin can be directly traced by the circular polarized luminescence of both complexes. The spin dynamic of resident electrons in QWs and donor electrons is accessible via the bleaching of the initial state of the  $X^-$  and  $D^0X$ , respectively, photo-excitation.

Hole spin relaxation times of 80 and 140 ps are found for  $D^0X$  and  $X^-$ , respectively. The only marginal increase found for the reduced dimensionality of a QW is attributed to the fact that the conditions favorable for a slow hole spin relaxation via spin-orbit coupling are already present in the bulk case. The quantum confinement of holes in ZnO QWs do only marginally vary the A-B valence band splitting since the rather congeneric orbital symmetry of  $\Gamma_7^-$  and  $\Gamma_9^-$ -holes leads to practically the same strain-induced shift and similar confinement energies.

The spin relaxation of resident electrons in QWs and donor electrons in epilayers is dominated at zero external magnetic field by the hyperfine interaction which can be practically completely suppressed by a by a proper magnetic field applied along the ZnO  $c$ -axis. A field strength of 2 mT is already large enough proving the extremely small value of the Overhauser field in ZnO caused by the very restricted number of magnetic nuclei interacting with an electron inside the volume of the exciton complex.

- [1] M.I. Dyakonov (Ed.), Spin Physics in Semiconductors, Springer-Verlag, Berlin 2008.
- [2] S. Ghosh, V. Sih, W. H. Lau, and D. D. Awschalom, Appl. Phys. Letters **86**, 232507 (2005).  
H. Horn, A. Balocchi, X. Marie, A. Bakin, A. Waag, M. Oestreich, and J. Hübner  
Phys. Rev. B **87**, 045312 (2013)  
S. Kuhlen, R. Ledesch, R. de Winter, M. Althammer, S. T. B. Gönnenwein, M. Opel, R. Gross, T. A. Wassner, M. S. Brandt, and B. Beschoten, Phys. Stat. Sol. (b) **251**, 1861 (2014).
- [3] D. Lagarde, A. Balocchi, P. Renucci, H. Carrère, F. Zhao, T. Amand, X. Marie, Z. X. Mei, X. L. Du, and Q. K. Xue, Phys. Rev. B **78**, 033203 (2008)  
W.M. Chen, I.A. Buyanova, A. Murayama, T. Furuta, Y. Oka, D. P. Norton, S.J. Pearton, A. Osinsky, and J. W. Dong, Appl. Phys. Letters **92**, 092103 (2008).
- [4] J. Puls, S. Sadofev, and F. Henneberger, Phys. Rev. B **85**, 041307(R) (2012).

## Long-range $p$ - $d$ exchange interaction in a ferromagnet-semiconductor hybrid structure

V. L. Korenev<sup>1,2</sup>, M. Salewski<sup>2</sup>, I. A. Akimov<sup>1,2</sup>, V. F. Sapega<sup>1,3</sup>, L. Langer<sup>2</sup>, I. V. Kalitukha<sup>1</sup>,  
J. Debus<sup>2</sup>, R. I. Dzhioev<sup>1</sup>, D. R. Yakovlev<sup>1,2</sup>, D. Müller<sup>2</sup>, H. Hövel<sup>4</sup>, G. Karczewski<sup>5</sup>, M.  
 Wiater<sup>5</sup>, T. Wojtowicz<sup>5</sup>, Yu. G. Kusrayev<sup>1</sup>, and M. Bayer<sup>1,2</sup>

<sup>1</sup>IoFFE Physical-Technical Institute, Russian Academy of Sciences, St. Petersburg, Russia

<sup>2</sup>Experimentelle Physik 2, TU Dortmund, Dortmund, Germany

<sup>3</sup>Physical Faculty of St. Petersburg State University, St. Petersburg, Russia

<sup>4</sup>Experimentelle Physik 1, TU Dortmund, Dortmund, Germany

<sup>5</sup>Institute of Physics, Polish Academy of Sciences, Warsaw, Poland

Correlated magnetism in condensed matter, such as ferro-, antiferro- or ferrimagnetism, originates from exchange interactions. In magnetic semiconductors, the exchange occurs between free charge carriers and localized magnetic atoms and is determined by their wavefunction overlap. Hybrid structures consisting of a ferromagnetic layer and a semiconductor quantum well (QW) are appealing objects to assess and control this overlap. In particular, for a two-dimensional hole gas (2DHG) in a QW, the overlap of the hole wavefunction with the magnetic atoms in a nearby ferromagnetic layer is believed to result in a  $p$ - $d$  exchange interaction. In the effective magnetic field of that  $p$ - $d$  exchange the 2DHG spin system can become polarized. Recently, it was shown that additionally to this equilibrium 2DHG polarization there is an alternative mechanism involving spin-dependent capture of charge carriers from the semiconductor into the ferromagnet [1]: for ferromagnetic GaMnAs on top of an InGaAs QW, the capture of electrons induces their spin polarization in the QW, thus representing a dynamical effect in contrast to the exchange-induced equilibrium polarization.

Here, we report on a different ferromagnet/semiconductor hybrid system consisting of a cobalt layer and a CdTe QW separated by a non-magnetic barrier. Due to negligible hole tunneling, this hybrid combination shows mostly the quasi-equilibrium ferromagnetic proximity effect due to the  $p$ - $d$  exchange interaction between Co atoms and heavy holes in the CdTe layer. For conventional  $p$ - $d$  exchange via wavefunction overlap, an exponential decay with the barrier width of about a nanometer would be expected. Surprisingly, we found that the proximity effect, measured through the spin polarization of the heavy holes in the QW, is almost constant over long distances of more than 10 nm barrier width. This novel exchange coupling effect is therefore truly long-range, which is highly advantageous because it is robust with respect to hybrid interface variations. As possible origin of this long-range proximity effect we suggest an effective  $p$ - $d$  exchange interaction mediated by elliptically polarized phonons emitted from the ferromagnet into the QW.

[1] V. L. Korenev, I. A. Akimov, S. V. Zaitsev et al., Nature Commun. **3**, 959 (2012).

## (Al)GaAs:Be/Zn(Mn)Se Heterovalent Quantum Well Heterostructures: Electrical and Structural Properties

T.A. Komissarova\*, G.V. Klimko, S.V. Gronin, I.V. Sedova, S.V. Sorokin, B.Ya. Ber,  
A.A. Toropov, and S.V. Ivanov  
Ioffe Institute, St. Petersburg, Russia  
\*komissarova@beam.ioffe.ru

Ferromagnetic semiconductors with high Curie temperature  $T_C$  have been intensely studying last two decades. Maximum achieved  $T_C$  value is 185K for GaMnAs epitaxial films [1]. However, further increase of the  $T_C$  in GaMnAs is prevented by its specific growth conditions. Namely, it is known that the  $T_C$  value of diluted magnetic semiconductors (DMS) is governed by the concentrations of holes and Mn ions [2]. In case of GaMnAs layers, it is difficult to increase hole concentration and Mn ion density simultaneously, since the high Mn solubility in this material can be achieved only at low growth temperature (300°C), which, in turn, leads to increasing the donor defect density and limits the hole concentration. This problem might be overcome by using the (Al)GaAs:Be/Zn(Mn)Se heterovalent heterostructures involving the high quality GaAs/AlGaAs quantum well (QW) with the lower AlGaAs barrier modulation-doped with Be acceptors and the upper II-Mn-VI barrier proposed to be a source of Mn ions for the GaAs QW [3].

This work is devoted to study of electrical and structural properties of the (Al)GaAs:Be/Zn(Mn)Se QW heterovalent heterostructures grown by molecular beam epitaxy (MBE). Complex design of the structures with several conductivity channels and the close position of the GaAs QW and the heterovalent interface (HI), which can result in influence of the interdiffusion effects on the QW electrical properties, need in detailed consideration. The growth mode of the HI (the GaAs surface reconstruction and the growth initiation technique of the II-VI part) and the distance from the GaAs QW to the HI were varied for different samples. II, VI and III, V elements diffusion was studied by secondary ion mass spectroscopy. DC and AC (up to 1 MHz) electrical measurements were carried out in the temperature range of (4.2-300)K. The values of the hole concentration and mobility were determined from the Hall measurements. The results of the AC measurements were analyzed in terms of the Nyquist plot (dependence of the imaginary part of the impedance on its real part).

It has been shown that the total conductivity of the heterovalent heterostructures is governed by two conductivity channels: GaAs QW and AlGaAs:Be barrier layer. Conductivity through the GaAs QW is strongly influenced by the space charges at the GaAs/AlGaAs interface and HI, which leads to occurrence of the capacitive contribution to the QW conductivity and prevents the reliable magnetic measurements. Relationships between the space charge values at the HI, effects of II,VI and III, V element interdiffusion and growth conditions were studied. As a result, the method of the HI formation which allows the significant reduction of the relaxation processes related to the space charges at the HI has been determined. Optimized structure design for decreasing the influence of the space charge at the GaAs/AlGaAs interface has been proposed.

The work is partially supported by the Russian Foundation for Basic Research (grant ## 15-52-12014) and the Deutsche Forschungsgemeinschaft in the frame of International Collaborative Research Center TRR 160.

- [1] Wang M., Campion R.P., Rushforth A.W., Edmonds K.W., Foxon C.T., and Gallagher B.L., *Appl. Phys. Lett.* **93**, 132103 (2008).
- [2] Dietl T., Ohno H., Matsukura F., Cibert J., and Ferrand D., *Science* **287**, 1019 (2000).
- [3] Evropeytshev E.A., Klimko G.V., Komissarova T.A., Sedova I.V., Sorokin S.V., Gronin S.V., Kazantsev D.Yu., Ber B.Ya., Ivanov S.V., and Toropov A.A., *Semiconductors* **48**, 30 (2014)

**Wednesday September, 16 - Oral Session - WeB**

**10:45-12:15**

**ZnO, Plasmonic and optical engineering**

Chair: Joachim Puls, *Institute of Physics, Humboldt-University, Berlin (Germany)*

## **ZnO-based Plasmonics**

Kalusniak S\* and Sadofev S

Institut für Physik, Humboldt-Universität zu Berlin, Newtonstr. 15, 12489 Berlin, Germany

\*kalus@physik.hu-berlin.de

In this special talk, devoted to the memory of Prof. Fritz Henneberger, we recall his main scientific achievements, which had a strong impact on the II-VI community during the last decade. We focus on ZnO-based plasmonics, which was one of his last main research areas. We will show that strongly n-type doped ZnO is an excellent plasmonic material in the infrared spectral range and discuss the surface plasmon polariton dispersion curves, in particular thus obtained in epitaxial multi-layer structures of different doping level. We will show resonant coupling of such surface plasmon polaritons to molecular vibrations and finally discuss the realization of metamaterials with ZnGaO as a plasmonic component.

## Free-electron concentration and polarity inversion domains in plasmonic (Zn,Ga)O

Sadofev S\*, Kalusniak S, Schäfer P, Kirmse H and Henneberger F

Institut für Physik, Humboldt-Universität zu Berlin, Newtonstr. 15, 12489 Berlin, Germany

[\\*sergey.sadofev@physik.hu-berlin.de](mailto:sergey.sadofev@physik.hu-berlin.de)

Highly  $n$ -doped ZnO is attracting increasing attention as an alternative tunable plasmonic material [1]. It has been recently shown that free carrier concentrations of  $n \approx 10^{21} \text{ cm}^{-3}$  are readily achievable in ZnO doped with several mol.% of Al or Ga [2, 3]. Such high electron densities extend the metallic range with negative real part of the dielectric function from the mid to the near infrared reaching thus the wavelengths important for telecommunication processes. Recently we have demonstrated that in single crystalline (Zn,Ga)O layers grown on a-plane sapphire by molecular beam epitaxy (MBE) the zero-crossover wavelength of the dielectric function can reach  $\lambda_c = 1.36 \mu\text{m}$  at about 6 mol.% of incorporated Ga, while the plasmonic damping does not exceed 50 meV [4]. In order to address processes limiting  $n$  and increasing damping in (Zn,Ga)O, we performed a study of the layers grown on bulk ZnO wafers, aiming to probe the material with substantially better crystalline quality.

The MBE growth of (Zn,Ga)O is found to proceed in a two-dimensional mode coherently with substrate up to the carrier concentration of  $n \approx 8 \times 10^{20} \text{ cm}^{-3}$ . The layers show high crystalline perfection documented by full-widths at half maxima of the X-ray omega curves of 30-50 arcsec and distinct interference fringes in the  $\omega$ - $2\theta$  scans. The out-of-plane lattice constant increases linearly as  $n$  increases with a slope of  $1.4 \times 10^{-23} \text{ \AA} \cdot \text{cm}^3$ . At higher doping levels a gradual transition from two- to three-dimensional growth accompanied by overall degradation of material quality is observed. Transmission electron microscopy and convergent beam electron diffraction measurements reveal that the transition occurs via formation of Zn-polar inversion domains in the O-polar ZnO matrix [5]. The domain formation can be inhibited by low deposition temperatures or larger excess of Zn during the growth. This results in up to 1.4 times increase of free carrier concentration and a short-wavelength shift of a surface plasmon resonance of  $\hbar\Delta\omega = 100 \text{ meV}$  covering now fully the telecommunication spectral region.

Despite more than 40 times smaller width of the omega curves compared to the layers grown on sapphire no remarkable improvement of the plasmonic properties of (Zn,Ga)O is observed. Thus, in the carrier concentration range of  $n \approx 10^{20} \text{ cm}^{-3}$  the plasmonic damping is mainly defined by intrinsic scattering processes in (Zn,Ga)O, while a degree of crystalline perfection of the ZnO matrix plays a minor role.

[1] A. Boltasseva and H. A. Atwater, Science **331**, 290 (2011)

[2] D. Look, T. Droubay, and S. Chambers, Appl. Phys. Lett. **101**, 102101 (2012)

[3] H.Y. Liu, V. Avrutin, N. Izyskaya et al., J. Appl. Phys. **111**, 103713 (2012)

[4] S. Sadofev, S. Kalusniak, P. Schäfer, and F. Henneberger, Appl. Phys. Lett. **102**, 181905 (2013)

[5] S. Sadofev, S. Kalusniak, P. Schäfer, H. Kirmse and F. Henneberger, Phys. Status Solidi B, **252**, 607 (2015)

## Enhanced luminescence excitation via efficient optical energy transfer

Roy Aad<sup>1</sup>, Komla Nomenyo<sup>1</sup>, Christophe Couteau<sup>1</sup>, Vincent Sallet<sup>2</sup>, Corinne Sartel<sup>2</sup>, Gaëlle Amiri<sup>2</sup>, Laurent Divay<sup>3</sup>, Christophe Galindo<sup>3</sup>, Pierre Le Barny<sup>3</sup>, and Gilles Lérondel<sup>2\*</sup>

<sup>1</sup>Laboratoire de Nanotechnologie et d'Instrumentation Optique (LNIO), Institut Charles Delaunay, CNRS UMR 6281, Troyes France.

<sup>2</sup>Groupe d'Etude de la Matière Condensée (GEMAC), CNRS-UVSQ, Versailles, France.

<sup>3</sup>THALES Research and Technology, Campus Polytechnique, 1 avenue Augustin Fresnel, 91767 Palaiseau, France.

\*E-mail of the corresponding author: lerondel@utt.fr

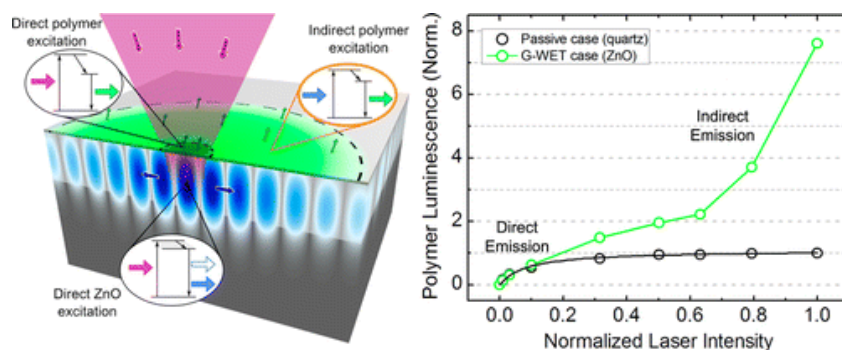


Figure 1. To the left, an illustration of the G-WET concept. To the right, photoluminescence measurements showing an 8-fold increase in the luminescence intensity. [1]

Luminescent nanoscale materials (LNMs) have received widespread interest in sensing and lighting applications due to their enhanced emissive properties. For sensing applications, LNMs offer improved sensitivity and fast response time which allow for lower limits of detection. Meanwhile, for lighting applications, LNMs, such as quantum dots, offer an improved internal quantum efficiency and controlled color rendering which allow for better lighting performances. Nevertheless, due to their nanometric dimensions, nanoscale materials suffer from extremely weak luminescence excitation (i.e. optical absorption) limiting their luminescence intensity, which in turn results in a downgrade in the limits of detection and external quantum efficiencies. Therefore, enhancing the luminescence excitation is a major issue for sensing and lighting applications.

In this work, we report on a novel photonic approach to increase the luminescence excitation of nanoscale materials. Efficient luminescence excitation increase is achieved via a gain-assisted waveguided energy transfer (G-WET). The G-WET concept consists on placing nanoscale materials atop of a waveguiding active (i.e. luminescent) layer with optical gain. Efficient energy transfer is thus achieved by exciting the nanoscale material via the tail of the waveguided mode of the active layer emission. The G-WET concept is demonstrated on both a nanothin layer of fluorescent sensitive polymer and on CdSe/ZnS quantum dots coated on ZnO thin film, experimentally proving up to an 8-fold increase in the fluorescence of the polymer and a 3-fold increase in the luminescence of the CdSe/ZnS depending of the active layer emission regime (stimulated vs spontaneous emission). Furthermore, we will discuss on the extended G-WET concept which consists on coating nanoscale materials on a nanostructured active layer. The nanostructured active layer offers the necessary photonic modulation and a high specific surface which can presumably lead to a more efficient G-WET concept. Finally, the efficiency as well as the observation conditions of the GWET will be discussed and compared with more conventional charge transfer or dipole-dipole energy transfer.

[1] Roy Aad *et al.*, ACS Photonics, **1**, 246-253, (2014).

[2] Roy Aad *et al.*, accepted in Materials (2015).

## Interface engineering in ZnO/organic hybrid structures for optimized excitonic coupling and charge transfer

Bianchi F<sup>1</sup>, Sparenberg M<sup>1</sup>, Sadofev S<sup>1</sup>, Schlesinger R<sup>1</sup>, Kobin B<sup>2</sup>, Hecht S<sup>2</sup>, Koch N<sup>1</sup>, and Blumstengel S<sup>1\*</sup>

<sup>1</sup>Institute of Physics, Humboldt University Berlin, Berlin, Germany

<sup>2</sup>Institute of Chemistry, Humboldt University Berlin, Berlin, Germany

\*Sylke.Blumstengel@physik.hu-berlin.de

ZnO is currently attracting significant interest as a candidate for hybrid photovoltaic and light-emitting devices. The key for achieving improved device performance or even new functionality is the control and engineering of the hybrid interface. We studied - in an all-ultrahigh vacuum approach - the interface formation of ZnO with various prototypical conjugated organic molecules, including perylene derivatives, oligo(phenylenes) as well as ladder-type oligo(phenylenes), whose fundamental optical excitation is resonant with the ZnO excitonic transition, employing *in-situ* scanning probe microscopies, photoemission and differential reflectance spectroscopy, complemented by *ex-situ* transmission electron microscopy and X-ray diffraction analysis. The talk will summarize our recent efforts to control the morphology and the electronic structure of the hybrid interface [1,2]. By appropriate interfacial design, we are able to manipulate electron-hole separation at the ZnO/organic interface and, alternatively, to achieve excitonic energy transfer from ZnO quantum wells to organic overlayers with efficiencies of up to 80 % [2,3].

[1] Sparenberg M. et al., Phys. Chem. Chem. Phys. 16, 26084, (2014).

[2] Schlesinger R. et al., Nat. Commun. 6:6754 doi: 10.1038/ncomms 7754 (2015).

[3] Bianchi F. et al., Appl. Phys. Lett. 105, 233301, (2014).

## Colloidal Quantum Dot-Based Excitonic Light-Emitting Devices

Seonghoon Lee\*

School of Chemistry, Seoul National University, Seoul, Korea 151-747

\*E-mail address: shnlee@snu.ac.kr

Colloidal nanobuilding blocks called gigantic artificial atoms or quantum dots have been well-developed and provide us with tremendous opportunities for the creation of new materials. The various artificial atoms with constituent interaction ranging from ionic to covalent are generated by wet chemical methods. The nanoscopic phenomenon of quantum confinement effect in artificial atoms allows us to control excitonic energies by tuning their sizes and understand broad absorption and narrow emission of light, phonon bottleneck, and energy transfer. The creation, recombination, annihilation, and separation, transport of excitons are investigated in artificial atoms-embedded conducting matrix or inorganic-organic hybrid materials. The portable, thin flexible highly bright, efficient, low-voltage driven red, green, blue, and natural white light-emitting devices (R/G/B/white-LEDs), enabled by the direct exciton formation within gigantic artificial atom-embedded active layers in a conducting polymer matrix or organic materials, have been demonstrated. The luminances of red-, green-, and blue-emitting devices are 23040, 218800, and 2250  $\text{cd/m}^2$  at the maximum, respectively. In addition, the external quantum efficiencies (EQEs) of the RGB devices were 7.3, 5.8, and 1.7%, respectively. White-QLEDs with a luminance of 5,000  $\text{cd/m}^2$  at an applied bias less than 6 V and external quantum efficiency of 1% or more have been successfully realized. Practicable everyday applications to traffic signals, display back-lights, and solid-state white illumination sources for the next generation are also exemplified.

- [1] W. K. Bae, J. Lim, D. Lee, M. Park, H. Lee, K. Char, C. Lee, Seonghoon Lee, *Adv. Mater.*, **26**, 6387-6393, (2014).
- [2] J. Lim, M. Park, W. K. Bae, D. Lee, Seonghoon Lee, C. Lee, K. Char, *ACS Nano*, **7(10)**, 9019-9026, (2013).
- [3] J. Kwak, W. K. Bae, D. Lee, I. Park, J. Lim, M. Park, H. Cho, H. Woo, D. Y. Yoon, K. Char, Seonghoon Lee, C. Lee. *Nano Lett.*, **12(5)**, 2362-2366, (2012). Also reported in C&E News in April 10, 2012 and in PHYSORG.com in April 20, (2012).
- [4] J. Lim, W. K. Bae, D. Lee, M. K. Nam, J. Jung, C. Lee, K. Char, Seonghoon Lee, *Chem. Mater.*, **23**, 4459-4463, (2011).
- [5] W. K. Bae, J. Kwak, J. Lim, D. Lee, M. K. Nam, K. Char, C. Lee, Seonghoon Lee, *Nano Lett.*, **10(7)**, 2368-2373, (2010). Also highlighted in MRS Bulletin, 35, Aug, (2010).

**Thursday September, 17 - Oral Session - ThA**

**08:30-10:00**

**Colloidal systems**

Chair: Grzegorz Karczewski, *Institute of Physics, Polish Academy of Sciences (Poland)*

## Preparation and study of semiconductors with a honeycomb nanogeometry

W. H. Evers<sup>1</sup>, M. P. Boneschanscher<sup>1</sup>, J. J. Geuchies<sup>1</sup>, J. Peters, C. Overbeek<sup>1</sup>, C. de Morais Smith<sup>2</sup>, E. Kalesaki<sup>3</sup>, C. Delerue<sup>3</sup>, and D. Vamaekelbergh<sup>1\*</sup>

<sup>1</sup>Debye Institute for Nanomaterials Science, University of Utrecht, Utrecht, NL

<sup>2</sup>Institute for Theoretical Physics, University of Utrecht, Utrecht, NL

<sup>3</sup>IEMN-ISEN, University of Lille, Lille, France

[\\*d.vanmaekelbergh@uu.nl](mailto:d.vanmaekelbergh@uu.nl)

The interest in 2-dimensional systems with a honeycomb lattice and related Dirac-type electronic bands has exceeded the prototype graphene. Currently, 2-dimensional atomic and nanoscale systems are extensively investigated in the search for materials with novel electronic properties that can be tailored by geometry. I will show how atomically coherent honeycomb superlattices of rock salt (PbSe, PbTe) and zinc blende (CdSe, CdTe) semiconductors can be obtained by nanocrystal self-assembly, covalent attachment, and subsequent cation exchange. A detailed analysis with STM, GISAXS, and HAADF-STEM of these systems learned that self-assembly and oriented attachment leads to buckled (i.e. silicene-type) honeycomb structures with a periodicity of about 6 nm.

Atomistic and analytical theory predict that these artificial graphene systems combine Dirac-type electronic bands with the beneficial properties of a semiconductor, such as the presence of a band gap and strong spin-orbit coupling, leading to the quantum spin Hall effect. Finally, I will present the first experimental results on the opto-electrical characterization of PbSe and CdSe honeycomb semiconductors.

- [1] Boneschanscher, M. P., Evers, W. H., Geuchies, J. J., Altantzis, T., Goris, B., Rabouw, F. T., van Rossum, S. A. P., van der Zant, H. S. J., Siebbeles, L. D. A., Van Tendeloo, G., Swart, I., Hilhorst, J., Petukhov, A. V., Bals, S., Vanmaekelbergh, D., *Science* **344**, 1377 (2014).
- [2] Kalesaki, E., Delerue, C., Smith, C. Morais, Beugeling, W., Allan, G., Vanmaekelbergh, D., *Physical Review X* **4**, 011010 (2014)

## Transport properties of 2D colloidal nanoplatelets to achieve enhanced photoconduction properties

Emmanuel Lhuillier<sup>1\*</sup>, Adrien Robin<sup>1,2</sup>, Jean-Francois Dayen<sup>3</sup>, Benoit Dubertret<sup>2</sup>

<sup>1</sup>Nexdot, 10 rue Vauquelin, Paris, France

<sup>2</sup>Laboratoire de Physique et d'Etude des Matériaux, ESPCI-ParisTech, PSL Research University, Sorbonne Université UPMC Univ Paris 06, CNRS, 10 rue Vauquelin 75005 Paris, France.

<sup>3</sup>Université de Strasbourg, IPCMS-CMRS UMR 7504, 23 Rue du Loess, 67034 Strasbourg, France

\*Emmanuel.lhuillier@espci.fr

2D colloidal nanoplatelets (NPL) made of cadmium chalcogenides offer unique optical properties (fast and narrow PL) thanks to the atomic control of their surface [1]. The use of these new materials for optoelectronic devices also requires to reach a high level of control on their conduction properties. In particular the photoconductivity of NPL film remains limited by traps and the high exciton binding energy which prevents an efficient electron hole dissociation. Here we present two strategies to achieve enhanced photoconduction properties in thin film on NPL.

To reduce the effect of trap our strategy is to control the carrier density and to bring the fermi level close to the conduction band which will prevent electron trapping. The tuning of the Fermi level is achieved thanks to ion gel electrolyte gating [2]. The latter allows a large current modulation ( $>10^7$  on-off ratio) with limited gate bias (2V). In this phototransistor configuration the photocarrier lifetime is significantly enhanced which lead to a rise of the material responsivity by three decades [3].

Further improvement of the material photoconductance can be obtained by achieving a larger electron hole pair dissociation. In this case larger voltage drop per particle has to be applied, which can be done connecting NPL over a nanotrench. In this case the mechanism of transport switches from a hopping process to a single tunnel event. Again the photoresponse is significantly boosted by 7 decades and leads to the highest value reported in CdSe nanomaterial ( $R \approx kA \cdot W^{-1}$ ) [4], while the noise level in the system also drops.

- [1] E. Lhuillier, S. Pedetti, S. Ithurria, B. Nadal, H. Heuclin, B. Dubertret, *Accounts for chemical research* 22, 48 (2015).
- [2] E. Lhuillier, S. Pedetti, S. Ithurria, H. Heuclin, B. Nadal, A. Robin, G. Patriarche, N. Lequeux and B. Dubertret, *ACS nano* 8, 3813(2014).
- [3] E. Lhuillier, A. Robin, S. Ithurria, H. Aubin, B. Dubertret, *Nano Lett.* 14, 2715(2014).
- [4] E. Lhuillier, J.F. Dayen, D. O. Thomas, A. Robin, B. Doudin, B. Dubertret, *Nano Lett* 15,1736 (2015).

## Polarimetric Determination of CdSe/Cds Dipole Orientation

C. Lethiec<sup>1</sup>, L. Thu N'Guyen<sup>1</sup>, J. Laverdant<sup>1,2</sup>, M. Nasilowski<sup>3</sup>, C. Javaux<sup>3</sup>, B. Dubertret<sup>3</sup>, F. Pisanello<sup>4</sup>, L. Carbone<sup>4</sup>, L. Coolen<sup>1</sup>, A. Maître<sup>1\*</sup>

1. Institut des Nanosciences de Paris, Université Pierre et Marie Curie, 4 place Jussieu, 75252 Paris cedex 05, France

2. Institut Lumière Matière, Université de Lyon, Université Lyon 1, Villeurbanne, France

3. Laboratoire de Physique et d'Etude des Matériaux, ESPCI, UPMC, CNRS, 10 rue Vauquelin, 75005 Paris, France

4. Università del Salento, via per Monteroni, 73100 Lecce, Italy

\*agnes.maitre@insp.upmc.fr

Efficient coupling of nanoemitters to photonic or plasmonic structures requires specific orientation of their emitting dipoles which remains an experimental challenge. We propose in this paper to determine the nature and the orientation of II-VI nanoemitter dipoles by polarization analysis of their emission[1].

A nanoemitter can be considered either by a single radiating dipole (molecule or nanorod for example), or by the sum of two orthogonal incoherent dipoles (CdSe / ZnS nanocrystal for example) - known as 2D dipole [2]. By analogy, 200 nm spheres filled with a large number of dye molecules, can be modeled of a 3D dipole (sum of three orthogonal incoherent dipoles). The polarization anisotropy distribution, defined as  $(I_x - I_y)/(I_x + I_y)$ , of a statistical collection of several hundreds of individual emitters randomly oriented[3], reveals the dimensionality of the dipoles. For colloidal CdSe/CdS nanocrystals, the anisotropy shows a clear signature of a 2D dipole, whereas CdSe/CdS nanorods are 1D dipoles.

Once the dimensionality of the emitter is known, at the single scale, its orientation can be determined by considering the phase and the contrast of the sinusoidal curves obtained by turning an emission polarizing analyzer. This analysis has been performed as well in the case of II-VI colloidal nanocrystals [1], nanorods [2] and nanoplatelets.

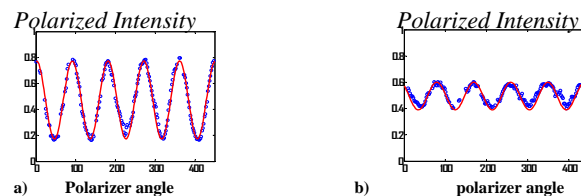


**Fig 1:** intensity transmitted by the polarizer for a single nanoemitter as a function of the polarizer rotation angle. red line simulation, blue points : experimental points. a) CdSe/CdS nanorod, (1D dipole) , b) CdSe/CdS nanocrystals (2D dipole)

This determination of dipole orientation by polarization analysis is complementary to defocused microscopy, and can give information even when defocused microscopy is not suited (2D dipole at a metallic interface...). The knowledge of the dimensionality and orientation of II-VI nanoemitter dipoles ensures a better control of their emission properties especially when they are included in photonic structures.

### References

- [1] C. Lethiec et al, "Three-dimensional orientation measurement of a single fluorescent nanoemitter by polarization analysis", *Phys. Rev. X* **4**, 021037 (2014)
- [2] C. Lethiec et al, "Polarimetry-based analysis of dipolar transitions of single colloidal CdSe/CdS dot-inrods", *New Journal of Physics* **16**, 093014 (2014)
- [3] I. Chung, et al, "Room temperature measurements of the 3D orientation of single CdSe quantum dots using polarization microscopy", *Proc. Nat. Ac. Sci.* **100**, 405 (2003)

## Alignment of Rod-Shaped Single-Photon Emitters Driven by Line Defects in Liquid Crystals

PelliserLaurent<sup>1</sup>, ManceauMathieu<sup>2</sup>, LethiecClotilde<sup>1</sup>, CoursaultDelphine<sup>1</sup>, VezzoliStefano<sup>2,3</sup>, LeménagerGodefroy<sup>2</sup>, CoolenLaurent<sup>1</sup>, DeVittorioMassimo<sup>4,5,6</sup>, PisanelloFerruccio<sup>5</sup>, CarboneLuigi<sup>6</sup>, MaitreAgnes<sup>1</sup>, BramatiAlberto<sup>2</sup>, and LacazeEmmanuelle<sup>1\*</sup>

<sup>1</sup>Institut des NanoSciences de Paris (INSP), CNRS, UMR 7588, Paris, France

<sup>2</sup>Laboratoire Kastler Brossel, Collège de France, Paris, France

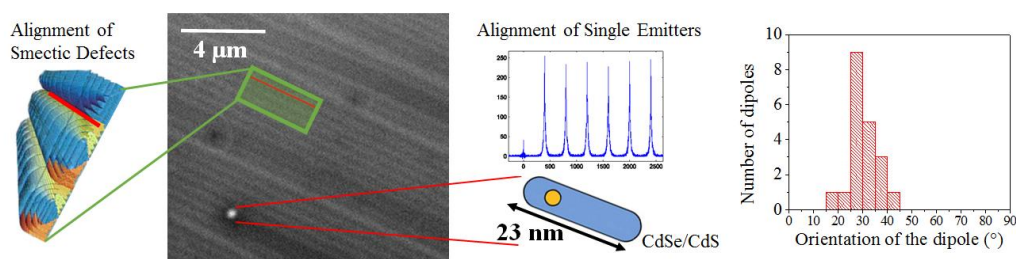
<sup>3</sup>Centre for Disruptive Photonic Technologies, Singapore

<sup>4</sup>Dipartimento di Ingegneria dell'Innovazione, Università del Salento, Lecce, Italy

<sup>5</sup>Center for Biomolecular Nanotechnologies @Unile, Istituto Italiano di Tecnologia (IIT), Lecce, Italy

<sup>6</sup>National Nanotechnology Laboratory (NNL), CNR-Istituto Nanoscienze, Lecce, Italy

Arrays of liquid crystal defects—linear smectic dislocations—are used to trap semiconductor CdSe/CdS dot-in-rods which behave as single-photon emitters. Measurements of the emission diagram are combined together with measurements of the emitted polarization of the single emitters whose unicity was verified through antibunching measurement. It is shown that the dot-in-rods are confined parallel to the linear defects to allow for a minimization of the disorder energy associated with the dislocation cores. It is demonstrated that the electric dipoles associated with the dot-in-rods, tilted with respect to the rods, remain oriented in the plane including the smectic linear defects and perpendicular to the substrate, most likely due to dipole/dipole interactions between the dipoles of the liquid crystal molecules and those of the dot-in-rods. Using smectic dislocations, nanorods can consequently be oriented along a unique direction for a given substrate, independently of the ligands' nature, without any induced aggregation, leading as well to a fixed azimuthal orientation for the dot-in-rods' dipoles. These results open the way for the fine control of nanoparticle anisotropic optical properties, in particular, fine control of single-photon emission polarization.



Pelliser L. et al., Alignment of Rod-Shaped Single-Photon Emitters Driven by Line Defects in Liquid Crystals, *Advanced Functional Materials*, 25, 11, 1719-1726, 2015

## Gold Plated and Thick Shell Quantum Dots: Two Examples of Colloidal Quantum Dots with Much Improved Optical Properties

M. Nasilowski, P. Spinicelli and B. Dubertret\*

LPEM, ESPCI, 10 rue Vauquelin, 75005 Paris, France

\*e-mail : benoit.dubertret@espci.fr

The quest for the perfect quantum dot (QD) is a drive for both chemists and physicists. Many studies have tried to understand and limit QD emission blinking in time[1].

The most widely accepted explanation for the emission intensity flickering is the presence of an excess charge, in or in close proximity to the nanocrystal[2] that can recombine non radiatively with the exciton through Auger processes. This results in lower quantum yield and fluctuation of the QD emission in time when observed at the single particle level.

Recently, two routes have been proposed to decrease the efficiency of Auger recombination: composition gradient between the core and the shell[3] and thick shell QDs[4]. While these two routes have led to QDs with improved fluorescent properties, they both have their limitations: limited quantum yields for gradient QDs and strongly temperature dependent quantum yield for thick shell QDs.

We present here two new generations of quantum dots with unmatched optical properties. The first one, a CdSe/CdS QD with a thick CdS shell and a gradient interface between the core and the shell, exhibit a quantum yield of 100% at room temperature, with a perfectly stable, non-blinking, fluorescence emission over long periods of time (hours). We measured a similar quantum yield for the monoexciton and for the biexciton, which shows that Auger recombinations are completely suppressed in these QDs. At high excitation powers, these QDs show multiexcitonic emission even at the single dot level, another proof of the complete suppression of Auger recombination.

The second one consists of a single quantum dot encapsulated in a silica shell coated with a continuous gold nanoshell.[5] It provides a system with a stable and Poissonian emission at room temperature. This novel hybrid quantum dot/silica/gold structure behaves as a plasmonic resonator with a strong Purcell factor. The gold nanoshell also enhances the QDs' resistance to high-power photoexcitation or high-energy electron beams.

These two types of new QDs bring a rupture in the family of colloidal QDs in the sense that they are the first examples of 100% quantum yield QD at room temperature even at high excitation power, regardless of their charge state and with robust optical properties.

- [1] M. Nirmal, B. O. Dabbousi, M. G. Bawendi, J. J. Macklin, J. K. Trautman, T. D. Harris, and L. E. Brus, *Nature*, vol. **383**, no. 6603, pp. 802–804, Oct. 1996.
- [2] M. Kuno, D. P. Fromm, H. F. Hamann, A. Gallagher, and D. J. Nesbitt, *J. Chem. Phys.*, vol. **115**, no. 2, p. 1028, 2001.
- [3] G. E. Cragg and A. L. Efros, *Nano Lett.*, vol. **10**, no. 1, pp. 313–7, Jan. 2010.
- [4] C. Javaux, B. Mahler, B. Dubertret, A. Shabaev, A. V Rodina, A. L. Efros, D. R. Yakovlev, F. Liu, M. Bayer, G. Camps, L. Biadala, S. Buil, X. Quelin, and J.-P. Hermier, *Nat. Nanotechnol.*, vol. 8, no. 3, pp. 206–12, Mar. 2013.
- [5] B. Ji, E. Giovanelli, B. Habert, P. Spinicelli, M. Nasilowski, X. Xu, N. Lequeux, J.-P. Hugonin, F. Marquier, J.-J. Greffet, and B. Dubertret, *Nat Nano*, vol. **10**, no. 2, pp. 170–175, Feb. 2015.

**Thursday September, 17 - Oral Session - ThB**

**10:30-12:15**

**ZnO, Transport and Doping**

Chair: Chong-Xin Shan, *Changchun Institute of Optics, Chinese Academy of Sciences (China)*

## Novel Quantum Transport of 2D Electrons in MBE-Grown ZnO Heterostructures

Yusuke Kozuka<sup>1\*</sup>

<sup>1</sup>Department of Applied Physics, University of Tokyo, Tokyo, Japan

\*kozuka@ap.t.u-tokyo.ac.jp

High-mobility electron gas has been formed at heterointerfaces of clean materials, including Si, GaAs and CdTe. In such a two-dimensional electron gas (2DEG), a novel quantum phenomenon called quantum Hall effect emerges at low temperature under high magnetic field. However, the physics of the quantum Hall effect has developed mainly using GaAs heterostructures owing to the extremely high electron mobility exceeding 10 million  $\text{cm}^2/\text{Vs}$ .

Here we show that crystal quality of ZnO heterostructures is now comparable to GaAs heterostructures. Based on our continuous effort, the mobility of the ZnO heterostructure reaches 1 million  $\text{cm}^2/\text{Vs}$ , which corresponds to  $\sim 5$  million  $\text{cm}^2/\text{Vs}$  for GaAs in terms of the transport scattering time [1]. Furthermore, the quantum scattering time, which more precisely reflects total scattering rate, is nearly the same value as that of the best-quality GaAs system. This outstanding property enabled the observation of the unprecedented even-denominator fractional quantum Hall effect [2]. The case of ZnO clearly demonstrates that the improvement of crystal quality of semiconductors is fundamentally important, leading to new physics or applications [3].

- [1] J. Falson, D. Maryenko, Y. Kozuka, A. Tsukazaki, and M. Kawasaki, *Appl. Phys. Express* **4**, 091101 (2011).
- [2] J. Falson, D. Maryenko, B. Friess, D. Zhang, Y. Kozuka, A. Tsukazaki, J. H. Smet, and M. Kawasaki, *Nature Phys.* *in press*.
- [3] Y. Kozuka, A. Tsukazaki, and M. Kawasaki, *Appl. Phys. Rev.* **1**, 011303 (2014).

## ZnO-Based Oxide Semiconductors for Transparent Electronics

Jianguo Lu\*, Qingjun Jiang, Lisha Feng, Genyuan Yu, and Zhizhen Ye  
 State Key Laboratory of Silicon Materials, School of Materials Science and Engineering,  
 Zhejiang University, Hangzhou 310027, China  
 \* lujianguo@zju.edu.cn

ZnO is an II-VI compound semiconductor with a wide bandgap of 3.37 eV. ZnO-based oxides are ideal semiconductors for transparent electronics. In this report, we will present the growth, properties, and applications of ZnO:Al (AZO) and ZnMSnO (M=Al and Si) films. The two materials are indium-free and very promising for transparent electronic devices.

AZO is a typical transparent conductive oxide (TCO) that can replace commercial ITO and FTO for practical applications. The optimal Al content was determined to be 4 at. % [1,2]. At optimized conditions, high-quality AZO films could be grown at room temperature [3], with a low resistivity  $\sim 10^{-4}$   $\Omega\text{cm}$  and high visible transmittance  $\sim 90$  %. AZO films were used as transparent electrodes in GaN light-emitting diodes (LEDs) [4], having a forward voltage of 3.36 V, an electroluminescence emission at 526 nm, and a light output power of 386 mcd at 20 mA. AZO films, with texture surfaces produced by ammonium acetate, were used as front transparent electrodes in solar cells [5], for example, showing a high conversion efficiency of 10.75% for single-junction amorphous silicon thin-film solar cells. AZO films could be widely used in various fields including flexible devices.

For replacing InGaZnO, we have developed a new amorphous semiconductor (AOS), ZnMSnO (M=Al and Si). Sn is a competitive alternative for In due to the similar electron configurations ( $4d^{10}5s^0$ ) of  $\text{Sn}^{4+}$  and  $\text{In}^{3+}$  [6]. The lower standard electrode potential (SEP) of Al (-1.66 V) and Si (-0.91 V) indicates a much effective substitution for the traditional suppressor of Ga (-0.55 V). The introduction of Al and Si could enhance the stability, densify the active layers, and suppress the formation of oxygen vacancies [7-9]. Amorphous ZnMSnO (M=Al and Si) is an ideal channel material for thin-film transistors (TFTs). For example, the *a*-ZnAlSnO TFTs exhibited acceptable performances, with an on/off current ratio of  $\sim 10^7$ , field-effect mobility of  $2.33 \text{ cm}^2\text{V}^{-1}\text{S}^{-1}$ , threshold voltage of 2.39 V, and subthreshold swing of 0.52 V/decade [9]. The indium-free ZnAlSnO TFTs may be very promising for practical applications in flat panel and next-generation displays.

By using *a*-ZnAlSnO as the channel and AZO as the electrodes, fully transparent TFTs have been fabricated recently. We will also present the results in this report. The study in this work can be expected to facilitate the development of transparent electronics.

- [1] J. G. Lu, Z. Z. Ye, Y. J. Zeng, L. P. Zhu, L. Wang, J. Yuan, B. H. Zhao, and Q. L. Liang, *J. Appl. Phys.* **100**, 073714, (2006).
- [2] J. G. Lu, S. Fujita, T. Kawaharamura, H. Nishinaka, Y. Kamada, T. Ohshima, Z. Z. Ye, Y. J. Zeng, Y. Z. Zhang, L. P. Zhu, H. P. He, and B. H. Zhao, *J. Appl. Phys.* **101**, 083705, (2007).
- [3] Y. P. Wang, J. G. Lu, X. Bie, L. Gong, X. Li, D. Song, X. Y. Zhao, W. Y. Ye, and Z. Z. Ye, *J. Vac. Sci. Technol. A* **29**, 031505 (2011).
- [4] D. Chen, J. G. Lu, J. Y. Huang, Y. Z. Jin, H. X. Zhang, and Z. Z. Ye, *J. Inorg. Mater.* **28**, 649, (2013).
- [5] Q. J. Jiang, J. G. Lu, J. Zhang, Y. L. Yuan, H. Cai, C. J. Wu, R. J. Sun, B. Lu, X. H. Pan, and Z. Z. Ye, *Sol. Energy Mater. Sol. Cells*, **130**, 264, (2014).
- [6] Q. J. Jiang, J. G. Lu, J. P. Cheng, X. F. Li, R. J. Sun, L. S. Feng, W. Dai, W. C. Yan, and Z. Z. Ye, *Appl. Phys. Lett.* **105**, 132105, (2014).
- [7] C. J. Wu, X. F. Li, J. G. Lu, Z. Z. Ye, J. Zhang, T. T. Zhou, R. J. Sun, L. X. Chen, B. Lu, and X. H. Pan, *Appl. Phys. Lett.* **103**, 082109 (2013).
- [8] P. Wu, J. Zhang, J. G. Lu, X. F. Li, C. J. Wu, R. J. Sun, L. S. Feng, Q. J. Jiang, B. Lu, X. H. Pan, and Z. Z. Ye, *IEEE Trans. Electron Dev.* **61**, 1431, (2014).
- [9] Q. J. Jiang, L. S. Feng, C. J. Wu, R. J. Sun, X. F. Li, B. Lu, Z. Z. Ye, and J. G. Lu, *Appl. Phys. Lett.* **106**, 053503, (2015).

## Electrical properties, and Optical properties of p-n and p-i-n heterostructures based on p-ZnO, n-GaN and i-Al<sub>2</sub>O<sub>3</sub>

E. Przeździecka\*, S. Chusnutidinow, M. Stachowicz, E. Guziewicz, D. Snigurenko,  
K. Kopalko, R. Jakiela, A. Kozanecki

<sup>1</sup>Institute of Physics, Polish Academy of Sciences, Warsaw, Poland

\*eilczuk@ifpan.edu.pl

Zinc oxide (ZnO) is a promising candidate for applications as ultraviolet (UV) photodetectors due to its large direct band gap and the high absorption coefficient in the UV spectral range. UV detectors based on wide bandgap semiconductors as GaN and ZnO have recently received a lot of attention due to their chemical and thermal stability in harsh environment. In the case of ZnO the *p*-type doping is required for many applications. It is known, however, that the *p*-type doping of ZnO is a difficult task due to the background *n*-type centers.

The *p-n* structures consisting of acceptor doped ZnO:N films were grown by plasma-assisted molecular beam epitaxy (MBE) on *n*-type GaN on sapphire templates. In the case of *p-i-n* heterostructure a thin isolating Al<sub>2</sub>O<sub>3</sub> layer was deposited on GaN template by atomic layer deposition before the growth of ZnO layer by MBE. In both cases the ZnO was doped by nitrogen using rf N<sub>2</sub> plasma cell. The concentration of nitrogen in ZnO, measured with secondary ion mass spectroscopy, is about  $2 \cdot 10^{20}$  at/cm<sup>-3</sup> and acceptor-related lines in temperature dependence photoluminescence are observed. We show that the maximum forward-to-reverse current ratio  $I_F/I_R$  in the obtained diodes is relatively high (about  $10^7$ ) for the applied voltage of  $\pm 5$  V [1] which is 2–5 orders of magnitude higher than previously reported values for this type of heterojunctions. The very low dark current of  $10^{-11}$  A and the high breakdown voltage (<-7V) are characteristic of this type of the obtained diodes. Electron Beam Induced Current (E-BIC) measurements confirmed the formation of the junctions [2, 3] at the *p*-ZnO:N/*n*-GaN interface. The presence of isolating Al<sub>2</sub>O<sub>3</sub> layers is also visible, with the E-BIC scan superimposed on cross-sectional SEM image, which is an unusual result. The diffusion length and activation energy of charge carriers have been calculated from E-BIC scan profiles. It was shown that heterostructures exhibit strong and selective absorption in the UV range and the photocurrent signal was modified by adding an isolating Al<sub>2</sub>O<sub>3</sub> layer at the interface. The difference between the light and dark currents is above four orders of magnitude and it strongly depends on the powers of UV light. The investigated ZnO:N/GaN and ZnO:N/Al<sub>2</sub>O<sub>3</sub>/GaN structures are promising for UV sensor application.

The research was partially supported by the NCN project DEC-2013/09/D/ST3/03750.

[1] E. Przeździecka, M. Stachowicz, S. Chusnutidinow, R. Jakiela and A. Kozanecki, *Appl. Phys. Lett.* **106**, 062106 (2015).

[2] L. Chernyak, C. Schwarz, E. Flitsyan, S. Chu, J. L. Liu, and K. Gartsman, *Appl. Phys. Lett.* **92**, 102106 (2008).

[3] O. Lopatiuk-Tirpak, L. Chernyak, L. J. Mandalapu, Z. Yang, J. L. Liu, K. Gartsman, Y. Feldman, and Z. Dashevsky, *Appl. Phys. Lett.* **89**, 142114 (2006).

## Stabilization of p-type N-doped Zn-deficient ZnO Nanoparticles

Renaud A.<sup>1</sup>, Chavillon B.<sup>1</sup>, Rocquefelte X.<sup>1</sup>, Faulques E.<sup>1</sup>, Deniard P.<sup>1</sup>, Boujtita M.<sup>2</sup>, Pellegrin Y.<sup>2</sup>, Blart E.<sup>2</sup>, Odobel F.<sup>2</sup>, Cheviré F.<sup>3</sup>, Tessier F.<sup>3</sup>, Cario L.<sup>1</sup> and Jobic S.<sup>1\*</sup>

<sup>1</sup>Institut des Matériaux Jean Rouxel, Université de Nantes, CNRS, 2 rue de la Houssinière, 44322 Nantes cedex 3, France

<sup>2</sup>CEISAM, Université de Nantes, CNRS, 2 rue de la Houssinière, 44322 Nantes cedex 03, France

<sup>3</sup>Institut des Sciences Chimiques de Rennes, Université de Rennes 1, CNRS, 263 Avenue du General Leclerc, 35042 Rennes cedex, France

\*stephane.jobic@cnrs-imn.fr

Nowadays zinc oxide is regarded as a very promising material deemed to compete in the near future with GaN for optoelectronic applications. Unfortunately, the durability of p-type ZnO is yet a blockage that singularly slows down the launching of ZnO based devices. In that context, we embarked recently on the synthesis as powdered samples of a p-type zinc oxide material with the wurtzite structure by ammonolysis at low temperature (e.g. 250 °C) of zinc peroxide [1]. The nature of the charge carriers was identified without ambiguity by photo-electrochemistry, complex impedance spectroscopy and transient spectroscopy. P-typeness in ZnO would result from an extraordinary huge amount of Zn vacancies (up to 20%) coupled with the insertion of nitrogen within nanoscale spherical particles. Remarkably, the p-type conductivity remains stable for periods longer than two years and a half in ambient conditions. Here the chemical route to produce p-type ZnO, as well the optical and electrical properties of the synthesized material, will be described. In addition, the origin of the strong Zn deficit, which probably plays a major role in the establishment of p-typeness, will also be addressed [2].

[1] Chavillon B., Cario L., Renaud A., Tessier F., Cheviré F., Boujtita M., Pellegrin Y., Blart E., Smeigh A., Hammarström L., Odobel F. and **Jobic S.**, *J. Am. Chem. Soc.* **134**, 464, (2012)

[2] Renaud A. et al., submitted (2015)

## Research on p-type Doping, Bandgap Engineering and Stability of Thin-Film Transistors in ZnO and its Related Oxide

Z.Z. Ye\*, S.S. Chen, X.H. Pan, C. Chen, H.H. Zhang, J. Zhang, J.Y. Huang, L.X. Chen  
<sup>1</sup>School of Materials Science and Engineering, Zhejiang University, Hangzhou, People's Republic of China

\* E-mail address: yezz@zju.edu.cn

Among all wide band gap semiconductors, ZnO with its direct band gap of 3.37 eV and large exciton binding energy has attracted much attention in optoelectronics and electronics. High-quality p-n homojunction is the main factor to realize its applications in light emitting devices. Reliable p-type ZnO has always been a major challenge. We report repeatable p-type conductivity with a hole concentration of about  $3.0 \times 10^{16} \text{ cm}^{-3}$  in ZnO:Na films. Na doping behavior has been further studied, and two acceptor levels have been confirmed in different ZnO:Na films. In addition, bandgap engineering which is also a crucial step in designing modern light emitting devices has been carried out to obtain high luminescent efficiency. Zn<sub>1-x</sub>Mg<sub>x</sub>O is considered as a desired barrier material of ZnO based multiple quantum wells (MQWs). High-quality Zn<sub>1-x</sub>Mg<sub>x</sub>O film and ZnO/Zn<sub>1-x</sub>Mg<sub>x</sub>O MQWs have been fabricated and analyzed.<sup>[1]</sup> The valence band offsets of ZnO/Zn<sub>1-x</sub>Mg<sub>x</sub>O heterojunctions were measured by photoelectron spectroscopy. A systematic investigation of the valence and conduction band offsets at ZnO/Zn<sub>1-x</sub>Mg<sub>x</sub>O heterojunctions with various Mg compositions, and the Mg composition dependent band alignment is revealed and analyzed.<sup>[2]</sup> Meanwhile, the increased conduction band offsets and the control of local strain are supposed to benefit Na doping by alloying Mg in ZnO. The design of desired band structure has been further studied for p-type doping by doping and polarity control.<sup>[3, 4]</sup>

On the other hand, ZnO and its related oxide semiconductors thin-film transistors (TFTs) have numerous advantages including high mobility, high optical transparency and low processing temperature, making them suitable to be used in transparent and flexible display. Our work focused on three different oxide semiconductors: ZnO, InGaZnO (IGZO) and InAlZnO (IAZO). Annealing treatment was used to control the carrier concentration in ZnO films and achieve the operation of ZnO TFTs.<sup>[5]</sup> The stability of IGZO TFTs was investigated, and two instability mechanisms were observed. The first one is shallow trap mechanism, and the other one is interface trapping mechanism.<sup>[6]</sup> Besides, oxygen and water in air may be the dominant factors for threshold voltage instability for unpassivated or not-well passivated devices. Therefore, we proposed a model to explain how the ingredients of ambient affect the TFT performance by investigating amorphous IAZO TFTs under vacuum conditions and an oxygen atmosphere with different rates of relative humidity. The mechanism of water assisted oxygen absorption on the back channel is proposed to explain the phenomenon that wet oxygen leads to a larger positive threshold voltage shift than dry oxygen.<sup>[7]</sup>

[1] H. Zhang, X. Pan, P. Ding, J. Huang, H. He, W. Chen, Y. Li, B. Lu, J. Lu, Z. Ye, *Opt. Commun.* **96**, 301, (2013).

[2] H. Zhang, X. Pan, B. Lu, J. Huang, P. Ding, W. Chen, H. He, J. Lu, S. Chen, Z. Z. Ye, *Phys. Chem. Chem. Phys.* **15**, 11231, (2013).

[3] H. Zhang, X. Pan, Y. Li, Z. Ye, B. Lu, W. Chen, J. Huang, P. Ding, S. Chen, H. He, J. Lu, L. Chen, C. Ye, *Appl. Phys. Lett.* **104**, 112106, (2014),.

[4] S. Chen, X. Pan, W. Chen, H. Zhang, W. Dai, P. Ding, J. Huang, B. Lu, Z. Ye, *Appl. Phys. Lett.* **105**, 122112, (2014).

[5] J. Zhang, X. Li, J. Lu, P. Wu, J. Huang, Q. Wang, B. Lu, Y. Zhang, B. Zhao, Z. Ye, *AIP Advances* **2**, 022118, (2012).

[6] J. Zhang, X. Li, J. Lu, Z. Ye, L. Gong, P. Wu, J. Huang, Y. Zhang, L. Chen, B. Zhao, *J. Appl. Phys.* **110**, 084509, (2011).

[7] J. Zhang, X. Li, J. Lu, N. Zhou, P. Guo, B. Lu, X. H. Pan, L. X. Chen, Z. Z. Ye, *RSC Adv.* **4**, 3145, (2014).

## The ZnO:(N, Al)-based homojunction deposited at low temperature

D. Snigurenko\*, T. A. Krajewski, K. Kopalko, R. Jakiela, B. S. Witkowski, P. Dluzewski and E. Guziewicz

Institute of Physics, Polish Acad. of Sciences, al. Lotnikow 32/46, 02-668 Warsaw, Poland  
\*snigurenko@ifpan.edu.pl

Zinc oxide (ZnO) is a II-VI semiconducting material with a series of unique physical properties such as transparency ( $E_g = 3.4$  eV) and a very high exciton binding energy (60 meV) at RT. The main obstacle in using this material for various electronic and optoelectronic purposes is the lack of reliable, reproducible and tunable p-type doping. For this reason ZnO-based homojunctions suffer from a rather poor electrical characteristic and low time stability [1].

Nitrogen, as a group V element with the ionic radius very similar to the one of oxygen, has been regarded as the best candidate for a p-type dopant in ZnO. However, the p-type conductivity of ZnO:N material is usually not stable in time and obtained homojunctions lose their rectification behavior even after a few days [2]. Recently N and Al co-doping has been reported as an effective way to achieve p-type conductivity in ZnO [3]. Theoretical investigations show that (N, Al) co-doping leads to the formation of (Al-2N) acceptor complexes with ionization energy lower than that of the single nitrogen acceptor [4].

In this work we present the ZnO homo-junction fabricated by Atomic Layer Deposition with p-type ZnO achieved by nitrogen and aluminium co-doping. ZnO films were grown using diethylzinc and water precursors. Nitrogen has been introduced to the ZnO films during the ALD growth process by replacing the water precursor with the ammonia water one at every fourth ALD cycle, which resulted in 0.15% of nitrogen content in the grown films. As an aluminum precursor we used trimethylaluminium, which was introduced alternately with diethylzinc. We investigated ZnO:N films with aluminum content at the level of 1% as measured with EDS. All deposited layers of ZnO (p-ZnO and n-ZnO) are obtained at low (100°C) temperature. The ZnO:(N, Al) films show hole conductivity type without any post-growth treatment on the contrary to ZnO:N films obtained in the same technology, which require post-growth annealing to achieve p-type conductivity. The concentration of acceptors is up to  $10^{18}$  cm<sup>-3</sup> with hole mobility varying between 1 to 6 cm<sup>2</sup>/Vs. The ZnO-ALD based homojunction obtained with Al and N co-doping exhibits good technical characteristics ( $I_{ON}/I_{OFF}$  at the order of  $4 \times 10^4$ ). Noteworthy, it is obtained in one technological ALD process at low temperature which makes it an interesting device for applications in transparent organic electronics.

[1] Z.P. Wei, Y.M. Lu, D.Z. Chen, Z.Z. Zhang, B. Yao, B.H. Li, J.Y. Zhang, D.X. Zhao, X.W. Fan, Z.K. Tang, Appl. Phys. Lett. 90, 042113 (2007)

[2] J.G. Lu, S. Fujita, T. Kawaharamura, H. Nishinaka and Y. Kamada, Phys.stat.sol(c) 5, 3088 (2008)

[3] G.D. Yuan, Z.Z. Ye, L.P. Zhu, Q. Qian, B.H. Zhao, R.X. Fan, C.L. Perkins, S.B. Zhang, Appl. Phys. Lett. 86, 202106 (2005)

[4] X.M. Duan, C. Stampfl, M.M. Bilek, D.R. McKanzie, Phys. Rev. B 79, 235208 (2009)

The Authors [D.S., E.G. and K.K. and P.D.] were supported by the Polish NCN project DEC-2012/07/B/ST3/03567 and the author T.A.K. was supported by the Polish NCN project DEC-2013/09/D/ST5/03879.

**Thursday September, 17 - Oral Session - ThC**

**13:45-15:15**

**Photovoltaic 2**

Chair: Henri Mariette, *Institut Néel (France)*

## Progress in Polycrystalline CdTe PV Beyond 21%

Markus Gloeckler

First Solar, Inc., Perrysburg, Ohio, USA

In 2015, First Solar announced a record cell efficiency of 21.5% and record module efficiency of 18.6%. The module efficiency is 2% higher than the 16.7% cell result by Wu et al. [1], which held the cell record for over 10 years and was believed by many to be the highest achievable efficiency for polycrystalline CdTe. Starting in 2011, with the announcement of a 17.3% cell by First Solar, a frenzy of new records was started [2], which was initially fueled by competition and later by collaboration [3] between First Solar and General Electric research teams.

The record cell efficiency is higher than the current multi-crystalline Si efficiency record [4] and yet has higher upside relative to fundamental and practical limits of single-junction energy conversion. The paper will review the areas of progress achieved in the past five years and compare the progress against fundamental limits and secondary device metric. The future of CdTe technology remains bright with upside demonstrated on individual metrics such as short-circuit current, fill factor, or lifetime. Open-circuit voltage is key to this next frontier of the technology and the least understood due to the complexity of defect structure and multitude of recombination sources. Simple models can be used to predict toward efficiency up to 25%, at which point polycrystalline CdTe would match very high quality MBE-grown single-crystal efficiencies of GaAs.

[1] Wu X, Keane JC, Dhere RG, DeHart C, Duda A, Gessert TA, Asher S, Levi DH, Sheldon P, Proceedings of the 17<sup>th</sup> European PV Solar Energy Conf., Munich, 22-26 October 2001; 995-1000

[2] Markus Gloeckler, Igor Sankin, and Zhibo Zhao, 39th IEEE Photovoltaic Specialists Conference, June 16-21, 2013, Tampa, Florida, USA

[2] First Solar, Inc., press release, August 6<sup>th</sup>, 2013. [http://investor.firstsolar.com/release\\_detail.cfm?ReleaseID=783197](http://investor.firstsolar.com/release_detail.cfm?ReleaseID=783197)

[4] Green MA, Emery K, Hishikawa Y, Warta W, Dunlop ED, Prog. Photovolt: Res. Appl., **23**, 805-812 (2015)

## Chemical engineering of CdTe and Cd<sub>x</sub>Zn<sub>1-x</sub>Te surfaces in aqueous HBr/Br<sub>2</sub> solutions

A-Vallée<sup>1</sup>, I. Gérard<sup>1</sup>, Tommy Vairon<sup>1</sup>, L. Mollard<sup>2</sup>, J. Baylet<sup>2</sup>, J. Vigneron<sup>1</sup>, M. Bouttemy<sup>1</sup>  
and A. Etcheberry<sup>1,\*</sup>

<sup>1</sup> Institut Lavoisier Versailles, UMR CNRS-UVSQ 8180, Université de Versailles St Quentin  
en Yvelines, 45 ave des Etats Unis 78035 Versailles, France

<sup>2</sup> CEA, LETI, 17 rue des Martyrs, 38054 Grenoble, France

E mail : arnaud.etcbeberry@uvsq.fr

In this work, the surface modification of CdTe (CT) and CdZnTe (CZT) surfaces using a HBr/Br<sub>2</sub> chemical etching is studied. A multi-scale characterization of the surface composition and morphology is performed enabling for a precise description of the surface evolution combining large area and local considerations. SEM and AFM observations reveal the surface topography modification after aqueous bromine etching with the formation of nanometric pillars randomly dispersed on the surface. AFM phase contrast images suggest a chemical heterogeneity. XPS and Auger characterizations determine the global and local surface composition immediately after the HBr/Br<sub>2</sub> treatment and after ageing of the surfaces. XPS show an oxide free surface, just after the treatment, with a tellurium excess due to the presence of elemental Te (Te<sup>0</sup>). The XPS and ARXPS analyses of the same sample surface after air ageing evidence an additional ultra- thin layer which seems mainly ascribed to a direct oxidation of the CZT matrix with the formation of a thin Cdox-Teox mixed layer, the oxidation of the surface happening mainly in-between the pillars. The nano-Auger local analyses (14nm spot size) enable to separately analyze the pillars and surroundings. It shows that the extreme surface of the pillars is only composed of Te whereas, around the pillars, the surface is constituted of a Cd and Te rich mixture. This is in agreement with AFM phase contrast images which suggest a chemical heterogeneity. Based on these complementary results, we propose a schematic kinetic mechanistic model of the complex structuration of the CZT surface after HBr/Br<sub>2</sub> etching and ageing, with pillars covered by Te<sup>0</sup> and surrounded by a Cd-Te oxide mixture. The complementary use of reductive solutions just after the bromine treatment enables to eliminate the Te<sup>0</sup> on top of pillars while conserving the topography of the surface. This surface structuration (with or without Te<sup>0</sup>) is particularly interesting as it represents a direct mean to prepare contacts for Cd(Zn)Te based solar cells or others devices with specific surface morphology and chemical modulation.

## Valence band offsets between CdX (X=S,Se,Te) and CdCl<sub>2</sub>

Mark Lundie and Stanko Tomić\*

Joule Physics Laboratory, University of Salford, Manchester M5 4WT, UK

\*E-mail: s.tomic@salford.ac.uk

Recent advances in synthesis of colloidal quantum dot (QD) make possible the design of complex core/shell structures in order to alternate the interfaces between QD and the colloid. In this way fundamental QD properties that rely on the interplay between quantum confinement, Coulombic interaction between charges and dielectric confinement can be tailored to provide for desired functionalities of optoelectronic devices like solar cells, semiconductor lasers or single photon sources in quantum information processes. It has been found recently that the QD surface treatment with CdCl<sub>2</sub> dramatically increases the yield from Cd-based multi-exciton generation (MEG) solar cells [1]. However very little is known about the band alignment and the nature of the conduction and valence band offset across the CdX (X=S, Se, Te) and CdCl<sub>2</sub> interface [2]. We demonstrate our methodology on CdTe/CdCl<sub>2</sub> interface. Band alignments across the interface between two semiconducting materials are influenced by two effects: (1) “chemical” alignment that provides information on the position of the edges relative to the common chemical potential, and (b) “mechanical” or “strain” component of the alignment which is due to lattice mismatch between the two crystals forming the interface. As a first step we use all electron basis approach in the ab initio density functional theory (DFT), as implemented in the CRYSTAL code [3]. From that we compare the Kohn-Sham eigenvalue spectra of the constituent materials to align the Cd (which is common cation on both sides of the interface) 1s core state as a reference level. We have found that CdTe/CdCl<sub>2</sub> forms type I band alignment with the top of unstrained CdCl<sub>2</sub> valence band at 1.37 eV below the CdTe VB edge. It is also worth mentioning that the energy gap of CdCl<sub>2</sub>, estimated by hybrid B3LYP DFT [4], is 5.7 eV. As a second step we form a model heterojunction from CdTe [111] and CdCl<sub>2</sub> [001] surfaces. In plane lattice mismatch is estimated to be 11%. This choice of interface both minimizes the lattice mismatch and preserves the greatest symmetry. From the planar average microscopic and macroscopic electrostatic potentials across the interface [5], we have found the strained valence band offset to be 1.91 eV, where VBE is measured again relative to the bulk macroscopic potentials. Our analysis for the first time estimated the valence band offsets between CdX (X=S,Se,Te) and CdCl<sub>2</sub> and reveal qualitatively its character and distinguish quantitatively both chemical and mechanical contributions to VBO. We will discuss effect of piezoelectric field and spontaneous polarization on VBO too.

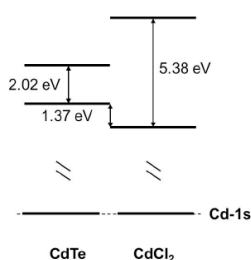


Fig 1 Chemical VBO between CdTe and CdCl<sub>2</sub>

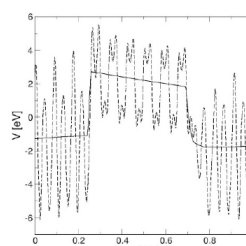


Fig 2 Micro and macroscopic average of electrostatic potentials across CdTe/CdCl<sub>2</sub> interface.

- [1] Robert C. Page et al, *Small*, 2014, DOI: 10.1002/smll.201402264
- [2] M.A. Lourenco, W.L. Ng, K.P. Homewood, K. Durose, *Appl. Phys. Lett.* **75**, 277 (1999)
- [3] I.J. Bush, S. Tomić, B.G. Searle, et al, *Proceedings of the Royal Society A* **467**, 2112 (2011)
- [4] S. Tomić, B. Montanari, and N.M. Harrison, *Physica E* **40**, 2125 (2009)
- [5] A. Baldereschi, S. Baroni, and R. Resta, *Phys. Rev. Lett.* **61**, 734 (1988)

## Molecular Beam Epitaxy of Short-Period Zn(S)Se/CdSe/In<sub>0.3</sub>Ga<sub>0.7</sub>As Superlattices with the Effective Bandgap Energy of 2.1-2.2 eV

S.V. Sorokin\*, G.V. Klimko, E.A. Evropeytsev, S.V. Gronin, I.V. Sedova, A.A. Sitnikova, A.A. Toropov, and S.V. Ivanov  
Ioffe Institute, 194021, Politekhnicheskaya 26, St.-Petersburg, Russia  
\*E-mail: sorokin@beam.ioffe.ru

One of the promising applications of wide-gap II-VI compounds is realization of the widest gap cascade in the heterovalent multijunction solar cells (SC) based on Ge-A<sup>3</sup>B<sup>5</sup> [1]. The using of In<sub>x</sub>Ga<sub>1-x</sub>As (x~0.3) metamorphic buffer layer (MBL) in such SCs to accommodate the lattice mismatch between the Ge substrate and the In<sub>x</sub>(Al,Ga)<sub>1-x</sub>As cascades, having the optimum  $E_g$  values of 1.0 and 1.4 eV, potentially allows realization of 4-junction SCs with the conversion efficiency of more than 55% (under AM0:500 suns conditions), if the upper wide gap cascade has  $E_g=2.0-2.1$ eV. In this case, the short-period CdSe/Zn(S)Se superlattices (SLs) grown coherently on InGaAs with the independently varied effective bandgap ( $E_g^{eff}$ ) and lattice constant are considered as a perspective material for the wider-gap cascade.

The paper presents the results on molecular beam epitaxy (MBE) growth of In<sub>x</sub>Ga<sub>1-x</sub>As MBLs with low density of threading dislocations on GaAs (001) substrates as well as reports on MBE growth of the CdSe/Zn(S)Se SLs having  $E_g^{eff}=2.1-2.2$ eV on the In<sub>0.3</sub>Ga<sub>0.7</sub>As "virtual substrates". The structural properties of linearly graded (with the rate of 30mol.% In/μm) In<sub>x</sub>Ga<sub>1-x</sub>As MBLs, which are the key element of the SCs, were studied in detail by X-ray diffraction (XRD) and transmission electron microscopy (TEM) techniques. The data on XRD reciprocal space mapping suggest that the optimum feedback step in the In content ( $\Delta x$ ) of the linearly graded In<sub>x</sub>Ga<sub>1-x</sub>As MBL is in a good agreement with calculations reported in Ref. [2].

The CdSe/Zn(S)Se SL structures were grown coherently on the In<sub>0.3</sub>Ga<sub>0.7</sub>As "virtual substrates" by MBE at  $T_S\sim 250-280^\circ\text{C}$  using a double-chamber setup (SemiTEq, Russia). The sulfur content in SLs was varied from  $x=0$  to  $x=0.3$ . The thicknesses of the SL layers provided the strain balance between the tensile-strained Zn(S)Se and compressively strained CdSe layers. The sulfur-free CdSe/ZnSe SLs look more preferable taking account of the higher growth temperature and better reproducibility. In contrast to the CdSe/Zn(S)Se SLs lattice-matched to GaAs [3,4], the effective bandgap of the {CdSe/Zn(S)Se}/In<sub>0.3</sub>Ga<sub>0.7</sub>As SLs can be lowered down to the 2.1 eV range corresponding to the calculated maximum of the 4-junction SC efficiency. However, the calculations carried out in the envelope function approximation predict that the lowest value of the CdSe/ZnSe SL  $E_g^{eff}$  is limited to ~ 2.15 eV only due to the steep narrowing of the heavy-hole miniband width (< 10 meV), which hinders the vertical transport of photo-excited carriers in the SLs. Alternatively, the main disadvantage of the CdSe/ZnS<sub>0.3</sub>Se<sub>0.7</sub> SLs is low  $T_S\sim 250^\circ\text{C}$  which is governed by the temperature dependence of S incorporation coefficient. Good agreement between the calculated and experimental SL parameters has been demonstrated. The studies of crystalline quality of the {CdSe/Zn(S)Se}/In<sub>0.3</sub>Ga<sub>0.7</sub>As SLs by using XRD and TEM techniques as well as the results on p-type doping of the SLs using a nitrogen plasma source will be presented. This work was supported by the Ministry of Education and Science of RF (project #14.604.21.0008 from 17.06.2014 with the applied research unique identifier RFME-FI60414X0008).

- [1] M.A. Green, K. Emery, Y. Hishikawa, W. Warta and E.D. Dunlop, Prog. Photovolt: Res. Appl. **21**, 1 (2013)
- [2] A. Sacedón et al., Appl. Phys. Lett. **66**, 3334 (1995)
- [3] E.A. Evropeytsev et al., Acta Phys. Polonica A **126**(5), 1156 (2014)
- [4] S.V. Sorokin et al., J. Cryst. Growth, (2015) (in print) (<http://dx.doi.org/10.1016/j.jcrysgro.2015.02.007>).

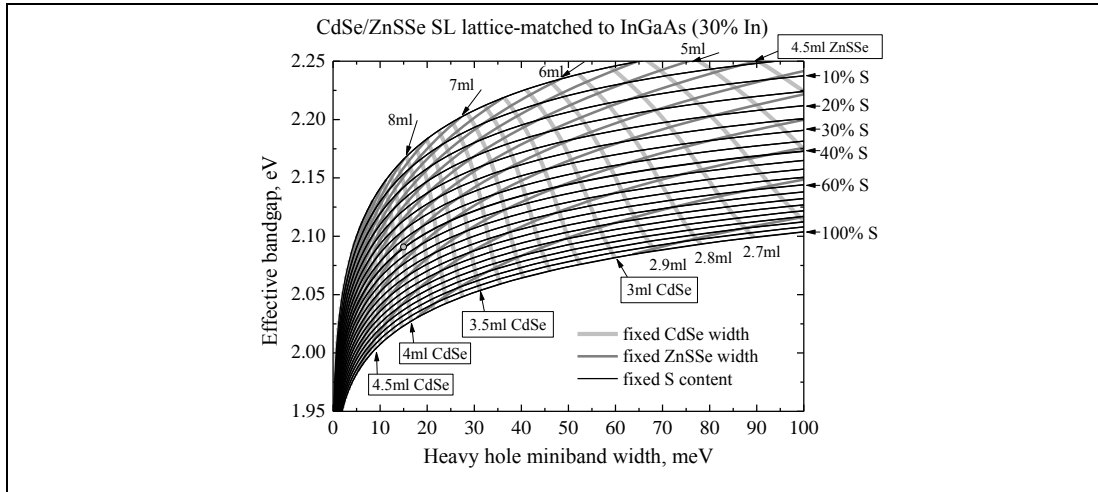


Fig 1. The parametric dependence of the effective bandgap and heavy-hole miniband width on the SL layer thicknesses and S content for CdSe/ZnSse SLs lattice-matched to  $In_{0.3}Ga_{0.7}As$ .

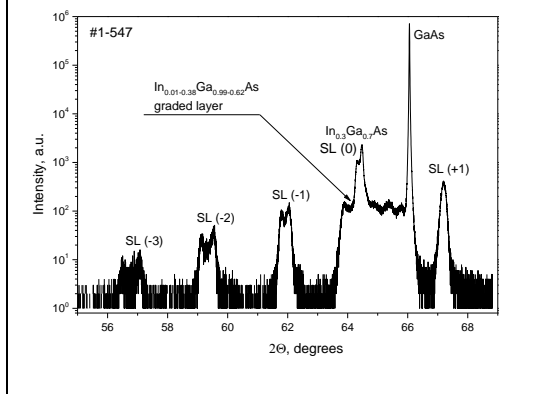


Fig 2. XRD curve of the structure with {CdSe-3.8ml/ZnSe-8ml} SL lattice-matched to  $In_{0.3}Ga_{0.7}As$

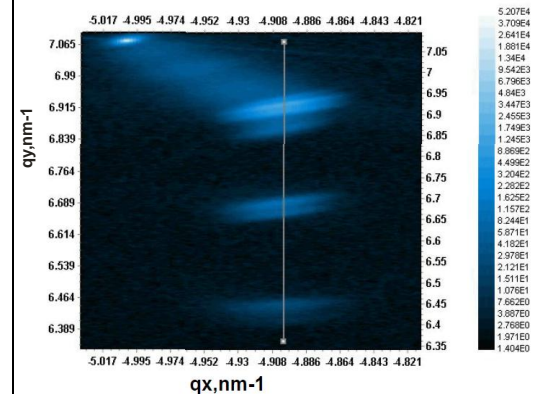


Fig 3. XRD reciprocal space mapping of the structure with {CdSe-3.8ml/ ZnSe-8ml} SL lattice-matched to  $In_{0.3}Ga_{0.7}As$

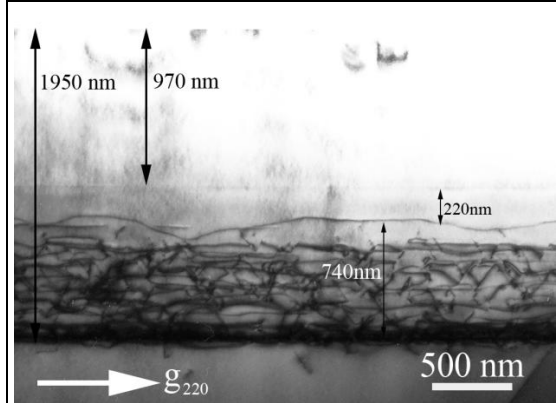


Fig 4. Cross-section TEM image of the structure with  $1\mu m$ -thick  $In_{0.3}Ga_{0.7}As$  layer grown on top of the linearly graded  $In_xGa_{1-x}As$  MBL

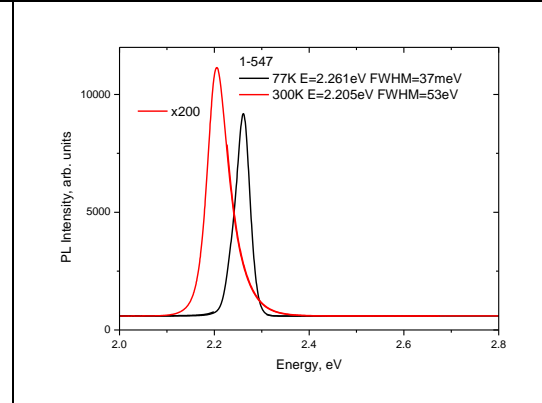


Fig 5. PL spectra of the structure with {CdSe-3.8ml/ ZnSe-8ml} SL lattice-matched to  $In_{0.3}Ga_{0.7}As$

## Four-Junction Heterovalent Solar Cells Based on II-VI/III-V/Ge Coherent and Metamorphic Heterostructures

A.A. Toropov\*, E.A. Evropeytsev, S.V. Sorokin, G.V. Klimko, S.V. Gronin, I.V. Sedova,  
V.S. Kalinovskii, E.V. Kontrosh, A.A. Usikova, N.D. Il'inskaya, and S.V. Ivanov  
Ioffe Institute, Politekhnikeskaya 26, 194021, St. Petersburg, Russia

\*E-mail: toropov@beam.ioffe.ru

Multijunction semiconductor heterostructures are currently among the best candidates for ultra-high efficiency concentrator solar cells (SCs). Current state-of-the-art SCs take advantage of triple-junction heterostructures based on III-V semiconductors and Ge or III-V semiconductors alone. The heterostructures can be either completely lattice-matched or use metamorphic buffer layers matching junctions with different lattice constants. In the former case, the SC performance is limited by the lack of a lattice-matched 1.0-1.3 eV bandgap semiconductor. On the other hand, the metamorphic structures suffer from increased defect density, which causes enhanced recombination losses. The efficiency of these monolithic SCs is limited by the value ~44% for terrestrial- and ~35% for space applications. Further improvement implies increasing the number of junctions that is hampered by the lack of suitable III-V semiconductors with wide enough bandgap. Note that application of wafer bonding technique has allowed recently fabrication of a four-junction III-V SC with the efficiency 46% [1].

In this paper we present original design and performance simulations of four-junction heterovalent SCs with monolithically integrated junctions based on Ge, III-V, and II-VI semiconductors. Furthermore, experimental results are reported, demonstrating ability of molecular beam epitaxy (MBE) to fabricate all key elements of such SC heterostructures grown atop of a Ge junction formed on a Ge substrate. Both lattice-matched and metamorphic designs are considered. The first one consists of two III-V junctions (InGaAs and InGaAlAs) and a II-VI junction (ZnCdSSe), grown pseudomorphically to Ge. In the metamorphic SC, all three junctions are grown pseudomorphically to a metamorphic  $\text{In}_{0.3}\text{Ga}_{0.7}\text{As}$  buffer deposited atop the Ge structure. The photoactive region of the II-VI junction in both structures is represented by a short-period alternately-strained CdSe/ZnSSe superlattice with its bandgap energy optimized within the 2.1-2.5 eV range. The performance calculations show that the developed optimized four-junction designs may have significant advantage over the existing monolithic three-junction ones. For the metamorphic SCs, the expected efficiency exceeds 46% for terrestrial applications (AM1.5, 500 suns) and can be as high as 44% for space applications (AM0, 500 suns). The pseudomorphic four-junction design also provides enhanced efficiency for space applications, while it is practically ineffective for terrestrial ones. Experimentally, most of the key components of the four-junction SCs are developed using a two-chamber MBE setup (SemiTEq) including a III-V and II-VI chambers interconnected by an ultrahigh-vacuum transfer module. In particular, we demonstrate possibility to produce the CdSe/ZnSSe superlattice providing simultaneously the required bandgap energy, efficient vertical transport of photoexcited carriers, and relatively low density of extended defects. The tunneling structures needed for efficient electrical interconnection of separate junctions are produced within the III-V part of the SC, using Si and Be as n- and p-type dopants, respectively, as well as the efficient InGaAs metamorphic buffer matching the lattice constants of Ge and  $\text{In}_{0.3}\text{Ga}_{0.7}\text{As}$ . Furthermore, as an intermediate result we developed the heterovalent III-V/II-VI SC, including the III-V photoactive junction and the n-type ZnSSe wide-bandgap-window/contact layer. Fabrication of the four-junction heterovalent SC is currently on the way. The work was supported by the Ministry of Education and Science of RF (Project #14.604.21.0008 of 17.06.2014 with ARUI - RFMEFI60414X0008).

[1] <http://www.ise.fraunhofer.de/en/press-and-media/press-releases/press-releases-2014/new-world-record-for-solar-cell-efficiency-at-46-percent>

**Thursday September, 17 - Oral Session - ThD**

**15:45-17:15**

**ZnO, Device**

Chair: Michael Lorenz, *Institut für Experimentelle Physik II, Universität Leipzig (Germany)*

## **Recent Progress on Electrically Pumped ZnO Lasers**

Jianlin Liu

Department of Electrical and Computer Engineering,  
University of California, Riverside, CA 92521, USA  
\*jianlin@ece.ucr.edu

Ultraviolet (UV) semiconductor lasers have many potential applications, such as photonics, information storage, and medical therapeutics. As a direct wide bandgap (3.3 eV) semiconductor material with a large exciton binding energy (60 meV) at room temperature, ZnO is an important candidate for UV lasers. Although a great deal of research effort has been spent on achieving optically pumped ZnO lasers, there lacks high-efficiency electrically pumped laser diodes. In this presentation, we report our recent progress on various electrically pumped ZnO lasers. These lasers include both thin film and nanowire based lasers. Both random lasers and Fabry-Perot (FP) lasers will be reported.

## 10 GHz Operation of Schottky Diodes Based on IGZO

Jiawei Zhang<sup>1</sup>, Qian Xin<sup>2</sup>, and Aimin Song<sup>1,2\*</sup>

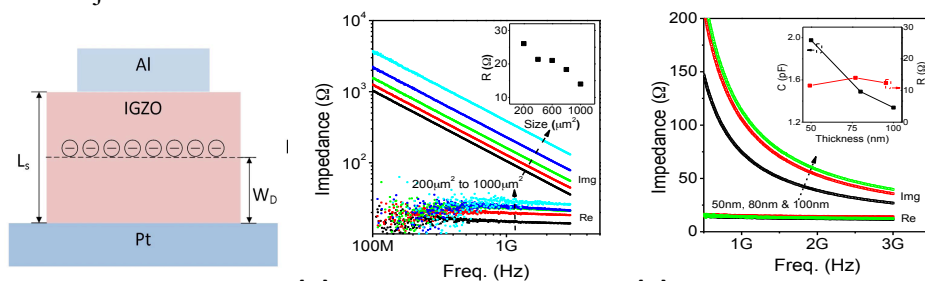
<sup>1</sup>School of Electrical and Electronic Engineering, University of Manchester, Manchester, United Kingdom

<sup>2</sup>School of Physics, Shandong University, Jinan, China

\*A.Song@manchester.ac.uk

Amongst the available amorphous semiconductor films that are suitable for large-area electronics, IGZO has shown perhaps the most commercial potential due to its high electron mobility and possibility of low-temperature film deposition on glass or plastic substrates. So far, however, most efforts have been focused on IGZO-based thin-film transistors, and very limited attention has been paid on Schottky diodes. On the other hand, metal-IGZO Schottky diodes can be used in a variety of other devices such as metal semiconductor field effect transistors (MESFETs), radio-frequency harvesters, and switch elements in memory arrays.

It has long been envisaged that transparent or semi-transparent mobile phones may one day be built on a glass substrate. To achieve this, the most speed-demanding components in such a phone, namely the front-end diode, needs to operate at 2.45 GHz to cover cellular communications, Bluetooth and IEEE 802.11b/g/n WiFi frequency bands. Even more desired is an even higher speed of 5 GHz in order to cover the newest 4G LTE band at 3.8 GHz and 802.11a/h/j/n/ac WiFi channels at 5 GHz.



Schematic of the IGZO diode structure, and the curves of reactance and resistance versus frequency that are obtained from S-parameter of the device, in log and linear scales, respectively.

Previous publications have shown that IGZO-based Schottky diodes are able to operate at radio frequencies. The most recently achieved speeds of IGZO Schottky diodes include 900 MHz in 2012,<sup>1</sup> 1.8 GHz in 2013,<sup>2</sup> and 3 GHz in 2014.<sup>3</sup> However, this is still short of the speed requirement for the newest 4G network and WiFi channels. In this work, we demonstrate the first IGZO Schottky diode fabricated at room temperature on glass substrate that operates beyond 10 GHz. First, we analyze the characteristics of Schottky diodes on glass substrates with different IGZO thicknesses, deposition conditions, and device area sizes in a coplanar mesa structure. The cut-off frequencies of the diodes are then extracted from their S-parameters. The crossing point of the extrapolated reactance and resistance curves yield diode speeds as high as 10.2 GHz, which is to the best of our knowledge the highest achieved to date in IGZO-based diodes. Finally, we study the low-frequency noise of the Schottky diodes and show that it exhibits  $1/f$  behavior. Analysis reveals that the noise follows mobility fluctuation model in the thermionic emission limited region and Hooge's empirical theory in the series resistance limited region. The demonstrated low noise properties are ideal in applications as switch elements in memory devices, photosensors, and mixer diodes.

- [1] A. Chasin, et al., Proceedings of 2012 IEEE International. Electron Devices Meeting (IEDM).
- [2] A. Chasin, et al. IEEE Transactions on Electron Devices, 60, 3407-3412 (2013).
- [3] A. Chasin, et al. IEEE Transactions on Electron Devices, 61, 3289-3295 (2014).
- [4] Jiawei Zhang, Linqing Zhang, Xiaochen Ma, Josh Wilson, Jidong Jin, and Aimin Song, to be published.

## Resistive-switching Memory and Ultraviolet Light-emitting Diodes Based on ZnO related Materials

Yichun Liu,\* Haiyang Xu, Jiangang Ma, Zhongqiang Wang, Weizhen Liu  
Key Laboratory for UV Light-Emitting Materials and Technology of Ministry of Education,  
Northeast Normal University, Changchun, China

\* ycliu@nenu.edu.cn

Wide band gap (3.37 eV) and high exciton binding energy (60 meV) make ZnO a promising candidate for ultraviolet (UV) light-emitting diodes (LEDs) and low-threshold lasing diodes (LDs). Recently, doping and alloying techniques of ZnO-based materials extends their applications into some novel optoelectronic fields such as RRAM and memristor. Herein, we will present our recent studies on ZnO-based RRAM and UV LEDs.

Firstly, we will discuss our group's recent progress in the developing RRAM and synaptic emulation. Our study shows that the performance of ZnO-based RRAM devices can be improved by introducing Ag nanoclusters into the switching layer.<sup>[1]</sup> The enhanced local electric field around Ag NCs leads to the localization of resistive switching sites, which is responsible for improving memory device performance. On the other hand, we also demonstrated the synaptic emulation based on dual-layer InGaZnO devices. Several essential learning abilities of synapse can be achieved, including the nonlinear transmission characteristic, synapse plasticity, long-term/short-term plasticity, and learning behavior with experience. The physical mechanism of device operation, which does not strictly follow the memristor model, has been attributed to oxygen ion migration and diffusion. A correlation between short term memory and ion diffusion is established by studying the temperature dependence of the relaxation processes of short-term plasticity and ion diffusion.<sup>[2]</sup>

Secondly, size-controlled ZnO-based nanostructures (e.g. ZnO/MgZnO core/shell nanowires, ZnO/MgO core/shell nanowires and MgZnO/MgO strained multi-quantum-well nanorods) were fabricated by hydrothermal synthesis and pulsed laser deposition (PLD) technique. Based on these nano-heterostructures, two types of heterojunction LEDs, including MIS and PN junctions, were demonstrated. The PN-heterojunction LEDs employing ZnO/MgZnO core/shell nanowire arrays as active layers show higher efficiency and stability than the one using bare ZnO nanowire array.<sup>[3]</sup> While, electrically pumped near-UV random lasing was achieved in the MIS-heterostructure devices that based on ZnO/MgO core/shell nanowire array. To further improve internal quantum efficiency and light-extraction efficiency of the LEDs, localized surface plasmon of Ag nanoparticles were introduced into above two kinds of devices. By optimizing structural parameters, the UV EL efficiency and spatial distribution uniformity were remarkably improved due to a combined effect of exciton-LSP coupling and photon-LSP coupling.<sup>[2, 3]</sup> Additionally, by employing thin Cu sheets as bottom electrodes, the emission efficiencies of both LEDs and LDs were greatly improved due to the good thermal dissipation of Cu.

- [1] Z. Q. Wang, H. Y. Xu\*, L. Zhang, X. H. Li, J. G. Ma, X. T. Zhang and Y. C. Liu\*, *Nanoscale*, 5, 4490, (2013).
- [2] Z. Q. Wang, H. Y. Xu\*, X. H. Li, H. Yu, Y. X. Liu, Y. C. Liu\*, Z. J. Zhu, *Adv. Funct. Mater.*, 22(13), 2759(2012).
- [3] W. Z. Liu , H. Y. Xu, J. G. Ma , C. Y. Liu, Y. X. Liu, Y. C. Liu, *Appl. Phys. Lett.*, 100, 203101 (2012).
- [4] C. Y. Liu, H. Y. Xu, Y. Sun, J. G. Ma, Y. C. Liu, *Opt. Express*, 22, 16731 (2014).
- [5] C. Zhang, C. E. Marvinney, H. Y. Xu, W. Z. Liu, C. L. Wang, L. X. Zhang, J. N. Wang, J. G. Ma, Y. C. Liu, *Nanoscale*, 7, 1073 (2015).

## ZnO-Based Avalanche Photodetectors

C. X. Shan

<sup>1</sup> State Key Laboratory of Luminescence and Applications, Changchun Institute of Optics, Fine Mechanics and Physics, Chinese Academy of Sciences, Changchun 130033, China

<sup>2</sup> Department of Physics, Zhengzhou University, Zhengzhou 450001, China

Email: [shancx@ciomp.ac.cn](mailto:shancx@ciomp.ac.cn)

Zinc oxide (ZnO) has a wide bandgap of 3.37 eV and relatively large electron saturation velocity and high resistance to irradiation, which makes it a promising candidate for ultraviolet (UV) photodetection. There have been many reports on ZnO-based UV photodetectors including metal-semiconductor-metal, Schottky, photoconductive type have been reported in recent years. Nevertheless, to realize both high gain and high response speed, avalanche structure is almost indispensable. However, since the efficient *p*-type doping of ZnO is still a huge challenging issue, none report on ZnO-based avalanche photodetectors has been demonstrated before.

In this presentation, Au/MgO/ZnO structures have been designed and prepared, by applying a bias onto the structures, carrier impact ionization will occur in the MgO layer due to its high resistivity, and carrier multiplication will be induced in the impact ionization process. By separating the multiplied carriers, ZnO-based avalanche photodetectors have been realized for the first time. Furthermore, by injecting the holes generated in the impact ionization process into ZnO, intense emission resulting from the recombination of the injected holes and the residual electrons in the ZnO has been observed.

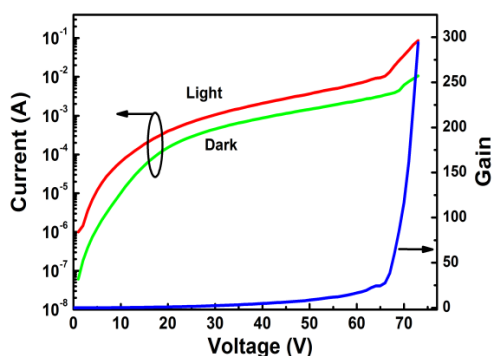


Fig. 1 Current-voltage curve of the Au/MgO/ZnO structured avalanche photodetectors under dark and illumination.

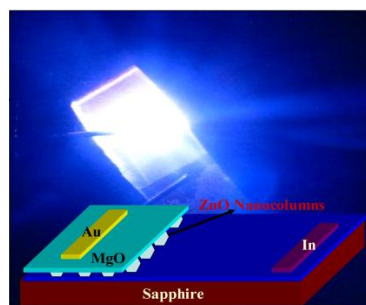


Fig. 2 The structural illustration and emission image of the Au/MgO/ZnO nanostructure devices.

- 【1】 H. Zhu, C.X. Shan, J. Y. Zhang, Z. Z. Zhang, B. H. Li, D. X. Zhao, B. Yao, D. Z. Shen, X. W. Fan, Z. K. Tang, X. H. Hou, K. L. Choy, *Adv. Mater.* 22, 1877 (2010).
- 【2】 H. Zhu, C. X. Shan, L. K. Wang, J. Zheng, J. Y. Zhang, B. Yao, D. Z. Shen, *J. Phys. Chem. C* 114, 7169 (2010).
- 【3】 J. Yu, C. X. Shan, X. M. Huang, X. W. Zhang, S. P. Wang, D. Z. Shen, *J. Phys. D: Appl. Phys.* 46, 305105 (2013).
- 【4】 J. Yu, C. X. Shan, H. Shen, X. W. Zhang, S. P. Wang, D. Z. Shen, *Chin. Phys. B* 22, 077307 (2013).
- 【5】 J. Yu, C. X. Shan, J. S. Liu, X. W. Zhang, B. H. Li, D. Z. Shen, *Phys. Status Solidi RRL* 7, 425 (2013).
- 【6】 X. Y. Liu, C. X. Shan, S. P. Wang, H. F. Zhao, D. Z. Shen, *Nanoscale* 5, 7746 (2013).

## High Performance Indium-Gallium-Zinc-Oxide-Based Schottky Diodes Fabricated at Room Temperature

Qian Xin<sup>1</sup>, Linlong Yan<sup>1</sup>, Lulu Du<sup>1</sup>, Yi Luo<sup>1</sup>, and Aimin Song<sup>1,2,\*</sup>

<sup>1</sup>School of Physics, Shandong University, Jinan, China

<sup>2</sup>School of Electrical and Electronic Engineering, University of Manchester, Manchester, United Kingdom

\*A.Song@manchester.ac.uk

Amorphous metal oxides semiconductors, particularly In-Ga-Zn-O (a-IGZO), have attracted great attention due to their superior properties, such as high electron mobility ( $> 10 \text{ cm}^2/\text{Vs}$ ), excellent optical transparency in visible light region, large-area uniformity, and long-term stability against bias stress by conventional sputtering methods even at room temperature. To date, most research on IGZO-based devices has focused on thin-film transistors, but the effort on pn and Schottky diodes is yet much limited. Like transistor, diode is also a basic building block in most circuits. In many thin film electronics, e.g., radio frequency identification tags, solar cells, amplifiers, logic gates, as well as the recently developed oxide-semiconductor-based metal-semiconductor field-effect transistors (MESFETs), high quality Schottky contacts are crucial. So far, the limited studies on IGZO-based Schottky diodes generally focused on the device performance and the influences of thermal treatment, anode and cathode materials, and anode treatments for diodes with particular IGZO-thicknesses (e.g. only one or two thicknesses) sputtered at particular oxygen contents (e.g. only 0 and 20%).<sup>1-3</sup> Systematic studies on the relationship between the preparation conditions (e.g. RF powers, various oxygen contents, various IGZO-thickness, etc) and the device characteristics, as well as the device characteristics at high reverse bias were rarely reported,<sup>4</sup> although these aspects are key factors for designing high quality applicable Schottky diodes.

We have systematically investigated the dependence of the performance of Schottky diodes with a structure of Pd/a-IGZO/Ti/Au on the preparation conditions. The a-IGZO layer was deposited by RF magnetron sputtering method. All diodes are fabricated on glass but at room temperature without any thermal treatment, so that the results are relevant to possible applications on flexible plastic substrate. During the sputtering process, various conditions including RF powers (50~130 W), oxygen content (0~15%), and thicknesses of a-IGZO layers (25~200 nm) were applied to probe the optimized process parameters. The results indicate that high performance Schottky diodes with high rectification ratio (e.g.  $\sim 10^7$ ), high barrier height (maximum 1.01 eV), low ideality factor (minimum 1.04), and high breakdown voltage ( $\sim 15 \text{ V}$  for the diode with 200-nm-IGZO) can be realized by using a-IGZO layers sputtered at relatively low RF powers ( $\leq 70 \text{ W}$ ) and oxygen content of  $\sim 2.5\text{-}5\%$ . The breakdown voltage shows no clear dependence on the RF powers and oxygen contents but a near linear dependence on the a-IGZO thickness. These results give important hints on designing high quality flexible a-IGZO based rectifying diodes and MESFETS, etc.

- [1] D. H. Lee, K. Nomura, T. Kamiya, and H. Hosono, *IEEE Electron. Dev. Lett.*, **32**, 1695 (2011).
- [2] A. Chasin, S. Steudel, K. Myny, M. Nag, T.-H. Ke, S. Schols, J. Genoe, G. Gielen, and P. Heremans, *Appl. Phys. Lett.*, **101**, 113505 (2012).
- [3] A. Chasin, E. Simoen, A. Bhoolokam, M. Nag, J. Genoe, G. Gielen, and P. Heremans, *Appl. Phys. Lett.*, **104**, 082112 (2014).
- [4] Q. Xin, L. Yan, Y. Luo, and A. Song, *Appl. Phys. Lett.*, **106**, 113506, (2015).

**Friday September, 18 - Oral Session - FrA**

**08:30-10:00**

**Optical and Excitonic properties**

Chair: Irina Buyanova, *Linköping University (Sweden)*

## Second-Harmonic Generation Spectroscopy of Excitons in ZnO

V. V. Pavlov<sup>1\*</sup>, M. Lafrentz<sup>2</sup>, D. Brunne<sup>2</sup>, A. V. Rodina<sup>1</sup>,  
R. V. Pisarev<sup>1</sup>, D. R. Yakovlev<sup>1,2</sup>, A. Bakin<sup>3</sup>, and M. Bayer<sup>2</sup>

<sup>1</sup>Ioffe Physical-Technical Institute, Russian Academy of Sciences, St. Petersburg, Russia

<sup>2</sup>Experimentelle Physik 2, Technische Universität Dortmund, Dortmund, Germany

<sup>3</sup>Institut für Halbleitertechnik, Technische Universität Braunschweig, Braunschweig, Germany

\*pavlov@mail.ioffe.ru

In semiconductors the optical properties in close vicinity to the band gap are largely determined by excitons or electron-hole bound complexes. The exciton energy levels including their spin properties have been intensely studied using both linear and nonlinear optical methods such as absorption, reflection, photoluminescence, two-photon absorption, four-wave mixing, etc. However, the contributions of excitons to optical harmonics generation have remained essentially unexplored. Typically harmonics generation studies lack a microscopic theoretical explanation, with rare exceptions.

Among nonlinear optical phenomena, the most prominent is the coherent three-photon process of optical second-harmonic generation (SHG) [1]. We report results of a comprehensive experimental and theoretical study of the SHG in the noncentrosymmetric hexagonal wide-band-gap semiconductor ZnO in the photon energy range of 3.2–3.5 eV which comprises the exciton resonances. ZnO crystallizes preferably in the wurtzite-type hexagonal structure, having the noncentrosymmetric point group  $6mm$  for which SHG is allowed in the electric-dipole approximation. Hexagonal ZnO is characterized by a large exciton binding energy of 60 meV and a rich exciton level structure. Three exciton series are formed in ZnO by a  $\Gamma_7$  electron and a hole from one of the  $A(\Gamma_7)$ ,  $B(\Gamma_9)$ , or  $C(\Gamma_7)$  valence bands.

Resonant crystallographic SHG is observed for the  $1s(A, B)$ ,  $2s(A, B)$ ,  $2p(A, B)$ , and  $1s(C)$  excitons. We show that SHG signals at these exciton resonances can be induced by the application of an external magnetic field perpendicular to the incident and the SHG light wave vectors directed along the hexagonal  $z$ -axis of ZnO crystal. In this geometry the crystallographic SHG response vanishes. A microscopic theory of the exciton SHG is developed, which shows that the nonlinear interaction of coherent light with excitons has to be considered beyond the electric-dipole approximation. Depending on the particular symmetry of the exciton states the SHG can originate from the electric- and magnetic-field-induced perturbations of the excitons due to the Stark effect, the spin and orbital Zeeman effects, as well as the magneto-Stark effect [2, 3]. The importance of each mechanism is analyzed and discussed by confronting experimental data and theoretical results for the dependences of the SHG signals on photon energy, magnetic field, electric field, crystal temperature, and light polarization. A good agreement is obtained between experiment and theory proving the validity of our approach to the complex problem of nonlinear interaction of light with ZnO excitons. This general approach can be applied also to other semiconductors. Tailoring these symmetry reductions of the exciton level structure opens new degrees of freedom in the nonlinear spectroscopy of excitons.

This work was supported by the Deutsche Forschungsgemeinschaft, the Russian Foundation for Basic Research 15-52-12015 and the Government of the Russian Federation through the Program P220 14.B25.31.0025.

[1] M. Fiebig, V. V. Pavlov, R. V. Pisarev, *JOSA B* **22**, 96 (2005).

[2] M. Lafrentz, D. Brunne, B. Kaminski, V. V. Pavlov, A. V. Rodina, R. V. Pisarev, D. R. Yakovlev, A. Bakin, M. Bayer, *Phys. Rev. Lett.* **110**, 116402 (2013).

[3] M. Lafrentz, D. Brunne, A. V. Rodina, V. V. Pavlov, R. V. Pisarev, D. R. Yakovlev, A. Bakin, M. Bayer, *Phys. Rev. B* **88**, 235207 (2013).

## Spectroscopy of Trion states in non-polar ZnO Quantum Wells and their use to monitor Spin Injection

C. Morhain<sup>1\*</sup>, C. Deparis<sup>1</sup>, M. Teisseire<sup>1</sup>, B. Vinter<sup>1,2</sup>, J.-M. Chauveau<sup>1,2</sup>, J. Zúñiga-Pérez<sup>1</sup>

<sup>1</sup> Centre de Recherche sur l'Hétéro -Epitaxie et ses Applications, Centre National de la Recherche Scientifique (CRHEA-CNRS), Rue B. Gregory, F-06560 Valbonne Sophia Antipolis, France

<sup>2</sup> University of Nice Sophia Antipolis, Parc Valrose, F-06102 Nice Cedex 2, France  
\*cm@crhea.cnrs.fr

We have grown high quality non-polar m-plane ZnO/ (Zn,Mg)O quantum well (QW) heterostructures on ZnO substrates. The photoluminescence of the structures display narrow and well resolved lines from the QW emission. They are identified as the free exciton line, X, and the trion singlet ground state line, X<sub>S</sub>. We have performed the optical spectroscopy of these structures. Under external magnetic field, we could identify for the first time in ZnO QWs, the first excited states of the trions, X<sub>T</sub>, the first state having 2 electrons ferromagnetically aligned. We will report on the electronic structure and properties of the singlet, X<sub>S</sub>, and triplet states, X<sub>T</sub>.

In addition, ZnO QW heterostructures containing a thin (Zn,Mg,Mn)O spin aligner were grown, the ZnO QW acting as a spin detector. We demonstrate the successful electron spin injection into these structures. We will show that there is no possibility to analyze the spin injection in nonpolar ZnO QWs by studying the circular polarization of the emitted light, as traditionally done, for example, in spin LEDs. Instead, we propose to a different way of monitoring the spin injection which does not rely on circular polarization of the luminescence.

## Exciton-polariton thermodynamics in ZnSe-based microcavities

S. Klembt<sup>1\*</sup>, E. Durupt<sup>1</sup>, S. Datta<sup>2</sup>, T. Klein<sup>3</sup>, Y. Léger<sup>4</sup>, A. Baas<sup>1</sup>, C. Kruse<sup>3</sup>, D. Hommel<sup>3</sup>,  
A. Minguzzi<sup>2</sup>, and M. Richard<sup>1</sup>

<sup>1</sup>Institut Néel, CNRS-CEA-Université Grenoble Alpes, BP166, 38042 Grenoble, France

<sup>2</sup>CNRS-Université Grenoble Alpes, LPMMC, BP166, 38042 Grenoble, France

<sup>3</sup>IFP, Universität Bremen, Otto-Hahn-Allee NW1, 28359 Bremen, Germany

<sup>4</sup>CNRS, Laboratoire FOTON, Insa de Rennes, 35708 Rennes, France

\*Corresponding author: sebastian.klembt@neel.cnrs.fr

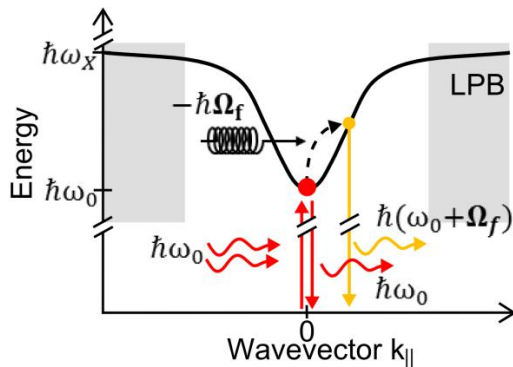
In the last two decades exciton-polaritons have attracted considerable interest since they allowed for fundamental understandings of light-matter interactions such as polariton Bose-Einstein condensation and superfluidity [1]. At high density, microcavity-polaritons constitute indeed a driven dissipative quantum fluid of half-light half-matter integer spin quasi-particles, which is embedded in a solid-state crystalline environment.

So far, the thermodynamic properties of polariton fluids have been mostly overlooked. An intriguing specificity of polariton condensates and superfluids is that they are in contact with three different reservoirs: the thermal phonon bath, the exciton bath and the electromagnetic vacuum. A first interesting question is whether heat can be transferred from the phonon bath to the polariton fluid.

To be able to study polariton thermodynamics, we use high-quality ZnSe-based microcavities, since they provide a large Rabi splitting of  $\hbar\Omega_R=29$  meV, low local disorder and Q-factors well above 5000, and allow to have access to a high temperature phonon bath (up to  $T=270$  K) interacting with stable microcavity-polaritons.

We show experimentally and theoretically that indeed phonons can be efficiently absorbed by inelastic scattering with polaritons. In this context we present a Raman spectroscopy based technique using anti-Stokes fluorescence (ASF) [2]. Resonant excitation of ground state polaritons ( $k_{\parallel} = 0, \hbar\omega_0$ ) and subsequent phonon absorption is used to optically extract thermal energy out of the system and thus cool it down. Owing to polariton's cavity-like dispersion, Stokes fluorescence (phonon emission) is fully inhibited while ASF is permitted and enhanced by the polariton's excitonic fraction (see Fig. 1). By carrying out angle-resolved Raman spectroscopy, we measured the cooling power generated by polariton ASF. We determine the temperature and laser power range where a net cooling rate is achievable. Our experiments show that the highest cooling power is achieved at an initial temperature of only 50 K [3].

The interaction between polariton condensates at temperatures up to  $T=270$  K with the respective phonon baths is also investigated in this context.



[1] I. Carusotto et al., Rev. Mod. Phys. 85, 299 (2013)

[2] P. Pringsheim, Z. Phys. A **57**, 739-746 (1929).

[3] S. Klembt et al., arXiv 1412.2630 (2014)

Figure 1: Diagram of polariton anti-Stokes scattering. Thermal phonons of average energy  $\hbar\Omega_f$  are absorbed by ground-state polaritons.

## Interaction of Tamm plasmons with cavity photons and excitons in ZnSe-based microcavities

SK. S. Rahman<sup>1\*</sup>, M. Cornelius<sup>1</sup>, T. Klein<sup>2</sup>, S. Klemmt<sup>2\*\*</sup>, C. Kruse<sup>2</sup>, D. Hommel<sup>2\*\*\*</sup>, J. Gutowski<sup>1</sup>, K. Sebald<sup>1</sup>

<sup>1</sup>Semiconductor Optics, <sup>2</sup>Semiconductor Epitaxy, Institute of Solid State Physics, University of Bremen, P.O. Box 330440, 28334 Bremen, Germany

\*rahman@ifp.uni-bremen.de

Cavity polaritons are formed via strong interaction between excitons and photons. These light-matter quasiparticles are extremely interesting for various optoelectronic applications including polariton lasers. ZnSe-based microcavities (MCs) are very promising to realize polariton-based devices at elevated temperatures due to the high oscillator strength and large binding energy of the exciton [1]. Electromagnetic modes called Tamm plasmons (TP) can be formed at the interface between a metallic layer and the distributed Bragg reflector (DBR) [2]. Their in-plane wave vector is close to zero, thus they can be excited via photons. In order to manipulate the light-matter interaction these TP can easily be obtained in our existing MC structures, since their formation doesn't require any complicated device processing steps.

In this contribution, we present the influence of TP on the optical properties of ZnSe-based MCs grown by molecular beam epitaxy. The investigated cold MCs consist of a 12-fold bottom DBR, a  $\lambda/2$  cavity and a 1.5-fold top DBR. Ag layers with thicknesses between 30 and 50 nm were deposited on the MC samples. Micro-reflectivity measurements on the cold MC covered by a 40 nm Ag layer show a blue shift of the cavity resonance by 36 meV compared to the metal-free areas, due to the influence of TP. When the top DBR layer thickness is reduced by chemically assisted ion-beam etching, the bare TP resonance can be observed besides the cavity resonance. The spectral position of TP can be tuned inside the stopband by further reducing the top DBR layer thickness. The observed energy shift of the cavity resonance and the tuning of the bare TP resonance can theoretically be reproduced by simulations based on the transfer matrix method. Furthermore, we will present the interaction of QW excitons with the bare TP resonance. For this investigation, we used an open cavity sample consisting of an 18-fold bottom DBR and a  $\lambda$  cavity including 3 ZnSe QWs. The TP resonance is formed in this sample by depositing a 35 nm Ag layer. At room temperature, the TP resonance is largely detuned from the QW energies. By changing the sample temperature, the QW emission can be tuned. An anticrossing is observed between the QW exciton and the TP resonance in temperature dependent micro-reflectivity measurements, being in good agreement with simulations. This is a clear indication for the strong coupling regime being achieved in this sample and showing a Rabi splitting of 18 meV. Our findings are very promising in order to realize electrically tunable polariton devices with a simple sample configuration. In addition, we will also present hybrid states of TP and exciton polaritons in a complete MC sample.

[1] K. Sebald, et al., Eur. Phys. J. B **84**, 381 (2011).

[2] M. Kaliteevski, et al., Phys. Rev. B **76**, 165415 (2007).

Current affiliation: \*\*Institute Néel, CNRS/UJF Grenoble, France; \*\*\*Institute of Experimental Physics, University of Wrocław and Wrocław Research Center EIT, Poland.

## Effect of parity in magneto-optical spectra of quantum wells

V.Kochereshko<sup>1,2</sup>, V.Kats<sup>1,2</sup>, A.Platonov<sup>1</sup>, L.Golub<sup>1</sup>, L.Besombes<sup>3</sup>, D.Woverson<sup>4</sup>, H.Mariette<sup>3</sup>

<sup>1</sup>*A.F.Ioffe Physical-Technical Institute, 194021, St. Petersburg, Russia*

<sup>2</sup>*Spin Optics Laboratory, St Petersburg State University, St. Petersburg, Russia*

<sup>3</sup>*Institut Neel, CNRS, Grenoble, France*

<sup>4</sup>*University of Bath, Bath, UK*

E-mail: [Vladimir.kochereshko@mail.ioffe.ru](mailto:Vladimir.kochereshko@mail.ioffe.ru)

We have studied reflectivity spectra in magnetic fields from heterostructures with wide quantum wells CdTe/CdZnTe and GaAs/AlGaAs. The well width was much larger than the exciton Bohr radius. In such wells quantization of the exciton center of mass motion was observed.

In the Vogt geometry,  $K \perp H$  the effect of “**magnetic field inversion**” was observed in which the reflection spectrum depends on the mutual direction of the exciton wave vector and the magnetic field [1].

In the Faraday geometry  $K \parallel H$  the “**effect of parity**” was found. This means that the increasing of magnetic field induces redistribution of intensities between even and odd exciton states. This redistribution depends on the polarization of the incident and reflected light. Such redistribution looks very unusual because the odd and even states should be absolutely equivalent to each other.

In the case if the incident light was circularly polarized and the circularly polarized components of the reflected light was analyzed, the normal Zeeman (Faraday) effect was observed in the spectra. (But as it was shown previously [2] the exciton Zeeman splitting was proportional to the kinetic energy of the exciton center of mass.) In the linearly polarized light when the incident light was polarized along the (110) axis and analyzed light was polarized along (110) or (1-10) we also observed normal Zeeman effect.

In the case if the sample was illuminated by linearly polarized light along (100) axis and the circularly polarized components of the reflected light was analyzed, the intensity of the lines of the even and odd states was depending on the sign of the circular polarization of the analyzed light. If you change the sign of the polarization, there was a redistribution of the intensity of the even and odd states. This effect was completely symmetric according to the changes of the polarization of the incident light from (100) to (010). The effect was also symmetric if the incident light was circularly polarized and linearly polarized component was detected.

The observed phenomenon is explained by the effect of magnetic field induced non-reciprocal birefringence [3]. That is, cubic crystal in a magnetic field in the Faraday geometry acquired properties of the uniaxial crystal and the direction of the optical axis depends on the sign of the magnetic field and exciton wave vector.

[1] D.G.Thomas and J.J.Hopfield // Phys.Rev.**124**, 657 (1961); E.F.Gross, B.P.Zakharchenia, O.V.Konstantinov // Sov.Phys. Solid State **3**, 305 (1961)

[2] J.J.Davies, D.Wolverson, V.P.Kochereshko, et al. // Phys. Rev. Lett. **97**, 187403 (2006)

[3] E.L.Ivchenko, V.P.Kochereshko, G.V.Mikhailov, I.N.Uraltsev // Phys.Stat.Sol. (b), **121**, 221 (1984)

## Laser Induced Tellurium Formation Detected by Coherent Phonon Excitation in Plasmonic Crystals

Lars E. Kreilkamp<sup>1\*</sup>, Martin Pohl<sup>1</sup>, Maciej Wiater<sup>2</sup>, Tomasz Wojtowicz<sup>2</sup>, Grzegorz Karczewski<sup>2</sup>, Boris A. Glavin<sup>3</sup>, Leonid Litvin<sup>4</sup>, Axel Rudzinski<sup>4</sup>, Michael Kahl<sup>4</sup>, Ilya A. Akimov<sup>1,5</sup>, Dmitri R. Yakovlev<sup>1,5</sup> and Manfred Bayer<sup>1</sup>

<sup>1</sup>Experimentelle Physik 2, Technische Universität Dortmund, D-44221 Dortmund, Germany

<sup>2</sup>Institute of Physics, Polish Academy of Sciences, PL-02668 Warsaw, Poland

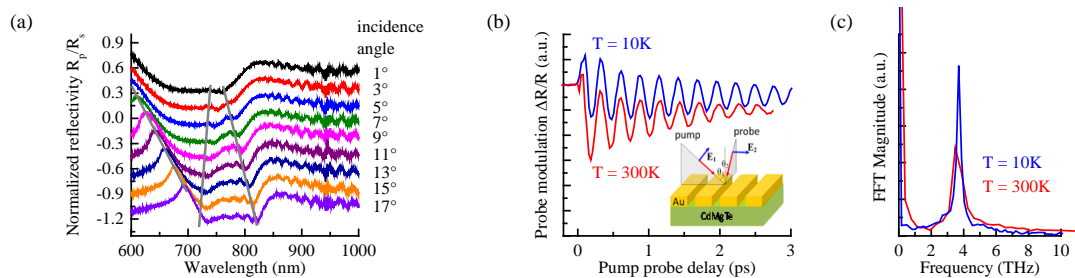
<sup>3</sup>Lashkaryov Institute of Semiconductor Physics, 03028 Kyiv, Ukraine

<sup>4</sup>Raith GmbH, Konrad-Adenauer-Allee 8, 44263 Dortmund, Germany

<sup>5</sup>A. F. Ioffe Physical-Technical Institute, Russian Academy of Sciences, 194021 St. Petersburg, Russia

\*lars.kreilkamp@tu-dortmund.de

Ultrashort-pulse lasers can be used to study the time-evolution of coherently excited vibrations in crystalline materials. When the pulse duration is considerably smaller than the period of an ionic vibration, impulsive excitation and subsequent phase-sensitive detection in the time domain can be achieved via pump-probe experiments. [1] In order to enhance the detection efficiency of such transient optical measurements, the electronic response near a surface plasmon polariton (SPP) resonance can be employed to probe small changes in the dielectric environment induced e.g. by the coherent motion of the crystal lattice. [2]



Here, we present the results of ultrafast time-resolved pump-probe studies in hybrid structures which consist of an epitaxially grown CdMgTe crystal capped with a one-dimensional gold grating. The patterning allows for the excitation of propagating SPPs at the metal-semiconductor interface which give rise to characteristic dispersive features in the reflectivity spectrum shown in Fig. 1(a). In Fig. 1(b) differential reflectivity transients of such a plasmonic crystal sample are presented. The signal shows pronounced oscillations with a frequency of 3.6 THz (see Fig. 1(c)), which we attribute to coherent oscillations of the  $A_1$  breathing mode of a thin Tellurium layer forming on the sample surface upon laser illumination, an effect that has been observed via CW micro-Raman experiments in several other II-VI compounds. [3] The build-up of this layer can be monitored over time by analyzing the change in oscillation amplitude and frequency during prolonged exposure to the pump beam. In contrast to the results obtained on the plasmonic sample, the oscillatory signal is barely visible when no gold grating is patterned onto the semiconductor. By performing polarization and energy resolved measurements and changing the angle of light incidence, we find that SPPs lead to the observed enhancement of both, impulsive excitation of coherent phonons and detection of crystal deformation in our structures.

[1] R. Merlin, *Solid State Communications* **102**(2–3), 207 – 220 (1997).

[2] Z. Chen and M. F. DeCamp, *Journal of Applied Physics* **112**(1), 013527 (2012).

[3] Wiedemeier et al., *Semicond. Sci. Technol.* **26**(10), 105023 (2011)

**Friday September, 18 - Oral Session - FrB**

**10:30-12:00**

**Dots and Nanowires 2**

Chair: Maria Chamarro, *Institut des NanoSciences de Paris (France)*

## Dangling Bond Magnetic Polaron in CdSe Nanocrystals

A.V. Rodina<sup>1\*</sup>, and Al. L. Efros<sup>2</sup>

<sup>1</sup>Ioffe Physical-Technical Institute, Russian Academy of Sciences, St. Petersburg, Russia

<sup>2</sup>Naval Research Laboratory, Washington DC, USA

\*anna.rodina@mail.ioffe.ru

We predict theoretically that non-magnetic CdSe nanocrystals may possess macroscopic momentums due to the formation of dangling-bond magnetic polarons. We suggest that interaction between excitons localized inside a CdSe nanocrystal and spins of dangling bonds at the nanocrystal surface activates the ground-state "dark" exciton radiative recombination by flipping the spins of the dangling bonds. At temperatures below critical, the unpolarized state of the exciton and of the dangling bond spins (DBSs) becomes unstable provided that the interaction between the electron spin and the DBS is ferromagnetic and that the rate of optical pumping of the DBSs is faster than the DBS relaxation rate. As result, the optical pumping of the nanocrystal and dangling-bond-assisted recombination of the dark exciton lead to dynamic polarization of the dangling bond spins and formation of the dangling-bond magnetic polaron. In turn, the formation of the dangling-bond magnetic polaron partly suppresses the dangling-bond-assisted radiative recombination of the dark exciton and leads to a temperature-dependent polaron contribution to the Stokes shift of the photoluminescence.

The dangling bond magnetic polaron model consistently explains experimentally observed low-temperature photoluminescence features of non-magnetic CdSe nanocrystals as manifestations of their spin-related magnetic properties.

## Magnetic Polaron Formation in (Cd,Mn)Te Quantum Dots inserted in ZnTe Nanowires

A. Artioli<sup>1,2\*</sup>, P. Rueda-Fonseca<sup>1,2,3</sup>, M. Orrù<sup>1,2,3</sup>, T. Cremel<sup>1,3</sup>, S. Klembt<sup>1,2</sup>, K. Kheng<sup>1,3</sup>,  
 F. Donatini<sup>1,2</sup>, E. Bellet-Amalric<sup>1,3</sup>, M. Den Hertog<sup>1,2</sup>, C. Bougerol<sup>1,2</sup>, J.-F. Motte<sup>1,2</sup>,  
 Y. Genuist<sup>1,2</sup>, M. Richard<sup>1,2</sup>, R. André<sup>1,2</sup>, E. Robin<sup>1,3</sup>, S. Tatarenko<sup>1,2</sup>, J. Cibert<sup>1,2</sup>  
 and D. Ferrand<sup>1,2</sup>

<sup>1</sup>Univ. Grenoble Alpes, F-38000 Grenoble, France

<sup>2</sup>CNRS, Institut Néel, F-38000 Grenoble, France

<sup>3</sup>CEA, INAC-SP2M, F-38000 Grenoble, France

\* Corresponding author: [alberto.artioli@neel.cnrs.fr](mailto:alberto.artioli@neel.cnrs.fr)

II-VI diluted magnetic semiconductor nanostructures have been studied, in the last 20 years, as model systems in spintronics [1]. The interest in using II-VI nanowires has recently increased thanks to the possibility to realize new attractive systems (core-shell heterostructures, multi-dot systems...) and the advantage to easily manipulate these structures allowing the combination of optical and transport measurements. Moreover, using the nanowire geometry, it is possible to have a stronger confinement and a better control of the quantum dot (QD) allowing a more efficient coupling between the photocarriers and the magnetic atoms [2].

We show, for the first time, the evidence of a magnetic polaron formation in (Cd,Mn)Te quantum dots inserted in ZnTe-(Zn,Mg)Te core-shell nanowires grown by molecular beam epitaxy [3,4]. Nanowires, transferred onto home-made Si<sub>3</sub>N<sub>4</sub> membranes using a ZEISS Cross Beam NVision 40 nano-manipulator, were studied by means of different techniques (Fig. 1). We used energy-dispersive X-ray spectroscopy (EDX) to check the insertion of the (Cd,Mn)Te QD (Fig. 1 (b)) and cathodoluminescence (CL) to characterize its emission energy (Fig. 1 (a)). Afterwards we performed a magneto-optical characterization of the QD emission to check the good Mn incorporation: these studies were done at different temperatures showing a clear Giant Zeeman Effect (Fig. 1 (c)). Temperature dependence (Fig. 1 (d)) and time resolved PL (to be shown in the presentation) shows a clear red shift both in temperature and in time: this is the sign of a ferromagnetic ordering of the Mn's spins in the (Cd,Mn)Te QD induced by photocarriers, a clear evidence of the magnetic polaron formation, first time observed in a nanowire geometry.

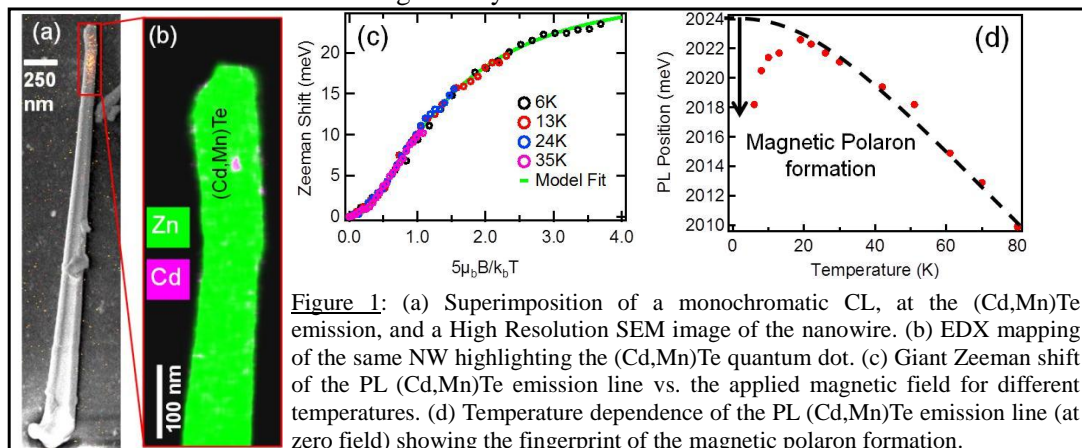


**Figure 1:** (a) Superimposition of a monochromatic CL, at the (Cd,Mn)Te emission, and a High Resolution SEM image of the nanowire. (b) EDX mapping of the same NW highlighting the (Cd,Mn)Te quantum dot. (c) Giant Zeeman shift of the PL (Cd,Mn)Te emission line vs. the applied magnetic field for different temperatures. (d) Temperature dependence of the PL (Cd,Mn)Te emission line (at zero field) showing the fingerprint of the magnetic polaron formation.

- [1] L. Besombes et al., *Int. J. of Nanotechnology* **7**, 641 (2010)  
 [2] L. Klopotoski et al., *Physical Review B* **83**, 081306(R) (2011)  
 [3] P. Rueda et al., *Nano Lett.* **14**, 1877 (2014)  
 [4] A. Artioli et al., *Appl. Phys. Lett.* **103**, 222106 (2013)

## Magneto-photoluminescence of Tellurium Isoelectronic Bound Excitons in Zn-Se-Te in the Presence of Type-II Submonolayer Quantum Dots

Siddharth Dhomkar<sup>1,6</sup>, Haojie Ji<sup>1,6</sup>, Vasilios Deligiannakis<sup>2,6</sup>, Jonathan Ludwig<sup>3,4</sup>, Dmitry Smirnov<sup>3,4</sup>, Carlos Meriles<sup>5,6</sup>, Maria C. Tamargo<sup>2,6</sup>, and Igor L. Kuskovsky<sup>1,6\*</sup>

<sup>1</sup>Department of Physics, Queens College of CUNY, Queens, New York 11367, USA

<sup>2</sup>Department of Chemistry, City College of CUNY, New York, New York 10031, USA

<sup>3</sup>National High Magnetic Field Laboratory, Tallahassee, Florida 32310, USA

<sup>4</sup>Department of Physics, Florida State University, Tallahassee, Florida 32306, USA

<sup>5</sup>Department of Physics, City College of CUNY, New York, New York 10031, USA

<sup>6</sup>The Graduate Center, CUNY, New York, New York 10016, USA

\*Igor.Kuskovsky@qc.cuny.edu

Isoelectronic centers (ICs) have recently been proposed as a promising platform for quantum information processing [1]. Here we report our recent study on Te-IC bound excitons in Zn-Se-Te multilayer system grown via migration enhanced epitaxy with submonolayer insertion of Te. Photoluminescence (PL) spectrum of such a sample has been reported [2] to demonstrate coexistence of the isoelectronic centers along with the type-II quantum dots. Spectrally, the band edge emission, originating from the IC bound excitons, is observed as characteristic ‘sharp lines’ and their phonon replicas, whereas the low energy side is dominated by spatially indirect, type-II excitons bound to the quantum dots.

Here we report a high resolution spectral analysis of the magneto-PL spectra of various samples with relatively low Te content. The quantum dot bound excitons exhibit robust Aharanov-Bohm oscillations in the PL intensity as well as energy of the magneto-PL up to 30 K, while no such effect is expected for the excitons bound to Te-ICs. This analysis reveals additional features in magneto-PL intensity as well as energy appearing at much lower temperatures (< 3 K). These features emerge at specific magnetic fields and only in the spectral region dominated by the ‘sharp lines’. Circular polarization dependent magneto-PL measurements show that these unique features are highly polarized indicating that the spin selection rules is an important parameter to understand this behavior. The energy of one of the sharp lines shows non-monotonic dependence on the external magnetic field and the experimentally measured value of diamagnetic coefficient comes out to be about  $1.2 \mu\text{eV}/\text{T}^2$ , much smaller than that of the donor bound exciton in ZnSe. Although the precise origin of these distinctive peaks in intensity of magneto-PL is still unknown, they are thought to be arising due to crossing between multiple IC bound excitonic states.

This research is supported by the Department of Energy, Office of Basic Energy Sciences, Division of Materials Sciences and Engineering under Award No. DE-SC003739.

[1] G. Éthier-Majcher, P. St-Jean, G. Boso, A. Tosi, J. F. Klem, S. Francoeur, Nat. Commun. **5**, 3980 (2014)

[2] Y. Gu, I.L. Kuskovsky, M. van der Voort, G.F. Neumark, X. Zhou, M.C. Tamargo, Phys. Rev. B **71**, 045340 (2005)

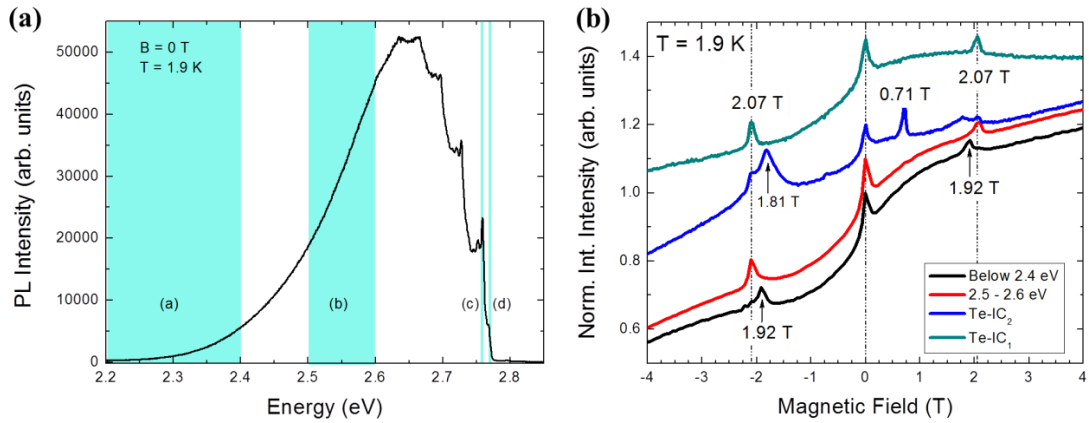


Figure 1. (a) PL spectrum of the investigated samples. Shaded Regions ‘c’ and ‘d’ correspond to the emission from Te-IC<sub>2</sub> and Te-IC<sub>1</sub> respectively, whereas regions ‘a’ and ‘b’ are dominated by quantum dot emissions. (b) Magneto-PL intensity as a function of magnetic field for various spectral regions.

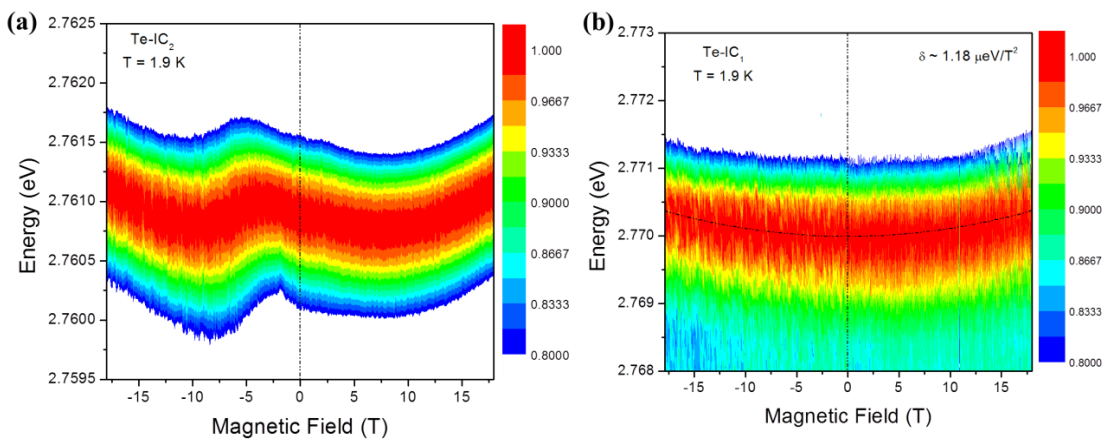


Figure 2. PL energy as a function of magnetic field for (a) Te-IC<sub>2</sub> and (b) Te-IC<sub>1</sub>. Here positive field corresponds to  $\sigma^+$  polarized PL, while negative field corresponds to  $\sigma^-$  polarized PL.

## Strain induced energy gap variation and valence band mixing in (Zn,Mn)Te/(Zn,Mg)Te core/shell nanowires

P. Wojnar<sup>1\*</sup>, M. Szymura<sup>1</sup>, Ł. Kłopotowski<sup>1</sup>, M. Wiater<sup>1</sup>, W. Zaleszczyk<sup>1</sup>, J. Suffczyński<sup>2</sup>, T. Smoleński<sup>2</sup>, P. Kossacki<sup>2</sup>, E. Janik<sup>1,2</sup>, M. Zieliński<sup>3</sup>, S. Kret<sup>1</sup>, T. Wojciechowski<sup>1</sup>, L. T. Baczewski, G. Karczewski<sup>1</sup>, T. Wojtowicz<sup>1</sup>, J. Kossut<sup>1</sup>

<sup>1</sup> Institute of Physics, Polish Academy of Sciences, Warsaw, Poland

<sup>2</sup> Institute of Experimental Physics, University of Warsaw, Warsaw, Poland

<sup>3</sup> Institute of Physics, Faculty of Physics, Astronomy and Informatics, Nicolaus Copernicus University, Toruń, Poland

\*E-mail of corresponding author: wojanr@ifpan.edu.pl

The high aspect ratio being the characteristic of semiconductor nanowires results in several novel and exciting properties of these structures, such as, e.g., the linear polarization of the optical emission [1] and possibility of matching semiconductors with relatively large lattice mismatch [2].

In this work, strain-induced changes of ZnTe nanowire energy gap, arising from the lattice mismatch between the core and the shell semiconductor in radial ZnTe/ZnMgTe core/shell structures, are studied by means of optical methods. It is shown that the increase of the Mg content in the shell, as well as the increase of the shell thickness result in an effective redshift of the near band edge emission from ZnTe nanowire cores. This reflects directly the decrease of energy gap under tensile strain conditions. The conclusions are supported by theoretical calculations in terms of the valence force field model. The maximum observed change of ZnTe energy gap is as large as 120 meV with respect to the unstrained conditions and can be tuned in a continuous manner by adjusting shell parameters, which opens a path towards an effective band gap engineering using these structures [3].

The tensile strain acting on the ZnTe nanowire core lifts also the degeneracy of the light and heavy hole band with the heavy hole band being the ground state of optical transitions. This effect has been investigated in individual (Zn,Mn)Te/(Zn,Mg)Te core/shell nanowires with the Mn molar fraction of about 5%. As shown previously [4], the presence of magnetic Mn-ions enhances the spin splitting of the bands by an order of magnitude due to the presence of the *s,p-d* exchange interaction. Most importantly, it is demonstrated that the value of the spin splitting of the bands depends strongly on the direction of the applied magnetic field with respect to the nanowire axis. When the magnetic field is applied along the axis the spin splitting is up to 5 times larger than in the case of a perpendicular configuration. This effect is attributed directly to the strain induced light and heavy hole level splitting with the value being of the order of tens of meV and with the anisotropy axis corresponding to the nanowire axis [5].

The research has been partially supported by National Centre of Science (Poland) grants 2011/01/D/ST5/05039 and DEC-2012/06/A/ST3/00247.

### References

- [1] J. Wang *et al.*, Science **293**, 1455, (2001).
- [2] F. Glas, Phys. Rev. B **74**, 121302 (2006).
- [3] P. Wojnar *et al.*, Appl. Phys. Lett. **104**, 163111 (2014).
- [4] P. Wojnar *et al.*, Nano Lett. **12**, 3404, (2012).
- [5] M. Szymura *et al.*, Nano Lett. **15**, 1972 (2015).

## Cd(Se,Te)/ZnSe Quantum Dots: Beyond the Crossroad of Se and Te Based Systems

M. Ścieszek<sup>1</sup>, W. Pacuski<sup>1</sup>, M. Parlińska-Wojtan<sup>2</sup>, P. Kossacki<sup>1</sup>, J. Suffczyński<sup>1\*</sup> and A. Golnik<sup>1</sup>

<sup>1</sup>Institute of Experimental Physics, Faculty of Physics, University of Warsaw, Warsaw, Poland

<sup>2</sup>Facility of Electron Microscopy & Sample Preparation, Center for Microelectronics and Nanotechnology, Faculty of Mathematics and Natural Sciences, University of Rzeszow, Rzeszow, Poland

\*Jan.Suffczynski@fuw.edu.pl

The efficiency of photoluminescence from typical CdTe/ZnTe QDs is limited by low confinement energy of holes. We design, produce and study Cd(Se,Te) Quantum Dots (QDs) embedded in ZnSe barrier. This system is beneficial for enhanced confinement of carriers of both types [1]. Advanced structural, optical and magneto-optical methods are employed to uncover Cd(Se,Te)/ZnSe QDs properties which, contrary to expectations, reach beyond a range of properties typical for two, Te and Se based, combined systems.

Transmission electron microscope imaging involving energy dispersive X-ray spectroscopy indicates the average tellurium content in Cd(Se,Te) QDs of  $\sim 0.2$ . However, different Te content in different QDs might be expected. Low QDs density induced by Mn assisted epitaxial growth allowed us to observe individual Cd(Se,Te)/ZnSe QD emission lines.

Some properties of the studied QDs are quite similar to the ones of CdSe/ZnSe QDs, including values of anisotropic exchange splitting and of diamagnetic shift of excitonic lines. However, other, like energy difference between exciton and biexciton transitions vary from 25 meV (as for CdSe/ZnSe QDs), through 14 meV (as for CdTe/ZnTe QDs), down to values of the order of 3 meV. Such a small exciton-biexciton energy difference has not been reported for neither of the two, Se and Te based, systems. Moreover, one could predict that g-factor should be a resultant of values typical for CdTe/ZnTe QDs ( $g_{\text{CdTe}} \sim 2$ ) and CdSe/ZnSe ( $g_{\text{CdSe}} \sim 1.6$ ) QDs. This, however, is not the case, with Cd(Se,Te)/ZnSe QDs g-factor attaining values below 1.

Wide range of observed values of exciton-biexciton energy difference allows discovering of its correlation: positive with excitonic g-factor and negative with anisotropic splitting of excitonic lines (see Figure 1).

The photoluminescence (PL) measurements as a function of temperature from 2 K to 300 K show that quantum yield of such QDs is more robust with respect to increasing temperature than quantum yield of both, CdTe/ZnTe and CdSe/ZnSe QDs.

[1] Y. Hinuma, A. Grüneis, G. Kresse, and F. Oba, Physical Review B **90**, 155405 (2014).

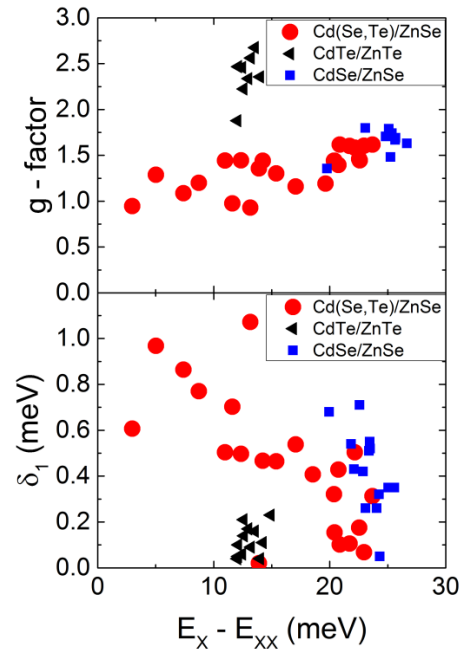


Figure 1: Excitonic g-factor and anisotropic splitting vs exciton - biexciton energy difference for the QD systems indicated.

**Monday September, 14 - Poster Session 1 - MoP**

**17:15-18:45**

<b>Growth and characterization , doping and defects</b>	146
<b>ZnO , related oxydes and Transparent conductors (devices and physics)</b>	181
<b>Detectors and new devices: X and gamma high energy sensors , Infrared, visible, and UV materials and devices</b>	200

**Poster Session 1 - MoP**

**Growth and characterization , doping and defects**

## Deuterium diffusion in nitrogen-doped ZnO at room temperature

N. Temahuki<sup>1</sup>, F. Jomard<sup>1</sup>, A. Lusson<sup>1</sup>, I. Stenger<sup>1</sup>, J. Chevallier<sup>1</sup>, J. Barjon<sup>1\*</sup>,  
J.M. Chauveau<sup>2,3</sup>, C. Morhain<sup>2</sup>

<sup>1</sup> GEMaC, Université Versailles Saint Quentin, CNRS, 78035 Versailles, France

<sup>2</sup> CNRS-CRHEA, Rue Bernard Grégory, 06560 Valbonne, France

<sup>3</sup> Université de Nice Sophia-Antipolis, 06103 Nice, France

\* julien.barjon@uvsq.fr

In this work, the diffusion of deuterium is investigated by secondary ion mass spectrometry (SIMS) in nitrogen-doped homoepitaxial ZnO layers. They were grown by molecular beam epitaxy on m-plane ZnO substrates [1] with a nitrogen content varying from non-intentionally-doped ( $<10^{17}$  at.cm<sup>-3</sup>) up to  $5 \times 10^{18}$  at.cm<sup>-3</sup>. These layers having different nitrogen contents were all treated with the same protocol, namely an exposure to a RF deuterium plasma during 1h at room temperature.

Deuterium diffusion is observed in all epilayers. The penetration depth of deuterium in the epilayer decreases as the nitrogen concentration increases. This is a first evidence of a diffusion mechanism limited by the trapping of deuterium on a nitrogen-related trap.

The SIMS profiles are further analyzed using a two-trap model including a shallow trap, associated with a fast diffusion, and a deep trap related to nitrogen. The capture radius of the nitrogen-related trap is determined. It presents a strong discrepancy with the value expected for ND pairs formed by a coulombic attraction between H<sup>+</sup> and N<sup>-</sup>. Other kinds of nitrogen-deuterium complexes which could be formed during the deuterium diffusion are discussed.

[1] D. Taïnoff et al., Appl. Phys. Lett. **98**, 131915, (2011).

## Electronic Band Structure Engineering of $\text{ZnO}_{1-x}\text{S}_x$ and $\text{ZnO}_{1-x}\text{Te}_x$ Highly Mismatched Alloys

Maribel Jaquez<sup>1,2</sup>, Min Ting<sup>1,2</sup>, O. D. Dubon<sup>1,3</sup>, Kin Man Yu<sup>1,4</sup>, and W. Walukiewicz<sup>1\*</sup>

<sup>1</sup>Materials Sciences Division, Lawrence Berkeley National Laboratory, Berkeley, CA 94720

<sup>2</sup>Mechanical Engineering Department, University of California, Berkeley, CA 94720

<sup>3</sup>Materials Science & Engineering Department, University of California, Berkeley, CA 94720

<sup>4</sup>Department of Physics and Materials Science, City University of Hong Kong, Kowloon, Hong Kong

\*E-mail of the Corresponding Author: w\_walukiewicz@lbl.gov

The high demand and need for renewable energy has triggered a vast exploration of potential materials for energy applications. Zinc Oxide (ZnO) is a material of great interest because it is non-toxic, earth abundant and relatively inexpensive. The band gap of ZnO is too wide to absorb visible light, which hinders its usefulness for solar energy conversion. Band gap engineering is an attractive method that can make ZnO accessible for solar applications. Our previous work on band gap engineering of O-rich Zinc Oxide Selenide ( $\text{ZnO}_{1-x}\text{Se}_x$ ) highly mismatched alloys (HMA) [1] has shown that substituting a small amount of the less electronegative Se element for O in ZnO results in a large upward shift of the valence band maximum (VBM). HMA are alloys that comprise of semiconductor compounds where the anions are partially substituted with isovalent atoms of considerably different size and/or electronegativity. The electronic band structure of HMA is well described by the band anticrossing (BAC) model that considers an interaction between localized states introduced by the minority anions and the extended states of the host conductor/valence band in the dilute alloy composition limit.

In this work, we synthesized Zinc Oxide Sulfide ( $\text{ZnO}_{1-x}\text{S}_x$ ) and Zinc Oxide Telluride ( $\text{ZnO}_{1-x}\text{Te}_x$ ) to study the effects of the electronegativity and anion size on the bandgap of ZnO. Based on the BAC model, the larger the electronegativity difference and anion size is between the substituted anion and O, the larger the effect in the electronic structure. With our results, we show that incorporating 10% S in a ZnO matrix results in a 0.46 eV upward shift of the VBM; and a 10% Te incorporation results in a 1.5 eV [2] VBM upward shift.

Thin films of  $\text{ZnO}_{1-x}\text{S}_x$  alloys with  $0 \leq x \leq 1$  and  $\text{ZnO}_{1-x}\text{Te}_x$  alloys with  $x < 0.23$  were deposited by radio frequency magnetron sputtering and pulsed laser deposition respectively. The composition of the alloys were measured by Rutherford Backscattering Spectrometry (RBS) and the concentration of substitutional S in ZnO and Te in ZnO were calculated from shifts in the X-Ray Diffraction (0002) peak using a linear extrapolation of the lattice parameter between that of wurtzite ZnO and ZnS (or ZnTe). The band structures of these alloys were determined by fitting the absorption coefficient spectra data with the calculated absorption coefficient utilizing the BAC model. The upward shift of the VBM has been verified by X-ray photoelectron spectroscopy (XPS). The structural properties, optical properties and the electronic band structures of the II-VI mismatched alloy system will be compared. Potential applications of these materials for solar power conversion devices will be discussed.

[1]. M. A. Mayer, D. T. Speaks, K. M. Yu, S. S. Mao, E. E. Haller, and W. Walukiewicz, *Appl. Phys. Lett.* **97**, 022104 (2010).

[2] M. Ting, R. dos Reis, M. Jaquez, O.D. Dubon, K.M. Yu and W. Walukiewicz, *Appl. Phys. Lett.* **106**, 092101 (2015).

## Quasiamorphous ZnO layers produced by the ALD technique

A.Turos<sup>1-2\*</sup>, E. Guziewicz<sup>3</sup>, D. Snigurenko<sup>3</sup>, B.S. Witkowski<sup>3</sup>, R.Diduszko<sup>1</sup>, A.Stonert<sup>2</sup>,  
M. Behar<sup>4</sup>

<sup>1</sup>Institute of Electronic Materials Technology, Wolczynska 133, 01-919 Warsaw, Poland

<sup>2</sup>National Centre for Nuclear Research, Soltana 7, 04-500 Otwock, Poland

<sup>3</sup>Institute of Physics, Polish Academy of Sciences, 02-668 Warsaw, Poland

<sup>4</sup>Instituto de Fisica, Universidade do Rio Grande de Sul, 91501 Porto Alegre, Brasil

e-mail: [andrzej.turos@itme.edu.pl](mailto:andrzej.turos@itme.edu.pl)

Although zinc oxide has been widely investigated for many important applications like laser diodes, photovoltaics, sensors etc. some basic properties of this materials has not been established up to now. One of these is stopping power measurements which are crucial for the Rutherford Backscattering Spectrometry analysis [1]. For this kind of measurements amorphous materials should be used.

In this paper we show the results of stopping power measurements for ZnO films grown by Atomic Layer Deposition with diethylzinc (DEZn) and water precursors. The films were grown on silicon (100) substrate and parameters of the growth were chosen in a way that prevent crystallization of ZnO films [2] e.g. the temperature of the growth was very low (100°C) and short purging times were used (2s after DEZn and 6s after water). We grown a series of ZnO films with thickness between 20 and 160 nm. The surface of the films was very smooth. The RMS value of the surface roughness as measured by Atomic Force Microscopy was between 0.8 and 1.6 nm depending of the thickness, which far below this value obtained for highly crystalline ZnO films obtained by ALD [2].

Siemens D500 powder diffractometer using  $K_{\alpha 1,2}Cu$  radiation ( $\lambda = 0.15418$  nm) has been applied for X-ray diffraction measurements. The diffraction patterns were measured in a  $(\theta - 2\theta)/2\theta$  scanning mode. Accordingly, polycrystalline structure of the layers without any texture has been revealed and the average crystallite size of about 25 nm has been estimated. Very low background level in diffraction profiles indicates only small contribution of amorphous phase. The width of 002 diffraction line of ZnO is broader than those for other indexes. This can be explained by partial relaxation of crystallites along c axis i.e. perpendicular to the surface as compared to full relaxation of crystallites of other orientations.

ZnO films have been used for precise stopping power measurement of MeV H- and He-ions in the energy range from 200 to 150 keV. These results provided indispensable data for ion beam modification and analysis of ZnO. They show that the obtained nanopolycrystalline ZnO films can be considered as truly amorphous with respect to ion beam applications, and we obtained the perfect agreement of our measurements and theoretical predictions using the SRIM code.

**Acknowledgements.** The work was supported by the Polish National Centre for Research and Development (NCBiR) through the project DZP/PBSII/1699/2013.

### References

- [1] M. Behar et al., Eur. Phys. J. D59 (2010) 209.
- [2]. I.A. Kowalik et al., J. Cryst. Growth 311 (2009) 1096.

## MOCVD growth of ZnO nanowires on Ni-W metallic substrates

Halaoui M<sup>1</sup>, Amiri G<sup>1</sup>, Montenegro DN<sup>2</sup>, Galtier P<sup>1</sup>, Sallet V<sup>1\*</sup>

<sup>1</sup>Groupe d'Etude de la Matière Condensée (GEMAC), CNRS - Université de Versailles  
St Quentin, 45 avenue des Etats Unis, 78035 Versailles, France

<sup>2</sup>Department of Physics, Universidad del Atlantico, km 7 antigua via Puerto Colombia,  
Barranquilla, Colombia

\*corresponding author : vincent.sallet@uvsq.fr

Research on semiconductor nanowires has opened new fields of investigation in fundamental physics, and offers unique opportunities for the future generation of (opto)-electronics, photonics, sensors... applications. For example, this has motivated the preparation of ZnO nanowires on sapphire substrate completely free of defects although these two materials exhibit a large lattice mismatch. Up to now, most of the investigations were undertaken using semiconductors as substrate or insulating oxides (sapphire, SrTiO<sub>3</sub>, silicon) An alternative route that we present here is to study and demonstrate the possibility to grow “perfect” semiconductor nanowires on “imperfect” metallic substrates.

ZnO nanowires were grown by metalorganic chemical vapor deposition (MOCVD) on Ni-W alloys substrates. These metallic substrates exhibit (001) textured crystalline structure. DEZn and N<sub>2</sub>O were used as zinc and oxygen precursors, and growths were carried out at 800°C. Samples were characterized by scanning electron microscopy (SEM) to assess the morphology and uniformity of the nanowires. Direct growth on Ni-W substrates shows no deposition of nanowires, and rather a rough layer (although C-axis oriented nanowires are easily achieved on sapphire using the same growth conditions). The effect of a ZnO buffer layer has been studied. Doing so, nanowires growth is observed, but depends on the grain orientation.

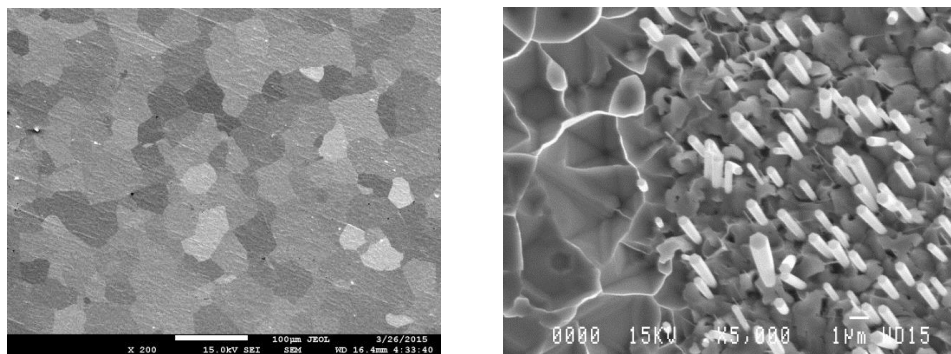


**Figure** : SEM images of Ni-W metallic substrate (left), and ZnO nanowires grown on this surface (right)

Baran N<sup>1</sup>, Korsunskaya N<sup>1\*</sup>, Polishchuk Yu, Kladko V, Stroyuk O<sup>2</sup>, Kryshtab T<sup>3</sup> and Stara T<sup>1</sup>

<sup>1</sup>VE Lashkaryov Institute of Semiconductor Physics of NAS of Ukraine, Kyiv, Ukraine

<sup>2</sup>LV Pysarzhevsky Institute of Physical Chemistry of NAS of Ukraine, Kyiv, Ukraine

<sup>3</sup>Department of Material Sciences, ESFM-IPN, Av. IPN, Ed.9 U.P.A.L.M., 07738, Mexico D.F.

\* korsunskaya@ukr.net

Nanocrystalline zinc sulfide and ZnS-based solid solutions are broadly used in technologies of scintillators and luminophors, light-emitting devices and UV light photodetectors, catalysts and photocatalysts. Typically, nanocrystalline ZnS exhibits intense photoluminescence (PL) and high photosensitivity, but at the same time, is prone to destructive photolysis when excited by UV light. The photolysis of ZnS can have both positive and negative effects. In particular, it is an intrinsic primary stage of many photocatalytic reactions with the participation of ZnS and simultaneously, it can be a deteriorating factor in optoelectronic devices. Meanwhile, mechanisms of the photolysis of ZnS nanocrystals as well as factors resulting in acceleration/inhibition of the photolysis, such as doping, require still to be understood in more details.

The present work reports on a study of the influence of ZnO addition and doping with Co<sup>2+</sup> on the photolytic and post-photolytic behavior of the nanocrystalline ZnS by means of PL spectroscopy, electron paramagnetic resonance (EPR) and X-ray diffraction (XRD). It was found that illumination of ZnS by UV light in ambient air atmosphere results in PL quenching and rise of two EPR signals as well as a shift of the XRD peaks to smaller angles. The EPR signals were identified as those belonging to two types of paramagnetic centers localized within the products of the photolysis – metallic zinc clusters and elemental sulfur. The results showed that the oxidative photolysis yields not only sulfur vacancies and oxygenated S-containing products but also the individual S<sub>8</sub> phase indicating on the partial character of the photolytic ZnS transformation.

After termination of the photolysis and keeping of the ZnS samples in the dark the photo-induced changes continue to develop resulting in non-monotonous character of EPR signals changing that can be interpreted in terms of charge transfer between zinc and S<sub>8</sub> islands and formation of additional radical centers followed by their extinction at longer times. The EPR data also showed that photolytic transformation of ZnS nanocrystals imparts them with the capability to undergo dark oxidative decomposition that is uncharacteristic for the non-illuminated ZnS nanocrystals.

It was found that the UV-induced shift of the XRD peaks to lower angles originates from photogeneration of sulfur vacancies and oxygen inclusion. The latter conclusion is supported by the light-induced changes in the Auger spectra of irradiated ZnS nanocrystals.

Doping of ZnS nanocrystals with Co<sup>2+</sup> results in considerable increase of the photolysis rate manifesting itself in much higher intensity of EPR signals as well as faster extinction of S-related paramagnetic centers during the post-photolytic ageing. The Co(II) influence interpreted in terms of catalytic activity of cobalt(II) ions and CoS phase in the processes of charge transfer from sulfur species (S<sup>2-</sup>, S<sup>0</sup>, paramagnetic species) to O<sub>2</sub>.

Mixing of the ZnS nanocrystals with ZnO nanocrystals or partial oxidation of ZnS samples was found to result in considerable acceleration of the UV-induced photolysis. The most probably reason for the effect is the spatial separation of the photogenerated charge carriers between the phases of zinc sulfide and zinc oxide that is favoured by the offsets between the conduction and valence bands of ZnS and ZnO.

## ZnO microstructures Obtained by HFCVD and Its Characterization.

García Salgado G<sup>1\*</sup>, Ramos Serrano R<sup>1</sup>, Morales Ruiz C<sup>1</sup>, Diaz Becerril T<sup>1</sup>, Rosendo Andrés E<sup>1</sup>, Juarez Santiesteban H<sup>1</sup>, Pacio Castillo M<sup>1</sup>, Nieto Caballero G<sup>1</sup>, Galeazzi Isasmendi R.  
<sup>1</sup>Benemerita Universidad Autónoma de Puebla, Puebla, Mexico  
 \*godgarcia@yahoo.com

ZnO microstructures with microspheres and hexagonal faceted shapes using a solid source and atomic hydrogen in a CVD home made reactor are presented in this work. Structural and optical characterization was performed to samples obtained with growth temperatures of 200, 300, 350 and 400°C during 3 min. the hydrogen flow was set up to 120 sccm. The analysis shows that the microstructures are composed by metallic zinc and zinc oxide in a core shell disposition. The ZnO presents the wurtzite structure and the metallic zinc the hexagonal structure. The presence of both components is depending of the temperature, showing at growth low temperatures more quantity of metallic zinc. However a photoluminescence peak around 550 nm is present in any case with a shift to high energies with growth low temperatures. With the deconvolution realized to the photoluminescence peaks it is suggested that interstitial defects ( $O_i$ ) predominate at high temperatures over the substitutional defects ( $O_{Zn}$ ). EDS studies support the photoluminescence results. The growth temperature influence on the morphology too; SEM micrographs show at low temperatures hexagonal sheets stacked and microspheres at high temperatures. Finally TEM studies show core shell type nanostructures, with zinc metallic in the core and ZnO in the shell.

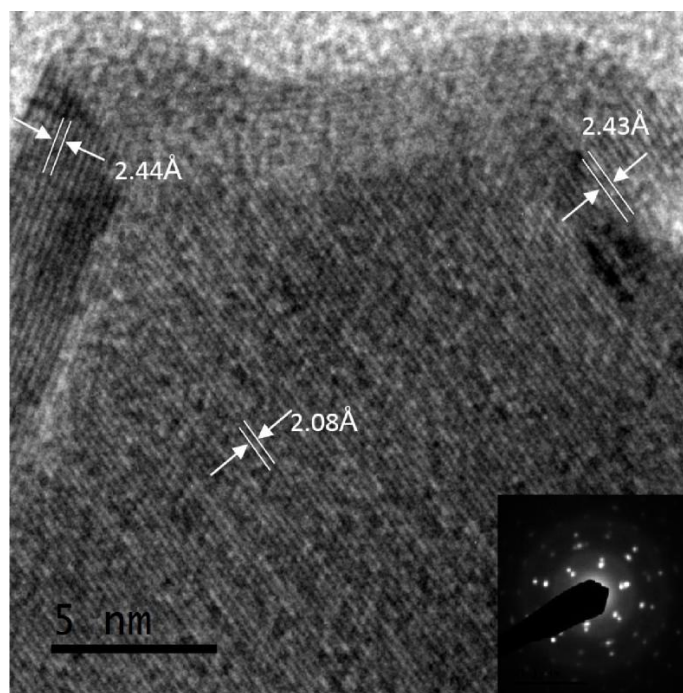


Fig. 1. Core shell structure growth for HFCVD, showing the metallic zinc crystalline in the core and ZnO in the shell

## High quality ZnO nanotube on conductive substrate by pulsed laser deposition

*Tahani H Flemban, Iman S Roqan\**

Physical Sciences and Engineering Division, King Abdullah University of Science and Technology (KAUST), Thuwal 23955-6900, Saudi Arabia.

E\*-mail: [iman.roqan@kaust.edu.sa](mailto:iman.roqan@kaust.edu.sa)

Nanotube (NT) structures attracted attentions due to the higher aspect ratio and oxide has much better output efficiency compared to other nanostructures. Particularly, ZnO NTs have potential for several electronic and optoelectronic applications such as biosensors.[1] Controlling the growth conditions to provide homogeneous dimensions remains a challenge. In this work, we were successful to produce ZnO NTs on conductive Si (001) substrate by pulsed laser deposition (PLD), which has never been accomplished before according to our knowledge. We used standard Excimer laser KrF PLD system with laser frequency of 10 Hz, target-substrate distance of  $\sim 9$ cm, and laser energy density on target were fixed at  $\sim 2.5$  J/cm<sup>2</sup>. The scanning electron microscopy (SEM) image (Figure 1) shows ZnO NTs with homogeneous length ( $\sim 650$  nm) and diameter ( $\sim 60$  nm) obtained at partial oxygen pressure ( $P(O_2) = 100$  mTorr). We study the growth mechanism by transmission electron microscopy (TEM). We investigate the optical properties of these NTs by mean of micro-photoluminescence ( $\mu$ PL) and cathodoluminescence (CL). Room temperature  $\mu$ PL measurements show a strong and sharp bandedge peak at 378.8 nm with very weak defect band, indicating high optical quality. CL maps show luminescence properties of a single NT. Hall measurements are carried out to study the electrical properties. These novel findings demonstrate that PLD system has significant potential to grow high quality oxide NTs.

[1] J.L. Gomez, O. Tigli, Journal of Materials Science, 48 (2013) 612-624.

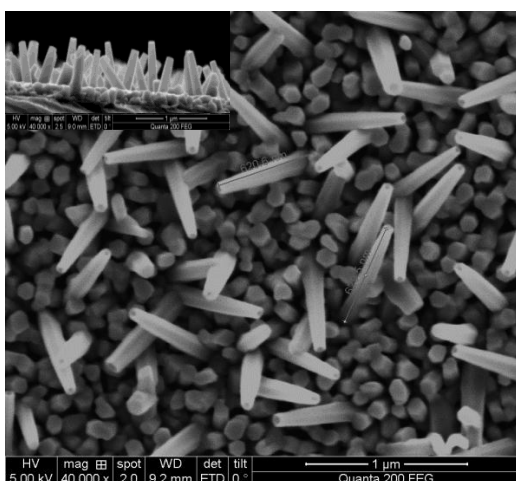


Figure 1. SEM top view of ZnO nanotubes on silicon substrate obtained at  $P(O_2) = 100$  mTorr. The inset shows the side view.

## Influence of Substrate Temperature on Crystalline Characteristics and Optical Properties of Tourmaline/ZnO Thin Film

Qing Huang Zhang, Yun Guo \*, Ji Wei Xu, Ting Wu, Lin Jun Wang

School of Materials Science and Engineering, Shanghai University, Shanghai 200444, China

\* guoyun@shu.edu.cn

As a kind of wide band gap semiconductor material, ZnO has multitudinous advantages of high chemical stability, low dielectric constants, excellent performances in optics, piezoelectricity and electromechanical coupling properties [1-2]. Tourmaline is a unique type of crystalline material and silicate mineral with thermoelectric, piezoelectric and spontaneous polarization [3-4]. The structure and function of ZnO material are rather similar to that of tourmaline, the spontaneous polarization and the intrinsic surface electric field of tourmaline crystal can produce beneficial influence on the ZnO epitaxial growth, so as to improve the physical properties of ZnO material, then advance the further applications of ZnO-based optoelectronic devices.

In present work, the ultrasonic spray pyrolysis deposition technique (USP) was taken to grow nano-ZnO films on glass slides (BL/ZnO) and XJ/ZnO and tourmaline (XJ/ZnO) slices under different deposition temperature devised to 300°C, 400°C and 500°C respectively. Raman spectroscopy (Raman), X-ray diffraction (XRD), Scanning Electron Microscopy (SEM) and UV-Visible absorption spectrum (UV-Vis) were utilized to systematically analyze the crystal structure, microscopic morphology of ZnO films, and the influence of deposition temperature on the optical properties of ZnO thin films on different substrates materials.

XRD and Raman results indicated that the as-prepared ZnO crystal were wurtzite polycrystalline structure with greater intensity of Raman characteristic peaks at  $435\text{cm}^{-1}$  and more preferential orientation along (002) plane, simultaneously better crystallinity and bigger-sized grain had been achieved at higher substrate temperature. Nearly round sheet of ZnO nano-crystals stacked along the direction parallel to the substrate and crystaled into flowery micro-column. As the substrate temperature increased, ZnO nanosheets and the crystalline columns became wider. The crystal particle sizes of BL/ZnO and XJ/ZnO were calculated as 43.7nm/45.4nm/59.2nm and 29.0nm/33.5nm/38.4nm respectively at different heating temperature. Comparing with the UV-Vis spectra of composite films, the maximum absorption peak intensity in XJ/ZnO had increased to 1.70 while that was 1.08 in BL/ZnO. Due to the effective counteraction for the grain boundaries charge by the surface electric field effect of tourmaline substrate material, the absorption edges of ZnO had occurred red shifts, with relatively smaller wavelength shift at higher heating temperature. Therefore, under different deposition temperature circumstances, so taking tourmaline slices as the substrate materials can have regulatory effect on the crystal structure and growth morphology, and exert certain influence on the optical absorption characteristics for the nano-crystalline ZnO thin films.

- [1] Ü Özgür, Ya I Alivov, C Liu, A Teke, M A Reshchikov, S Doan, V Avrutin, S J Cho, H Morkoç, *Journal of Applied Physics*, **98**, 1-25, (2005).
- [2] S H Choi, D S Shim, S H Jung, E Oh, B R Lee, K H Lee, *Materials Letters*, **63**, 739-741, (2009)
- [3] S Yamaguchi, *Applied Physics A*, **31**, 183-185, (1983).
- [4] J Zhan, X P, Hao H Liu, B B Huang, X T Tao, *Journal of Functional Materials*, **37**, 524-527, (2006)

## Enhanced Photocatalytic Activity of Hierarchical ZnO Nanostructure for Water Purification

Yamina-Ghozlane HABBA, Martine Capo-Chichi, Linda Serairi, and Yamin Leprince-Wang\*  
 ESYCOM – EA2552, Université Paris-Est, UPEM, Marne-la-Vallée, France

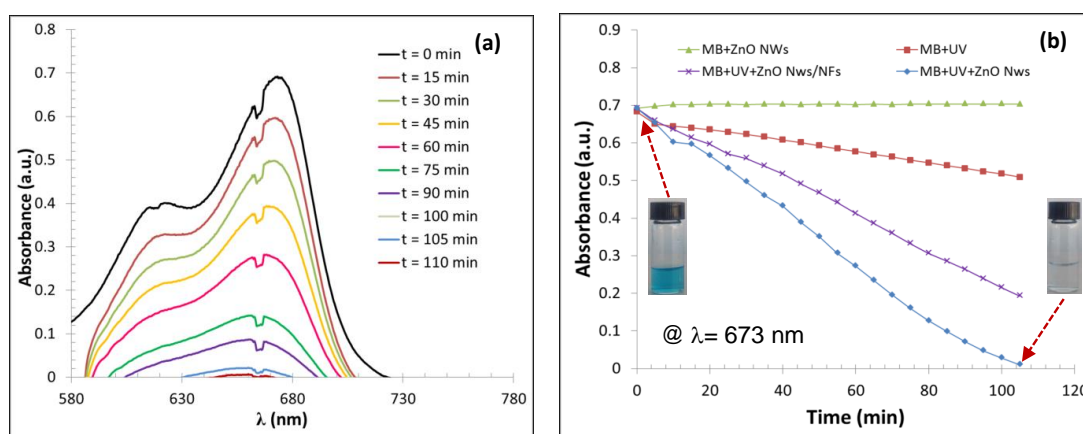
\*Corresponding author: [yamin.leprince@u-pem.fr](mailto:yamin.leprince@u-pem.fr)

Nowadays the water pollution by industry and urban effluents has become a major threat to the lives of humans. These pollutants pose a severe ecological problem because of their biodegradation is generally very slow and conventional treatments are mostly ineffective and not environmentally benign. On the other hand, the nontoxic and environmental friendly zinc oxide (ZnO) is a remarkable and very promising semiconductor in the development of new materials for the environment, due to its interesting multi-properties such as wide band gap of 3.37 eV, large energy binding of 60 meV, and low cost. ZnO owns also excellent bulk electron mobility and high transparency in visible region, which make it a good candidate for photocatalyst [1].

We report here a study of the depollution properties of nanostructured ZnO in aqueous medium. A comparative study of the photocatalytic activity has been carried out between the classical ZnO nanowire array and the hierarchical ZnO nanofiber-nanowire architecture. The classical well controlled ZnO nanowire array was obtained via two-step hydrothermal method and the hierarchical ZnO nanofiber-nanowire architecture was obtained by combining the electrospinning and hydrothermal methods, both frequently used as the low temperature and cost-effective synthesis methods.

Toxic organic compounds such as methylene blue (MB), methylene orange (MO) or acid red 14 (AR14) dyes were used to test the photocatalytic water purification performance of the nanostructured ZnO with UV or white light illumination. The UV-absorption spectra were recorded during the sensing process for monitoring photodegradation process in the aqueous solution.

We noticed that the photodegradation efficiency of the polluted aqueous medium can be enhanced by the presence of the nanostructured ZnO and the nanostructure morphology can also influence on the water purification performance.



(a) UV-Vis spectra evolution of MB aqueous solution (10 μM) with photocatalytic activity of ZnO nanowires. (b) The comparison of the variations of the absorbance of methylene blue aqueous solutions (10 μM) at different conditions with ZnO nanostructures.

[1] S.Baruah, S.Pal, J.Dutta, Nanoscience & Nanotechnology-Asia, **2**,90-102 (2012).

## Chemical and Physical Growth Mechanisms of Zinc Sulfide and Zinc Oxide Thin Films Grown by Mist Chemical Vapor Deposition

Kazuyuki Uno<sup>1\*</sup>, Yuichiro Yamasaki<sup>1</sup>, Ping Gu<sup>2</sup>, and Ichiro Tanaka<sup>1</sup>

<sup>1</sup>Faculty of Systems Engineering, Wakayama University, Wakayama, Japan.

<sup>2</sup>Faculty of Education, Wakayama University, Wakayama, Japan.

\*kuno@sys.wakayama-u.ac.jp

Mist chemical vapor deposition (mist-CVD) method, which uses ultrasonically atomized solutions as sources, is an environmental friendly and cost-effective technology for the growth of compound semiconductors [1]. This growth process is realized under atmospheric pressure and allows us to use many kinds of salts, complexes, and compounds. Using the oxidizability of water including the source, most of the previous reports of the mist-CVD method are on oxide materials [2]. In this report, we fabricated zinc sulfide (ZnS) films by the mist-CVD method using thiourea (CH<sub>4</sub>N<sub>2</sub>S) -based water + methanol solutions for VI-group sources and investigated the roles of chloride complex and vaporized process of dry-mist sources in the growth of ZnS [2]. Especially for the growth of ZnO, we determined the origin of oxygen atom composed of ZnO films using oxygen isotope water.

Our mist-CVD apparatus is originally constructed. 1.6 MHz ultrasonic transducers were used for the mist generators. A horizontal quartz furnace and a quartz fine-channel susceptor was used in its reactor. Carrier gas was nitrogen and controlled by flow-meters.

We successfully grew ZnS thin films using 0.01-0.1 mol/L zinc chloride and thiourea mixed solutions with VI/II ratio = 1. The growth temperature was around 500°C. However, using zinc sulfate and zinc acetate as II-group sources, any film did not grow. In cases using zinc acetate, ZnS films can be grown by adding hydrochloric acid (HCl). Their thickness was proportional to the ratio of [Cl<sup>-</sup>]/[Zn<sup>2+</sup>] and saturated when the ratio reached to 2. This result indicates that the zinc-chloride complex is necessary for the formation of ZnS in the mist-CVD.

Currently, two types of models are proposed on the growth mechanism of mist-CVD: vaporized model (VM) and Leidenfrost effect model (LEM). According to the VM, the mist sources are vaporized and then a ZnS film is formed. On the other hand, according to the LEM, the mists run on the substrate and ZnS is grown at the interface between the mists and the substrate. Considering which model is appropriate, we tried to grow ZnS films with the setup of separated supply of Zn and S sources individually using two mist generators. If the growth is carried out in the manner of LEM, ZnS is difficult to form with this setup. The result was that the thickness of ZnS was almost the same as that grown by mixed supply of Zn and S sources. This indicates that VM is appropriate to the growth model of ZnS by mist-CVD.

We also carried out the growth of ZnO with the setups of separated and mixed supply of a Zn acetate solution and a water including H<sub>2</sub><sup>18</sup>O (Taiyo-Nissan Corp.). Examining the ratio of [<sup>18</sup>O]/[<sup>16</sup>O] by SIMS, the ratio is almost the same in these two setups. This indicates that the VM is reasonable also for the growth of ZnO. As well, considering the ratio of [<sup>18</sup>O]/[<sup>16</sup>O] in the films and the solutions, the origin of oxygen in ZnO films was determined to be water, not to be acetyl group of Zn sources or hydroxyl group of methanol in solutions.

In conclusion, VM is basically appropriate to the physical growth model of mist-CVD. In addition, Zn-Cl complexes is necessary for the growth of ZnS and water is the oxygen source of ZnO. These result would be helpful for the growth-optimization of mist-CVD.

[1] S. Fujita *et al.*, Jpn. J. Appl. Phys. **45**, L857 (2006); **47**, 4669 (2008); **47**, 7311 (2008).

[2] K. Uno *et al.*, JSAP Meetings, 17p-A12-6, Sept. 2014; 14a-D1-9, Mar. 2015.

## Energy Harvesting Based on ZnO Nanostructure

Linda Serairi, Martine Capo-Chichi, Yamina-Ghozlane Habba, and Yamin Leprince-Wang\*

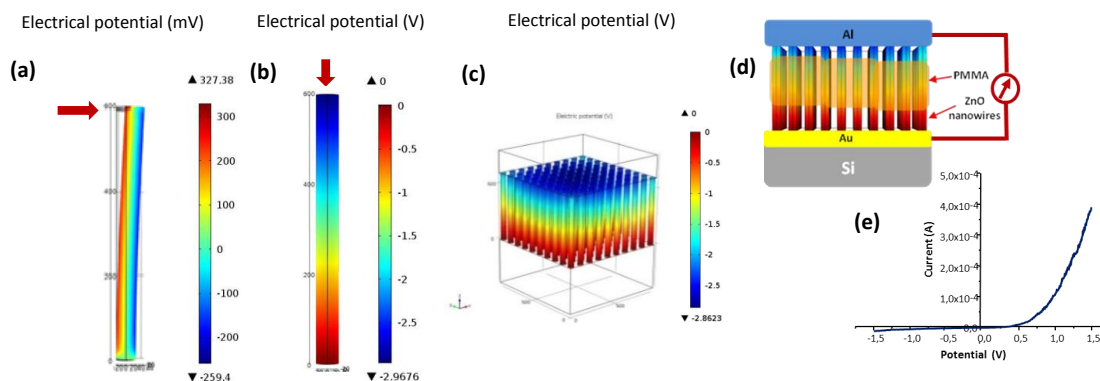
ESYCOM – EA2552, Université Paris-Est, UPEM, Marne-la-Vallée, France

\*Corresponding author: [yamin.leprince@u-pem.fr](mailto:yamin.leprince@u-pem.fr)

ZnO is a typical II-VI group wide direct band gap (3.37 eV) compound semiconductor. Due to its multi-functional properties, the environmental friendly ZnO can be considered in a wide range of applications such as optics, optoelectronics, sensors, actuators, energy, biomedical sciences and spintronics. In this work, our effort is mainly focused on the ZnO nanostructure-based piezoelectric nanogenerators for self-powered micro-/nanodevices, by converting ambient mechanical energy into electric energy.

In order to have a better understanding of the energy harvesting mechanism in the ZnO nanowire (NW) based nanogenerator device, some simulations have been carried out on the mechano-electrical properties using the finite element method. Both bending and compression configurations have been considered. In each case, a systematic study on the influence of the NW morphology (such as diameter, length, and aspect ratio) on the generated electrical potential has been performed. Our approach consists of a progressive method: from one NW to a NW array. The ZnO NW array has been undergone both in static and in vibrational strain for piezoelectric potential and current generation, in order to estimate the harvestable output power from such device. These calculations allow a better control during the ZnO NW array synthesis leading a better performance of the nanogenerator.

The ZnO NW arrays have been synthesized via hydrothermal method showing a high monocrystallinity along *c*-axis growth direction. The output potential measurements have been carried out both from single NW using the AFM and from NW array under low frequency vibration. The experimental data were compared to the numerical calculations.



(a) & (b) Simulation of the single ZnO nanowire under bending and compression modes, respectively; (c) Nanowire arrays under periodic compression; (d) Sketch of electrical measurements and (e) Schottky junction between ZnO nanowires and Au.

## ZnO Nanostructure Synthesis via Hydrothermal and Electrospinning Methods for Gas Sensor

Martine Capo-Chichi, Yamina-Ghozlane Habba, Linda Serairi, and Yamin Leprince-Wang\*  
ESYCOM – EA2552, Université Paris-Est, UPEM, Marne-la-Vallée, France

\*Corresponding author: [yamin.leprince@u-pem.fr](mailto:yamin.leprince@u-pem.fr)

Zinc oxide (ZnO) is a typical II-VI group wide direct band gap (3.37 eV) compound semiconductor. Due to its multifunctional properties, the environmental friendly ZnO has become a very promising semiconductor material in the development of new materials for renewable energy and the environment such as chemical sensors or photovoltaic cells. Nowadays, the ZnO nanowire arrays become the promising building blocks for various micro-/nanodevices and the important effective surface due to their high aspect ratio of this kind of structure is especially interesting for gas sensing.

In this work, we present two synthesis methods to obtain different ZnO nanostructures. The first one is the growth of narrow and well oriented ZnO nanowire arrays by a low temperature hydrothermal process. The second one consists in growing a single crystal ZnO nanowire array by hydrothermal process on polycrystalline ZnO nanofibers produced by electrospinning process [1]; this second part aims to improve the surface/volume ratio which will increase the sensing efficiency.

SEM observations showed a quite homogeneous morphology under optimized elaboration conditions in both cases; while DRX patterns revealed a preferred orientation towards the c-axis for the ZnO nanowire arrays obtained via hydrothermal process and a polycrystalline structure for nanofibers obtained via electrospinning method.

Gas such as ethanol, acetone and ammoniac, usually employed in laboratory, are used for gas sensing tests. A comparative study of the gas sensing performance has been carried out for the two types of ZnO nanostructure using optical measurements. As shown in Figure 1c, we can note that the hierarchical ZnO nanostructure owns a better performance for gas sensing due to its larger effective surface exposed to gas flow.

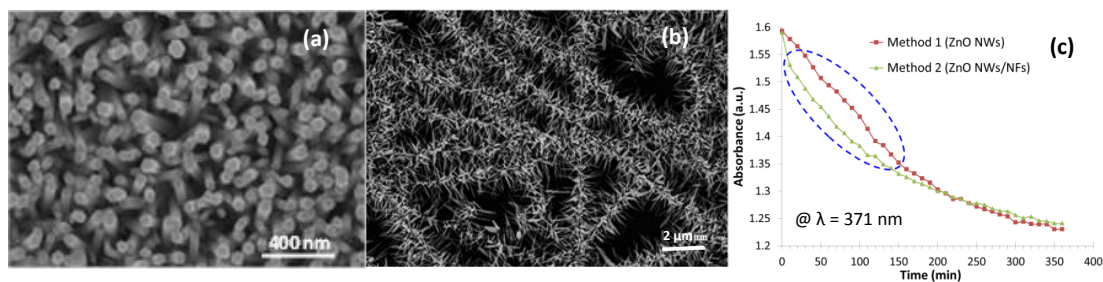


Figure 1. (a) Well controlled ZnO nanowire arrays grown toward c-axis with an excellent crystallinity, obtained via hydrothermal method. (b) Hierarchical nanostructure: ZnO nanowires grown on the polycrystalline ZnO nanofibers (as seeds). (c) The comparison of the variations of the absorbance during the gas detection by the various methods of synthesis.

[1] A.Sugunan, V.Guduru, A.Uheida, M.Toprak, M.Muhammed, Division of Functional Materials, Royal Institute of Technology (KTH), Stockholm 16440, Sweden.

## Polarity Effects on the Formation of ZnO Nanowires and Related Heterostructures with CdSe and CdTe

V. Consonni<sup>1\*</sup>, S. Guillemin<sup>1,2</sup>, L. Gérard<sup>3</sup>, L. Rapenne<sup>1</sup>, E. Sarigiannidou<sup>1</sup>, A. Bocheux<sup>1,4</sup>, G. Renou<sup>5</sup>, H. Roussel<sup>1</sup>, F. Donatini<sup>3</sup>, E. Rauch<sup>5</sup>, G. Brémond<sup>2</sup>, E. Appert<sup>1</sup>, and R. André<sup>3</sup>.

<sup>1</sup> Univ. Grenoble Alpes & CNRS, LMGP, F-38000 Grenoble, France

<sup>2</sup> Université de Lyon, Institut des Nanotechnologies de Lyon, F-69621, Villeurbanne, France

<sup>3</sup> Univ. Grenoble Alpes & CNRS, Institut Néel, «Nanophysique et Semiconducteurs» group, F-38000 Grenoble, France

<sup>4</sup> CEA, LETI, MINATEC Campus, F-38054 Grenoble, France

<sup>5</sup> Univ. Grenoble Alpes & CNRS, SIMAP, F-38402 Saint-Martin d'Hères, France

\*E-mail of the corresponding author: [vincent.consonni@grenoble-inp.fr](mailto:vincent.consonni@grenoble-inp.fr)

ZnO / II-VI core shell nanowire (NWs) heterostructures have recently received increasing interest as building blocks for the next generation of photovoltaic devices. They offer several crucial assets over planar thin films such as reduced material consumption, improved crystallinity, efficient light trapping [1], and efficient charge carrier management. The core can be composed of ZnO NWs as electron transporting layer and is usually deposited by low-cost and surface scalable deposition techniques such as the low-temperature chemical bath deposition (CBD). The shell can consist of CdSe or CdTe as absorbing layer in order to form type II radial heterostructures [2].

In this work, the formation mechanisms of ZnO NWs by CBD are discussed in details with a special emphasis on the effects of crystal orientation and polarity of the ZnO nucleation surface [3]. The combination with selective area growth using electron beam lithography is demonstrated by growing both O- and Zn-polar ZnO NWs with high structural uniformity and optical quality [4]. The ZnO NW arrays are further covered with a CdTe shell or a CdSe shell by molecular beam epitaxy. The resulting structural properties of these heterostructures are investigated by scanning and transmission electron microscopy (TEM) as well as by out-of-plane and in-plane x-ray diffraction. The occurrence of epitaxial relationships and of different crystalline phases is shown by advanced scanning TEM experiments, showing the strong interest of these heterostructures. Eventually, their optical absorption process is revealed by UV-visible-NIR spectrophotometry.

[1] J. Michallon, D. Bucci, A. Morand, M. Zanucoli, V. Consonni, and A. Kaminski-Cachopo, *Optics Express* **22**, A1174 (2014).

[2] C. Lévy Clément, R. Tena-Zaera, M.A. Ryan, A. Katty, and G. Hodes, *Advanced Materials* **17**, 1512 (2005).

[3] S. Guillemin, L. Rapenne, H. Roussel, E. Sarigiannidou, G. Brémond, and V. Consonni, *The Journal of Physical Chemistry C* **117**, 20738-20745 (2013).

[4] V. Consonni, E. Sarigiannidou, E. Appert, A. Bocheux, S. Guillemin, F. Donatini, I.C. Robin, J. Kioseoglou, and F. Robaut, *ACS Nano* **8**, 4761-4770 (2014).

## Spatially Controlled Growth of Highly Crystalline ZnO Nanowires by an Inkjet-Printing Catalyst-Free Vapor-Solid Method

Güell F<sup>1\*</sup>, Rubio-Garcia J<sup>1</sup>, Martínez-Alanis P R<sup>1</sup>, Khachadorian S<sup>2</sup>, Franke A,<sup>2</sup> Wagner M R<sup>2</sup>, Hoffmann A<sup>2</sup>, and Morante J R<sup>1,3</sup>

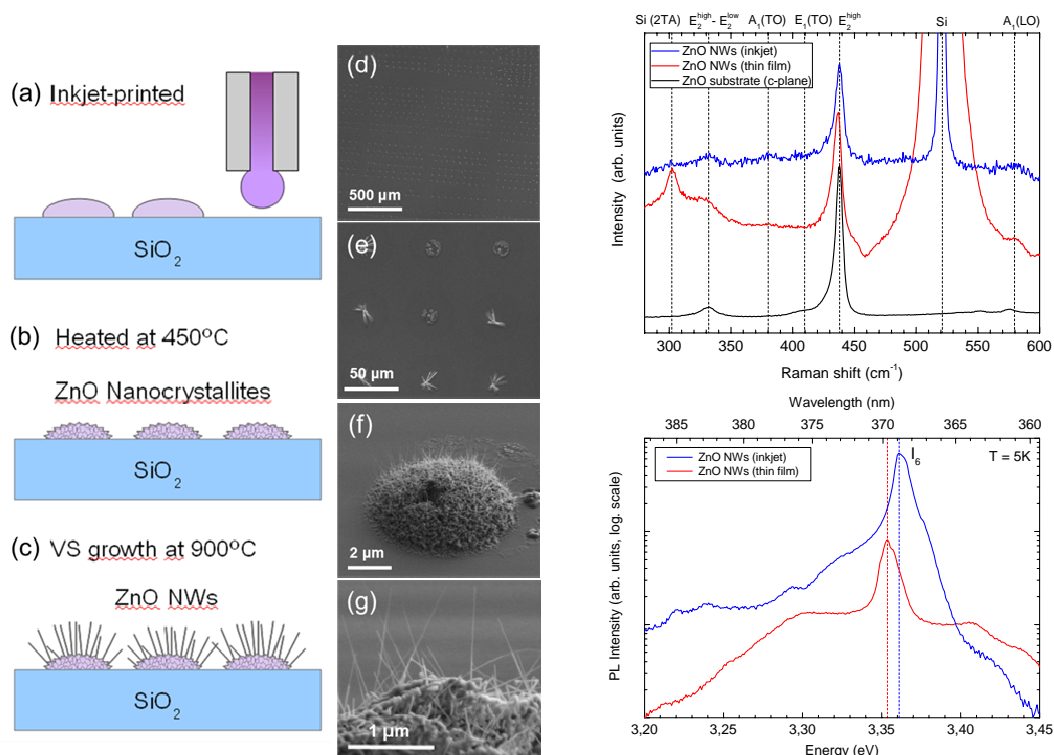
<sup>1</sup>Departament d'Electrònica, Universitat de Barcelona, Barcelona, Catalunya, Spain

<sup>2</sup>Institut für Festkörperphysik, Technische Universität, Berlin, Germany

<sup>3</sup>Institut de Recerca en Energia de Catalunya, Sant Adrià del Besòs, Catalunya, Spain

\*frank@el.uib.edu

High-density arrays of uniform ZnO nanowires (NWs) with a high-crystal quality have been synthesized by a catalyst-free vapor-transport method. Two different approaches for the growth preparation of the NWs were investigated. First, a thin ZnO film was grown on a Si substrate as nucleation layer for the NWs. In a second approach, spatially selective, mask-less growth of ZnO NWs was achieved using inkjet-printed patterned islands as the nucleation sites on a SiO<sub>2</sub>/Si substrate. Raman scattering and low temperature micro-photoluminescence ( $\mu$ -PL) measurements were applied to characterize the optical and structural properties of the ZnO NWs. The results reveal negligible amounts of strain and defects in the mask-less ZnO NWs as compared to the ones grown on the ZnO thin film which underlines the potential of the inkjet-printing approach for the growth of high-crystal quality NWs.



Schematic illustration of the vapor-transport growth of ZnO NWs using the ZnO inkjet-printed islands as seeds on a SiO<sub>2</sub>/Si substrate: (a) printed zinc nitrate drops, (b) ZnO nanocrystallites formed after annealing at 450°C and (c) ZnO NWs growth at 900°C by the VS process; FESEM images of the ZnO NWs (d) and (e), view of a single island (f) and side view (g). Raman spectra of ZnO NWs grown on ZnO inkjet-printed patterned islands (blue) and ZnO thin film seeding layers (red), respectively. ZnO c-plane substrate (black) as comparison. Low-temperature (5 K)  $\mu$ -PL spectra of ZnO NWs grown on ZnO inkjet-printed patterned islands (blue) and ZnO thin film seeding layers (red) on SiO<sub>2</sub>/Si and Si substrates, respectively.

## Controlling the structural uniformity of ZnO nanowires grown by chemical bath deposition

E. Appert<sup>1,2</sup>, R. Parize<sup>1,2</sup>, S. Guillemin<sup>1,2,3</sup>, E. Sarigiannidou<sup>1,2</sup>, A. Bocheux<sup>1,2</sup>, B. Doisneau<sup>1,2</sup>, H. Roussel<sup>1,2</sup>, G. Brémond<sup>3</sup> and V. Consonni<sup>1,2</sup>

1) *Univ. Grenoble Alpes, LMGP, F-38000 Grenoble, France*

2) *CNRS, LMGP, F-38000 Grenoble, France*

3) *Université de Lyon, Institut des Nanotechnologies de Lyon, UMR 5270 CNRS INSA Lyon 69621 Villeurbanne, France.*

\*Email of corresponding author: [estelle.appert@grenoble-inp.fr](mailto:estelle.appert@grenoble-inp.fr)

ZnO nanowires (NWs) grown in solution have attracted much attention over the last decade due to their high technological potential in optoelectronic and photovoltaic devices. However, for real-world device integration, the technological and fundamental challenge is still the precise control of their morphology, space arrangement, vertical alignment and polarity. These structural properties depend both on the morphology of the ZnO seed layer and on the growth conditions used in chemical bath deposition (CBD) [1, 2].

In this context, the influence of the solution concentration and the withdrawal speed are deeply investigated on the structural properties of ZnO seed layer deposited by dip coating as well as the possibility for using high temperature annealing treatments during the crystallization step. The effects of the chemical precursors (i.e. zinc nitrate and hexamethylenetetramine (HMTA)) on the structural properties of ZnO NWs are also studied by CBD, resulting in a better understanding of the role of HMTA. The density, diameter, length and vertical alignment of ZnO NWs are characterized by scanning electron microscopy imaging and x-ray diffraction measurements. In order to further control the uniformity of the structural properties of ZnO NWs, c-plane ZnO single crystals with either O- or Zn- polarity are patterned by electron-beam lithography or nano-imprint lithography and then used as substrates. The resulting selective area growth by CBD offers the possibility to form ZnO NWs with great structural uniformity [3]. Both nucleation mechanisms and polarity effects are investigated by high-resolution TEM imaging as well as convergent beam electron diffraction (CBED).

[1] S. Guillemin, V. Consonni, E. Appert, E. Puyoo, L. Rapenne, H. Roussel, *J. Phys. Chem. C* 116, 25106 (2012).

[2] S. Guillemin, L. Rapenne, H. Roussel, E. Sarigiannidou, G. Brémond, V. Consonni, *J. Phys. Chem. C* 117, 20738 (2013).

[3] V. Consonni, E. Sarigiannidou, E. Appert, A. Bocheux, S. Guillemin, I.-C. Robin, J. Kioseoglou, F. Robaut. *ACS Nano* 8, 4761 (2014)

## Structural and optical characterization of hybrid ZnO/polymer core-shell nanowires fabricated by oxidative chemical vapor deposition

Stephanie Bley<sup>1,\*</sup>, Max Rückmann<sup>1</sup>, Alejandra Castro-Carranza<sup>1</sup>, Florian Meierhofer<sup>2</sup>, Lutz Mädler<sup>2</sup>, Tobias Voss<sup>1,3</sup> and Jürgen Gutowski<sup>1</sup>

<sup>1</sup> Institute of Solid State Physics, Semiconductor Optics, University of Bremen, 28359 Bremen, Germany

<sup>2</sup> Foundation Institute of Material Science (IWT), Department of Production Engineering, University of Bremen, Bremen, Germany

<sup>3</sup> Institute of Semiconductor Technology, Braunschweig University of Technology, 38106 Braunschweig, Germany

\*E-mail of the corresponding author: bley@ifp.uni-bremen.de

Hybrid inorganic ZnO/organic polymer nanowire structures have recently attracted considerable attention since they provide new functionalities that cannot be achieved with either the inorganic or the organic part alone. In general, there are exist no suitable procedures for p-doping of ZnO, however, organic p-conductive polymers adsorbed at the ZnO surface can form a pn-junction together with the ZnO. In particular, core/shell nanowires with inorganic ZnO cores and organic p-conductive polymer shells have shown to possess a huge potential for the realization of efficient light-emitting or photovoltaic devices. For such structures, a controlled deposition of the polymer shell with a thickness control in the nm range is required to tailor the electronic and optical properties of the hybrid nanostructure.

For the fabrication of hybrid ZnO/polymer core-shell nanowires, oxidative chemical vapor deposition (oCVD) is used. oCVD, compared to wet-chemical processes, is a completely solventless dry process where both the oxidizing agent and the monomer are provided in the gaseous phase. Together with a constant flow of nitrogen carrier gas, the desired monomer is passed through the reaction chamber. The polymerization reaction occurs directly on the sample and is initiated by introducing the oxidizing agent vapor which additionally leads to the doping of the polymer and thereby increases its hole conductivity. We show the coating of ZnO nanowires with the p-conductive polymers polypyrrole (PPy) and poly(3,4-ethylenedioxythiophene) (PEDOT).

SEM and TEM characterization of the hybrid ZnO/polymer core-shell nanowires show that the thickness and homogeneity of the polymer coating depend on the amount of the oxidizing agent (here FeCl<sub>3</sub>) and the substrate temperature. Photoluminescence spectroscopy shows a broadening of the exciton lines of the ZnO nanowires after polymer coating (especially for PEDOT) which is attributed to etching processes of the wire surface occurring during the application of FeCl<sub>3</sub>. The results point to the importance of the initial etching processes induced by FeCl<sub>3</sub> at that surface for the subsequent deposition of the polymer shell. Another observable effect is the decrease of the defect luminescence of the ZnO nanowires what is attributed to passivation of the defect states on the ZnO nanowire surface by adsorption of the polymers.

## Transparent Conducting Magnetic V:ZnO

E. Chikoidze<sup>1</sup>, M. Boshta<sup>2</sup>, M. M. Gomaa<sup>2</sup>, J. Papierska<sup>3</sup>, J. Suffczyński<sup>3</sup>,  
C. Villard<sup>1</sup>, M. Neumann Spallart<sup>1</sup> and Y. Dumont<sup>1</sup>

<sup>1</sup>*Groupe d'Etudes de la Matière Condensée (GEMaC), Université de Versailles– CNRS,  
Versailles, France*

<sup>2</sup>*Solid State Physics Department, National Research Center, El-Behooth st., 12311Dokki,  
Giza, Egypt*

<sup>3</sup>*Faculty of Physics, University of Warsaw, Warsaw, Poland  
boshta2000@yahoo.com*

Wide band gap ZnO is well known as a transparent conducting oxide (TCO), a very interesting and promising material for transparent electronics [1]. We wish to further enhance its functionalities and a range of possible applications, e. g. in magnetophotonic devices, by doping of ZnO with magnetic ions. We aim to combine a cheap deposition technique, use of cheap amorphous substrates and a low deposition temperature with attractive properties of this material.

ZnO thin films doped with a nominal composition of 2%, 5% and 10% of Vanadium (V) have been grown by home built spray pyrolysis technique [2] on a fused silica substrate. ZnO:V growth by other physical and chemical growth methods have been reported previously [3-5]. EDS measurement confirms incorporation of vanadium in ZnO matrix. XRD spectra show that polycrystalline samples have (101) preferential growth direction.

Room temperature resistivities of the samples are between 14 Ohm.cm and 22 Ohm.cm. Resistivity versus temperature exhibits a semiconducting behavior, with estimated activation energy of conductivity equal to 30 meV. Carrier mobility and concentrations have been determined from Hall Effect measurements as:  $n = 2 \times 10^{17} \text{cm}^{-3}$  and  $2.6 \times 10^{18} \text{cm}^{-3}$  correspondingly for 2% and 10% V doped samples. Increase of carrier concentration with the V content, that vanadium occupies an  $V^{3+}$  state and plays role of a donor in the studied samples This is consistent with room temperature transmission measurements carried out in the energy range from 0.4 eV to 6.2 eV (3000 nm – 200 nm) indicating lack of absorption related to  $V^{+2}$  ions [5]. All studied samples are found to be fully transparent below the absorption edge of ZnO (3.3 eV), that is in VIS and NIR spectral region. No broadening of absorption edge upon V doping indicates a good crystalline quality of the layers.

Magnetoresistance (MR) of the films at  $T = 80 \text{ K}$  and  $T = 300 \text{ K}$  shows a positive sign. At  $B = 1.6 \text{ T}$ :  $MR = 7\% - 12\%$  varying with the V content.

Macroscopic magnetization measurement by VSM shows almost no magnetization for V concentrations below 10%, and a weak ferromagnetic response persisting up at room temperature for the 10% V doped sample.

Our results indicate that transparent, ferromagnetic at room temperature, with large room temperature magnetoresistance - polycrystalline ZnO:V is an interesting material for applications in “invisible” magnetoelectronics.

[1] H. Ohta and H. Hosono, ISSN:1369 7021 © Elsevier Ltd, (2004).

[2] E. Chikoidze et al., Journal of Applied Physics, **113**, 043713 (2013).

[3] K.Asano, S.Doi, H.Yamaguchi et al, J. Vac. Sci. Techn. A 29, 03A119, (2011).

[4] M.K.Gupta, B.Kumar, J. Mat. Chem. 21,14559, (2011).

[5] H.Saeki, H.Tabata, T.Kawai, Solid. State. Commun. 120, 439, (2001).

## Unambiguous DEFECT IDENTIFICATION in compound semiconductors by POSITRON ANNIHILATION SPECTROSCOPY

A. Sarkar<sup>1\*</sup>, M. Chakraborti<sup>2</sup>, S. Chattopadhyay<sup>3</sup>, and D. Sanyal<sup>4</sup>

<sup>1</sup>Department of Physics, Bangabasi Morning College, Kolkata 700009, India.

<sup>2</sup>Department of Physics, University of Calcutta, Kolkata 700009, India

<sup>3</sup>Department of Physics, Maulana Azad College, Kolkata 700013, India

<sup>4</sup>Radioactive Ion Beam division, Variable Energy Cyclotron Centre, Kolkata 700064, India

\*sarkarcal@gmail.com

We are engaged in unambiguous identification of vacancy defects in compound semiconductors such as ZnO, CdO, ZnS, CdS, TiO<sub>2</sub>, SnO<sub>2</sub> etc. using positron annihilation spectroscopy (PAS) [1-5]. Defects in the samples have been incorporated using annealing, mechanical milling and ion irradiation. Whenever possible, such defective samples have been compared with their single crystal counterparts. Also, modifications of electrical, magnetic and optical properties have been monitored with the nature of vacancy defects in the systems. We feel that the defect probing methodology we have adopted here can be extended to large family of compound semiconductor systems. Few of our interesting results are given below.

Granular ZnO samples, annealed at different temperatures between 200 and 1000 °C have been investigated using Doppler broadening of electron positron annihilation radiation lineshape (DBEPARL) measurements with two HPGe detectors in coincidence. Ratio curve [1,2] for each DBEPARL spectrum has been constructed with respect to that of the spectrum of as-supplied (unannealed) and single crystalline ZnO. Two prominent peak-like structures at  $p_L \sim 16.8 \times 10^{-3} m_0c$  and  $\sim 22.6 \times 10^{-3} m_0c$  for 1000 °C annealed sample can be clearly seen (here  $p_L$  represents electron momentum along the direction of the detectors). On the contrary, sample annealed at 400 °C or below show prominent dip (ratio less than 1) in nearby  $p_L$  values. Detailed analysis [3,4,6] of the peak/dip positions shows that they arise due to more/less annihilation of positrons with Zn 3p and 3s electrons. So generation and recovery of Zn vacancy defects as well as the relevant temperature zones can be clearly understood. In similar methodology, hydrogen defects in ZnO single crystal [3], Sn vacancies in ion irradiated SnO<sub>2</sub> [4] and Cd and O vacancies in CdO [5,7] have been identified.

Preferential segregation of atoms is another important topic in doped compound semiconductors like Zn(Ag)S, studied here by measuring positron lifetime in the material [8]. The lifetime of positrons trapped at grain surface defects in Zn(Ag)S is found to be  $\sim 350$  ps which is characteristic of Zn and S divacancy clusters. The defect lifetime is increased with the duration of mechanical milling of the material. However, after one hour milling defect lifetime (so also the average positron lifetime [1]) is slightly reduced. In the XRD data of the same material, a weak signal of Ag can be seen. Combining results of two different probes, segregation of Ag from ZnS host lattice to grain surface is clearly identified. This observation opens the scope to monitor evolution of ferromagnetism in nanocrystalline Zn(Mn)O or Zn(Co)O with the change of PAS parameters.

- [1] Dutta S, Chakraborti M, Chattopadhyay S, et al., J. Appl. Phys. **98**, 053513, (2005).
- [2] Dutta S, Chattopadhyay S, Sarkar A, et al., Prog. Mater. Sci. **54**, 89, (2009).
- [3] Sarkar A, Chakraborti M, Sanyal D, et al., J. Phys.: Condens. Matter **24**, 325503, (2012).
- [4] Sarkar A, Sanyal D, Nath P, et al., RSC Adv. **5**, 1148, (2015).
- [5] Sarkar A, Chattopadhyay S and De U, Phys. Status Sol. **6**, 2526, (2009)
- [6] Myler U and Simpson P. J., Phys. Rev. B **56**, 14303, (1997).
- [7] Sanyal D and Sarkar A, (to be submitted)
- [8] Sanyal D and Sarkar A and Chattopadhyay S, (In preparation).

## Dependence of the Structural, Chemical and Electrical Properties of GaAs/ZnSe Heterovalent Interface on MBE Growth Mode

T.A. Komissarova<sup>1\*</sup>, S.V. Sorokin<sup>1</sup>, I.V. Sedova<sup>1</sup>, G.V. Klimko<sup>1</sup>, M.V. Lebedev<sup>1</sup>, W. Calvet<sup>2</sup>,  
S.V. Gronin<sup>1</sup>, and S.V. Ivanov<sup>1</sup>

<sup>1</sup>Ioffe Institute, St. Petersburg, Russia

<sup>2</sup>Helmholtz-Zentrum Berlin (HZB), Berlin, Germany

\*komissarova@beam.ioffe.ru

Heterovalent III-V/II-VI semiconductor heterostructures are the perspective materials for optoelectronic, spintronic and photovoltaic applications. Special features of the heterovalent interface (HI) in contrast to the isovalent one can provide ample opportunities for heterostructure design with varied electronic structure and band offsets. Study of the HI properties depending on growth conditions is necessary for realization of these opportunities.

Three series of GaAs/ZnSe heterostructures grown by MBE on n-type GaAs (100) substrate were studied in this work. The structures of the first series (I) consist of a 0.2- $\mu\text{m}$ -thick GaAs:Si buffer layer and thin ZnSe layer with the thickness  $d = 2$  nm and were measured by Soft X-Ray Photoelectron Spectroscopy (SXPS). Other two series of samples (II and III) were intended for electrical (I-V curves) and structural (secondary ion mass spectroscopy (SIMS)) measurements and contain GaAs:Si and ZnSe:Cl layers with equal  $d$  (50 nm and 300 nm) and  $n$  ( $n = 2 \times 10^{17} \text{ cm}^{-3}$  and  $n = 8 \times 10^{17} \text{ cm}^{-3}$ ) values for II and III series, respectively. For the samples of each series, three growth mode of HI formation were used:

- (1) (2x4)As surface reconstruction after GaAs growth, start of the ZnSe growth on (2x1) surface decorated by Se, growth of ZnSe in MBE mode at 280°C;
- (2) (2x4)As surface reconstruction after GaAs growth, ZnSe growth by migration-enhanced epitaxy (MEE) at low temperature (210°C) with a Zn pre-exposure;
- (3) c(4x4)As surface reconstruction after GaAs growth, start of the ZnSe growth on (2x1) surface decorated by Se, growth of ZnSe in MBE mode at 280°C.

Analysis of the SXPS data has revealed that the average value of the valence band offset  $\Delta E_V$  at the GaAs/ZnSe HIs does not depend on the HI growth mode and is equal to  $\sim 0.77 \text{ eV}$ . At the same time, it has been shown that  $\Delta E_V$  value varies in rather wide range for each structure depending on a distance from the GaAs/ZnSe interface: 0.76-0.79 eV for HI of type (1), 0.71-0.81 eV for HI of types (2) and (3), i.e. band offset formation is realized within a finite thickness of the near-interface layer. It has been shown that the HIs are not chemically sharp and their chemical structure (deviation from the stoichiometry, diffusion of Ga and As into ZnSe layer) depends on the HI formation mode. The more abrupt and stoichiometric HI was obtained by the low-temperature MEE growth of ZnSe on (2x4)As surface. Se decoration results in chemical blurriness of the HI with the predominant Ga diffusion in case of the (2x4)As surface reconstruction and As diffusion for structures with the c(4x4)As surface reconstruction of the GaAs buffer.

The values of the potential barrier heights at HI of (570-640 meV) and (680-740 meV) for forward and reverse current direction, respectively, were determined from the I-V curve measurements for different structures. It has been shown that these values do not depend on the HI growth mode, that corresponds well to the SXPS results. However, the potential barrier values are higher than those of the conduction band offset  $\Delta E_C$  at the HI determined from the SXPS measurements ( $\Delta E_C$  should be  $\sim 0.5 \text{ eV}$  at  $\Delta E_V = 0.77 \text{ eV}$ ). This fact is explained by influence of the electrical fields at the HI arising due to the interdiffusion effects. Joint analysis of the SXPS, I-V and SIMS data allowed us to determine the relationship between chemical structure, interdiffusion effects, electrical fields and space charges at the HIs versus the HI growth mode. This work is partially supported by RFBR (grant ##13-02-01063).

## Significantly improved interface recombination velocity and minority carrier lifetime for CdTe/MgCdTe double heterostructures

Shi Liu<sup>1,2</sup>, Xin-Hao Zhao<sup>1,3</sup>, Calli M. Campbell<sup>1,3</sup>, Maxwell B. Lassise<sup>1,2</sup>, Yuan Zhao<sup>1,2</sup>, and Yong-Hang Zhang<sup>1,2,\*</sup>

<sup>1</sup>Center for Photonics Innovation, Arizona State University, Tempe, AZ 85287, USA

<sup>2</sup>School of Electrical, Computer, and Energy Engineering, Arizona State University, Tempe, AZ 85287, USA

<sup>3</sup>School for Engineering of Matter, Transport and Energy, Arizona State University, Tempe, AZ 85287, USA

\*Email: yhzhang@asu.edu

Recombination through surface states is a major undesirable carrier loss mechanism for solar cells. MgCdTe has been proposed as a barrier layer for CdTe to form a double heterostructure (DH) which offers sufficient carrier confinement and demonstrates a low interface recombination velocity of  $(4.7 \pm 0.4) \times 10^2$  cm/s [1]. This allows for the enhancement of single-crystal CdTe carrier lifetimes up to a value of  $0.34 \mu\text{s}$  [1-5]. In the present work, we have studied the dependence of interface recombination velocity on barrier height in several CdTe/Mg<sub>x</sub>Cd<sub>1-x</sub>Te DHs. A significant reduction in the interface recombination velocity and a much improved minority carrier lifetime are reported.

The samples studied are categorized into three groups, which feature 20 nm Mg<sub>0.36</sub>Cd<sub>0.64</sub>Te barriers, 15 nm Mg<sub>0.46</sub>Cd<sub>0.54</sub>Te barriers, and 30 nm Mg<sub>0.46</sub>Cd<sub>0.54</sub>Te barriers, respectively. The time-resolved PL decays for the studied samples are shown in Figure 1. They clearly show that the minority carrier lifetime decreases with CdTe layer thickness for all the samples, meaning the recombination velocities at the CdTe/MgCdTe interfaces are nonzero. A longest minority carrier lifetime of  $2.6 \mu\text{s}$  has been observed. The interface recombination velocities can be extracted by the linear fitting of  $1/\tau$  versus  $2/d$  plots, as shown in Figure 2. The extracted interface recombination velocities for Group I and II are  $66 \pm 17$  cm/s and  $43 \pm 20$  cm/s, respectively, and the interface recombination velocity for Group III is estimated to be below 10 cm/s. Detailed analysis of the recombination mechanisms will be presented at the conference.

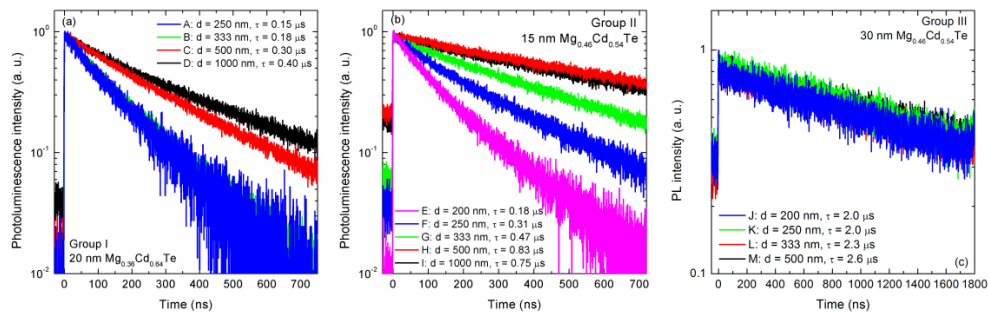


Figure 1 Time-resolved photoluminescence decays of the studied samples.

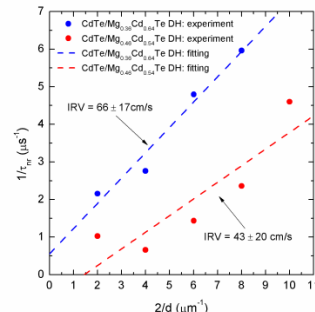


Figure 2 Extraction of interface recombination velocities by linear fittings of  $1/\tau_{tr}$  vs.  $2/d$  plots.

Table I. Structural parameters of the CdTe/Mg<sub>x</sub>Cd<sub>1-x</sub>Te double heterostructure samples.

Group	Sample	Parameters		
		$d_{\text{CdTe}}$ (nm)	$d_{\text{MgCdTe}}$ (nm)	$x$
I	A	250	20	0.36
	B	333		
	C	500		
	D	1000		
II	E	200	15	0.46
	F	250		
	G	333		
	H	500		
	I	1000		
III	J	200	30	0.46
	K	250		
	L	333		
	M	500		

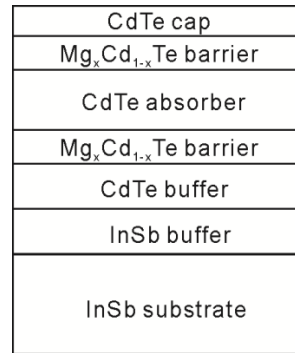


Figure 3 Schematic layer structure of the studied CdTe/MgCdTe double heterostructure samples.

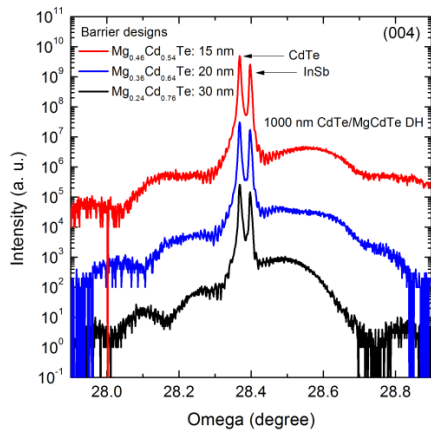


Figure 4 X-ray diffraction patterns of three CdTe/MgCdTe DHs showing excellent crystalline qualities.

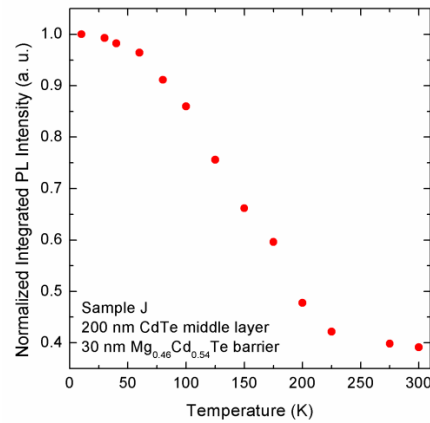


Figure 5 Integrated photoluminescence intensity as a function of temperature for sample J, showing an internal quantum efficiency of ~40% at 300 K.

**References**

[1] X.-H. Zhao, M. J. DiNezza, S. Liu, C. M. Campbell, Y. Zhao, and Y.-H. Zhang, Appl. Phys. Lett. **105**, 252101 (2014).  
 [2] M. J. DiNezza, X.-H. Zhao, S. Liu, A. P. Kirk, and Y.-H. Zhang, Appl. Phys. Lett. **103**, 193901 (2013).  
 [3] X.-H. Zhao, M. J. DiNezza, S. Liu, S. Lin, Y. Zhao, and Y.-H. Zhang, J. Vac. Sci. Tech. B **32**, 040601 (2014).  
 [4] S. Liu, X.-H. Zhao, C. Campbell, M. J. DiNezza, Y. Zhao, and Y.-H. Zhang, J. Vac. Sci. Tech. B **33**, 011207 (2015).  
 [5] C. H. Swartz, M. Edirisooriya, E. G. LeBlanc, O. C. Noriega, P. A. R. D. Jayathilaka, O. S. Ogedengbe, B. L. Hancock, M. Holtz, T. H. Myers, and K. N. Zaunbrecher, Appl. Phys. Lett. **105**, 222107 (2014).

## Influence of Source Transport Rate upon Compositions of Mg and Se in $Zn_{1-x}Mg_xSe_yTe_{1-y}$ Layers grown by Metalorganic Vapor Phase Epitaxy

K. Saito\*, M. Abiru, E. Mori, Y. Araki, D. Tanaka, T. Tanaka, Q.X. Guo, and M. Nishio

Department of Electrical and Electronic Engineering and  
Synchrotron Light Application Center, Saga University, Saga 840-8502, Japan

\*saito@o.m.saga-u.ac.jp

$Zn_{1-x}Mg_xSe_yTe_{1-y}$  quaternary alloy system is expected to be one of the best materials as a cladding layer of ZnTe based pure-green light-emitting devices (LEDs), because of the wide band-gap in the range from 2.26 to ~3.2 eV under lattice-matching to ZnTe. It is important to study this material for improving the performance of ZnTe based LED, therefore, since it has been demonstrated that even ZnTe pure-green LED with homo-junction structure shows an efficiency comparable to GaP LED [1]. Furthermore,  $Zn_{1-x}Mg_xSe_yTe_{1-y}$  is an interesting alloy system, since ambipolar doping is possible as suggested by theoretical investigation [2]. So far, several investigations have been reported on the preparation of  $Zn_{1-x}Mg_xSe_yTe_{1-y}$  by means of molecular beam epitaxy. Unfortunately there are only a few reports on the growth of  $Zn_{1-x}Mg_xSe_yTe_{1-y}$  using metalorganic vapor phase epitaxy (MOVPE), which is a potential epitaxial growth technique for mass production. Since the investigation on MOVPE growth of  $Zn_{1-x}Mg_xSe_yTe_{1-y}$  layer is in its infancy, therefore, information about the influence of the growth conditions upon the compositions of Mg and Se and crystal quality of  $Zn_{1-x}Mg_xSe_yTe_{1-y}$  layer is very important. In the previous studies[3,4], the effect of substrate temperature upon the Mg and Se compositions, surface morphology, roughness and Raman spectrum of  $Zn_{1-x}Mg_xSe_yTe_{1-y}$  layer has been clarified together with a trial on phosphorus doping. In this study, we perform growth work to investigate the relationship between the compositions and bis-methylcyclopentadienyl-magnesium ((MeCp)<sub>2</sub>Mg) or diethylselenide (DESe) transport rate.

The growth of nominal undoped  $Zn_{1-x}Mg_xSe_yTe_{1-y}$  layers was performed on semi-insulating gallium-doped (100) ZnTe substrates by using a horizontal-type atmospheric pressure MOVPE system. Dimethylzinc, (MeCp)<sub>2</sub>Mg, diethyltelluride and DESe were used as source materials. (MeCp)<sub>2</sub>Mg or DESe transport rate was varied between 1 and 11  $\mu\text{mol}/\text{min}$  while the other source transports were fixed. As (MeCp)<sub>2</sub>Mg transport rate increased, the Mg composition ( $x$ ) increased monotonically until 0.74 whereas the Se one ( $y$ ) was kept at ~0.23. Similar tendency was obtained when DESe transport rate was varied, although  $y$  was less than 0.35 due to a use of low substrate temperature. Then, it was demonstrated that the Mg and Se compositions in  $Zn_{1-x}Mg_xSe_yTe_{1-y}$  layer can be controlled successfully by these source transport rates. Also it was shown that  $Zn_{1-x}Mg_xSe_yTe_{1-y}$  layer nearly lattice-matched to ZnTe substrate is attainable by choosing proper source transport rate. Furthermore, the behaviors of the surface roughness and two Raman peaks corresponding to ZnSeTe-like longitudinal optical phonon mode and MgSeTe-like one in  $Zn_{1-x}Mg_xSe_yTe_{1-y}$  layer as a function of (MeCp)<sub>2</sub>Mg or DESe transport rate were clarified.

- [1] T. Tanaka, K. Saito, M. Nishio, Q. Guo, and H. Ogawa, *Applied Physics Express* **2**, 122101 (2009).
- [2] D. J. Chadi, *Phys. Rev. Lett.* **72**, 534 (1994).
- [3] M. Nishio, K. Saito, R. Ito, K. Tanaka, K. Urata, Y. Nakamura, T. Tanaka, and Q.X. Guo, *physica status solidi (c)* **11**, 1202 (2014).
- [4] M. Nishio, K. Saito, K. Urata, Y. Okamoto, D. Tanaka, Y. Araki, M. Abiru, E. Mori, T. Tanaka, and Q. Guo, *J. Crystal Growth*, **414**, 114 (2015).

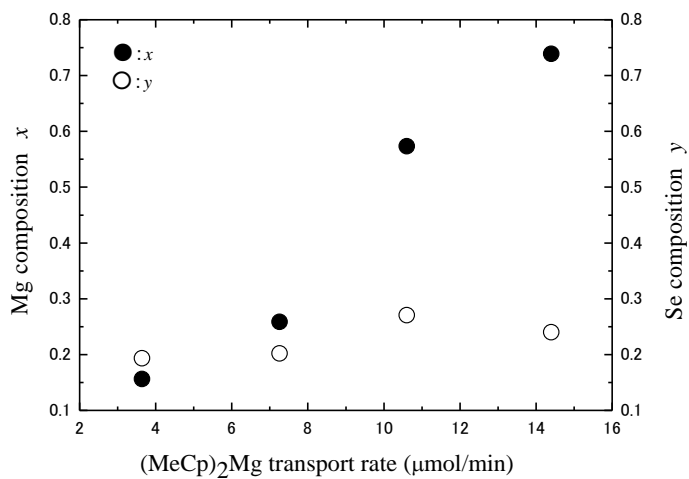


Fig.1. The compositions of Mg and Se versus (MeCp)<sub>2</sub>Mg transport rate.

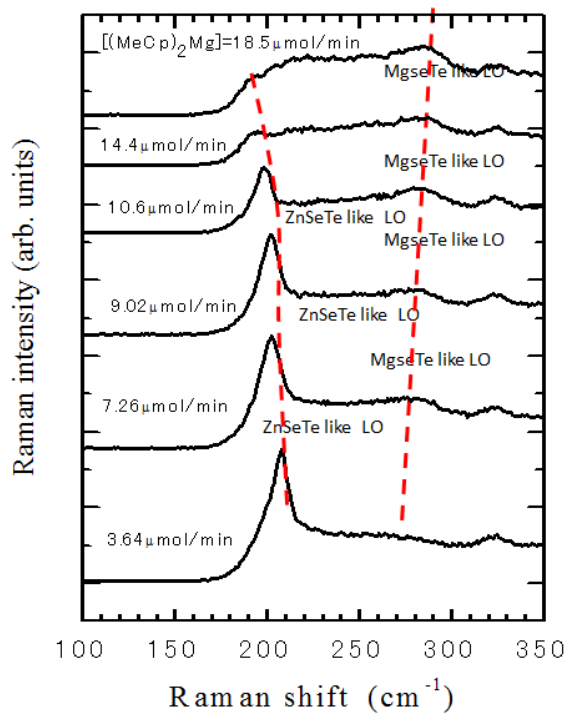


Fig.2. The change of Raman spectrum of Zn<sub>1-x</sub>Mg<sub>x</sub>Se<sub>y</sub>Te<sub>1-y</sub> layer when (MeCp)<sub>2</sub>Mg transport rate was varied.

## ZnSTe Lattice-matched to GaP Substrates Grown by Molecular Beam Epitaxy Using ZnS Buffer Layers

K. Ichino\*, S. Kashiya, N. Nanba, H. Hasegawa, and T. Abe

<sup>1</sup>Department of Information and Electronics, Graduate School of Engineering,  
Tottori University, Tottori, Japan

\*ichino@ele.tottori-u.ac.jp

ZnS has been known as efficient phosphors for cathode-ray tubes as well as a wide bandgap semiconductor, and thus considered as a possible material for semiconductor visible/UV light emitting devices. It has also been known, however, that achieving p-type conduction in ZnS is very difficult. We have previously reported p-type conduction in ZnS<sub>1-x</sub>Te<sub>x</sub>:N layers in the range of 0.1 <  $x$  < 0.3, and the operation of pn-junction light-emitting diodes [1,2]. The properties of the p-type layers such as conductivity and luminescence characteristics, however, were not satisfactory for practical applications. For the improvement, one of the problems seems to be insufficient crystal quality of the ZnS<sub>1-x</sub>Te<sub>x</sub> layers. Since these ZnS<sub>1-x</sub>Te<sub>x</sub>:N layers were grown on thick ZnS layers, a lattice-mismatch between ZnS<sub>1-x</sub>Te<sub>x</sub> and ZnS seems to cause deterioration of the crystals.

ZnS<sub>1-x</sub>Te<sub>x</sub> can be lattice-matched to GaP at a Te content  $x$  of 0.06, and superior crystal quality is expected under such a condition. Therefore, it is worthwhile to do p-type doping experiments on the lattice-matched layers. To date, there have been only a limited number of reports on ZnS<sub>1-x</sub>Te<sub>x</sub> growth on GaP, and almost no reports on the clear effect of lattice-matching of ZnS<sub>1-x</sub>Te<sub>x</sub> to GaP.

In this paper, we report the growth of ZnS<sub>1-x</sub>Te<sub>x</sub> layers lattice-matched to GaP substrates, and the improvement in the crystal quality by the use of thin ZnS buffer layers coherently grown on GaP substrates.

ZnS<sub>1-x</sub>Te<sub>x</sub> layers were grown on GaP substrates by molecular beam epitaxy using elemental sources of Zn, S and Te. Since S is preferentially incorporated into the films compared to Te, the S beam flux must be reduced to increase the Te content to a certain extent. The layers were characterized by X-ray diffraction (XRD), XRD reciprocal space maps (RSMs), and transmission electron microscope (TEM), etc.

First, ZnS<sub>1-x</sub>Te<sub>x</sub> layers were directly grown onto GaP substrates. Even the layers with  $x = 0.06$ , the lattice-matching condition, show only broad XRD peaks, suggesting poor crystal quality. This seems to be due to the deviation of the Te content in the initial stage of the growth, i.e., the growth on GaP surface, probably because the Te incorporation ratio depends on underlying materials.

In order to avoid this problem, a thin ZnS buffer layer was inserted between a ZnS<sub>1-x</sub>Te<sub>x</sub> layer and a GaP substrate. The ZnS buffer layer must be thinner than the critical thickness to avoid the generation of misfit dislocations since there is a lattice-mismatch of 0.77% between ZnS and GaP. We have previously reported that the critical thickness of a ZnS layer on a GaP substrate is less than 30nm [3]. Taking this value into account, ZnS<sub>1-x</sub>Te<sub>x</sub> layers with  $x \sim 0.06$  were grown onto 25-nm-thick ZnS buffer layers on GaP substrates. The ZnS<sub>1-x</sub>Te<sub>x</sub> layers thus grown are coherent with GaP substrates as confirmed by RSM, and exhibit narrow and intense XRD peaks, which clearly indicate an improvement in the crystal quality by the lattice-matching effect. p-type doping experiments to these layers are also reported.

[1] K. Ichino *et. al.*, Appl. Phys. Express, **6**, 112102, (2013).

[2] K. Ichino *et. al.*, Phys. Status Solidi C **11**, 1282, (2014).

[3] K. Ichino *et. al.*, Phys. Status Solidi C **9**, 1744, (2012).

## Low Pressure MOVPE Growth and Characterization of ZnTe Homoepitaxial Layers

M. Nishio, K. Saito\*, M. Abiru, E. Mori, Y. Araki, D. Tanaka, T. Tanaka, and Q.X. Guo

Department of Electrical and Electronic Engineering and  
Synchrotron Light Application Center, Saga University, Saga 840-8502, Japan

\*saito@o.m.saga-u.ac.jp

ZnTe is promising for application in a variety of optoelectronic devices such as pure-green light-emitting devices, terahertz detectors, solar cells and waveguides. So far, several efforts have been made to establish the epitaxial growth technique of high quality ZnTe layer. As for metalorganic vapor phase epitaxy (MOVPE), which is a powerful growth technique for mass production, undoped ZnTe layers of good quality have been achieved under atmospheric-pressure growth [1-3] based on a lot of experimental results on the effects of the growth condition on the quality. Low pressure MOVPE is promising for accurate control of the thickness of epitaxial layer. Since there is only a few studies on the effect of reactor pressure on MOVPE growth of ZnTe [4], however, the optimum growth conditions to obtain ZnTe layer of good quality in the case of low pressure MOVPE are still ambiguous, different from the case of atmospheric pressure MOVPE of ZnTe. In this work, low pressure MOVPE growths and characterizations of surface morphologies and photoluminescence (PL) properties of ZnTe layers have been carried out systematically by varying the substrate temperature or reactor pressure.

Undoped ZnTe layers have been homoepitaxially grown by using a horizontal-type low pressure MOVPE. Dimethylzinc (DMZn) and diethyltelluride (DETe) were used as source materials. The growth has been carried out by varying the substrate temperature or reactor pressure while DMZn and DETe transport rates and hydrogen flow rate were kept at 45 and 44  $\mu\text{mol}/\text{min}$  and 2.4 slm, respectively. The surface morphologies of ZnTe layers have been investigated using atomic force microscopy. Characterization of low temperature PL properties has also been carried out using a 488 nm  $\text{Ar}^+$  laser as an excitation light source. The growth characteristics such as growth rate behavior and variation of surface morphologies of ZnTe epilayers as a function of substrate temperature or reactor pressure were investigated. The growth conditions corresponding to the transition part between the mass-transport and the surface kinetics regimes provided an optimum growth for obtaining ZnTe layer with smooth surface, independent of reactor pressure. All PL spectra of ZnTe layers were marked by a free excitonic emission (FE) and the emission from excitons bound to neutral acceptors (Ia), indicating that ZnTe layer of good quality is obtainable under low pressure growth. The optimum growth condition for achieving a better PL property of undoped ZnTe layer, i.e., the PL spectrum with strong FE peak and weak Ia one, was in good agreement with that for obtaining smooth surface mentioned above.

- [1] T. Tanaka, K. Hayashida, S. Wang, Q. Guo, M. Nishio, and H. Ogawa, *J. Crystal Growth* **248**, 43 (2003).
- [2] M. Traversa, N. Loverginea, P. Prete, T. Di Luccio, G. Scalia, M. Pentimalli, L. Tapfer, P. Morales, and A. M. Mancini, *J. Appl. Phys.* **96**, 1230 (2004).
- [3] M. Nishio, K. Saito, T. Tanaka, and Q. Guo, *J. Crystal Growth* **370**, 348 (2013).
- [4] Y. Kume, Q. Guo, T. Tanaka, M. Nishio, H. Ogawa, and W. Shen, *J. Crystal Growth* **298**, 441 (2007).

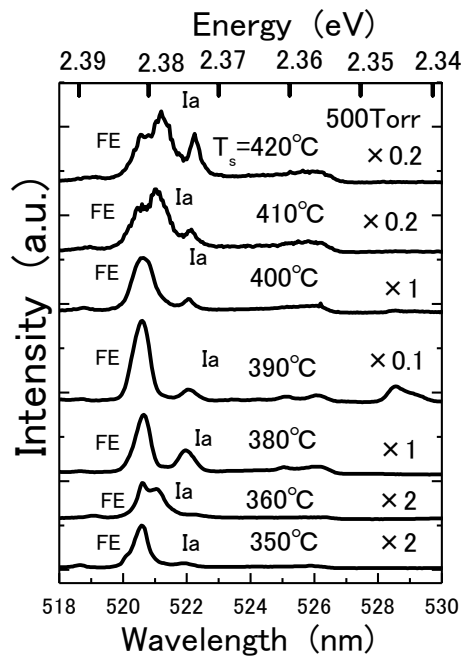


Fig.1. Change of low temperature PL spectrum of ZnTe layer when substrate temperature was varied.

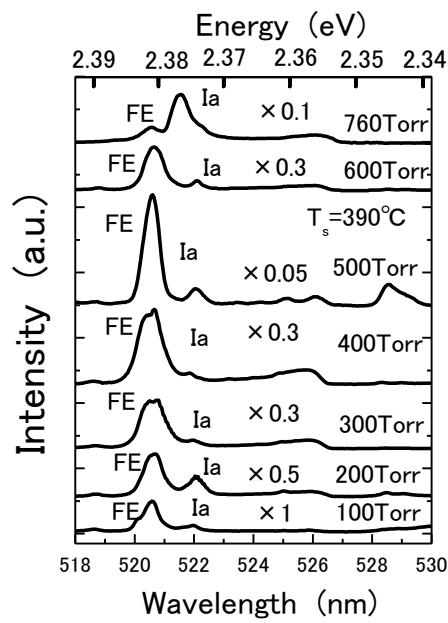


Fig.2. Change of low temperature PL spectrum of ZnTe layer when reactor pressure was varied.

## Diffusion Driven Growth of Nanowires: The case of ZnTe

Orrù M.<sup>1\*</sup>, Rueda-Fonseca P.<sup>1,2</sup>, Artioli. A.<sup>1</sup>, Den Hertog M.<sup>1</sup>, Genuist Y.<sup>1</sup>, André R.<sup>1</sup>, Ferrand D.<sup>1</sup>, Tatarenko S.<sup>1</sup>, Cibert J.<sup>1</sup> and Bellet-Amalric E.<sup>2</sup>

<sup>1</sup>Inst. NEEL, CNRS, Univ. Grenoble Alpes, F-38042 Grenoble, France

<sup>2</sup>INAC, CEA, Univ. Grenoble Alpes, 17 rue des Martyrs, 38054 Grenoble, France,

\*marta.orrù@neel.cnrs.fr

Semiconductor nanowires offer new opportunities for many potential applications and a great flexibility. However the precise control of their growth is very challenging. In the case of ZnTe, the coexistence of nanowires with zinc-blende and wurtzite structure, homogeneously distributed on the whole sample, is observed under stoichiometric growth conditions [1].

Nanowires with the zinc blende structure exhibit a low diffusion length on the sidewalls, accompanied by a significant lateral growth which gives rise to a cone shape structure. Their height distribution on a same sample is dramatically broad (see Fig A). To explain the morphology of these cone-shaped nanowires we have used a purely diffusion-driven growth model where the nanowires do not start growing all at the same time. This particular fact was confirmed using a series of CdTe insertions as markers during the nanowire growth. Transmission electron microscopy experiments on different nanowires of this sample show that the distance between insertions is constant but the number of insertions can vary from 1 to at least 8 (see Fig B).

By contrast, nanowires with the wurtzite structure assume a cylinder shape and show a narrow height distribution (see Fig. A) probably limited by nucleation mechanism at the nanowire – catalyst interface.

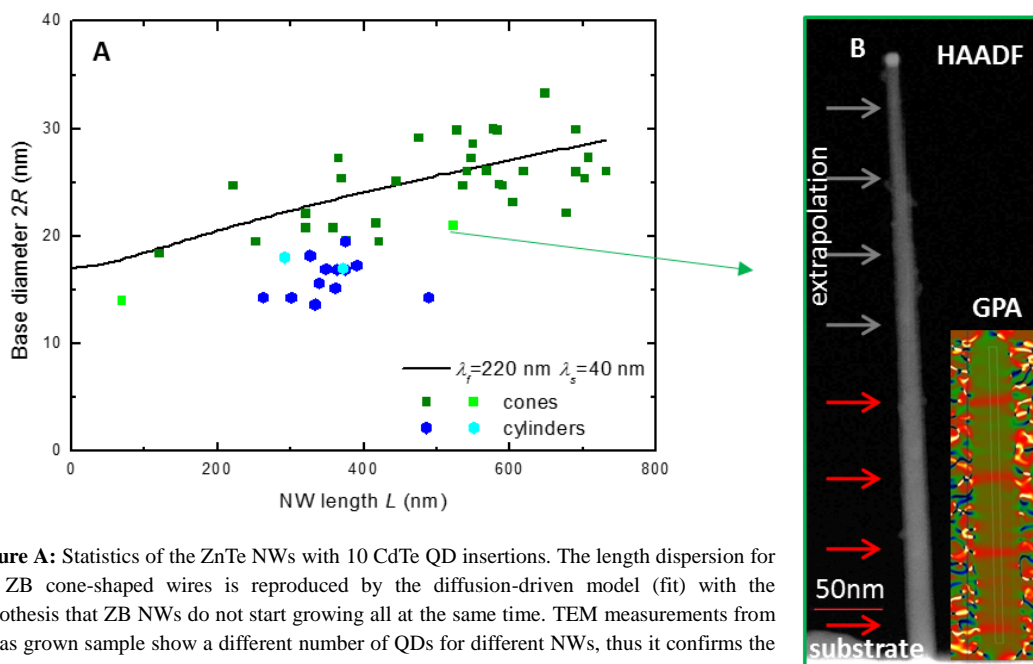


**Figure A:** Statistics of the ZnTe NWs with 10 CdTe QD insertions. The length dispersion for the ZB cone-shaped wires is reproduced by the diffusion-driven model (fit) with the hypothesis that ZB NWs do not start growing all at the same time. TEM measurements from the as grown sample show a different number of QDs for different NWs, thus it confirms the hypothesis.

**Figure B:** Example of TEM measurement of the as grown NW.

[1] P. Rueda-Fonseca et al., Nano Letters **14**, 1877, (2014).

## Photoluminescence of High-Resistivity ZnTe Crystals Doped with Gallium and Indium

Satoru Seto<sup>1\*</sup> and Kazuhiko Suzuki<sup>2</sup>

<sup>1</sup>Ishikawa National College of Technology, Tsubata, Kahoku, Ishikawa 929-0392, Japan

<sup>2</sup>Hokkaido University of Science, Maeda, Teine, Sapporo 006-8585, Japan

\*seto@ishikawa-nct.ac.jp

ZnTe is a unique II-VI compound semiconductor that p-type conduction can be easily obtained by phosphorous doping. Group III elements such as gallium or indium are expected to act as donors in ZnTe. However, these elements act as dopants for high resistivity and not as donors in ZnTe. It is therefore still difficult to obtain n-type low conductive ZnTe. In CdTe, on the other hand, group III elements act as donors substituting on Cd sites. In this study, we measured low temperature and temperature dependent PL spectra of high resistive ZnTe crystals doped with gallium or indium and compared the spectra with those of high resistive CdTe.

High resistive ZnTe single crystals we used in the present study were purchased from JX Nippon Mining & Metals Corp. The resistivity of the indium and gallium doped ZnTe crystals are  $5 \times 10^5$  and  $5 \times 10^7$   $\Omega\text{cm}$ , respectively. PL spectra in the near-band edge region at 10 K are shown in Fig. 1. We notice that the spectrum structure is very similar to each other. Emission peaks from free exciton (FX) and excitons bound to donors ( $D^0X$ ) and acceptors ( $A^0X$ ) can be clearly resolved. In addition to these excitonic peaks, a characteristic peak appears in the lower energy side of the  $A^0X$ . This peak has also been observed in ZnTe films grown on GaAs substrate [1] and high-resistive CdTe [2]. By comparison with a similar PL peak observed in high resistive CdTe, we identified the characteristic peak at 2.363 eV as emission from excitons bound to complex defects arising from a Zn vacancy and gallium or indium donor ( $V_{\text{Zn}}\text{-D}$ ) [2]. We also observed a broad emission band having a peak at 1.0 eV. The intensity of the deep emission in high-resistive ZnTe crystals is much stronger than that in undoped one. The deep levels related to the deep emission band is responsible for the high resistivity. At the conference, we will show temperature dependent of the deep emission band and discuss the mechanism of high resistivity in ZnTe doped with group III elements.

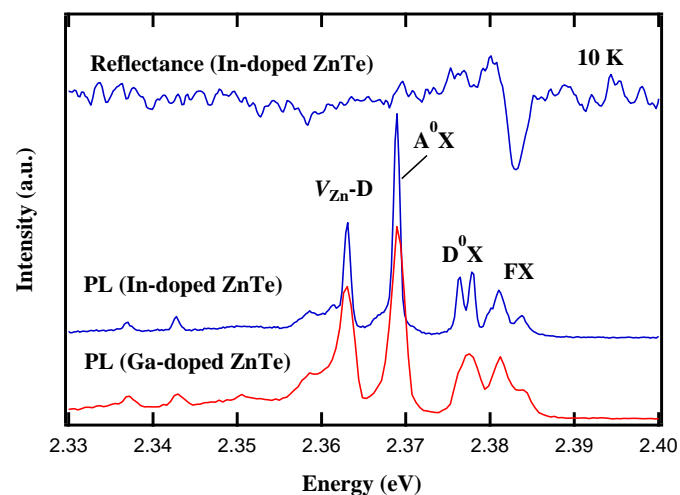


Figure 1. PL and reflectance spectra of In-doped and Ga-doped ZnTe single crystals.

[1] S. Seto, N. Mochida, K. Inabe, K. Suzuki, T. Kuroda, F. Minami, Phys. Stat. Sol (b) **229**, 587–590, (2002).

[2] S. Seto, K. Suzuki, V.N. Abastillas Jr, K. Inabe, J. Cryst. Growth **214/215**, 974-978, (2000).

## Ultrasonic-Assisted Mist Chemical Vapor Deposition for Oxide and Sulfide Semiconductor Thin Films

Shizuo Fujita<sup>1\*</sup>, Kazuaki Akaiwa<sup>2</sup>, Sam-Dong Lee<sup>2</sup>, Yoshito Ito<sup>2</sup>,  
Kenta Suzuki<sup>2</sup>, Ryosuke Takagi<sup>2</sup>, and Kentaro Kaneko<sup>1</sup>

<sup>1</sup>Photonics and Electronics Science and Engineering Center, Kyoto University, Kyoto, Japan

<sup>2</sup>Department of Electronic Science and Engineering center, Kyoto University, Kyoto, Japan

\*fujitasz@kuee.kyoto-u.ac.jp

We report the recent successful applications of mist chemical vapor deposition (CVD) technology for the growth of not only oxide but also sulfide thin films. The basic equipment in the mist CVD is an ultrasonic atomizer, which generates small ( $\sim 3 \mu\text{m}$  in diameter, depending on the ultrasonic frequency) mist particles of the precursor solution containing metal elements (Zn, Mg, Ga, In, etc.) of the target material. Safe and inexpensive chemicals such as acetylacetonates and chlorides may be used as sources, being solved in such as water and alcohol. Because the film deposition occurs in the atmosphere containing oxygen in the solvents, we have originally developed this technology for oxides growth [1]. However, recently, the growth of sulfides has been evidenced by the use of thiourea ( $\text{CH}_4\text{N}_2\text{S}$ ) in the solution [2,3]. The mist CVD, therefore, may be expensively applied to the growth of a variety of oxides and sulfide, not only II-VI but also other (I, III, IV)-VI compounds for their wide use as devices.

ZnO is an important material which can be grown by the mist CVD and exhibit excellent performance as a single crystal [4] and a polycrystal [5]. One of the post-ZnO applications of the mist CVD, brought by our group, is for III-oxides.  $\text{Ga}_2\text{O}_3$  is an attractive material for unexplored optical [6] and electrical [7,8] devices. We have developed structural and property control of corundum-structured  $\alpha\text{-Ga}_2\text{O}_3$  and  $\alpha\text{-In}_2\text{O}_3$  compounds, followed by  $\alpha\text{-(Al,Ga)}_2\text{O}_3$  and  $\alpha\text{-(Ga,In)}_2\text{O}_3$  alloys. MOSFETs of  $\alpha\text{-In}_2\text{O}_3$  was demonstrated, showing the effective mobility of  $217 \text{ cm}^2/\text{Vs}$  and the current on-off ratio of  $>10^6$ . Together with the wide gap of 3.7 eV, which is wider than those of SiC and GaN, we may infer that electron devices of  $\alpha\text{-In}_2\text{O}_3$  grown by the mist CVD are advantageous as high power devices due to their high performance and low cost. MOSFETs of  $\alpha\text{-Ga}_2\text{O}_3$  are now under investigation, where the control of electrical properties by doping is an unresolved issue at the present stage.

Recently, attempts have been given to apply the mist CVD technology to the growth of non-oxide materials. By solving thiourea in the source together with the metal sources, we could grow sulfides without severe contamination of oxygen. The successive mist sulfurization with the solution of thiourea was found to be effective to reduce the residual oxygen and to realize the stoichiometric composition of the target sulfides. Examples will be demonstrated for  $\text{Cu}_2\text{ZnSnS}_4$  (CZTS) and  $\text{CuInS}_2$  (CIS) thin films. It is very interesting why the reaction of source materials with sulfide overrides that with oxides.

We may conclude that the mist CVD technology can contribute to the marked evolution of oxides and sulfides, not only II-VI but also a variety of (I, III, IV)-VI compounds.

- [1] S. Fujita *et al.*, Jpn. J. Appl. Phys. **45**, L857 (2006); **47**, 4669 (2008); **47**, 7311 (2008).
- [2] K. Uno *et al.*, Jpn. Soc. Appl. Phys. Meetings, Mar. 2014, Sept. 2014, and Mar. 2015 [in Japanese].
- [3] K. Shibayama *et al.*, J. Soc. Mat. Sci. Jpn. (in press) [in Japanese].
- [4] H. Nishinaka *et al.*, Jpn. J. Appl. Phys. **48**, 121103 (2009).
- [5] Toshiba Mitsubishi-Electric Industrial Corporation (TMEIC), exhibitions in Japan and Korea.
- [6] T. Oshima *et al.*, Jpn. J. Appl. Phys. **48**, 011605 (2009).
- [7] M. Higashiwaki *et al.*, Appl. Phys. Lett, **100**, 013504 (2012); **103**, 123511 (2013)
- [8] K. Sasaki *et al.*, Appl. Phys. Express **5**, 035502 (2012).

## Percolation-type Multi-phonon Pattern of Zn(Se,S): Ambient/High-pressure Backward/Near-forward Raman Scattering and *Ab Initio* Calculations

Hajj Hussein R.,<sup>1</sup> Pagès O.,<sup>1\*</sup> Schuler S.,<sup>1</sup> Dicko H.,<sup>1</sup> Postnikov A.V.,<sup>1</sup> Polian A.,<sup>2</sup> Firszt F.,<sup>3</sup> Marasek A.,<sup>3</sup> Paszkowicz W.,<sup>4</sup> Maillard A.,<sup>5</sup> Broch L.<sup>1</sup> and Gorochov O.<sup>6</sup>

<sup>1</sup>LCP-A2MC / Institut Jean Barriol, Université de Lorraine, Metz, France

<sup>2</sup>IMPMC, CNRS, Université Pierre et Marie Curie, Paris, France

<sup>3</sup>Institute of Physics, Nicolaus Copernicus University, Toruń, Poland

<sup>4</sup>Institute of Physics, Polish Academy of Sciences, Warsaw, Poland

<sup>5</sup>LMOPS, Université de Lorraine – Sup'elec, Metz, France

<sup>6</sup>Laboratoire de Physique des Solides de Bellevue, CNRS, Meudon, France

\*Corresponding author: olivier.pages@univ-lorraine.fr

Based on a careful far-infrared study, supported by *ab initio* phonon calculations, Vynogradov *et al.* have proposed that the phonon modes of the Zn(Se,S) zincblende-type mixed crystal obey an exceptional pseudo-two-mode behavior [1]. In this work we further explore the nature of the phonon mode behavior of Zn(Se,S) by using a combination of backward / near-forward Raman scattering, with particular attention to the transverse optical modes.

Besides the three [1x(Zn-Se),2x(Zn-S)] known Raman modes apparent in the conventional backscattering geometry, one novel Zn-Se mode is revealed in the unusual near-forward scattering geometry, suggesting a four-mode [2x(Zn-Se),2x(Zn-S)] behavior for Zn(Se,S) falling into the scope of our so-called percolation scheme (1-bond→2-mode). Remarkably, the Zn(Se,S) Raman pattern appears to violate most admitted rules behind the current version of the percolation scheme for a zincblende alloy or a diamond one, in reference to GaAsP [2] and GeSi [3], respectively, concerning (i) the number of Raman modes, as well as the composition dependence of their (ii) frequencies and (iii) intensities.

The four-mode Zn(Se,S) Raman pattern is explained within a refined version of the percolation scheme, now suggested, in which the 1-bond→2-mode behavior is echoed among all constituent bonds of an alloy – in reference to (i), the phonon dispersion is taken into account besides the local strain – in reference to (ii), and both the Zn-Se and Zn-S bonds exhibit an unusual sensitivity to their local environment at the second-neighbor scale – in reference to (iii).

Last, the pressure dependence of the Zn(Se,S) percolation-type Raman pattern is studied in the phonon-polariton regime by near-forward scattering. It is a matter to decide whether the pressure-induced percolation-type phonon freezing earlier detected in backscattering with the model percolation-type (Zn,Be)Se mixed crystal when approaching its zincblende→rocksalt structural phase transition [4], tentatively attributed to the large contrast in the pressure transitions of its parent ZnSe (~10 GPa) and BeSe (~70 GPa) compounds, is preserved, or not, with Zn(Se,S), characterized by quasi identical pressure transitions of its parent compounds.

The discussion is supported by *ab initio* phonon calculations using prototype percolation-type (S,Se)-impurity motifs, and by a contour modeling of the multi-phonon-polariton Zn(Se,S) near-forward Raman spectra within the formalism of the linear dielectric response, based on ellipsometry measurement of the Zn(Se,S) refractive index. Particular attention is awarded to the coupling of neighboring transverse optical modes via their developing transverse electric field when entering the phonon-polariton regime.

[1] Vinogradov E. A., Mavrin B. N., Novikova N. N., and Yakovlev V. A., Phys. Sol. State **48**, 1940 (2006).

[2] Pagès O., Souhabi J., Postnikov A. V. and Chafi A., Phys. Rev. B **80**, 035204 (2009).

[3] Pagès O., Souhabi J., Torres V. J. B., Postnikov A. V. and Rustagi K. C., Phys. Rev. B **86**, 045201 (2012).

[4] Pradhan G. K., Narayana C., Pagès O., Breidi A., Souhabi J., Postnikov A. V., Deb S. K., Firszt F., Paszkowicz W., Shukla A. and El Hajj Hassan F., Phys. Rev. B **81**, 115207 (2010).

## Growth and Characterization of $\text{Mg}_{1-x}\text{Cd}_x\text{O}$ Thin Films.

L.M. Guia<sup>1\*</sup>, V. Sallet<sup>2</sup>, C. Sartel<sup>2</sup>, C. Martínez-Tomás<sup>1</sup>, and V. Muñoz-Sanjosé<sup>1</sup>

<sup>1</sup>Applied Physics Department, University of València, València, Spain

<sup>2</sup>Groupe d'Etude de la Matière Condensée, UVSQ-CNRS, Versailles, France

\*luis.m.guia@uv.es

The development of new optoelectronic materials has received significant attention from the materials science community. More concretely the II-VI compounds such as Mg, Zn and Cd oxides and its ternary alloys, namely  $\text{Mg}_{1-x}\text{Zn}_x\text{O}$  and  $\text{Cd}_{1-x}\text{Zn}_x\text{O}$ , have been and are being widely studied due to their huge physical properties. However there are only few reports regarding the alloys of CdO and MgO cubic binary oxides. Recently some theoretical papers were published showing the interesting properties that this alloy should present [1-3]. Since then, some experimental work has been carried out synthesizing CdO:Mg layers, with a concentration up to 6% of Mg content, by using the Spray Pyrolysis technique [4-5]. On the other hand, the growth of isolated nanoparticles on r-sapphire substrates of the new ternary compound  $\text{Cd}_{1-x}\text{Mg}_x\text{O}$  has been proved and characterized in the whole range of Mg content ( $0 \leq x \leq 1$ ) [6].

In this communication, we extend the work to the growth of thin films of the new  $\text{Mg}_{1-x}\text{Cd}_x\text{O}$  alloy in a large range of compositions by using the Metal Organic Chemical Vapour Deposition (MOCVD) method at low pressure. The selection of experimental conditions has been revealed as fundamental for obtaining the alloy.

By using XRD analysis the compound formation and the progressive incorporation of  $\text{Cd}^{2+}$  ions into the cubic MgO lattice has been demonstrated. Both, single-cubic phase  $\text{Mg}_{1-x}\text{Cd}_x\text{O}$  and layers with a phase separation where  $\text{Cd}_{1-x}\text{Mg}_x\text{O}$  and  $\text{Mg}_{1-x}\text{Cd}_x\text{O}$  co-exist have been studied. Finally, a morphological study of the  $\text{Mg}_{1-x}\text{Cd}_x\text{O}$  thin films has been carried out using Scanning Electron Microscopy (SEM) and the composition of the layers has been measured by using Energy Dispersive X-Ray analysis (EDX).

- [1] Y. Z. Zhu, G. D. Chen and H. Ye, Phys. Rev. B: Condens. Matter Mater. Phys. **77**, 245209, (2008).
- [2] B. Amin, I. Ahmad, M. Maqbool, N. Ikram, Y. Saeed, A. Ahmad and S. Arif, J. Alloys Compd. **493**, 212, (2010).
- [3] K. B. Joshi, U. Paliwal, K. L. Galav, D. K. Trivedi and T. Bredow, J. Solid State Chem. **204**, 367, (2013).
- [4] F. Atay, I. Akyuz, S. Kose, E. Ketenci and V. Bilgin, J. Mater. Sci.: Mater. Electron. **22**, 492, (2011).
- [5] M. Vigneshwaran, R. Chandiramouli, B. G. Jeyaprakash and D. Balamurugan, J. Appl. Sci. **12**, 1754, (2012).
- [6] Sreekumar Rajappan Achary, Said Agouram, Juan F. Sánchez-Royo, M Carmen Martínez-Tomás and Vicente Muñoz-Sanjosé. CrystEngComm **16**, 8969, (2014).

## Electronic spectrum of Bi-related defects in crystalline cadmium telluride

Bagaev V.<sup>1</sup>, Krivobok V.<sup>1\*</sup>, Klevkov U.<sup>1</sup>, Kolosov S.<sup>1</sup>, Nikolaev S.<sup>1</sup>, Onishchenko E.<sup>1</sup>, Pruchkina A.<sup>1</sup> and Skorikov M.<sup>1</sup>

<sup>1</sup>Lebedev Physical Institute, Moscow, Russia

\*krivobok@lebedev.ru

Bismuth doped cadmium telluride (CdTe:Bi) is of interest, because Bi doping enhances the photosensitivity of crystalline CdTe and allows to achieve high resistivity even at a moderate doping level ( $\sim 10^{17} \text{ cm}^{-3}$ ), which is important for  $\gamma$ -ray detectors [1]. The ab-initio modeling of Bi-related defects in CdTe predicts a strong dependence of Bi behavior on the Fermi energy, resulting in the formation of both acceptor ( $\text{Bi}_{\text{Te}}$ ) and donor ( $\text{Bi}_{\text{Cd}}$ ) centers [2]. Moreover, for the  $\text{Bi}_{\text{Cd}}$  donor, low symmetry DX-like state should be stable [2]. Thus, one would expect that a high resistivity of CdTe:Bi is a result of amphoteric Bi properties in CdTe lattice.

Using measurements of conductivity, photoconductivity and low-temperature photoluminescence, we have studied electronic levels in the band gap of CdTe:Bi (Bi concentration  $\sim 10^{18} \text{ cm}^{-3}$ ), CdTe:Bi,Cl (bismuth concentration  $\sim 10^{18} \text{ cm}^{-3}$ , chlorine concentration  $\sim 10^{17} \text{ cm}^{-3}$ ) single crystals grown by the modified Bridgman technique. All CdTe:Bi samples were p-type with a resistivity falling in the range of  $10^5$ - $10^9 \text{ Ohm}\cdot\text{cm}$ . The conductivity of CdTe:Bi with a lower resistivity is determined by two deep levels of 0.29 eV and 0.4 eV. At low temperatures ( $< 120 \text{ K}$ ), these samples reveal persistent photoconductivity. For samples with higher resistivity the conductivity is determined by a deep level with an energy of 0.72 eV. CdTe:Bi,Cl samples exhibited n-type conductivity with a resistivity of 1-2  $\text{Ohm}\cdot\text{cm}$ . The relatively high conductivity is due to  $\text{Cl}_{\text{Te}}$  shallow donors.

Low temperature (5K) PL spectra of all of the samples under study reveal a shallow Bi-related acceptor with an activation energy of 36 meV. For CdTe:Bi, this defect is responsible for the acceptor bound exciton (PL line at 1.5905 eV) and the strong free-to-bound transition (band at  $\sim 1.571 \text{ eV}$ ). In CdTe:Bi,Cl, distant donor-acceptor pairs (DAP) related to the  $\text{Cl}_{\text{Te}}$  hydrogen-like donor and shallow Bi related acceptor were surely observed. This fact allows us to restore the electronic spectrum of the Bi-related shallow acceptor using the analysis of the selectively excited DAP PL (details of the experimental technique can be found in ref. [3]). The data obtained indicate that the effective potential for a hole bound to the shallow acceptor has a reduced symmetry. The effective potential consists of a negative non-tetrahedral central cell correction as well as of a low-symmetry long-range part which is apparently due to local lattice distortion. Using similar measurements of selectively excited PL, we have shown that the defect bands in the region of 1.35-1.5 eV are due to residual impurities ( $\text{Ag}_{\text{Cd}}$ ,  $\text{Cu}_{\text{Cd}}$ ) or Cl-related A-centre [3]. Thus, we have shown that there are no Bi-related donor/acceptor states in CdTe whose energies fall in the range of 0.05-0.25 eV.

- [1] E. Saucedo, O. Martinez, C.M. Ruiz, O. Vigil-Galan, I. Benito, L. Fornaro, N.V. Sochinskii, and E. Dieguez. *J. Cryst. Growth* 291, 416 (2006)
- [2] M.-H. Du. *Phys. Rev. B* 78, 172105 (2008)
- [3] Pruchkina A.A., Krivobok V.S., Nikolaev S.N., Onishchenko E.E., Belov A.G., Denisov N.A., Merinov V.N. *JETP Letters* 98, 450 (2013)

## Application of the difference spectroscopy for studying of complex acceptors in Cd(Zn)Te

Bagaev V.<sup>1</sup>, Krivobok V.<sup>1\*</sup>, Nikolaev S.<sup>1</sup>, Onishchenko E.<sup>1</sup>, Pruchkina A.<sup>1</sup> and Skorikov M.<sup>1</sup>

<sup>1</sup>Lebedev Physical Institute, Moscow, Russia

\*krivobok@lebedev.ru

Using differential optical spectroscopy we have studied electronic spectra of complex acceptors in compensated Cd(Zn)Te single crystals. The method applied is based on the fact that a compensated semiconductor usually contains distant donor-acceptor pairs (DAPs). The excited states of the donor and the acceptor in a specified DAP form a set of absorption bands, typically located close to the fundamental absorption edge. Analysis of the low temperature photoluminescence (PL) spectra recorded using selective excitation of these bands in a high-quality undoped single crystal allows one to restore the energies of the excited states for donors and acceptors in a given type of DAP [1,2]. Inhomogeneous broadening and/or excitation transfer between selectively excited DAPs strongly complicate the application of this approach for doped semiconductors or semiconductor alloys. The wavelength modulation of the excitation source and the analysis of the differential PL signal allowed us to the extend above mentioned well-known approach to the case of doped single crystals (CdTe:Cl, CdTe:Ag,Cl, CdTe:Bi,Cl) and undoped alloys CdZnTe.

Using the approach described above we have measured the energies of five excited states for the tetrahedral  $\text{Ag}_{\text{Cd}}$  acceptor in CdTe:Ag,Cl. The values obtained are in good agreement with the  $\text{Ag}_{\text{Cd}}$  spectrum in CdTe known from the literature. In the case of small DAP (the distance between the donor and acceptor  $R_{\text{DA}} < 10\text{nm}$ ); the splitting of the fourfold degenerate  $2\text{P}_{3/2}$  and  $2\text{S}_{3/2}$   $\text{Ag}_{\text{Cd}}$  excited states has been surely observed. This splitting results from the degeneracy lifting due to the low symmetry of DAPs. For the acceptor with an activation energy of  $\sim 120\text{ meV}$ , commonly referred to in the literature as Cl-related A-centre, the energies of eight excited states have been determined, see fig. The observed energy spectrum indicates the mixing of S-like and P-like acceptor states and confirms a low symmetry of the A-centre. From the analysis of the data obtained, it follows that the A-centre is characterized by a strong low-symmetry central-cell correction, while at large distances ( $> 1\text{ nm}$ ) from the defect there is only a weak non-tetrahedral perturbation.

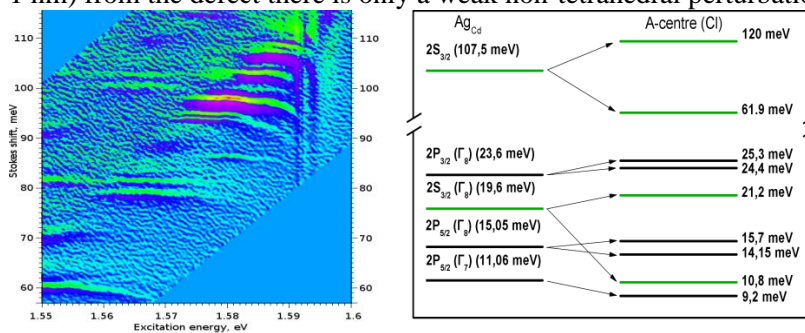


Fig. (Left) Map of the satellites detected in the PL spectra of CdTe:Cl under selective excitation of A-centre related DAPs. (Right) Scheme of the measured A-centre electronic spectrum in comparison with the energy spectrum of  $\text{Ag}_{\text{Cd}}$  acceptor.

Similar studies have been carried out for CdTe:Bi,Cl and CdZnTe single crystals. In particular, the electronic spectrum of Bi-related shallow (36 meV) acceptor has been revealed. The data obtained indicate that this acceptor is characterized by strong low symmetry lattice distortion. For  $\text{Cd}_{1-x}\text{Zn}_x\text{Te}$  ( $x < 0.1$ ) alloys, the influence of zinc concentration on the electronic spectrum of phosphorous ( $\text{P}_{\text{Te}}$ ) acceptor has been shown.

[1] V. S. Bagaev, V. S. Krivobok, E. E. Onishchenko, M. L. Skorikov, A. A. Shepel. JETP, **113**, 808 (2011)

[2] E. Molva, J. L. Pautrat, K. Saminadayar, G. Milhberg, and N. Magnea. Phys. Rev. **30**, 3344 (1984)

## Preparation of $\text{Cu}_2\text{ZnSnSe}_4$ films from selenization of Cu-Zn-Sn spin-coated precursors by dimethyl selenide

Masahiro Tahashi<sup>1\*</sup>, Ryota Yamada<sup>1</sup>, Kenji Yoshino<sup>2</sup>, Makoto Takahashi<sup>3</sup>, and Hideo Goto<sup>1</sup>

<sup>1</sup>Department of Electrical Engineering, Chubu University, Kasugai, Japan

<sup>2</sup>Department of Electrical and Electronic Engineering, University of Miyazaki, Japan

<sup>3</sup>Department of Applied Chemistry, Chubu University, Kasugai, Japan

\*tahashi@isc.chubu.ac.jp

$\text{Cu}_2\text{ZnSn}(\text{S},\text{Se})_4$  (CZTSSe) is a promising candidate to replace  $\text{Cu}(\text{In}, \text{Ga})\text{Se}_2$  in thin film photovoltaic modules. CZTSSe has a direct band gap of 1.0-1.5 eV and a high absorption coefficient of  $10^4\text{cm}^{-1}$ . Solar cells based on CZTSSe have achieved a conversion efficiency of 12.6%. Furthermore, CZTSSe does not contain any toxic or low-abundance elements. Various fabrication methods for CZTSSe have been investigated. Generally, the two-step process for the formation of CZTSSe is the most commonly used one. The first step is preparation of Cu-Zn-Sn precursor. Non-vacuum technique for precursor has been required for low-cost fabrication of solar cells. Next, the second step is sulfurization/selenization process using elemental S/Se vapor, or  $\text{H}_2\text{S}/\text{H}_2\text{Se}$  gas. In particular,  $\text{H}_2\text{S}/\text{H}_2\text{Se}$  gas is highly toxic and is stored in high-pressure cylinders; consequently, it must be handled carefully to prevent leakage. The organometallic compound is an alternative source material which offers several advantages over  $\text{H}_2\text{S}/\text{H}_2\text{Se}$  gas, and it is a liquid at room temperature and can be stored in a stainless steel bubbler at atmospheric pressure, so that it has a much lower risk of leakage than  $\text{H}_2\text{S}/\text{H}_2\text{Se}$  gas.

In this paper, we prepared the Cu-Zn-Sn precursor using spin-coating technique with copper naphthenate, zinc naphthenate, and tin octinate solutions. These solutions are used for adhesive and paint so that they are suitable for spin-coating technique. And, polycrystalline  $\text{Cu}_2\text{ZnSnSe}_4$  (CZTSe) films were prepared by thermal treatment of the precursor in the presence of dimethyl selenide (DMSe).

Copper naphthenate, zinc naphthenate, and tin octinate solutions were used as starting materials for Cu-Zn-Sn precursors and mixed in molar ratios, Cu : Zn : Sn = 2 : 1.5 : 1. The homogeneous solution was spin-coated at 3000 rpm for 30 s onto soda lime glass substrates. The coated films were calcined at 450 °C and kept for 15 min in nitrogen gas. The procedure of coating and calcination was repeated 5 times to obtain the precursor films having thickness of 1  $\mu\text{m}$ . Finally, the calcined precursor films were selenized in DMSe at 400–600 °C for 90 min. The supply rate of DMSe was set to 10  $\mu\text{mol}/\text{min}$ , and the total flow rate of nitrogen carrier gas was 100 mL/min at atmospheric pressure.

Figure 1 shows X-ray diffraction patterns of samples obtained at 400–600 °C. The formation of CZTSe was promoted at the treatment temperature of 500 °C.

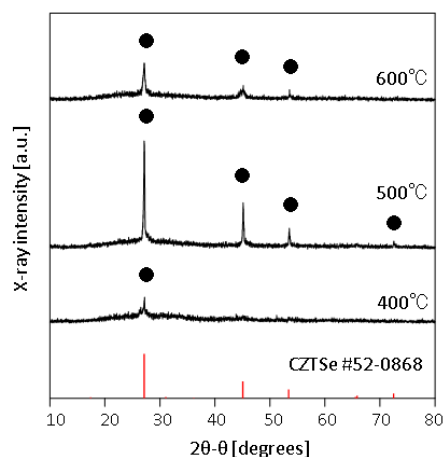


Fig.1 XRD patterns of samples obtained at different treatment temperatures.

**Poster Session 1 - MoP**

**ZnO , related oxydes and Transparent conductors (devices and physics)**

## Persistent photoconductivity of ZnO nanowires under varying ambient conditions

Florian Huber<sup>1\*</sup>, Manfred Madel<sup>1</sup>, Raphael Müller<sup>1</sup>, Martin Dickel<sup>1</sup>, Bruno Amann<sup>1</sup>,  
and Klaus Thonke<sup>1</sup>

<sup>1</sup>Institute of Quantum Matter /Semiconductor Physics Group, Ulm University, Ulm, Germany

\*florian.huber@uni-ulm.de

Zinc oxide, with a wide direct band gap ( $\sim 3.4$  eV) and large exciton binding energy (60 meV), is a promising candidate for visible range optoelectronic and sensing devices. After excitation with UV light, ZnO shows persistent photoconductivity (PPC), which is mostly attributed to intrinsic defects or adsorption and desorption processes of oxygen at the surface. As intrinsic defects, especially oxygen vacancies are discussed as a possible reason for the long persistence of the photocurrent. Following theoretical calculations, these oxygen vacancies can be excited by UV light from an electron trapping deep DX state into a shallow donor state [1]. The PPC depends strongly on the oxygen concentration in the ambient gas and can persist over days at room temperature [2,3].

To further understand the PPC, we investigated in detail the kinetics of the photoinduced conductivity processes of ZnO nanowires on the short and long time scale at different temperatures, in different ambient gases, and for different excitation wavelength.

The nanowires used here were grown by chemical vapor deposition at high temperature on silicon substrates using gold as catalyst. After separation from the substrate, they were deposited on a structure with two closely spaced Au contacts using a dielectrophoresis method allowing to contact a high number of wires in parallel (see Figure 1).

The photoconductivity of these structures shows a clear photon energy threshold slightly below the bandgap energy  $E_g$ , and follows the temperature dependence of  $E_g$ . In measurements with short and long illumination times the decay process follows a stretched exponential function. The decay time of the PPC depends on the illumination time interval, and is slower after longer exposure times (see Figure 2). From temperature dependent measurements, an activation energy for the decay process, which changes with the ambient gas atmosphere, could be determined. We found this activation energy to be lower in pure oxygen atmosphere as in atmospheres with reduced oxygen content.

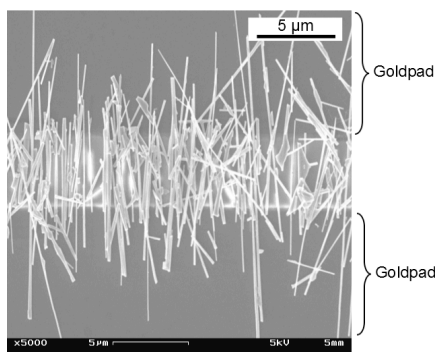


Fig. 1: SEM picture of the ZnO nanowires on a contact structure.

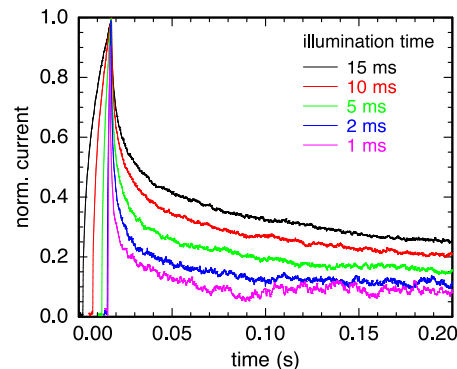


Fig. 2: Photocurrent of ZnO nanowires after short UV-excitation.

- [1] S. Lany and A. Zunger, Physical Review B **72**, 035215, (2005).
- [2] J. Bao et al., Nanoscale Research Letters **6**, 404, (2011).
- [3] B. Claflin et al., Journal of Crystal Growth **287**, 16 (2006).

Additional page – not included in the abstract booklet:

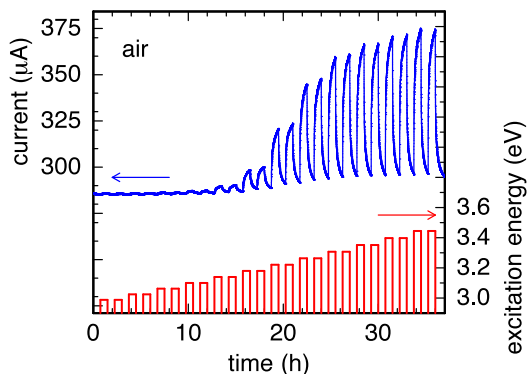


Fig. 3: Photocurrent at different excitation wavelength in air.

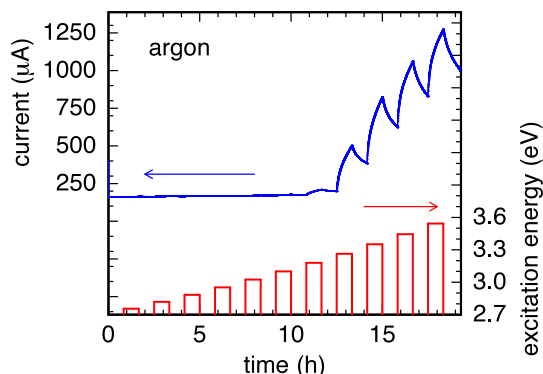


Fig. 4: Photocurrent at different excitation wavelength in argon. The current increase is much higher and the decay process slower compared to the measurement in air.

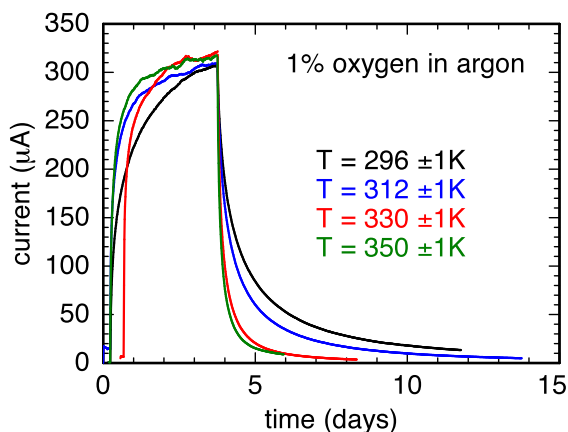


Fig. 5: Temperature dependency of the long-term decay process.

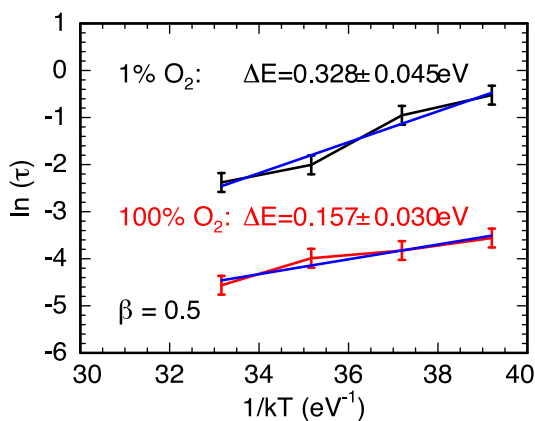


Fig. 6: Arrhenius plot of the long-term decay times. The activation energy for the decay process is doubled in 1% oxygen compared to pure oxygen atmosphere.

## Band Tail Induced Photoluminescence Broadening in Heavily-Doped n-Type ZnO Nanowires

Haiping He\*, Hongfeng Duan, and Zhizhen Ye

College of Materials Science and Engineering, Zhejiang University, Hangzhou, China

\*E-mail: hphe@zju.edu.cn

n-type doping of ZnO nanowires is the key to construct various nanoscale optoelectronic devices for light-emitting, transparent conductive, and plasmonic applications. However, the determination of doping level is more difficult for ZnO nanowires when compared with thin films. For semiconductor nanowires, generally field effect transistor (FET) based on individual nanowire is fabricated to measure the electrical properties. Unfortunately, this method is difficult to be employed in heavily-doped semiconductor nanowires.[1] Therefore, there are few reports on the electrical properties of heavily-doped n-ZnO nanowires so far. The optical characterization of such nanowires is also limited.

In this work, we demonstrate that photoluminescence (PL) is a non-damaging and powerful tool for the characterization of heavily-doped semiconductor nanostructures such as n-ZnO nanowires. Using a conventional vapor phase transport method, ZnO nanowires with controllable doping of indium (In) as high as 3.3 at% can be grown. The low temperature PL shows clear redshift and broadening with increasing doping concentration. The near band edge PL shows FWHM as large as 171 meV even at 15 K. The PL has a Gaussian-shaped low-energy wing, indicating a broadening mechanism governed by impurity band rather than the Burstein-Moss effect.[2] We highlight that the electron concentration of ZnO nanowires can be estimated from the PL linewidth according to the model of tail-induced broadening. For example, the electron concentration in ZnO nanowires doped with 3.3 at% of In is estimated to be  $\sim 5 \times 10^{20} \text{ cm}^{-3}$ , indicating a high doping efficiency.

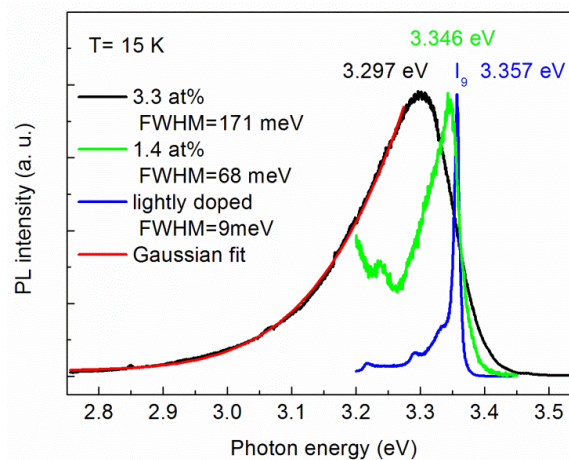


Figure 1. Low temperature PL spectra of the lightly- and heavily-doped ZnO nanowires. The low-energy tail of the heavily-doped PL can be well fitted by Gauss function.

- [1] G. D. Yuan, W. J. Zhang, J. S. Jie, X. Fan, J. X. Tang, I. Shafiq, Z. Z. Ye, C. S. Lee, and S. T. Lee, *Adv. Mater.* **20**, 168, (2008).  
 [2] E. Iliopoulos, D. Doppalapudi, H. M. Ng, and T. D. Moustakas, *Appl. Phys. Lett.* **73**, 375, (1998).

## Annealing effects on nitrogen-doped ZnO nanowires.

Sartel C.<sup>1</sup>, Hassani Said<sup>1</sup>, Vilar C<sup>1</sup>, Lusson A<sup>1</sup>, Sallet V. and Galtier P.

<sup>1</sup> GEMaC, Université de Versailles-Saint-Quentin-en-Yvelines 45, avenue des Etats-Unis –  
78035 Versailles Cedex, France

\*Email of corresponding author: [corinne.sartel@uvsq.fr](mailto:corinne.sartel@uvsq.fr)

The ZnO nanowires (NW) were grown at 650°C by low-pressure MOCVD, using DEZn, O<sub>2</sub> and NH<sub>3</sub> as zinc, oxygen and nitrogen doping sources respectively. The ZnO NWs were annealed under different conditions (gas and temperature). They were characterized by scanning electron microscopy (SEM), photoluminescence (PL), and micro-Raman.

The undoped (sample A) and doped (sample B), ZnO NWs were vertically aligned along their c-axis (fig1). The undoped NWs diameter is less than of doped NWs. The Raman spectra of nitrogen-doped NWs, as-grown or annealed, exhibited three additional Raman peaks (276, 510 and 580cm<sup>-1</sup>), related to the nitrogen incorporation, in addition to the classical Raman modes (fig.2). Bound and surface exciton (I<sub>6</sub> and X<sub>s</sub>) are observed on PL spectra of sample A (fig.3). All PL spectra collected on doped ZnO NWs, as-grown and annealed after doping, exhibit also a DAP transition and phonon replicas. We observed that the intensity of surface exciton X<sub>s</sub> is strongly decreased after annealing.

In conclusion, the annealing conditions do not affect the morphology of NWs, the additional Raman modes, and the DAP, but only the surface exciton X<sub>s</sub>.

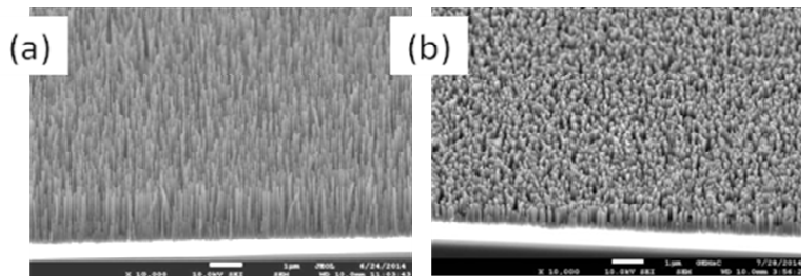


Fig 1 : SEM images Sample undoped A (a) and sample B doped as-grown(b)

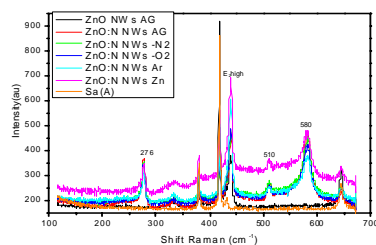


Fig2: Raman spectra collected on sample A and B as-grown and annealing

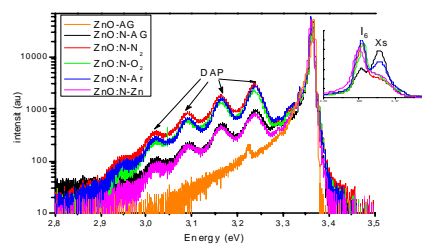


Fig3: PL spectra collected on sample A and B as-grown and annealing

## Enhanced Ultraviolet Luminescence of ZnO Nanorods Treated by High-Pressure Water Vapor Annealing

A. Al-Nafiey<sup>1,2</sup>, B. Gelloz<sup>3</sup>, B. Sieber<sup>2,\*</sup>, A. Addad<sup>2</sup>, M. Moreau<sup>4</sup>, J. Barjon<sup>5</sup>  
and R. Boukherroub<sup>1</sup>

<sup>1</sup> IRI, USR CNRS 3078, Université Lille 1, 59658 Villeneuve d'Ascq Cédex, France

<sup>2</sup> UMET, UMR CNRS 8207, Université Lille 1, 59655 Villeneuve d'Ascq Cédex, France

<sup>3</sup> Department of Applied Physics, Nagoya University, Nagoya, 464-8603 Aichi, Japan

<sup>4</sup> LASIR, UMR CNRS 8516, Université Lille1, 59655 Villeneuve d'Ascq Cédex, France

<sup>5</sup> GEMAC, UMR CNRS 8635, Université de Versailles, 78035 Versailles, France

\*Brigitte.Sieber@univ-lille1.fr

The luminescence intensity of ZnO nanostructures is very much surface-dependent as a result of their large surface area to volume ratio. Thus, whatever the bulk luminescence intensity, the more defective the surface is, the lower the total luminescence emitted by the nanostructure. One way to reduce the density of surface defects is to anneal the nanostructures at high temperature. In such high temperature post-annealing leading to an improvement of the optical properties of ZnO, air, oxygen and argon are the most used atmospheres. To the best of our knowledge, the influence of high-pressure water vapor annealing (HWA) on ZnO nanostructures has never been reported. HWA has been successfully used to improve the photoluminescence (PL) of porous silicon<sup>1</sup> and silicon nanowires substrates.

In this work, we show that HWA of ZnO nanorods at a temperature as low as 260°C leads to a large enhancement of their UV luminescence. The ZnO nanorods were prepared via a chemical bath deposition method at low temperature (96°C) on silicon substrates.<sup>2</sup> Then the samples were post-annealed for 3 h either in air, or using HWA with pressures in the range 1.3 -3.9 MPa. Figure 1 shows the PL spectra of as-grown and annealed ZnO nanorods. It is clear that while annealing in air allows the appearance of the UV band (very weak in the as-prepared samples), the HWA treatment leads to a further threefold increase of its intensity. Also the visible band is strongly decreased after post-annealing.

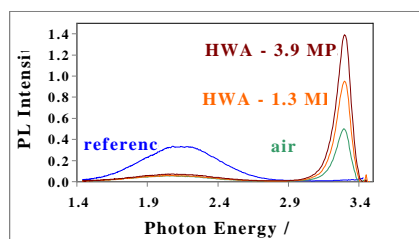


Fig. 1 Room temperature PL spectra of ZnO nanorods before and after annealing under shown conditions (Excitation: 325 nm).

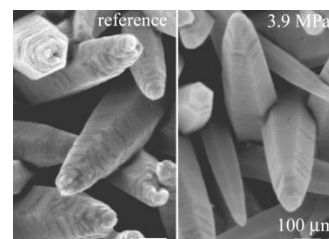


Fig. 2 SEM image of as-grown and HWA treated ZnO nanorods showing the decrease of surface roughness.

The characterization of the nanostructures using micro-Raman spectroscopy, cathodoluminescence, transmission electron microscopy and scanning electron microscopy (SEM-Fig 2) demonstrates that the main origin of the UV enhancement is reconstruction of the nanorods surface.

[1] B. Gelloz, A. Kojima and N. Koshida, Appl. Phys. Lett. **87**, 031107 (2005)

[2] G. Perry, Y. Coffinier, V. Thomy and R. Boukherroub, Langmuir, **28**, 389-395 (2012)



## Enhanced ultraviolet emission from Au/Ag-nanoparticles@MgO/ZnO heterostructure light-emitting diodes: A combined effect of exciton- and photon- localized surface plasmon couplings

W. Z. Liu,\* H. Y. Xu, and Y. C. Liu

Key Laboratory for UV Light-Emitting Materials and Technology of Ministry of Education, Northeast Normal University, Changchun 130024, China

\*liuwz455@nenu.edu.cn

Localized surface plasmon (LSP)-enhanced ultraviolet light-emitting diodes (LEDs) based on a Au/MgO/ZnO metal/insulator/semi-conductor heterostructure were fabricated by embedding Ag nanoparticles (Ag-NPs) into MgO dielectric layer. A ~6-fold electroluminescence (EL) enhancement was achieved from the Ag-NPs decorated device. Time-resolved spectroscopy studies, as well as theoretical estimations based on experimental data, reveal that the internal quantum efficiency and light extraction efficiency of the heterojunction LED are increased ~3-fold and ~2-fold, respectively, as a result of the introduction of Ag LSPs. This result indicates that the observed EL enhancement originates from a combined effect of both exciton-LSP coupling and photon-LSP coupling.[1-3]

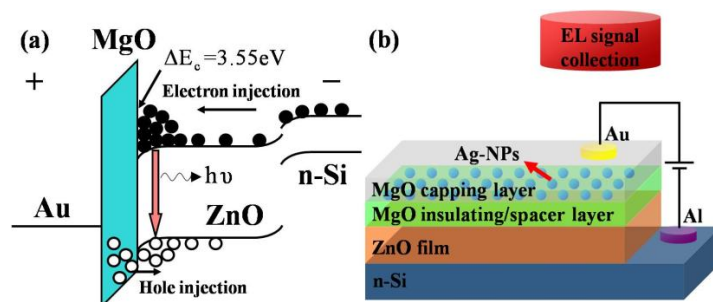


Fig. 1. (a) Energy-band alignment of Au/MgO/ZnO/n-Si heterostructure under forward bias. (b) Schematic diagram of LSP-enhanced Au/Ag-NPs@MgO/ZnO MIS heterojunction LED.

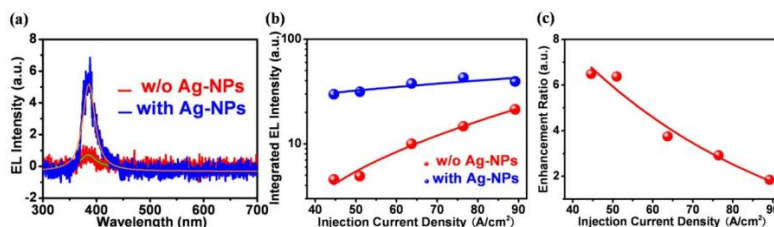


Fig. 2. (a) EL spectra of the LEDs with (blue line) and without (red line) Ag-NPs decoration. (b) The variations of integrated UV EL intensity with the injection current density for the devices with and without Ag-NPs. (c) EL enhancement ratio of the two LEDs as a function of the injection current density.

- [1] W. Z. Liu, H. Y. Xu, L. X. Zhang, C. Zhang, J. G. Ma, J. N. Wang, Y. C. Liu, *Appl. Phys. Lett.*, **101**, 142101 (2012).
- [2] W. Z. Liu, H. Y. Xu, C. L. Wang, L. X. Zhang, C. Zhang, S. Y. Sun, J. G. Ma, X. T. Zhang, J. N. Wang, Y. C. Liu, *Nanoscale*, **5**, 8634 (2013).
- [3] C. Zhang, C. E. Marvinney, H. Y. Xu, W. Z. Liu, C. L. Wang, L. X. Zhang, J. N. Wang, J. G. Ma, Y. C. Liu, *Nanoscale*, **7**, 1073 (2015).

## Improvement of thermal stability of p-ZnO:(Al,N) thin films by oxidizing Zn<sub>3</sub>N<sub>2</sub>:Al thin films

B. S. Li,<sup>1\*</sup> Y. F. Wang,<sup>2</sup> B. Yin,<sup>2</sup> A. Shen<sup>3</sup>

<sup>1</sup>Academy of Fundamental and Interdisciplinary Sciences, Harbin Institute of Technology, Harbin 150080, China

<sup>2</sup>Department of Physics, Harbin Institute of Technology, Harbin 150080, China.

<sup>3</sup>Department of Electrical Engineering, City College of New York, New York, NY 10031, USA

\*E-mail address: libingsheng@hit.edu.cn.

The authors report a p-ZnO thin film with improved thermal stability has been achieved by oxidizing Zn<sub>3</sub>N<sub>2</sub>:Al thin films in an oxygen ambient. The Zn<sub>3</sub>N<sub>2</sub>:Al and Zn<sub>3</sub>N<sub>2</sub> both samples were deposited on at 100 °C by magnetron sputtering. XRD shows the ZnO, oxidized from Zn<sub>3</sub>N<sub>2</sub>:Al thin film, is (002) preferred orientation and, on the other hand, the diffraction pattern of ZnO from Zn<sub>3</sub>N<sub>2</sub> thin film varied with different annealing temperature. The optical band gap (3.294 eV) of ZnO from Zn<sub>3</sub>N<sub>2</sub>:Al thin film, annealed at 800 °C, is narrower than the ZnO (3.31 eV) from Zn<sub>3</sub>N<sub>2</sub>, annealed at 500 °C. These results are summarized in Fig. 1. Shown in Fig.2 are the dependence of carrier density and conductive type for the ZnO thin films obtained from Zn<sub>3</sub>N<sub>2</sub>:Al and Zn<sub>3</sub>N<sub>2</sub> thin films. With thermal annealing, Zn<sub>3</sub>N<sub>2</sub>:Al turned to ZnO at 500 °C and the films turn to p-type at around 600 °C. With further lift up annealing temperature, the hole density increases and reaches 1.4 x 10<sup>16</sup> cm<sup>-3</sup> at 800 °C. After then, the carrier density decreases, but still keep p-type behavior even up to 900 °C. In completely contrast, oxidizing Zn<sub>3</sub>N<sub>2</sub> can only produce n-ZnO and the films then become insulating after further increasing the annealing temperatures (above 700 °C). This indicates that the Al can stabilize the acceptor of N in ZnO thin films.

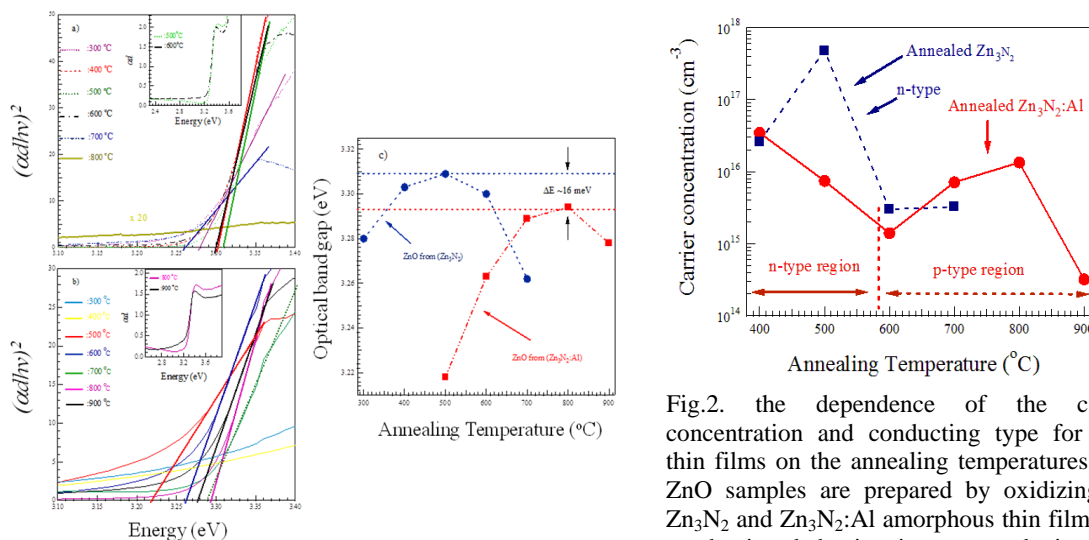


Fig.1. optical absorptions of ZnO thin films obtained from thermal annealing Zn<sub>3</sub>N<sub>2</sub>( a) and Zn<sub>3</sub>N<sub>2</sub>:Al thin films. (c) are the dependence of optical band gap for (a) and (b), respectively.

Fig.2. the dependence of the carrier concentration and conducting type for ZnO thin films on the annealing temperatures. The ZnO samples are prepared by oxidizing the Zn<sub>3</sub>N<sub>2</sub> and Zn<sub>3</sub>N<sub>2</sub>:Al amorphous thin film. The conducting behavior is p-type obtained for Zn<sub>3</sub>N<sub>2</sub>:Al.

## Characterization of ZnO thin film grown on vicinal-cut sapphire (0001) substrates by MOCVD

M. A. Boukadhaba<sup>1</sup>, A. Fouzri<sup>1,2,\*</sup>, V. Sallet<sup>3</sup>, S. S. Hassani<sup>3</sup>, G. Amiri<sup>3</sup>, A. Lusson<sup>3</sup> and M. Oumezzine<sup>1</sup>.

<sup>1</sup>Laboratoire Physico-chimie des Matériaux ; Unité de Service Commun de Recherche « High resolution X-ray diffractometer », Département de Physique, Université de Monastir, Faculté des Sciences de Monastir, Avenue de l'Environnement, 5019 Monastir, Tunisia.

<sup>2</sup>Institut Supérieur des Sciences Appliquées et de Technologie de Sousse, Université de Sousse, Tunisia.

<sup>3</sup>Groupe d'Etude de la Matière Condensée, Centre National de la Recherche Scientifique/Université de Versailles Saint Quentin en Yvelines 78035 Versailles, France.

\*Corresponding author: Fouzri.Afif@gmail.com

In recent years, ZnO thin films have attracted much attention because of their potential applications such as transparent electrodes, solar cells, surface acoustic wave devices, optical wave guides, varistors, LDs, LEDs, etc... Many different deposition methods have been used to grow ZnO thin films on various substrates such as sapphire, silicon, GaAs, and glass. Among them, the sapphire substrate plays an important role in applying ZnO thin films to optoelectronic devices. Despite the large differences in the thermal expansion coefficient and lattice constant between the ZnO thin films and sapphire substrates, it's widely used as a substrate because of its physical robustness and high-temperature stability. It is now well recognized that the surface treatment of the substrate prior to growth has crucial effects on both the growth mechanism and the material properties. Furthermore, there are few reports on the surface treatment effects of sapphire substrates on the epitaxial ZnO thin films. Among the stable surface orientations, the c-plane Al<sub>2</sub>O<sub>3</sub> (0001) substrate is so far the most widely studied and most commonly used surface. These templates have recently attracted additional interest as they offer the possibility of reconstructing their surfaces into a hill and valley structure [1]. It was demonstrated that annealing of the (0001) surface can produce periodic step-and-terrace arrangements with a step height  $h = 1.2$  nm [2]. The step rearrangements of c-plane -Al<sub>2</sub>O<sub>3</sub> have been previously investigated as a function of parameters such as annealing temperature [2, 3], time [1, 3], pressure [4], off-cut angle [3, 5] and orientation [3].

In this work, we report epitaxial growth, by metal organic chemical vapor deposition (MOCVD), of ZnO films on c-plane (0001) sapphire substrates with a nominally vicinal-cut angle of  $\alpha$  ( $\alpha = 0^\circ$ ,  $\alpha = 0.25^\circ$  toward the a-plane  $(11\bar{2}0)$  and  $\alpha = 0.25^\circ$  toward the m-plane  $(10\bar{1}0)$ ) at different annealing temperature substrates. We are interested on the influence of substrates annealing temperature and  $\alpha$  vicinal-cut angle on the microstructural and optical properties thin films.

[1] J. R. Heffelfinger, M. W. Bench, C. B. Carter. Surf. Sci, **370**,188 (1997).

[2] L. P. Van, O. Kurnosikov, J. Cousty, Surf. Sci, **411**, 263 (1998).

[3] O. Kurnosikov, Surf. Sci, **459**, 256 (2000).

[4] L. P. Van, J. Cousty, C. Lubin, Surf. Sci, **549**, 157 (2004).

[5] F. Cuccureddu, S. Murphy, I. Shvets, M. Porcu, H. Zandbergen, N. Sidorov, S. Bozhko, Surf. Sci. **604**, 1294 (2010).

## GROWTH, OPTICAL AND STRUCTURAL PROPERTIES OF ZnO/ZnMgO CORE-SHELL QUANTUM WELLS.

S. A. Said Hassani\*, C. Sartet, C. Vilar, A. Lusson, V. Sallet et P. Galtier

Groupe d'Etude de la Matière Condensée, CNRS Université de Versailles Saint Quentin en Yvelines, 45 Avenue des Etats-Unis, 78035, Versailles Cedex France.

\*Author e-mail: said.hassani@uvsq.fr

ZnO vertical nanowires have been grown by metal-organic-chemical-vapour-deposition (MOCVD) on sapphire substrates. The use of  $N_2O$  and diethylzinc,  $DEZn$  ( $(C_2H_5)_2$ ) as oxygen and zinc precursors combined with high temperature growth ( $> 600^\circ C$ ) lead to spontaneous growth of ZnO nanowires (NWs) on underlying three dimensional islands present at the bottom of each nanowire. ZnO nanowires with the wurtzite structure are grown, free of extended defects, along the c axis and they exhibit m-type, non-polar, facets. This configuration is favorable to band-gap engineering because Stark effect is not observed when heterostructures are grown on non-polar surfaces leading to efficient optical band-gap recombination. Based on this, we have grown a series of radial ZnO/ZnMgO quantum wells with different thicknesses and Mg concentrations using oxygen,  $(MCP)_2Mg$  and  $DEZn$  as oxygen, magnesium and zinc precursors. Low temperature Photoluminescence spectroscopy (PL) and Transmission Electron Microscopy (TEM) using EDX were used to estimate the Mg concentrations in the shell which can reach  $x=0.2$ . The figure below shows a TEM image of a single ZnO/ZnMgO quantum well structure with a ZnO core of 32 nm and a well of 10 nm surrounded by two ZnMgO barriers of 18 nm. Electron diffraction reveals that ZnMgO alloy is, at least partially, ordered. Dislocations are also observed for the highest magnesium concentrations. Micro-photoluminescence performed on single ZnO/ZnMgO quantum well exhibit excellent luminescence properties with a strong emission of the ZnO and ZnMgO band edges. Furthermore, between these two emissions, additional contributions appear that could be attributed to the lateral quantum well.

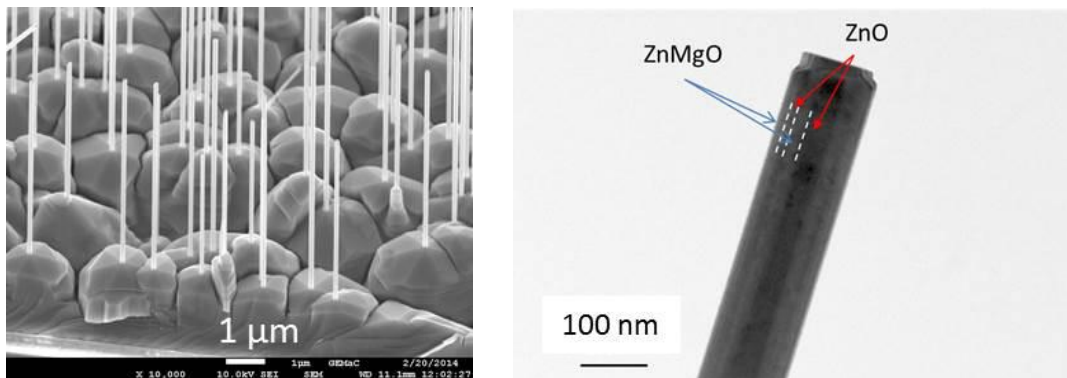


Figure: Scanning Electron Microscope image for ZnO nanowires (left) and Transmission Electron Microscope (right) of  $ZnO/Zn_{0.86}Mg_{0.14}O$  based quantum well (right).

## MgZnO growth on (0001)sapphire by mist chemical vapor deposition

Ryosuke GOTO, H. NAGAI, T. YAMAGUCHI, T. ONUMA, M. SATO and T. HONDA\*

Department of Applied Physics, School of Advanced Engineering, Kogakuin University  
2665-1 Nakano-machi, Hachioji, Tokyo 192-0015, JAPAN

\*e-mail: ct11761@ns.kogakuin.ac.jp

ZnO and its related materials have been much attention for the application to transparent electrodes with transistors [1, 2]. In particular, MgZnO is a crucial material for the application to transparent electrodes in UV spectral regions. These cost-effective fabrication is a key for the applications. Previously, the fabrication of MgZnO films by molecular precursor method (MPM) was reported [3, 4]. The MPM is one of the spin-coating techniques. Zinc-butyl-ammine dehydrate and magnesium-ethylene-diamine-N,N,N',N'-tetra-acetic acid (edta) were used as precursors. The spin-coated films was annealed subsequently at 650 °C. Although the films showed a good transparency in near UV spectral regions, their resistivity was higher than  $10^0 \Omega\cdot\text{cm}$  (their thickness was 80 nm), which was insufficient for the application to transparent electrodes.

For the improvement of these properties, MgZnO films were grown by mist chemical vapor deposition (mist CVD) using the molecular precursor as sources, which was the same as a case of MPM. Nitrogen carrier gas was used for the CVD and the substrate temperature was kept at 500 °C. The source dosed ammonia-based aqueous solution was formed and it was supplied as mist conditions into the reactor.

The resistivity of the ZnO film grown by mist-CVD was dramatically improved ( $10^{-1} \Omega\cdot\text{cm}$ ). The surface images of ZnO films observed using atomic force microscopy (AFM) are shown in Fig. 1. The smooth surface of ZnO films grown by mist-CVD was obtained, compared with those fabricated by MPM. The carbon concentration in the films grown by mist-CVD were also reduced. We consider these lead to the improvement of their resistivity.

- [1] T. Minami, MRS Bull. **25**, 38 (2000).
- [2] T. Kawaharamura, H. Nishinaka and S. Fujita, Jpn. J. Appl. Phys. **47**, 4669 (2008).
- [3] Y. Mashiyama, K. Yoshioka, S. Komiyama, H. Nomura, S. Adachi, M. Sato and T. Honda, Phys. Stat. Sol. C**6**, 596 (2009).
- [4] T. Honda, T. Oda, Y. Mashiyama, H. Hara and M. Sato, Phys. Stat. Sol. C**7**, 2471 (2010).

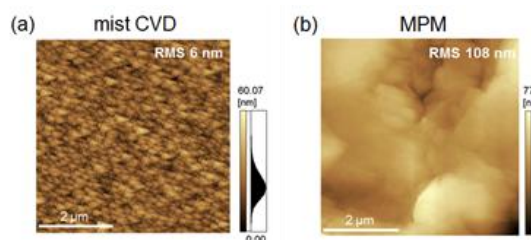


**Fig. 1** AFM images of ZnO films grown by (a) mist-CVD and (b) MPM.

## Properties of ZnO/ZnMgO Nanostructures Grown on R-plane Al<sub>2</sub>O<sub>3</sub> Substrates by MBE

M.A. Pietrzyk\*, M. Stachowicz, D. Jarosz, E. Przewdziecka, R. Minikayev, A. Kozanecki  
Institute of Physics, Polish Academy of Sciences, Al. Lotnikow 32/46, 02-668 Warsaw,  
Poland

\*pietrzyk@ifpan.edu.pl

Ternary Zn<sub>1-x</sub>Mg<sub>x</sub>O alloys present suitable material system which allows widening of the band-gap up to 3.9 eV for  $x = 0.33$  before any structural phase transition to cubic ZnMgO occurs. Using this alloy system in ZnO quantum well structures the exciton binding energy can be increased from 60 meV in bulk ZnO up to ~100 meV in quantum wells (QWs).

We report on the growth conditions, optical and structural properties of ZnO/ZnMgO nanostructures grown on semi-polar r-plane sapphire substrates by molecular beam epitaxy. We show that it is possible to grow self-organized ZnMgO nanocolumns without employing a catalyst. Use of low-temperature ZnO buffer layer enables to obtain good quality planar layers. The samples consist of 10 pairs of ZnO/ZnMgO QWs of 2 nm separated by 3 nm ZnMgO barriers.

XRD pattern shows two types of peaks coming from ZnMgO nanocolumns. First ( $11\bar{2}0$ ) peak and the second one (0002) indicates on non-polar a-plane and polar c-plane orientation of ZnO/ZnMgO, respectively. The nanocolumn structures exhibit 62 deg tilt with respect to the sapphire substrate, which is connected with mutual placement of r-plane Al<sub>2</sub>O<sub>3</sub> and a-plane ZnMgO. SEM images reveal that density and diameter of ZnMgO nanocolumns can be controlled by the growth temperature.

Optical properties of ZnO/ZnMgO MQWs using room and low temperature photoluminescence (PL) techniques were studied. The spectrum measured at 10K temperature contains of a sharp, dominant peak, located at 3.392 eV. It is recombination of excitons in the 2 nm ZnO MQW structures. One can find another weak peaks on the low energy slope of the main transition. These peaks can obviously be attributed to 1LO, 2LO and 3LO longitudinal optical phonon replicas of the NBE emission from the MQWs. At the high energy part of the spectra a weak peak with maximum at about 3.700 eV, which originates from emission in ZnMgO barrier.

The energy position of excitonic transition in the 2 nm MQWs where the barrier thickness is only 3 nm is lower than in case of quantum wells separated by thick barriers. For this width of barrier exists high probability of localized exciton wave function penetration of barrier layers and interacting or influencing with the neighboring QW excitonic wave function. In the case of MQWs it leads to lowering of the energy levels in the QW. The transition energy of the excitons localized in the single or separated 2 nm QWs is much higher than in case described above.

**Acknowledgements** The project was supported by the Polish National Science Centre (NCN) based on the decision No: DEC-2013/09/D/ST5/03881.

## Structural, Electrical and Optical Properties of Ga-Doped ZnO Films Grown on Flexible Substrates by Using Plasma-assisted Molecular Beam Deposition

T. Muranaka<sup>1\*</sup>, Y. Oyaizu<sup>1</sup>, K. Takasho<sup>1</sup>, S. Nakajima<sup>1</sup>, K. Okajima<sup>1</sup>, K. Nakashima<sup>1</sup>, Y. Nabetani<sup>1</sup>, T. Matsumoto<sup>1</sup>, S. Iwamoto<sup>2</sup>, S. Hiraki<sup>2</sup>, H. Kono<sup>3</sup>, and S. Hagihara<sup>3</sup>

<sup>1</sup>Department of Electrical and Electronic Engineering, University of Yamanashi, Kofu, Japan

<sup>2</sup>Nakaya Corporation, Showa, Yamanashi, Japan

<sup>3</sup>Yamanashi Industrial Technology Center, Kofu, Japan

\*tmuranaka@yamanashi.ac.jp

Zinc oxide (ZnO) is promising material for future invisible electronics technology due to its wide band gap (3.3 – 3.4 eV), low cost, abundant ability and non-toxicity. Well-controlled carrier doping technique is essential issue for realization of high quality transparent electrode or TFT based on ZnO-related materials. In particular, applications for transparent conducting oxide (TCO) films such as Ga-doped ZnO (GZO), Al-doped ZnO (AZO), In-doped ZnO (IZO) films were prepared by many kinds of growth techniques. However, the substrate material most extensively used is glass, and there have been few reports on deposition onto plastic substrates. TCO films using ZnO-related materials on plastic substrates are interested for new applications to flexible display panels, electronic papers, etc.

In order to prepare ZnO films on non-heat-resistant and low-cost plastic substrates, growth temperature should be reduced lower than 100°C. From such a viewpoint, we have recently demonstrated highly transparent and conductive ZnO films grown by plasma-assisted molecular beam deposition (PAMBD) [1]. In this study, the GZO films grown under various Ga/Zn supply ratios were carefully characterized by X-ray diffraction (XRD), scanning electron microscope (SEM), Hall measurements and optical transmittance measurements to investigate the structural, electrical and optical properties of the GZO films on polyethylene naphthalate (PEN), polyethylene terephthalate (PET) and polycarbonate (PC) substrates.

All the growth procedures of the GZO films were carried out in our plasma-assisted MBE system. The low temperature growth at 50°C on PEN, PET and PC substrates were performed. Zinc (Zn) vapor was supplied by heating of metallic Zn from 340°C to 390°C, and oxygen was excited in a microwave cavity and only neutral atomic radicals were supplied onto substrates. Therefore, grown film is free from ion bombardment. Gallium (Ga) vapor was also supplied by heating of metallic Ga from 500°C to 800°C. The resistivity, Hall carrier density and mobility of the GZO films were obtained by the Van der Pauw method at room temperature. Optical transmittance spectra of the GZO films were also taken in the range from 300 nm to 800 nm at room temperature.

The GZO films on PEN, PET and PC substrates were highly c-axis orientated and showed the resistivity less than  $1 \times 10^{-3} \Omega\text{cm}$ . The highest carrier density was  $9 \times 10^{20} \text{ cm}^{-3}$  and almost the same value as that of the GZO films on glass substrates, but the resistivity increased due to the lower mobility. The GZO films on PEN, PET and PC substrates also showed visible transparency as good as that of the GZO films on glass substrate, and the average transmittance in the visible region was higher than 85 %.

[1] T. Matsumoto, K. Mizuguchi, T. Horii, S. Sano, T. Muranaka, et al., Jpn. J. Appl. Phys. 50, 05FB13 (2011).

## ZnO:Tb Films Grown by RF Magnetron Sputtering: the dependence of structural and luminescent properties on the type of the substrate

Khomenkova L<sup>1\*</sup>, Ziani A<sup>2</sup>, Frilay C<sup>2</sup>, Polishchuk Yu<sup>1</sup>, Kolomys O<sup>1</sup>,  
Kladko V<sup>1</sup>, Borkovska L<sup>2</sup> and PortierX<sup>2</sup>

<sup>1</sup>V. Lashkaryov Institute of Semiconductor Physics of NAS of Ukraine,  
45 Pr. Nauky, Kyiv 03028, Ukraine

<sup>2</sup>CIMAP (CNRS/CEA/Ensicaen/UCBN, 6 Blvd. Maréchal Juin, 14050 Caen Cedex 4, France  
\*khomen@ukr.net

Zinc oxide (ZnO) is a wide band gap semiconductor with unique electronic and optical properties that makes it suitable for a wide range of applications photovoltaic, photonic and optoelectronic devices. Rare earth doping of ZnO is used to achieve a broad luminescent spectrum of ZnO required for white LEDs.

In the present work we studied structural and light emitting properties of Tb-doped ZnO films fabricated by radio frequency magnetron sputtering from composed target by means of X-ray diffraction, Raman scattering and photoluminescence methods. The films were grown on different substrates (silicon, fused quartz and sapphire) and annealed at 600 and 900°C for 1 h in air.

The as-deposited films were found to be polycrystalline with the grains oriented preferably in (002) direction. The grain sizes were estimated to be about 11, 20 and 27 nm in the films grown on sapphire, silicon and fused quartz substrates, respectively. The films were found to be stressed in direction perpendicular to the film surface. Thermal treatment stimulated the increase of ZnO grain sizes with the annealing temperature, keeping the same trend versus type of substrate.

In the photoluminescence (PL) spectra of as-deposited films, only a weak emission in the ultraviolet spectral range caused by exciton recombination in the ZnO grains was observed. Thermal annealing caused its enhancement and simultaneous appearance of visible PL band in the range of 540-600 nm related to native defects in ZnO as well as Tb<sup>3+</sup> PL transitions. The strongest PL was detected in the films grown on a quartz substrate and annealed at 900°C that have the largest ZnO grains. At the same time this annealing results also in some quenching of the emission of Tb<sup>3+</sup> ions due to their possible agglomeration. This was confirmed by the appearance of Tb<sub>2</sub>O<sub>3</sub> grains with (222) orientation and an average size of about 30 nm. The effect of the type of substrate on structural and luminescent properties is discussed in details.

## Effects of band anticrossing on the temperature dependence of the band gap of Zn(Cd)TeO

**M. Welna<sup>1,4\*</sup>, R. Kudrawiec<sup>1</sup>, T. Tanaka<sup>2,3</sup>, and W. Walukiewicz<sup>4</sup>**

<sup>1</sup>*Department of Experimental Physics, Wrocław University of Technology, Wybrzeże Wyspińskiego 27, 50-370 Wrocław, Poland*

<sup>2</sup>*Department of Electrical and Electronic Engineering, Saga University, 1 Honjo, Saga 840-8502, Japan*

<sup>3</sup>*PRESTO, Japan Science and Technology Agency (JST), Kawaguchi, Saitama 332-0012, Japan*

<sup>4</sup>*Materials Sciences Division, Lawrence Berkeley National Laboratory, Berkeley, California 94720, USA*

\*monika.welna@pwr.edu.pl

Dilute group II-VI oxides in which anion atoms are partially replaced by oxygen belong to a new class of semiconductors called highly mismatched alloys (HMAs). The energy band structure of the HMAs is described by the band anticrossing (BAC) model in which localized O states interact with the extended states of the host matrix [1, 2]. The interaction leads to formation of a narrow band of states in the larger gap semiconductor. This unusual modification of the electronic band structure has been used to demonstrate an intermediate band solar concept [3, 4].

We have investigated the effects of BAC interactions on the electronic band structure of the conduction band of  $\text{Zn}_{1-y}\text{Cd}_y\text{Te}_{1-x}\text{O}_x$  HMA. A great advantage of this quaternary alloy is that it can be lattice matched to ZnTe substrate offering a potential for detail studies of the BAC interactions in a dilute II-VI oxide. In addition varying of the Cd content allows for changing the location of the conduction band edge of the semiconductor matrix relative to the localized O energy level. The  $\text{Zn}_{1-y}\text{Cd}_y\text{Te}_{1-x}\text{O}_x$  films were grown by MBE on ZnTe substrates. We have used photoreflectance (PR) spectroscopy to study temperature dependence of the interband optical transition in  $\text{ZnTe}_{1-x}\text{O}_x$  with oxygen content  $x$  up to 0.016 and  $\text{Zn}_{1-y}\text{Cd}_y\text{Te}_{1-x}\text{O}_x$  with  $x < 0.01$  and  $y < 0.1$ . We observe two interband absorption edges corresponding to optical transitions from the valence band to two conduction band subbands  $E_-$  and  $E_+$ . The observed weak dependence of  $E_+$  and  $E_-$  absorption edges on temperature is explained by BAC interaction between weakly temperature dependent energy of the O states and the conduction band edge of the ZnCdTe matrix. Assuming temperature independent energy of the O level relative to the vacuum level we were able to separately determine temperature induced shift of the conduction band and the valence band edges. Thus we find that in the case of  $\text{Cd}_{0.1}\text{Zn}_{0.9}\text{Te}$  host matrix the total band gap reduction of 100 meV between 20 and 300K is almost evenly distributed between a downward shift of the CBE and an upward shift of the valence band.

[1] W. Shan, et al., Phys. Rev. Lett. 82, 1221 (1999)

[2] W. Walukiewicz, et al., Phys. Rev. Lett. 85, 1552 (2000)

[3] T. Tanaka, et al., Appl. Phys. Lett. 102, 052111 (2013)

[4] K. M. Yu, et al., Phys Rev Lett. 91 24 (2003)

## Positron lifetime spectroscopy of vacancy-related defects in ZnO

Šedivý L.<sup>1\*</sup>, Čížek J.<sup>2</sup>, Belas E.<sup>1</sup>, Valenta J.<sup>3</sup>, Grill R.<sup>1</sup> and Vlček M.<sup>2</sup>

<sup>1</sup>Institute of Physics, Charles University in Prague, Ke Karlovu 5, CZ-121 16, Prague 2, Czech Republic

<sup>2</sup>Department of Low-Temperature Physics, Charles University in Prague, V Holešovičkách 2, CZ-180 00, Prague 8, Czech Republic

<sup>3</sup>Department of Chemical Physics and Optics  
Charles University in Prague, Ke Karlovu 3, CZ-121 16, Prague 2, Czech Republic

\*luky.sedivy@seznam.cz

Single crystalline Zinc Oxide represents promising material to manufacture blue and UV light emitters and high-temperature and high-power transistors. The main advantages of ZnO as a light emitter are the large exciton binding energy (60 meV) and the existence of well-developed bulk and epitaxial growth processes. The producing of UV laser, at both low and high temperatures, has already been experimentally demonstrated, although efficient electrical lasing awaits the further development of defect-free material [1]. An engineering of point defects existing in ZnO crystals represents principal task for routine productions of high quality crystals for such application.

Divalent donors oxygen vacancy ( $V_O$ ) or zinc interstitial ( $Zn_i$ ) and their complexes with extrinsic substituting impurities are considered to be the most important defects for the n-type conductivity [2]. The divalent acceptor zinc vacancy ( $V_{Zn}$ ) is usually present in ZnO, but deep donor self-compensation precludes successful production of p-types. In spite of the enormous effort made in the past decades to fix properties of native defects in ZnO, namely formation and ionization energies, there remains unsatisfactory information and large scatter of these quantities found in the literature.

The aim of this work was to examine the defect structure in eight ZnO samples obtained from different vendors and grown by different technology (HTG - hydrothermal growth, PMG - pressurized melt growth, BG - Bridgman growth, CVT - chemical vapour transport, VPG - vapour phase growth). The defect structure of ZnO was investigated using combination of multiple methods – Positron annihilation spectroscopy (PAS), Photoluminescence (PL), galvanomagnetic measurements (GM) and inductively coupled plasma mass spectrometry (ICP-MS). Combination of measurements allowed us extensive analysis of the defects properties.

The most distinguished result was obtained with PAS where we have proven that HTG yields a single component spectrum with the positron lifetime of  $\approx 180$  ps, which is in contrast to other growth methods producing a single component spectrum with the lifetime of  $\approx 165$  ps. This finding was independent of the concentration of impurities determined by ICP-MSP. We explained this difference by the positron trapping and annihilation in hydrogen-stabilized Zn vacancy ( $V_{Zn} - H$ ) in the former case and by the bulk positron annihilation in the latter case. The interpretation was confirmed by PL measurements where more pronounced green luminescence induced by ( $V_{Zn}$ ) [3] was observed in HTG samples. The interpretation of GM was more complicated—due to different impurity concentration in various samples, but it was helpful for self-compensation study and determination of defects activation energy.

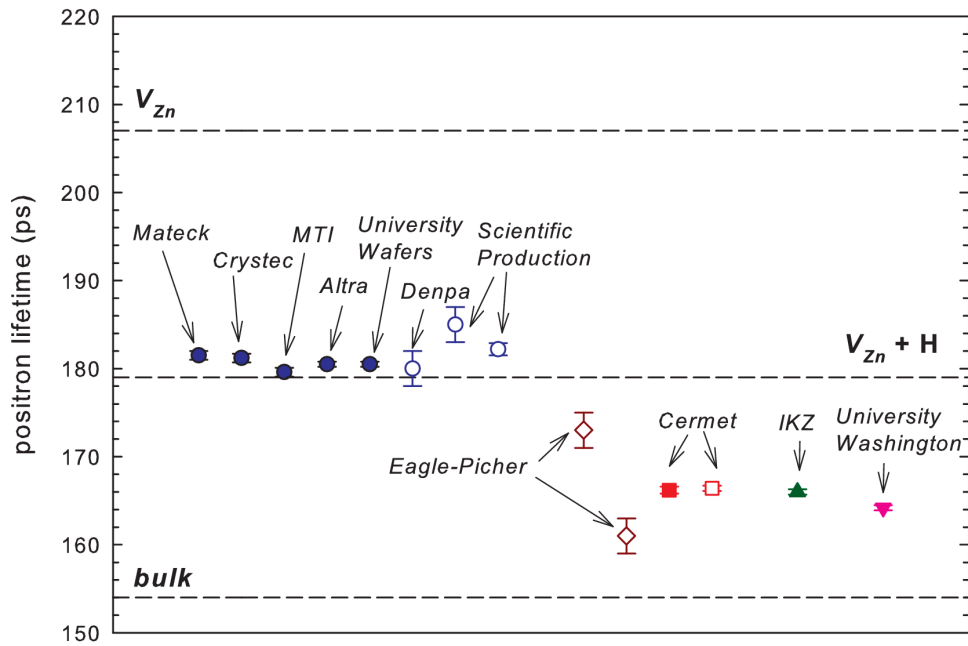
[1] Look D. C., Mat. Sci. Eng. B-Solid, **80**, 383-387, (2001).

[2] Janotti A., Van de Walle C. G., Phys. Rev. B, **76**, 165202, (2007).

[3] Fabbri, F. et al., Sci. Rep. **4**, 5158, (2014).

Positron lifetimes determined for ZnO crystals grown by various methods (shape of symbols) and supplied by various producers (marked by arrow). The data from literature was added for the comparison (open symbols).

- HTG
- PMG
- ▲ BG
- ▼ CVT
- HTG, Tuomisto 2007, Chen 2005
- PMG, Brauer 2009
- ◇ VPG, Brunner 2001



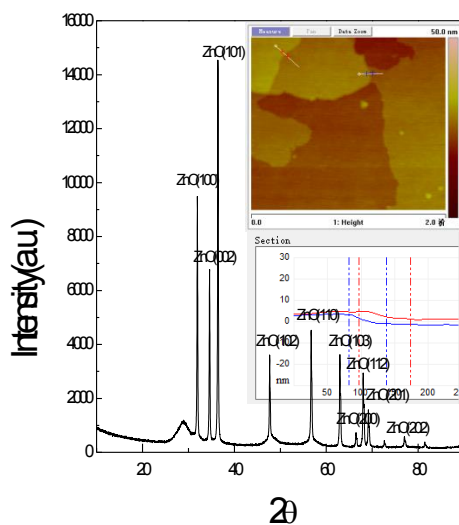
## Fabrication of Flexible and Freestanding ZnO Few Layers

Zheng Wang, Haiping He\*, Zhizhen Ye

School of Materials Science & Engineering, Zhejiang University  
hphe@zju.edu.cn

### Abstract

II-IV compound semiconductors have attracted enormous attention due to their unique properties and wide applications in semiconductor industries. Recently, controlling the physical dimensions of II-IV compound semiconductors has been a new way to systematically tune their optical and electronic properties[1]. Two dimensional (2D) semiconductors have attracted enormous attentions for their unique electronic, optical, and biocompatible properties with respect to the traditional bulk semiconductors[2]. 2D semiconductors have broad application prospects in the area of optical and optoelectronic devices. ZnO is a wide band-gap semiconductor with a direct band gap of 3.37eV and a large exciton binding energy of 60meV at room temperature. We have successfully fabricated large-area freestanding few layers of ZnO with several-atomic thickness by the method of hydrothermal process. Firstly, we fabricated few layer ZnS after exfoliation and removal of organic species. Secondly, few layer ZnS was oxidated to few layer ZnO in a tube furnace. Strong quantum confinement effect leads to significantly enhanced electronic and optical properties like blue shift in optical absorption spectra. Atomic Force Microscopy(AFM) measurement shows the area of ZnO layer is about 1  $\mu\text{m}^2$  while its thickness as little as 3nm.



[1] Xiaoying Huang, Jing Li, J.Am.Chem.Soc, **129**, 3157, (2007).

[2] Kun Xu, Pengzuo Chen, and Yi Xie, **52**, 10477, (2013).

**Poster Session 1 - MoP**

**Detectors and new devices: X and gamma high energy sensors , Infrared, visible,  
and UV materials and devices**

## 20 MHz Operation of Organic Nano-Diodes

Leszek A. Majewski and Aimin Song\*

School of Electrical and Electronic Engineering, University of Manchester, Manchester, UK

\*A.Song@manchester.ac.uk

Recent years have seen active and passive radio frequency identification (RFID) tags and smart cards widespread in a range of applications. It is envisaged that solution-processed polymer semiconductors may enable a dramatic cost reduction because of the potentially low material cost and high-throughput printability as compared with silicon technology. A key challenge is however the low carrier mobility in conducting polymers which significantly limits device speed. In an RFID tag, the most demanding component in terms of switching speed is the front-end rectifier that must rectify an AC signal received from a resonant antenna in order to provide quasi-DC power supply to the logic circuit of the tag. The rest of the logic circuitry can operate at much lower frequencies (i.e. several kHz). Recently, solution-processed polymer rectifiers operating at MHz and higher frequencies using conventional device designs have been demonstrated. However, these multi-layered device structures require a high degree of vertical alignment and process control to fabricate, which are not compatible to standard printing technology. Here we propose an alternative approach to these, and show that a single-layered nano-device can offer MHz operation but is also suitable to be fabricated by a single-step nano-imprint technology.

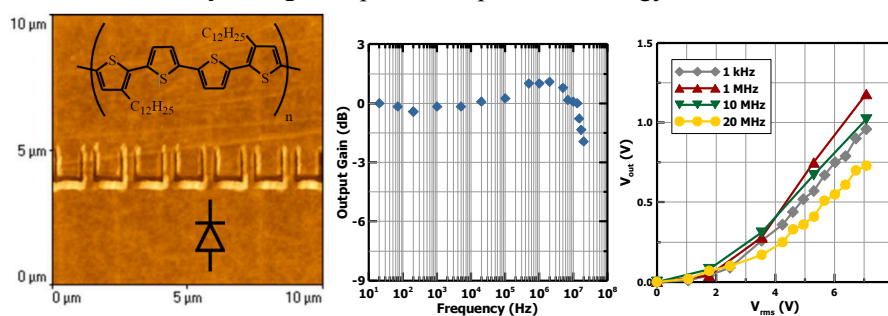


Fig. 1 AFM micrograph of an SSD array. Output voltage ( $V_{out}$ ) versus frequency and input voltage ( $V_{rms}$ )

Figure 1 is an atomic-force micrograph of a self-switching diode (SSD) array fabricated in a 15nm thin PQT12 layer. The SSDs consist of U-shaped insulating trenches structured in such a fashion that breaks the geometric symmetry and forces the electrical current to flow only through the nanochannels formed between the U-shaped trenches. The rectification is achieved by a self-induced field-effect that enhances conduction through the nanochannels in one direction, while suppressing it in the opposite direction [1]. SSDs have been demonstrated to operate at THz frequencies using conventional InGaAs semiconductors at room temperature [2-5]. Figure 1 shows the rectified output voltage ( $V_{out}$ ) versus frequency and input voltage ( $V_{rms}$ ) characteristic, confirming the quadratic dependency of  $V_{out}$  on  $V_{rms}$  that was predicated theoretically. The 20MHz operation is one of the highest speeds achieved in conducting polymers, and this is high enough for the common 13.56 MHz RFID communication band.

- [1] Song, A. M. et al. *Appl. Phys. Lett.* 83, 1881–1883 (2003).
- [2] Balocco, C. et al. *Nano Lett.* 5, 1423–1427 (2005).
- [3] Balocco, C. et al. *Appl. Phys. Lett.* 98, 223501 (2011).
- [4] Kasjoo S. R. et al. *IEEE Elec. Dev. Lett.* 34, 1554 (2013).
- [5] Pan Y. et al. *Appl. Phys. Lett.* 105, 253901 (2014).

## Multi-Band Radiation Detector Based on HgCdTe Heterostructure

T. Kryshchab<sup>1</sup>, A. B. Smirnov<sup>2</sup>, and R. K. Savkina\*<sup>2</sup>

<sup>1</sup> Department of Physics, Instituto Politécnico Nacional – ESFM, Mexico D.F., Mexico

<sup>2</sup> V. Lashkaryov Institute of Semiconductor Physics, NAS of Ukraine, Kiev, Ukraine  
\*r\_savkina@isp.kiev.ua

Radiation detectors are the eyes of many modern scientific, medical, industrial and security systems which obtain the information about the environment by absorbing electromagnetic waves from hard X-rays and visible light to microwave spectral range. Development of multi-band detector technology is critical and remains one of the important directions for the successful development of active and passive vision.

In this work, HgCdTe-based detector structure considering different semiconductor device concepts is presented. Narrow-gap HgCdTe (MCT) technologies are well developed now, and today this material is one of the basic semiconductor for photon detectors from MWIR ( $\lambda \sim 3\text{--}5 \mu\text{m}$ ) to LWIR ( $\lambda \sim 8\text{--}14 \mu\text{m}$ ) spectral range and is used in large-scale arrays with silicon CMOS readouts. Here, we describe multi-band radiation detector based on HgCdTe/Si heterostructure which exhibit sensitivity in the middle and long wavelength IR spectral range without cryogenic cooling to achieve useful performance. MCT-based heterostructure was also considered as sub-THz detector.

MCT multilayer structures were grown by MBE with intermediate CdTe/ZnTe buffer layers on [310]-oriented Si substrates. It was observed that  $\text{Hg}_{0.68}\text{Cd}_{0.32}\text{Te}/\text{CdTe}/\text{ZnTe}/\text{Si}$  heterostructure exhibits photo-response under IR photoexcitation without electrical bias and amplification. The measured value of responsivity was from  $\sim 0.5 \text{ V/W}$  to  $\sim 4.3 \text{ V/W}$  at  $0.5 \text{ mW}$  incident power in MWIR region. An element of the prototype achieves photovoltaic spectral sensitivity on a level  $10^9 \text{ (W}^{-1} \text{ cm Hz}^{1/2})$  at  $300 \text{ K}$ . It was also found out that the prototype of photovoltaic detector is sensitive to  $\text{CO}_2$  laser radiation on the level of  $\sim 0.04 \text{ V/W}$  at  $1 \text{ mW}$  laser beam power in focal spot.

The sensitivity of MCT-based heterostructures for sub-THz radiation (the source with  $\sim 140 \text{ GHz}$  frequency was used for testing) was found after the ion beam bombardment of the sample investigated. The value of the measured signal was about  $7\text{--}15 \mu\text{V}$  at output power  $\sim 7 \text{ mW}$ . These measurements were performed using a lock-in detection scheme with modulation at  $190 \text{ Hz}$ . The signal was detected without antenna and amplification. The properties of the heterostructure samples subjected to the ion beam bombardment were studied. It was found that, as a result of the silver ion implantation with the energy and dose about  $140 \text{ keV}$  and  $4.8 \cdot 10^{13} \text{ cm}^{-2}$ , respectively, a uniform array of nanostructures with a height from  $5$  to  $10 \text{ nm}$  and a base diameter from  $50$  to  $80 \text{ nm}$  is formed on the surface of MCT-based structures. The metal oxide phase ( $\text{Ag}_2\text{O}$ ) precipitation in the subsurface ( $<100 \text{ nm}$ ) region of the host material was also detected.

## II-VI Quantum Cascade Emitters in the 6-8 $\mu$ m range

Thor Axtmann Garcia<sup>1,5</sup>, Joel De Jesus<sup>2,5</sup>, Arvind P. Ravikumar<sup>3</sup>, Aidong Shen<sup>4</sup>, Claire Gmachl<sup>3</sup>, and Maria C. Tamargo<sup>1\*</sup>

<sup>1</sup>Department of Chemistry, The City College of New York, New York, NY, USA

<sup>2</sup>Department of Physics, The City College of New York, New York, NY, USA

<sup>3</sup>Department of Electrical Engineering, Princeton University, Princeton, New Jersey, USA

<sup>4</sup>Department of Electrical Engineering, The City College of New York, New York, NY, USA

<sup>5</sup>The Graduate Center, CUNY, New York, New York 10016, USA

\*mtamargo@ccny.cuny.edu

We present the growth and characterization of ZnCdSe/ZnCdMgSe quantum cascade (QC) heterostructures grown by molecular beam epitaxy (MBE) and designed to operate at 6-8 $\mu$ m. Since they were first demonstrated in 1994<sup>1</sup>, QC lasers have had great success using the AlInAs/InGaAs/InP material system. Due to a limiting conduction band offset (CBO) of 0.72 eV, it is difficult to obtain a good performance at the shorter wavelengths with those materials. The ZnCdSe/ZnCdMgSe material system is an attractive alternative<sup>2</sup>. ZnCdSe/ZnCdMgSe has a direct bandgap, no intervalley scattering and a CBO as high as 1.12 eV making it a good candidate for devices operating in a broad range of range of infrared wavelengths<sup>4,5,6</sup> including the possibility of wavelengths as low as 1.55  $\mu$ m. We have previously reported electroluminescence in this material system in the 4 to 5  $\mu$ m range<sup>5,6</sup>. However, lasing from those structures has not yet been observed, likely due to non-optimized materials. In order to understand the source of these problems, devices were designed and grown to operate at the 6-8  $\mu$ m range. These structures utilize the better understood ZnCdMgSe with InP lattice matched compositions yielding a bandgap of 2.80 eV. Here we present results from that effort, including the first long wavelength quantum cascade emitters made from II-VI materials with higher performance than the short wavelength devices.

[1] J. Faist, F. Capasso, D. L. Sivco, C. Sirtori, A. L. Hutchinson, and A. Y. Cho, *Science* **264**, 553 (1994).

[2] W. Charles, A. Shen, K. Franz, C. Gmachl, Q. Zhang, Y. Gong, G. Neumark, and M.C. Tamargo, *J. Vac. Sci. Tech. B* **26**, 1171 (2008).

[3] M. Sohel, X. Zhou, H. Lu, M. N. Perez-Paz, M. Tamargo, and M. Muñoz, *J. Vac. Sci. Tech. B* **23**, 1209 (2005).

[4] K. J. Franz, W. O. Charles, A. Shen, A. J. Hoffman, M. C. Tamargo, and C. Gmachl, *Appl. Phys. Lett.* **92**, 121105 (2008).

[5] Y. Yao, A. Alfaro-Martinez, K.J. Franz, W.O. Charles, A. Shen, M.C. Tamargo, and C.F. Gmachl, *Appl. Phys. Lett.* **99**, 041113 (2011).

[6] T. A. Garcia, J. de Jesus, A. P. Ravikumar, S. Hong, A. Shen, C. F. Gmachl M. Tamargo, *J. Vac. Sci. Technol. B*, **31**, 3 (2013).

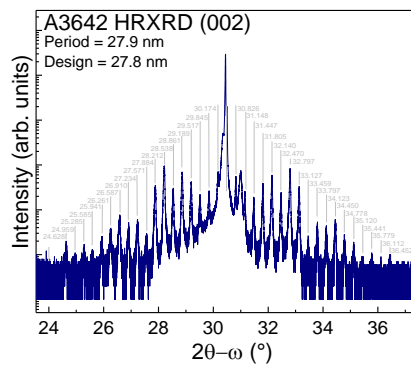


Figure 1: High Resolution X-ray Diffraction (002) of quantum cascade laser structure

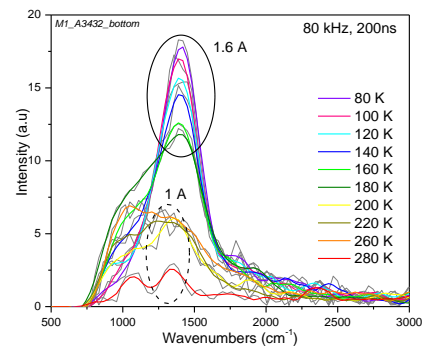


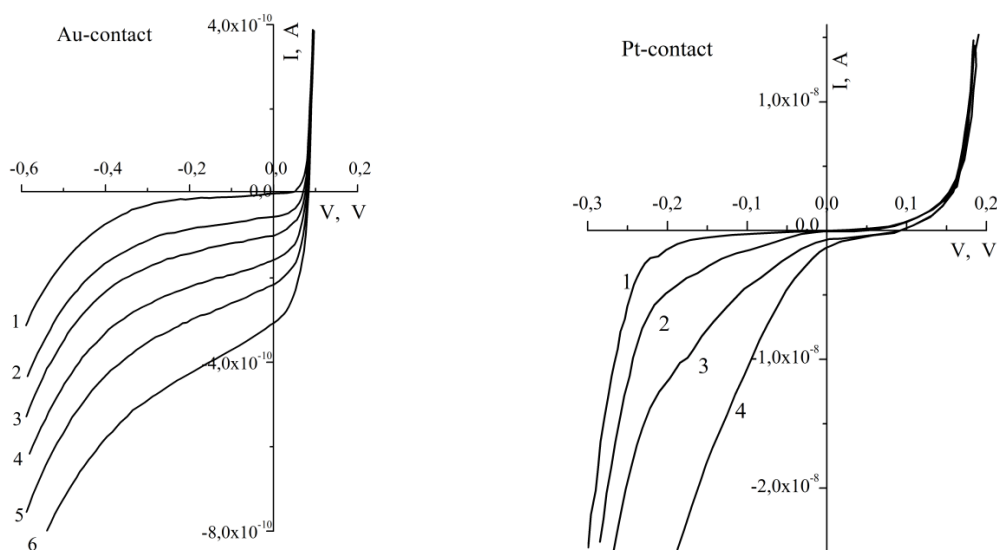
Figure 2: Temperature dependence on electroluminescence spectra of fabricated quantum cascade device

## Photosensitive MIS Structures with Ultrathin Dielectric Based on $\text{Cd}_x\text{Hg}_{1-x}\text{Te}$ ( $x \sim 0.4$ )

V.G. Kesler, A.A. Guzev, S.A. Dvoretzkiy, E.R. Zakirov, A.P. Kovchavtsev,  
Z.V. Panova, M.V. Yakushev

Federal State Budgetary Institution A.V. Rzhzanov Institute of Semiconductor Physics,  
Siberian Branch of the Russian Academy of Sciences, Novosibirsk, Russia.  
\*kesler@isp.nsc.ru

One of the key operations for production of infrared photodetectors based on solid solutions of  $\text{Cd}_x\text{Hg}_{1-x}\text{Te}$  is passivation of a semiconductor device with thin dielectric films for minimizing surface parasitic leakage currents. We present the results of the pilot studies aimed at developing the new method for MCT surface passivation with ultrathin dielectric films ( $\sim 3$  nm). The research is aimed to determine the nature and degree of stoichiometric imbalance in a near-surface layer of MCT films during necessary production operations (chemical etching, vacuum annealing, oxidation in glow-discharge plasma, platinum and aluminum dioxide deposition) and to study electrophysical characteristics of the produced structures. The experimental studies were carried out using heteroepitaxial structures  $\text{Cd}_x\text{Hg}_{1-x}\text{Te}$  ( $x \sim 0.4$ ) of n-type conductance produced by MBE. The chemical composition of the surface was studied *in situ* using X-ray photoelectron spectroscopy (XPS) in the high-vacuum chamber "SSC Riber". The electrophysical properties of the test MIS structures with tunnel-thin dielectric ( $< 2$  nm) with golden or platinum electrodes were studied on the basis of current-voltage and capacitance-voltage characteristics. The structures are characterized by rectifying barrier properties and are sensitive to light exposure from the ABB imitator with cavity temperature of 583 K (diaphragm  $1 < \dots < 6$ ) (see figure).



Evaluation of detectivity of the best structures with gold contacts by shot noise of dark current is  $1.2 \cdot 10^{14} \text{ cm Hz}^{1/2} \text{ W}^{-1}$  (quantum yield is assumed equal 1, temperature is 78 K and voltage is  $-0.1$  V).

The study was supported by the RFBR, project 13-07-12151 - ofi-m.

## Application of Indium Tin Oxide to the p-cladding Layers of Yellow/Green II-VI Compound Semiconductor Laser Diode Structures on InP Substrates

Koji Fukushima, Tomohiro Shiraishi, Ryohei Kobayashi, Katsumi Kishino,  
and Ichirou Nomura,

Department of Engineering and Applied Sciences, Sophia University  
7-1 Kioi-cho, Chiyoda-ku, Tokyo, 102-8554 Japan  
[i-nomura@sophia.ac.jp](mailto:i-nomura@sophia.ac.jp)

We examined application of indium tin oxide (ITO) to the p-cladding layers of yellow/green II-VI compound semiconductor laser diodes (LDs) on InP substrates. Waveguide analyses of the LD structures with ITO p-cladding layers were performed to obtain optical confinement factors ( $\xi$ ) in the active layer. Compared with the theoretical electromagnetic field distributions in the LD structures with ITO cladding and the conventional structures (i.e., with not ITO but MgSe/BeZnTe superlattices (SLs) p-cladding layers), it is shown that the optical confinements are enhanced by using ITO cladding. For example,  $\xi$  values are 27% and 15% for the ITO cladding and the conventional structure, respectively, when the emission wavelength is 580 nm. We fabricated LD structures consisting of a BeZnTe/ZnSeTe SL active layer sandwiched by MgSe/BeZnTe SL barrier layers, MgSe/ZnCdSe SL n-cladding, ZnTe p-contact, and ITO cladding layers on InP substrates. The II-VI layers were grown employing a double-chamber molecular beam epitaxy system. The ITO layers were deposited by a magnetron sputtering. Yellow emissions at 580 nm were observed by current injections.

ITO is widely applied to many optical devices such as display and solar cells as a transparent electrode, because of high electrical conductivity and high transparency in visible and infrared range. On the other hand, we noticed another merit of ITO, that is, a low refractive index, and that ITO is a promising cladding layer material of LDs because of these merits. In this study, we examined application of ITO to the p-cladding layers of II-VI LD structures on InP substrates. However, ITO cannot be directly applied to p-cladding layers because it is an n-type conductivity material. Thus, we proposed the LD structure with hole-injection layers consisting of a p-type MgSe/BeZnTe SL barrier and p-ZnTe contact layer between the active and ITO cladding layer. In our previous work, it was shown that excellent electrical characteristics were obtained for ITO/p-ZnTe combinations [1]. Here, we analyzed and optimized the waveguide structures of the LDs with ITO cladding, and characterized the fabricated LD structures.

[1] T. Shiraishi, I. Nomura, K. Murakami, S. Takamatsu, T. Kobayashi, and K. Kishino, *Proc. SPIE*, 9198, p. 1278 (2014).

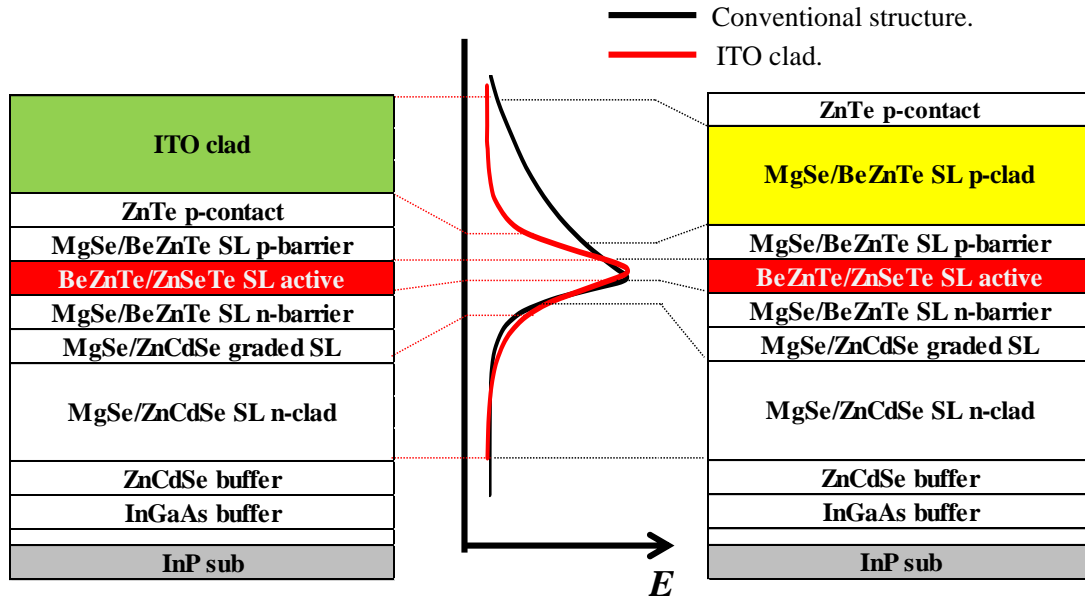


Fig. 1 Schematic diagrams of the LD structures with an ITO cladding layer (left side) and the conventional structure (right side), and theoretical electromagnetic field distributions for each structure (a red solid line for ITO and a black one for the conventional structure). The optical confinement is enhanced by using the ITO cladding layer.

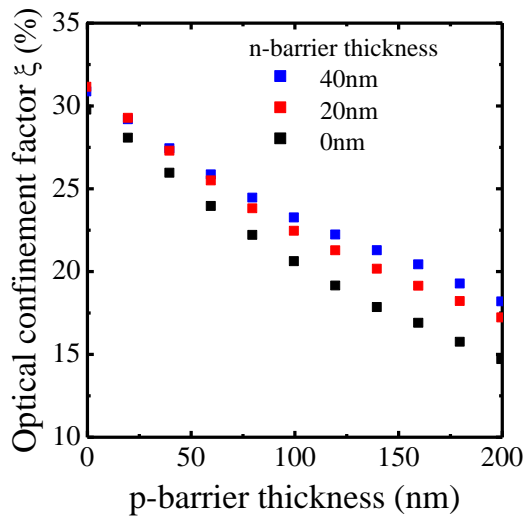


Fig. 2 Theoretical optical confinement factors ( $\xi$ ) as a function of the SL p-barrier thickness with changing the SL n-barrier thickness.  $\xi$  is calculated to be 27% when the p- and n-barrier thicknesses are 40 nm.

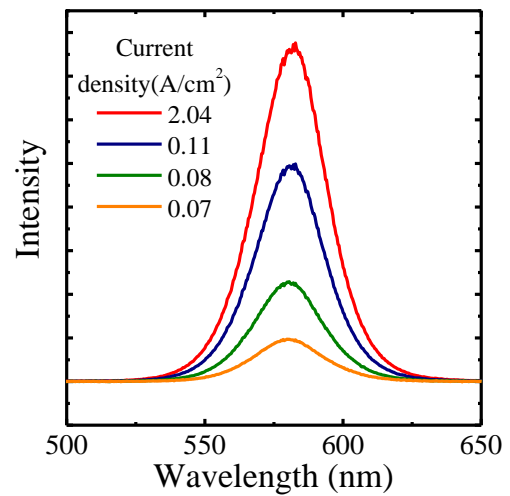


Fig. 3 Emission spectra of the LD structure under current injections.

## Molecular Beam Epitaxy of II-VI/GaAs Laser Heterostructures for Yellow-Orange Spectral Range

S.V. Gronin<sup>1,\*</sup>, S.V. Sorokin<sup>1</sup>, I.V. Sedova<sup>1</sup>, G.V. Klimko<sup>1</sup>, S. Rouvimov<sup>1,2</sup>, K.G. Belyaev<sup>1</sup>,  
A.A. Toropov<sup>1</sup>, E.V. Lutsenko<sup>3</sup>, A.G. Vainilovich<sup>3</sup>, G.P. Yablonskii<sup>3</sup>, and S.V. Ivanov<sup>1</sup>

<sup>1</sup>Ioffe Physical-Technical Institute, St.-Petersburg, Russia

<sup>2</sup>NDIIF, University of Notre Dame, Notre Dame, USA

<sup>3</sup>Stepanov Institute of Physics, NASB, Minsk, Belarus

\* Corresponding author; e-mail: gronin\_sergey@yahoo.com

Lasers emitting in the visible spectrum play significant role in numerous medical applications, e. g. ophthalmology, where green and yellow lasers are used for photocoagulation purposes [1]. At the same time, the yellow light in comparison with the green one is better absorbed by both oxyhemoglobin and deoxyhemoglobin, and less absorbed by melanin. The DPSS lasers commonly used as the sources of coherent yellow light have a fixed wavelength as well as relatively high cost, which makes the development of yellow direct-emitting semiconductor lasers of great importance. The II-VI wide-gap CdSe/Zn(Cd)Se quantum dot (QD) based heterostructures look as a promising candidates to cover the whole yellow range (550-590 nm). In particular, the yellow lasing ( $\lambda = 567$  nm) has been recently demonstrated in II-VI CdSe/ZnSe QD heterostructures with CdSe nominal thickness slightly above 3 monoatomic layer (ML) [2]. Nevertheless, to achieve the “true” yellow emission the nominal thickness of CdSe/ZnSe QDs should exceed the critical one ( $\sim 3.1$  MLs [3]), which inevitably results in both defect arising and drastic decrease in the QD photoluminescence (PL) efficiency. The alternative approach assuming the molecular beam epitaxy (MBE) growth of CdSe QDs in a strained  $\text{Zn}_{1-x}\text{Cd}_x\text{Se}$  quantum well (QW) has resulted in efficient room temperature PL up to 590 nm. It has been predicted theoretically and confirmed experimentally that to achieve the yellow emission the QW composition  $x$  should exceed 0.35-0.4, while the thickness could vary within 2-4 nm [5]. The tensile-strained ZnSSe/ZnSe waveguide SLs compensating partly the strain induced by the ZnCdSe QW is the key element of yellow structure design enabling one to avoid the onset of plastic relaxation in highly compressively-strained active region. This paper reports on MBE growth and studies of laser structures with the asymmetric ZnSe/ $\text{Zn}_{1-x}\text{Cd}_x\text{Se}$  QW/2.8 ML-CdSe QDs active region embedded in the tensile-strained waveguide SLs and emitting in “true” yellow and orange ranges of the visible spectrum. The structures were grown on GaAs (001) substrates via a GaAs buffer at  $T_S \sim 290^\circ\text{C}$  and consisted of bottom (1-1.5)  $\mu\text{m}$  and top (10-20) nm ZnMgSSe claddings, graded-index waveguide (GIW) composed of short-period Zn(Mg)SSe/ZnSe SLs. The active region has been formed by growing of 2.8 ML CdSe QDs on the surface of the ZnSe barrier, followed by deposition of the ZnCdSe QW. The parameters of the  $\text{Zn}_{1-x}\text{Cd}_x\text{Se}$  QWs (thickness and  $x$ ) were chosen as (5 nm and 0.35) and (2 nm and  $x=0.5$ ) for structures #A and #B, respectively. The Cd content in ZnCdSe QW as well as ZnCdSe growth rate were controlled *in situ* via measuring of RHEED specular spot intensity oscillations at the II-VI initial growth stage. The structures demonstrate room temperature lasing at  $\lambda=573$  nm (#A,  $L_{\text{cav}}=734$   $\mu\text{m}$ ) and  $\lambda=593$  nm (#B) with the threshold power density of 1.3 kW/cm<sup>2</sup> and 2.53 kW/cm<sup>2</sup>, respectively. The results of structural (XRD and HRTEM) and optical (PL excitation and T-dependent PL) characterization will be discussed in detail. The work is supported by RSF Project #14-22-00107.

[1] M.A. Mainster, *Ophthalmology* **93**, 952-8 (1986); [2] E.V. Lutsenko et al., *Quantum El.* **43**(5), 418-422 (2013), [3] D. Schikora et al., *Appl. Phys. Lett.* **76**, 418 (2000), [4] S.V. Gronin et al., *Acta Physica Polonica A* **126**(5), 1096 (2014)

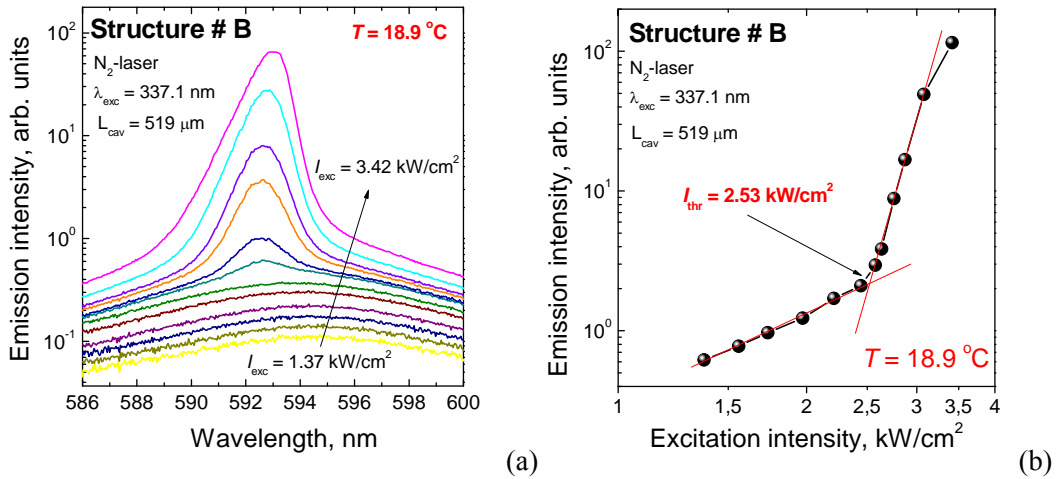


Fig.1. RT lasing spectra (a) and laser threshold (b) of the orange GIW laser heterostructure with ZnSe/2nm-Zn<sub>0.5</sub>Cd<sub>0.5</sub>Se QW /2.8 ML-CdSe QDs active region.

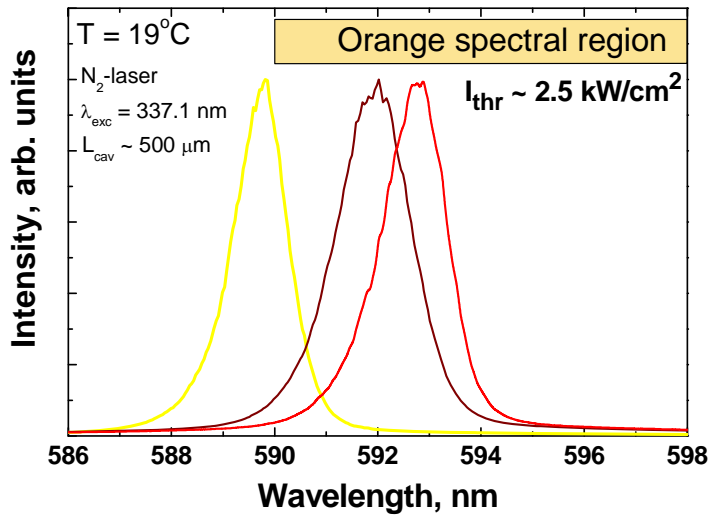


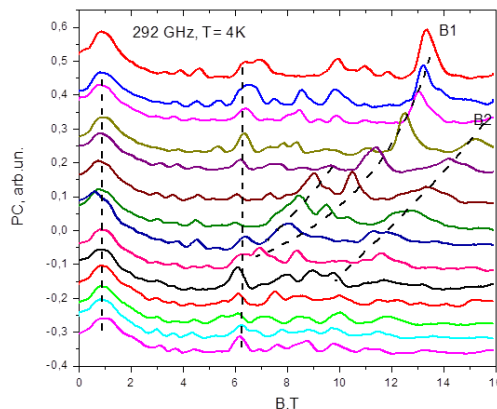
Fig.2. RT lasing spectra of a set of laser structures emitting in the yellow-orange spectral range.

## Terahertz Excitations in HgTe-based Field Effect Transistors

A. Kadykov<sup>1,3</sup>, F. Teppe<sup>1\*</sup>, C. Consejo<sup>1</sup>, N. Diakonova<sup>1</sup>, D. Coquillat<sup>1</sup>, S. Ruffenach<sup>1</sup>, W. Knap<sup>1</sup>, L. Viti<sup>2</sup>, M. Vitiello<sup>2</sup>, S. Morozov<sup>3</sup>, V. Gavrilenko<sup>3</sup>, N. N. Mikhailov<sup>4</sup>, S. A. Dvoretiskii<sup>4</sup>

<sup>1</sup>UMR CNRS 5221, GIS-TERALAB, Université Montpellier II, 34095 Montpellier, France; <sup>2</sup>Institute for Physics of Microstructures, RAS, Nizhny Novgorod, Russia; <sup>3</sup>NEST, Istituto Nanoscienze-CNR and Scuola Normale Superiore, I-56127 Pisa, Italy <sup>4</sup>ISP, Siberian Branch, RAS, pr. Akademika Lavrent'eva 13, Novosibirsk, 630090 Russia  
\*Frederic.teppe@univ-montp2.fr

Recently, a type of topological invariance was predicted in materials with band inversion (semiconductor with a gap between the upper p-type and lower s-type energy bands) due to strong spin-orbit coupling [1]. In this case, one speaks of topological insulators [2]. This kind of topologically protected surface state was first demonstrated to exist in two-dimensional HgTe/CdTe quantum wells (QWs) [3,4]. In this work, we report on a Terahertz magneto-photoconductivity study of inverted band structure HgTe-based Field Effect Transistor (FET) : i) We observe a resonance that could be attributed to topological phase transition related to anticrossing of the zero-mode Landau levels at a critical value of the magnetic field [5-7]. ii) We also observe unknown resonances in the direct band structure regime which are shifting to higher magnetic field values with increasing gate voltage. These resonances cannot be attributed to magnetoplasmons and may be linked with impurity resonant transitions. iii) We finally observe the cyclotron resonance line giving electron effective mass  $m^* = 0.03 m_0$ .



*Photoconductivity spectra as a function of magnetic field for different values of gate bias, at 292 GHz and 4K.*

- [1] C. L. Kane and E. J. Mele, Phys. Rev. Lett. 95, 146802 (2005).
- [2] M. Z. Hasan and C. L. Kane, Rev. Mod. Phys. 82, 3045 (2010).
- [3] Andrei Bernevig, T. L. Hughes, and S.-C. Zhang, Science 314, 1757 (2006).
- [4] M. König, S. Wiedmann, C. Brüne, A. Roth, H. Buhmann, L. W. Molenkamp, X.-L. Qi, and S.-C. Zhang, Science 318, 766 (2007).
- [5] M. Zholudev, F. Teppe, M. Orlita, et al., Phys. Rev. B 86, 205420 (2012).
- [6] M. Zholudev, F. Teppe, M. Orlita, et al. Proceedings of IRMMW conference, Mainz, Germany (2013).
- [7] M. Zholudev, F. Teppe, C. Consejo, et al. Unpublished (2015).

## Growth and characterization of ZnCdSe/ZnCdMgSe two-color quantum-well infrared photodetectors

Guopeng Chen<sup>a</sup>, Arvind P. Ravikumar<sup>b</sup>, Thor A. Garcia<sup>c</sup>, Joel de Jesus<sup>c</sup>,  
 Maria C. Tamargo<sup>c</sup>, Claire Gmachl<sup>b</sup>, and Aidong Shen<sup>a,\*</sup>

<sup>a</sup>Department of Electrical Engineering, The City College of New York, USA

<sup>b</sup>Department of Electrical Engineering, Princeton University, USA

<sup>c</sup>Department of Chemistry, The City College of New York, USA

\*ashen@ccny.cuny.edu

Two-color infrared (IR) photodetectors operating in the mid-wavelength IR (MWIR) and long-wavelength IR (LWIR) regions are key elements for IR focal plane arrays that have important military, medical and industrial applications. Quantum-well infrared photodetectors (QWIPs) grown by molecular beam epitaxy (MBE) with high material quality and uniformity are intersubband (ISB) photonic devices suitable for this application. Two-color QWIPs working in the MWIR and LWIR ranges are mostly fabricated from III-V semiconductors, typically consist of multi-stacks of InGaAs/AlGaAs and GaAs/AlGaAs multiple quantum wells (MQWs) grown on GaAs substrates. We have recently shown that QWIPs with high performance can be fabricated from ZnCdSe/ZnCdMgSe MQWs [1, 2]. The wide band gap II-VI material system can be grown lattice-matched on InP substrates with a large tunable band gap, which makes it especially suitable for multi-color QWIP applications.

In this work, we report the growth of II-VI two-color QWIPs by MBE. The samples were grown on InP substrates with InGaAs buffer layers in a dual-chamber Riber MBE system. In each sample, MWIR and LWIR ZnCdSe/ZnCdMgSe MQWs are sandwiched between Cl-doped ZnCdSe bottom, middle and top contact layers. The barrier height and well thickness were designed to have the bound-to-quasi-bound transition in both MQWs. X-ray diffraction and photoluminescence measurements demonstrated the high structural and optical properties of the samples. Room temperature ISB absorption spectrum obtained by FTIR for a typical sample is shown in Fig. 1.

This work is supported in part by MIRTHE (NSF-ERC # EEC-0540832) and by PSC-CUNY Award.

<sup>1</sup> A.P. Ravikumar, et al., Appl. Phys. Lett. 102, 161107 (2013).

<sup>2</sup> A. Shen, et al., J. Vac. Sci. Technol. B 31, 03C113 (2013).

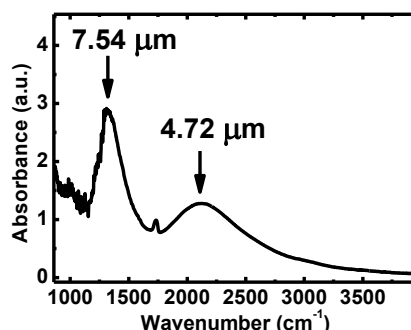


Fig. 1 ISB absorption measured at RT for a ZnCdSe/ZnCdMgSe two-color QWIP.

## Mid-infrared light sensitive p-CdZnTe/i-CdTe/n-CdTe diode structures with PbTe nano-inclusions

S. Chusnutdinov\*, M. Szot, S. Kret, L. Kowalczyk,  
T. Wojtowicz and G. Karczewski  
Institute of Physics, Polish Academy of Sciences, Warsaw, Poland  
\*chusnut@ifpan.edu.pl

Devices based on cadmium telluride (CdTe) are widely used in renewable energy applications and medicine, due to its favorable physical and chemical properties (wide and direct band gap, high radiation resistance, low Auger recombination rate etc.) Detection range of CdTe-based detectors can be extended toward longer wavelengths by incorporation into the device structures of inclusions from a narrow-gap semiconductor, such as lead telluride (PbTe) having the energy gap of 0.31 eV at 300K. CdTe and PbTe have almost identical crystal lattice parameters, thus the lattice mismatch is only  $\sim 0.3\%$ . However, CdTe and PbTe crystallize in the zinc blend and rock salt, respectively. As a result of the difference in crystal lattice structures these materials are almost immiscible. Limited miscibility allows creation of high-quality quantum size inclusions with high efficiency of electro- and photoluminescence even at room temperature [1, 2].

Here we report on optical and photoelectrical investigations of p-CdZnTe/i-CdTe/n-CdTe thin-film diodes with PbTe nano-inclusions produced inside the intrinsic CdTe absorption layer. The thin-film heterojunctions were grown by molecular beam epitaxy (MBE) on monocrystalline, semi-insulating (100) GaAs substrates from elemental sources. The n-type CdTe films were produced by iodine doping. Depending of the growth parameters either PbTe quantum dots or PbTe quantum wells were formed in the intrinsic CdTe layer. The CdZnTe layers were doped with nitrogen supplied from nitrogen-plasma source. The investigated structures exhibit a very strong photoluminescence (PL) emission in the infrared spectral range in the entire temperature range from liquid He temperatures up to room temperatures. At low temperatures strong PL signal centered at wavelength of 4.9  $\mu\text{m}$  is detected. The full width at half maximum of the emission spectrum is 0.4  $\mu\text{m}$ , which corresponds to 17 meV in energy terms. With the increasing temperature the emission peak narrows down to 7 meV and shifts towards higher energies reaching 3.49  $\mu\text{m}$  at  $T=290$  K. The temperature coefficient of the peak emission, 0.44 meV/K is in perfect agreement with those of the PbTe energy gap. The current-voltage characteristics of a p-CdZnTe/i-CdTe/n-CdTe diodes were measured in darkness and under infrared illumination (wide spectral range: 1- 20  $\mu\text{m}$ ). The dark forward-to-reverse current ratio for this diode is  $10^6$  at the bias of 0.8 V and the diode ideality factors is about 1.5. The leakage current of  $1 \times 10^{-10}$  A in reverse bias is observed. The reverse current increases under infrared illumination. Photocurrent is generated in diode due to absorption of the infrared light by PbTe quantum structures. The peak spectral response is observed at about 5.30  $\mu\text{m}$  at 10 K. Reference CdTe diodes without PbTe nano-inclusions do not show any sensitivity in the mid-infrared spectral region. The investigated p-CdZnTe/i-CdTe/n-CdTe structures with PbTe nano-inclusions proved to be very promising for IR sensor applications.

This work was partially supported by the Foundation of Polish Sciences by the Master program № Mistrz5./2013

- [1] A. Hochreiner, T. Schwarzl, M. Eibelhuber, W. Heiss, G. Springholz, V. Kolkovsky, G. Karczewski, and T. Wojtowicz, *Appl. Phys. Lett.* **98**, 021106 (2011).
- [2] G. Karczewski, M. Szot, S. Kret, L. Kowalczyk, S. Chusnutdinov, T. Wojtowicz, S. Schreyeck, K. Brunner, C. Schumacher and L. W. Molenkamp. *Nanotechnology* **26** 135601 (2015).

## Investigation of Yellow/Green II–VI Compound Semiconductor Laser Diode Structures on InP Substrates

Ryohei Kobayashi, Shingo Takamatsu, Koji Fukushima, Katsumi Kishino,  
and Ichirou Nomura,

Department of Engineering and Applied Sciences, Sophia University  
7-1 Kioi-cho, Chiyoda-ku, Tokyo, 102-8554, Japan  
[i-nomura@sophia.ac.jp](mailto:i-nomura@sophia.ac.jp)

We investigated yellow/green laser diode (LD) structures consisting of a BeZnTe/ZnSeTe superlattice (SL) active layer sandwiched by MgSe/BeZnTe SL barrier (optical guide) layers, MgSe/ZnCdSe SL n-cladding and MgZnSeTe p-cladding layers on InP substrates. By device simulation using SiLENSe (STR Group, Inc.), it is shown that the n-side barrier layer prevents electron injections from the n-cladding to the active layer, which reduces radiative recombination carriers and emission intensity in the active layer. On the other hand, waveguide analyses of the LD structures show that there are not so large differences between the optical confinement factors ( $\xi$ ) in the active layer of the LD structures with and without the n-barrier. For example,  $\xi$  values are 25.8 and 23.3% for the structures with and without the n-barrier, respectively, when the emission wavelength is 580 nm. In experiments, we characterized the LD structures fabricated on InP substrates by a molecular beam epitaxy. In injection current density versus applied voltage (J-V) characteristics, turn-on voltages of the devices without the n-barrier were lower than those of the devices with the n-barrier by about 7 V. Orange emissions at 603 nm were observed by current injections for the devices without the n-barrier. These results show that the LD structure without n-barrier is more suitable.

II-VI compound semiconductors such as ZnCdSe and BeZnTe are very attractive materials in the development of yellow/green LDs and LEDs. For example, BeZnTe/ZnSeTe SLs [1] have the direct bandgap energies in a yellow to green wavelength range. In addition, the SLs include BeTe, which is effective for strengthening the lattice bonds and enhancing the device reliability. Therefore, the SLs are expected to be active layer materials of highly reliable yellow/green LDs and LEDs. Besides, MgSe/ZnCdSe SLs and MgZnSeTe quaternaries are promising cladding layer materials because of high doping properties and low refractive indices. Using these materials, we have developed yellow/green LDs and LEDs so far [2,3]. In this study, we investigated the LD structures consisting of the materials and SLs mentioned above by device simulation, waveguide analyses, and characterization of the fabricated devices.

[1] T. Kobayashi, I. Nomura, K. Murakami, and K. Kishino, *J. Cryst. Growth*, 378, p.263 (2013).

[2] I. Nomura, Y. Nakai, K. Hayami, T. Saitoh, and K. Kishino, *pss(b)*, 243, p. 924 (2006).

[3] I. Nomura, Y. Sawafuji, and K. Kishino, *Jpn. J. Appl. Phys.*, 50, 031201 (2011).

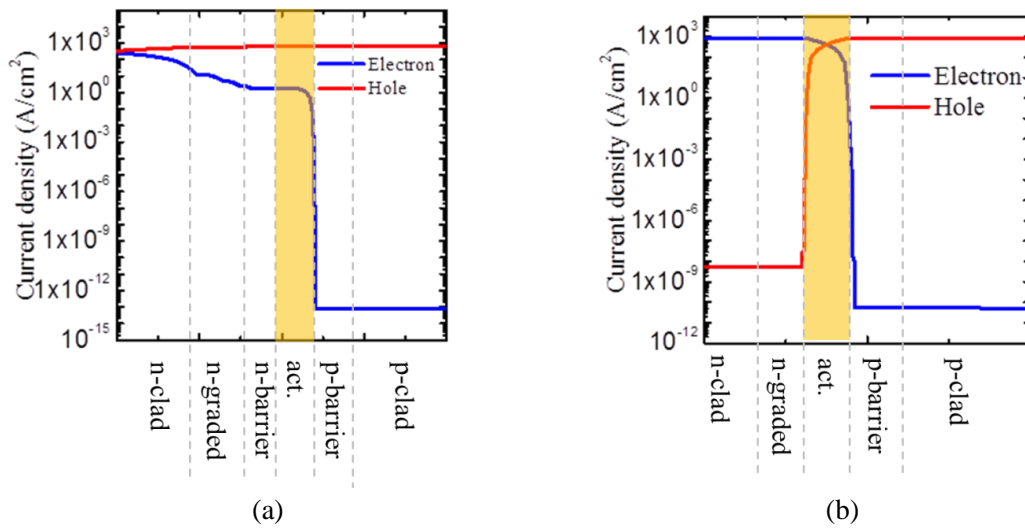


Fig. 1 Theoretical electron and hole current profiles in the LD structures with (a), and without the n-barrier (b) when the total current densities are  $0.6(a)$  and  $0.8 \text{ kA/cm}^2$  (b), respectively. In (a), the electron injection from the n-cladding to the active layer is prevented by the n-barrier. On the other hand, electrons and holes are injected into the active layer efficiently in (b).

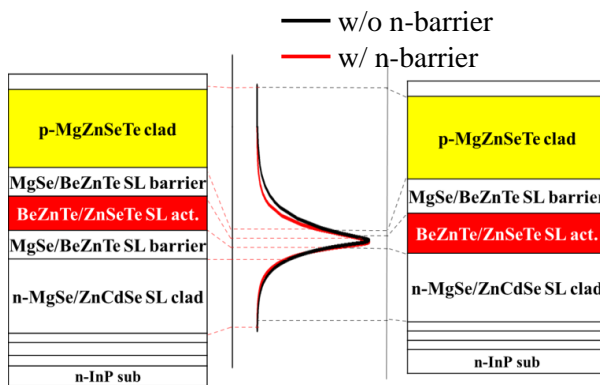


Fig. 2 Schematic diagrams of the LD structures with (left) and without the n-barrier (right) and theoretical electromagnetic field distributions for each LD structure. There are not so large differences between both the distributions.

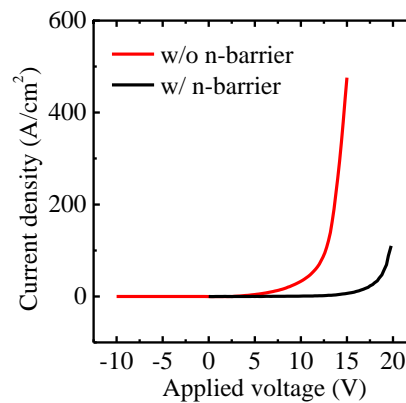


Fig. 3 J-V characteristics of the fabricated LD structures with and without the n-barrier. Turn-on voltages of the devices without the n-barrier were lower than those of the devices with the n-barrier by about 7 V.

## Analysis of the diffusion of charge carriers in the photosensing film of photovoltaic n-on-p HgCdTe IR FPA detectors

A.V. Vishnyakov, V.A. Stuchinsky\*, D.V. Brunev, A.V. Zverev, and S.A. Dvoretzky  
Institute of Semiconductor Physics, Russian Academy of Science, Siberian Branch,  
Novosibirsk 630090, Russia  
\*stuchin@isp.nsc.ru

In our report, we present a general scheme for analyzing the diffusion of charge carriers in the photosensing film (PF) of 2D HgCdTe (MCT) IR FPA detectors on the basis of spot-scan measurements performed at different levels of photocurrents  $j_{ph}$  being extracted by the readout circuits out of the PF. The starting point in our analysis was the consideration that, in an FPA with suppressed surface recombination of charge carriers at film boundaries, the lifetime  $\tau$  and, hence, the diffusion length of charge carriers in the PF are defined, first, by their bulk recombination in the absorber material and, second, by the extraction of photocurrents out of the PF. The bulk diffusion length of minority carriers  $l_d$  in the film can therefore be determined as the extreme value of their effective diffusion length  $l_{d\,eff}$  (at  $j_{ph} \neq 0$ ) achieved as  $j_{ph} \rightarrow 0$ . The influence of readout circuits on the diffusion length of charge carriers can be minimized by decreasing the gate potential of input FETs  $V_g$  in the photoelectric cells of the detector [1]. At sufficiently large lengths  $l_{d\,eff}$ , the asymptotic behavior of  $l_{d\,eff}(j_{ph})$  for  $j_{ph} \rightarrow 0$  can be analytically revealed within a continuum approach assuming that the excess charge carriers are extracted out of the PF, instead of the discrete diode array, by a large suction electrode continuously covering the whole PF area occupied by FPA, while the carriers themselves diffuse out of the illumination spot into adjacent non-illuminated film regions over an MCT film of zero thickness ( $d=0$ ). The latter assumption is applicable because, at a low rate of photocurrent suction, the distribution of excess charge carriers flattens across the film. In such a model, the action of FPA on the lateral distribution of excess carriers in the film  $n_s(x)$  can be allowed for via an additional term, introduced into 1D diffusion equation, implying that the local photocurrent density  $j_{ph}$  nondimensionalized by the lifetime  $\tau$  varies in proportion (with some coefficient  $k$ ) to the local value of the sheet density of excess carriers  $n_s$  in the film ( $j_{ph} = k \times n_s / \tau$ ). As a result, the bulk diffusion length  $l_d$  can easily be determined from spot-scan data obtained at low values of  $V_g$ . In normal operational regime of the detectors (with large values of  $V_g \approx 1\text{V}$  and FPA diodes being back-biased with a sufficiently large reverse bias voltage), both assumptions of the previously adopted model become violated. Yet, the model itself proved to still be applicable to the analysis of spot-scan scan data for large values of  $V_g$  providing that the discrete structure of FPA is taken into account. The latter modification of the model can be achieved by assuming that  $k=0$  in the film region in between FPA diodes while the local effective diffusion-length value  $l_{d\,eff}$  of excess charge carriers in the film regions under the diodes,  $l_{d\,eff}^*$ , is defined by a local non-zero value of  $k$ ,  $k_{ph}$ , to be deduced from a comparison of measured with calculated spot-scan profiles. With the obtained value of  $k_{ph}$ , the length  $l_{d\,eff}^*$  can therefore be determined ( $l_{d\,eff} = l_d / \sqrt{1+k_{ph}}$ ). The obtained values of  $l_d$  in the MCT films of examined MWIR and LWIR FPA detectors (19.5 to 24  $\mu\text{m}$ ) proved to be in a good agreement with relevant literature data. Simultaneously, the estimated values of  $l_{d\,eff}$  in the film region under FPA diodes proved to be consistent with an *a priori* estimate of this length,  $l_{d\,eff} \approx 2d / \pi$ , obtained from an analysis of the typical shape of cross-film distributions  $n(z)$  in that region.

- [1] A.V. Vishnyakov, V.A. Stuchinsky, D.V. Brunev, A.V. Zverev, and S.A. Dvoretzky, Appl. Phys. Lett. **104**, 092112 (2014)

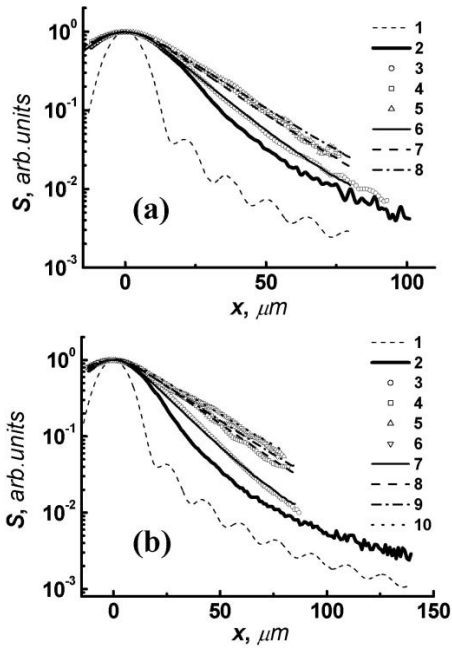


FIG. 1. Distribution of the IR radiation intensity in the vicinity of the illumination spot (curve 1) and spot-scan profiles  $S(x)$  registered in examined MWIR (D-1) (a) and LWIR (D-2) (b) detectors at several values of  $V_g$  (the rest data) from which the diffusion-length values were determined.

(a) Input-FET gate potential:  $V_g=1.068$  V (curve 2), and 0.96, 0.88, and 0.82 V (symbols 3, 4, and 5 and curves 6, 7, and 8, respectively). Symbols 3–5 and curve 2 show the measured spot-scan profiles  $S(x)$ ; curves 6–8 show the profiles  $S(x)$  calculated for small values of  $V_g$  by the 1D diffusion model.

(b) Input-FET gate potential:  $V_g=0.95$  V (curve 2), and 0.90, 0.85, 0.74, and 0.73 V (symbols 3, 4, 5, and 6, and curves 7, 8, 9, and 10, respectively). Symbols 3–6 and curve 2 show the measured spot-scan profiles  $S(x)$ ; curves 7–10 are the profiles  $S(x)$  calculated for small values of  $V_g$  by the 1D diffusion model.

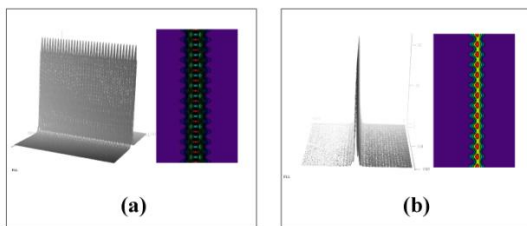


FIG. 3. 2D plots and contour lines of the sheet density of excess minority carriers  $n_s$  for the measuring diode position at the centerline of the illumination spot (a) and for the diode center position  $10 \mu\text{m}$  aside from the spot axis (b). The data were obtained for the D-1 detector in the calculation with  $k_{ph}=40$ .

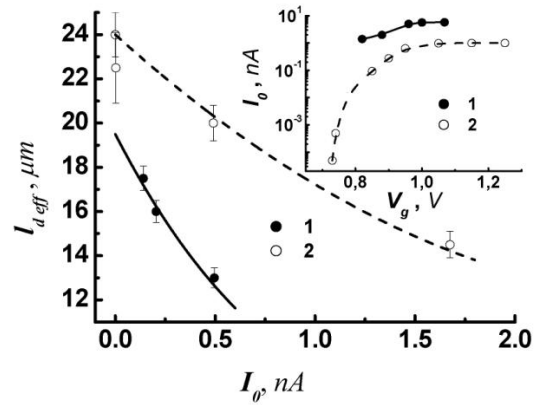


FIG. 2. Effective minority-carrier diffusion length  $l_{d,eff}$  versus the photocurrent  $I_0$  registered by the measuring diode at the maximum of the spot-scan profiles  $S(x)$ . Symbols 1 and 2 are the data for the D-1 and D-2 detectors; the curves are the dependences calculated by formula (3) with  $\alpha/I_0=0.9$  and  $0.33 \text{ nA}^{-1}$  for D-1 and D-2, respectively.

The inset shows the dependence of  $I_0$  on  $V_g$  for the D-1 and D-2 detectors at fixed (yet different for the D-1 and D-2 detectors) levels of the IR radiation intensity in the illumination spot. Symbols 1 and 2 are the data for the D-1 and D-2 detectors, respectively.

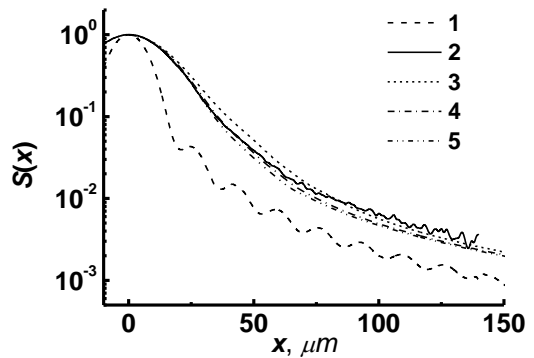


FIG. 4. Spot-scan profile  $S(x)$  in the D-2 detector measured at  $V_g=0.95$  V (curve 2) in comparison with the profiles  $S(x)$  calculated by the 2D diffusion model with  $k_{ph}=20$ , 40, and 60 (curves 3, 4, and 5, respectively). Curve 1 is the distribution of the IR radiation intensity.

## **640×512 Focal Plane Assemblies based on HgCdTe heterostructures grown by MBE**

Yakushev M.V.\*, Brunev D.V., Dvoretzky S.A., Marchishin I.V., Mikhailov N.N.,  
Predein A.V., Sabinina I.V., Sidorov Y.G., Sidorov G.Y., Vasilyev V.V., Varavin V.S.,  
Vishnyakov A.V.

A.V. Rzhanov Institute of Semiconductor Physics, SB RAS, Novosibirsk, Russia  
[\\*yakushev@isp.nsc.ru](mailto:*yakushev@isp.nsc.ru)

640×512 on 25- $\mu\text{m}$  pitch Infrared Focal Plane Assemblies (IRFPA) based on MCT heterostructures (HS) for MWIR (3-5  $\mu\text{m}$ ) and LWIR (8-10  $\mu\text{m}$ ) has been designed and fabricated by ISP SB RAS

MCT HS were grown by MBE on GaAs (013) and Si (013) substrates. The density of morphological V-shaped defects was as lower than 500  $\text{cm}^{-2}$ .

As-grown MCT MBE had n-type conductivity with electron concentration of  $(2-5)\times 10^{14}\text{cm}^{-3}$ . After thermal annealing in helium atmosphere n-type MCT MBE HS were converted into p-type with hole concentration of  $(5-15)\times 10^{15}\text{cm}^{-3}$ .

The photovoltaic arrays “n-on-p” type were manufactured by  $\text{B}^+$  ion doping at implantation into p-type MCT MBE HS. The diodes current-voltage characteristics were measured in wide temperature range. We determined the current mechanism through n-p junction and its changing with temperature.

640×512 IRFPA were fabricated by flip-chip technology of matrix photosensitive element and Read-Out Integrated Circuit (ROIC) through In bumps. 640×512 CMOS ROIC had been designed for 0,6- $\mu\text{m}$  technology and could be operated in following formats as 640×512, 640×480, and 512×512, “snap shot” regime and in ITR and IWR modes. The ROIC allows controlling exposure time and framing rate with an external signal using the serial and parallel interfaces.

The photoelectric characteristics were measured for MWIR and LWIR IRFPA at at 80 - 120 K and 70 - 85 K respectively (see in Table for fixed temperature measurements). At measurements temperature of a background and the absolutely black body made 295 and 501K respectively. Frequency of poll of an output signal made 2.0 MHz.

Characteristic	Value	
	MWIR	LWIR
Cut-off wavelength ( $\lambda_{0,5}$ ), $\mu\text{m}$	4,86	10,2
NETD, mK	19,9	34,8
Defective pixels, %	1,59	4,57
Operating temperature, K	97	72

The defective pixels were determined for those in which  $\text{NETD} > 3 \times (\text{NETD}_{\text{mean}})$ .

## Investigation of Au/Zn composite electrode on CdZnTe detector

Xiao-yan LIANG<sup>1</sup>, Jia-hua MIN<sup>1\*</sup>, Ji-jun ZHANG<sup>1</sup>, Lin-jun Wang<sup>1</sup>

<sup>1</sup> School of Materials Science and Engineering, Shanghai University 1, Shanghai, P.R.China

\* minjh@shu.edu.cn

Electrode fabrication is a key procedure for preparation of high-performance CdZnTe detectors, and metal-semiconductor contact contributes greatly to the performance of detectors. Electrode materials employment, crystal surface treatments and electrode thermal annealing are used to improve CdZnTe metal-semiconductor contact. In recent years, composite electrodes on CdZnTe detector are reported to achieve better spectrum response. However, composite electrode on different CdZnTe lattice plane was rather studied.

In the present paper, CdZnTe (111) Cd (A) plane and (111) Te (B) plane were distinguished by etch liquid. Au/Zn composite electrode was deposited on the (111) B plane of P-CdZnTe by vacuum evaporation method. Based on the AFM, SEM and EDS, XRD, the barrier heights and spectrum response, effects of Au/Zn composite electrode on metal-semiconductor contact were investigated. The results showed that Zn has effectively diffused into the internal CZT crystal, which would accommodate the surface element component without the introduction of other metal impurities, decreasing the influence of Te enriched surface on the metal-semiconductor contact. Furthermore, combination of Zn and Te plane increased the electrode adhesion and prevented Au atom diffusion into CZT, which might introduce deep level defects, giving rise to electron capture. A lower Schottky barrier height and better spectrum response were attained by depositing Au/Zn composite electrode than Au electrode on (111) B surface, suggesting Au/Zn composite electrode on (111) B surface is a preferred ohmic contact for CdZnTe detector.

- [1] Niraula M, Nakamura A, Aoki T. Nucl Instr Meth A **491**,168, (2002).
- [2] Bolotnikov A E, Camarda G C, Wright G W, et al., Nuclear Science, IEEE Transactions on **52**,589-598, (2005).
- [3] Chen H, Awadalla SA, Harris F, Lu P, Redden R, Bindley G. IEEE Trans Nucl Sci. **255**,59, (2008).
- [4] Nelson K A, Geuther J A, Neihart J L, et al., Nuclear Instruments and Methods in Physics Research Section A: Accelerators, Spectrometers, Detectors and Associated Equipment **680**, 97-102, (2012).
- [5] Zha G, Jie W, Bai X, et al. . Journal of Applied Physics **106**. 053714. (2009).
- [6] Prokesch M, Szeles C. , Journal of applied physics **100**, 014503, (2006).
- [7] Liang XY, Min JH, Wang CJ, Sang WB. Rare Metal Mater Eng **563**,2085. (2009).
- [8] Bell S J, Baker M A, Chen H, et al. , Journal of Physics D: Applied Physics **46**,455502, (2013).
- [9] Tripathi J K, Harilal S S, Hassanein A. Materials Research Express **1**,035904, ( 2014).
- [10] Gangqiang Zha, Wanqi Jie, Tingting Tan, et al.. Chemical Physics Letters **427**. 197-200. (2006).
- [11] Jianrong Y, Huiming G, Xinqiang C, et al., Journal of crystal growth **234**, 337-342,(2002).
- [12] Tung R T. , Physical review B **64**, 205310, (2001).
- [13] Al-Shibani K. M. , Physica B **322**, 390-396, (2002).

**Tuesday September, 15 - Poster Session 2 - TuP**

**17:15-18:45**

<b>Low-dimensional structures and related physics (novel 2D systems, nanostructures, quantum dots, colloidal nanocrystals)</b>	<a href="#">220</a>
<b>Spin related phenomena (topological insulators , magnetic semiconductors , magnetic devices)</b>	<a href="#">248</a>
<b>Growth and characterization , doping and defects</b>	<a href="#">268</a>
<b>New materials : Biomaterials, hybrid organic-inorganic structures</b>	<a href="#">294</a>

**Poster Session 2 - TuP**

**Low-dimensional structures and related physics (novel 2D systems, nanostructures, quantum dots, colloidal nanocrystals)**

## Influence of Shell Thickness on the Charge Transfer Dynamics from Photoexcited PbS/CdS Quantum Dots to Metal Oxides

Sohel, M.<sup>1\*</sup>, and Yakadze, B.<sup>1</sup>

<sup>1</sup>Natural Sciences Department, Hostos College of The City University of New York, Bronx, U.S.A.

\*msohel@hostos.cuny.edu

Lead chalcogenide quantum dots (QDs) like PbSe and PbS specially core/shell PbS/CdS are promising near-infrared nanomaterials due to their quantum confinement properties, phonon confinement features, and potential for electronic and optoelectronics application. [1] In photovoltaics, charge recombination is a detrimental process that reduces the efficiency of a solar device as photons are lost by charge recombination. A compromise is needed between charge separation and charge recombination and this can be achieved by control of the QD shell thickness for optimized functionality of devices based on QD core/shell structures. It is important to explore and understand the role of QD core size and shell thickness on the hole transfer taking place between PbS/CdS core/shell QDs and metal oxides. In this collaborative study with Cotlet's group at the Center for Functional Nanomaterials at Brookhaven National Laboratory, using time-resolved confocal photoluminescence (PL) microscopy, NIR emitting PbS/CdS QDs as a function of core, and the role of varying CdS shell thickness on charge transfer initially exhibited an exponential dependency on the varying thickness of the CdS shell similar to previously reported varying core CdSe/ZnS core/shell QDs and titanium oxides providing the tunneling barrier character of the CdS shell toward hole transfer. [2, 3]

- [1] Y. Pan, M. A. Sohel, L. Pan, Z. Wei, H. Bai, M. C. Tamargo, and J. R. Lombardi, *Materials Today*, Accepted for publication (2015).
- [2] Z. Xu, C. Hine, M. Maye and M. Cotlet, *ACS NANO*, **6** (6), 4984-4993, (2012).
- [3] H. Zhao, Z. Fan, H. Liang, G. S. Selopal, B. A. Gonfa, L. Jin, A. Soudi, D. Cui, F. Enrichi, M. M. Natile, I. Concina, D. Ma, A. O. Govorov, F. Rosei, A. Vomiero, *Nanoscale*, **6**, 7004, (2014).

## Electric field imaging in single ZnO nanowire Schottky diodes

F. Donatini<sup>1,2</sup>, A. De Luna Bugallo<sup>1,2</sup>, P. Tchoufian<sup>1,2,3</sup>, V. Sallet<sup>4</sup>, C. Sartel<sup>4</sup>, J. Pernot<sup>1,2,5\*</sup>

<sup>1</sup> Univ. Grenoble Alpes, Inst NEEL, F-38042 Grenoble, France

<sup>2</sup> CNRS, Inst NEEL, F-38042 Grenoble, France

<sup>3</sup> CEA-LETI, MINATEC Campus, 17 rue des Martyrs, F-38054 Grenoble Cedex 9, France

<sup>4</sup> GEMAC, Université de Versailles St-Quentin en Yvelines– CNRS, 45 Avenue des  
Etats-Unis, 78035 Versailles, France

<sup>5</sup> Institut Universitaire de France, 103 boulevard Saint-Michel, F-75005 Paris, France

\*julien.pernot@neel.cnrs.fr

Due to its direct-band gap and large exciton binding energy, ZnO semiconductor is a promising material for devices applications such as UV emitters-photodetectors. Nanostructuring of ZnO in the form of nanowires (NWs) brings additional advantages for the next device generation such as light trapping, improved crystal quality, low cost substrate integration. Nevertheless, NW properties often diverge from their bulk counterparts due to the high surface-to-volume ratio. Therefore, a detailed comprehension on the electronic transport and electrostatics properties is essential for the design of NW based devices. In the scope this work, we present a systematic study of ZnO NW Schottky diodes using two complementary techniques, electron beam induced current (EBIC) and cathodoluminescence (CL) to map the space charge region, and induced electric field formed by the metal-semiconductor junction and to determine the exciton diffusion length in ZnO NWs. The ZnO NWs used in this study, were grown on a-plane sapphire or c-plane ZnO substrates by metalorganic chemical vapor deposition (MOCVD).

In order to fabricate Schottky diodes, Ohmic (Ti-Au) and Schottky (Ni-Au) contacts were achieved on single NWs dispersed on a Si/SiO<sub>2</sub> substrate template using a hybrid lithography process that integrates e-beam lithography and CL imaging [1]. Spatially resolved CL and EBIC images were recorded at room temperature over several Schottky devices with different nanowire diameters ranging from 50 nm to 350 nm. The physical properties measured by CL (optical) and EBIC (electrical) will be compared. The exciton diffusion lengths were obtained by analyzing the CL and EBIC profiles taken along the NW axis. The exciton diffusion lengths were found to be strongly diameter dependent. This behavior will be discussed and described in terms of surface recombination mechanisms. Less expected, the extension of the space charge region induced by the Schottky barrier is found to vary linearly versus the reverse bias voltage applied to the Schottky diodes. The spatial extension versus bias (close to 30 nm/V) is similar to the one previously reported by some of us for ZnO wires grown by MOCVD in another lab [2] and found here to be independent to the NWs diameter. These data will be correlated to resistivity measurements (4 probe resistance measurements between 4 K and 300 K) [3] and finite element simulations (nextnano3) in order to explain the origin of this unexpected voltage dependence of the depleted area in semiconducting NW.

[1] F. Donatini and Le Si Dang, *Nanotechnology*, **21**, 375303 (2010)

[2] J.S. Hwang, F. Donatini, J. Pernot, R. Thierry, P. Ferret, Le Si Dang. *Nanotechnology*, **22**, 475704 (2011)

[3] A.De Luna Bugallo, F. Donatini, C. Sartel, V. Sallet, and J. Pernot, *Appl. Phys. Express* **8**, 025001 (2015).

## Polarization Resolved Photoluminescence Excitation Studies of Individual CdSe Quantum Dots Emitting in Yellow Spectral Range

J. Piwowar<sup>1,2</sup>, M. Goryca<sup>1</sup>, T. Smoleński<sup>1</sup>, A. Bogucki<sup>1</sup>, A. Golnik<sup>1</sup>, P. Kossacki<sup>1</sup>,  
M. Nawrocki<sup>1</sup>, W. Pacuski<sup>1</sup>, J. Suffczyński<sup>1\*</sup>

<sup>1</sup>Institute of Experimental Physics, Faculty of Physics, University of Warsaw, Warsaw, Poland

<sup>2</sup>Biological and Chemical Research Centre, Department of Chemistry, University of Warsaw, Warsaw, Poland

\*Jan.Suffczynski@fuw.edu.pl

Selenium based Quantum Dots (QD) act as efficient light sources, what makes them suitable for applications, e.g., in high quantum yield lasing devices. Incorporation of magnetic ions, like Mn, would further enhance their functionalities. Operation of such magneto-optical devices requires, however, QDs emission below the energy of Mn internal transition (at 2.1 eV), which competes with excitonic radiative recombination.

We present design, a Molecular Beam Epitaxy growth, and optical properties of CdSe Quantum Dots embedded in an innovative,  $Zn_{1-x}Cd_xSe$  ( $x$  up to 30%) barrier. As demonstrated by micro-Photoluminescence ( $\mu$ -PL) measurements (0.5  $\mu$ m spatial resolution, temperatures between 1.7 K and 300 K), introducing cadmium to ZnSe barrier enables tuning of the QDs energy emission from 2.3 – 2.5 eV, proper for CdSe/ZnSe system, down to 1.9 eV, that is below the Mn internal transition energy.

The QDs are characterized by non-resonant  $\mu$ -PL (excitation at 3.06 eV) in magnetic field up to 10 T. A typical pattern of excitonic emission spectrum of a single CdSe/(Zn,Cd)Se QD is determined, along with values of exciton fine structure splitting, g-factor and diamagnetic shift.

Photoluminescence Excitation (PLE) measurements on individual QDs are performed with tunable Rhodamine 590 dye laser operating in energy range 2.05-2.20 eV, acting as the excitation source. Sharp (FWHM down to 200  $\mu$ eV) maxima are found in PLE spectra, reflecting the resonant transfer of photoexcitation to the emitting QD state. The PLE carried out with a circularly polarized excitation and detection reveals that a significant degree of circular polarization is conserved during the excitation transfer to charged exciton state. Its efficiency is as large as 18%.

Some of the studied QD layers are doped with a very low density of  $Mn^{2+}$  ions during the growth. A characteristic six-fold splitting of the excitonic lines confirms presence of QDs containing a single  $Mn^{2+}$  ion.

Possibility of incorporation of single  $Mn^{2+}$  ions combined with an ability of resonant excitation makes them promising for efficient optical orientation of single magnetic ions spin. Present study opens also a perspective for studies of selenium based QDs doped with many  $Mn^{2+}$  ions. Moreover, the emission energy of presented CdSe/(Zn,Cd)Se QDs corresponds to the short wavelength transmission window of plastic optical fibers.

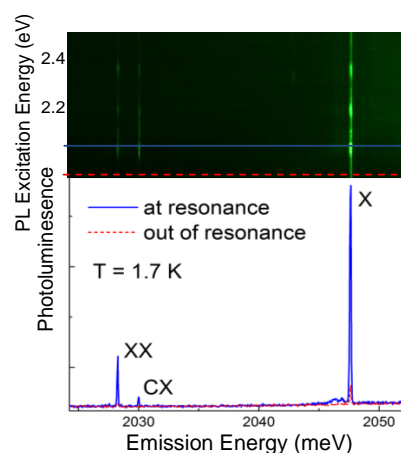


Figure 1. The PLE and  $\mu$ -PL spectra of a CdSe/(Zn,Cd)Se QD excited at resonance and out of resonance.

## Photoinduced Transformations of Optical Properties of the CdSe and AgInS<sub>2</sub> Quantum Dots Embedded in the Films of Polyvinyl Alcohol

L. Borkovska<sup>1\*</sup>, O. Stroyuk<sup>2</sup>, A. Raevskaya<sup>2</sup>, T. Kryshchab<sup>3</sup>

<sup>1</sup>V Lashkaryov Institute of Semiconductor Physics of NAS of Ukraine, Kyiv, Ukraine

<sup>2</sup>L Pysarzhevsky Institute of Physical Chemistry of NAS of Ukraine, Kyiv, Ukraine

<sup>3</sup>Instituto Politécnico Nacional – ESFM, Mexico D.F., Mexico

\*bork@isp.kiev.ua

The interest to colloidal semiconductor nanocrystals (quantum dots, QDs) is highly motivated by their potential application in opto- and photoelectronics, biology, medicine, etc. Luminescent QDs based on II-VI compounds (CdSe, CdS, CdTe and their alloys) are characterized by high quantum yield, narrow excitonic emission band and a broad absorption spectrum, which make them well suited to multicolor labeling. In turn, the QDs of I-III-VI materials (CuInS<sub>2</sub>, AgInS<sub>2</sub> and their alloys) also show high quantum yield, but are composed of the elements with reduced toxicity that is especially important for *in vivo* imaging. To improve the stability and bio-compatibility of the QDs, different polymer materials are applied as surface stabilizing and coating agents. Among them, polyvinyl alcohol (PVA), a hydrophilic noncarcinogenic optically transparent polymer, is considered as a good host material for metal nanoparticles and semiconductor QDs.

Here we present the results of the investigation of photostability of CdSe and AgInS<sub>2</sub> QDs embedded in the PVA matrix. The QDs were synthesized at room temperature in aqueous media in the presence of mercaptoacetic acid as a stabilizer. A part of bare QDs was coated with a ZnS shell. To produce the composite polymer films, the QD solutions were mixed with PVA, dropcasted onto glass plates and dried at room temperature. The photoluminescence (PL) and optical absorption spectra of the films were studied in the 77-300 K temperature range. The films were annealed for 5 minutes at about 100 °C in the atmospheric ambience in dark or under illumination with a 409-nm light from a light-emitting diode (LED).

The PL spectra of the CdSe QDs in the PVA matrix showed two bands, i.e. a weak band ascribed to exciton radiative recombination in the QDs and an intense broad band caused by surface defects of the QDs. The PL spectra of the AgInS<sub>2</sub> QDs embedded in the PVA film demonstrated only the intense broad PL band caused by defects in the QDs.

It is found that thermal annealing of the films in the dark stimulates the increase of the room-temperature emission from the QDs of both types. This is ascribed to the improvement of QD surface defect passivation by functional group of PVA. However, the annealing under illumination produces different effects on the intensity of QD-related emission. Specifically, the irradiation enhances the effect of annealing for the CdSe QDs and decreases for the AgInS<sub>2</sub> QDs. When the composite films were irradiated with a LED's light at room temperature, the PL intensity of the QDs also changed: the PL intensity of the CdSe QDs gradually increased, while those of the AgInS<sub>2</sub> QDs decreased. These effects were accompanied by a darkening of the films under irradiation. The changes occurred in the PL and optical absorption spectra under irradiation are found to be reversible and only weakly affected by a ZnS shell. The mechanisms of the effects are discussed.

## Defect composition in acceptor doped ZnO quantum structures

Tchelidze T\*, Kereslidze T, Nadareishvili T

Department of Physics, Faculty of Exact and natural Sciences, Ivane Javakhishvili Tbilisi State University, Tbilisi, Georgia

[\\*tchelidze@tsu.ge](mailto:tchelidze@tsu.ge)

We investigated defect composition in ZnO quantum structures – quantum wells (QW), quantum wires (QW) and Quantum dots doped with different impurities. The motivation is that ZnO suffers from the doping asymmetry problem, in that it can be doped n-type rather easily, but highly p-type doping is still problematic. This fact continues to impede the development of ZnO-based light emitters. The difficulties of p-type doping can arise from a variety of causes. One of the main reasons that makes difficult obtaining low ohmic hole conductivity is compensation of dopants by low energy native defects, such as  $V_O$  or  $Zn_i$ , or background impurities.

Compensating processes is strongly affected by electronic structure of system: band gap, ionization energies of donors, acceptors and their compensation centers, formation enthalpy of defects. Our aim was to reveal the way size confinement alters compensation processes, and to find optimal sizes of quantum structures for which it can be suppressed. For this purpose we calculated acceptor and donor ionization energies for ZnO QW, QD, and NW of different size. The space and dielectric confinement is taken into account. These activation energies were used then in the Kroger method of quasi-chemical equations, which gives defect, impurities and charge carriers concentrations vs. temperature and oxygen pressure. The calculation for Ag doped ZnO NW shows that for NW of definite radius p-conductivity becomes achievable. We defined optimal for p-conductivity geometric sizes for ZnO QD and QW doped with Li and Na atoms too.

The existence of optimal sizes in ZnO quantum structures is connected to the fact that acceptor ionization energy is less sensitive to space and dielectric confinement, than those for compensating donors. In NW, e.g., the ionization energy of oxygen vacancy remains higher than corresponding bulk value until  $r=8\text{nm}$ , while ionization energy of acceptor impurity returns to its bulk value for  $r=3.5\text{ nm}$ .

## Application of DBRs for the Enhancement of CdTe Quantum Dots Photoluminescence in Single Emitter Studies

J.-G. Rousset<sup>1\*</sup>, J. Kobak<sup>1</sup>, A. Janaszek<sup>1</sup>, E. Janik<sup>1</sup>, M. Parlinska-Wojtan<sup>2</sup>, T. Slupinski<sup>1</sup>,  
J. Suffczyński<sup>1</sup>, M. Nawrocki<sup>1</sup>, A. Golnik<sup>1</sup>, P. Kossacki<sup>1</sup>, and W. Pacuski<sup>1</sup>

<sup>1</sup> Institute of Experimental Physics, Faculty of Physics, University of Warsaw, Poland

<sup>2</sup> Institute of Nanotechnology, University of Rzeszow, Poland

\*rousset@fuw.edu.pl

Microcavities embedding quantum dots are of great interest from the point of view of fundamental physics (quantum electrodynamics, light-matter coupling) and applications in the active field of optoelectronics. Intense investigations on such structures carried out in many laboratories lead to the realization of, among others, vertical cavity surface emitting lasers (VCSELs) and resonant cavity light emitting diodes (RCLEDs). Pillar microcavities, etched by focused ion beam (FIB), and containing a single QD allow controlling spatial, energetic and temporal properties of light emission [1, 2]. In such structures, the coherent coupling between light and matter is of great interest for quantum information processing. On the other hand, investigations on single quantum emitters suffer from the low light extraction coefficient crucial for example in the time resolved studies of QDs with single magnetic dopant.

In this work we report on MBE growth and characterization of ZnTe based photonic structures exhibiting a wide cavity-like mode allowing for the amplification of the QD PL intensity by one order of magnitude. We use the distributed Bragg reflectors (DBRs) which are based on ZnTe and the digital alloy ZnTe|MgTe|ZnTe|MgSe layers [3] lattice matched to ZnTe. We compare the PL spectra of self-organized CdTe/ZnTe quantum dots grown on a ZnTe buffer and embedded in a microcavity structure or on top of DBRs [4]. We show that in the case of quantum dots grown on a Bragg reflector, the photoluminescence intensity is enhanced by more than one order of magnitude compared to quantum dots grown on a ZnTe buffer. Unfortunately at the same time broadening of the single quantum dots lines occurs. High resolution transmission electron microscopy (HRTEM) analysis allows to identify incorporation of residual selenium as a source of line broadening. Unwanted ZnSe or CdSe monolayers (instead of nominal ZnTe or CdTe) are observed in places, where growth was interrupted for change of substrate temperature [5]. The recovery of sharp single emission lines (FWHM below 0.1 meV) is obtained by growing the CdTe/ZnTe QDs 24 hours after growing the DBR to get rid of the Se background in the growth chamber. This technique allowed us to resolve sixfold splitting of CdTe/ZnTe QDs containing single Mn ions, grown on DBRs. It is an important step towards combining cavity electrodynamics with the emerging field of solotronics [6,7].

[1] J. M. Gerard et al., Phys. Rev. Lett. **81**, 1110 (1998).

[2] T. Jakubczyk et al., Appl. Phys. Lett. **101**, 132105 (2012).

[3] W. Pacuski et al., Appl. Phys. Lett. **94**, 191108 (2009).

[4] J.-G. Rousset et al., J. Cryst. Growth **401**, 644 (2014).

[5] J.-G. Rousset et al., arXiv:1411.0525.

[6] W. Pacuski et al., Cryst. Growth Des. **14**, 988 (2014).

[7] J. Kobak et al., Nat. Commun. **5**, 3191 (2014).

## Magneto-Optical Studies of Semimagnetic Cavity Polaritons in a (Cd,Zn,Mg)Te Based Microcavity

J.-G. Rousset\*, B. Piętko, M. Król, R. Mirek, K. Lekenta, J. Szczytko, T. Kazimierczuk, M. Goryca, J. Suffczyński, P. Kossacki, A. Golnik, M. Nawrocki, W. Pacuski

Institute of experimental physics, Faculty of Physics, University of Warsaw, Poland

\*rousset@fuw.edu.pl

In the past fifteen years, investigations on cavity polaritons led to the observation of several fundamental physical phenomena like Bose – Einstein condensation of polaritons, or superfluidity. In this multidirectional field of research, a particular interest has arisen from polaritons spin related effects theoretically discussed in [1]. Investigations provided on GaAs based microcavities lead to the observation of the vanishing and sign change of the Zeeman splitting [2] that could be interpreted as a spin Meissner effect [3].

In this work, we present magneto-optical investigations on a new microcavity structure specially designed for the study of semimagnetic cavity polaritons. In opposite to previous telluride based microcavity structures [4], the Mn free DBRs are made of (Cd,Zn,Mg)Te layers lattice matched to MgTe [5] embedding dilute magnetic semiconductor (Cd,Zn,Mn)Te QWs lattice matched to the whole structure (fig.1). In such a structure, the *sp-d* exchange interaction between magnetic ions and the carriers in the QWs results in an enhancement of the magneto-optical effects such as the giant Zeeman splitting. In our structure, the cavity polaritons resulting from the strong exciton – photon coupling deserve then the denomination of semimagnetic cavity polaritons. As shown by our angle resolved PL measurement, these semimagnetic cavity polaritons exhibit: a magnetic field controlled wide range detuning and a dependence of the polariton laser threshold on the magnetic field (fig.2).

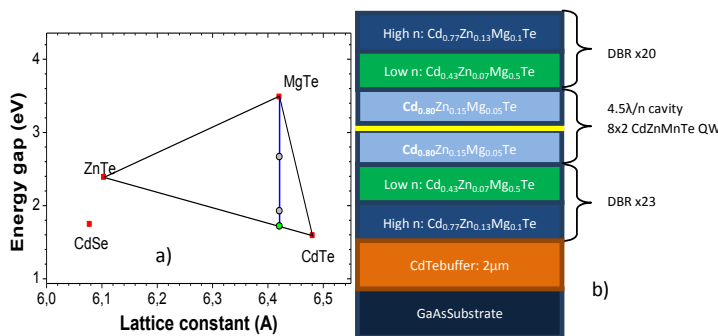


Fig.1: a) Map showing the energy gap as a function of the lattice constant for chosen tellurides. Blue line: compounds lattice matched to MgTe. Grey points: (Cd,Zn,Mg)Te layers of the DBRs. green point: (Cd,Zn,Mn)Te quantum well lattice matched to the whole structure. b) example of a microcavity structure.

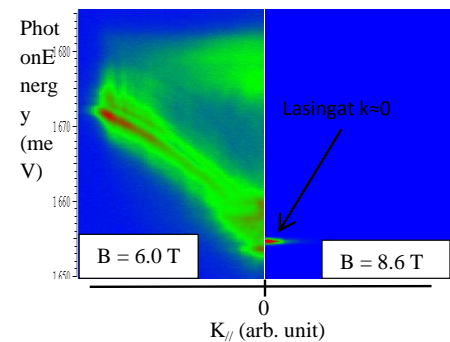


Fig.2: Polariton dispersion under the same excitation conditions in two different magnetic field: B=6.0 T – under lasing threshold, B=8.6 T – above lasing threshold

- [1] D. D. Solnyshkov et al., Phys. Rev. B **78**, 165323 (2008).  
 [2] A. V. Larionov et al., Phys. Lett. **105**, 256401 (2010).  
 [3] J. Fischer et al., Phys. Lett. **112**, 093902 (2014).  
 [4] H. Ulmer-Tuffigo et al., Superlattices and Microstructures **22**, 383 (1997).  
 [5] J.-G. Rousset et al., Journal of Crystal Growth **378**, 266 (2013).

## Collinear Four-Wave Mixing using Laguerre-Gauss modes in CdTe quantum well

Déborah Persuy<sup>1\*</sup>, Marc Ziegler<sup>1</sup>, Olivier Crégut<sup>1</sup>, Kuntheak Kheng<sup>2</sup>, Mathieu Gallart<sup>1</sup>, Bernd Hönerlage<sup>1</sup> and Pierre Gilliot<sup>1</sup>

<sup>1</sup>Institut de Physique et Chimie des Matériaux de Strasbourg, UMR7504 CNRS-Université de Strasbourg, Strasbourg, France

<sup>2</sup>Univ. Grenoble Alpes and CEA, INAC-SP2M, F-38000 Grenoble, France

\*E-mail of the corresponding author: [persuy@ipcms.u-strasbg.fr](mailto:persuy@ipcms.u-strasbg.fr)

Four-wave mixing experiments are usually performed in *a non-collinear configuration*. In this case, the signal is selected by means of its wave-vector that has to fulfill the phase matching condition: for time and space overlapped incident beams with wave vectors  $\vec{k}_a$  and  $\vec{k}_b$ , respectively, signals are observed in the  $2\vec{k}_a - \vec{k}_b$  and  $2\vec{k}_b - \vec{k}_a$  directions.

We demonstrate the possibility to perform four-wave mixing (FWM) experiments in *a collinear configuration* with Laguerre-Gauss beams that would enable a precise cartography of both nonlinear response and local dynamics of semiconductor samples.

Laguerre-Gaussian (LG) modes differ from usual Gaussian modes by an azimuthal phase dependence  $e^{-il\phi}$  of their amplitudes. Therefore their cross sectional intensity has an annular character, i.e. a “donut” profile [1]. Moreover, we know since 1992, that this type of light beams carry a well-defined orbital angular momentum (OAM) with a value of  $L = l\hbar$  per photon [2].

First, we demonstrate theoretically that the OAM of the generated beams in a FWM process obey a conservation law similar to the phase-matching condition that determines the direction of the generated signal in non-collinear FWM [3].

Then, we check, by performing time-resolved experiments on excitons in a CdTe/CdZnTe quantum well, that this conservation law is actually satisfied: the OAM of the exciting pulses is transferred and conserved by the electronic excitations during the excitonic coherence time. Using  $l_a = 2$  and  $l_b = 1$  LG modes for the incident beams, we obtain signals in the  $2\vec{k}_a - \vec{k}_b$  direction with an OAM value of  $l = 2l_a - l_b = 3$  and in the  $2\vec{k}_b - \vec{k}_a$  direction with  $l = 2l_b - l_a = 0$ . Furthermore, the same decay time of  $0.5ps$  is obtained in time-resolved FWM using Gaussian beams or LG modes. The signal decay is attributed to the dephasing time of the polarization excited at the energy of the charged exciton transition.

Finally we show that it is possible to perform *collinear* degenerate FWM experiments by detecting the generated FWM signal with OAM  $l=0$  at the center of the beams. Indeed only this LG mode  $l=0$  shows a non-zero intensity at the center of the beam, all the others LG modes have an annular profile, i.e. with no intensity at the center.

The main original feature here is that we take advantage of the specific intensity profile of Laguerre-Gauss modes for spatially discriminate the FWM signal from the exciting pulses. Unlike the conventional FWM technique which requires well-defined wave-vectors of incident and signal beams, our collinear FWM using Laguerre-Gauss modes allows the use of large numerical aperture leading to a sharper beam focusing and a better spatial resolution. This new type of FWM opens the way for investigation of electronic coherences and their dynamics in semiconductor nanostructures or in disordered systems where these properties need to be precisely mapped over the sample.

[1] M. Padgett, J. Courtial and L. Allen, *Physics Today* **5**, 35 (2004)

[2] L. Allen, M.W. Beijersbergen, R.J.C. Spreeuw and J.P. Woerdaman, *Phys. Rev. A* **11**, 8185 (1992)

[3] R. Levy, M.J.M. Gomes, B. Kippelen and B. Hönerlage, *Phys. Stat. Sol. (b)* **158**, 391 (1990)

## Comparative studies of CdSe/ZnSe Quantum Dot Structures Epitaxially Grown either with or without a Sub-monolayer CdTe Stressor

M. V. Rakhlin\*, I. V. Sedova, S. V. Sorokin, S. V. Gronin, A. A. Usikova, A. A. Sitnikova,  
S. V. Ivanov, and A. A. Toropov

Ioffe Institute, Russian Academy of Sciences, Politeknicheskaya 26, 194021

St. Petersburg, Russia

\*E-mail: [maximrakhlin@mail.ru](mailto:maximrakhlin@mail.ru)

Epitaxially grown heterostructures with CdSe/ZnSe quantum dots (QDs) have potential application both as an active region of low-threshold optically pumped lasers [1] and as sources of single-photon emission, operating up to room temperature [2]. These two kinds of applications demand for the QD nanostructures with essentially different properties. The QD laser structures particularly benefit from the dense array of QDs with narrow size distribution, resulting in a sharp and strong spectral peak of the optical gain. Quite the contrary, the QD single-photon emitters require the small QD density and broad size distribution to facilitate optical addressing of a single individual QD and to avoid spectral overlap of photoluminescence bands of different QDs. Until recently the CdSe QDs have been mostly fabricated either by conventional molecular beam epitaxy (MBE) or migration-enhanced epitaxy (MEE). An alternative technique implies deposition of an ultra-thin layer of CdTe (stressor) prior formation of the CdSe QDs [3].

In this work we apply a micro-photoluminescence ( $\mu$ -PL) spectroscopy to compare emission properties of individual CdSe QDs grown by MEE either with (sample A) or without (sample B) predeposition of the sub-monolayer CdTe stressor. In both samples the single sheets of QDs were inserted in ZnSe barrier layers. The emission of a limited number of QDs was registered by the confocal  $\mu$ -PL spectroscopy through 500-nm-size round apertures opened in a non-transparent gold mask by a ball-assisted etching technique. The QD density and size distribution in the structures were estimated by means of transmission electron microscopy (TEM).

In both structures, the  $\mu$ -PL measurements reveal a number of relatively narrow lines, assigned to the emission of excitons, trions, and biexcitons in either individual QDs or certain groups including a few QDs. The QD density obtained by calculating the overall number of narrow emission lines is roughly similar in both samples and correlates with the plane images obtained by TEM. Nevertheless, there is a striking difference between the two samples in the typical spectral width of the emission lines. In sample B, the typical full width at half maximum (FWHM) of the narrow PL lines is in the range of 0.3-0.6 meV at 5 K that is typical for most previously reported studies of single epitaxial CdSe QDs. In sample A, the emission lines are always wider than 1 meV that may be explained by the enhanced jitter of the line position, induced by trapping of charged carriers in the type-II ZnSe/CdTe nanostructures formed presumably in the vicinity of the CdSe QDs [3]. Moreover, some individual lines tend to overlap, forming composite emission bands with FWHM larger than 2-3 meV. In fact, both effects are disadvantageous for the observation of single-photon emission. On the other hand, the FWHM of the spatially integrated PL spectrum of sample A is smaller than in sample B, indicating the better homogeneity of the QD ensemble. Therefore, one can assume that the CdSe QD ensembles formed by using the CdTe stressor are better suited for the laser application. This work was supported by Russian Science Foundation (Project #14-22-00107).

[1] S. V. Ivanov, A. A. Toropov, S. V. Sorokin et al., *Appl. Phys. Lett.* **74**, 498 (1999).

[2] O. Fedorych, C. Kruse, A. Ruban et al., *Appl. Phys. Lett.* **100**, 061114 (2012).

[3] A. A. Toropov, I. V. Sedova, O. G. Lyublinskaya et al., *Appl. Phys. Lett.* **89**, 123110 (2006).

## Direct determination of zero field splitting of a $\text{Co}^{2+}$ ion in a CdTe/ZnTe QD

Kobak J.\*, Smoleński T., Papaj M., Golnik A., and Pacuski W.  
 Institute of Experimental Physics, Faculty of Physics, University of Warsaw,  
 ul. Pasteura 5, 02-093 Warsaw, Poland  
 \*jakub.kobak@fuw.edu.pl

We report on magneto-optical study and theoretical description of influence of local strain on individual cobalt ion in CdTe/ZnTe quantum dot (QD). Using molecular beam epitaxy we have grown self assembled CdTe/ZnTe QDs with small amount of  $\text{Co}^{2+}$  ions introduced by delta doping in the middle of CdTe layer [1]. The low temperature magneto-photoluminescence (PL) measurements and modelling allow us to identify PL lines related to QDs containing exactly one cobalt ion. Exciton and biexciton lines are 4-fold split due to 4 possible spin projections of  $\text{Co}^{2+}$ :  $\pm 3/2$ ,  $\pm 1/2$  [1], similarly to QDs with single  $\text{Mn}^{2+}$  where exciton and biexciton are split by 6 due to 6 spin projection of  $\text{Mn}^{2+}$  [2,3]. However, the intensity of the lines related to  $\text{Co}^{2+}$  spin projections  $\pm 3/2$  (outer lines) can be significantly different from those related to the spin projections  $\pm 1/2$  (inner lines). In contrast to  $\text{Mn}^{2+}$ , the  $\text{Co}^{2+}$  ion has non-zero orbital momentum and thus is very sensitive to a local anisotropy and the strain, which lead to the splitting of  $\pm 3/2$  and  $\pm 1/2$  states and a difference in their occupancy [1]. Moreover, we have found experimentally that the sign of  $\text{Co}^{2+}$  strain can be positive and negative. Therefore, depending on strain both  $\pm 3/2$  and  $\pm 1/2$  spin state can be the ground state of  $\text{Co}^{2+}$  in QD. In order to obtain a deeper understanding of the impact of local strain on the ground state of cobalt ion we performed theoretical simulations (Fig. 1). We were able to achieve perfect agreement between experiment and simulation when we took into account that the quantization direction of the cobalt ion ground state does not have to be parallel to the quantization axis of the quantum dot.

However, precise determination of the splitting of  $\pm 3/2$  and  $\pm 1/2$   $\text{Co}^{2+}$  states (parameter  $2D$ ) cannot be obtained from the evolution of 4 main emission lines (Fig. 1). We show that direct determination of cobalt ion anisotropy (parameter  $2D$ ) can be obtained by observation of very weak, partially allowed optical transitions for which initial and final state of Co ion is not the same, as shown in Fig. 2. We present results of magneto-optical and theoretical study of such lines.

- [1] Kobak J., et al., Nature Communications **5**, 3191 (2014)
- [2] Besombes L., et al., Phys. Rev. Lett. **93**, 207403 (2004)
- [3] Goryca M., et al., Phys. Rev. Lett. **103**, 087401 (2009)

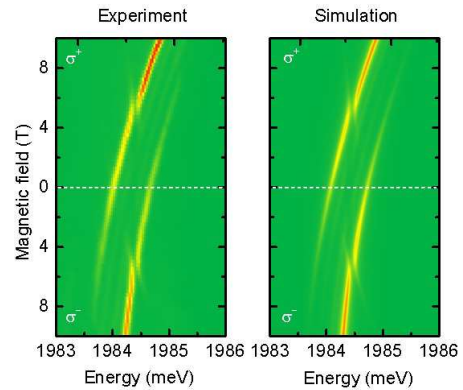


Fig. 1: Perfect agreement of magneto-optical spectroscopy and simulation of neutral exciton in QDs with single cobalt ion.

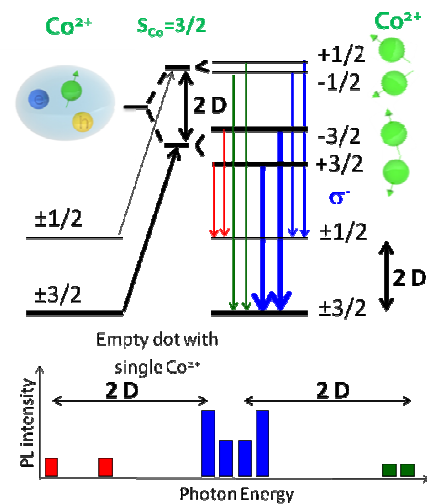


Fig. 2: Scheme of excitonic transitions. Energy difference between main, strong (blue), and weak (red and green) emission lines gives directly anisotropy parameter ( $2D$ ) of  $\text{Co}^{2+}$ .

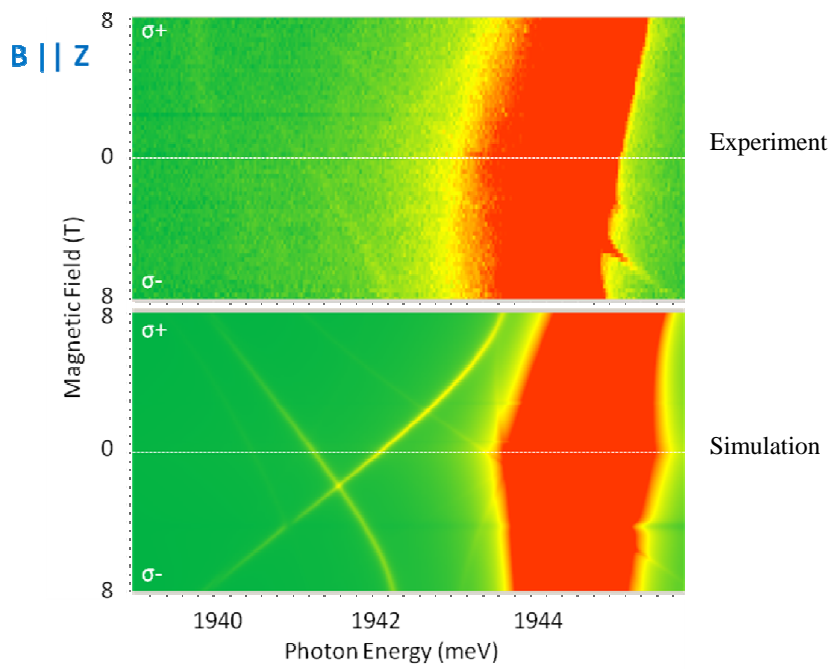


Fig 3. Magneto-optical spectroscopy and simulation of weak emission lines related to transitions for which initial and final  $\text{Co}^{2+}$  spin state is not the same. Such emission lines are few orders of magnitude weaker than emission lines related to transitions with conserved spin of  $\text{Co}^{2+}$ .

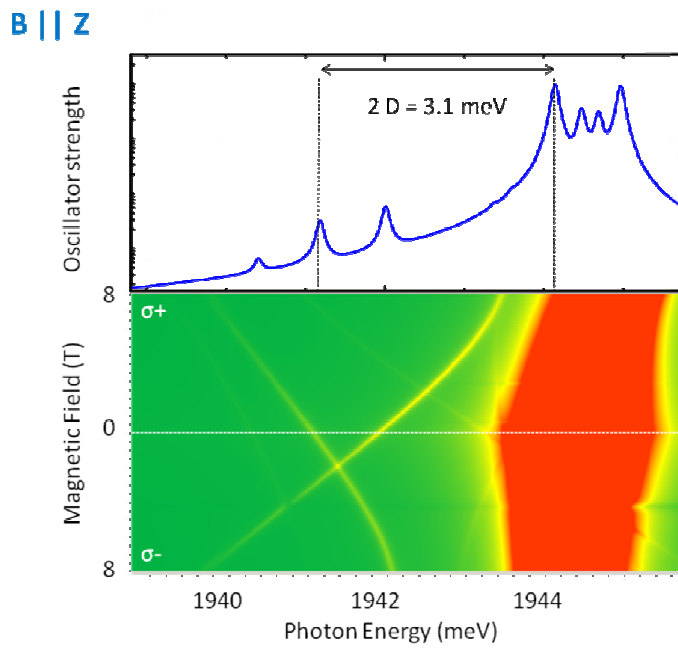


Fig 4. Determination of cobalt ion anisotropy (parameter  $2D$ ).

## Coherent spin evolution of acceptor-bound excitons in a CdTe quantum well

P. Grinberg<sup>1</sup>, B. Eble<sup>1</sup>, F. Bernardot<sup>1</sup>, B. Siarry, G. Karzeczewski<sup>2</sup>, C. Testelin<sup>1</sup>  
and M. Chamarro<sup>1</sup>

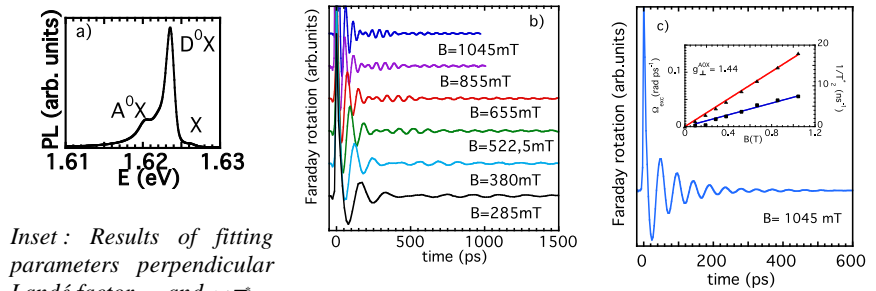
1 Sorbonne Universités, UPMC Univ. Paris 06, UMR 7588, Institut des Nanosciences  
de Paris (INSP), F-75005 Paris, France.

2 Institute of Physics, Polish Academy of Sciences, Al. Lotnikow 32/46 02-668  
Warsaw, Poland

As with trapped ions in cold gases, paramagnetic impurities trapped on a semiconductor lattice have uniform properties, relatively long spin lifetimes and are promising spin-qubit candidates [1]. Their semiconductor environment provides a natural localization and ease of fabrication and scalability that is absent in atomic and ion qubit systems. In particular, single electrons, holes or excitons trapped by individual donors or acceptors in direct band-gap semiconductors are particularly interesting spin-qubit candidates because they show an excellent scalability with strong optical transitions and higher homogeneity than electrons, holes or excitons confined in self-assembled quantum dots (QDs).

Here, we show a study of the coherent evolution of the electron spin (e-spin) of acceptor-bound excitons,  $A^0X$ , immersed in a 80Å CdTe/CdMgTe quantum well (QW) nominally undoped by using the Photo-induced Faraday Rotation (PFR). The 2K photoluminescence (PL) spectrum of the sample shows that the QW contains donors and acceptors in very small concentration (Figure 1a). When pump and probe beam energy is tuned between 1.622 et 1.614 eV, the temporal behaviour of the PFR signal in a transverse magnetic field shows beating patterns between a long signal associated to e-spin bound to neutral donors,  $D^0$ , [2] and a short-living one associated to  $A^0X$  (Figure 1b). At lower energy of 1.614eV we are able to isolate the coherent evolution of  $A^0X$  (Figure 1c). This complex contains three particles, two holes with spin in antiparallel configuration and an electron. The spin of  $A^0X$  is then fixed by the photo-created e-spin. The  $A^0X$  lifetime, 220ps, has been determined by measuring the differential transmission and does not change until  $B=1.2T$ . We have fitted the PFR curves in Figure 1c to damped cosinus. For 95mT we obtain an e-spin dephasing time in the order of  $T_2^* \gg 4$  ns. This value is much larger than the value obtained previously [3] for the relaxation time of e-spin in a positively charged exciton in CdTe QW, 60ps, but is comparable to the value obtained for resident electrons in n-doped CdSe QDs at 250mT [4] and with the value obtained for  $D^0$  in this work and in a previous work [2]. In conclusion, due to the acceptor localization potential the e-spin of  $A^0X$  is completely frozen during its lifetime.

**Figure 1** a) 2K- PL of the studied sample.  $X$  and  $D^0X$  denote free and donor-bound excitons emission peak. b) PFR signal versus time for different magnetic fields. Energy of pump and probe is 1.621 eV. c) PFR signal versus time delay. Energy of pump and probe is 1.614eV.



[1] P.M. Koenraad and M. Flatté. « Single dopants in semiconductors » Nature Materials, 91, (2011).

[2] J. Tribollet *et al.* Phys. Rev. B 75, 205304 (2007).

[3] E. Vanelle *et al.* Phys. Rev. B 62, 2696, (2000)

[4] M. Syperek *et al.* Phys. Rev. B. 84, 085304 (2011)

## Spectral selection of excitonic transitions in a dense array of epitaxial CdSe/ZnSe quantum dots

T. V. Shubina<sup>1\*</sup>, A. V. Rodina<sup>1</sup>, M. A. Semina<sup>1</sup>, A. A. Golovatenko<sup>1</sup>, A. A. Toropov<sup>1</sup>,  
M. V. Rakhlin<sup>1</sup>, I. V. Sedova<sup>1</sup>, S. V. Sorokin<sup>1</sup>, S. V. Gronin<sup>1</sup>, A. A. Sitnikova<sup>1</sup>,  
D. I. Kuritsyn<sup>2</sup>, S. M. Sergeev<sup>2</sup>, Z. F. Krasil'nik<sup>2</sup>, and S. V. Ivanov<sup>1</sup>

<sup>1</sup>Ioffe Institute, 26 Politekhnicheskaya, St Petersburg 194021, Russia

<sup>2</sup>Institute for Physics of Microstructures, GSP 105, Nizhniy Novgorod 603950, Russia

\*shubina@beam.ioffe.ru

Epitaxial quantum dots (QDs) have certain advantage over the colloidal ones for quantum light emitters, namely, the absence of blinking. However, their lateral density is usually too high for easy separation of a single QD from a dense array. Solving this problem requires either formation of a mesa by advanced nanolithography or insertion of a QD sheet in a thin nanowire. We propose a new approach for selection of a limited number of single excitonic lines, which can be combined with other methods. In contrast to the spatial isolation, it is realized spectrally via the resonant energy transfer from a huge ensemble of small QDs towards a limited set of massive nano-islands.

This approach was proved by the studies of QD structures with the density of  $10^{11}$ - $10^{12}$  cm<sup>-2</sup> fabricated by molecular beam epitaxy via inserting  $\leq 3$  monolayers of CdSe within a ZnSe matrix. Such QD sheets were commonly considered as disordered ZnCdSe quantum wells, though recent transmission electron microscopy (TEM) studies have shown that they consist of distinct nano-islands, whose characteristic lateral sizes are distributed within the 2-12 nm range with maximum at 2-4 nm. The small dots are placed predominantly over the large ones due to the Cd segregation during growth of the top ZnSe barrier, that can promote the energy transfer between these dots at optical pumping. The photoluminescence (PL) line has a width of  $\sim 50$  meV, which apparently contradicts the QD size dispersion. The single-exponential PL decay has a characteristic time of 300-400 ps, which is close to the calculated radiative lifetime of excitonic transitions in the QDs. Micro-PL studies, performed using apertures in a non-transparent metal mask, showed a limited number of narrow lines, which is an order of magnitude less than it may be predicted from the TEM data. However, their number reasonably corresponds to the density of the nano-islands possessing the sizes of 5-7 nm (the larger islands are likely non-radiative due to defect formation).

Theoretical modeling was developed for QDs with a Gaussian potential profile, whose shape is varied from sphere to oblate spheroid. To simulate the PL spectra the calculation of the density of states of the ground excitonic levels,  $I_{DOS}$ , was done firstly assuming that the number and energies of these levels are defined by the QD size distributions given by TEM. The calculated  $I_{DOS}$  peak is at 2.6-2.7 eV that is markedly higher than the PL line observed at 2.4-2.5 eV, however it matches well with the higher-energy peak in PL excitation spectra. The calculations also showed that at least one excited level for electrons, situated 100-200 meV above the ground level, and a number of closely spaced levels for holes exist in the 5-7 nm nano-islands with Cd content in the center  $>50$ mol.%. Respective excited excitonic levels coincide well with the  $I_{DOS}$  peak. Such architecture of the quantum levels allows the resonant energy transfer from the ground levels in the small QDs, responsible mainly for the  $I_{DOS}$  peak, to the excited excitonic levels of the large QDs, followed by the energy relaxation to their ground levels. We have achieved reasonable modeling the emission spectra taking into account the energy transfer process, possessing the two orders of magnitude less transfer time than the radiative time of the excitonic transitions. The probable contribution of non-resonant energy transfer involving LO phonons is also discussed.

These studies are supported by Russian Science Foundation (Project № 14-22-00107).

## Using single CdTe nanocrystals to study excitons from the quantum confined to the bulk regime [1]

Jenya Tilchin<sup>1</sup>, Freddy T. Rabouw<sup>2</sup>, Relinde Moes<sup>2</sup>, Roman Vaxenberg,<sup>1</sup> Maya Isarov,<sup>1</sup> Efrat Lifshitz,<sup>1\*</sup> Daniel Vanmaekelbergh<sup>2\*\*</sup>

<sup>1</sup>Schulich Faculty of Chemistry, Russell Berrie Nanotechnology Institute, Technion, Solid State Institute, Haifa 32000, Israel (\*ssefrat@technion.ac.il.)

<sup>2</sup>Department of Chemistry, University of Utrecht, Utrecht, The Netherland (\*\*d.vanmaekelbergh@uu.nl)

Confinement of charge carriers in a colloidal semiconductor nanocrystal (NC), when its size reaches bulk exciton Bohr radius, becomes weak or marginal. In this regime, the Coulomb attraction between the photo-generated electrons and holes becomes comparable or even stronger than the intraband spacing between electron (or hole) levels. Thus, the energy level structure of the NC is no longer governed by spatial confinement but rather by Coulomb interaction. Hence, large nanocrystals may form a bridge between the regime of strong confinement and the bulk crystal.

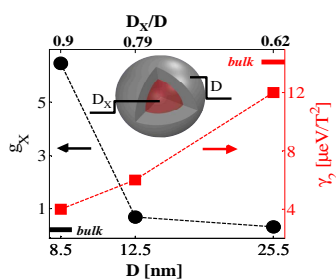


Fig. 1: The Landé g-factor ( $g_X$ ); black circles, left axis) and the diamagnetic shift ( $\gamma_2$ ); red squares, right axis) as a function of NC size. The top axis presents the ratio between exciton diameter ( $D_X$ ) and NC size ( $D$ ). The bulk values of  $g_X$  and  $\gamma_2$  are presented as horizontal black and red lines on the respective axes.

In this work we explore the effect confinement effects on the exciton ( $X$ ) in CdTe/CdSe “giant” CQDs. The studied samples are CdTe of different sizes, passivated with two monolayers of CdSe revealing total particle diameter ( $D$ ) of 8.5, 9.5, 12.5 and 25.5 nm. The impact of the confinement on  $X$  is explored using low temperature (4.2 K) single dot spectroscopy with/without external magnetic field ( $B$ -field). This allows following the size evolution of Landé g-factor ( $g_X$ ) and diamagnetic shift constant ( $\gamma_2$ ). Those parameters are a measure of the  $X$  effective mass and its spatial localization, respectively.

The  $\gamma_2$  and  $g_X$  extracted for the different samples investigated are shown in Fig. 1. The plot reveals gradual change in  $g_X$  and  $\gamma_2$  with increasing NC size, approaching the bulk values (see black and red horizontal lines on left and right axis in Fig. 1). The  $\gamma_2$  in a good approximation is equal to [2]:  $\gamma_2 = e^2 \langle r_X^2 \rangle / 8\mu$ . Here,  $e$  is electron charge,  $\mu$  the electron-hole reduced mass, and  $\langle r_X^2 \rangle^{1/2}$  the exciton localization region. The estimated ratio between the effective exciton diameter  $D_X = 2 \langle r_X^2 \rangle^{1/2}$  and the actual NC size ( $D_X / D$ ) is shown on a top axis in Fig. 1.

This localization reflects the special behavior under weak and spatial confinement regime, presumably due to a dominance of Coulomb interactions, confining at least the  $X$  into a regime that is substantially smaller than the actual size of the NCs. It has been theoretically shown [3] that  $X$  is focused at the central part of the NC, keeping a uniform dielectric surrounding, resembling self-assembled quantum dots within a semiconductor host, and neatly approaching exciton behavior of bulk semiconductors.

[1] Submitted for publication

[2] Walck *et al.*, *Physical Review B* **57**, 9088-9096 (1998).

[3] Efros *et al.*, *Sov. Phys. Semicond.* **16**, 772 (1982).

## Mobility of the Two-Dimensional Electron Gas in Modulation Doped CdTe Quantum Well Structures with Gate Controlled Electron Concentration

V. Kolkovsky<sup>1\*</sup>, Z. Adamus<sup>1</sup>, M. Wiater<sup>1</sup>, A. Sulich<sup>1</sup>, G. Karczewski<sup>1</sup>, A. Kazakov<sup>2</sup>,  
L.P. Rokhinson<sup>1</sup> and T. Wojtowicz<sup>1</sup>

<sup>1</sup>Institute of Physics, Polish Academy of Sciences, 02-668 Warsaw, Poland

<sup>2</sup>Department of Physics and Astronomy, Purdue University, West Lafayette, IN 47907, USA  
\* kolkova@ifpan.edu.pl

Recent progress in fabrication of high mobility 2DEG in CdTe quantum well (QW) in our laboratory allowed not only to achieve highest mobility of electrons in wide gap telluride semiconductors, but also to observe fragile fractional quantum Hall effect (FQHE) in this structures [1]. A fundamental asset of high mobility CdTe quantum wells is the possibility to incorporate magnetic ions to form diluted magnetic semiconductors QWs, which offer potential applications in the fields of spintronics and quantum computing [2,3]. It is presumed that incorporation of paramagnetic manganese (Mn) ions into a modulation doped CdTe quantum well will provide a strong enough s-d coupling to 2DEG, but without any considerable reduction of the mean free path or broadening of the quantum levels. Additionally, it is expected that the electron-electron correlation effects in CdTe are stronger as compared to GaAs, the material in which the record 2DEG mobility of  $3.5 \times 10^7$  cm<sup>2</sup>/Vs was observed [4].

Here, we report on the studies of scattering mechanisms, which limit the mobility of the 2D electron gas in CdTe QWs. To the best of our knowledge, no results of such studies have yet been published. To this end, the evolution of the mobility of 2DEG as function of the electron concentration, spacer width and temperature was analyzed. The experimental results were compared with theoretical calculations. All the structures studied here were grown by molecular beam epitaxy and contained a single, 30 nm wide CdTe quantum well, remotely doped on one side by iodine donors, and embedded between Cd<sub>1-x</sub>Mg<sub>x</sub>Te barriers (with Mg content x of about 0.26). In order to analyze the mobility of 2DEG as function of spacer width, the series of structures with different spacer layer thickness - from 2.5 nm to 50 nm - were studied. All structures had 60 nm thick cap made of Cd<sub>0.74</sub>Mg<sub>0.26</sub>Te that was separating Iodine doped barrier region (supplying electrons to the QW) from the structure surface. The electron concentration in a given structure was varied by gating electric fields in a field-effect transistor configuration. Hall bar devices with golden gates were produced by electron beam lithography, wet etching and lift-off techniques.

Low-temperature studies of Hall- and longitudinal- magnetoresistance revealing well-developed Integer Quantum Hall (IQH) plateaus were performed as a function of gate voltage in temperatures down to 1.4 K and in magnetic fields up to 9 T. Both the change of the slope of low field Hall voltage and the shift of IQH plateaus were used to measure variation of electron concentration. Next-nano software package was used for theoretical simulation of the dependence of electron mobility on temperature, spacer width and 2DEG concentration by taking into account various scattering mechanisms.

The research was partially supported by National Science Centre (Poland) grant DEC-2012/06/A/ST3/00247 and by the ONR grant N000141410339. T. W. acknowledges support from the Foundation for Polish Science through the International Outgoing Scholarship 2014.

- [1] B. A. Piot *et al.*, Phys. Rev. B **82**, 081307 (2010).
- [2] R. Rungsawang *et al.*, Phys. Rev. Lett. **110**, 177203 (2013).
- [3] C. Betthausen *et al.*, Science **337**, 324 (2012).
- [4] V. Umansky *et al.*, J.Cryst. Growth **311**, 1658 (2009).

## Magneto-optical studies of CdTe and CdSe quantum dots

Kobak J.<sup>1\*</sup>, Pacuski W.<sup>1</sup>, Smoleński T.<sup>1</sup>, Rousset J.-G.<sup>1</sup>, Bogucki A.<sup>1</sup>, Kossacki P.<sup>1</sup>, Płachta J.<sup>2</sup>,  
Wojnar P.<sup>2</sup>, Kruse C.<sup>3</sup>, Hommel D.<sup>3</sup>, Potemski M.<sup>4</sup>, Golnik A.<sup>1</sup>, and Kazimierczuk T.<sup>1</sup>

<sup>1</sup>Institute of Experimental Physics, Faculty of Physics, University of Warsaw,  
ul. Pasteura 5, 02-093 Warsaw Poland

<sup>2</sup>Institute of Physics, Polish Academy of Sciences,  
al. Lotników 32/64, 02-688 Warsaw, Poland

<sup>3</sup>Institute of Solid State Physics, Semiconductor Epitaxy, University of Bremen,  
PO Box 330 440, D-28334 Bremen, Germany

<sup>4</sup>Grenoble High Magnetic Field Laboratory,  
CNRS-UJF-UPS-INSA F-38042 Grenoble Cedex 09, France

\*jakub.kobak@fuw.edu.pl

We present a systematic study of parameters describing photoluminescence of a quantum dot (QD) in external magnetic field: the pattern of emission line energies for different excitonic complexes, their effective Landè factor  $g$  and diamagnetic shift  $\gamma$ . Our analysis is based on measurements of over 130 individual QDs in CdSe/ZnSe and CdTe/ZnTe systems. The data was collected in a microphotoluminescence ( $\mu$ PL) setup at low temperatures (1.5K) and high magnetic field (up to 28T).

Samples were grown in three different Molecular Beam Epitaxy (MBE) laboratories using a method of amorphous Te (Se) proposed by Tinjod et al. [1,2,3]: after deposition of thin CdTe (CdSe) layer by ALE (Atomic Layer Epitaxy), substrate was cooled down with presence of Te (Se) flux in order to deposit amorphous Te (Se), next the substrate was heated to growth temperature, Te (Se) was evaporated and ZnTe (ZnSe) cap was grown.

In each case we identified emission lines related to different charge states of a single QD by measurement of polarization resolved PL and PL dependence on the excitation power. The values of diamagnetic shift and  $g$ -factor were obtained by fitting a second-order polynomial to magnetic field dependence of emission energy.

For both II-VI QD systems we observed characteristic energetic patterns of emission lines related to recombination of neutral exciton X, biexciton 2X, and charged excitons ( $X^+$ ,  $X^-$ ). Although energy distances between various lines of a single QD vary from dot to dot, energy distances  $X-X^+$  and  $X-X^-$  stay roughly proportional to  $X-XX$  distance in each system.

Our studies confirmed systematic differences between the values of QD parameters between CdSe and CdTe systems. For telluride QDs average value of fine-structure splitting was about 0.14 meV while for selenide QDs we found few times higher average value (0.48 meV). For CdTe QDs we determined slightly higher average  $g$ -factors (2.12) than for CdSe QDs (1.63). More significant differences we obtained by studying diamagnetic shift, which was found to be approximately 2 times higher for telluride QDs ( $0.0025 \text{ meV/T}^2$ ) compared with selenide QDs ( $0.0013 \text{ meV/T}^2$ ).

The most surprising results are related to correlations between effective Landè factors for different excitonic complexes. Since each of observed lines was related to recombination of  $s$ -shell hole with  $s$ -shell electron, all these transitions should exhibit the same excitonic  $g$ -factor. Nevertheless, our measurements clearly show a systematic deviation between  $g$ -factors of  $X$ ,  $X^+$ , and  $X^-$  transitions. Such a systematic difference was found in both systems, but with opposite sign. We discuss the relation of the observed effect to the bulk  $g$ -factor values of CdTe/ZnTe and CdSe/ZnSe pairs.

- [1] Tinjod F., et al., Appl. Phys. Lett. **82**, 4340 (2003).
- [2] Kobak J., et al., Acta Physica Polonica A **119**, 627 (2011).
- [3] Kobak J., et al., Journal of Crystal Growth **378**, 274 (2013)

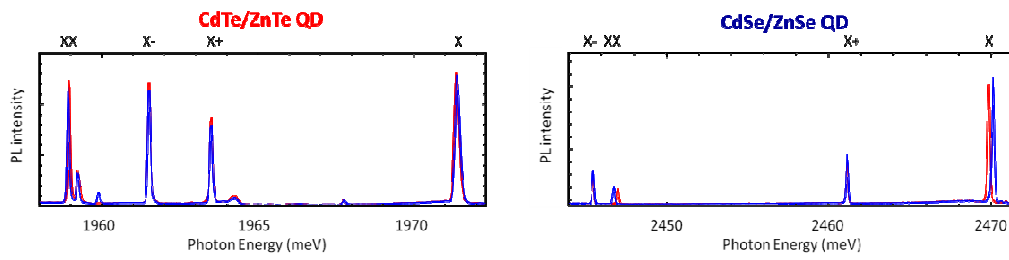


Fig 1. Emission lines of CdTe/ZnTe (left) and CdSe/ZnSe (right) QD show typical anisotropy properties: neutral exciton and biexciton have opposite linear polarization and trions are not linearly polarized.

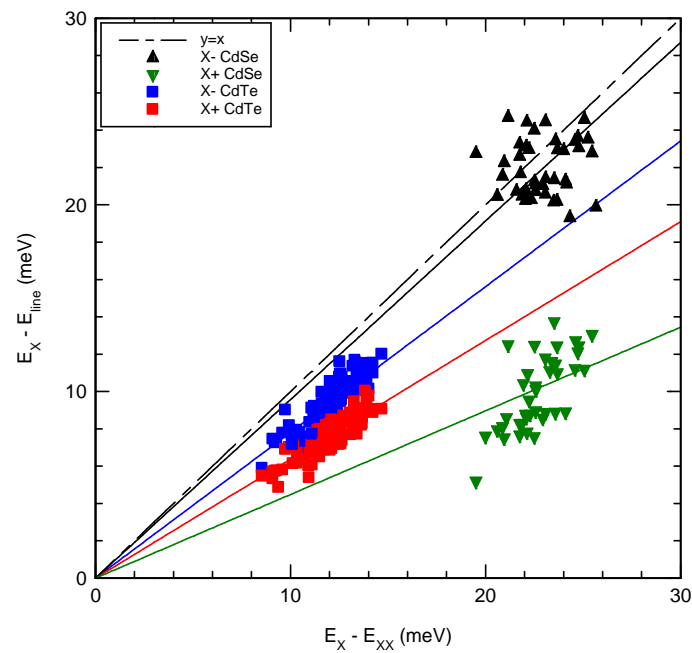


Fig 2. Spectral patterns of emission lines associated with optical transitions in single CdTe/ZnTe (red and blue) and CdSe/ZnSe (black and green) quantum dot.

## Quantum confined Stark effect of polar and non-polar ZnO/ZnMgO quantum wells grown by MBE

T. Abe, T. Motoyama, M. Yamamoto, A. Yamamoto, H. Kasada, K. Ando, and K. Ichino  
Department of Information and Electronics, Graduate School of Engineering,  
Tottori University, Tottori, Japan  
E-mail: abe@ele.tottori-u.ac.jp

ZnO has attracted increasing interest as promising material for ultraviolet optoelectronic devices because of its wide band gap (3.37eV) and large exciton binding energy (60meV). This large exciton binding energy is an advantage in quantum confined Stark effect (QCSE) of excitonic transition, which has potential applications for optical functional devices such as high speed optical modulators and switches in the ultraviolet region. In this paper, we report on the QCSE of polar and non-polar ZnO/ZnMgO quantum wells (QWs) grown by molecular beam epitaxy (MBE).

ZnO/ZnMgO QWs used in this study were grown by plasma-assisted MBE using Zn, Mg, Ga and plasma O<sub>2</sub>\*. The ZnO/ZnMgO QW structures were grown on n-type ZnMgO:Ga contact layer and buffer layer on sapphire substrate. The c-plane sapphire substrates were used for polar (O-polar) QWs, and r-plane sapphire substrates were used for non-polar (a-plane) QWs. The buffer layer for polar QW was LT-ZnO(~30nm)/MgO(1nm), and for non-polar QW was LT-ZnO(~30nm). QW structures were 10 or 20 periods ZnO(3nm)/ZnMgO(10nm). QW excitonic transition energies were determined by electroabsorption (EA) experiments at room temperature. We used poly(3,4-ethylenedioxythiophene):poly(styrenesulfonate) (PEDOT: PSS) as Schottky window layers formed by inkjet printing technique on the ZnO top layers. In the EA experiments, DC reverse bias (0 ~ 10 V) and AC modulation ( $\pm 2$  V) voltages were applied between the PEDOT:PSS Schotky contact and the n-type ZnMgO:Ga bottom layer.

By applying the reverse bias in the EA experiment, the QW excitonic transition energies show blue-shift (~20meV) for non-polar QWs, and red-shift (~40meV) for non-polar QWs. The blue shifts of polar QWs are due to reverse QCSE in the tilted potential QWs caused by built-in Piezo electric-field in the polar ZnO/ZnMgO QWs. On the other hand, the red shifts of non-polar QWs are due to normal QCSE in the flat potential QWs. In polar ZnO/ZnMgO QWs, built-in electric-field is estimated as ~ 1 MV/cm. This large electric-field may cause an exciton dissociation. Thus, energy-shift is smaller than non-polar QWs. However, non-polar QW has a Schottky build-in electric-field only. Therefore, excitons were maintained from zero bias to the reverse bias of ~10 V. The transmission spectral shows clear exciton absorption peak in the case of non-polar QW but only shoulder was observed in the case of polar QW. These results show that non-polar ZnO/ZnMgO QWs are promising for QCSE devices such as optical modulators in the new ultraviolet wavelength region.

## Magnetic Ground State of an Individual Fe<sup>2+</sup> Ion in a Strained Semiconductor Quantum Dot

T. Smoleński<sup>1,\*</sup>, T. Kazimierczuk<sup>1</sup>, J. Kobak<sup>1</sup>, M. Goryca<sup>1</sup>, A. Golnik<sup>1</sup>,  
P. Kossacki<sup>1</sup>, and W. Pacuski<sup>1</sup>

<sup>1</sup>Institute of Experimental Physics, Faculty of Physics, University of Warsaw, Warsaw, Poland

\*Tomasz.Smolenski@fuw.edu.pl

Spin manipulation of individual impurities has attracted a lot of research attention over the last years [1-5]. Important contribution to this field can be done using II-VI quantum dots (QDs) containing various single transition metal ions, as was recently shown by the measurements of Mn<sup>2+</sup> and Co<sup>2+</sup> spin relaxation dynamics in different QD systems [3,4] or by our observation of coherent precession of a single Mn<sup>2+</sup> spin [5].

One of the strongest motivations for the research in this area is a possibility to obtain long spin coherence time of an individual magnetic moment. From that perspective the nuclear-spin free Fe<sup>2+</sup> ion embedded in a QD seems a promising system. However, it was not considered as a candidate for quantum information applications, since the Fe<sup>2+</sup> ion in bulk zinc-blende or wurtzite II-VI semiconductors was found to inherently exhibit a single non-degenerate ground state and thus regarded as not able to store any quantum information.

In this work we demonstrate that by using the strain of a semiconductor QD it is possible to tailor the energy spectrum of the Fe<sup>2+</sup> ion to exhibit doubly degenerate (i.e., magnetic) ground state. Moreover, this ground state is composed of states corresponding to the ion spin projections  $S_z = \pm 2$ , which makes those two states less prone to decoherence, e.g., by residual in-plane magnetic field. Our concept is evidenced both theoretically and experimentally. From the theoretical side, we find that strong structural strain of the QD alters the spectrum of the ion orbital states, which in turn induces a distinctive changes in the ordering of the ion spin levels due to the spin-orbit coupling. The experimental proof is based on the results of photoluminescence (PL) studies of a novel II-VI QD system: self-assembled CdSe/ZnSe quantum dots doped with individual Fe<sup>2+</sup> ions. A direct fingerprint of a nonzero spin of the Fe<sup>2+</sup> ion ground state is a pronounced twofold splitting of the emission lines visible in a QD PL spectrum, which is observed for all three excitonic complexes (Fig. 1). In each case, the splitting originates from the  $s,p-d$  exchange interaction between the ion and confined carriers, which leads to two different energies of the optical transitions depending on the Fe<sup>2+</sup> spin projection. Our analysis is complemented by the measurements of a QD PL spectrum evolution in magnetic field, which allow us to determine the character and strength of the  $s,p-d$  exchange and to obtain the ion g-factor of 2.0, exactly as expected for the Fe<sup>2+</sup>.

An excellent agreement between our model and experimental results unequivocally confirms the strain-induced magnetic character of a single Fe<sup>2+</sup> ion in a CdSe/ZnSe QD. Such a novel II-VI QD system is thus a prominent candidate for quantum information processing, since both the CdSe lattice and Fe<sup>2+</sup> ion can be free of any nuclear spin fluctuations.

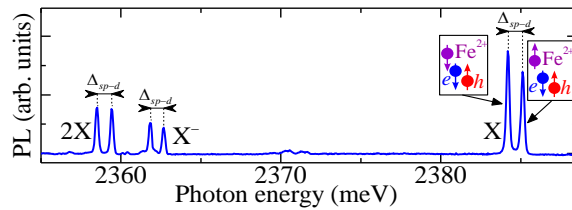


Fig. 1: PL spectrum of a CdSe/ZnSe QD with an individual Fe<sup>2+</sup> ion ( $\Delta_{sp-d}$  represents the  $s,p-d$  exchange splitting visible for all excitonic complexes).

- [1] C. Yin *et al.*, Nature **497**, 91 (2013).
- [2] T. Smoleński *et al.*, Phys. Rev. B **91**, 045306 (2015).
- [3] J. Kobak, T. Smoleński *et al.*, Nat. Commun. **5**, 3191 (2014).
- [4] B. Varghese *et al.*, Phys. Rev. B **90**, 115307 (2014).
- [5] M. Goryca *et al.*, Phys. Rev. Lett. **113**, 227202 (2014).

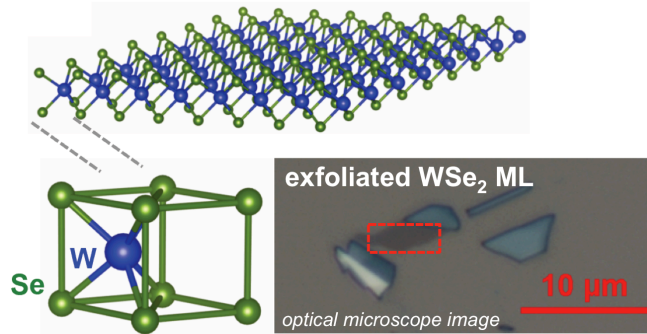
## Strong excitonic effects dominate linear and nonlinear optical response in monolayer WSe<sub>2</sub> and MoSe<sub>2</sub>

Gang Wang, Louis Bouet, Iann Gerber, Delphine Lagarde, Andrea Balocchi,  
Thierry Amand, Xavier Marie and Bernhard Urbaszek\*

Université de Toulouse, INSA-CNRS-UPS, LPCNO, 135 Avenue de Rangueil, Toulouse, France

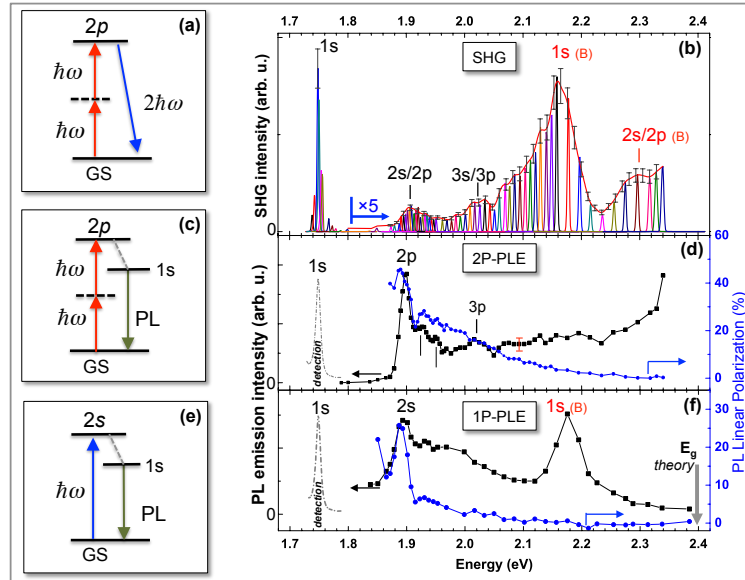
\*urbaszek@insa-toulouse.fr

Monolayers (MLs) of transition metal dichalcogenides (TMDC) such as WSe<sub>2</sub>, MoSe<sub>2</sub> and MoS<sub>2</sub> are an exciting class of two-dimensional (2D) materials for (opto-)electronics and for exploring electron k-valley physics. Crystal inversion symmetry breaking together with the spin-orbit interaction lead to a unique coupling of carrier spin and k-space valley physics, initially described in a single particle picture [1]. When electrons



and holes are simultaneously present, they will form excitons as the Coulomb interaction is enhanced by the strong quantum confinement, the large effective masses and the reduced dielectric screening in these ideal 2D systems. Large exciton binding energies  $E_b$  of typ. 0.5eV have been confirmed experimentally [2,3] i.e. the energy of the lowest lying optical transition (optical bandgap in the visible) is about 0.5eV below the electronic bandgap  $E_g$ .

Here we demonstrate at  $T=4K$  a variation over several orders of magnitude of the non-linear and linear optical response of ML WSe<sub>2</sub> and MoSe<sub>2</sub>. This is achieved by tuning the optical excitation *on* and *off* resonance with respect to the ground (1s) and excited (2s,2p...) exciton states. At these particular energies, identified in 1 and 2-photon excitation spectroscopy (PLE), the light-matter interaction is strongly enhanced [3]. We perform second harmonic generation (SHG) spectroscopy (for an application in ZnO see [4]) i.e. monitor the SHG signal as a function of laser energy and polarization in Fig. (b). We find an enhancement of the SHG efficiency of up to 3 orders of magnitude when scanning the 2-photon laser energy across the excitonic spectrum. Another important consequence of exciting the 2s (see Fig.(f)) or 2p (see Fig.(d)) exciton state resonantly, is to maximize valley coherence and valley polarization in 2- and 1-photon absorption, providing an ideal starting point for valley index manipulation [1]. We evaluate the energy position of the electronic bandgap  $E_g$  with respect to the excited exciton states with ab initio GW-BSE calculations and extract an exciton binding energy in ML WSe<sub>2</sub> of about 600 meV.



- [1] D. Xiao et al, Phys. Rev. Lett. **108**, 196802 (2012) & K.F. Mak et al, Science **344**, 1489 (2014).  
 [2] *for example* PRL **113**, 026803 (2014) & PRL **113**, 076802 (2014) & Nature **513**, 214 (2014)  
 [3] Gang Wang et al, Phys. Rev. Lett. **114**, 097403 (2015)  
 [4] M. Lafrentz et al, Phys. Rev. B **88**, 235207 (2013).

## Marking of individual CdTe/ZnTe Quantum Dots containing a single Mn<sup>2+</sup> ion using *single-color, in situ* photolithography technique

K. Sawicki, F. K. Malinowski, K. Gałkowski, T. Jakubczyk, P. Kossacki, W. Pacuski  
and J. Suffczyński\*

Institute of Experimental Physics, Faculty of Physics, University of Warsaw,  
Pasteura 5 St., PL-02-093 Warsaw, Poland

\* Jan.Suffczynski@fuw.edu.pl

Epitaxially grown Quantum Dots (QDs) are typically randomly distributed in a semiconductor matrix. An indispensable prerequisite for fabrication of any kind of functional device, as well as for any systematic research involving QDs is thus a possibility of permanent marking of their position. One of the most efficient methods of QD marking developed so far combines  $\mu$ -Photoluminescence ( $\mu$ -PL) with photolithography [1]. It requires two aligned to a common path laser beams: one for determination of a QD position through  $\mu$ -PL mapping and the second one, of a higher energy, for the exposure of a photoresist deposited on the sample surface.

We present a much simpler method for the photolithography marking of the position of individual semiconductor QDs then applied so far [2]. It involves a single laser beam. Switching from the mapping to the marking stage is achieved through increase the power of laser beam. In that way, any possible inaccuracies resulting from an imperfect alignment of two laser beams of different colors are avoided. We confirm the utility of the method by systematic  $\mu$ -PL studies of individual QDs containing a single Mn<sup>2+</sup> ion.

A sample containing a layer of CdTe/ZnTe QDs doped with individual Mn<sup>2+</sup> ions is grown by Molecular Beam Epitaxy. An uniform  $\sim 1$   $\mu$ m layer of negative photoresist (SU-8 2002) is spin-coated on the sample surface. Laser emitting at 3.06 eV is used as the light source for both:  $\mu$ -PL excitation and for photoresist exposure. The power density of hundreds of W/cm<sup>2</sup>, found to not affect the photoresist, is applied in the  $\mu$ -PL measurement. The power density of tens of kW/cm<sup>2</sup> is applied for the photoresist exposure. The  $\mu$ -PL mapping and *in situ* photolithography is performed in a cold finger helium cryostat at T = 10 K. The exposed photoresist is wet developed and as a result, permanent spots above the selected QDs (50 nm accuracy) are formed on the sample surface. The sample is placed in a pumped helium cryostat for  $\mu$ -PL measurements in magnetic field of up to 10 T. Laser beam is focused to 1  $\mu$ m spot on the sample surface in both experimental setups.

Typically, the chance of finding a signal from the same QD after a change introduced to the experimental setup is very low. Here, thanks to QD marking, we are able to perform a measurement on the same QD, even after rotation of the cryostat by 90 deg. Evolution with magnetic field of the sixfold-split QD exciton line coming from the marked QD with a single Mn<sup>2+</sup> ion is thus observed in both Faraday and Voigt configurations. The set of experimental data is well reproduced with a theoretical model yielding values of constants characterizing exciton-Mn<sup>2+</sup> ion coupled system.

The process yield of the presented method is close to 100%. We have checked that the markers act as a durable protection of the sample against dry etching. It provides a chance for the preparation of mesa structures, e. g., micropillars or photonic trumpets containing the selected QD, using of the markers as protection masks. The ease of application and flexibility of the presented technique allows one to extend its application to other systems, including those requiring high energy of the PL excitation, like NV centers in diamond.

[1] A. Dousse *et al.*, *Phys. Rev. Lett.* **101**, 267404 (2008).

[2] K. Sawicki *et al.*, *Appl. Phys. Lett.* **106**, 012101 (2015).

## Synthesis and characterization of opto-magnetic ZnO/MgO core/shell doped copper ions nanoparticles.

Mikulski J\*, Sikora B, Fronc K, Kłopotowski Ł, Aleshkevych P, Kret S, Kossut J  
Institute of Physics, Polish Academy of Sciences, al. Lotników 32/46, 02-668 Warsaw,  
Poland.

\* mikulski@ifpan.edu.pl

Colloidal semiconductor nanocrystals are a class of materials with great potential for applications in low-cost optical, magnetic and electrical signal processing devices (eg., photovoltaics, light emitting diodes (LED), as well as new advanced equipment characterized by, e.g., "zero-threshold" optical gain).

As part of this work, ZnO/MgO core/shell nanoparticles doped by copper ions, were synthesized. The absorption and luminescence characteristics at different temperatures was measured. Samples with several concentrations of copper have been characterized by transmission electron microscopy (TEM) and electron paramagnetic resonance (EPR). An attempt was made to observe the magnetic properties.

To prove the presence of copper ions inside the crystal ZnO core, the EPR technique was used. The EPR spectra were measured for various amounts of Cu additives. Copper ions built into ZnO grids are described by the axial spin-Hamiltonian:  $g_{\text{perp}}=2.055$ ,  $g_{\text{par}}=2.42$ ,  $A_{\text{perp}}=0.0025 \text{ cm}^{-1}$ ,  $A_{\text{par}}=0.0080 \text{ cm}^{-1}$ [1]. The obtained parameters of the EPR spectra confirmed that the  $\text{Cu}^{2+}$  built into the ZnO without precipitates of copper(II) oxide, even for 10% dopant concentration. The EPR and TEM measurements do not confirm also the presence of copper ions in magnesium oxide shell.

The bandgap is defined by the edge of the absorption band, which in this case strongly depends on the particle size ( $\Phi \sim 5 \text{ nm}$ ). The band gap in the resulting material were around 3.53 eV, indicating the bandgap shift toward the blue relative to the bulk crystal of ZnO (3.44 eV), which is associated with quantum confinement in such small nanoparticles. Studies failed to confirm unambiguously the influence of concentrations of  $\text{Cu}^{2+}$  on the absorption spectra of ZnO/MgO nanoparticles.

Photoluminescence (PL) spectra of the nanoparticles with various concentration of Cu doped were examined. The two bands characteristic for ZnO were observed, the first narrow band in the UV region corresponding to across-the-bandgap transition, and a second broad band with a maximum in green related to luminescence of defects. Increasing concentration of  $\text{Cu}^{2+}$  led to luminescence quenching of both the UV and VIS PL. The influence of magnetic field on the luminescences test samples was insignificant. The intensity for the sample containing 1% of Cu has increased by several percent. When magnesium oxide shell was modified by an additional organic outer shell (oleic acid), intensity of the photoluminescence in a magnetic field increases considerably compared to ZnO/MgO without oleic acid coverage.

### Acknowledgements

The research was partially supported by the grant of Polish National Science Center NN UMO-2013/08/A/ST3/00297

[1] B. Babu, T. Aswani, G. Thirumala Rao, R. Joyce Stella, B. Jayaraja, R.V.S.S.N. Ravikumar, J. Magn. Mater., **355**, 76, (2014).

## Influence of Phonon Confinement on Optical Phonon-Mediated Carrier Capture into CdSe/ZnS/H<sub>2</sub>O Quantum Dots

Vartanian A\*, Vardanyan K, and Kirakosyan A

Department of Solid State Physics, Yerevan State University, Yerevan, Armenia

\*E-mail: vardan@ysu.am

Chemically synthesized CdSe quantum dots are interesting for many of their applications in optoelectronics, nonlinear optics, and biology due to their bright luminescence, which is size tunable across the visible spectrum from 470 to 625 nm [1]. An important characteristic of quantum dot (QD) structures is the timescale on which the excited charge carriers relax to their equilibrium state in QD. The understanding of ultrafast carrier dynamics in QDs is important for operation of optoelectronic devices. The inhomogeneous nature of CdSe/ZnS/H<sub>2</sub>O QD nanostructures leads to strong modifications of the electronic properties as well as the phonon spectrum. New types of confined, interface, and surface optical phonon

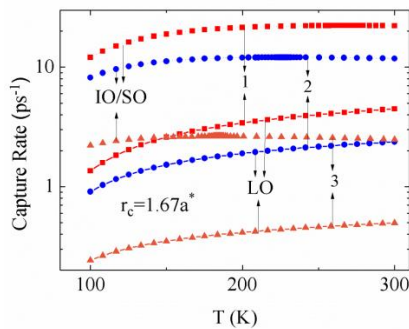


**Fig. 1.** The capture rate dependence in CdSe/ZnS/H<sub>2</sub>O QD on temperature, via emission of LO- and IO/SO-phonons for electron densities 1)  $10^{17} \text{ cm}^{-3}$ , 2)  $5 \cdot 10^{16} \text{ cm}^{-3}$ , and 3)  $10^{16} \text{ cm}^{-3}$ .

modes can occur in QD-quantum wells [2]. In this work the polar-optical-phonon-mediated capture processes in spherical CdSe/ZnS/H<sub>2</sub>O QD-quantum well structure has been studied by taking into account the phonon confinement. The numerical results of the capture rate as function of dot radius, lattice temperature and electron density in CdSe/ZnS/H<sub>2</sub>O QD systems are obtained. It has been shown that the capture rate of an electron from the barrier region to the quantum dot ground-state due to the emission of confined or interface optical phonons, exhibits strong resonances versus dot radius. In contrast with this case, the electron capture rate dependence on the radius of the GaAs QDs, the

wider areas with a high rate of electron capture appear with [3] and without [4] phonon confinement effect. In Fig.1 we show the temperature dependence of the capture rate of the LO- and IO/SO-phonon modes. The behavior of the capture rate with temperature follows mainly the behavior of the Bose-Einstein distribution. In Fig.1, it can be seen the increase of the capture rate due to emission of the LO phonons with increasing temperature. We note that this contradicts to the results obtained in Ref. [4]. One should note, nevertheless, that the experimentally determined capture rate for InAs/GaAs QD system obviously increases with increasing temperature [5].

This work was supported by the SCS MES RA (Projects No.13-1C196, 13IE-038, 13RF-093, 13YR-1C0044) and the research grant (condmatth-3821) from the Armenian National Science and Education Fund (ANSEF) based in New York, USA.

- [1] Alivisatos A P, Science **271**, 933, (1996).
- [2] Zhang L, Xie H-J, and Chen C-Y, Phys. Rev. B **66**, 205326, (2002).
- [3] Vardanyan K A, Vartanian A L, Mughnetyan V N, Dvurechenskii A V, and Kirakosyan A A, Physica E **66**, 268, (2015).
- [4] Magnusdottir I, Uskov A V, Bischoff S, Tromborg B, and Mørk J, Journ. Appl. Phys., **92**, 5982, (2002).
- [5] Feldmann J, Cundiff S T, Arzberger M, Böhm G, and Abstreiter G, Journ. Appl. Phys. **89**, 1180, (2001).

## Tuning the emission energy from CdTe and CdSe quantum dots by copper doping

**P. Wojnar**<sup>1,\*</sup>, **M. Wiater**<sup>1</sup>, **K. Fronc**<sup>1</sup>, **J. Mikulski**<sup>1</sup>, **L. Kłopotowski**<sup>1</sup>, **J. Kossut**<sup>1</sup>

<sup>1</sup>*Institute of Physics, Polish Academy of Sciences, Al Lotników 32/46, 02-668 Warsaw, Poland*

Doping II-VI semiconductors with copper attracts a great interest because of a recent observation of a strong spin-exchange interaction between paramagnetic Cu<sup>2+</sup> dopants and the band carriers in copper-doped chalcogenide nanocrystals [1]. This finding gives raise to explore diluted magnetic systems based on Cu<sup>2+</sup> magnetic ions.

In this work, we report on the fabrication of copper doped self assembled CdTe/ZnTe and CdSe/ZnSe quantum dots (QDs) by molecular beam epitaxy containing various Cu concentrations. The samples are investigated by means of low-temperature photoluminescence and micro-photoluminescence. The most important result is that we observe a pronounced spectral blue shift of the excitonic emission from CdTe and CdSe QDs as result of incorporation of copper inside of them.

The growth of the samples is performed in the following way. First, a ZnSe barrier layer is grown on 100-GaAs substrate and is followed by 3 monolayers of CdSe grown by alternating opening of Cd and Se effusion cells for 5 seconds at 280°C. Simultaneously to the Cd flux the copper effusion cell has been opened for 5 seconds. Its flux is characterized by the beam equivalent pressure being of the order of 10<sup>-9</sup> – 10<sup>-8</sup> torr depending on the sample. The estimated Cu content is, therefore, relatively low - of the order of maximum a few percent. The quantum dots formation process is induced by the Se-covering at low temperature and its subsequent thermal desorption. The quantum dots are finally covered with 50 nm ZnSe barrier layer.

In the case of Te-based structures, CdTe QDs are formed on a ZnTe barrier layer from 6 monolayers CdTe grown by alternating exposing to Cd and Te fluxes for 5 seconds. After the 3<sup>rd</sup> Cd-layer the sample is moved to another MBE chamber equipped with Cu effusion cell without breaking the high vacuum conditions. Cu is deposited for 5 seconds. Subsequently, the sample is moved back to the main growth chamber for the deposition of further 3 CdTe monolayer. The QDs formation process is induced by the Te covering method [2]. The growth is accomplished by a 50 nm thick ZnTe cap layer.

The samples are characterized by low temperature (5 K) photoluminescence and micro-photoluminescence measurements. We observe that the copper doping has a significant impact on the emission energy from CdSe and CdTe quantum dots despite of a relatively low Cu concentrations being of the order of only a few percent. The energy shift is as large as 250meV for CdTe quantum dots and 220 meV for CdSe quantum dots. The micro-photoluminescence technique confirms that the observed emission is originating indeed from QDs excitonic emission for all Cu compositions. When the excitation spot is reduced to 3μm the relatively broad emission from the QDs-ensemble splits into several emission lines origination from individual dots. Interestingly, the isolating of individual emission lines is much easier in the case of quantum dots containing copper which suggests a decrease of the density of optically active QDs. On the other hand the blue shift of the emission can also be observed for Cu containing ZnCdSe quantum wells which indicates that the quantum dot formation process only cannot be responsible for the observed spectral blue shift.

The research has been supported by National Centre of Science (Poland) grant 2013/08/A/ST3/00297

[1] Pandey, A.; Brovelli, S.; Viswanatha, R.; Li, L.; Pietryga, J.; Klimov, V., I; Crooker, S. *Nature Nanotechnology* **2012**, 7, 792

[2] Tinjod, F.; Robin, I. C.; Andre, R.; Kheng, K.; Mariette, H. *Journal of Alloys and Compounds* **2004**, 371: 63-6

\*Contact: wojnar@ifpan.edu.pl

## A correlative study of interfacial structure in type-II ZnTe/CdSe Superlattices.

R. André<sup>1</sup>, E. Bellet-Amalric<sup>2</sup>, J. Bleuse<sup>2</sup>, B. Bonef<sup>2</sup>, C. Bougerol<sup>1</sup>, L. Gérard<sup>1</sup>, A. Grenier<sup>3</sup>,  
P.H. Jouneau<sup>2</sup>, H. Mariette<sup>1</sup>.

Univ. Grenoble Alpes, F-38000 Grenoble, France

<sup>1</sup>CNRS, Inst. Néel, "Nanophysique et Semiconducteurs" group, F-38000 Grenoble <sup>2</sup>CEA,  
INAC-SP2M, F-38000 Grenoble, France

<sup>3</sup>CEA, LETI, MINATEC Campus, F-38000 Grenoble, France

S. Boyer-Richard, J.M. Jancu

Université Européenne de Bretagne, INSA, FOTON, UMR 6082, 35708 Rennes, France

We combine various optical studies (photoluminescence, absorption, time resolved spectroscopy) with structural quantitative analyses (Z-contrast images from STEM using a High-Angle Annular Dark Field detector, Atom probe tomography, X-ray diffraction) to provide a precise measurement of interfacial profiles in ZnTe/CdSe superlattices (SLs) at the atomic scale. These specific heterostructures grown by molecular beam epitaxy are interesting for their optoelectronic properties. In particular the type-II band gap alignment observed in these SLs allows an efficient absorption of light in a tunable energy range [1,2]. This prospect is however strongly dependent on the chemical structure of the interfaces: indeed, in type-II structures, the spatially indirect transition due to electron-hole overlap, arises only within an extremely narrow region adjacent to the interface. Moreover, quantum structures without a common atom have nonequivalent normal and inverted interfaces which can induce giant optical anisotropy.

We perform photoluminescence experiments on various CdSe/ZnTe SLs: for short periods, the SL emission energy is strongly dependent on the chemical species at the interfaces and a fast exponential decay is observed; by contrast for large periods SLs, the emission energy does not vary as much with the interface structure and a slow hyperbolic decay is obtained. To account for all these results, an accurate tight binding simulation has been done: a good agreement has been obtained with the insertion of 1.5 monolayer ZnSe at the normal interface (i.e. ZnTe on CdSe) whereas the inverted one (CdSe on ZnTe) is found to be broader with alloyed layers.

These findings are in perfect harmony with the chemical nature directly deduced from structural analysis. Indeed, Z-contrast atomic resolution imaging achieved in a STEM – HAADF, Atom Probe Tomography, and X-ray diffraction reveal the presence of a thin ZnSe layer at each interface of these SLs [3].

[1] D. Mourad, J.P. Richters, L. Gérard, R. André, J. Bleuse, H. Mariette  
Determination of valence-band offset at cubic CdSe/ZnTe type-II heterojunctions: A combined experimental and theoretical approach, Phys. Rev B86, 195308 (2012).

[2] S. Boyer-Richard, C. Robert, L. Gérard, J.P. Richters, R. André, J. Bleuse, H. Mariette, J. Even and J.M. Jancu. Atomistic simulations of the optical absorption of type II CdSe/ZnTe superlattices  
Nanoscale Research Letters, 7, 543 (2012).

TuP-23

[3] B. Bonef, L. Gérard, J.L. Rouvière, A. Grenier, P.H. Jouneau, E. Bellet-Amalric, H. Mariette, R. André, C. Bougerol, *Appl. Phys. Lett.* 106, 051904 (2015); C. Bougerol et al. Invited paper at the 17<sup>th</sup>IntConf on II-VI Compounds and related materials.

## Mn-enhanced collective emission of CdMnSe quantum dots

T. Schmidt<sup>2</sup>, D. F. Cesar<sup>1</sup>, L. Cabral<sup>1</sup>, F. Hartmann<sup>2</sup>, K. Brunner<sup>3</sup>, L. Worschech<sup>2</sup>,  
E. Menendez-Proupin<sup>4,5</sup>, A. Forchel<sup>2</sup>, T. Slobodskyy<sup>3</sup>, G. Schmidt<sup>3</sup>, L. W. Molenkamp<sup>3</sup>,  
G. E. Marques<sup>1</sup>, V. Lopez-Richard<sup>1\*</sup>

<sup>1</sup>Departamento de Física, Universidade Federal de Sao Carlos, Sao Carlos, Brazil

<sup>2</sup>Technische Physik, Universität Würzburg, Würzburg, Germany

<sup>3</sup>Experimentelle Physik III, Universität Würzburg, Würzburg, Germany

<sup>4</sup>Departamento de Física, Universidad de Chile, Santiago, Chile

<sup>5</sup>Instituto de Energia Solar and Departamento de Tecnologías Especiales,  
Universidad Politecnica de Madrid, Madrid, Spain

\*vlopez@df.ufscar.br

Differently sized arrays of semimagnetic CdMnSe quantum dots (QDs) have been studied by time-resolved luminescence spectroscopy. They constitute ensembles of light emitters that couple to each other via their electromagnetic radiation field [1,2]. In these systems, it has been observed that the QD exciton lifetime reduction due to the Mn incorporation, which is commonly attributed to Mn-induced non-radiative channels, is by far more pronounced in large quantum dot ensembles compared to small mesas containing a low number of QDs.

The effect can be attributed to a polarization of the Mn system which locks to the polarization of the exciting laser. In this work we show that the introduction of Mn into CdSe QDs can indeed enhance the initial polarization, thus leading to radiative coupling. We demonstrate that due to the presence of Mn, the luminescence quantum yield in ensembles of QDs is more than one order of magnitude larger than for only a few QDs. The Mn ions can adapt to the polarization of excited carriers and thus increase the initial polarization in a quantum dot system excited by polarized light. This additional initial polarization enhances the radiative coupling between the dots and leads to a decrease of the radiative lifetime. However, we observe a decrease of the luminescence yield with decreasing mesa size. This analysis has been developed within the framework of the Density Functional Theory between systems with and without Mn and the results of these ab-initio calculations have been used to tract the nature of the polarization transfer.

[1] Dicke, R. H.: "Coherence in Spontaneous Radiation Processes", Physical Review **93**, 99 (1954).

[2] Scheibner, M. *et al.*: "Superradiance of quantum dots", Nature Physics **3**, 106 (2007).

**Poster Session 2 - TuP**

**Spin related phenomena (topological insulators , magnetic semiconductors ,  
magnetic devices)**

## Growth, Structure, Electronic and Vibrational properties of Epitaxial $\text{Bi}_2\text{Se}_3$ Topological Insulator Films on GaAs(111) Substrates.

*M. Eddrief<sup>1,2, a)</sup>, T. Phuphachong<sup>3</sup>, F. Vidal<sup>1,2</sup>, B. Jusserand<sup>1,2</sup>,  
S. Hidki<sup>1,2</sup>, Y. Zheng<sup>1,2</sup>, D. Demaille<sup>1,2</sup>, L. Largeau<sup>4</sup>, M. Marangolo<sup>1,2</sup>, P. Atkinson<sup>1,2</sup>,  
L.-A. De Vaultier<sup>3</sup> and Y. Guldner<sup>3</sup>*

<sup>1</sup> *Sorbonne Universités, UPMC Univ Paris 06, UMR 7588, Institut des NanoSciences de Paris, 4 place Jussieu, F-75005, Paris, France*

<sup>2</sup> *CNRS, UMR 7588, Institut des NanoSciences de Paris, 4 place Jussieu, F-75005, Paris, France*

<sup>3</sup> *Laboratoire Pierre Aigrain (UMR 8551), Ecole Normale Supérieure- PSL Research University, 24 rue Lhomond, 75005 Paris*

<sup>4</sup> *Laboratoire de Photonique et de Nanostructures (CNRS-LPN), Route de Nozay, 91460 Marcoussis, France*

*a) Electronic mail : eddrief@insp.jussieu.fr*

Discovery of a new class of materials, called topological insulators (TIs), has opened up a whole new research area. Topological insulators behave in the bulk like ordinary insulators but support in addition a conducting two-dimensional topological surface state. This surface state has a linear energy-momentum dispersion shaped like a Dirac cone, resulting from a band inversion generated by strong intrinsic spin-orbit coupling. The electron momentum in these surface states is locked to the spin orientation and spin-flip scattering is prohibited by time reversal symmetry [1], offering great advantages for spintronic or quantum computation applications [2].

For practical device applications, considerable effort has been made to grow epitaxial  $\text{Bi}_2\text{Se}_3$  layers on different substrates as a first step towards large-scale monolithic integration of TIs in gated heterostructures, which allow the Fermi level to be tuned through the Dirac point and enable electric-field control of the spin polarized currents in devices.

The group at the INSP has optimized the epitaxial growth of  $\text{Bi}_2\text{Se}_3$  thin films on GaAs (111)B substrates, with state-of-the-art thin film structural and electronic quality [3,4]. The crystalline quality of the  $\text{Bi}_2\text{Se}_3/\text{GaAs}(111)$  interface has been investigated using high resolution X-ray diffraction and atomic resolution high-angle annular dark field scanning transmission electron microscopy (HAADF-STEM) demonstrating a quasi-van der Waals hetero-epitaxy mastered from the first-quintuple layer (QL) film-thickness. We present the Raman properties from the first to few-QL film-thickness, in particular the phonon sensitivity to the QL-thickness [3].

From angle resolved photoemission spectroscopy (ARPES) measurements, we discuss the evolution of the electronic structure as a function of QL-thickness of the films, across the critical thickness where transition occurs between gapless topological insulators and conventional gapped insulator [4]. For more information on the electronic band structure, ARPES observations will be compared with optical and magneto-optical infrared transmission measurements. The electronic properties will be related to the growth conditions and the concentration of intrinsic Se vacancies.

### References :

- [1] L. Fu, C. L. Kane, and E. J. Mele, *Phys. Rev. Lett.* **98**, 106803 (2007).
- [2] P. Roushan, J. Seo, C.V. Parker, Y. S. Hor, D. Hsieh, A. Richardella, D. Qian, M. Z. Hasan, R. J. Cava, and A. Yazdani, *Nature (London)* **460**, 1106 (2009).
- [3] M. Eddrief, P. Atkinson, V. Etgens and B. Jusserand, *Nanotechnology* **25**, 245701 (2014).
- [4] F. Vidal, M. Eddrief, B. Salles, I. Vobornik, E. Velez-Fort, G. Panaccione and M. Marangolo, *Phys. Rev. B* **88(R)** 241410 (2013).

## Rhenium monoselenide: an investigation by density functional theory

D. Wolverson<sup>1</sup>

<sup>1</sup>Department of Physics, University of Bath, Bath BA2 7AY, UK

\*d.wolverson@bath.ac.uk

The drive to combine magnetism and semiconducting properties within the same material has revealed an wide range of fascinating and fundamental spin-dependent physics in both III-V and II-VI semiconductors but, at present, it is still unclear whether many of the aims of spintronics can be realised, and what the most promising materials may be for practical applications. It is therefore a priority to explore ideas for novel materials that may address the technological challenges and may also present interesting new physics.

Here we consider the hypothetical zincblende compound ReSe, asking whether it can form an analogy to MnSe, since atomic Re and Mn are similar in having electronic configurations [Xe] 5d<sup>5</sup>6s<sup>2</sup> and [Ar] 3d<sup>5</sup>4s<sup>2</sup> respectively. Although the most stable known selenide of rhenium is the layered transition metal dichalcogenide ReSe<sub>2</sub> [1,2], it is likely to be possible to obtain metastable zincblende ReSe layers by non-equilibrium growth techniques such as molecular beam epitaxy, as has been demonstrated for numerous other non-equilibrium compound semiconductors [3]. To achieve this, some guidance concerning the likely metastable zincblende (ZB) lattice parameter is essential in order to identify promising epitaxial substrates and so we have carried out calculations within density functional theory using the projector augmented wave method as implemented within Quantum Espresso to obtain an approximate equation of state for ZB ReSe. From this, a zero-temperature cubic lattice parameter of 5.45 to 5.57 Å is obtained (depending on the choice of LDA or GGA functionals, which generally under- and overestimate respectively) and the zone-centre phonon energies and bulk modulus are also predicted.

Within the same calculations, we also obtain the predicted electronic band structure, and spin-polarised density of states, from which we can investigate possible ferro- and simple antiferromagnetic phases. Via the use of fully relativistic pseudopotentials, we take into account the effects of spin-orbit coupling on the predicted bandstructure. In order to investigate possible long-range electronic correlations, we also investigate the effects of including a Hubbard U term (the DFT+U model) whose value can be derived using a linear response method [4]. We shall show that, in the above models, ReSe is in fact not predicted to be closely analogous to MnSe, but is instead expected to form a non-magnetic semiconductor. Finally, therefore, we shall discuss the prospects for introducing magnetic behavior through alloying and doping.

[1] Wilson JA and Yoffe AD, *Advances in Physics* **18**, 193, (1969).

[2] Wolverson D, Crampin S, Kazemi, A, Ilie A and Bending SJ, *ACS Nano*, **8**, 11154, (2014).

[3] Moug RT and Prior KA, *phys. stat. sol. C* **11** 1206 (2014)

[4] Cococcioni M and de Gironcoli S, *Phys. Rev. B* **71** 035105 (2005)

## Sum rule constraints on the surface state conductance of topological insulators

D.N. Basov

University of California San Diego

I will discuss THz and infrared experiments aimed at probing the Drude oscillator strength ( $\mathbf{D}$ ) and the magnitude of the bulk band gap ( $\mathbf{E}_g$ ) of the epitaxially grown, topological insulator  $(\text{Bi,Sb})_2\text{Te}_3$ . The magnitude of  $\mathbf{E}_g$ , in conjunction with the model independent  $\mathbf{f}$ -sum rule, allowed us to establish an upper bound for the Drude weight expected in a typical Dirac like system composed of linear bands. The model was extended to include hexagonal band warping, and electron hole asymmetry, as is typical in topological insulator systems. The experimentally observed Drude weight is found to be at or below this theoretical upper bound, demonstrating the effectiveness of alloying in eliminating bulk charge carriers. Moreover, Hall effect parameters and the weak anti-localization observed in transport on the same sample support assignment of the low-energy conduction to topological surface states. Complimentary insights in the response of surface states of  $(\text{Bi,Sb})_2\text{Te}_3$  is provided by cyclotron resonance and Faraday rotation experiments in THz frequencies.

## Spin Dynamics of Tellurium Isoelectronic Bound Excitons in Zn-Se-Te Nanostructures

V. Deligiannakis<sup>1,4\*</sup>, S. Dhomkar<sup>3,4</sup>, H. Ji<sup>3,4</sup>,

I.L. Kuskovsky<sup>3,4</sup>, M.C. Tamargo<sup>2,4</sup>, C. Meriles<sup>1,4</sup>

<sup>1</sup>Department of Physics, The City College of New York, CUNY

<sup>2</sup>Department of Chemistry, The City College New York, CUNY

<sup>3</sup>Department of Physics, Queens College, CUNY

<sup>4</sup>The Graduate Center, CUNY

\*vdeligia@gmail.com

Three-dimensionally confined structures such as quantum dots (QDs) have been of considerable interest due to their ability to closely imitate isolated atoms on mesoscopic length scales. Recently, single impurity states in bulk semi-conductors have also attracted attention due to their ability to optically address quantum states. Here we show results pertaining to the optical and spin properties of type-II sub-monolayer ZnTe QDs embedded in a ZnSe matrix. Photoluminescence studies show two prominent bands centered around 2.5 eV (green band) and 2.7eV (blue band) at low temperatures. The green band has been correlated with the contribution from QDs, while the high energy blue band is attributed to contributions from the ZnSe spacer including Te isoelectronic centers present in them. Time resolved Kerr rotation (TRKR) measurements were performed using a degenerate pump-and-probe setup. Attempts to probe the dots directly via the green band did not show any results most likely due to the weak oscillator strength of this transition resulting from their type-II nature. Centering the pump and probe pulses around the band edge of ZnSe (blue band) and performing TRKR vs energy measurements, we were able to address the spin dynamics of Te-isoelectronic centers present in the spacer layer. Results show that the  $\tau_2^*$  lifetimes exhibit a bi-exponential decay and persist up to 1 ns. Further measurements will be done on samples with varying Te concentration, as well as a function of applied magnetic-field to understand the spin properties of this defect.

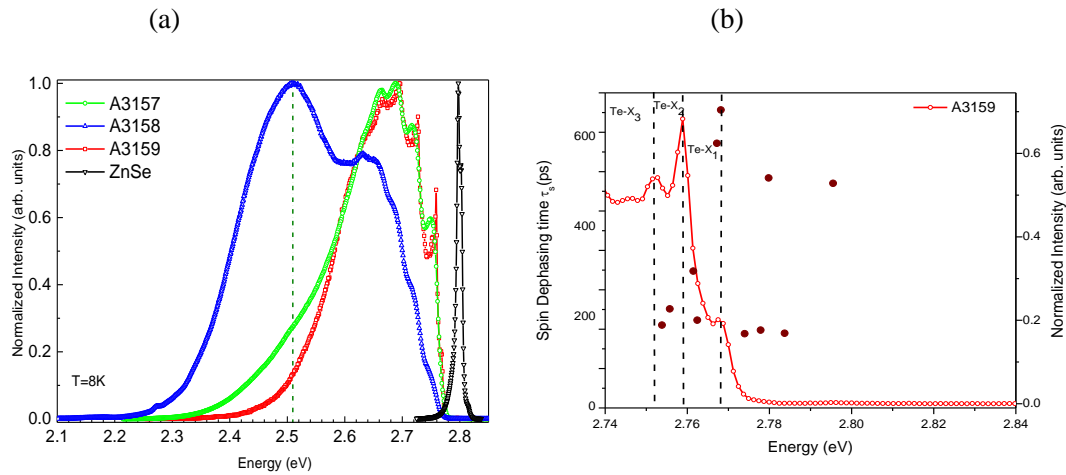


Fig1. (a) Low temperature photoluminescence for three different samples with varying Te concentration A3158, A3157 and A3159 having 3%, >.3%, >>.3% respectively and 100 nm ZnSe reference. (b) Closed circles represent the spin life times measured for different pump and probe energies.

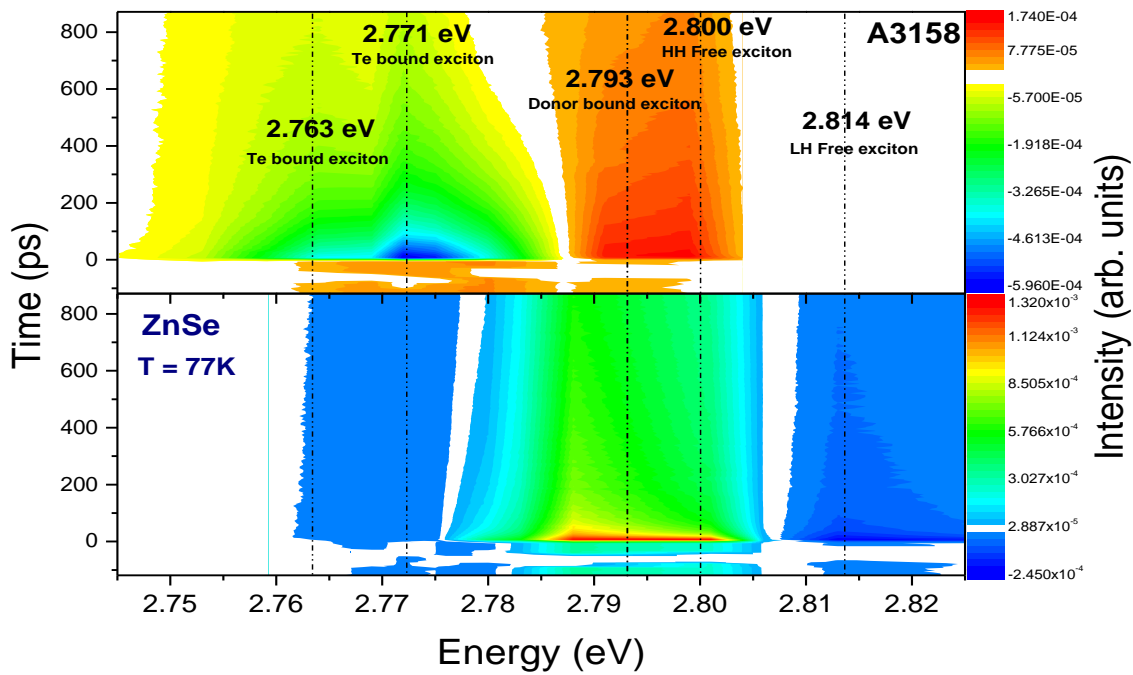


Fig2. TRKR vs Energy at 77K for A3158 and Bulk ZnSe. A3158 shows a strong signal near Te bound excitons and the signal becomes very weak for above HH-FX excitation. Also, the TRKR signal decreases and then flips when scanning to different excitonic complexes, suggesting an interplay in the hyperfine structure of the sample.

## Peculiarities of Room Temperature Magnetic Properties of single ZnO:Mn Nanowires revealed by Magnetic Force Microscopy

Lytvyn P.<sup>1</sup>, Strelchuk V.<sup>1</sup>, Kolomys O.<sup>1</sup>, Rarata S.<sup>1</sup>, Syngaiivska O.<sup>1</sup>, Tronc P.<sup>2</sup>, Chan Oeurn Chey<sup>3</sup>, Omer Nur<sup>3</sup>, and Magnus Willander<sup>3</sup>

<sup>1</sup> V. Lashkaryov Institute of Semiconductor Physics NAS Ukraine, Kyiv, Ukraine

<sup>2</sup> École Supérieure de Physique et de Chimie Industrielles (ESPCI), Paris, France

<sup>3</sup> Department of Science and Technology, Linköping University, 601 74 Norrköping, Sweden  
peter.lytvyn@ccu-semicond.net

Mn-doped ZnO nanowires (NWRs) have attracted much interest for their potential in spintronic applications. We present a magnetic and microstructure characterization of individual upright standing and lying ZnO:Mn NWRs using magnetic atomic force microscopy (MFM) and Raman imaging. Arrays of undoped and ZnO:Mn NWRs with nominal Mn concentrations of 10, 15 and 30% were synthesized by aqueous chemical growth. NWRs had clear hexagonal facets and average diameter varied from 50 to 500 nm depending on the nominal Mn content. For carrying out MFM and Raman measurements the NWRs were extracted from the glass substrate and deposited from the water suspension onto glass substrates coated with a golden film. MFM is used to record 2D magnetization maps simultaneously with topography. Single ZnO:Mn NWRs showed clear magnetic contrast in 2D magnetization maps, providing the evidence of in-plane ferromagnetic magnetization in individual upright standing ZnO:Mn NWRs at room temperature. Variation of the magnetic contrast at different magnetic field polarities of the MFM tip is shown on fig.1,c,d. The ring-shaped complex structures are clearly visible, that transforms corresponding to the MFM tip polarity. This can be caused by (i) increased Mn concentration near the surface of the NWRs due to segregation of Mn in the growth process and/or (ii) formation of structural defects and/or spinel structural phases in the near-surface region of the NWRs mediating ferromagnetism in Mn-alloyed ZnO. The fine magnetic structure of individual NWR transformation in external magnetic field of different directions and magnitude is also analyzed.

Lateral Raman mapping of single NWR with lateral step of 0.1  $\mu\text{m}$  was performed. The Raman spectra of ZnO:Mn NWRs show the Raman-active vibrational modes of wurtzite phase ZnO and two local vibration modes associated with Mn- $\text{V}_\text{O}$  complexes at 275 and 526  $\text{cm}^{-1}$ . In addition, at high Mn concentration, strong vibrational modes related to spinel phase  $\text{ZnMn}_2\text{O}_4$  at near 321, 384, 677  $\text{cm}^{-1}$  and  $\text{Mn}_3\text{O}_4$  at near 319, 375 and 662  $\text{cm}^{-1}$  were found in the nanowires. Both phases coexist along the entire length of the NW, even if with variable contributions. Additionally,  $\text{ZnMn}_2\text{O}_4$  two-dimensional "seed" layers is formed.

Found peculiarities of spatial distribution of structural phase composition considerably depend on Mn concentration and the technological conditions of the NWs growth. This work was supported by NATO Grant SfP 984735.

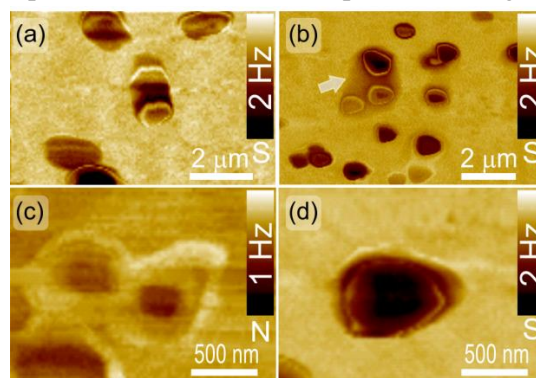


Fig.1. a-d) MFM images of upright standing ZnO:Mn (Mn15%) NWRs measured by MFM tip with opposite polarity of apex, north (N) or south (S). Arrow shows 2D "seed" layer. (e)

## Spin dependent energy transfer in II-Mn-VI DMS nanostructures

Vitalii Yu. Ivanov<sup>1\*</sup>, Jörg Debus<sup>2</sup>, Matthias Salewski<sup>2</sup>, Dmitri R. Yakovlev<sup>2,3</sup>,  
Marek Godlewski<sup>1,4</sup> and Grzegorz Karczewski<sup>1</sup>

<sup>1</sup>Institute of Physics Polish Acad. Sci., 02-668 Warsaw, Al. Lotników 32/46, Poland

<sup>2</sup>Experimental Physics 2, TU Dortmund University, 44221 Dortmund, Germany

<sup>3</sup>Ioffe Physical-Technical Institute, RAN, 194021 St. Petersburg, Russia

<sup>4</sup>Dept. Mathematics and Natural Sciences College of Science,  
Cardinal S. Wyszyński University, Warsaw, Poland

\*e-mail: [ivanov@ifpan.edu.pl](mailto:ivanov@ifpan.edu.pl)

Giant enhancement (up to two orders of magnitude) of integral exciton photoluminescence (PL) in II-Mn-VI DMS nanostructures in magnetic fields was observed together with quenching of intra-shell  $Mn^{2+}$  emission. This phenomenon has been reported [1,2], but its origin was not clarified. Two mechanisms have been under consideration: (i) spin dependent direct transfer between excitons and  $3d^5$ -shell of  $Mn^{2+}$  ions and (ii) spin dependent Auger recombination of excitons, mediated by population of excited states of  $Mn^{2+}$  ions.

In this communication we summarize the results of comprehensive studies of spin-dependent energy transfer processes between excitons and  $3d$ -shell levels of  $Mn^{2+}$  ions in quantum well (QW) structures of  $(Zn,Mn)Se/(Zn,Be)Se$ ,  $(Zn,Mn)Te/(Zn,Mg)Te$  and  $(Cd,Mn)Te/(Cd,Mg)Te$  with  $Mn^{2+}$  content varied from  $x=0.004$  to  $x=0.12$ . Dependencies of intensities of exciton photoluminescence and intra-shell  $Mn^{2+}$  PL on magnetic field, as well as, PL excitation (PLE) spectra and kinetics of both emission processes were studied. Optically detected magnetic resonance (ODMR) spectra were monitored by studying intensity changes and energy shift of exciton PL and intensity change of  $Mn^{2+}$  PL.

In the ODMR experiments we observed a strong decrease of an integral exciton intensity against an increase of  $Mn^{2+}$  intra-shell emission under the electron spin resonance condition, i.e., at the magnetic resonance of  $Mn^{2+}$  ions in the ground state. Under the same conditions the spin-lattice relaxation (SLR) time, measured by time-resolved ODMR technique, decreases, as well as decay time of  $Mn^{2+}$  ions intra-shell emission. At the same time, exciton PL decay time was not affected by magnetic field. It is important to note that, PLE spectra of excitons and  $Mn^{2+}$  intra-shell emission are matched basically and determined by exciton absorption in QW and barrier.

Results of comprehensive studies of the above-mentioned effects show, that simple mechanism of resonant excitation transfer could not be used for their explanation. Otherwise, mechanism of Auger-recombination suppression in magnetic field [2,3] or/and mechanism of exchange scattering of carriers on the  $Mn^{2+}$  localized spins [4] looks to be available. The absence of magnetic field influence to exciton radiative life time and polarization dependence of ODMR spectra are evident on the strong effects of exchange scattering.

This work was supported in the part by Polish National Science Center "Harmonia" Grant and EAGLE EU Project FP7-REGPOT-2012-2013-1 (Project Number: 316014)

[1] V. Yu. Ivanov, M. Godlewski, D. R. Yakovlev, et al., *PRB* **78**, 085322 (2008)

[2] A.V.Chernenko, P.S.Dorozhkin, V.D.Kulakovskii, et al., *PRB* **72**, 045302, (2005)

[3] M.Nawrocki, Yu.G.Rubo, J.P.Lascaray, et al., *PRB*, **52**, R2241, (1995)

[4] Yu.G.Semenov, S.M.Ryabchenko., Sov. Phys. *JETP* **57**, 4, 825,(1983)

## Highly Spin-Polarized Green Electroluminescence Achieved by Spin Filter in Semimagnetic Semiconductor Bicrystals

Le Van Khoi, A. Avdonin, K. Dybko, V. Kolkovsky, R.R. Gałazka  
 Institute of Physics, PAS, al. Lotników 32/46, 02-668 Warsaw, Poland  
 \*E-mail: lkhoi@ifpan.edu.pl

The wide bandgap II-Mn-VI semimagnetic semiconductors (SMSs) are very attractive materials for fabrication of the semiconductor spin filters due to the large Zeeman splitting of the conduction and valence bands. Recently, we have reported that application of a bias voltage of  $\sim 4$  V to a  $\text{Zn}_{1-x}\text{Mn}_x\text{Te}$  bicrystal causes an avalanche breakdown in the grain boundary junction (GRJ). In the post-breakdown regime the bicrystal emits an intense and highly circularly polarized green light. The degree of circular polarization ( $P$ ) reached a value as high as  $\approx 95\%$  [1]. In this communication, we report that the GRJ in the  $p\text{-Zn}_{1-x}\text{Mn}_x\text{Te}$  bicrystal can act as a spin filter for a current flowing across the bicrystals. We present results of the magnetoresistance measurements for the  $\text{Zn}_{1-x}\text{Mn}_x\text{Te}$  emitting bicrystal. We demonstrate that when the Zeeman splitting values of the conduction and valence bands saturate, there is a highly spin-polarized electron current ( $I_{e\downarrow}$ ) injected from the first grain into the second one. This  $I_{e\downarrow}$  strongly interacts with the sample magnetization ( $M$ ), leading to an abrupt increase in the sample resistance, electroluminescence (EL) intensity and  $P$ .

The  $\text{Zn}_{0.97}\text{Mn}_{0.03}\text{Te}$  bicrystal was p-type, doped with phosphorus to a level of  $5 \times 10^{18} \text{ cm}^{-3}$ . The  $I$ - $V$  and  $C$ - $V$  measurements have revealed a symmetrical electric barrier with a height of  $0.50 \pm 0.05$  eV and a width of  $150 \text{ \AA}$  at the GBJ, within the  $\text{ZnMnTe}$  bicrystal. Figure 1(a) presents the magnetoresistance (MR) of the  $\text{Zn}_{0.99}\text{Mn}_{0.01}\text{Te}$  single crystal grain at different temperatures  $T$ . It is seen that the values of the MR monotonically decrease with decreasing  $T$  and saturate at high fields. The MR curves resemble the magnetization curves of the sample. The decrease in the sample MR is due to the suppression of the magnetic disorder, caused by the compositional fluctuations.

This picture strongly changes for the  $\text{Zn}_{0.97}\text{Mn}_{0.03}\text{Te}$  bicrystals containing a GRJ. Figure 1(b) presents the MR measured for a single crystal grain GR1 and for the GBJ. It is seen that when the applied magnetic field increases, the MR of both the GR1 and GRJ first decreases reaching a minimum at a same switching field  $B_{sw} \approx 3$  T, then the MR of the GR1 (GRJ) sharply increase by one-step (two-step) from  $-12\%$  ( $-0.25\%$ ) to  $+75\%$  ( $+9\%$ ). Simultaneously, the emission intensity increases sublinearly [2]. Moreover, we observed that the  $B_{sw}$  increases with increasing current and depends on the current direction. All these features indicate that at  $B > B_{sw}$  the  $I_{e\downarrow}$  occurs and it interacts with the  $M$  via the  $s$ - $d$  exchange interaction. The two-step increase of the MR at GRJ shows the different response of the  $M$  in the neighboring grains composing the bicrystal. We suggest that the  $I_{e\downarrow}$ - $M$  interaction causes the change in the  $M$  direction (spin transfer torque effect) that leads to increases of the sample resistance.

In conclusion, we are successful in the fabrication of the SMS spin filter using the GRJ in the  $\text{Zn}_{0.97}\text{Mn}_{0.03}\text{Te}$  bicrystal. This spin filter allows us to achieve highly spin polarized green emission, which is of an importance for the spin-based optoelectronic devices.

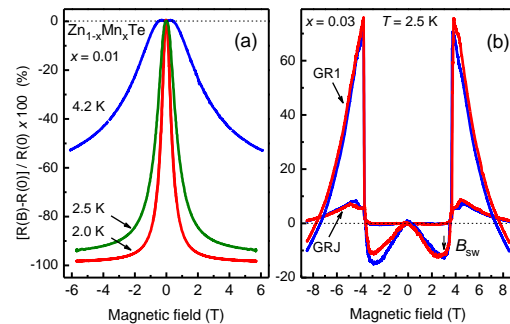


Figure 1

[1] Le Van Khoi and R.R. Gałazka, Appl. Phys. Lett. **98**, 112103 (2011).

[2] Le Van Khoi, et al., J. Appl. Phys. **106**, 036102 (2009).

## Long Spin-Flip Time and Large Zeeman Splitting of Holes in Type-II ZnTe/ZnSe Submonolayer Quantum Dots

H. Ji<sup>1,3,\*</sup>, S. Dhomkar<sup>1,3</sup>, J. Ludwig<sup>4,5</sup>, D. Smirnov<sup>4</sup>, M. C. Tamargo<sup>2,3</sup>, and I. L. Kuskovsky<sup>1,3</sup>

<sup>1</sup>Department of Physics, Queens College of CUNY, Queens, NY 11367, USA

<sup>2</sup>Department of Chemistry, City College of CUNY, New York, NY 10031, USA

<sup>3</sup>The Graduate Center of CUNY, New York, NY 10016, USA

<sup>4</sup>National High Magnetic Field Laboratory, Tallahassee, FL 32310, USA

<sup>5</sup>Department of Physics, Florida State University, Tallahassee, FL 32306, USA

\*HJI1@qc.cuny.edu

In recent years there has been intense interest in semiconductor quantum dots (QDs) for application in spintronics and quantum information processing, since the confinement of the wavefunction of the charge carriers in QDs plays a key role in the enhancement of Zeeman splitting and the prolongation of spin-flip time [1, 2]. These effects have been seen for electrons in several material systems, while experimental results of  $g$ -factors or spin-flip time of holes in QD systems are rarely reported.

Herein we report the  $g$ -factors of excitons, electrons and holes in type-II submonolayer ZnTe/ZnSe QDs obtained via studying circularly polarized magneto-photoluminescence. The  $g$ -factor of the QD-bound type-II excitons (with holes confined in ZnTe QDs and electrons located in ZnSe barriers) was extracted from the Zeeman splitting of the polarized spectra, as shown in Fig. 1(a). The energy and intensity relations between the  $\sigma^+$  and the  $\sigma^-$  polarized emissions are explained by a model, for which  $g$ -factor of holes is positive and the hole spin-flip time is longer than the recombination lifetime of excitons, which for this system is more than 100 ns. Within this model, the  $g$ -factor of electrons was fitted via the temperature dependence of the degree of circular polarization (DCP) to

$$DCP = \frac{I_{\sigma^+} - I_{\sigma^-}}{I_{\sigma^+} + I_{\sigma^-}} = \frac{1 - \exp(\ln(r) - g_e \mu_B B / kT)}{1 + C_s + \exp(\ln(r) - g_e \mu_B B / kT)}, \quad (1)$$

as shown in Fig. 1(b). The  $g$ -factor of holes confined within ZnTe QDs is then calculated from the  $g$ -factors of excitons and electrons, and is found to be positive and one order of magnitude larger than the values reported for bulk ZnTe. We attribute the enhancement of  $g$ -factor of holes to the strong confinement of the hole wavefunction due to submonolayer nature of QDs in this system.

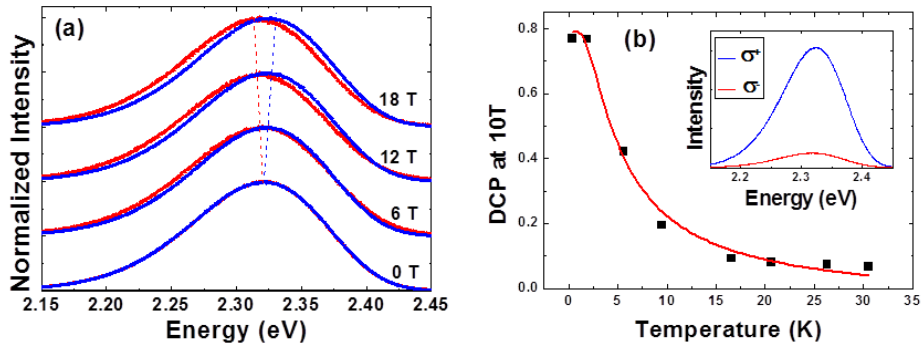


**Figure 1.** (a) Normalized PL spectra under different magnetic field at 0.36 K.  $\sigma^+$  is shown in blue while  $\sigma^-$  is shown in red. (b) Temperature dependence of DCP at 10 Tesla. The line is fitted to Eq. 1. The inset shows PL spectra at 0.36 K of  $\sigma^+$  and  $\sigma^-$  polarized emission under magnetic field 10 Tesla.

[1] R. Kotlyar, T. L. Reinecke, M. Bayer, and A. Forchel, Phys. Rev. B **63**, 085310 (2001).

[2] A. V. Khaetskii and Y. V. Nazarov, Phys. Rev. B **64**, 125316 (2001).

## Vibrational and Magnetic Properties of Co-doped Hexagonal ZnO

I.M. Kupchak<sup>1</sup>, V.V. Strelchuk<sup>1</sup>, N.F. Serpak<sup>1</sup>, D.V. Korbutyak<sup>1</sup>, P.Tronc<sup>2</sup>

<sup>1</sup> V. Lashkarev Institute of Semiconductor Physics of National Academy of Sciences of Ukraine, Kiev, Ukraine

<sup>2</sup> École Supérieure de Physique et de Chimie Industrielles (ESPCI), Paris, France  
[strelch@isp.kiev.ua](mailto:strelch@isp.kiev.ua)

Zinc oxide (ZnO), due to the large direct band gap ( $E_g \sim 3.3$  eV) at RT, large exciton binding energy ( $E_x \sim 60$  meV) and strong excitonic emission, is widely used as a material for filters and detectors of UV radiation [1]. Doping with transition metal atoms opens another field of ZnO applications. Such diluted magnetic semiconductor are the interesting materials for spintronics. Particularly, they can serve as memory cells and even as the logic elements for data processing due to their ability to store both electric charge and spin.

Despite ZnO is already well studied and widely used in technology, the nature of its magnetic properties, which appear due to transition metal doping, is still far from clear understanding.

One of the most informative methods for studying such structural disorders is the Raman light scattering. In particular, micro-Raman studies are applicable even in the case of nanocrystals, while the X-ray analysis does not always allow to identify their structure distinctly. In contrast to undoped ZnO samples, Raman spectra of ZnO:Co samples demonstrate additional bands between LO and TO phonon modes, the intensity of which increases with the Co atoms concentration. Thereby, our aim was to model different Co complexes in bulk ZnO, calculate corresponding vibrational density of states and magnetic structure, and compare them with existing experimental data (Raman, magnetic force microscopy) where possible.

Vibrational density of states of 12.5% cobalt doped bulk hexagonal ZnO has been studied by the density functional theory method using generalized gradient approximation (GGA). We have considered various mutual positions of cobalt atoms in the structure including cases of single atoms and their complexes, as well as the possibility of secondary structure formation (spinel-like  $\text{Co}_3\text{O}_4$  or metal CoO clusters). It has been shown, that cobalt introducing into ZnO leads to appearing of additional vibrational modes with their frequencies dependent on the relative positions of the cobalt atoms. The magnetic and vibrational properties have been studied also of highly Co-doped ZnO samples, which are characterized by a high possibility of the metal clusters formation. The interface ZnO/ $\text{Co}_3\text{O}_4$  [2] has been modelled with different mutual orientation of hexagonal ZnO and cubic spinel  $\text{Co}_3\text{O}_4$ , to minimize the intrinsic stresses induced by the lattice mismatch. For such interfaces, the magnetic structure was calculated.

Particularly, in this work we found that two cobalt atoms forming Co-O-Co chain lead to a redistribution of vibrational density of states, and its maximum shifts to the region between TO and LO modes of ZnO. In addition, the cobalt clustering also may lead to appearing of additional modes with frequencies between TO and LO modes frequencies of ZnO, which are associated with the vibrations of Co-O-Co chains.

[1] Ü. Özgür, Y. I. Alivov, C. Liu, a. Teke, M. a. Reshchikov, S. Doğan, V. Avrutin, S. J. Cho, and H. Morkoç, *J. Appl. Phys.* **98**, 1 (2005).

[2] T. Il Lee, S. H. Lee, Y.-D. Kim, W. S. Jang, J. Y. Oh, H. Baik Koo, C. Stampfl, A. Soon, and J. M. Myoung, *Nano Lett.* **12**, 68 (2012).

## Enhanced Conduction- to Valence-Subband Overlap in the HgTe Double Quantum Well

M.V. Yakunin<sup>1\*</sup>, A.V. Suslov<sup>2</sup>, E.G. Novik<sup>3</sup>, M.R. Popov<sup>1</sup>,  
N.N. Mikhailov<sup>4</sup>, and S.A. Dvoretzky<sup>4</sup>

<sup>1</sup>Institute of Metal Physics UB RAS, Ekaterinburg, Russia

<sup>2</sup>NHMFL, FSU, Tallahassee, Florida, USA

<sup>3</sup>Physical Institute, University of Wurzburg, Wurzburg, Germany

<sup>4</sup>Institute of Semiconductor Physics SB RAS, Novosibirsk, Russia

\*yakunin@imp.uran.ru

HgTe layer wider than 6.3 nm have an inverted energy dispersion of spatially quantized conduction and valence subbands, which overlap for still wider layer resulting in a coexistence of 2D electron and hole systems. This creates new physics like a formation of the topological insulator state, electron-hole correlation phases etc. We suggest a technique to enhance and regulate this overlap combining it with an interlayer overlap in a double quantum well (DQW) consisting of two HgTe layers separated by a thin barrier. It is based on an energy shift between the two layers either built into the structure initially and/or introduced by application of the voltage  $V_g$  to the gate. We measured the Hall and longitudinal magnetoresistivities (MR)  $\rho_{xy}$  and  $\rho_{xx}$  as a function of field  $B$  and  $V_g$  of the samples consisting of two 20 nm wide HgTe layers separated by 6–10 nm  $\text{Cd}_x\text{Hg}_{1-x}\text{Te}$  barrier.

The band overlap manifests itself in the weak field  $N$ -shaped  $\rho_{xy}(B)$  concomitant with the parabolic  $\rho_{xx}(B)$  and in a specific behavior of  $\rho_{xy}(B)$  in the Quantum Hall (QH) range of fields. The latter displays the plateau  $h/e^2$  for filling factor  $i = +1$  in the hole conductivity, which moves to weaker fields with increasing  $V_g$  at  $V_g \leq 0$  but stops moving at  $B_c \approx 15$  T and sinks down to negative values with the further increase of  $V_g$ . This field indicates the moment when the gap between the arrays of electron and hole levels is closed. Our value of  $B_c$  is much larger than  $B_c \approx 2$  T observed in a similar single QW [1] indicating a much larger overlap in the DQW. We estimated the overlap for  $B_c = 15$  T using a calculated picture of magnetic levels as of  $\sim 10$  meV for interlayer overlap plus the intrinsic overlap in a layer of 6.5 meV resulted in the net value of  $\sim 17$  meV. The observed value of  $B_c$  and the corresponding overlap in a DQW may depend on the impurity content in the sample but generally it would be much larger than in a single QW.

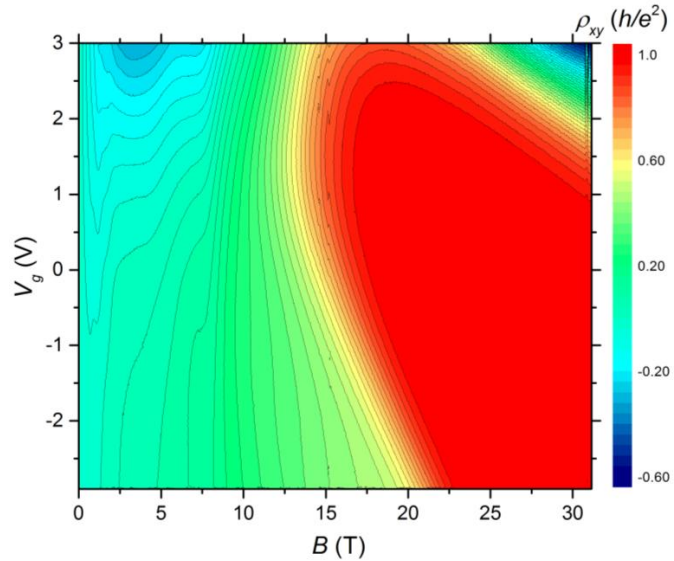


Fig.1. An example of  $\rho_{xy}(B, V_g)$  in the HgTe DQW.

[1] O.E. Raichev, G.M. Gusev, E.B. Olshanetsky, Z.D. Kvon et al., Phys. Rev. B **86**, 155320 (2012).

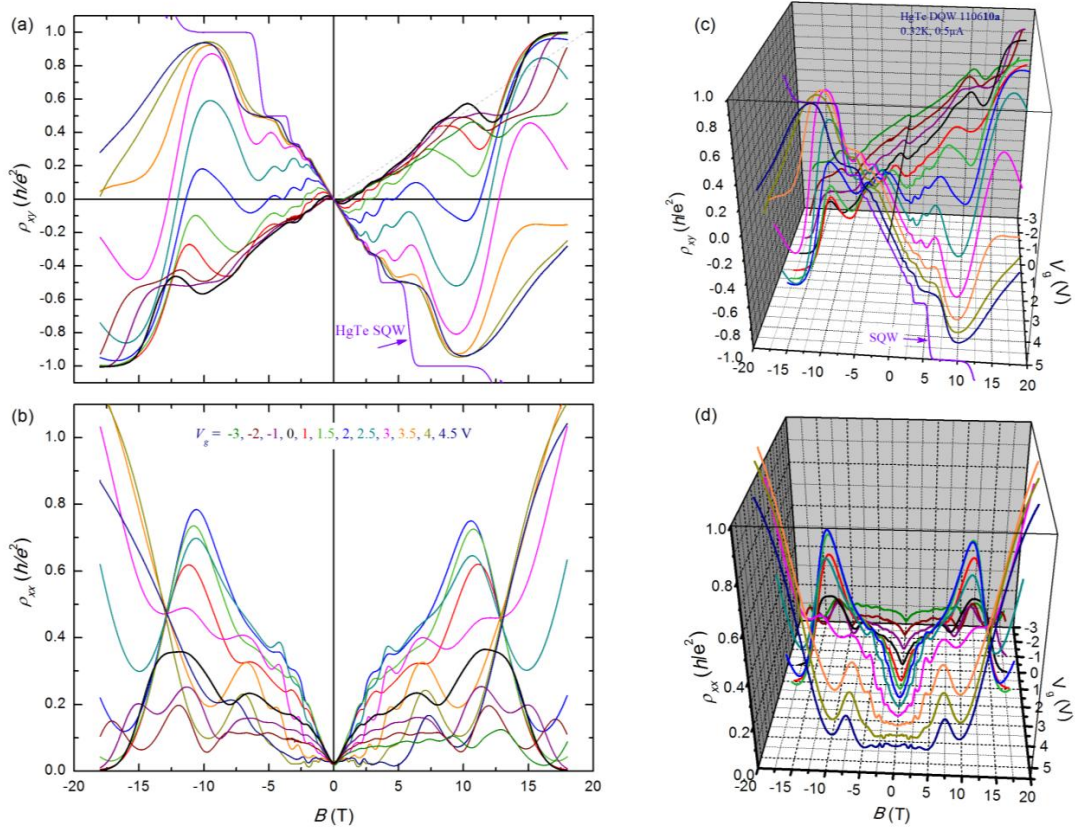


Fig.2. Other example of magnetotransport in a HgTe DQW. (a)  $\rho_{xy}(B)$  and (b)  $\rho_{xx}(B)$  in a series of  $V_g = -3 \div +4.5$  V [see description in (b) for different colors]. (c) and (d) – the same in the bulk graph presentation.  $\rho_{xy}(B)$  at large positive  $V_g$  are compared with the QH trace for an identical Single QW.

## Electron Spin Flip Raman Spectroscopy and Magneto-Resistance of the Diluted Magnetic Semiconductor $\text{Zn}_{1-x}\text{Mn}_x\text{Se}$ below the Metal-Insulator Transition

A. G. Knapp<sup>1\*</sup>, S. Petznick<sup>2</sup>, F. Jansson<sup>3</sup>, M. Wiemer<sup>3</sup>, M. Hetterich<sup>4</sup>, F. Gebhard<sup>3</sup>,  
S. D. Baranovskii<sup>3</sup>, P. J. Klar<sup>2</sup>, and J. Geurts<sup>1</sup>

<sup>1</sup>Physikalisches Institut (EP3), University of Würzburg, D-97074 Würzburg, Germany

<sup>2</sup>Institute of Experimental Physics I, Justus-Liebig-University Giessen, D-35392 Giessen,  
Germany

<sup>3</sup>Department of Physics and Material Sciences Center, Philipps University, D-35032  
Marburg, Germany

<sup>4</sup>Institute of Applied Physics and DFG Center for Functional Nanostructures (CFN),  
Karlsruhe Institute of Technology (KIT), D-76131 Karlsruhe, Germany

[\\*Alexander.Knapp@physik.uni-wuerzburg.de](mailto:Alexander.Knapp@physik.uni-wuerzburg.de)

The diluted magnetic wide-gap semiconductor  $\text{Zn}_{1-x}\text{Mn}_x\text{Se}$  offers the opportunity for the independent tuning of its magnetic properties and its electronic transport behavior by variation of the Mn-content  $x$  and the concentration of nonmagnetic dopant atoms (e.g. Cl), respectively. Furthermore, the strong exchange interaction coupling between the d-levels of the Mn-ions and the electron s-wavefunctions gives rise to a giant Zeeman splitting of the latter states in an external magnetic field. This also applies for the donor-bound electrons, which determine the transport behavior at low temperature for dopant concentrations below the metal-insulator transition via hopping processes (Mott hopping). Because of the short-range character of the exchange interaction, the value of the Cl-donor-level splitting is expected to depend strongly on the magnetization of the Mn atoms in the immediate vicinity of the respective Cl-atom. Therefore, the random spatial Mn distribution should lead to a field-induced broadening of the donor energy distribution.

We have investigated this effect for Cl-doped  $\text{Zn}_{1-x}\text{Mn}_x\text{Se}$  with  $x = 0.05 - 0.06$  and various Cl-concentrations up to  $4.5 \cdot 10^{17} \text{ cm}^{-3}$ , which is  $\sim 64\%$  of the Mott density. For this purpose, we applied low-temperature electronic spin flip Raman spectroscopy (ESFRS) and magneto-transport measurements.

In ESFRS, the spin flip transition of the donor-bound electron is mediated by optically induced donor-bound excitons ( $D^0, X$ ), which results in a sharp resonance of the ESFRS efficiency when the exciting laser photon energy matches the ( $D^0, X$ ) energy [1]. Therefore, the spectral dependence of the ESFRS-efficiency (resonance profile) reflects the energy distribution of the donor states.

We observed a significant broadening of the ESFRS resonance profiles with increasing B-field, up to 11.5 meV (FWHM) for B=5 T, which confirms the field-induced broadening of the level distribution.

These spectroscopy results agree very well with those of our magneto-transport experiments, which show a positive magneto-resistance up to 200%, which implies that the electron hopping processes are progressively hindered by the broadening of the level distribution.

These experimental results are explained by a modelling of the B-dependent characteristic width  $\sigma$  of the donor energy distribution, using for the magneto-resistance general scaling arguments based solely on the dependence of hopping rates on temperature and on the energies of hopping sites [2, 3].

[1] M. Hirsch, R Meyer and A. Waag, Physical Review B **48**, 5217 (1993)

[2] F. Jansson et al., Journal of Applied Physics **116**, 083710 (2014)

[3] A. V. Nenashev et al., Physical Review B **88**, 115210 (2013)

## Evidence of Exchange Interaction of Localized Carriers and Transition Metals in Diluted II-VI nanostructures: ODMR Study

Baranov P.G<sup>1\*</sup>, Romanov N.G<sup>1</sup>, Tolmachev D.O<sup>1</sup>, Gurin A.S<sup>1</sup>, Namozov B.R<sup>1</sup>, Kusrayev Yu.G<sup>1</sup>, Karczewski G<sup>2</sup>, Orlinskii S.B<sup>3</sup>, De Mello Donegá C<sup>4</sup>, Schmidt J<sup>5</sup>,

<sup>1</sup>Ioffe Institute, St. Petersburg, 194021 Russia

<sup>2</sup>Institute of Physics, Polish Academy of Sciences, PL-02608 Warsaw, Poland

<sup>3</sup>Federal Center of Shared Facilities, Kazan State University, Kazan 420008, Russia

<sup>4</sup>Debye Institute for Nanomaterials Science, Utrecht University, Netherlands

<sup>5</sup>Huygens Laboratory, Leiden University, 2300 RA Leiden, Netherlands

\*pavel.baranov@mail.ioffe.ru

Optically detected magnetic resonance (ODMR) study of (CdMn)Te quantum wells allowed to reveal fine structure splitting of Mn ions due to low dimensionality, formation of exchange-coupled complexes Mn ions and localized holes in quantum wells with excess hole concentration, and directional electron tunneling towards wider wells in multiple quantum well structures.

Mn and Co - doped ZnO quantum dots (QDs), which are promising classes of diluted magnetic semiconductors and consist of a ZnO nanocrystal core and Zn(OH)<sub>2</sub> shell have been studied. A direct evidence of Co (Mn) interaction with shallow donors in the core and hyperfine coupling with <sup>1</sup>H in the shell of QD has been demonstrated. The shape of the EPR spectrum of cobalt ions was shown to change as a result of Co<sup>2+</sup> coupling with optically created shallow donors. This, along with a shift of shallow donors EPR line, is a direct demonstration of interaction between the magnetic ion and donor electron in confined system of ZnO QD.

Spin-dependent electron-hole recombination has been studied by optically detected magnetic resonance (ODMR). ODMR techniques which are based on EPR detection via photoluminescence or via tunneling afterglow that can be observed for a long time after preliminary X-ray or UV irradiation proved to be very useful to study colloidal ZnO nanocrystals. The higher sensitivity of ODMR allowed its application for characterization of ZnO QDs dispersed in transparent media, which cannot be studied by conventional EPR and ESE. This is an important advantage, since these systems are more relevant for a number of practical applications.

The work has been supported by Russian Science Foundation under Agreement № 14-12-00859 and RFBR #13-02-00821.

## Optical probing of the spin state of a single Cr<sup>2+</sup> ion in a quantum dot

A. Lafuente-Sampietro<sup>1,2</sup>, H. Boukari<sup>1,2</sup>, L. Besombes<sup>1,2\*</sup>,  
F. Nakazawa<sup>3</sup>, H. Utsumi<sup>3</sup>, S. Kuroda<sup>3</sup>

<sup>1</sup>Univ. Grenoble Alpes, Grenoble, France

<sup>2</sup>CNRS, Institut Néel, Grenoble, France

<sup>3</sup>Institute of Materials Science, University of Tsukuba, Tsukuba, Japan

\*lucien.besombes@grenoble.cnrs.fr

Controlling the state of single spins in semiconductors is very attracting for fundamental issues and the potential of such ultimate spin based memories in the field of quantum information storage and processing. It has already been shown that the spin of a magnetic ion in II-VI semiconductor quantum dots (QDs) can be controlled optically. Among the variety of magnetic transition elements, Chromium (Cr) is of particular interest. Cr is incorporated in II-VI compounds as a Cr<sup>2+</sup> ion carrying a localized electronic spin  $S=2$  with an angular momentum  $L=2$  and 90 % of Cr isotopes have no nuclear spin limiting the number of spin states to 5. The non-zero angular momentum provides a large sensitivity of the ion spin to local strain making Cr<sup>2+</sup> a very promising spin *qubit* for the realization of hybrid spin-mechanical systems.

Here we demonstrate that the spin state of a single Cr<sup>2+</sup> ion embedded in a CdTe/ZnTe QD can be detected optically (Figure 1). The exchange interaction between the confined carriers and localized spin is strong enough to allow a mapping of the spin state of the Cr<sup>2+</sup> into the QD optical transitions observed in photoluminescence (PL). The PL of neutral and charged Cr-doped QD reveals a large magnetic anisotropy of the spin of the Cr<sup>2+</sup> which is induced by biaxial strain in the plane of the QDs. This leads to the zero field splitting of the 0,  $\pm 1$  and  $\pm 2$  spin states (Figure 1a) and the difference in their occupancy as revealed by the PL intensity distribution (Figure 1b and 1c). The PL spectra can be significantly affected by the presence of in-plane strain anisotropy which acts on the Cr<sup>2+</sup> ion through the crystal field and on the confined heavy-hole wave-function producing some valence band mixing. The sensitivity to the strain is typically 100 times larger for Cr<sup>2+</sup> than for Mn<sup>2+</sup>.

A large photon bunching, with a characteristic time in the 100 ns range, is measured for individual lines of the PL. This dynamics, controlled by carriers and Cr<sup>2+</sup> spin-flips, is not affected by a transverse magnetic field up to 0.5T confirming the large Cr<sup>2+</sup> magnetic anisotropy. CW and time resolved polarization rate measurements show that the PL is strongly co-circularly polarized. This is a signature of the good stability of the exciton-Cr<sup>2+</sup> spin at zero magnetic field.

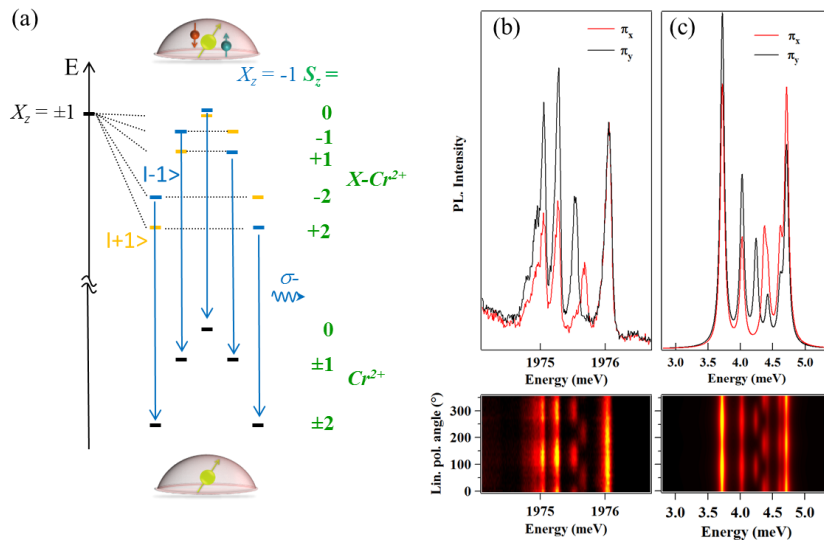


**Figure 1:** Single Cr<sup>2+</sup> in a CdTe/ZnTe QD: (a) Energy levels of the ground state (Cr<sup>2+</sup>) and bright exciton ( $Xz=\pm 1$ ) coupled to the magnetic ion ( $X-Cr^{2+}$ ). (b) Linearly polarized PL spectra and intensity map at  $T=5K$ . (c) Calculated PL spectra and linear polarization intensity map.

## EPR Study of Layers Obtained from ZnCrTe Target by PLD Method

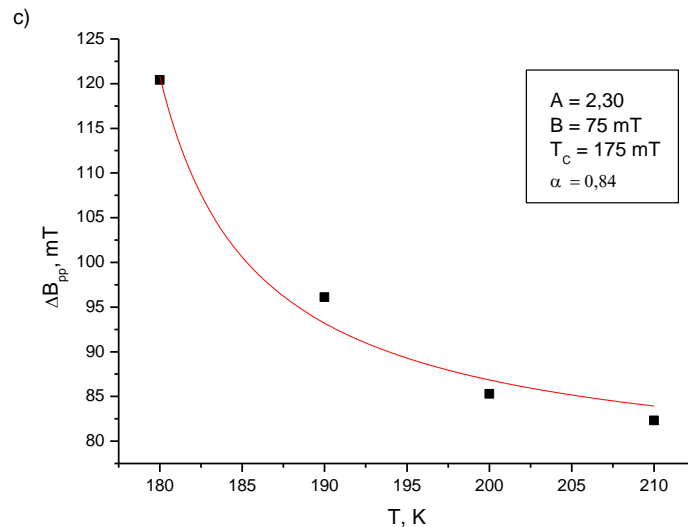
Bester M<sup>1\*</sup>, Cieniek B<sup>1</sup>, Kuzma M<sup>1</sup>, and Dubiel L<sup>1</sup>

<sup>1</sup>Faculty of Mathematics and Natural Sciences, University of Rzeszow, Pigionia. 1 St.,  
35-959 Rzeszow, Poland

\*mbester@ur.edu.pl

The Cr-doped ZnTe crystals have been studied as a new class of diluted magnetic semiconductors with high Curie temperature [1-4]. The replacement of Zn atom with Cr in ZnTe crystal lattice introduces not only magnetic impurity but yields p-type doping as well [5], what results in a net ferromagnetic exchange interaction [6-7]. Magnetic properties of epitaxial films of this material were studied on films obtained by molecular beam epitaxial (MBE) method [8]. We report EPR measurements of thin films obtained by pulsed laser deposition method (PLD) from target in which the amount of Cr was large in respect to Zn content.

Thin ZnCrTe layers were obtained by pulsed laser deposition method (PLD) on quartz substrate. We performed EPR measurements in temperature of 120 – 300 K using Bruker Elexsys E 580 spectrometer operating in the X-band (9.43GHz). In the temperature range 150-210 K the shape of spectra are of Dyson type and show typical paramagnetic-ferromagnetic behavior with magnetic transition. Huber's theory approximates Curie temperature on  $T_C=175$  K.



- [1] Pekarek T M, Luning J E., Miotkowski I, and Crooker B C, Phys. Rev. B **50**, 16914, (1994).
- [2] Guo X G, Cao J C, Chen X S, Lu W, , Solid State Commun. **138**, 275, (2006).
- [3] Fukushima T, Sato K, Katayama-Yoshida H, and Dederichs P. H, Phys. Stat. Sol. (a) **203**, 2751, (2006),
- [4] Soundararajan D, Mangalaraj D., Nataraj D, Dorosinskii L, and. Kim H K, Solid State Commun. **87**, 113, (2012).
- [5] Kepa H, Le Van Khoi, Brown C. M, Sawicki M., Furdyna J K, Giebułtowicz T. M, and. Dietl T, Phys. Rev. Lett. **91**, 087205, (2003).
- [6] Kacman P, Semicond. Sci. Technol. **16**, R25, (2001).
- [7] Dietl T, and Ohno H, Rev. Mod. Phys. **86**, 187, (2014).
- [8] Soundararajan D, Mangalaraj D, Nataraj D, Dorosinskii L, Santoyo-Salazar J, and Riley M J, J. Magn.

TuP-38

Magn. Mater. **321**, 4108, (2009).

## Optical and magnetic studies of MBE-grown ferromagnetic CrSe and CrS layers in zincblende structure

Röder J<sup>1</sup>, Moug R T<sup>2</sup>, Prior K A<sup>2</sup>, Krug von Nidda H-A<sup>3</sup>, Loidl A<sup>3</sup> and Heimbrodt W<sup>1</sup>

<sup>1</sup>*Department of Physics and Material Science Center, Philipps University, Marburg 35032, Germany*

<sup>2</sup>*Institute of Photonics and Quantum Sciences, SUPA, School of Engineering and Physical Sciences, Heriot-Watt University, Edinburgh EH144AS, United Kingdom*

<sup>3</sup>*Experimental Physics V, Center for Electronic Correlations and Magnetism, University of Augsburg, Augsburg 86159, Germany*

Half-metallic ferromagnets have been suggested as promising spin contacts for semiconductorbased spintronic devices since they exhibit a hundred percent spin alignment at the Fermi level. Theoretical calculations predicted Chromium chalcogenides in the zinc blende (ZB) structure to be promising candidates to be half-metallic spin-aligner at room temperature<sup>1,2</sup>.

Unfortunately, the thermodynamically stable phase of CrSe and CrS is the hexagonal NiAs-structure. In the NiAs-phase the Cr-chalcogenides are, however, antiferromagnetic semiconductors and do not possess half-metallic character. In recent papers we have shown, that the growth of ZB transition metal chalcogenides can be stabilized by growing on appropriate ZB substrates<sup>3,4</sup>.

In the present contribution we use similar methods to stabilize the ZB structure of CrS and CrSe films. Different configurations have been successfully tested. (i) CrSe have been grown on InAs substrates with ZB CdSe buffer layers or as CrSe/CdSe superlattices, (ii) CrSe layers on GaAs substrates with either ZnSe or ZnSe/MgS as buffer layers. (iii) The CrS-layers have been embedded between ZnMgS layers. All the samples have been grown by MBE in a V80H MBE System using Zn, Mg, Se and Cr elemental sources and ZnS to supply the sulphur. The cubic symmetry has been ensured in situ by RHEED-measurements and later by X-ray reflection (see Ref.4 for more details).

We investigated the ferromagnetic properties and magnetic phase transition and the respective optical properties of all the films and nanostructures. The magnetic properties and the magnetic phase transition have been studied by temperature dependent SQUID measurements. The aim was to reveal the ferromagnetism of the samples and the dependence of the Curie temperature of CrSe and CrS on the preparation conditions and film thicknesses. The appearance of a ferromagnetic phase transition is an important and independent proof for the stabilization of the ZB crystal structure, as it is well established that the NiAs-structure exhibits solely an antiferromagnetic phase transition. The so far determined Curie-temperatures were found to be below room temperature. Nevertheless, a correlation of the strain state and  $T_C$  could be revealed. Obviously the exchange interaction strength can be changed by changing the lattice parameters and the respective Cr-Cr distance. This may open new pathways to further enhance the Curie temperature in the future by growing appropriate strained layer systems.

All the samples have been studied also by polarization dependent photoluminescence and reflection spectroscopy in the temperature range between 2 K and room temperature. The results will be discussed in detail with the aim to reveal the minority spin gap of CrSe and CrS and its behaviour in an external magnetic field as fundamental parameters for any feasible application.

<sup>1</sup>K. Yao, G. Gao, Z. Liu, and L. Zhu, Solid State Commun. **133**, 301 (2005)

<sup>2</sup>N. H. Long, M. Ogura, and H. Akai, J. Appl. Phys. **106**, 123905 (2009)

<sup>3</sup>M. Demper, W. Heimbrodt, C. Bradford, K.A. Prior, H.A. Krug von Nidda, A. Loidl, Appl. Phys. Lett. **100**, 132405 (2012)

<sup>4</sup>R.T. Moug, K.A. Prior, phys. stat. sol.(c) **11**, 1206 (2014)

## Magnetic Phase Transitions in ZnO Doped by Transition Metals

Sh. U. Yuldashev, V. Sh. Yalishev, Z. A. Yunusov, Y. H. Kwon and T. W. Kang

Quantum-Functional Semiconductor Research Center, Dongguk University, 3-26 Pil-dong, Chung-gu, Seoul 100-715, Korea (E-mail: shavkat@dongguk.edu)

ZnO based diluted magnetic semiconductors (DMS) have attracted much interest since Dietl *et al.* [1] predicted ferromagnetic ordering in these materials with a Curie temperature  $T_C$  exceeding room temperature. However, the magnetic properties of ZnO DMS reported so far by different research groups are quite contradictory. Some groups observed high-temperature ferromagnetism in low-temperature grown bulk and thin films of ZnO doped by transition metals such as Mn, Co, Cr and etc., whereas others have observed paramagnetic or even spin-glass behaviors.

Here we present the results on experimental study of magnetic phase transitions in ZnO thin films doped by Mn and Co by using the specific heat and thermal diffusivity measurements. The main advantage of using these methods is the possibility to determine the critical exponents for the magnetic phase transition without using an external magnetic field, which can suppress the magnetization fluctuations near the critical temperature. By establishing the universality class for the phase transition, one can obtain information on the range of the exchange interactions determining magnetic order in the system in question. Moreover, the useful quantity that can be extracted from the specific heat measurements is the magnetic entropy, associated with the number of the local magnetic moments involved in the establishing of the magnetic ordering.

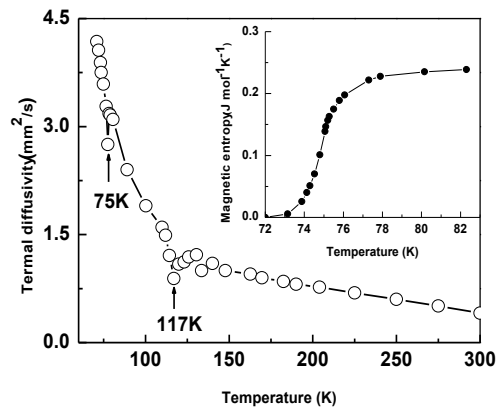


Fig.1. Temperature dependence of the thermal diffusivity of the ZnO doped by Mn. The inset shows the magnetic entropy of the phase transition observed at  $T = 75$  K.

The detailed analysis of the critical exponent of the specific heat near the critical temperature provides the information on the universality class of observed phase transitions and the number of magnetic ions involved in the magnetic ordering.

[1] T. Dietl, H. Ohno, F. Matsukura, J. Cibert and D. Ferrand, *Science* **287**, 1019 (2000).

**Poster Session 2 - TuP**

**Growth and characterization , doping and defects**

## Spectroscopic and Kinetic Studies of ZnSe and ZnSe:Mn Colloidal Quantum Dots

Thiago G. Silva<sup>1</sup>, Igor M. R. Moura<sup>2</sup>, Paulo E. C. Filho<sup>2</sup>, Maria I. A. Pereira<sup>2</sup>, Goreti Pereira<sup>1</sup>, Giovannia A. L. Pereira<sup>2</sup>, Adriana Fontes<sup>3</sup>, Beate S. Santos<sup>1\*</sup>

<sup>1</sup>Pharmaceutical Sciences Dept, Federal University of Pernambuco, Recife, Brazil.

<sup>2</sup>Fundamental Chemistry Dept, Federal University of Pernambuco, Recife, Brazil.

<sup>3</sup>Biophysics and Radiobiology Dept, Federal University of Pernambuco, Recife, Brazil.

\*beate@ufpe.br

Among the diverse promising known technological applications of semiconductor quantum dots (QDs) their main application in the biomedical interface is due to their efficient fluorescent biolabeling properties<sup>1</sup>. Doping metal elements in QDs add other discrete energy levels within the intrinsic energy bands enriching the energy dynamics of excitons resulting new optical profiles<sup>2</sup> enabling new biolabeling possibilities. In special zinc based QDs present as less cytotoxic alternatives to this class of fluorescent markers. In the present study we present the optimization of the optical properties of Mn<sup>2+</sup> doped ZnSe QDs coated with positive and negative alkylthiols in aqueous media. The optimization procedures rely on chemometric experimental design and post procedures based on the controlled UV photoactivation of the systems. The nanoparticles were characterized by using Ionic Coupled Plasma, Electron Paramagnetic Resonance, Transmission Electronic Microscopy and X-Ray diffractometry. We obtain efficient 2-3 nm UV-blue (390, 400 or 420 nm emission bands related to exciton relaxation) and orange emitting QDs (<sup>4</sup>T<sub>1</sub>→<sup>6</sup>A<sub>1</sub> transition centered 580 nm)<sup>3</sup>. The results point out a doping fraction smaller than 1% and that the Mn<sup>2+</sup> ions are preferentially located close to the surface of the particles. We also show that the surface activation has a great influence on the emission quantum yield and on the colloidal stability of the particles. The overall results are discussed in terms of the growth kinetic of the particles and on the chemical modifications of the surface during the photoactivation.

### References

[1] Y. G. Zheng, S. J. Gao and J. Y. Ying, *Adv. Mater.*, 2007, 19, 376–380.

[2] A. P. Alivisatos, *Perspectives on the physical chemistry of semiconductor nanocrystals*, *J. Phys. Chem.*, 1996, 100, 13226–13239.

[3] S. C. Erwin, L. Zu, M. I. Haftel, A. L. Efros, T. A. Kennedy and D. J. Norris, *Nature*, 2005, 436, 91–94.

### Acknowledgments

We are grateful to the following agencies: Conselho Nacional de Desenvolvimento Científico e Tecnológico (CNPq), Fundação de Amparo à Ciência e Tecnologia do Estado de Pernambuco (FACEPE) for financial support and student fellowships. We are also grateful to the National Institute of Science in Photonics (INFo) for financial support.

## Application of Diffuse X-ray Scattering and Polarization Dependent Photoluminescence for Realistic Modeling of Ultra-thin Quantum Dots

Siddharth Dhomkar<sup>1,4</sup>, Nicolas Vaxelaire<sup>2</sup>, Haojie Ji<sup>1,4</sup>, Vasilios Deligiannakis<sup>3,4</sup>, Jean Jordan-Sweet<sup>5</sup>, Maria C. Tamargo<sup>3,4</sup>, I. C. Noyan<sup>2</sup> and Igor L. Kuskovsky<sup>1,4\*</sup>

<sup>1</sup>Department of Physics, Queens College of CUNY, Queens, New York 11367, USA

<sup>2</sup>Department of Applied Physics and Applied Mathematics, Columbia University, New York, New York 10027, USA

<sup>3</sup>Department of Chemistry, City College of CUNY, New York, New York 10031, USA

<sup>4</sup>The Graduate Center, CUNY, New York, New York 10016, USA

<sup>5</sup>National Synchrotron Light Source, T. J. Watson Research Center, IBM, Yorktown Heights, New York 10598, USA

\*Igor.Kuskovsky@qc.cuny.edu

Characterization of so-called submonolayer quantum dots (QDs) (i.e., QDs formed from deposition of less than a monolayer of material) is challenging due to their small thicknesses and, for common cation systems, due to a low electron density contrast between the embedded QDs and the host. A good example is ZnTe/ZnSe type-II submonolayer QDs grown via migration enhanced epitaxy, in which the contrast between Te- and Se-containing sublattices is very low.

We have devised a systematic diffraction analysis to obtain quantitative structural information about such hard-to-image systems. In this procedure, a large portion of the reciprocal space is mapped to acquire both out-of-plane and in-plane information. Vertical self-ordering of quantum dots is determined from out-of-plane and non-specular reflectivity maps, while diffuse scattering analysis is used to check in-plane correlations. A specific model taking into account realistic quantum dot shape and dispersion has been developed and the simulations confirm the findings about quantum dot shape anisotropy.

This in-plane anisotropy has been further confirmed by azimuthally resolved polarization dependent photoluminescence (PL) measurements. We obtained the anisotropic exchange energy splitting from the degree of linear polarization of PL, which agrees with the magnetic field dependence of circular polarization of PL, and X-ray diffraction data.

We also present quantitative analysis of the anisotropy based on the anisotropic confinement of wavefunctions of the charge carriers. This work greatly enhances the potential for extracting structural information of complex embedded 3D QD structures.

This research is supported by the Department of Energy, Office of Basic Energy Sciences, Division of Materials Sciences and Engineering under Award No. DE-SC003739.

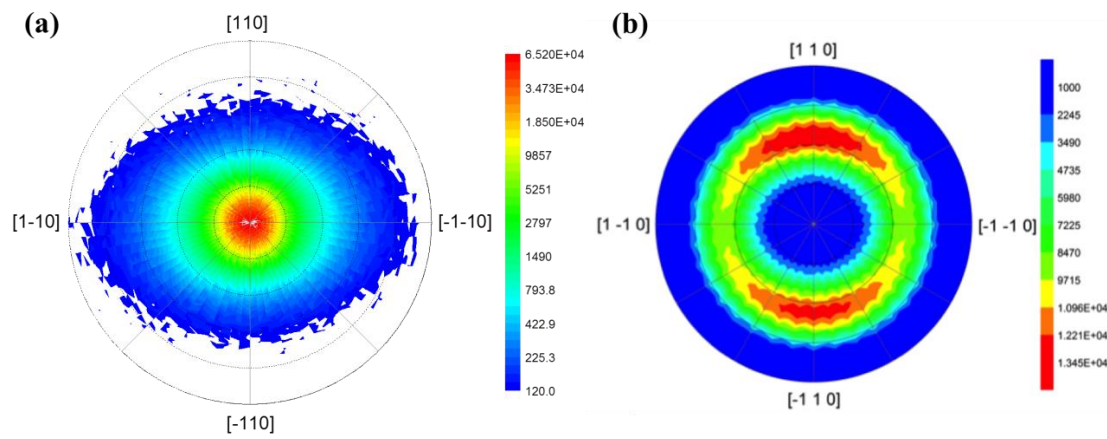


Fig 1.(a) X-ray diffraction map showing in-plane anisotropy, (b) Linear polarization dependent photoluminescence spectrum confirming the presence of QD shape anisotropy.

## Microchip Laser Converter based on InGaN LD and ZnCdSe QDs Heterostructure

E.V. Lutsenko<sup>1\*</sup>, A.G. Vainilovich<sup>1</sup>, V.N. Pavlovskii<sup>1</sup>, G.P. Yablonskii<sup>1</sup>, S.V. Gronin<sup>2</sup>, S.V. Sorokin<sup>2</sup>, I.V. Sedova<sup>2</sup>, S.V. Ivanov<sup>2</sup>, M. Aljohenii<sup>3</sup>, A. Aljerwii<sup>3</sup> and A. Alyamani<sup>3</sup>

<sup>1</sup>Stepanov Institute of Physics, National Academy of Science of Belarus,  
220072 Minsk, Nezhaleznyy 68 str., Belarus

<sup>2</sup>Ioffe Physico-Technical Institute, Russian Academy of Science,  
194021, 26 Politekhnicheskaya str., St. Petersburg, Russia

<sup>3</sup>KACST, National Nanotechnology Center. P.O. BOX 6086, 11442 Riyadh, Saudi Arabia

\**e.lutsenko@ifanbel.bas-net.by*

Modern InGaN laser diodes allow to reach  $\lambda_{\text{las}}=540$  nm in the green region. The DPSS lasers allow obtaining laser emission only at discrete wavelengths. But numerous applications require arbitrary laser wavelength choose in the 500-560 nm interval. The optically pumped QD lasers allow to change the emission wavelength by variation the QD dimensions and composition. Besides, there exists a possibility to change the laser wavelength by variation of useful laser losses (laser cavity length). Therefore we consider the optically pumped semiconductor laser based on the QD heterostructures as promising for multiple applications.

Laser converter comprising low threshold ZnCdSe QDs heterostructure optically pumped by emission of commercial InGaN laser diode has proved to be perspective compact laser source from green up to yellow spectral region [1]. Recently, a microchip laser converter ( $\lambda=510$  nm) based on single QDs sheet heterostructure with the output power of  $\sim 1$  W has been demonstrated [2]. However single QDs sheet active region performance suffers from gain saturation and rather low differential laser efficiency. The use of multiple QD sheets active region could overcome these limitations without leading to a significant increase in threshold power density [3].

The new heterostructure with active region composed of three electronically coupled ZnCdSe QD sheets in one ZnSe QW inside SL waveguide was designed and grown. High laser quality of the heterostructure was confirmed by internal laser parameters obtained at pumping by pulsed nitrogen laser emission ( $\lambda=337$  nm,  $\tau=8$  ns,  $f=600$  Hz). Growth details and internal laser characteristics are described in [4]. Relatively low transparency threshold  $I_T \sim 1.27$  kW/cm<sup>2</sup> and high characteristic gain  $\Gamma G_0 = 155$  cm<sup>-1</sup> could provide rather low laser threshold for short cavity length. This will allow to ensure pumping by InGaN laser diode emission with intensity value exceeding considerably the laser threshold, that is important to obtain maximal values of the efficiency and power.

Using the value of the characteristic gain, the optimal cavity length with the lowest threshold pumping power was determined as  $\sim 100$  microns for the cleaved cavity. The microchip laser converter was comprised of ZnCdSe QDs laser chip having  $\sim 100$   $\mu\text{m}$  cavity length emitting at  $\lambda > 540$  nm and commercial InGaN LD chip ( $\lambda=438$  nm,  $P_{\text{cw}}=1.6$  W) placed in TO-18 standard package. The threshold pumping power was  $\sim 0.5$  W. The maximal output power and conversion efficiency of  $\sim 1.5$  W and  $\sim 15\%$  respectively were reached.

[1] E.V. Lutsenko et al., Quantum Electron. 43(5), 418-422 (2013)

[2] S.V. Ivanov, S.V. Sorokin, S.V. Gronin, et.al., 16 Int. Conf. "Laser Optics 2014", St. Petersburg, Russia, (2014)

[3] G. P. Yablonskii et al., Journal of Non-Crystalline Solids. **356**, p. 1928-1934 (2010).

[4] I.V. Sedova et al, this conference

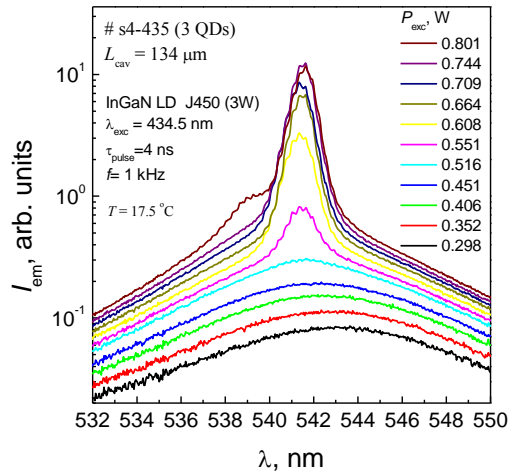


Fig. 1 – Emission spectra of microchip laser converter as a function of output power of InGaN laser diode.

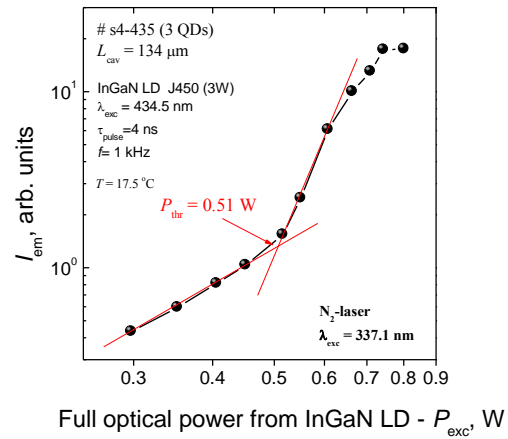


Fig. 2 – Integral emission intensity of microchip laser converter as a function of output power of InGaN laser diode.

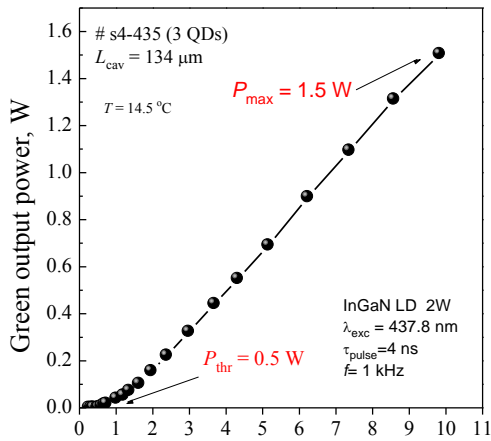


Fig. 3 – Output optical power of microchip laser converter as a function of output power of InGaN laser diode.

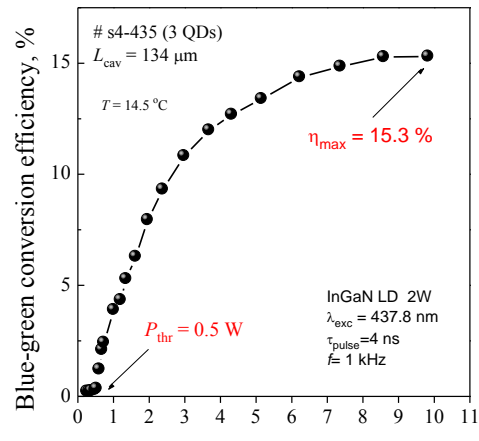


Fig. 4 – Blue-green conversion efficiency of microchip laser converter as a function of output power of InGaN laser diode.

## **Cd<sub>x</sub>Zn<sub>1-x</sub>Se quantum dots: Correlation between chemical composition and optical properties**

**H. Benallali<sup>a</sup>, T. Cremel<sup>b</sup>, K. Hoummada<sup>a</sup>, K. Kheng<sup>b</sup>, R. André<sup>b</sup>, S. Tatarenko<sup>b</sup>, D. Manginck<sup>a</sup>**

<sup>a</sup>*Aix-Marseille Université, IM2NP-CNRS, Case 142, 13397 Marseille Cedex 20, France.*

<sup>b</sup>*CEA-CNRS group "Nanophysique et Semiconducteurs" Institut Nanosciences et Cryogénie, 17 rue des martyrs, 38054 Grenoble, France*

[hammouda.benallali@im2np.fr](mailto:hammouda.benallali@im2np.fr)

Recently, the CdSe/ZnSe quantum dots (QDs) have attracted much interest because of its possible application for optoelectronic such as source of single photon operating at room temperature. The physical properties of QDs depend on many parameters such as morphology, chemical composition and chemical environment. In order to adjust specific properties, nanoscale information on the dots and their surroundings is required. However, the analysis of embedded QDs is challenging. The CdSe/ZnSe QDs have been already analyzed by transmission electron microscopy (TEM) giving a first estimation of the average chemical composition of intermixing between CdSe and ZnSe layers. The key strength of TEM is that it can directly visualize the atomic structure of a material, a recent approach aimed at a direct compositional analysis of CdSe quantum dots using high resolution TEM (HRTEM). However, such TEM techniques are still essentially two-dimensional. However, the Atom Probe Tomography (APT) is a technique able to give more information about the chemical composition at atomic scale in 3-D of all elements in the material.

In this work, we report for the first time the chemical composition analysis by APT of Cd<sub>x</sub>Zn<sub>1-x</sub>Se QDs embedded in ZnSe on (001) GaAs substrate. The sample was grown by molecular beam epitaxy (MBE). First, 60 nm thick ZnSe buffer layer was grown at 280°C on a (100) GaAs substrate. Then 3 monolayers (MLs) of CdSe were deposited on the ZnSe layer by Atomic layer Epitaxy (at 280°C). To induce the 2D–3D transition of the strained CdSe layer, amorphous selenium were first deposited at low temperature (10°C) and then desorbed by heating up to 240°C where spotty 3D RHEED (reflection high-energy electron diffraction) patterns appear and typically indicate QD formation. Finally, the CdSe QD layer was capped with ZnSe layer (2 min at 240°C then 5 min at 280°C).

The APT analysis shows the presence of several Cd-rich regions attributed to QDs with Cd content ranging from 0.39 to 0.65 surround by poor Cd region ( $x = 0.26 \pm 0.04$ ) and an average Cd content of 0.37 in the Cd<sub>x</sub>Zn<sub>1-x</sub>Se wetting layer. In addition, Cd concentrations measured by TEM are similar to the 15-nm-in-depth profile. Due to its ability of 3D local chemical analysis, APT provides more accurate size and Cd concentration within the QDs, which is indeed higher than the Cd concentration deduced by TEM. The QDs have an average surface of  $5 \times 5 \text{ nm}^2$  and a height of  $3.5 \pm 0.3 \text{ nm}$ . This study has revealed the variability of dot size and shape, the complexity of their chemistry, and a strong intermixing between the Cd and the Zn in the quantum dots. The comparison between the PL emission energy and the calculation of the transition energies including excitonic and strain effects shows that the PL measurements and the APT study are quantitatively consistent.

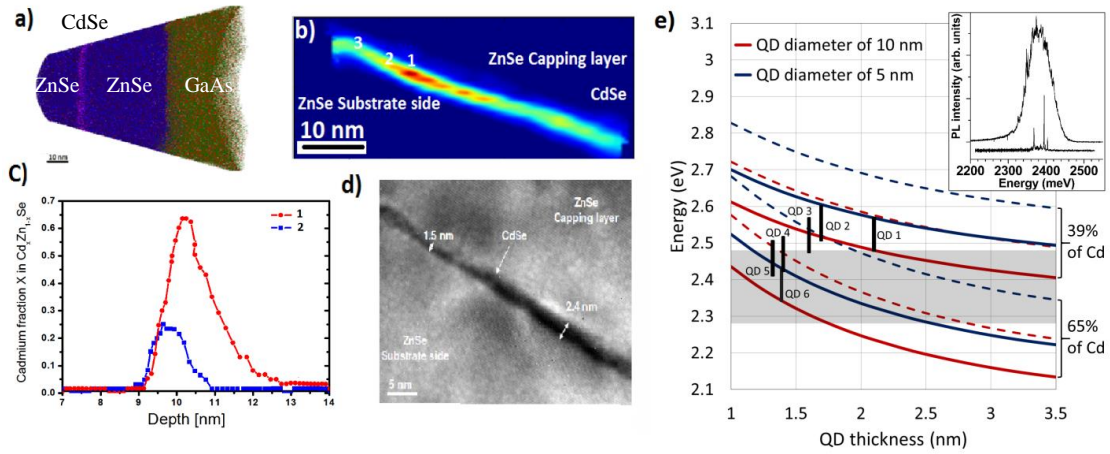


Figure 1: **a)** 3D APT volume **b)** 2D map concentration obtained from 3 nm slice through the CdZnSe layer along the growth direction. **c)** 1D Cd composition profiles from two different regions in the CdZnSe layer using a 3 nm diameter cylinder; Profile 1 corresponds to Cd rich (QDs) region and profile 2 corresponds to cadmium-poor region (wetting layer). **d)** TEM image for the CdSe QDs. **e)** PL transition energies as a function of the QD thickness. Two sets of four curves are displayed; the higher set corresponds to a Cd concentration of 39% and the lower set to 65% of Cd. Solid (dashed) curves are the transition energies with (without) excitonic and strain effects. Blue (red) curve is the transition energies for QD diameter of 5 nm (10 nm). Within the 5-10 nm diameters, the expected transition energies are represented by vertical black rectangles for each QD whose thickness and composition has been measured by APT. The inset shows the PL spectra of an ensemble of QDs, and of a few QDs PL measured on a mesa of about 100 nm lateral sizes. The PL energy distribution is displayed by the shaded area in the figure.

## Peculiarities of CdS Nanocrystals Formation at Annealing of a Langmuir-Blodgett Matrix

Svit K, Protasov D, Teys S, Sveshnikova L, Yakushev M, and Zhuravlev K.  
Rzhanov Institute of Semiconductor Physics, Novosibirsk, Russia

Semiconductor nanocrystals (NC) are promising materials for novel optical and electronic devices due to their properties different from the bulk material. II-IV compound NC are very attractive materials for development and fabrication of photosensitive and photovoltaic devices, lasers, sensors, displays and solar cells [1].

Among the ways of NC preparation a chemical approach occupies a special place due to its cheapness and low labor costs. The chemical approach [2] includes a colloidal synthesis and a Langmuir-Blodgett (LB) technique [3] used in this work. The LB technique is one of the most promising methods for synthesizing PbS, CdS and ZnS NC.

In this work arrays of CdS NC obtained using the LB technique on a highly ordered pyrolytic graphite (HOPG) substrate were investigated using atomic force microscopy (AFM) method and scanning tunneling microscopy (STM) and spectroscopy (STS) methods. The cadmium chloride solution was used as a liquid sub-phase. Monolayers of cadmium behenate ( $\text{CdBh}_2$ ) were transferred from the surface of liquid sub-phase on highly ordered pyrolytic graphite (HOPG) substrate. CdS NC were formed in the solid behenate acid matrix by sulphidizing of the  $\text{CdBh}_2$  films in  $\text{H}_2\text{S}$  ambient. Removal of the matrix was carried out by evaporation of the LB film matrix at temperature of about 200 °C in ammonia atmosphere. To study the process of NC assembly, the density of NC in the initial film was varied systematically by increasing the number of monolayers (MLs) from 1 to 20 ML.

AFM and STM data showed that at a small LB ML number from 1 to 2 ML individually standing NC are formed on the substrate. When increasing ML number from 3 to 8 NC began to self-organize into arrays with ribbon-like structure due to diffusion limited aggregation and from 10 ML sub-monolayer NC film arises. It was found that only a small part of CdS molecules form into NC by diffusion along the plane of LB layers and with an increase of the ML number, the interlayer diffusion arises that leads to almost full binding of CdS molecules into NC. By analyzing occurrences of small arrays, pair bond energy of NC was found to be about 48meV.

STS investigation indicated the presence of high density of intra-band states in NC located near the arrays edges. It was found that a distance from the array edge at which the unusual NC can be met reaches several tens of nanometers, however, some clusters do not contain the unusual NC. A defect-induced gap states model was used to explain this feature. Spatial distribution of unusual NC was explained by peculiarities of the LB matrix evaporation.

- [1] Hullavard N, Hullavard S, Karulkar P, J. Nanosci. Nanotechnol. **8**, 3272, (2008).
- [2] Hu H, Kung S, Yang L, Nicho M, Penner R, Sol. Energy Mater. Sol. Cells **93**, 51, (2009)
- [3] Bagaev E, Zhuravlev K, Sveshnikova L, Badmaeva I, Repinskii S, Voelskow M, Semiconductros **37**, 1321, (2003).

## Cu<sub>2</sub>ZnSnSe<sub>4</sub> thin film grown by molecular beam epitaxy on GaAs

Y. Curé<sup>1,2</sup>, V. Reita<sup>1,3</sup>, S. Pouget<sup>1,2</sup>, C. Bougerol<sup>1,3</sup>, E. Robin<sup>1,2</sup> and H. Boukari<sup>1,3,\*</sup>

<sup>1</sup>Univ. Grenoble Alpes, Grenoble, France

<sup>2</sup>CEA, INAC-SP2M, Grenoble, France

<sup>3</sup>CNRS, Institut Néel, Grenoble, France

\* herve.boukari@neel.cnrs.fr

Cu<sub>2</sub>ZnSn(S,Se)<sub>4</sub> is an attracting compound because of its potential to be used as an absorber in high efficient, low cost, thin film solar cells. The absorption coefficient is around  $4 \cdot 10^4 \text{ cm}^{-1}$  with a tunable band gap in the 1-1,5~eV range depending on the S/Se ratio. This is suited for an optimum photovoltaic conversion with a single junction solar cell. The advantages over existing materials used in thin film solar cells is that all the constituents of this material are non toxic and abundant in the earth crust. The record conversion efficiencies are 8.4% for Cu<sub>2</sub>ZnSnS<sub>4</sub> [1], 9.7% for Cu<sub>2</sub>ZnSnSe<sub>4</sub> [2], and 12,6% for Cu<sub>2</sub>ZnSn(S,Se)<sub>4</sub> [1]. The record efficiencies do not increase as fast as expected and are still too small to think of a possible transfer of such solar cells to the research and development stage.

Our goal is to fabricate monocrystalline Cu<sub>2</sub>ZnSnSe<sub>4</sub> thin layers to set the intrinsic properties of this compound and investigate the impact of the defects on the electronic properties. So far, only one group has reported data on such an approach for Cu<sub>2</sub>ZnSnSe<sub>4</sub> [4].

Here we report on Cu<sub>2</sub>ZnSnSe<sub>4</sub> layers that were grown by molecular beam epitaxy on GaAs(001). We performed simultaneous deposition of Cu, Zn, Sn and Se through 4 effusion cells. In-situ Reflection of High Energy Electron Diffraction (RHEED) has widely been used to set the growth conditions. The layers were then characterized by Scanning Electron (SEM) and Transmission Electron Microscopy (TEM), Energy Dispersive Spectroscopy (EDS), Fourier Transform Infrared (FTIR) and Raman spectroscopy, X-ray diffraction, and photoluminescence (PL). We show that epitaxial films are oriented with the c-axis of Cu<sub>2</sub>ZnSnSe<sub>4</sub> being along the growing direction. The 500nm to 1000nm thick layers are almost fully relaxed and the band gap of our 'best' layer, as extracted from FTIR, is 0,95 eV. The best layers were obtained for a growth at 460°C in a large excess of Selenium. The presence of secondary phases will be discussed in correlation with the growth parameters.

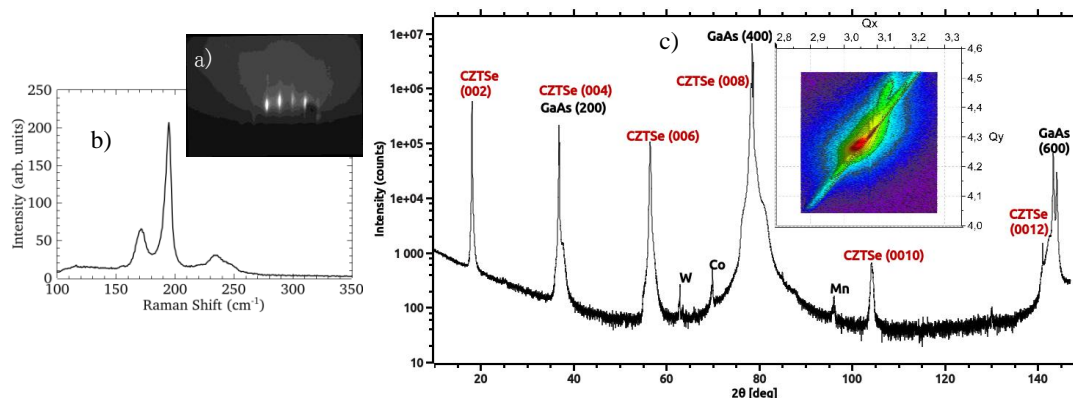


Figure 1: a) RHEED diffraction pattern at the surface of a 1 μm thick Cu<sub>2</sub>ZnSnSe<sub>4</sub> layer grown by MBE on GaAs(001). b) corresponding Raman spectrum and c) X-ray diffraction:  $\theta$ -2 $\theta$  scan and reciprocal space map of Cu<sub>2</sub>ZnSnSe<sub>4</sub>(228) and GaAs(224) reflections.

[1] B. Shin et al., Progress in Photovoltaics: research and Application **21**, 72, (2013)

[2] G. Brammertz et al., Applied Physics Letters **103**, 163904, (2013)

[3] W. Wang et al., Advanced Energy Materials **4**, 1301465, (2014)

[4] A. Redinger et al., Photovoltaic Specialists Conference (PVSC), 2013 IEEE **39th**, 0420, (2013)

## Synthesis and characterization of CuZnSe<sub>2</sub> thin film structures

H.H. Güllü<sup>1,2</sup>, Ö. Bayraklı<sup>1,2</sup> and, M. Parlak<sup>1,2</sup>

<sup>1</sup>*Department of Physics, Middle East Technical University (METU), Ankara 06800, Turkey*

<sup>2</sup>*Center for Solar Energy Research and Applications (GÜNAM), METU, Ankara 06800, Turkey*

Currently, applications of thin film solar cells are concentrated on the CuInSe<sub>2</sub> and Cu(In,Ga)Se<sub>2</sub> chalcopyrite hetero-junctions. These structures have been extensively studied because of their thin film properties, especially their absorption characteristics. On the other hand, with new and better technologies and increasing demand for the cheap photovoltaic devices these structures start to be out of interest. Because of containing rare earth elements, In and Ga, these two types of solar cells cannot meet the future development of solar cells [1]. Therefore, in the case of Zn and Sn usage attracts significant interest as an alternative material for these rare elements in the well-known chalcopyrite structures. In this work, CuZnSe<sub>2</sub> ternary chalcopyrite structure has been studied with the Cu and Zn in the ratio 1:1 to form this new combination. In fact, the motivation has been developed on the CuInSe<sub>2</sub>-like chalcopyrite system in which In is replaced by Zn and also as the important constituents in Cu<sub>2</sub>ZnSn(S,Se)<sub>4</sub> material, CuZnSe<sub>2</sub> has not been well understood in material properties [2-4]. Thus, this structure was thermally deposited on commercial soda-lime glass substrates by using Cu, Se and ZnSe evaporation sources in a stacked layer form. During the deposition, the substrate temperature was kept at 200°C and the vacuum was controlled at about 10<sup>-6</sup> Torr. The deposited thin films were analyzed under the effect of thermal annealing in the temperature interval of 300-500°C. The as-grown and annealed films were showed the polycrystalline structure with the preferred orientation along in (112) direction [4]. The compositional analysis of the films showed that there was a slight change in the elemental contribution to the structure with annealing process. In the visible and near-visible region, the absorption coefficient of the as-grown and annealed samples was in between 10<sup>3</sup> and 10<sup>4</sup> and the band gap values of the samples calculated from transmission data were about 2.6 eV. In addition, the room temperature resistance values were measured in the order of 10<sup>7</sup> Ω and the temperature dependent dark conductivity values showed Arrhenius behavior. Furthermore, a slight response in the conductivity of the samples was determined in the low temperature regions.

### References

- [1] S.R. Kodigala, "Thin Film Solar Cells from Earth Abundant Materials" (Elsevier, USA, 2014)
- [2] D.P. Joseph and C. Venkateswaran, "Room temperature ferromagnetism in Cr doped chalcopyrite type Cu-Zn-Se compound", *Physica Status Solidi A* 207, 2549-2552 (2010)
- [3] D.P. Joseph, S. Ganesan, M. Kovendhan, S.A. Suthanthiraraj, P. Maruthamuthu and C. Venkateswaran, "Fabrication of dye sensitized solar cell using Cr doped Cu-Zn-Se type chalcopyrite thin film", *Physica Status Solidi A* 208, 2215-2219 (2011)
- [4] T.M. Chen, S.M. Lan, W.Y. Uen, T.N. Yang, K.J. Chang, C.C. Shen, C.F. Hsu and J.C. Jhao, "Fabrication of Cu<sub>3</sub>Zn<sub>3</sub>Se ternary compounds by AP-MOCVD", *Journal of Crystal Growth* 381, 144-147 (2013)

## Fabrication of $\beta$ -CuGaO<sub>2</sub> Thin Films

I. Suzuki<sup>1</sup>, H. Nagatani<sup>1</sup>, M. Kita<sup>2</sup>, T. Omata<sup>1,\*</sup>

<sup>1</sup>Graduate School of Engineering, Osaka University, Suita, Japan

<sup>2</sup>Toyama National College of Technology, Toyama, Japan

\* omata@mat.eng.osaka-u.ac.jp

$\beta$ -CuGaO<sub>2</sub> is one of the oxide semiconductors that possess the wurtzite-derived structure. It shows the interesting properties of direct and 1.47 eV of band gap and p-type electrical conduction. These properties enable to use  $\beta$ -CuGaO<sub>2</sub> as a thin-film solar cell absorber. In order to study the optical and electrical properties  $\beta$ -CuGaO<sub>2</sub> in detail and develop devices using this material, it is very important to study fabrication of the thin-films of  $\beta$ -CuGaO<sub>2</sub>. In our previous studies on  $\beta$ -CuGaO<sub>2</sub>,  $\beta$ -CuGaO<sub>2</sub> powder was synthesized by ion-exchange of Na<sup>+</sup> ions in the precursor  $\beta$ -NaGaO<sub>2</sub> with Cu<sup>+</sup> ions in CuCl [1]. In this study, we tried to fabricate  $\beta$ -CuGaO<sub>2</sub> films by ion-exchange of  $\beta$ -NaGaO<sub>2</sub> films.

$\beta$ -NaGaO<sub>2</sub> films were prepared by conventional rf-magnetron sputtering. The obtained films were placed on the CuCl pellet and heated at 300°C in a vacuum furnace for 6h. The films obtained were washed with acetonitrile and methanol to remove the residual CuCl and by-product NaCl, respectively.

Figs. 1 (a) and (b) show XRD patterns of  $\beta$ -NaGaO<sub>2</sub> film and the film after ion-exchange. The diffractions appeared in the film after ion-exchange can be indexed as those of orthorhombic system similar to the precursor film; however, diffraction angles of the films after ion-exchange are obviously larger than those of the film before ion-exchange and agree with those of  $\beta$ -CuGaO<sub>2</sub>. This indicates that the film transforms from  $\beta$ -NaGaO<sub>2</sub> into  $\beta$ -CuGaO<sub>2</sub> by the ion-exchange. The intensities ratios of respective diffractions are quite different from those of  $\beta$ -CuGaO<sub>2</sub> powder (Fig. 1 (c)), and are very close to those of the precursor  $\beta$ -NaGaO<sub>2</sub> film. This implies that the orientation of the precursor film is remained in the  $\beta$ -CuGaO<sub>2</sub> film.

Fig. 2 shows Tauc's plot of  $\beta$ -CuGaO<sub>2</sub> film. The optical band gap is determined to be ~1.45 eV; this value well agrees with that obtained from the powdered sample (1.47 eV). We will report fabrication of p/n-junction between  $\beta$ -CuGaO<sub>2</sub> and ZnO on the poster.

- [1] T. Omata, H. Nagatani, I. Suzuki, M. Kita, H. Yanagi, N. Ohashi, *J. Am. Chem. Soc.* **136**, 3378, (2014)

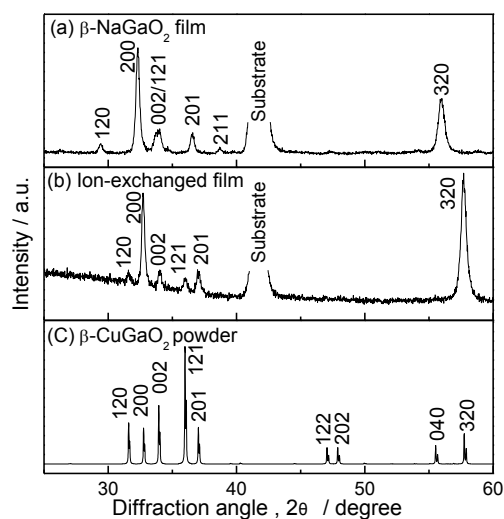


Fig.1 XRD patterns of (top) precursor  $\beta$ -NaGaO<sub>2</sub> film, (middle) ion-exchanged film and (bottom)  $\beta$ -CuGaO<sub>2</sub> powder.

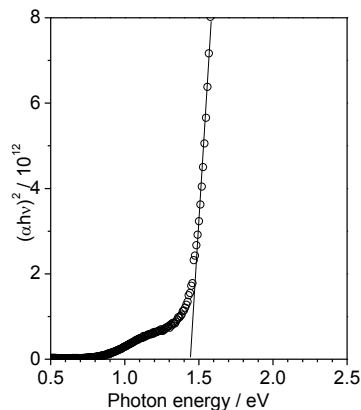


Fig.2 Tauc's plot of  $\beta$ -CuGaO<sub>2</sub> film.

## The electrical parameters of $\text{Hg}_{1-x}\text{Cd}_x\text{Te}$ epitaxial films with and without CdTe passivation layers

N. Mikhailov, S. Dvoretzky, V. Remesnik, Yu. Sidorov, V. Varavin  
Rzhanov Institute of Semiconductor Physics SB RAS, Novosibirsk, Russia  
mikhailov@isp.nsc.ru

The surface passivation of IR detectors based on  $\text{Cd}_x\text{Hg}_{1-x}\text{Te}$  by graded wide-gap or CdTe layers has been used.

MCT heteroepitaxial structures (HS) and CdTe layers on the surface was grown on (013) GaAs substrate using UHV "Ob-M" set with ellipsometric control of the composition and thickness in situ. The absorber layer has MCT composition of  $X_{\text{CdTe}} = 0,20 \div 0,23$  and thickness of  $6 \div 8 \mu\text{m}$  with graded wide-gap layers thickness of  $0.5 \div 1.5 \mu\text{m}$  at the interface of CdTe/ZnTe /GaAs substrate and at the HS surface.

After exposition in the growth chamber in mercury atmosphere the electron concentration, mobility and lifetime of minority carriers as grown MCT HS without CdTe layer were  $(2 \div 5) \times 10^{14} \text{ cm}^{-3}$ , more  $8 \times 10^4 \text{ cm}^2\text{V/s}$  and  $5 \div 8 \mu\text{s}$  at 80 K, respectively.

The exposition time was influenced on the electrical parameters of MCT HS. The decreasing of exposition time leads to decreasing in the electron density and lifetime of minority carriers of MCT HS.

The CdTe layer growth on the surface of MCT HS without stopping of the process leads to decreasing in the electron concentration up by 5-8 times lower. The lifetime of minority carriers were reduced by more than order of magnitude. Thermal annealing of electron conductivity MCT HS with CdTe layer in mercury atmosphere did not converted into hole conductivity type.

After the chemical removing of CdTe layer and the following thermal annealing of MCT HS in mercury atmosphere the electron concentration and the lifetime of minority carriers were became the same as the parameters of MCT HS after the growth and exposition in mercury atmosphere in the growth chamber. The electron concentration and mobility were  $(2 \div 5) \times 10^{14} \text{ cm}^{-3}$  and  $(2 \div 5) \times 10^4 \text{ cm}^2\text{V/s}$  and  $4 \div 10 \mu\text{s}$  at 80 K, respectively.

The experimental results shown that CdTe layer on the surface of MC HS MBE creates a barrier to the mercury diffusion in and from the volume of MCT absorber.

## Electrical and optical studies of a tellurium-related defect in molecular-beam epitaxy-grown HgCdTe

Yakushev M V<sup>1</sup>, Izhnin I I<sup>2,3</sup>, Świątek Z<sup>4</sup>, Ozga P<sup>4</sup>, Mynbaev K D<sup>5,6\*</sup>, Varavin V S<sup>1</sup>, Marin D V<sup>1</sup>,  
Mikhailov N N<sup>1</sup>, Dvoretzky S A<sup>1,3</sup>, Voitsekhovski A V<sup>3</sup>, Savytsky H V<sup>7</sup>, Bonchyk O Yu<sup>7</sup>

<sup>1</sup>Rzhanov Institute of Semiconductor Physics, Novosibirsk, Russia

<sup>2</sup>R&D Institute for Materials SRC “Carat”, Lviv, Ukraine

<sup>3</sup>National Research Tomsk State University, Tomsk, Russia

<sup>4</sup>Institute of Metallurgy and Material Science PAN, Krakow, Poland

<sup>5</sup>Ioffe Institute, Saint-Petersburg, Russia

<sup>6</sup>ITMO University, Saint-Petersburg, Russia

<sup>7</sup>Institute for Applied Problems of Mechanics and Mathematics NASU, Lviv, Ukraine

\*mynkad@mail.ioffe.ru

Molecular-beam epitaxy (MBE) has become the growth method of choice in the technology of HgCdTe (MCT), one of the main materials for infrared photodetectors. MBE allows for growing various types of structures with maximum flexibility in relation to chemical composition and thickness of the epitaxial films. The grown layers, however, are not free from defects, and while some of them seem to be typical of HgCdTe irrespective of the growth technique, other clearly depend on the specific technology. Reducing the concentration of defects is crucial for advancing parameters of photodetectors.

In this paper, we present the results of electrical and optical studies of tellurium-related defects in MCT films grown by MBE on GaAs and Si substrates. The existence of a specific type of neutral Te-related defects in MBE MCT was first reported on in 2007 [1], and since then has been a subject of controversy. The problem is that the electrical neutrality of the defects does not allow for detecting them with electrical measurements. After certain types of post-growth treatment such as ion-milling, however, the defects get electrically activated, which results in formation of donor-type centers with concentration up to  $10^{17}$  cm<sup>-3</sup>. A clear dependence of the concentration of the centers on the substrate temperature [2] allowed for relating their formation to growth conditions. Within the frames of the current work, we advanced these studies by investigating these defects in MCT doped with arsenic under different doping conditions and relating the results of these studies to those performed with Raman spectroscopy. The latter method was shown earlier to be capable of detecting tellurium nano-inclusions in MCT grown with liquid-phase epitaxy [3].

As a result of the studies, it was established that the concentration of the donor-type centers strongly depended on the form, in which arsenic was arriving to the surface of the growing film. Under doping with low-temperature cracking, arsenic arrived to the surface as As<sub>4</sub> and did not interact with tellurium, resulting in high concentration of the tellurium-related centers. With high-temperature cracking, most of the arsenic was incorporating in as-grown MCT in a donor-like form, which happened because As<sub>2</sub> interacted with tellurium producing donor complexes related to As<sub>2</sub>Te<sub>3</sub>. This reduced the concentration of centers related to pure tellurium. Generally, the ratio between the concentration of neutral (Te) and charged (As<sub>2</sub>Te<sub>3</sub>) complexes depended on the growth conditions (As<sub>4</sub> and As<sub>2</sub> fluxes). In our research, the results of the electrical studies are compared to those of Raman spectroscopy performed on MBE-grown films.

This work was supported by the Ministry of Education of the Russian Federation (Grant RFMEFI60414X0134).

- [1] Izhnin I I, Dvoretzky S A, Mikhailov N N, Sidorov Yu G *et al*, Appl. Phys. Lett., **91**, 132106 (2007)
- [2] Pociask M, Izhnin I I, Izhnin A I, Dvoretzky S A *et al*, Semicond. Sci. Technol., **24**, 025031 (2009)
- [3] Belogorokhov A I, Smirnova N A, Denisov I A *et al*, Phys. Stat. Sol. (c), **7**, 1624 (2010)

## Acceptor states in HgCdTe films grown by molecular-beam epitaxy on GaAs and Si substrates

Yakushev M V<sup>1</sup>, Mynbaev K D<sup>2,3\*</sup>, Bazhenov N L<sup>2</sup>, Varavin V S<sup>1</sup>, Mikhailov N N<sup>1</sup>,  
Marin D V<sup>1</sup>, Dvoretzky S A<sup>1</sup>, Sidorov Yu G<sup>1</sup>

<sup>1</sup>Rzhanov Institute of Semiconductor Physics, Novosibirsk, Russia

<sup>2</sup>Ioffe Institute, Saint-Petersburg, Russia

<sup>3</sup>ITMO University, Saint-Petersburg, Russia

\*mynkad@mail.ioffe.ru

Epitaxial films of HgCdTe (MCT), one of the main materials of infrared photo-electronics, are increasingly frequently grown on foreign substrates “alternative” to conventional Cd(Zn)Te substrates. Among the former, GaAs and Si substrates are the most popular. The technique for MCT growth on GaAs and Si (MCT/GaAs and MCT/Si) employs the advantage of the comparatively low cost of large-diameter GaAs and Si wafers, though the density of defects in the grown films remains an issue.

Recently, the focus of MCT/GaAs and MCT/Si technology has shifted from the simple analysis of dislocation density towards in-depth studies of point defects and their effect on the properties of the material. These defects, among other things, affect carrier lifetime, which in many cases limits the performance of MCT-based photodetectors. Our research has been focused on acceptor states in MCT films grown on GaAs and Si as revealed by photoluminescence (PL) and carrier lifetime measurements. The structures were grown by molecular-beam epitaxy and subjected to two types of post-growth anneals. The first one included a single high-temperature step and was used to convert the as-grown *n*-type films to *p*-type conductivity via generation of mercury vacancies, which are acceptors in MCT. The second type of anneal included both a similar high-temperature step and a low-temperature one under saturated mercury pressure.

It appeared that our as-grown MCT/GaAs films were mostly free of acceptor states. However, such states with energy of 18 and 27 meV could be generated in these films under certain growth and post-growth processing conditions associated with mercury deficiency. The first of these centers was related to a complex of defects, which could be destroyed by annealing, and the second, to a point defect constituting the complex. The key role in the formation of the complex was shown to be played by a mercury vacancy. It is of importance that the formation of the acceptor states was determined by specific features of the MBE growth conditions rather than by the chemical composition of the substrate. This was confirmed by observing similar states in some of MCT/Si films. At the same time, in MCT/Si films PL revealed an uncontrolled doping of the material. This doping caused generation of both shallow (energy depth ~10 meV) and deep (40 to 60 meV) acceptor levels.

The presence of specific states in the PL spectra was accompanied by certain features observed in the temperature dependencies of the carrier lifetime, where both the value of lifetime and the shape of the dependence indicated presence of centers of the Shockley-Read recombination. The two-step annealing significantly reduced the concentration of these centers. Thus, the results obtained in the study showed a clear relation of the PL data to those of the lifetime measurements. The lifetime data can be used together with the PL data for identification of defects in order to improve the technology and eliminate these defects completely, and also, for revealing the role of mercury vacancies and their complexes in MCT, which is a topic of the current interest [1].

This work was supported by the Ministry of Education of the Russian Federation (Grant RFMEFI60414X0134).

[1] Gemain F, Robin I C, De Vita M, Brochen S and Lusson A, Appl. Phys. Lett., **98**, 131901, (2011)

## Admittance of MIS-structures Based on Graded-Gap MBE HgCdTe with Al<sub>2</sub>O<sub>3</sub> Insulator

A. V. Voitsekhovskii<sup>1,2\*</sup>, S. N. Nesmelov<sup>1</sup>, S. M. Dzyadukh<sup>1</sup>, V. V. Vasil'ev<sup>3</sup>, V. S. Varavin<sup>3</sup>,  
S. A. Dvoret'skii<sup>3</sup>, N. N. Mikhailov<sup>3</sup>, M. V. Yakushev<sup>3</sup>, G. Yu. Sidorov<sup>3</sup>

<sup>1</sup>Siberian Physical-Technical Institute of the Tomsk State University, Tomsk, Russia

<sup>2</sup>Department of Radio Physics, National Research Tomsk State University, Tomsk, Russia

<sup>3</sup>Institute of Semiconductor Physics SB RAS, Novosibirsk, Russia

\*vav43@mail.tsu.ru

The narrow-band Hg<sub>1-x</sub>Cd<sub>x</sub>Te solid solution is widely used for manufacturing highly-sensitive infrared detectors operating in the spectral atmospheric transparency windows of 3–5 and 8–14 μm [1-3]. A new stage in the use of HgCdTe is associated with the development of epitaxial methods of growing of this material. The method of molecular-beam epitaxy (MBE) provides the possibility of growing HgCdTe films with a given thickness distribution of the CdTe content (x), which is used to optimize the performance of infrared detectors [4,5]. The aim of this work is an experimental investigation of the admittance of MIS structures based on graded-gap MBE n(p)-Hg<sub>x</sub>Cd<sub>1-x</sub>Te (x=0.22) with Al<sub>2</sub>O<sub>3</sub> insulator in a wide temperature range (8–150 K) and an analysis of the results.

Metal–insulator–semiconductor structures based on n(p)-Hg<sub>1-x</sub>Cd<sub>x</sub>Te (x=0.22) were grown by molecular-beam epitaxy on the GaAs (013) substrates. Near-surface graded-gap layers with high CdTe content were formed on both sides of the epitaxial HgCdTe. For all structures, a Al<sub>2</sub>O<sub>3</sub> insulator was created using by plasma enhanced atomic layer deposition technology [6]. Measurements were performed with an automated setup for spectroscopy of the nanoheterostructure admittance based on a non-optical cryostat Janis and an immittance meter Agilent E4980A.

The capacitance-voltage characteristics (CV-characteristics) of the MIS structure based on graded-gap MBE n(p)-HgCdTe were measured at different frequencies of the test signal at temperatures range (8-120) K. Cooling of MIS structures based on MBE HgCdTe (x=0.22) with the graded-gap layers from 77 K to 8 K significantly reduces the frequency of transition to the high-frequency behavior of CV-characteristics. In result the numerical solution of the Poisson equation the ideal CV-curves of MIS-structures were calculated at 77 K and densities of fixed and mobile charges were found. The spectra of the fast surface states on interface between HgCdTe and Al<sub>2</sub>O<sub>3</sub> were investigated by Terman method.

The dependences of the product of the differential resistance of the space charge region and area (R<sub>SCR</sub>A) on the inverse temperature for MIS structures based on MBE n(p)-HgCdTe (x=0.22) were investigated. Most likely that for MIS structures based on n(p)-HgCdTe (x=0.22) with the graded-gap layers, the differential resistance of space charge region is limited by the processes of Shockley-Reed-Hall generation. The value R<sub>SCR</sub>A for MIS structures based on epitaxial HgCdTe is a characteristic of the material and allows you to make a first estimation of the values of the differential resistance diodes of different configurations based on HgCdTe. It is shown that plasma enhanced atomic layer deposition of the Al<sub>2</sub>O<sub>3</sub> insulator provides high-quality passivation of graded-gap MBE HgCdTe.

- [1] Norton P., Opto-Electronics Review **10**, 159 (2002).
- [2] Saxena P.K., Infrared Physics & Technology **54**, 25, (2011).
- [3] Kinch M. A., Journal of Electronic Materials **39**, 1043 (2010).
- [4] Voitsekhovskii A.V., Nesmelov S.N., Dzyadukh S.M., Thin Solid Films **522**, 261 (2012).
- [5] Voitsekhovskii A.V., Nesmelov S.N., Dzyadukh S.M., Thin Solid Films **551**, 92 (2014).
- [6] Fu R., Pattison J., Optical Engineering **51**, 104003 (2012).

## Neutronographic characterization of II-VI cubic crystals highly doped by 3d-ions: on possible tendencies to structure rearrangements in the sphalerite crystal lattice.

Surkova T<sup>1\*</sup>, Maksimov V<sup>1\*</sup>, Dubinin S<sup>1</sup>, and Lopez-Rivera S A<sup>2</sup>

<sup>1</sup>Ural Branch of the RAS, Institute of Metal Physics, Ekaterinburg, Russia

<sup>2</sup>Universidad of de los Andes, Merida5101, Venezuela

\*Tatiana.Surkova@imp.uran.ru, kokailo@rambler.ru

Materials of II-VI compounds doped by magnetically active 3d- ions and known as diluted magnetic semiconductors (DMSs) are attractive for optoelectronics [1] and, possibly, spintronics applications [2]. In the present work  $\text{Zn}_{0.90}\text{Ni}_{0.10}\text{S}$ ,  $\text{Zn}_{0.90}\text{V}_{0.10}\text{Se}$  and  $\text{Zn}_{0.95}\text{Fe}_{0.05}\text{Se}$  single crystals were studied by neutron diffraction at  $T=300$  K in detail. Evidence of emergent pre-transition state of  $\text{FCC} \leftrightarrow \text{HCP}$  concentration transition is found by the total scanning of irreducible elements of reciprocal lattice for all investigated samples. The revealed superstructure reflections (an example is represented by fig 1) correspond with the wave vectors  $q=(1/3 \ 1/3 \ 1/3) 2\pi/a_c$  ( $a_c$  – the cubic lattice parameter), and their appearance is caused by correlated shear atomic displacements. Scanned in the vicinity of the strongest Bragg reflections of investigated crystals the neutron diffuse scattering pictures joined with neutronographic results regarded to II-VI crystals doped by extremely small content of 3d-impurity ([3] and refs therein) indicate on impurity-amount-dependent evolution in the subsystem of nanoscale regions of inhomogeneous distortions induced by 3d-ions incorporated in the sphalerite lattice. Such a complicated structure state determines a non-uniform deformation field supporting possibilities to form long-wave superstructures.

Cooperative lattice reaction arising from disturbances produced by foreign 3d-ions is under discussion. The obtained results may shed light on possible mechanisms of phase dissociations at high-level doping in II-VI DMSs based on 3d-ions.

The work was done at IVV-2M Neutron Material Science Complex within IMP Program “Potok” № 01201463334 with the partial support by the Program “Basic problems of material science and electrophysics” of the Ural Division of the RAS (project № 15-17-2-32).

- [1] Godlewski M, Guziewicz E, Kopalko K, Lusakowska E, Dynowska E, Godlewski M M, Goldys E M and Phillips M R, *J. Luminesc.* **102**, 455 (2003).
- [2] Dietl T, *Nature Materials* **9**, 965 (2010).
- [3] Maksimov V I, Dubinin S F, and Parkhomenko V D, *J. Surface Investigation* **7**, 105 (2013).

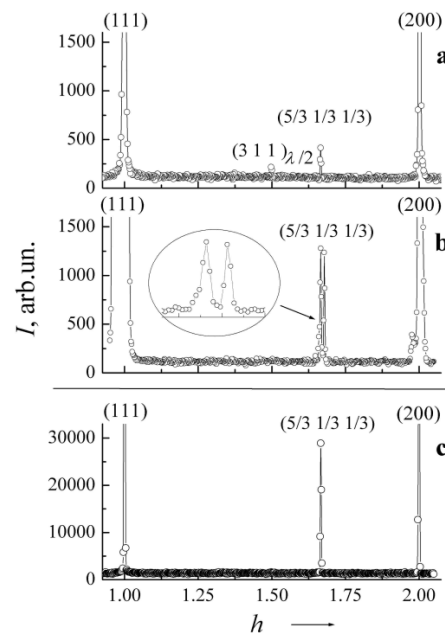


Fig.1. Neutron diffraction scans measured between (111) and (200) knots of reciprocal lattice of (0 1 1) plane of  $\text{Zn}_{0.90}\text{Ni}_{0.10}\text{S}$  (a),  $\text{Zn}_{0.90}\text{V}_{0.10}\text{Se}$  (b) and  $\text{Zn}_{0.95}\text{Fe}_{0.05}\text{Se}$  (c) crystals at 300K. Inset on the (b) panel illustrates splitting of the superstructure reflection.

## MBE Grown CdTe Absorber Layers on GaAs with In Assisted Thermal Deoxidation

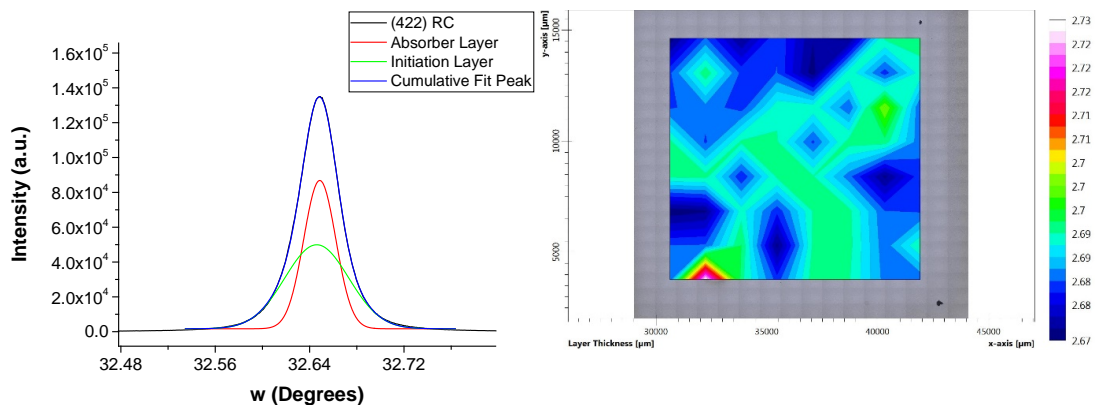
Ozan Ari<sup>1</sup>, Mustafa Polat<sup>1</sup>, Yusuf Selamet<sup>1</sup>

<sup>1</sup>Department of Physics, Izmir Institute of Technology, Izmir, Turkey,

Molecular Beam Epitaxy (MBE) grown single crystal CdTe absorbers have great potential for highly efficient solar cell devices[1]. CdTe absorber layers are considered to be less affected from the structural defects than the III-V absorber layers[1]. Dominant covalent bond characteristic between the III-V atoms makes III-V absorber layers more vulnerable to the structural defects for solar cell applications[2]. Recently, efficiency of the polycrystalline CdTe based polycrystalline PV solar cell has reached 21.0 % [3]. However this value is still far from theoretical maximum. Polycrystalline CdTe based PV solar cells suffer from the poor crystal quality of the CdTe absorber layer which leads to low open circuit voltages ( $V_{oc}$ )[1]. On the other hand, MBE grown CdTe absorber layers on GaAs substrates have potential to overcome structural defects related efficiency problems.

Thermal deoxidation of the GaAs wafers prior to the growth has important effect on the epitaxial grown layer.  $Ga_2O_3$  desorption creates surface pits with 50 to 200 nm size and 5 to 40 nm depth on the GaAs surface which may reduce the interface and overall layer quality of the CdTe absorbers. In order to overcome this problem, we have employed In assisted thermal deoxidation at lower surface temperatures than the usual As assisted thermal deoxidation temperatures. It has been reported that In atoms reacts to non-volatile  $Ga_2O_3$  molecules more effectively than the Ga atoms hence leaving atomically smooth and non-pit decorated surface[4] with the  $Ga_2O_3 + 4In \rightarrow Ga_2O \uparrow + 2In_2O \uparrow$  reaction.

We have found that As assisted deoxidation creates larger and deeper pits on the surface with respect to the In assisted deoxidation. Also population of the pits related to the missing Ga atoms ( $>50.5$  nm) on the GaAs surface were 15 % and 7 % in the As and In assisted cases, respectively. At the left side of the figure, HR XRD RC of the CdTe(422) reflection is shown. RC peak is deconvoluted into two peaks which they represent initiation and thick absorber layers. RC FWHM of the initiation and absorber layers estimated as 229 and 115 arc-seconds, respectively. At the right side of the figure, thickness map of the CdTe absorber is shown which is calculated from the interference fringes of the transmission map of the sample ( $2.7 \pm 0.03 \mu m$ ).



1. Garland, J. W., Biegala, T., Carmody, M., Gilmore, C. & Sivanathan, S. Next-generation multijunction solar cells: The promise of II-VI materials. *J. Appl. Phys.* **109**, 102425 (2011).
2. Çelebi, C., Ari, O. & Senger, R. Cleavage induced rows of missing atoms on ZnTe (110) surface. *Phys. Rev. B* **87**, 85308 (2013).
3. NREL. [http://www.nrel.gov/ncpv/images/efficiency\\_chart.jpg](http://www.nrel.gov/ncpv/images/efficiency_chart.jpg). (2014). at <[http://www.nrel.gov/ncpv/images/efficiency\\_chart.jpg](http://www.nrel.gov/ncpv/images/efficiency_chart.jpg)>
4. Li, L. H., Linfield, E. H., Sharma, R. & Davies, a. G. In-assisted desorption of native GaAs surface oxides. *Appl. Phys. Lett.* **99**, 061910 (2011).

Table 1. AFM results of the epi-ready and thermally deoxidized (As and In) GaAs wafers.

	Deox. Time (s)	Deox. Temp. (°C)	Peak to Peak (nm)	Roughness (RMS) (nm)	Skewness	Percentages of the Pits		Max. Pit Size (nm)
						35,7 nm (%)	50,5 nm (%)	
Epi-ready	-	-	4,76	0,42	0,229	17	6	61,8
As as. Deox.	245	585	5,12	0,35	-0,082	22	15	71,4
In as. Deox.	210	530	5,61	0,45	-0,068	18	7	71,4

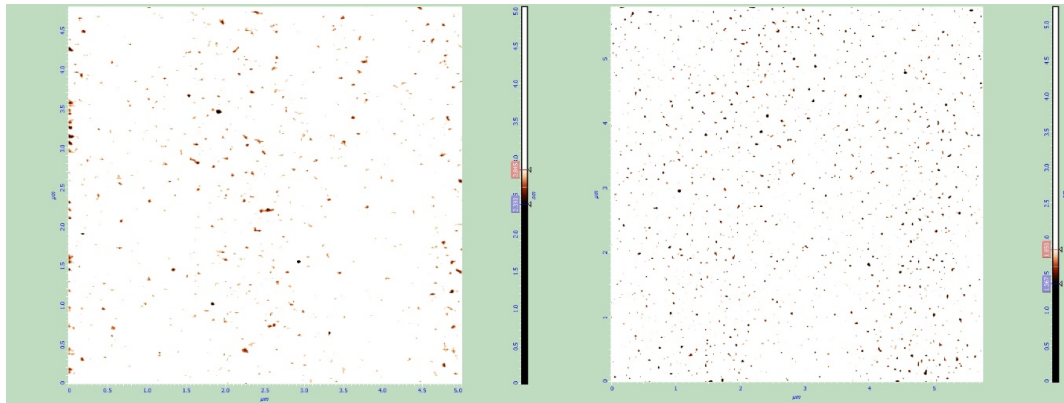


Figure 1. AFM images taken from the thermally deoxidized GaAs wafers with As overpressure (left) and In overpressure (right).

## Traveling Heater Growth and characterization of (Cd, Mn)Te crystals for radiation detectors

Jijun Zhang\*, Linjun Wang, Jiahua Min, Xiaoyan Liang, Lin Wang, Wenqi Wu, and Xuliang Wen

<sup>1</sup>School of Materials science and engineering, Shanghai University, Shanghai, PR China

\*zhangjijun222@shu.edu.cn

(Cd, Mn)Te is a new compound semiconductor for room-temperature X- and  $\gamma$ -ray detector applications, with advantages of large band gap (1.53 ~ 2.54 eV), high average atomic number (~ 50) and high density (5.2 ~ 5.9 g/cm<sup>3</sup>), etc. [1]. The (Cd, Mn)Te detector was demonstrated to be a good candidate to compete with CdTe and (Cd, Zn)Te detectors in nuclear detection applications, such as: nuclear medical, national security, environmental safety, and space science [2]. The CdMnTe crystal is usually grown by the Vertical Bridgman (VB) method [3]. However, the crystal grown by VB method were easy to generate twins, impurities, and inclusions, because of the high growth temperature, low stacking fault energy and solid-state phase transformation [4]. These defects reduce the electrical properties of CdMnTe crystals. Nowadays, the traveling heater method (THM) is demonstrated to be a promising way for growing high quality (Cd, Zn)Te and (Cd, Mn)Te crystals [5]. By THM, crystals can be grown at a lower temperature (800-900 °C) as compared to that of modified VB growth at 1150 °C, which favors to decrease the thermal stress and structural defects. In addition, THM is essentially a zone refine method, and the solvent zone has the purifying effect during the growth, which reduce the foreign impurity in the crystals.

In this paper, the (Cd, Mn)Te crystals were grown by the self-designed THM crystal growth system. The crystal and detector properties, including the Mn composition, Te inclusions, PL spectrum, electrical and energy response properties were characterized. The results showed that the (Cd, Mn)Te crystal grown by the THM had uniform Mn distribution and low impurity concentrations. The size of Te inclusion in the crystal grown by THM was  $\sim 10^4$  cm<sup>-3</sup> with the average diameter of 8 - 12  $\mu$ m. The resistivity were in the range of  $10^9$ - $10^{10}$   $\Omega$ ·cm with the conductivity of weak n-type. PL spectrum measurements revealed that the as-grown (Cd, Mn)Te crystal possessed high crystalline quality. The energy response spectroscopy of (Cd, Mn)Te detector fabricated on the crystals grown by THM was revealed under <sup>241</sup>Am radiation at room temperature. The relationship between the electrical properties and Te inclusions by THM method were discussed.

- [1] R. Rafiei, M. I. Reinhard, K. Kim, D. A. Prokopovich, D. Boardman, A. Sarbutt, G. C. Watt, A. E. Bolotnikov, L. J. Bignell, R. B. James, IEEE Trans. Nucl. Sci. 60, 1450 (2013).
- [2] S. Del Sordo, L. Abbene, E. Caroli, A. M. Mancini, A. Zappettini, P. Ubertini, Sensors 9, 3491 (2009).
- [3] Y. Y. Du, W. Q. Jie, T. Wang, Y. D. Xu, L. Y. Yin, P. F. Yu, G. Q. Zha, J. Cryst. Growth 318, 1062 (2011).
- [4] K. H. Kim, A. E. Bolotnikov, G. S. Camarda, R. Tappero, A. Hossain, Y. Cui, J. Franc, L. Marchini, A. Zappettini, P. Fochuk, G. Yang, R. Gul, R. B. James, IEEE Trans. Nucl. Sci. 59, 1510 (2012).
- [5] G. Wei, L. Wang, J. Zhang, et al., Growth and characterization of indium-doped Cd<sub>1-x</sub>Zn<sub>x</sub>Te crystal by traveling heater method, Nucl. Instrum. Meth. A. 704(2013) 127-130.

## **Dislocations in MCT heteroepitaxial structures on (013) substrates and possibilities of dislocation density reducing.**

Sidorov Y.G., Loshkarev I.D., Sabinina I.V., Trukhanov E.M., Varavin V.S.,  
Yakushev M.V.\*, Kolesnikov A.V.

A.V. Rzhanov Institute of semiconductor physics, SB RAS, Novosibirsk, Russia  
 \*yakushev@isp.nsc.ru

Fabrication of heterostructures with high crystal lattices parameter difference and reducing density of threading dislocations is the major problem of semiconductor material technology. In full, the problem is when HgCdTe (MCT) grown on substrates of gallium arsenide and silicon.

Investigation of the dislocation density dependence on thickness of buffer films CdTe (013) grown on gallium arsenide and silicon, detects different behavior of threading dislocations. In the buffer (013) CdTe films with a thickness of 6-7 microns, the dislocation density, defined as the etch pit density (EPD) reduces to  $10^7 \text{ cm}^{-2}$  for Si substrates and to  $10^6 \text{ cm}^{-2}$  for GaAs substrates. During the deposition of MCT on the cadmium telluride buffer layer the network of misfit dislocations with high density is also formed, despite a slight mismatch of the lattice parameters. As a result, at the interface between the CdTe buffer layer and HgCdTe film the threading dislocation density exceeds  $10^8 \text{ cm}^{-2}$  and with a thickness of 6-8 microns, the EPD reduces to  $10^7 \text{ cm}^{-2}$ .

X-ray data show that the film lattice angle of rotation relative to the substrate is equal to  $1.5^\circ$  for GaAs substrate and to  $4.5^\circ$  for Si one. Between HgCdTe and CdTe layers the rotation is absent. Introduction of misfit dislocations (MDs) in interface (013) is possible in framework of twelve  $\langle 110 \rangle \{ 111 \}$  slip systems. Experimental results are obtained for two of these systems, which form L-shape MDs. These MDs have the same Burgers vectors that alleviate the annihilation of threading dislocations.

Decrease of dislocation density due to the interaction between them may require the introduction or removal of crystal lattice atoms. Optimal conditions are different for input and output processes of various semiconductor compound components. With increasing component activity the probability of component entering into the crystal lattice increases and with decreasing - the probability of component leaving increases. For binary compound the component activities are associated by equilibrium constant  $K = a_{\text{Te}} \cdot a_{\text{Me}}$ , which implies that an increase in activity of one component at a constant temperature leads to a decrease in the activity of the other component. It is impossible to create optimal conditions simultaneously for all processes. Then, apparently, one needs to change the conditions during the heat treatment, in turn creating favorable conditions for the occurrence of different processes.

The most effective process for reducing the density of dislocations may be provided using a cyclic change of the annealing temperature at constant mercury vapor pressure. If for sequence of annealing cycles the temperature of MCT sample varies from 300 to  $500^\circ\text{C}$ , then the ratio  $a_{\text{Te}}/a_{\text{Hg}}$  will change from 0.0027 at  $300^\circ\text{C}$  to the value of 38 at  $500^\circ\text{C}$ , which will ensure conditions for effective input and output of tellurium and mercury atoms. Effectiveness of cyclic annealing has been shown in [1].

The cyclic annealing reduces the dislocation density an order of magnitude in the upper layer of MCT film, which is an active photodiode area. Reduction of the dislocation density is confirmed by X-ray studies. In double crystal diffraction curve the FWHM value of symmetric (026) peak changes from 148 to 91 seconds of arc during cycle annealing. For this case the FWHM value means the integral structure quality of the epitaxial film.

The research was supported by a grant of Ministry of Education of the Russian Federation RFMEFI60414X0134.

[1] S. Farrell, Mulpuri V. Rao, G. Brill, Y. Chen, P. Wijewarnasriya, N. Dhar, D. Benson, and K. Harris, J. Electron. Mater., **40**, 1727, (2011).

## Growth and Characterization of Cd<sub>0.9</sub>Zn<sub>0.1</sub>Te crystal by traveling molten zone method

Jia-hua Min<sup>1</sup>, Xiao-yan Liang<sup>1</sup>\*, Ji-jun Zhang<sup>1</sup>, Lin-jun Wang<sup>1</sup>

<sup>1</sup> School of Materials Science and Engineering, Shanghai University 1, Shanghai, P.R.China  
\* xxllllyy@gmail.com

As the preferred detector for the X-ray and low-energy gamma-ray detection, CdZnTe detector is the only room temperature detector employed under the state of serious shielding by lead or steel. Actually, the breakthrough of CdZnTe crystal preparation is the key to develop new-generation practical CdZnTe nuclear detector. In the recent years travelling heater method (THM) technique has proven to be the most viable technique to grow large-volume and high-resolution CdZnTe crystal.

In present paper, the In doped Cd<sub>0.9</sub>Zn<sub>0.1</sub>Te crystal has been prepared by traveling molten zone method of Te-rich alloy, which is the essence of THM technique, with the growth temperature of 800°C, the temperature gradient of 20°C/cm and the growth rate of 0.4mm/h. The Te inclusions distribution, IR transmittance, Hall characteristics and PICTS of the prepared crystal were analyzed, comparing with that of the CdZnTe crystal grown by vertical Bridgman (VB) method at the temperature of 1115°C. The results showed that the Te inclusions size was larger in the CdZnTe crystal grown by traveling solvent melting zone method, while the concentration and volume fraction of Te inclusions were smaller than that in the CdZnTe crystal by VB method, which contributed to the higher IR transmittance of CdZnTe crystal grown by traveling solvent melting zone method. Moreover, resistivity of CdZnTe crystals grown by traveling solvent melting zone method was one degree accurate higher than that of CdZnTe crystals grown by VB method. The PICTS test indicated that the primary defects concentrations in CdZnTe crystals grown by traveling solvent melting zone method were less than that in CdZnTe crystals grown by VB method.

- [1] Roy U N, Weiler S, Stein J. *Journal of Crystal Growth* **312**, 2840–2845, (2010).
- [2] Chen H, Awadalla S A, Iniewski K, et al. *J. Appl. Phys.* **103**, 014903, (2008).
- [3] Zhang N, Andrew Y, Arnold B, et al. *Journal of Crystal Growth* **325**, 10-19, (2011).
- [4] Wang L J, Sang W B, Shi W M, et al., *Nuclear Instruments and Methods in Physics Research A* **448**, 581-585, (2000).
- [5] Gamal G A, Zied M A, Ebnalwaled A A., *Physica B* **393**, 285–291, (2007).
- [6] Yue W, Katsuaki K, Yuko I, et al., *Journal of Crystal Growth* **284**, 406-411, (2005).
- [7] Komar V, Gektin A, Nalivaiko D., *Nuclear Instruments and Methods in Physics Research A* **458**, 113-122, (2001).
- [8] Zhang X W, Zhao Z L, Zhang P J, et al., *Journal of Crystal Growth* **311**, 286–291, (2009).
- [9] Mark Amman, Julie S. Lee, et al., *Nuclear Science, IEEE Transactions on.* **56**, 795-799, (2009).
- [10] S.A. Awadalla, J. Mackenzie, H. Chen, et al., *Journal of Crystal Growth* **312**, 507-513, (2010).
- [11] M. Fiederle, V. Babentsov, J. Franc, A. Fauler, J.-P. Konrath, *Cryst. Res. Technol.* **38**, 588-597, (2003).

## The local electron interaction with crystal defects in wurtzite CdS

O.P. Malyk <sup>1\*</sup>, V.M. Rodych <sup>2</sup>, G.A. Ilchuk <sup>2</sup>

<sup>a</sup> Semiconductor Electronics Department, Lviv Polytechnic National University, Lviv, Ukraine

<sup>b</sup> Physics Department, Lviv Polytechnic National University, Lviv, Ukraine  
\* omalyk@ukr.net

Usually the charge carrier scattering models in cadmium sulfide are considered in the relaxation time approximation. However, these models have essential shortcomings: a) they contradict the special relativity according to which the charge carrier would interact only with the neighboring crystal region; b) they contradict the atomistic hypothesis according to which the charge carrier interacts (and transfers the energy respectively) only with one atom but not simultaneously with many atoms which are situated in different points of space. From the other hand in [1-3] the short-range models of carrier scattering were proposed for  $A^{II}B^{VI}$  and  $A^{III}B^V$  semiconductors (zinc blende and wurtzite structure) in which the above mentioned shortcomings were absent. The purpose of the present paper is to use of short-range models to describe the electron scattering on the various crystal lattice defects taking into account the complex structure of optical vibrations in wurtzite CdS.

The CdS samples with defect concentration  $5.5 \times 10^{15} \div 2.77 \times 10^{17} \text{ cm}^{-3}$  were investigated. For the charge carrier scattering on the nonpolar optical and acoustic phonons, neutral defects and static strain potential the interaction radius of the short-range potential is limited by one unit cell. For the charge carrier scattering on the ionized impurity, polar optical and piezoelectric (piezoacoustic and piezooptic) phonons the interaction radius of the short-range potential is founded in a form  $R = \gamma \sqrt{3a_0^2 + c_0^2} / 2$  ( $a_0, c_0$  - lattice constants,  $\gamma$  - the respective adjustable parameters). To calculate the conductivity tensor components the method of the exact solution of the stationary Boltzmann equation was used [4].

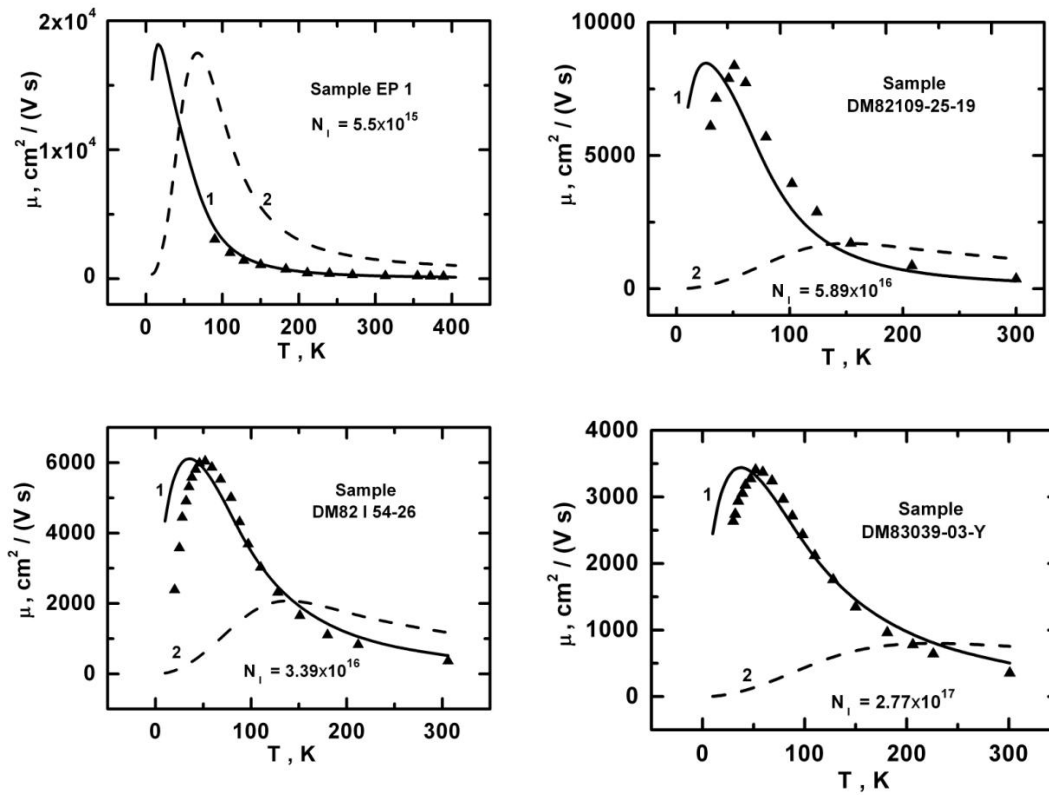
The temperature dependence of the electron mobility in the range  $10 \div 400 \text{ K}$  in wurtzite cadmium sulfide is calculated. The influence of the different scattering mechanisms on the charge carrier mobility is considered. The scattering parameters  $\gamma$  for different scattering modes are determined. The temperature dependence of the electron Hall factor is calculated.

[1] Malyk O.P., Physica B:Condensed Matter. **404**, 5022, (2009).

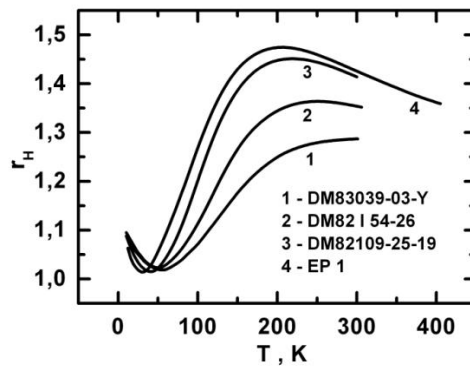
[2] Malyk O.P., Diamond Relat. Mater. **23**, 23, (2012).

[3] Malyk O.P., Can. J. Phys. **92**, 1372, (2014).

[4] Malyk O.P., WSEAS Trans. Math. **3**, 354, (2004).



The temperature dependence of electron mobility in CdS crystals with different impurity concentration. Experiment – [1,2]. Curve 1 – short-range scattering models; curve 2 – relaxation time approximation.



The temperature dependence of Hall factor (electrons) in CdS crystals.

[1] Boone J.L., and Cantwell G., J. Appl. Phys. **57**, 1171, (1985).  
 [2] Podor B., Balazs J., and Harsy M., Phys. Status Solidi A, **8**, 613, (1971).

## Vertical Transport of Photoexcited Carriers in a ZnSe/CdSe Superlattice Grown on an In<sub>0.3</sub>Ga<sub>0.7</sub>As Metamorphic Buffer Layer

E.A. Evropeytsev\*, S.V. Sorokin, G.V. Klimko, S.V. Gronin, I.V. Sedova, K.G. Belyaev,  
S.V. Ivanov, and A.A. Toropov

Ioffe Institute, 194021, Politekhnikeskaya 26, St.-Petersburg, Russia

\*E-mail: Evropeytsev@beam.ioffe.ru

The fabrication of a 4-junction solar cell with the constituent junctions based on Ge, In<sub>x</sub>Ga<sub>1-x</sub>As, Al<sub>x</sub>Ga<sub>y</sub>In<sub>1-x-y</sub>As and CdSe/ZnSe superlattice (SL) seems to be a promising way to increase the energy conversion efficiency in comparison with 3-junction solar cells involving Ge and III-V junctions alone. According to performance simulations made for AM0 solar spectrum, the optimal bandgap of the 4<sup>th</sup> II-VI cascade is in the range of 2.0-2.1 eV, provided that the III-V and II-VI junctions are lattice-matched to an In<sub>0.3</sub>Ga<sub>0.7</sub>As metamorphic layer separating them from the Ge junction. Although the optimal bandgap can be obtained in the CdSe/ZnSSe SL having sufficiently thick CdSe and ZnSSe layers, increasing the SL period leads to suppression of carrier mobility along the growth axis direction due to minibands narrowing. In this work we have studied the MBE grown short-period CdSe/ZnSe SL with a compromise effective band-gap energy ~2.180 eV (at 300 K) and estimated the vertical transport efficiency of the carriers by means of photoluminescence (PL) spectroscopy.

The CdSe/ZnSe SL with the nominal layer thicknesses of 4.3/9 monolayers (ML) and the total thickness exceeding 0.5 μm was grown by MBE pseudomorphically to the In<sub>0.3</sub>Ga<sub>0.7</sub>As metamorphic buffer layer using a double-chamber setup (SemiTEq, Russia). A wider CdSe quantum well (QW) with the nominal thickness of 5.5 ML was inserted into the SL at the distance of 0.1 μm from the buffer layer. Spectral positions of PL lines from the SL and the QW are 2.173 eV and 2.065 eV, respectively (at 300 K). In accordance with calculations carried out in the envelope functions approximation, the electron, heavy and light-hole miniband widths are 30, 8 and 160 meV, respectively. Taking into account the fact that the bottom of the light-hole miniband is only ~15 meV above the top of the heavy-hole miniband, the efficient hole transport is expected at 300 K due to thermal occupation of the light-hole states.

The vertical transport of carriers was studied by measuring temperature dependences of the integral PL intensity detected either in the SL or in the enlarged QW with the excitation energy well above the absorption edge of the SL. The dependences demonstrate the increase of the PL intensity in the QW and its simultaneous steep decrease in the SL with temperature rising in the interval 80-150 K. Such non-monotonous behavior of the PL intensity from the QW indicates the temperature activation of the carriers' vertical transport through the SL [1]. At higher temperatures the decrease of the PL intensity in the SL becomes slower that can be explained by the temperature activation of the carriers trapped in the QW back into the SL. These results indicate that the alternately-strained short-period CdSe/ZnSe SL is a suitable candidate for the 4<sup>th</sup> junction of a metamorphic solar cell, providing nearly the optimal bandgap and the efficient transport of photoexcited carriers. The expected higher critical thickness of SL with respect to the bulk layers of the same lattice mismatch [2] gives a chance to further reduction of the SL energy gap, making it slightly compressively strained by reducing the ZnSe barrier thickness.

- [1] S.V. Ivanov, A.A. Toropov, S.V. Sorokin, T.V. Shubina, A.V. Lebedev, P.S. Kop'ev, Zh.I. Alferov, H.-J. Lugauer, G. Reuscher, M. Keim, F. Fischer, A. Waag, and G. Landwehr, *Appl. Phys. Lett.* **73**, 2104 (1998)
- [2] Jan H. van der Merwe and W.A. Jesser, *J. Appl. Phys.* **63**, 1509 (1988).

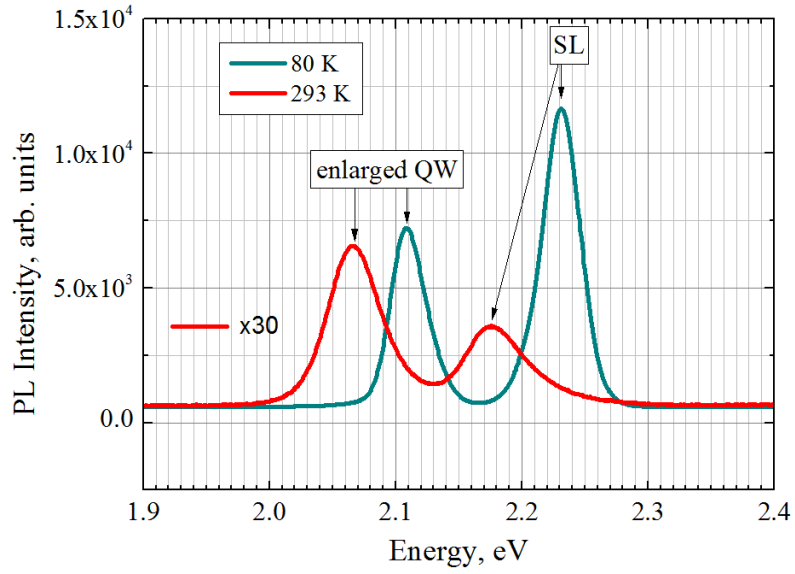


Fig. 1. PL spectra of the SL with the enlarged QW measured at 80 K and 293 K. PL spectrum measured at 293 K is multiplied by 30.

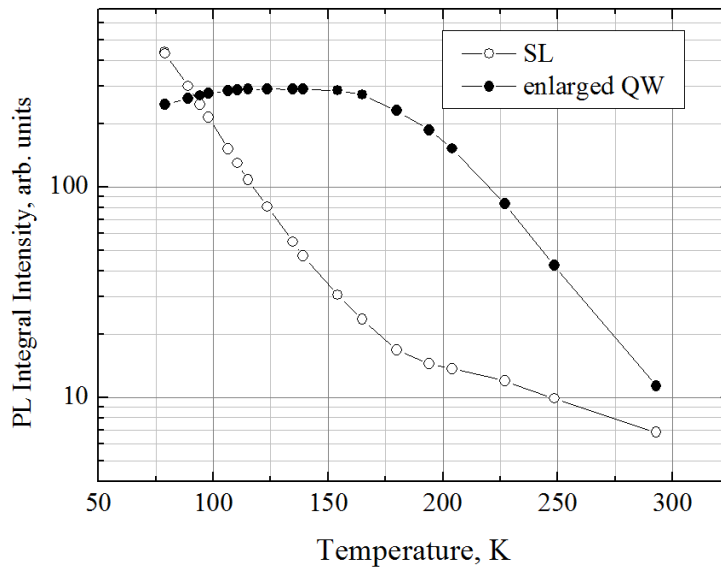


Fig. 2. Temperature dependence of integral PL intensity of the SL and the enlarged QW.

**Poster Session 3 - TuP**

**New materials : Biomaterials, hybrid organic-inorganic structures**

## Study of the effectiveness CdTe and Zn(II) tetraethyl-2-pyridil porphyrin conjugates as Photosensitizers in Photodynamic Therapy

Osnir S. Viana<sup>1</sup>, Martha S. Ribeiro<sup>2</sup>, Andréa C. D. Rodas<sup>2</sup>, C. G. Andrade<sup>4</sup>, Júlio S. Rebouças<sup>3</sup>, Adriana Fontes<sup>4</sup>, Beate S. Santos<sup>1\*</sup>

<sup>1</sup>Pharmaceutical Science Dept, Federal University of Pernambuco, Recife, Brazil.

<sup>2</sup>Center for Lasers and Applications, IPEN-CNEN/SP, São Paulo, Brazil,

<sup>3</sup>Chemistry Dept – Paraíba Federal University, João Pessoa, Brazil, <sup>4</sup>Biophysics and Radiobiology Dept, Federal University of Pernambuco, Recife, Brazil.

\*beate@ufpe.br

In the last decade semiconductor quantum dots have attracted great interest in different research areas. In health sciences quantum dots (QDs) applied as fluorescent labels showed a great potential in the development of image diagnostics, but more recently they are also being tested as photosensitizers (PS) in Photodynamic Therapy (PDT) free or conjugated to diverse molecules. In the present study we used CdTe QDs as PS for PDT upon cultures of the fungal pathogen *Candida albicans*, comparing their photodynamic effectiveness comparing free mercaptosuccinic acid coated CdTe QDs and the same QDs conjugated to cationic zincporphyrins [Zn(II)tetraethyl-2-pyridilporphyrin, ZnP]. The zeta potential of the bioconjugates was determined as a function of the QD:ZnP ratio. The spectroscopic analysis suggest that the expected energy transfer from the QDs to the ZnP is not effective, although a fluorescence quenching of the QDs is observed with increasing amounts of ZnP. All the systems produced ROS but at different levels. The cytotoxicity of the systems was tested under PDT irradiation in a fibroblast culture and none of the systems presented dark toxicity, but presented good photodynamic activity after irradiation which was increased in the QDs-ZnP conjugates. The TFD assays on *C. albicans* using LED (150 mW.cm<sup>-2</sup>) (exciting QDs only) showed that the QDs induced a cell inhibition of 1 log<sub>10</sub> while ~ 3 log<sub>10</sub> for ZnP porphyrin and < 1 log<sub>10</sub> for the conjugate. Under the conditions tested, the QD-ZnP conjugates did not present a good photodynamic inactivation on the tested cells. We suggest that the less effective PDT action of the QDs and their conjugates on the *C. albicans* reflect the lower capacity of the cellular uptake of these systems by the cells and that QDs did not act as efficient energy donors for the ZnP molecules. The overall results evidence that there is a potential application of the QDs as PS in PDT but the experimental conditions of the therapy and of the systems must be determined to increase their efficiency in ROS production in the cells.

### Acknowledgments

We are grateful to the following agencies: Conselho Nacional de Desenvolvimento Científico e Tecnológico (CNPq), Fundação de Amparo à Ciência e Tecnologia do Estado de Pernambuco (FACEPE) for financial support and student fellowships. We are also grateful to the National Institute of Science in Photonics (INFo) for financial support.

## Morphology and Photoluminescence of Multilayer PbTe/CdTe Heterostructures

G. Karczewski<sup>1</sup>, M. Szot<sup>1</sup>, S. Kret<sup>1</sup>, L. Kowalczyk<sup>1</sup>, S. Chusnutdinow<sup>1</sup>,  
T. Wojtowicz<sup>1</sup>, S. Schreyeck<sup>2</sup>, K. Brunner<sup>2</sup>, C. Schumacher<sup>2</sup>, L.W. Molenkamp<sup>2</sup>

<sup>1</sup>Institute of Physics, Polish Academy of Science, Warsaw, Poland

<sup>2</sup>Physikalisches Institut, Universität Würzburg, Würzburg, Germany

\*[karcz@ifpan.edu.pl](mailto:karcz@ifpan.edu.pl)

We study nanoscale morphology of PbTe/CdTe multilayer heterostructures grown by molecular beam epitaxy (MBE) on hybrid GaAs/CdTe (100) substrates. Nominally, the structures consist of 25 repetitions of subsequently deposited CdTe and PbTe layers with comparable thicknesses of 21 and 8 nm, respectively. However, the morphology of the resulting structures crucially depends on the growth temperature. The 2D layered, superlattice-like character of the structures remains preserved only when grown at low substrate temperatures, such as 230°C. The samples grown at the slightly elevated temperature of 270°C undergo a morphological transformation to structures consisting of CdTe and PbTe pillars and columns oriented perpendicular to the substrate as shown in Fig. 1. Although the pillar-like objects are of various shapes and dimensions these structures exhibit exceptionally strong photoluminescence in the near infrared spectral region. At the higher growth temperature of 310°C, PbTe and CdTe separate completely forming thick layers oriented longitudinally to the substrate plane. The observed topological transformations are driven by thermally activated atomic diffusion in the solid state phase. The solid state phase remains fully coherent during the processes. The observed topological transitions leading to the material separation in PbTe/CdTe system could be regarded as an analog of spinodal decomposition of an immiscible solid state solution and thus they can be qualitatively described by the Cahn-Hilliard model as proposed in Ref [1].

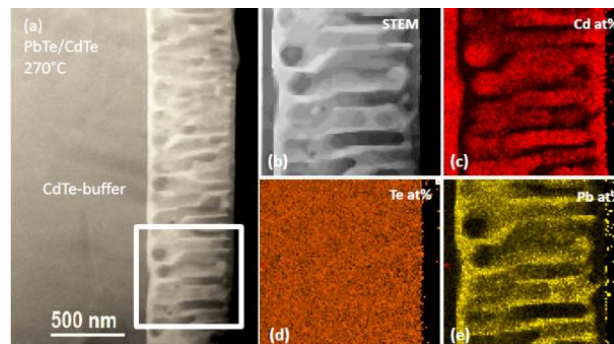


Fig. 1. (a) STEM image of PbTe/CdTe multilayer structure grown at 270°C. (b) Magnified TEM image of the area marked by white rectangle in figure (a). (c-e) Energy-dispersive X-ray (EDX) mappings over the marked area of elemental Cd, Te, and Pb, respectively.

**Acknowledgements.** This work was supported by the Foundation of Polish Sciences by the Master program.

- [1] H. Gross, I. Daruka, K. Koike, M. Yano, G. Hesser, G. Springholz, N. Zakharov, P. Werner, and F. Schäffler, *APL Materials* 2, 012105 (2014). Author X2, Author Y2, and Author Z2, *Name of Journal* 23, 556, (2010).

## Interfacial Bonds between CdS Nanoparticles and Polymeric Matrix

G.Yu. Rudko<sup>1</sup>, A.O. Kovalchuk<sup>1</sup>, V.I. Fediv<sup>2</sup>, W.M. Chen<sup>3</sup>, and I.A. Buyanova<sup>3\*</sup>

<sup>1</sup>V. Lashkaryov Institute of Semiconductor Physics of National Academy of Science of Ukraine, Kyiv, Ukraine

<sup>2</sup>Department of Biophysics and Medical Informatics, Bukovinian State Medical University, Chernivtsi, Ukraine

<sup>3</sup>Department of Physics, Chemistry and Biology, Linköping University, Linköping, Sweden  
\*irb@ifm.liu.se

The search for new nanoscale materials and structures that is stimulated by the necessity to miniaturize devices of electronics and optoelectronics is one of important trends in modern materials science. Among these materials, polymer-based composites containing semiconducting nanoparticles (NPs) are currently gaining an increasing attention due to relative simplicity of production and low costs. These nanocomposites can be fabricated via growing NPs directly in the solution of a polymer and further casting the so-obtained colloids to produce solid NP-containing films. In this colloidal synthesis routine, macromolecules of polymers provide an additional advantage of one-pot synthesis that produces a NP-containing colloid which is a feedstock for solid nanocomposite. The hybrid NP/polymer cannot be assumed, however, to be a simple sum of two components. Properties of both the NPs and the matrix can be significantly altered due to interactions between the polymer molecules and NPs surfaces. Because of a high surface-to-volume ratio of NPs, the contribution of NP/polymer interface to the properties of this material is of great importance. Thus, for a clear understanding of the nanocomposite properties it is essential to investigate interfacial interactions, which remain unknown for the CdS/PVA nanocomposite.

In the present study, we have applied Raman spectroscopy to analyze bonding between CdS NPs and macromolecules of the matrix. Several changes in Raman spectra of PVA after NPs incorporation are observed, including: 1) disappearance of an intense Raman doublet at 1717 cm<sup>-1</sup> and 1730 cm<sup>-1</sup> that corresponds to changing in C=O stretching vibrations [1]; 2) redistribution in crystallization-sensitive lines at 1127 cm<sup>-1</sup> and 1147 cm<sup>-1</sup> [2]; 3) modifications of a wide 3200-3500 cm<sup>-1</sup> band that corresponds to vibrations of hydroxyl groups O-H [3]; 4) redistribution between the Raman signal from symmetric C-H stretching vibrations at 2910 cm<sup>-1</sup> and asymmetric stretching vibrations at 2940 cm<sup>-1</sup> [2].

We have shown that the interfacial activity of PVA and CdS occurs via at least two types of interactions - coordination and hydrogen bonding. Coordination bonding arises either between a NP and C=O groups in the acetate residuals that are immanently present in commercially-produced PVA, or between a NP and ends of polymeric chains. Hydrogen bonding occurs between the hydroxyl groups allocated along the backbone of the macromolecule and the NPs surface. Besides the interfacial-related hydrogen bonds, formation of additional intra- and/or inter-molecular hydrogen bonds within the host polymeric matrix was observed. These changes in hydrogen bonding facilitate local organization of chains and, as a result, the crystallinity of the polymeric matrix as a whole increases. Based on these findings, a scheme of the interfacial bonds is proposed.

[1] J. Gaume, A. Rivaton, S. Therias, J.L. Gardette, RSC Adv. **1**, 1471, (2011).

[2] S. Krimm, C.Y. Liang, G. Sutherland, J. Polym. Sci. **22**, 227, (1956).

[3] M.A. Gauthier, J. Luo, D. Calvet, C. Ni, X. Zhu, Polymer. **45**, 8201, (2004).

**Thursday September, 17 - Poster Session 3 - ThP**

**17:15-18:45**

<b>ZnO , related oxydes and Transparent conductors (devices and physics)</b>	299
<b>Optical and electrical properties , photonic engineering</b>	319
<b>Theory and band structure</b>	350
<b>Solar cells</b>	362

**Poster Session 3 - ThP**

**ZnO , related oxydes and Transparent conductors (devices and physics)**

## Homogeneous vertical ZnO nanorod arrays on *in-situ* conductive Gd nanolayer

*Tahani H Flemban, Venkatesh Singaravelu, S. Assa Aravindh, Iman S Roqan\**

Physical Sciences and Engineering Division, King Abdullah University of Science and Technology (KAUST), Thuwal 23955-6900, Saudi Arabia.

E\*-mail: [iman.roqan@kaust.edu.sa](mailto:iman.roqan@kaust.edu.sa)

**ABSTRACT:** Simultaneously precise control density, spacing, height and vertical growth of well-defined hexagonal ZnO NRs is required in improving the performance of their potential applications, such as field emitters, solar cells, sensors, nanogenerators, and optoelectronic devices.[1] However, controlling these parameters (in particular the spacing between the NRs with a homogenous NR dimensions) remains a challenge.[2] In this work, we describe a novel one-step catalyst-free method for producing size-controlled vertical ZnO nanorod (NR) arrays of highly desirable characteristics is demonstrated by pulsed laser deposition using Gd doped ZnO target. Our discovery shows that an *in situ* transparent and conductive Gd nanolayer (with a uniform well-defined thickness of  $\sim 1$  nm) in the interface between a lattice-matched (11-20) *a*-sapphire substrate and ZnO NRs plays a significant role in the growth of such uniform ZnO NRs. The density of the NRs is well controlled by changing the partial oxygen pressure. The theoretical calculation indicates that the Fermi level shifts into the conduction band with Gd dopants, which explains the high mobility of these NRs ( $177 \text{ cm}^2 (\text{V.s})^{-1}$ ). The structural, electrical and optical properties confirm that this method can be used to obtain conductive and high quality NRs. Our approach have the potential to improve the performance of materials used in a wide range of electric and optoelectronic applications[3].

[1] R. Zhu, W.G. Zhang, C. Li, R.S. Yang, Nano Letters, **13**, 5171-5176 (2013).

[2] X.D. Wang, J. Zhou, C.S. Lao, J.H. Song, N.S. Xu, Z.L. Wang, Advanced Materials, **19**, 1627-1631, (2007)

[3] M. Willander, O. Nur, Q.X. Zhao, L.L. Yang, M. Lorenz, B.Q. Cao, J.Z. Perez, A. El-Shaer, A.C. Mofor, B. Postels, J. Guinard, D.L.S. Dang, Nanotechnology, **20**, 332001, (2009).

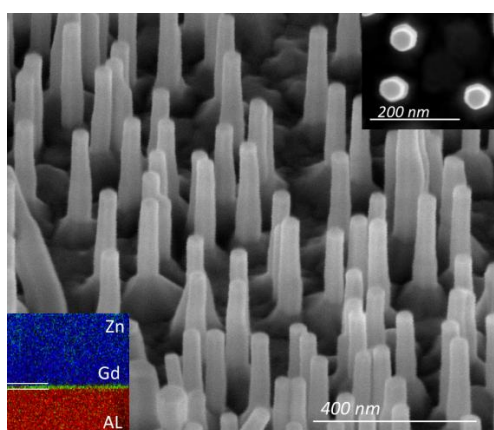


Figure 1. Scanning electron microscopy of ZnO NRs. Top inset shows the top view of the NRs indicating the vertical alignment. Bottom inset shows the energy dispersive x-ray map of  $40 \times 40$  nm transmission electron microscopy image near the interface between the NRs and the substrate, indicating the uniform Gd nanolayer.

## The Manifestation of Strong d-p – Hybridization in Photoluminescence Spectra of ZnO:Ni and ZnO:Co

Sokolov V.I.<sup>1\*</sup>, Gruzdev N.B.<sup>1</sup>, Pustovarov V.A.<sup>2</sup>, and Churmanov V.N.<sup>2</sup>

<sup>1</sup> M.N. Miheev Institute of Metal Physics of Ural Branch of Russian Academy of Sciences, 620990, S. Kovalevskaya Steet,18, Yekaterinburg, Russia

<sup>2</sup> Ural Federal University, 620002, Mira Street, 19, Yekaterinburg, Russia  
\*visokolov@imp.uran.ru , socolovvi@gmail.com

The significant difference of optical and luminescent properties of  $Zn_{1-x}M_xO$  ( $M$  –Co and Ni) in comparison to other II-VI:3d compounds was discovered as a result of many investigations. Preliminary analyses shows us that the reason of this difference is the strong hybridization between d-states of cation and p-states of  $O^{2-}$  ion caused by the smaller anion-cation distances in ZnO than in other II-VI:3d compounds.

The results of investigations of photoluminescence and photoluminescence excitation spectra of ZnO:Co and ZnO:Ni are presented in this work (Figure 1). As the excitation, we used the pulse synchrotron radiation in spectral region of 3.7-21 eV. This radiation has 1-ns pulses running at 96-ns intervals. The temperature during the measurements was 8 K. In photoluminescence spectra we can see two bands for ZnO:Ni and one band for ZnO:Co crystals. These bands are due to radiative transitions through donor and acceptor levels of  $Ni^{2+}$  and  $Co^{2+}$  ions. High energy edges of photoluminescence bands are in the good correlation with the low energy edges of charge transfer bands which was clearly observed in optical absorption spectra of ZnO:Co and ZnO:Ni compounds. Radiative transitions through donor and acceptor levels have large effectiveness due to the significant hybridization of d-functions with band states. In other II-VI compounds doped by Ni or Co radiative charge transfer transitions as a rule are not observed due to the Defect Auger Recombination process. In result of that the ion of 3d-impurity becomes in one of exciting states. After that, intracentral radiative or nonradioactive transitions take place.

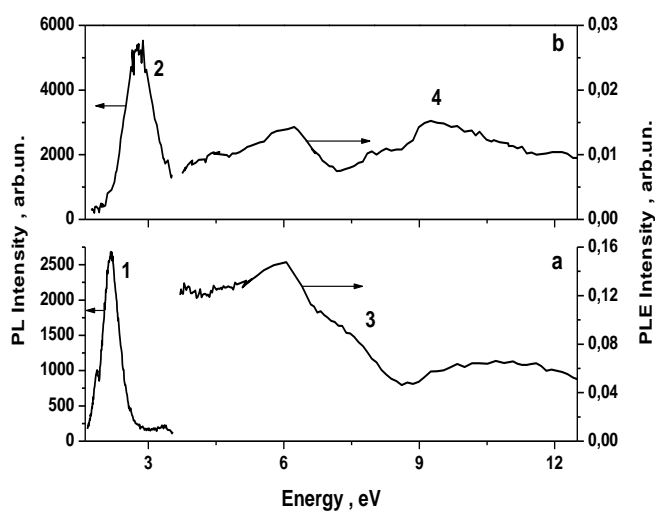


Figure 1. Photoluminescence (1,2) and photoluminescence excitation (3,4) time integrated spectra of ZnO:Ni (a) and ZnO:Co (b) crystals.

In photoluminescence excitation spectra at the energies larger than the energy band gap we can see the wide band with the maximum at the energy of 6 eV. We assumed that for  $Ni^{2+}$  and  $Co^{2+}$  ions in the lattice of ZnO the strong hybridization of its d-states with p-states of the oxygen ions manifests itself and the wide bands of transformed states arise in the valence bands of these materials. In this paper

we demonstrated that intensive bands of radiating recombination with charge transfer in the visible region of the spectrum are being excited in very wide region of ultraviolet part of the spectrum. This opens in principle a possibility of detection of ultraviolet radiation.

## Electrical properties of ZnO based heterojunctions deposited by Atomic Layer Deposition on 4H-SiC

R. Schifano<sup>1\*</sup>, M. Guziewicz<sup>2</sup>, T. A. Krajewski<sup>1</sup>, W. Jung<sup>2</sup>, K. Goscinski<sup>1</sup>, E. Przewdziecka<sup>1</sup>,  
J. Z. Domagala<sup>1</sup>, P. Dłuzewski<sup>1</sup>, E. Guziewicz<sup>1</sup>

<sup>1</sup>Institute of Physics, Polish Academy of Sciences, Al. Lotnikow 32/46, 02-668 Warsaw, Poland

<sup>2</sup>Institute of Electron Technology, Al. Lotnikow 32/46, 02-668 Warsaw, Poland  
\*e-mail: [schifano@ifpan.edu.pl](mailto:schifano@ifpan.edu.pl)

Inability to obtain reliable, reproducible and tunable p-type conductivity in ZnO is at the present stage one of the major obstacles in the realization of devices based on this promising semiconductor. Among the other wide gap semiconductors 4H-SiC represents a valid ZnO p-type counterpart considering that 4H-SiC has an established technology, same crystal structure as ZnO and the lattice mismatch between the two semiconductors is relatively small (equal to ~5%).

Till now the ZnO/4H-SiC heterojunctions were obtained by depositing the ZnO layer by thermal evaporator, filtered cathodic vacuum arc technique [1,2] and more recently Atomic Layer Deposition (ALD) [3] with diverse results concerning turn-on voltages, rectification ratios and overall electrical characteristics of the devices.

The present work is dedicated to n-ZnO/p-SiC (4H) heterojunctions where the ZnO layer has been deposited by ALD at 300°C. High resolution X-ray diffraction measurements (HR XRD) demonstrate that epitaxial ZnO with a FWHM of the 0002 reflection rocking curve as narrow as 0.345° has been obtained. Good crystallinity of the ZnO film has also been confirmed by TEM imaging. The Ohmic contact metallization to p-SiC (4H) was formed by deposition of a thin Ti-Al alloy film on the backside and subsequent annealing at 1000°C, while the contact metallization to ZnO was formed by deposition of a Ti/Au bilayer and *lift off* technique. It is shown that the resulting n-ZnO/p-SiC (4H) diode exhibits a rectification ratio as high as 10<sup>10</sup> at ± 2V with a flat dark reverse current density as low as ~5 · 10<sup>-9</sup> A/cm<sup>2</sup>. In addition, very good ideality factor ranging in the ~1.2-1.6 interval depending on the contact as well as a turn-on voltage of ~0.8 V have been measured. From capacitance vs voltage (C-V) dependence a conduction band offset of (1.3 eV ± 0.2) eV is obtained, in agreement with values recently obtained by X-ray photoelectron spectroscopy [4]. Furthermore, the n-ZnO/p-SiC (4H) diodes under UV illumination show a high UV-to-dark current ratio equal to ~10<sup>2</sup> in the reverse bias range suggesting a strong potential for the application of such devices as transparent UV sensors.

[1] J.F. Felix, E.F. da Silva Jr., E.A. de Vasconcelos, W.M. de Azevedoc, *Solid State Commun.* **151**, 1252 (2011)

[2] C. Yuen, S. F. Yu, S. P. Lau, Rusli, and T. P. Chen, *Appl. Phys. Lett.* **86**, 241111 (2005)

[3] Y.T. Shih, M.K. Wu, M.J. Chen, Y.C. Cheng, J.R. Yang, M. Shiojiri, *Appl. Phys. B* **98**, 767 (2010)

[4] H. B. Fan, G. S. Sun, S. Y. Yang, P. F. Zhang, R. Q. Zhang, H. Y. Wei, C. M. Jiao, X. L. Liu, Y. H. Chen, Q. S. Zhu, and Z. G. Wang, *Appl. Phys. Lett.* **92**, 192107 (2008)

**Acknowledgements.** The author R.S. was supported by the EU 7<sup>th</sup> Framework Programme project REGPOT-CT-2013-316014 (EAgLE). The authors T.A.K. and K.G. acknowledge support by the grant DEC-2013/09/D/ST5/03879 of NSC of Poland. The authors E.G. and P.D. were supported by Polish NCBiR project DZP/PBSII/1699/2013.

## Annealing of Frozen-in Defects in ZnO

Lott K<sup>1\*</sup>, Nirk T<sup>1</sup>, Krustok J<sup>1</sup>, Seeman V<sup>2</sup>, Gorokhova E<sup>3</sup>, Türn L<sup>1</sup>, Viljus M<sup>1</sup>, Öpik A<sup>1</sup>, and Vishnjakov A<sup>4</sup>

<sup>1</sup> Department of Materials Science, Tallinn University of Technology, Tallinn, Estonia

<sup>2</sup> Department of Physics, Tartu University, Tartu, Estonia

<sup>3</sup> S.I.Vavilov State Optical Institute, St.Petersburg, Russia

<sup>4</sup> Department of Physical Chemistry, D.Mendelejev University of Chemical Technology of Russia, Russia

\*kalju.lott@ttu.ee

Treated at  $T_{\text{ZnO}} = 1000^{\circ}\text{C}$  under saturated Zn vapor pressure  $P_{\text{Zn}}$ , ZnO gives Zn excess value in the concentration interval of  $10^{18} \div 10^{19} \text{ cm}^{-3}$  in dependent on the sample history [1]. Annealing of ZnO with excess Zn at elevated temperatures initiates a number of simultaneous unexpected effects [2-4]. From high temperature electrical conductivity (HTEC) it became clear: dominating native defects at elevated temperatures and at fixed  $P_{\text{Zn}}$  are connected to Zn excess in ZnO [5,6]. Used here HTEC relaxation measurement technique is described in Ref.[7]. The significant differences in HTEC relaxation curves were observed after step-wise change of  $T_{\text{ZnO}}$  or  $P_{\text{Zn}}$ . The connection between deviation from stoichiometric composition and appearance of differences in EPR spectra after frozen-in of high temperature defect equilibrium and between the subsequent vacuum annealing of frozen-in defects were investigated. Samples for EPR measurements were cut from single crystal as bars oriented on C-axis. Excess zinc was introduced into the crystal by heating the crystals at  $1000^{\circ}\text{C}$  at fixed zinc vapor pressure similar to [8]. As result the crystal color turned yellow and in EPR spectrum  $g \approx 1,96$  signal appeared with disappearing of all other EPR signals from contaminating impurities opposite to result of hydrogenation of ZnO [9] what enabled the detection of the Mn center. Annealing of crystals was performed in vacuum by 30 minutes cycles in 50 degrees temperature intervals from  $250^{\circ}\text{C}$  to  $1000^{\circ}\text{C}$ . EPR spectra were investigated after every annealing procedure. These EPR measurements had qualitative character to characterise the freeze-in and the annealing process in ZnO. EPR spectrum with  $g \approx 1,96$  gives donor concentration approximately 3 orders of magnitude lower than estimated from HTEC measurement data at  $1000^{\circ}\text{C}$  [5]. During annealing the crystal color turned from yellow to red, to brown and finally the annealing in vacuum at  $1000^{\circ}\text{C}$  removed as the coloration of the crystal as the EPR spectrum  $g \approx 1,96$ . The comparison of high temperature and low temperature experiments support the defect model where the main part of frozen-in excess Zn in ZnO exists in the form of Zn nanoclusters as found by optical method [3] and where the formation and dissolution of Zn precipitates takes place, facilitated by the low migration energy of interstitial zinc.

- [1] Lott K, Shinkarenko S, Kirsanova T, Türn L, Gorokhova E, Grebennik A, and Vishnjakov A, *Solid State Ionics*, **173**, 29, (2004).
- [2] Weber M H, Selim F A, Solodovnikov D, Lynn K G, *Applied Surface Science* **255**, 68, (2008).
- [3] Irmscher K, Albrecht M, Heimbrodt B, Naumann M, Remmele T, Schulz D, Schulz T, and Fornari R, *Physica Status Solidi C* **6**, 2658, (2009).
- [4] Weber M H, Lynn K G *Journal of Physics: Conference Series* 262, 012063, (2011).
- [5] Lott K, Nirk T, Türn L, Öpik A, Kortunova E, Shvanskiy P, Gorokhova E, and Vishnjakov A, *Physica Status Solidi C* **11**, 1481, (2014).
- [6] Lott K, Nirk T, Gorokhova E, Türn L, Viljus M, Öpik A, and Vishnjakov A, *Cryst. Res. Technol.* **50**, 10 (2015).
- [7] Lott K, Nirk T and Volobujeva O, *Cryst. Eng.*, **5**, 164, (2003).
- [8] Halliburton L E, Giles N C, Garces N Y, Luo M, Xu C, and Baic L, *Appl. Phys. Lett.* **87**, 172108 (2005).
- [9] Gluba M A, Friedrich F, Lips K, and Nickel N H, *Superlattices and Microstructures* **43**, 24 (2008).

## Identification of Localized Defects in ZnO Nanostructures and Thin Films

N. H. Nickel, N. Karpensky, and M. A. Gluba  
Helmholtz-Zentrum Berlin für Materialien und Energie,  
Institut für Silizium Photovoltaik, Kekuléstrasse 5, 12489 Berlin, Germany

Zinc oxide (ZnO) is attracting a lot of interest because of its electrical and optical properties for a variety of applications ranging from UV light emitting diodes and lasers to transparent conducting electrodes and nanostructures for organic-inorganic photovoltaic devices. Reliable doping and a low concentration of localized defects are key requirements for the successful integration of ZnO in high quality devices.

In this paper, we present experimental evidence of an enhanced concentration of localized defects in the near-surface region of ZnO nanowires and thin films. For this purpose undoped and doped ZnO layers and nanowire samples were grown on sapphire substrates using pulsed laser deposition. As dopants aluminum and nitrogen were used. Al doping was achieved by adding the desired amount of Al<sub>2</sub>O<sub>3</sub> to ZnO powder and fabricating a doped ceramic target. On the other hand, nitrogen doping was accomplished by microwave assisted plasma dissociation of N<sub>2</sub>O during the deposition of ZnO from an undoped target. The specimens were characterized with temperature dependent photoluminescence (PL) and photo-thermal deflection spectroscopy (PDS) measurements. The latter technique allows for a direct measurement of the sub band-gap absorption coefficient, which is an excellent measure for the concentration of localized defect states.

The nanowire specimens exhibit a pronounced photoluminescence band in the range of  $E = 1.8$  to  $2.8$  eV that involves transitions from or to localized defect states in the forbidden gap. With increasing nanowire density the PL band increases. This is accompanied by an increase of the sub band-gap absorption, which is directly proportional to the combined density-of-states. The enhanced optical absorption at an energy of about 1.6 and 1.9 eV is attributed to Zn vacancies and Zn vacancy clusters. When a 5 nm thick surface layer of the nanowires is etched off a pronounced decrease of the density-of-states is observed. This shows that the defects are predominantly located in the near-surface region of the nanowires. Nitrogen doped ZnO exhibits a similar density-of-states distribution. However, the peak located at about 1.9 eV vanishes with increasing doping concentration. The implications of these results for device applications will be discussed.

## **Defect Related Emission of ZnO and ZnO Cu Nanocrystals Prepared by Electrochemical method**

T. V. Torchynska<sup>1</sup>, B. El Filali<sup>2</sup>, A. Mosqueda<sup>2</sup> and L. Shcherbyna<sup>3</sup>

<sup>1</sup>ESFM-Instituto Politécnico Nacional, México D.F. México

<sup>2</sup>UPIITA-Instituto Politécnico Nacional, México D.F. México

<sup>3</sup>V.Lashkaryov Institute of Semiconductor Physics at NASU, Ukraine

\*torch@esfm.ipn.mx

Photoluminescence, X-ray diffraction, Scanning electron microscopy and Raman scattering have been used for the optical and structural characterization of ZnO and ZnO Cu nanocrystals (NCs) of various sizes. The samples prepared by an electrochemical method have a size from the range of 60 to 600 nm after a heat treatment for 2 hours at 400 oC in ambient air. X-ray diffraction diagrams present a small shift of peaks that testifies on a change in the lattice parameters of NCs with decreasing the NC size. The Raman scattering technique presents the several active modes including the surface phonon mode. The Raman intensity increases with decreasing the NC size is attributed to the surface enhanced Raman scattering (SERS) effect in ZnO Cu NCs. Photoluminescence spectra show a free exciton and defect-related emission. The peculiarities of defect related luminescence have been studied by means of the variation of temperatures and excitation light densities for the ZnO and ZnO Cu nanocrystals (NCs) of various sizes. The intensity stimulation of exciton-related PL bands with NC size decreasing up to 60 nm is attributed to the realization of the weak confinement and the exciton-light coupling with the formation of polariton in small size ZnO NCs.

## Effect of Al and/or Li Doping on Luminescent Properties of Highly Doped ZnO films

Khomenkova L, Kushnirenko V\*, Osipyonok N, and Borkovska L  
V. Lashkarev Institute of Semiconductor Physics, 45 Pr. Nauky, Kiev 03028, Ukraine  
\* E-mail: vl\_kush@ukr.net

Doping of materials plays a critical role in semiconductor device fabrication technology. The maximum level of dopant ions and their concentration in a crystalline structure of host materials are limited by their solid solubility. For polycrystalline semiconductors, this level varies, because the defects and grain boundaries can act as deposition sites, resulting in increase in the dopant concentration level. The segregation of dopant ions in grain boundaries may occur when the concentration of dopant ions is higher than its solid solubility limit, leading to the formation of trap states as new phases or clusters.

Zinc oxide is a wide bandgap semiconductor with unique electronic and optical properties at nanoscale which makes it suitable for a wide range of applications including fabrication of devices for photonics and optoelectronics. Similar to other semiconductors, ZnO may also be subject to property improvement by doping process. Different dopant ions such as Al, Li, Ga, etc. have been used to improve the performance and physical properties of ZnO nanostructures.

In present work, the peculiarities of doping of ZnO films with Li and/or Al ions which were produced by a screen-printing method on sapphire substrates were investigated. The doping of the films was performed from Al<sub>2</sub>O<sub>3</sub> (25 wt%) and LiNO<sub>3</sub> (5 wt%) during film sintering at T<sub>S</sub>=800–1000°C in air. The photoluminescence (PL) and PL excitation spectra were measured for the undoped and doped films at 77 and 300 K.

At low sintering temperature T<sub>S</sub>=800°C, the improvement of crystalline quality for the ZnO:Li films was found. This was confirmed by an enhancement of the excitonic PL band which was accompanied by a specific transformation of PL excitation spectra for the defect-related band. These changes are ascribed to the effect of LiNO<sub>3</sub> as a flux that lowers the melting point of the ceramic.

For the ZnO samples doped with Al ions only, the similar transformation of PL and PL excitation spectra was observed. The films sintered at 800°C were found to be with an improved crystalline quality in comparison with the pure and Li-doped ZnO films sintered at the same temperature. This effect is explained by a favorable outward diffusion of Zn ions from ZnO grains along with an Al diffusion inside them due to a significant difference in the diffusion coefficients of Zn and Al ions. The films sintered at higher temperatures showed a structural degradation due to the expected formation of ZnAl<sub>2</sub>O<sub>4</sub> phase that was accompanied by the quenching of excitonic PL band and the intensity increase of defect-related PL emission. However, for the (Al, Li)-co-doped films, the structural transformation was found to be more complicated. It was observed the competition of the diffusion of Li, Zn and Al ions and the preferable formation of Li<sub>x</sub>Al<sub>2</sub>O<sub>3</sub> phase and ZnAl<sub>2</sub>O<sub>4</sub> phases controlled the growth of ZnO grains and their structural performance. The effect of these phases on the PL properties of the films will be discussed in details.

## Effect of Al doping in Ag layer of MgZnO/Ag/MgZnO dielectric/metal/dielectric (DMD) UV-visible transparent conductive films

Yukiko Sugimoto, and Akihiko Kikuchi

Engineering and Applied Sciences, Sophia University, Tokyo, Japan

\*kikuchi@sophia.ac.jp

We report on dielectric/metal/dielectric (DMD) transparent conductive films [1] consisted of slightly Al-doped silver (Ag(Al)) metal and Al-doped  $\text{Mg}_{0.5}\text{Zn}_{0.5}\text{O}$  (AMZO) dielectric layer with high UV-visible transparency, low-sheet resistance and high thermal stability. The AMZO/Ag(Al)/AMZO-DMD films were prepared on  $\text{SiO}_2$  substrates by ion beam sputtering at room temperature with thicknesses of 7 nm for Ag(Al) and 50 nm for AMZO layers as shown in fig. 1. The Al composition of Ag(Al) layer was set to be 1.7 at%. The averaged transmittance in UV-visible region (315~780 nm)  $T_{\text{AVE}}$  and sheet resistance  $R_s$  of the DMD after annealing in vacuum at 300 °C for 60 min was 89.0 % and 8.9  $\Omega/\text{sq}$ , respectively.

To investigate the effect of Al doping in Ag layer, three DMD films with 7 nm-thick pure Ag, 10 nm-thick pure Ag and 7 nm-thick Ag(Al) layer were prepared. The thickness of AMZO layer were about 50 nm for all samples. Figure 2 shows transmission spectra of as deposited these DMD films. The DMD with 7 nm-thick Al layer showed low transparency in visible region and high  $R_s$  of 21.0  $\Omega/\text{sq}$ . due to island growth of thin Ag layer. For the DMD with 10 nm-thick Ag layer, the  $T_{\text{AVE}}$  increase to 82.1 % and  $R_s$  reduced to 13.6  $\Omega/\text{sq}$ . by a formation of continuous Ag layer, but the transmittance was limited by absorption of thicker Ag layer. For the case of DMD with 7 nm-thick Ag(Al), highest  $T_{\text{AVE}}$  of 88.0 % and  $R_s$  of 16.5  $\Omega/\text{sq}$ . were obtained. The superior transparency of DMD with Ag(Al) suggesting the suppression of plasmon resonant absorption due to island growth of thin Ag layer. Slightly high  $R_s$  is attributed to small thickness. Figure 3 shows annealing temperature dependency of  $T_{\text{AVE}}$  and  $R_s$  of DMDs with 10 nm-thick Ag and 7 nm-thick Ag(Al) layers. Remarkable change in  $T_{\text{AVE}}$  was not shown for both DMD up to 400 °C. The  $R_s$  of DMD with Ag layer reduced to 6.3  $\Omega/\text{sq}$ . at 300 °C but rapidly increased at 400 °C due to aggregation of Ag. On the other hand, the  $R_s$  of DMD with Ag(Al) layer reduced to 8.1  $\Omega/\text{sq}$ . at 400 °C and slightly increased to 10.0  $\Omega/\text{sq}$ . at 500 °C. The thermal stability of DMD with Ag(Al) is about 100 °C higher than that with pure-Ag layer [2].

We demonstrated that Al doping (1.7 at%) suppress the island growth and thermal aggregation of Ag layer, consequently brings about superior performance of Ag based DMD.

[1] R. Dragila, B. L-Davies, and S. Vukovic, Physical Review Letters, **55**, 1117, (1985).

[2] H. C. Kim and T. L. Alford, Journal of Applied Physics, **94**, 5393, (2003).

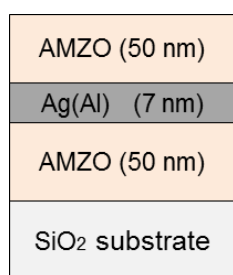


Fig. 1. Schematic diagram of AMZO/Ag(Al)/AMZO DMD.

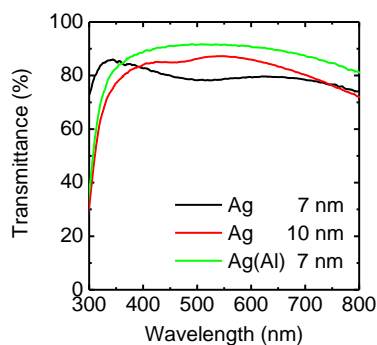


Fig. 2. UV-Visible transmission spectra of AMZO/Ag/AMZO- DMD films with different Ag layers of.

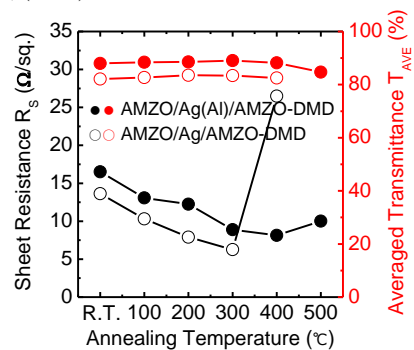


Fig. 3. Sheet resistance and averaged transmittance of AMZO based DMDs with and without Al doping in Ag layer.

## Photoconductive properties of non-doped and nitrogen-doped ZnO single crystals in various ambient gases

T. Abe<sup>1\*</sup>, S. Takahashi<sup>1</sup>, S. Kamada<sup>1</sup>, A. Nakagawa<sup>1</sup>, T. Chiba<sup>1</sup>, M. Nakagawa<sup>1</sup>, S. Chiba<sup>1</sup>,  
Y. Kashiwaba<sup>2</sup>, M. Daibo<sup>1</sup>, I. Niikura<sup>1</sup>, Y. Kashiwaba<sup>1</sup>, and H. Osada<sup>1</sup>

<sup>1</sup>Iwate University, Morioka 020-8551, Japan

<sup>2</sup>National Institute of Technology, Sendai College, Sendai 989-3128, Japan

\*E-mail : tabe@iwate-u.ac.jp

The effects of ambient gases on photoconductive properties of non-doped ZnO and nitrogen-doped ZnO (ZnO:N) single crystals are described and the role of adsorbed oxygen atoms on the ZnO surface is also discussed in this report.

ZnO is a promising material for a UV sensor without sensitivity in the visible light region because of its large band gap energy of 3.37 eV. In recent years, large single crystals of ZnO have become available, and their applications to various devices are expected. We have reported the characteristics of a photoconductive UV sensor using ZnO single crystals and have shown that the Zn face of ZnO:N single crystals is suitable for use in a photoconductive UV sensor [1, 2]. In this work, we examined the photoconductive properties of non-doped ZnO and ZnO:N single crystals in various ambient gases to determine the effects of ambient gases on photoconductivity.

Non-doped ZnO and ZnO:N single crystals were grown by the hydrothermal method (Tokyo Denpa Co., Ltd.). Samples were prepared by vacuum deposition of 1-mm-square Al electrodes with a 0.3-mm gap on non-doped ZnO and ZnO:N single crystals of  $5 \times 5 \times 0.5 \text{ mm}^3$  in size. The light source was a Xe-arc lamp and a grating monochromator was used for measurement of spectral response of the photocurrent. The applied voltage was 1.5 V. Ambient gases were air, O<sub>2</sub> gas and vacuum.

Fig. 1 shows timeresponse characteristics of the Zn face of non-doped ZnO and ZnO:N single crystals in O<sub>2</sub> gas (a) and of a ZnO:N single crystal in various ambient gases (b). The time response of the ZnO:N single crystal was faster than that of the non-doped ZnO single crystal, and the time response of the ZnO:N single crystal in O<sub>2</sub> gas was the fastest. It is thought that filling of defects related oxygen vacancies by nitrogen atoms caused a decrease of trap density in the ZnO single crystal and that the lifetime of photocarriers near the surface decreased because of an increase in surface recombination through adsorbed oxygen. We also confirmed that the time response of the Zn face was faster than that of the O face.

These results indicate that the use of the Zn face of ZnO:N single crystals with sealing in O<sub>2</sub> gas is appropriate for preparation of a photoconductive ZnO-UV sensor.

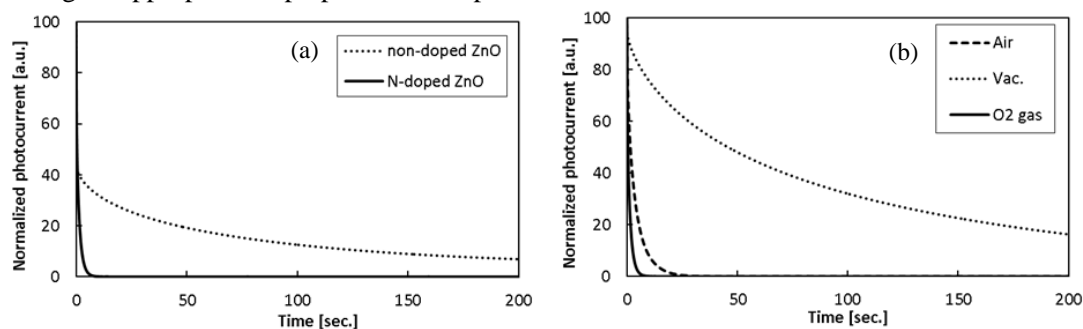


Fig. 1 Timeresponse characteristics of the Zn face of non-doped ZnO and ZnO:N single crystals in O<sub>2</sub> gas (a) and of a ZnO:N single crystal in various ambient gases (b).

[1] F. Masuoka et al., Phys. Stat. Sol. C 3, No. 4, 1238 (2006).

[2] S. Takahashi et al., Phys. Stat. Sol. C 11, No. 7-8, 1304 (2014).

## Strain-engineering and Electrical Performance of Aluminium-, Gallium-, and Indium-doped Homoepitaxial ZnO Thin Films

Michael Lorenz<sup>1\*</sup>, Tobias Weiss<sup>1</sup>, Florian Schmidt<sup>1</sup>, Holger von Wenckstern<sup>1</sup>, Marius Grundmann<sup>1</sup>

<sup>1</sup>Semiconductor Physics Group, Institut für Experimentelle Physik II, Universität Leipzig, D-04103 Leipzig, Germany

\*E-mail: mlorenz@physik.uni-leipzig.de

Aluminium-, Gallium-, and Indium-doped ZnO thin films with nominal source target compositions from 0.1 to 1 wt:% (Al), to 3% (Ga), and to 13.5% (In) were grown homoepitaxially and in-plane lattice matched on c-plane ZnO (00.1) single crystalline substrates by pulsed laser deposition (PLD). In dependence on dopant concentration and oxygen partial pressure during growth we found compressive or tensile out-of-plane epitaxial strain up to 0.1% for ZnO:Al and Ga [1]. Surprisingly, the crystallinity, i.e. intensity of X-ray diffraction peaks of the homoepitaxial ZnO:In films shows a much stronger dependence on oxygen partial pressure during PLD growth. The structural relaxation of ZnO:In films starts from about 4% In content, corresponding to about 1% out-of-plane strain. Below 4% In-doping, the ZnO:In films are in-plane lattice matched [2].

Electrical investigations showed that the conductivity of the substrates influences transport measurements at room temperature. Transport properties of the Al- and Ga-doped homoepitaxial ZnO layers can therefore only be interpreted correctly by performing variable temperature Hall effect measurements. These reveal, that besides the contribution of the substrate and the deposited thin film an additional conduction channel, likely located at the surface or the interface of the samples must be considered to explain and model the temperature dependence of the free electron concentration and their mobility [1]. The heavier doped ZnO:In films show very high carrier concentrations from  $10^{18}$  up to nearly  $10^{21}$   $\text{cm}^{-3}$  at 300 K [2].

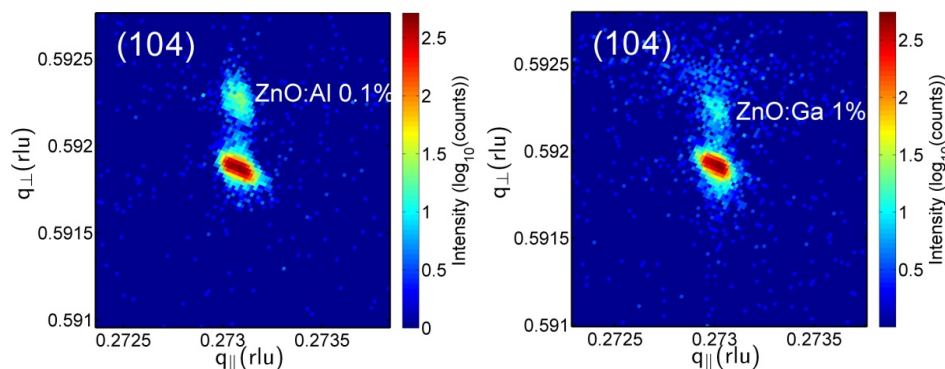


Fig. 1. X-ray diffraction reciprocal space maps around the (104) ZnO peaks, demonstrating in-plane lattice matched growth of the indicated ZnO:Al, Ga films. Adopted from [1].

[1] M. Lorenz, T. Weiß, F. Schmidt, H. von Wenckstern, M. Grundmann, submitted to Phys. Stat. Sol. A (2015)

[2] Sören Herath, BSc. Thesis, Universität Leipzig, Fakultät für Physik und Geowissenschaften (2015)

## Magnetospectroscopy Studies of $s, p-d$ Interaction in Nanocrystalline Zinc Oxide with $\text{Fe}^{3+}$ Ions

J. Papierska<sup>1</sup>, E. Chikoidze<sup>2</sup>, M. Boshta<sup>3</sup>, H.-J. von Bardeleben<sup>4</sup>, Y. Dumont<sup>2</sup>, M. M. Goma<sup>3</sup>,  
G. Kowalski<sup>1</sup>, M. Tokarczyk<sup>1</sup>, W. Pacuski<sup>1</sup>, M. Nawrocki<sup>1</sup>, and J. Suffczyński<sup>1\*</sup>

<sup>1</sup>Faculty of Physics, University of Warsaw, Warsaw, Poland

<sup>2</sup>Grouped'Etudes de la MatiereCondensee (GEMaC), Universite de Versailles  
St-Quentin en Yvelines – CNRS, Versailles, France

<sup>3</sup>Solid State Physics Department, National Research Center, El-Behoot st., 12622 Dokki,  
Giza, Egypt

<sup>4</sup>Sorbonne Universités, UPMC Université Paris 06, UMR7588, Institut des Nanosciences de  
Paris, F-75005, Paris, France

\*Jan.Suffczyński@fuw.edu.pl

Ultra long spin coherence time ( $>150 \mu\text{s}$ ) found recently for  $\text{Fe}^{3+}$  ions in ZnO[1] makes Fe doped ZnO one of the most promising, but still unexplored spintronic systems. The long relaxation time [1] suggests that  $\text{Fe}^{3+}$  ions in ZnO are decoupled from their environment. Hence, a question arises: do  $\text{Fe}^{3+}$  ions couple to band carriers by  $s, p-d$  exchange interaction?

The studied nanocrystalline ZnO layers with Fe ions are produced by a spray pyrolysis on glass and quartz substrates [2]. The respective pure ZnO layers serve as a reference. X-ray diffraction measurements reveal preferential c-axis orientation perpendicular to the layer plane. Polarization resolved reflectivity and photoluminescence (PL) measurements are performed in the Faraday configuration in magnetic field up to 10 T.

Clear transitions of three excitons, as expected for a wurtzite structure semiconductor, where the valence band is split into three subbands, are observed at energy around 3.38 eV, 3.39 eV and 3.43 eV in REF measurements. The integrated MCD intensity is determined basing on the acquired reflectivity spectra as a function of magnetic field for temperatures of 1.5 K, 5 K, 10 K, and 50 K. The results are well described by the paramagnetic Brillouin function with  $g$  factor of 1.997 (determined from independent Electron Paramagnetic Resonance measurement), spin 5/2 (as for  $\text{Fe}^{3+}$  ion) and experimental temperature.

Transitions of bound exciton at around 3.36 eV and the donor acceptor pairs (DAP) at around 3.32 eV are observed in the PL spectrum. It is evidenced that Fe doping promotes excitonic emission over other (in particular DAP) recombination channels.

Dependence of degree of polarization for the excitonic and DAP transitions on magnetic field is well described by the Brillouin function. The narrowing of bound exciton transition with the magnetic field is observed and attributed to reduction of the spin fluctuations of the  $\text{Fe}^{3+}$  ions. The increase of the intensity of excitonic emission in the magnetic field for both circular polarizations of the light is found. It indicates that magnetic field reduces efficiency of non-radiative Auger recombination involving excitation of the  $\text{Fe}^{3+}$  ion [3].

The dependences determined from the PL measurement show that magneto-optical response of the sample is proportional to the sample magnetization. In such a way, PL results provide a strong support for the conclusions drawn from the reflectivity measurements, what unequivocally confirms presence of the ion-carrier  $s, p-d$  interaction in the studied system.

[1] J. Tribollet *et al.*, Europhysics Letters **84**, 20009 (2008).

[2] E. Chikoidze *et al.*, Journal of Applied Physics **113**, 043713 (2013).

[3] M. Nawrocki *et al.*, Physical Review B **52**, R2241 (1995).

## **Peculiarities of Cu-Related and Self-Activated Green Emission Bands in ZnO and ZnMgO**

I.V.Markevich, T.R.Stara\*

V. Lashkaryov Institute of semiconductor physics of NASU, 03028 Kyiv, Ukraine

\*stara\_t@ukr.net

Doped with Cu and undoped Zn<sub>1-x</sub>Mg<sub>x</sub>O ceramics (x=0.20) were sintered at 1000 °C in air and Zn vapor accordingly. Photoluminescence (PL) and PL excitation (PLE) spectra were measured at room temperature using Xe-lamp light as an exciting source. In undoped samples sintered in Zn vapor, bright blue-green PL band was observed, peak position of this band shifting from 515 to 485 nm with increasing Mg content from x=0 to x=0.20. Doped with Cu and sintered in air samples exhibited intense green band peaked at 540nm whose spectral position was found to be independent on Mg content. In PLE spectra of the self-activated green emission, the only maximum at 380 nm whose position coincided with that of emission band related to free exciton was observed. At the same time, In PLE spectra of Cu-related green emission, extrinsic maximum at about 400 nm dominated. The peculiarities of interaction of self-activated and Cu-related emission centers with host crystal lattice and other local centers as well as electron-hole transitions responsible for observed green emission bands were discussed.

## Internal electric fields due to piezoelectric and spontaneous polarizations in ZnO/ZnOS quantum well

H. C. Jeon<sup>1</sup>, S. H. Park<sup>2</sup>, T. W. Kang<sup>1</sup>, S. J. Lee<sup>1\*</sup>

<sup>1</sup>Quantum-functional Semiconductor Research Center, Dongguk University, Seoul, Korea

<sup>2</sup>Department of Electronics Engineering, Catholic University of Daegu  
Kyeonbuk 712-702, Korea

\*E-mail of the corresponding author (leesj@dongguk.edu)

Wide band-gap wurtzite semiconductors have attracted much attention due to their potential applications for optoelectronic devices in blue and ultraviolet regions. So far, practical short-wavelength light-emitting diodes or laser diodes have been fabricated using GaN-related materials. On the other hand, ZnO and related oxides have been proposed as alternative wide band-gap semiconductors for short-wavelength optoelectronic applications. ZnO-based quantum well(QW) structures and their properties are of increasing interest for possible applications in light-emitting diodes (LEDs) and laser diodes (LDs) operating in the visible and ultraviolet region, owing to their direct wide band gap ( $E_g \sim 3.4\text{--}3.8$  eV) and large binding energy of excitons (60 meV) [1,2]. In order to design ZnO based optoelectronic devices, quantum confined structures are essential, which necessitate the modification of the band structure by alloying. In this regard, a change of the content of the anions or cations in ZnS by introducing the isoelectronic impurities is important in terms of a band-gap engineering.

Numerous works have been reported related to ZnMgO, ZnBeO and ZnCdO, which modify the band gap clearly toward higher and lower energies, respectively. However, fewer attentions have been paid to anions alloying such as S and Se in ZnO, which are also important from the viewpoint of band gap engineering. It is noted that the  $E_g$  of ZnS is larger than that of ZnO, so the band gap engineering might be possible. It was expected that the bowing parameter of ZnSO is large due to the large electronegativity differences between O and S and thus comparable with those of GaNP and GaNAs.

On the theoretical side, the above experimental result suggest that an understanding of the roles of internal electric fields due to piezoelectric (PZ) and spontaneous (SP) polarizations in wurtzite ZnO-based QW structures is very important in order to give guidelines on sample growth and a device design. For these results, we investigate electronic and optical properties of ZnO/ZnOS QW structures numerically with SP and PZ polarizations by considering many-body effects. The self-consistent (SC) band structures and wave functions for the QW structures are obtained by solving the Schrödinger equation for electrons and the 3x3 Hamiltonian for holes, similar to the Luttinger Hamiltonian. The strain-induced piezoelectric polarization and the spontaneous polarization can be reduced effectively using by the internal field engineering in the ZnO/ZnOS QW structures. That is, optical properties of ZnO/ZnOS QW structures resulting in the increased optical gain the fact that the QW potential is flattened as a result of the compensation of the internal field. We got very high laser gain spectrum compare with that of without considering droop prevention.

[1] A. Tsukazaki, A. Ohtomo, T. Kita, Y. Ohno, H. Ohno, and M. Kawasaki, *Science* **315**, 1388 (2007).

[2] B. P. Zhang, N. T. Binh, K. Wakatsuki, C. Y. Liu, Y. Segawa, and N. Usami, *Appl. Phys. Lett.* **86**, 032105-1 (2005).

## **Anisotropic Optical Properties of a Homoepitaxial (Zn,Mg)O/ZnO Quantum Wells growth on A plane**

Mohammed J. Mohammed Ali<sup>1</sup>, T. Bretagnon<sup>1\*</sup> and J.M. Chauveau<sup>2</sup>

<sup>1</sup>Laboratoire Charles Coulomb, CNRS - Université Montpellier, F-34095 Montpellier, France

<sup>2</sup>CRHEA–CNRS, Rue Bernard Grégory, F-06560 Valbonne, France

\* Thierry.Bretagnon@um2.fr

ZnO/(Zn,Mg)O hetero-structures have gained much interest in the last few years for its potential application. Zinc oxide is a well-known wide band gap semiconductor exhibiting a large exciton binding energy (~60meV). It is therefore of high interest in opto-electronic applications where robust excitons and/or large oscillator strengths are required.

In this communication, we report on the optical properties of homo-epitaxial non-polar (Zn,Mg)O/ZnO quantum wells (QWs) grown by molecular beam epitaxy (MBE) on A-plane (11-20) ZnO substrates. The optical properties of this quantum wells are investigated by using reflectance and continuous wave photoluminescence (CW-PL) spectroscopies.

The CW-PL and reflectivity spectra measured at low temperature reveal strong in-plane optical anisotropies and clear reflectance structures, as an evidence of good interface morphologies. The signatures of confined excitons analogous to C-exciton and (A ,B)-excitons in bulk ZnO, are detected using light polarized respectively along the c-axis and perpendicular to this axis.

Temperature dependence of CW-PL has been investigated in the two polarizations. For electric field of the light perpendicular to the c-axis the total intensity of the PL lines decreases by about an order of magnitude when the temperature increases from 10 K to room temperature. At low temperature a line associated to an excitonic complex dominates the PL spectrum. When the temperature increases the intensity of this line decreases as the intensity of the line associated to the free exciton increases. In the other polarization at about 80 K a new line appears in the spectrum. Its intensity increases with temperature. This feature is associated to the C free exciton.

## Luminescence transformation in mixture of ZnO and Carbon nanoparticles at mechanical processing

T. Torchynska<sup>1\*</sup>, B. Perez Millan<sup>2</sup>, M. Kakazey<sup>3</sup> and M. Vlasova<sup>3</sup>

<sup>1</sup>ESIME – Instituto Politécnico Nacional, México D. F. MEXICO

<sup>2</sup>UPIITA – Instituto Politécnico Nacional, México D. F. MEXICO.

<sup>3</sup>CIICAp - Universidad Autónoma del Estado de Morelos, Cuernavaca, MEXICO

\*torch@esfm.ipn.mx

The photoluminescence (PL), SEM and X ray diffraction (XRD) of the mixture of ZnO + xC nanoparticles have been studied before and after intensive mechanical processing (MP) with the aim to identify the native defects in ZnO nanocrystals (NCs). Three types of the ZnO + xC mixtures with the x equal to 0.1, 1.0 and 3.0 % wt have been investigated. The study reflects the diversity of physical and chemical processes occurring in samples during MP: the destruction of primary ZnO nanoparticle aggregates, crushing individual ZnO nanoparticles from the size of 250 nm down to 14 nm, crushing individual C nanoparticles, the development of pulse and accumulative thermal processes, the interaction of carbon atoms with oxygen in the treatment chamber and with the surface of ZnO nanoparticles etc. Two stages of PL spectrum transformation have been revealed and discussed. The new PL band peaked at 2.82-2.88 eV has been detected in PL spectra after 9 min of MP. The origin of this emission in ZnO has not been conclusively established and a number of hypotheses have been proposed. Using carbon content variation in the studied ZnO + xC mixture the new PL band at 2.82-2.88 eV has been studied and its nature has been discussed.

# Polariton condensates in ZnO microcavities: propagation Vs localization

R. Hahe<sup>2</sup>, L. Orosz<sup>3</sup>, S. Bouchoule<sup>4</sup>, C. Brimont<sup>2</sup>, P. Disseix<sup>3</sup>, T. Guillet<sup>2</sup>, X. Lafosse<sup>4</sup>, M. Leroux<sup>1</sup>, J. Leymarie<sup>3</sup>, Feng Li<sup>1</sup>, G. Malpuech<sup>3</sup>, F. Réveret<sup>2</sup>, F. Semond<sup>1</sup>, D. Solnyshkov<sup>3</sup>, and J. Zuniga-Perez<sup>1,\*</sup>

<sup>1</sup>CRHEA-CNRS, Rue Bernard Gregory, 06560 Valbonne, France

<sup>2</sup>Université de Montpellier 2, CNRS, Laboratoire Charles Coulomb, UMR 5221, 34095 Montpellier, France

<sup>3</sup>Institut Pascal, PHOTON-N2, Clermont Université, CNRS and Université Blaise Pascal, 24 Avenue des Landais, 63177 Aubière cedex, France

<sup>4</sup>LPN-CNRS, Route de Nozay, 91460 Marcoussis, France

Semiconductor planar microcavities operating in the strong-coupling regime are optical resonators in which the *eigenmodes* of the system are no longer purely excitonic nor purely photonic, but a mixture of these two states. These structures have been rapidly developed in the last years, especially since the demonstration of polariton Bose-Einstein condensation [1] and the observation of polariton condensate superfluidity [2]. However, all these experiments were carried out at low temperatures. In order to obtain polariton condensation at high temperature, i.e. room temperature or above, materials with large oscillator strengths and large exciton binding energies must be employed. This is the reason why so much attention has been paid lately to organic semiconductors, GaN and ZnO.

In this work we will address polariton propagation in two different ZnO-based microcavities. The first one consists of two dielectric Distributed Bragg Reflectors (DBRs) surrounding a ZnO active region made of ZnO bulk material [3]. This cavity displays polariton condensation from low to room-temperature as well as under very different detuning conditions, which leads to the generation of polariton condensates very different in nature [4]: indeed, it was possible to create polariton condensates ranging from 83% photon-like to 96% exciton-like, thanks to a large thickness gradient across the cavity. This allowed us to tune the polariton interaction constant by more than one order of magnitude and to understand how the excitonic/photonic potentials control the propagation of polariton condensates. This will be illustrated by spatially and spectrally-resolved images of the polariton condensate, both at low and room-temperatures, and the results will be compared to theoretical models describing polariton condensate propagation under similar conditions. The second cavity consists of a 30-pair AlN/AlGa<sub>N</sub> DBR, an epitaxial ZnO active region, and a top 11-pair SiO<sub>2</sub>/HfO<sub>2</sub> DBR: it displays a much smaller inhomogeneous photonic broadening [5]. However, it will be shown that even if the photonic disorder is negligible with respect to the measured Rabi splitting, it still has an influence on the properties of the polariton condensate.

[1] J. Kazprzak *et al.*, *Nature* **443** (2006) 409

[2] A. Amo *et al.*, *Nature* **457** (2009) 291

[3] Feng Li *et al.*, *Appl. Phys. Lett.* **102** (2013) 191118

[4] Feng Li *et al.*, *Phys. Rev. Lett.* **110** (2013) 196406

[5] J. Zuniga-Perez *et al.*, *Appl. Phys. Lett.* **104** (2014) 241113

\*Electronic mail: jzp@crhea.cnrs.fr

## EPR Investigations on Doped TiO<sub>2</sub> Nanopowders

Zhurovetski V<sup>1</sup>,  
Onisimchuk V<sup>1</sup>, Popovych D<sup>1</sup>, Serednytski A<sup>1</sup>  
 Buketov A<sup>2</sup>, Spronov O<sup>2</sup>, Brailo M<sup>2</sup>

<sup>1</sup>Institute of Applied Problems of Mechanics and Mathematics NASU,  
 Lviv, Ukraine, e-mail: [onisimchuk2info@gmail.com](mailto:onisimchuk2info@gmail.com)

<sup>2</sup>Kherson state maritime academy, Kherson, Ukraine

In our research we have been discovered electron-paramagnetic resonance (EPR) of TiO<sub>2</sub> nanopowders. EPR spectra were performed by means CMS-8400 spectrometr. During complex analysis of EPR spectra we do comparison of obtained peak characteristics one of them W (compute like the difference in points of minimum and maximum magnitudes of magnetic field) that is widely spread in practical use. Also analysis of concentration of paramagnetic centers was made (C) for as-prepared and doped TiO<sub>2</sub> nanopowders.

It was revealed that doping not only affects on concentration of paramagnetic centers but also make changes on external structure of TiO<sub>2</sub> nanopowders [1]. In our case conducted measurements of TiO<sub>2</sub> nanopowder samples showed changes of g-factors during Cu incorporation that we can see on changes parameters of the lower peak that can be induced by creation and appearance on the surface of oxygen radicals (OH, O<sub>2</sub>) catalytic reactions. Photocathalitic reactions generally formed hydroxide radicals (OH<sup>·</sup>) through water oxidation and superoxide radicals (O<sub>2</sub><sup>·-</sup>) induced by coupling and engaging of oxygen from the air [2,3]. Obtained values of spectra with resonance frequency of magnetic field  $\nu = 9423,558$  MHz for as-prepared TiO<sub>2</sub> shows W of resonance magnetic field peak  $W = 4,52$ . For conducted measurements of Cu-doped TiO<sub>2</sub> nanopowders  $W = 5,96$  concentration of the paramagnetic centers  $C = 5,05 \cdot 10^{21}$ . On this sample we observed shifting of the lower resonance peak and also higher concentration of the paramagnetic centers compared to as-prepared TiO<sub>2</sub> nanopowders (concentration of paramagnetic centers is  $C = 2,94 \cdot 10^{22}$ ). Treated by laser technics through the glass TiO<sub>2</sub> nanopowders showed a little lower concentration of paramagnetic centers compared to the as-prepared TiO<sub>2</sub> nanopowders. Resonance peak width W for the samples treated by laser through the glass was about  $W = 6,52$ .

Our experimental observations and obtained results showed that Cu as doping component can lead to significant increase in paramagnetic centers concentration in TiO<sub>2</sub> nanopowders. Cu dopant interaction with oxygen radicals on the nanopowder surface can also affect on photoluminescence of TiO<sub>2</sub> nanopowders. On our opinion changes in resonance peak width W also can be induced by interaction with hydroxyle groups and oxygen radicals. Furthermore, oxygen radicals on TiO<sub>2</sub> nanopowder surface take an active part in oxidation processes that can make changes to the structure and photoluminescence properties of TiO<sub>2</sub> nanopowders.

[1] Ao Y, Xu J, Zhang S, et al. A one-pot method to prepare N-doped titania hollow spheres with high photocatalytic activity under visible light. *Appl Surf Sci*, **256**: 2754–2758 (2010)

[2] Konaka R., E. Kasahara, W. C. Dunlap, Y. Yamamoto, K. C. Chien and M. Inoue Irradiation of titanium dioxide generates both singlet oxygen and superoxide anion. *Free Radic. Biol.Med.* **27**, 294–300 (1999)

[3] Reeves J. F., S. J. Davies, N. J. F. Dodd and A. N. Jha Hydroxyl radicals (OH) are associated with titanium dioxide (TiO<sub>2</sub>) nanoparticle-induced cytotoxicity and oxidative DNA damage in fish cells. *Mutat. Res.* **640**, 113–122 (2008)

## Vertical and Planar ZnO-based Schottky Junctions Obtained by the Atomic Layer Deposition – Influence of the Hafnium Dioxide Spacer on Rectifying Properties

Tomasz A. Krajewski<sup>1\*</sup>, Adam J. Zakrzewski<sup>1,2</sup>, Grzegorz Luka<sup>1</sup>, Krzysztof Goscinski<sup>1</sup>,  
Marek Godlewski<sup>1,2</sup> and Elzbieta Guziewicz<sup>1</sup>

<sup>1</sup>Institute of Physics, Polish Acad. of Sciences, Al. Lotnikow 32/46, 02-668 Warsaw, Poland

<sup>2</sup>Department of Mathematics and Natural Sciences, College of Science Cardinal Stefan Wyszyński University, ul. Dewajtis 5, 01-815 Warsaw, Poland

\*e-mail: krajew@ifpan.edu.pl

Zinc oxide is currently widely investigated as a very promising II-VI semiconducting material for various electronic and optoelectronic purposes. The ZnO applications include mainly thin film transistors [1], solar cells (photovoltaics) [2,3] where it acts as a transparent electrode and the new generation of 3D memories built in the so-called cross-bar architecture, in which the ZnO-based Schottky diode works as a selecting element [4,5]. The ZnO-based junctions can also be used as sensing devices. However, formation of ZnO-based Schottky rectifying structure dedicated to some of the above-mentioned purposes (e.g. memory arrays) still remains a scientific challenge as the advanced electronics often imposes very strict requirements on the electrical properties of the ZnO material. This concerns mainly the diode's rectification ratio ( $I_{ON}/I_{OFF}$ ) which in this case ought to be as high as  $10^6$ . This, in turn, requires low carrier density ( $n \sim 10^{16} \text{ cm}^{-3}$ ) and their high mobility (above  $10 \text{ cm}^2 \text{ V}^{-1} \text{ s}^{-1}$ ) being responsible for low reverse and high driving current of the junction, respectively [4].

This work shows results of modeling of current-voltage characteristics of Ag/ZnO/ITO(TiAu) Schottky diodes with ZnO fabricated in low temperature (around  $100^\circ\text{C}$ ) Atomic Layer Deposition process from diethylzinc and deionized water. The discussed structures contain also the interfacial layer of hafnium dioxide with thickness ranging from 1.25 to 7.5 nm. As it was found their forward characteristics can be described within the thermionic emission theory. Basing on this approach values of some relevant diodes' parameters were determined, including the ideality factor and the effective Schottky barrier height. Testing both types of the junction architecture (i.e. vertical and planar one) we found a satisfactory agreement of experimental and theoretical results proving that the 2.5 nm thick  $\text{HfO}_2$  spacer between ZnO and silver contact yields the highest effective Schottky barrier (about 0.5 – 0.7 eV), which is manifested by the enhanced rectification ratio (reaching  $10^5$  at  $\pm 2 \text{ V}$ ) of the examined structure [6].

- [1] R. Grundbacher, K. Chikkadi and C. Hierold, *J. Vac. Sci. Technol. B* **28** (6), 1173 (2010).
- [2] J. A. van Delft, D. Garcia-Alonso and W. M. M. Kessels, *Semicond. Sci. Technol.* **27**, 074002 (2012).
- [3] H. Saarenpää, T. Niemi, A. Tukiainen et al., *Solar Energy Materials and Solar Cells* **94**, 1379 (2010).
- [4] N. Huby, G. Tallarida, M. Kutrzeba et al., *Microel. Eng.* **85**, 2442 (2008).
- [5] M. Godlewski, E. Guziewicz, J. Szade et al., *Microel. Eng.* **85**, 2434 (2008).
- [6] T. A. Krajewski, G. Luka, S. Gieraltowska, A. J. Zakrzewski et al., *Appl. Phys. Lett.* **98**, 263502 (2011).

**Acknowledgements:** The work was supported by the grant of the National Science Center of Poland (decision number: DEC-2013/09/D/ST5/03879).

## Effects of the conduction band offset on the efficiency of n-ZnO/p-Si based heterojunctions for photovoltaic applications

R. Schifano<sup>1\*</sup>, R. Pietruszka<sup>1</sup>, T. A. Krajewski<sup>1</sup>, B. S. Witkowski<sup>1</sup>, E. Zielony<sup>2</sup>, K. Gwozdz<sup>2</sup>, P. Bieganski<sup>2</sup>, E. Placzek-Popko<sup>2</sup>, M. Godlewski<sup>1,3</sup>

<sup>1</sup>Institute of Physics, Polish Acad. of Sciences, Al. Lotnikow 32/46, 02-668 Warsaw, Poland

<sup>2</sup>Faculty of Fundamental Problems of Technology, Wrocław University of Technology  
ul. Wybrzeże Wyspińskiego 27, 50-370 Wrocław, Poland

<sup>3</sup>Dept. of Mathematics and Natural Sciences College of Science Cardinal S. Wyszyński  
University, ul. Dewajtis 5, 01-815 Warsaw, Poland

\*e-mail: [schifano@ifpan.edu.pl](mailto:schifano@ifpan.edu.pl)

Similarly to what has been shown for CIGS-based devices, numerical calculations indicate that reducing the conduction band offset ( $\Delta E_C$ ) appearing in n-ZnO/p-Si heterojunction solar cells strongly reduces the impact of recombination centers at the interface between the two semiconducting materials, thus enabling high efficiency solar cells.[1,2]

In the work here presented it is experimentally shown that there is a clear relation between higher efficiency n-ZnO/p-Si based heterojunction solar cells and lower  $\Delta E_C$  extracted from Capacitance vs. Voltage (C-V) measurements performed in the 250-1 kHz range. In detail, by decreasing  $\Delta E_C$  from ~0.63 eV to ~0.48 eV a corresponding rise in the solar cell efficiency from ~3.7% to ~6.0% under standard test conditions (STC) has been observed if the ideality factor,  $n$ , is below ~2. The increase in efficiency is occurring despite presence of defects and/or charging and de-charging of electric dipoles at the interface is observed in all samples. Existence of electrically active interfacial centers is suggested by the substantial deviation from the expected linear relationship of the  $1/C^2$  vs. V characteristics that has been detected in the reverse bias range when the probing voltage frequency is reduced to 1 kHz.[3] In addition, no significant variations for  $n$  obtained from Current vs. Voltage measurements (I-V) has been observed for samples with a STC efficiency above 3%. That is, an  $n$  value equal to ~1.5 has been extracted for these samples indicating that the current transport is not purely diffusion limited ( $n \sim 1$ ) or recombination limited ( $n \sim 2$ ) in the case of n-ZnO/p-Si based heterojunction with the highest efficiencies.

Finally, the ZnO based layer thickness and growth temperature have been optimized achieving in the case of the best sample a STC efficiency of ~7.5% corresponding to a Short Circuit Current ( $I_{SC}$ ), Open Circuit Voltage ( $V_{OC}$ ) and Fill Factor (FF) of 33.7 mA/cm<sup>2</sup>, 0.319 V and 66%, respectively.

[1] T. Minemoto, Y. Hashimoto, T. Satoh, T. Negami, H. Takakura, and Y. Hamakawa, J. Appl. Phys. 89 (12), 8327 (2001).

[2] K. E. Knutsen, R. Schifano, E. S. Marstein, B. G. Svensson, and A. Yu Kuznetsov, phys. stat. sol. (A) 210, 585 (2013)

[3] J. P. Donnelly, and A. G. Milnes, IEEE Trans. on Electron. Devices, 14, 63 (1967)

**Acknowledgments.** This work was partially supported by the National Science Centre (dec. No. DEC-2012/D6/A/ST7/00398) and National Centre for Research and Development through grant PBS1/A5/27/2012). The authors R. P. and T. A. K. acknowledge support by the grant DEC-2013/09/D/ST5/03879 of NSC of Poland. The author R.S. was supported by the EU 7th Framework Programme project REGPOT-CT-2013-316014 (EAgLE).

**Poster Session 3 - ThP**

**Optical and electrical properties , photonic engineering**

## Transparent and Flexible AC powder Electroluminescence Device with a Simple Structure of Ag Nanowire/ ZnS:Cu<sup>+</sup>, Mn<sup>2+</sup> /ITO

Seokgyu Lim<sup>1</sup>, Kwangwon Park<sup>1</sup>, Hyoungeak Jeong<sup>1</sup>, Daehan kim<sup>1</sup>, Jaehyeong Park<sup>1</sup>, and Jongsu Kim<sup>1\*</sup>

<sup>1</sup>Department of Display Science and Engineering, Pukyong National University, Busan 608-739, Korea

\*jsukim@pknu.ac.kr

ZnS: Cu, Mn nano phosphor was achieved by milling of the bulk phosphors to the nanoscale by a planetary miller, and then transparent and flexible ac powder electroluminescence (EL) device based on the ZnS: Cu, Mn nano phosphor was fabricated by spin coating and bar coating method, for the AgNW electrode layer and ZnS:Cu<sup>+</sup>, Mn<sup>2+</sup> phosphor layer, respectively. This transparent EL device have a simple structure of Ag nanowire (AgNW) electrode layer /ZnS:Cu<sup>+</sup>, Mn<sup>2+</sup> phosphor layer based on indium tin oxide (ITO) electrode PET film. Under forward biased condition, orange electroluminescence (EL) with its peak wavelength at about 580 nm was observed at room temperature. The peak position of the EL is very similar to that of the photoluminescence (PL) and the emitted EL intensity is proportional to the current density passing through the device. This orange electroluminescence (EL) is originated from impact excitation of Mn<sup>2+</sup> ions caused by accelerated electrons under a high electric field. [1] Transmittance of the EL device with simple structure was about ~ 70 % at 550 nm.

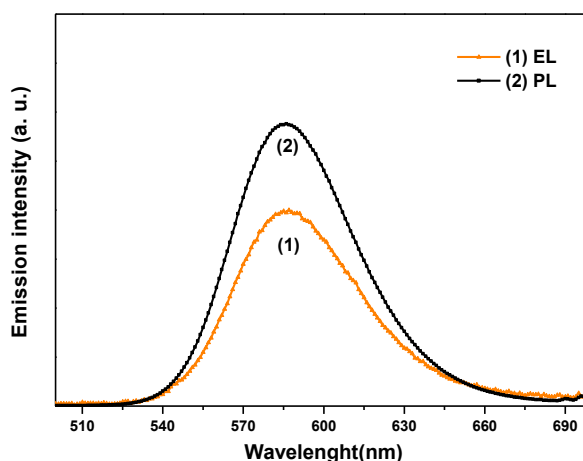


Fig. 1. Electroluminescence and photoluminescence spectra of the transparent ac powder EL device and nano powder, respectively.

[1] Y. A. Ono, "Electroluminescent Displays", World Scientific, USA, (1995)

## Structural, Optical, and Magnetic Characteristics of II-VI Semiconductor Nanocrystal - Graphene Hybrid Nanostructures

Savchuk A.I.<sup>1\*</sup>, Stolyarchuk I.D.<sup>1</sup>, Savchuk S.A.<sup>1</sup>, Sheregii E.M.<sup>2</sup>, and Polit J.<sup>2</sup>

<sup>1</sup>Department of Physics of Semiconductors and Nanostructures, Chernivtsi National University, Chernivtsi, Ukraine

<sup>2</sup>Centre for Innovation and Transfer of Natural Sciences and Engineering Knowledge, University of Rzeszow, Rzeszow, Poland

\*a.savchuk@chnu.edu.ua

Modern nanoscience with nanocrystals was born in the early 1980s, and II-VI semiconductor nanocrystals were among the first discovered zero-dimensional (0D) structures with exhibition of quantum size effect [1, 2]. Two decades later fascinated way has started for graphene, a one-atom-thick-layer of  $sp^3$ -bonded carbon atoms arranged in a two-dimensional (2D) honeycomb lattice structure [3]. Combination of semiconductor nanocrystals and graphene represents a new type of hybrid nanostructure that has attracted wide attention from point of view elucidation of interaction between the mentioned 0D and 2D structures. No doubt, this kind of hybrid structure has perspectives for various fields of practical applications from optoelectronics and nanoelectronics to biophysics and medicine.

The nanocrystal-graphene hybrid structures can be synthesized by combining various types of nanoparticles with graphene or its derivatives, graphene oxide, reduced graphene oxide and graphene quantum dots. In this work, we report on synthesis and characterization of II-VI semiconductor nanocrystal-graphene hybrid structures. We have focused our attention on case of nanocrystal-graphene composites, where the nanoparticles are attached to sheets of graphene.

Firstly, CdS and CdSe nanocrystals were synthesized by a solution-chemical route, which is widely used by many research groups [4] with some modifications. Then, trioctylphosphine oxide (TOPO) ligands of the semiconductor nanoparticles were exchanged with Pyridine (Py) by refluxing in anhydrous Py. Chemically converted graphene was prepared by reducing graphite oxide using a modified Hummers method. Nanocrystal-graphene hybrid materials were synthesized by mixing chemically converted graphene with Py-capped CdS and CdSe nanocrystals in aqueous solution. Nanocrystals of undoped zinc oxide (ZnO) and ZnO:Co were synthesized by a non-aqueous method in methanol. These nanoparticles were also mixed with chemically derived graphene in a certain ratio to form a mixture solution. For different characterizations and practical applications the obtained nanocrystal-graphene hybrids in solution were transformed in solid films. Both kinds of samples were imaged using transmission electron microscopy (TEM) and scanning electron microscopy (SEM). UV-vis absorbance spectroscopy has served for revealing of changes in related spectra depending on composition and component contents of the studied composites. On the base of results of magnetic and magneto-optical measurements for ZnO:Co nanocrystal-graphene hybrid, it was confirmed recent finding [5] of transition from paramagnetic to ferromagnetic behavior at room temperature.

- [1] Ekimov AI, Efros AIL, Onushchenko AA, Solid State Communications, **56**, 921, (1985).
- [2] Brus L, J. Phys. Chem. **90**, 2555, (1986).
- [3] Novoselov KS, Geim AK, Morozov SV, Jiang D, Zhang Y, Dubonos SV, Grigorieva IV, Firsov AA, Science, **306**, 666, (2004).
- [4] Kovalenko MV, Manna L, Cabot A et al. ACS Nano, **9**, 1012 (2015).
- [5] Sun Z, Yang X, Wang C, Yao T, Cai L, Yan W, Jiang Y, Hu F, He J, Pan Z, Liu Q, Wei S, ACS Nano, **8**, 10589, (2014).

## Polariton lasing in high-Q fully epitaxial wide-bandgap semiconductor microcavity pillars

T. Klein<sup>2</sup>, S. Klembt<sup>1\*</sup>, E. Durupt<sup>1</sup>, C. Kruse<sup>2</sup>, D. Hommel<sup>2</sup>,  
and M. Richard<sup>1</sup>

<sup>1</sup>Institut Néel, CNRS-CEA-Université Grenoble Alpes, BP166, 38042 Grenoble, France

<sup>2</sup>IFP, Universität Bremen, Otto-Hahn-Allee NW1, 28359 Bremen, Germany

\*Corresponding author: sebastian.klembt@neel.cnrs.fr

In the past decade exciton-polaritons in semiconductor microcavities have become a testing field of non-equilibrium dynamics of quantum fluids, that allowed for fundamental studies on light-matter interactions [1]. Polariton lasing has been demonstrated from 0D-modes in micropillars [2], and the confinement of cavity-polaritons has proven to be a versatile tool to study and tune interactions in polariton condensates [3,4,5]. Due to highly demanding requirements with respect to the crystalline and optical quality as well as disorder, experiments have mainly been done on GaAs-based structures so far.

Here we demonstrate polariton lasing from zero-dimensional states in fully epitaxial high-Q ZnSe-based micropillar cavities of various diameters as well as in a 2D planar microcavity.

These cavities show a Rabi splitting in the order of  $\hbar\Omega_R \approx 30$  meV. A linear blueshift with increasing state occupancy is found as a clear signature of polariton self-interaction. Q-factors well above 5000 and low polariton lasing thresholds between  $P_{\text{thr}}=2.41\mu\text{J}/\text{cm}^2$  and  $2.11\mu\text{J}/\text{cm}^2$  are found across all pillar diameters from  $1.5\mu\text{m}$  to  $10\mu\text{m}$ , pointing out the high crystalline quality and the low etching induced sidewall damage. Optical and structural properties compare well with the widely established GaAs- and CdTe-based microcavities, underlining furthermore the overall quality in these wide-bandgap semiconductor microstructures. We present this as a technical proof that in prospect can allow for e.g. the study of interactions at elevated temperatures.

[1] I. Carusotto and C. Ciuti, Rev. Mod. Phys. **85**, 299 (2013)

[2] D. Bajoni et al., Phys. Rev. Lett. **100**, 047401 (2008)

[3] T. K. Paraïso et al., Phys. Rev. B **79**, 045319 (2009)

[4] L. Ferrier et al. Phys. Rev. Lett. **106**, 126401 (2011)

[5] B. Besga et al., Phys. Rev. Appl. **3**, 014008 (2015)

## Enhanced stimulated emission in ZnO thin films by using top-down structuring

Komla Nomenyo<sup>1\*</sup>, Abdel-Sattar Gadallah<sup>1,2</sup>, Sergei Kostcheev<sup>1</sup>, Rafael Salas-Montiel<sup>1</sup>,  
Sylvain Blaize<sup>1</sup>, Dave Rogers<sup>3</sup>, and Gilles Lerondel<sup>1\*</sup>

<sup>1</sup>Laboratoire de Nanotechnologie et d'Instrumentation Optique, Institut Charles Delaunay, CNRS UMR 6281, Université de Technologie de Troyes, 12 rue Marie Curie, CS 42060, 10004 Troyes Cedex, France

<sup>2</sup>Department of Laser Sciences and Interactions, National Institute of Laser Enhanced Sciences, Cairo University, Giza, Egypt

<sup>3</sup>Nanovation, 8, route de Chevreuse, 78117 Châteaufort, France  
\*komla.nomenyo@utt.fr, gilles.lerondel@utt.fr

Lasers are more and more relevant for applications and especially compact UV laser diodes. Although GaN-based devices have a good performance and remains the material of choice in the semiconductor industry, ZnO is still interesting. Large exciton binding energy, efficient radiative recombination and simpler crystal-growth processes are significant for lower costs ZnO-based devices. On the other hand, ZnO structuring in order to realize planar photonic structures, has proved to be a critical issue that is faced up by the strong mechanical properties of ZnO, making of lithography one of the main challenges to confront for the fabrication of efficient ZnO lasers and LEDs.

In this work, ZnO microdisks were fabricated using top-down approach in planar thin film by combining electron beam lithography with a lift-off process after metal evaporation and reactive ion etching. The thin film was grown by pulse laser deposition (PLD) and has high optical gain and low losses [1]. Compared to a reference film, an enhancement of more than 200% of the stimulated surface emission from these micro-structured thin films was found [2]. Narrowing, reduction in lasing threshold and blue shifting of the emission wavelength were observed along with the enhancement in the emitted intensity. We find out that the light enhancement comes from the reduction of the spontaneous emission, the increase of the internal quantum efficiency of the thin film and the amplification of the stimulated emission. An analysis in terms of waveguiding is presented in order to explain these effects.

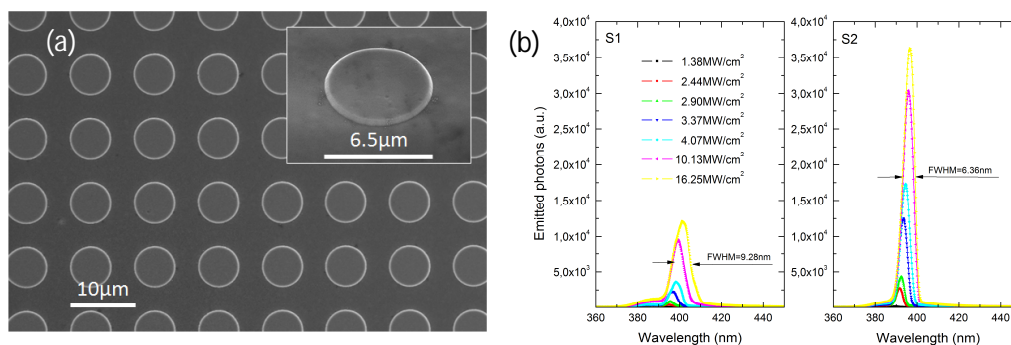


Figure: (a) Top view of the micro-structured planar ZnO thin film (electron micrograph), (b) Surface-emission spectra at different pumping intensities for a reference thin film, S1 and microdisk structured area S2.

- [1] A.-S. Gadallah, K. Nomenyo, C. Couteau, D. J. Rogers, and G. Léron del, *Appl. Phys. Lett.* 102, 171105 (2013).  
[2] K. Nomenyo, A.-S. Gadallah, S. Kostcheev, D. J. Rogers, and G. Léron del, *Appl. Phys. Lett.* 104, 181104 (2014).

## 2D-Localization and Delocalization Effects in Quantum Hall Effect Regime in HgTe Wide Quantum Wells

Arapov Yu.G.<sup>1</sup>, Gudina S.V.<sup>1\*</sup>, Neverov V.N.<sup>1</sup>, Podgornykh S.M.<sup>1</sup>, Popov M.R.<sup>1</sup>, Shelushinina N.G.<sup>1</sup>, Harus G.I.<sup>1</sup>, Yakunin M.V.<sup>1</sup>, Dvoretzky S.A.<sup>2</sup>, and Mikhailov N.N.<sup>2</sup>  
<sup>1</sup>M.N. Miheev Institute of Metal Physics of Ural Branch of Russian Academy of Sciences, Yekaterinburg, Russia  
<sup>2</sup>A.V. Rzhanov Institute of Semiconductor Physics of Siberian Division of Russian Academy of Sciences, Novosibirsk, Russia  
\*svpopova@imp.uran.ru

The longitudinal and Hall resistivities in the quantum Hall effect regime in an HgTe quantum well (well width 20.3 nm) with inverse energy spectrum at the temperatures (2÷50) K and in the magnetic field up to 9 T were measured. The experimental data both in the plateau-plateau transition region (metallic conductivity on delocalized states) and in the quantum Hall effect plateau regions (variable range hopping conductivity on localized states in the mobility gap between Landau levels) were analyzed.

The feasibility of the temperature scaling regime [1] for the plateau-plateau quantum phase transition for the 2D HgTe-based heterostructures from the temperature dependences of conductivity in the transition region between the first and second quantum Hall plateaus was proved. For the description of the temperature-induced conductivity in a quantum Hall plateau region the conception of variable range hopping conductivity [2] was used. The localization length critical exponent value corresponding to result of the classical percolation theory for long-range impurity potential [3] was received. It was shown that such a regime of hopping conductivity observing far from the Landau level center is agreed with hops on localized states in the tails of broadened Landau levels out of quantum tunneling regime, i.e. in the classical percolation theory region.

The work was supported by RFBR: grants № 14-02-00151 и №14-02-31164.

- [1] A. M. M. Pruisken, Phys. Rev. Lett. **61**, 1297 (1988).
- [2] D. G. Polyakov and B. I. Shklovskii, Phys.Rev.B **48**, 11167 (1993).
- [3] B. Huckestein, Rev. Mod. Phys. **67**, 367 (1995).

## Effect of Acoustic Vibrations on Electrical Properties of CdTe Crystals

Olikh Ya.M., Tymochko M.D.

V.E. Lashkaryov Institute of Semiconductor Physics, Nat. Acad. of Sci. of Ukraine, Kyiv  
[tymochko@ukr.net](mailto:tymochko@ukr.net)

It is known that the use of ultrasound (US) is one of the methods for the controlled modification of semiconductor structure and improvement of device characteristics on its basis. The phenomenon of US effect is connected with changes in the system of electrically- and optically-active defects. The important factor is the presence of metastable defect complexes of the crystal structure in dislocation-free semiconductor crystals [1]. Another mechanism of US effect is the acousto-dislocation interaction, mainly for II-VI semiconductors [2]. So, linear dislocations act as "agents" for the interaction between an acoustic wave and charged carriers. It is suggested that "trapping" or "removing" of mobile electrically-active point defects (acceptors or donors) from the dislocations occurs under the influence of an acoustic wave. The possibilities of these acoustic-wave-stimulated (AWS) defects modification processes are characterized by the content and structure of defects, the concentration of dislocations in the sample in particular.

This paper presents the AWS phenomena in CdTe monocrystal samples in dynamic regime (*in-situ*). It is known that CdTe monocrystals are used as uncooled X- and  $\gamma$ -ray detectors. Particularly interesting are the CdTe monocrystals with chlorine impurity to create metastable complexes with intrinsic defects. For identification of the nature of acoustically-active defects temperature investigations (77÷300 K) of Hall effect on CdTe:Cl monocrystals ( $N_{Cl}=(5\cdot 10^{17}\div 10^{19})\text{ cm}^{-3}$ ) *n* and *p*-type in conditions of US influence ( $f_{US}\sim(5\div 17)\text{ MHz}$ ,  $W_{US}\sim(0,1\div 1,0)\text{ W/cm}^2$ ) were carried out. It was observed that the dynamic AWS changes of the electrophysical characteristics (conductivity and mobility are decreasing at room temperature and increasing at low temperatures) are reversible. Long-term relaxation processes ( $10^0\text{--}10^3$  sec) at switching-on as well as at shutdown of US indicate the diffusion process modification of the point-defect structure of crystal.

The diverse nature of AWS relaxation of concentration and mobility of charge carriers is determined by the temperature of the sample. It shows different rebuilding mechanisms of the point-defect structure of crystal: instantaneous ( $< 0,1$  sec) – at the temperatures  $T > 200$  K and long-termed ( $10^0\text{--}10^3$  sec) at  $T < 160$  K. Various mechanisms of AWS changes for different temperature regions are discussed – an additional carriers scattering on the mobile dislocations and on AWS perturbation system of the thermal vibrations of the crystal lattice.

Therefore, in our opinion, the main rebuilding process in US switching-on consists of the transformation of an acceptor complex  $[(V_{Cd}^{2-}Cl_{Te}^+)]$  into a neutral one –  $[(V_{Cd}^{2-}2Cl_{Te}^+)^0]$ , with the diffusion of adding chlorine atoms that are situated on the dislocations in the equilibrium state. The AWS ionization of acceptors leads to increasing of the electron concentration. At the same time the decreasing number of  $[(V_{Cd}^{2-}Cl_{Te}^+)]$ , determining the efficiency of charge carriers scattering at low temperatures, has to increase their mobility. At US shutdown the process is reversing, because thermodynamic equilibrium probability of the complex formation  $[(V_{Cd}^{2-}Cl_{Te}^+)]$  is more than  $[(V_{Cd}^{2-}2Cl_{Te}^+)^0]$ .

Thus, we can assume that the use of ultrasound as an additional methodical approach to the investigation of rebuilding processes of crystal defects and also for the control of the device characteristics *in-situ*.

- [1] Olikh Ya.M., Tymochko M.D. Technical Physics Letters, **37**, 37-40, (2011).  
[2] Lysiuk I.O., Olikh Ya.M., Olikh O.Ya., Beketov G.V. Ukrainian Journal of Physics, **59**, 50-57, (2014).

## Epitaxial ZnO films implanted with Er and Yb

E. Guziewicz<sup>1\*</sup>, R. Ratajczak<sup>2</sup>, D. Snigurenko<sup>1</sup>, M. Stachowicz<sup>1</sup>, T.A. Krajewski<sup>1</sup>, A. Stonert<sup>2</sup>,  
A. Turos<sup>3</sup>

<sup>1</sup>Institute of Physics, Polish Academy of Sciences, Warsaw, Poland

<sup>2</sup>National Centre for Nuclear Research, Swierk, Poland

<sup>3</sup>Institute of Electronic Materials Technology, Warsaw, Poland

\*[guzel@ifpan.edu.pl](mailto:guzel@ifpan.edu.pl)

Rare Earth (RE) doped semiconductor materials have been widely investigated because of their optical properties and possible application as fiber lasers and amplifiers, plasma displays, phosphors in fluorescence lamps and solar cells. The *RE4f* electron shell is highly localized, so the intra-shell transitions of *4f* electrons are only slightly affected by the host material, therefore the radiative efficiencies are almost temperature independent. Wide bandgap semiconductors are especially interesting as host materials, because they are expected to overcome the temperature quenching observed in other materials (e.g. in Si) and to promote effective resonant pumping of the *f* shell [1]. GaN and ZnO have been the most investigated semiconductors in this field. Both materials have a similar bandgap (about 3.4 eV at RT) and nowadays they compete with each other as the most promising new materials for optoelectronics. ZnO, in contrary to GaN, still experiences a problem with reliable and stable p-type doping, but has such important advantages over GaN as much higher exciton binding energy (60 meV vs. 24 meV) and possibility to grow a high quality films by commercial and inexpensive deposition methods.

In the present work we report on Yb- and Er-ion implantation on epitaxial ZnO films grown by the Atomic Layer Deposition (ALD) method on a commercial GaN/Al<sub>2</sub>O<sub>3</sub> substrate. The samples of about 1 μm thick have been grown at temperature of 300°C using diethylzinc and deionized water precursors. The full width at half maximum (FWHM) of the rocking curve of the (006) diffraction peak was established as 0.05°. The collected channeling Rutherford Backscattering (RBS/c) spectra reveal  $\chi_{\min} = 3\%$  which is comparable with that for commercial single ZnO crystal (MaTecK).

The ZnO films have been implanted with Er or Yb ions to fluence of  $1 \times 10^{15}$ ,  $5 \times 10^{15}$  and  $1 \times 10^{16}$  at./cm<sup>2</sup>. Atomic Force Microscopy shows that Root Mean Square (RMS) of the surface roughness increases from 15 nm to 24 nm as a result of implantation. Photoluminescence measured at helium temperature for ZnO:Yb films shows a weak the *Yb4f* related emission between 970 and 1020 nm. Post-growth annealing performed at 800°C in an ambient atmosphere (30 and 60 min.) enhances the *Yb4f* emission by more than one order of magnitude. The structural effects of ion implantation has been studied by the RBS/c technique. It allows direct measurements of defect depth distributions and to perform lattice location of implanted species. It has been demonstrated that above 50% of implanted Yb ions occupy substitutional lattice positions. Subsequent thermal annealing of implanted samples leads to partial recovery of the crystal lattice but also reduces substitutional fraction of Yb atoms.

The work was supported by the Polish National Centre for Research and Development (NCBiR) through the project DZP/PBSII/1699/2013.

[1] A.J. Kenyon, Prog. Quntum El. **26**, 225 (2002)

[2] P.N. Favenec, H. L'Haridon, D. Moutonnet, M. Salvi, M. Gauneau, Rare Earth Doped Semiconductors, in: Pomrenke, Klein, Langer (Eds.), MRS Symposia Proceedings, Materials Research Society, Pittsburgh, PA, vol. 31, 181 (1993)

## P-d Charge Transfer Excitons in $\text{Zn}_{1-x}\text{Ni}_x\text{O}$ Under Inner Shell Excitation

Churmanov V<sup>1\*</sup>, Sokolov V<sup>2</sup>, Gruzdev B<sup>2</sup>, Pustovarov V<sup>1</sup>, and Ivanov V<sup>1</sup>

<sup>1</sup>Institute of Physics and Technology, Ural Federal University, Yekaterinburg, Russia

<sup>2</sup>Institute of Metal Physics UB RAS, Yekaterinburg, Russia

\*v.churmanov@ut.ee

Comprehension of energy spectrum of oxide compounds with 3d-transition metals remains one of the unresolved tasks of physics of binary oxides. There is still no coherent conception of structure of energy spectrum NiO and CoO. In general it is accepted that optical properties of aforementioned crystals are formed by p-d and d-d charge-transfer (CT) transitions. Nevertheless unambiguous distinction between these two types of transitions has not been achieved up to date. Investigation of oxide solid solutions  $\text{Zn}_x\text{Ni}_{1-x}\text{O}$  is believed to provide an additional possibility for solving of this problem.

The photoluminescence (PL) measurements were made on the samples of NiO and several oxide solid solutions  $\text{Zn}_x\text{Ni}_{1-x}\text{O}$  ( $x = 0.2, 0.3$  and  $0.6$ ) with rock salt crystal structure. The time-resolved PL spectra as well as the PL decay kinetics under soft X-ray (XUV) excitation have been measured on a BW3 beamline (SUPERLUMI, HASYLAB (DESY), Hamburg).

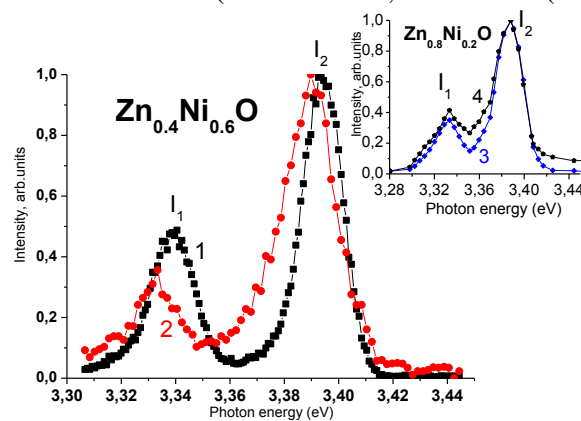


Figure 1. Time-resolved luminescence spectra of solid solution  $\text{Zn}_{0.4}\text{Ni}_{0.6}\text{O}$  (fast window) under excitation with energies  $E_{\text{exc}}=130$  eV (1) and 850 eV (2) at  $T=8$  K. Inset: luminescence spectra of  $\text{Zn}_{0.8}\text{Ni}_{0.2}\text{O}$  (integral window) under excitation with energy  $E_{\text{exc}}=130$  eV (3) and 450 eV (4) at  $T=8$  K.

Previous studies of oxide solid solutions  $\text{Zn}_{1-x}\text{Ni}_x\text{O}$  [1, 2] revealed two narrow lines  $I_1$  and  $I_2$  at the low-temperature ( $T=8\text{K}$ ) X-ray spectrum and found out a temperature dependences of these lines for solid solution  $\text{Zn}_{0.4}\text{Ni}_{0.6}\text{O}$  at the temperature range of 8-50 K.

Here we examine X-ray luminescence spectra of several solid solutions  $\text{Zn}_{1-x}\text{Ni}_x\text{O}$  in the region of  $I_1$  and  $I_2$  lines upon various photon excitation energies (130 eV, 450 eV and 850 eV) in the spectral region of absorption edges of the inner shells Zn M- and Ni L<sub>2,3</sub>- edges of Zn- and Ni- ions. PL decay kinetics of  $\text{Zn}_{1-x}\text{Ni}_x\text{O}$  under XUV excitation are discussed. The method of time-resolved luminescence spectroscopy with sub-nanosecond time resolution upon XUV excitation allows us to make a comparative analysis of the p-d and d-d CT transitions. We consider the origin of narrow lines  $I_1$  and  $I_2$  as a radiative annihilation of p-d CT excitons in NiO and  $\text{Zn}_{1-x}\text{Ni}_x\text{O}$ . We believe that the method may be used for successful distinguish of p-d CT transitions against d-d CT transitions in other  $\text{A}_{\text{II}}\text{B}_{\text{VI}}$  oxide compounds.

[1] Sokolov V. I., Pustovarov V. A., Churmanov V. N. et al., Phys. Rev. B., **86**, 115128 (2012).

[2] Sokolov, V.I., Pustovarov, V.A., Ivanov, V. Yu. et al., Optics and Spectroscopy, **116**, 5, 798-801 (2014).

## Hopping exciton model of photoluminescence in ZnSeO alloy

M. Baranowski<sup>1,\*</sup>, M. Welna<sup>1,2</sup>, R. Kudrawiec<sup>1</sup>, M. Latkowska<sup>1</sup>, Y. Nabetani<sup>3</sup>, J. Misiewicz<sup>1</sup>,  
and W. Walukiewicz<sup>2</sup>

<sup>1</sup>Department of Experimental Physics, Wrocław University of Technology,  
Wybrzeże Wyspiańskiego 27, 50-370 Wrocław, Poland

<sup>2</sup>Materials Sciences Division, Lawrence Berkeley National Laboratory, Berkeley,  
California 94720, USA

<sup>3</sup>Department of Electrical Engineering, University of Yamanashi,  
Takeda 4-3-11, Kofu 400-8511, Japan

\*michal.baranowski@pwr.edu.pl

The ZnSe<sub>1-x</sub>O<sub>x</sub> alloy belongs to the group of so called highly mismatch alloys (HMAs) [1] whose properties are determined by the interaction of host matrix bands with localized states isovalent impurities. The incorporation of a small amount of O, dramatically changes the electronic band structure. The reduction in the band gap of ZnSe<sub>1-x</sub>O<sub>x</sub> is around 130 meV per atomic percent of incorporated O [2]. Another important feature of HMAs is presence of the tail density of states below the bandgap which affects the carrier dynamics and emission properties of these alloys. The low temperature photoluminescence (PL) spectra of ZnSe<sub>1-x</sub>O<sub>x</sub> are very broad and asymmetric and the temperature dependence of PL peak energy exhibits S-shape like behavior. In addition the PL decay times are nonexponential and energy dependent. These features can be explained by the recombination of excitons localized on states below the bandgap [3]. Previous investigations of this complex carriers dynamics in ZnSe<sub>1-x</sub>O<sub>x</sub> have been restricted to qualitative description of the observed effects.

In this work we show that the carrier dynamics in ZnSe<sub>1-x</sub>O<sub>x</sub> alloy can be very well described by the model of hopping excitons [4–6]. The model provides a quantitative description of the complex PL decay process and allows for determination of disorder parameters. Numerical simulations of PL, micro-PL and time resolved PL (TRPL) spectra for different distributions of exciton localizing states are compared with the experimental data obtained for ZnSe<sub>1-x</sub>O<sub>x</sub> layers with different oxygen content. The simulations show how the distributions of the energy and the density of exciton localizing states affect PL characteristics such as, Stokes shift, dispersion of the PL decay time as well as broadening and temperature dependence of the PL spectra. A comparison of the numerical simulations with experiment has been used for determination of disorder parameters describing population of exciton localizing states in ZnSe<sub>1-x</sub>O<sub>x</sub> alloys. We will also discuss a general applicability of the hopping exciton model to analyze emission processes in other highly mismatched alloys.

- [1]. W. Shan, W. Walukiewicz, J. W. A. Iii, K. M. Yu, J. Wu, E. E. Haller, Y. Nabetani, T. Mukawa, Y. Ito, and T. Matsumoto, *Appl. Phys. Lett.* **83**, 299 (2003).
- [2]. R. Broesler, E. E. Haller, W. Walukiewicz, T. Muranaka, T. Matsumoto, and Y. Nabetani, *Appl. Phys. Lett.* **95**, 151907 (2009).
- [3]. Y. C. Lin, H. L. Chung, W. C. Chou, W. K. Chen, W. H. Chang, C. Y. Chen, and J. I. Chyi, *Appl. Phys. Lett.* **97**, 041909 (2010).
- [4]. S. D. Baranovskii, R. Eichmann, and P. Thomas, *Phys. Rev. B* **58**, 13081 (1998).
- [5]. M. Baranowski, M. Latkowska, R. Kudrawiec, and J. Misiewicz, *J. Phys. Condens. Matter* **23**, 205804 (2011).
- [6]. M. Baranowski, R. Kudrawiec, M. Latkowska, M. Syperek, J. Misiewicz, and J. A. Gupta, *Appl. Phys. Lett.* **100**, 202105 (2012).

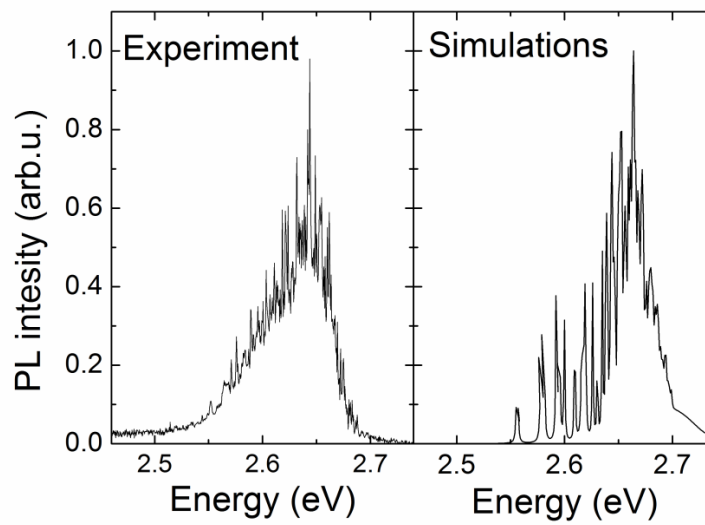


**Figure 1** Comparison of  $\mu$ -PL spectra with the results of hopping excitons model simulation

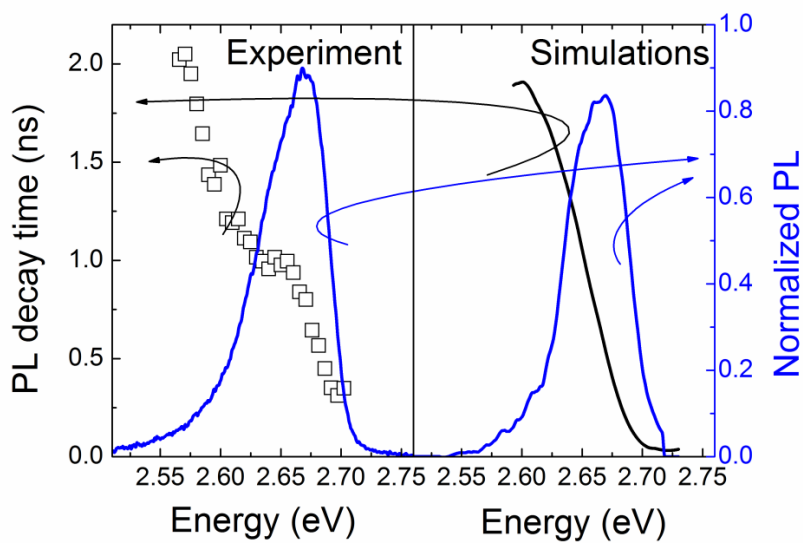


**Figure 2** Comparison PL decay time dispersion with hopping excitons model simulation

## Excited Electron and Multi-Phonon Coupling in Heavily Mn<sup>2+</sup> doped ZnS Phosphor

Daehan kim<sup>1</sup>, Kwangwon Park<sup>1</sup>, Jaehyeong Park<sup>1</sup>, Taehoon Kim<sup>2</sup>, and Jongsu Kim<sup>1\*</sup>

<sup>1</sup>Department of Display Science and Engineering, Pukyong National University, Busan 608-739, Korea

<sup>2</sup>R&D Institute of Lumimicro Co., Ltd. Yongin, Gyeonggi-do 449-883, Korea

\*jsukim@pknu.ac.kr

Heavily doped ZnS:Mn<sup>2+</sup> phosphors exhibited a strong photoluminescence excitation at 464 nm peak from the forbidden  ${}^6A_1({}^6S) \rightarrow {}^4A_1({}^4G)/{}^4E({}^4G)$  transitions of Mn<sup>2+</sup> ions [1] and a strong photoluminescence at 582 nm peak in comparison with the commercially available low doped ZnS:Mn<sup>2+</sup>. Their optical properties are investigated in terms of selection rule under the phonon triggered relaxation with increasing Mn<sup>2+</sup> ion concentrations. Under the direct excitation of Mn<sup>2+</sup> ions at 464 nm, they showed a higher thermal stability (97% @ 200 °C) in comparison with the band to band excitation at 340 nm (27% @ 200 °C). It indicates that heavily Mn<sup>2+</sup> doped ZnS phosphor can apply to the blue-light-emitting diode based pc-LED.

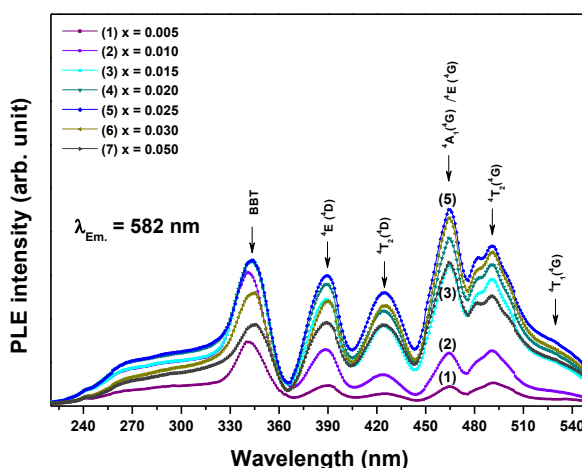


Fig. 1 PLE spectra of Zn<sub>1-x</sub>S:xMn<sup>2+</sup> monitored at 582 nm with varying Mn<sup>2+</sup> concentrations (x = 0.005, 0.01, 0.015, 0.02, 0.025, 0.03, and 0.05)

[1] G. Blasse, and B. C. Grabmaier, "Luminescent Materials," Springer-Verlag, Berlin-Heidelberg, 52, (1994).

## RT ZnSe-based Lasers and Laser Arrays Pumped by Low-Energy Electron Beam

M.M. Zverev<sup>1</sup>, N.A. Gamov<sup>1</sup>, E.V. Zhdanova<sup>1</sup>, V.B. Studionov<sup>1</sup>,  
I.V. Sedova<sup>2\*</sup>, S.V. Sorokin<sup>2</sup>, S.V. Gronin<sup>2</sup>, and S.V. Ivanov<sup>2</sup>

<sup>1</sup>Moscow State University of Radio Engineering, Electronics and Automations,  
Moscow 117454, Russia

<sup>2</sup>Ioffe Institute, St. Petersburg 194021, Russia

\*irina@beam.ioffe.ru

Low-temperature pulse electron-beam-pumped semiconductor lasers based on QW structures can be used for numerous applications, such as navigation system, optical communications, medicine etc. Minimum value of the room-temperature (RT) threshold current density for the green ZnSe-based lasers has been reported to be as low as of 0.4-0.5 A/cm<sup>2</sup> [1]. The peak light power up to 630W in green has been demonstrated for the laser array comprising 27 QW laser chips pumped by 24 keV electrons [2]. To decrease the electron energy in the pumping e-beam one should use the low-threshold QW structures. Since the maximum output pulse power from a chip is limited due to destruction of the laser crystal facets by its own laser radiation, one may use multi-element laser arrays to increase the peak output power. This paper reports on design and studies of “true” green ZnSe-based lasers and laser arrays pumped by a low-energy and high current density electron beam.

The laser structures were grown by molecular beam epitaxy on GaAs (001) substrates. The structures typically consist of a 1300 nm bottom ZnMgSSe cladding layer followed by the alternately strained ZnS<sub>0.15</sub>Se<sub>0.85</sub>/ZnSe superlattice waveguide lattice-matched to GaAs as a whole. The structures are capped with a thin (10 nm) Zn<sub>0.9</sub>Mg<sub>0.1</sub>S<sub>0.15</sub>Se<sub>0.85</sub> cladding layer. The active region includes two ZnSe (5nm) QW each centered by a CdSe quantum dot (QD) planes of 3 monolayer (ML) in a nominal thickness. The total width of waveguide is 310 nm.

The rectangular laser bars with a cavity length of 0.5-0.9 mm and the bar width up to 5 mm were cleaved from the QD laser structure. To avoid the effect of the amplification of the spontaneous emission along the laser bar the one-dimensional laser arrays were fabricated by scribing the bars surface across the bar through each 0.45 mm. The total laser array includes several (up to 6) one-dimensional arrays mounted on a copper heat sink in a staircase manner. The transverse excitation geometry was used. The electron beam with an energy of 3-12 keV, a pulse duration ~0.2 μs, and a current up to 20 mA was employed as a pumping source for studying the single-chip laser, while the laser array was pumped by the electron beam with the energy of 5.6 keV, the pulse duration of ~1 μs, and the current of 10A.

The lasing was observed for the electron energy range from 3.2 up to 12 keV. Lasing wavelength of ~550 nm was measured. The peak output power up to 80-100W was detected for the laser array pumped by electrons with the energy of 5.6 keV. Different ways to increase the laser array output power will be discussed. The work at the Ioffe Institute was supported by RSF Project #14-22-00107, and at MSU MEERA by RSF Project #13-02-00604 and RF Ministry of Education and Science (Task No. 3.611.2014/K).

[1] M.M. Zverev, N.A. Gamov, E.V. Zhdanova, et.al., Tech. Phys. Lett. **33**, 1 (2007).

[2] M.M. Zverev, S.V. Ivanov, N.A. Gamov, et.al., Phys. Stat. Sol. B **247**, 1561 (2010).

## Influence of the Number of Electronically Coupled CdSe/ZnSe QD Planes on Characteristics of Optically Pumped Green Lasers

I.V. Sedova<sup>1\*</sup>, E.V. Lutsenko<sup>2</sup>, S.V. Sorokin<sup>1</sup>, A.G. Vainilovich<sup>2</sup>, S.V. Gronin<sup>1</sup>, G.P. Yablonskii<sup>2</sup>,  
M. Aljohenii<sup>3</sup>, A. Aljerwii<sup>3</sup>, A. Alyamani<sup>3</sup>, and S.V. Ivanov<sup>1</sup>

<sup>1</sup>Ioffe Institute of RAS, 194021 St. Petersburg, Russia

<sup>2</sup>Stepanov Institute of Physics of NAS Belarus, 220072 Minsk, Belarus

<sup>3</sup>KACST, National Nanotechnology Center. P.O. BOX 6086, 11442 Riyadh, Saudi Arabia

\*irina@beam.ioffe.ru

Fabrication of efficient semiconductor green lasers for numerous applications still remains an actual problem. The integrated laser converters containing a II-VI-based green-emitting laser heterostructure optically pumped by the emission of an InGaN laser diode (LD) looks as one of promising ways to solve this problem. The micro-chip LD converters ( $\lambda=530-550\text{nm}$ ) comprising the low-threshold ( $<1\text{ kW/cm}^2$ ) II-VI laser structures with a single CdSe QD plane, optically pumped by the commercial InGaN LDs, have demonstrated recently the output power  $\sim 1\text{ W}$  (at  $\tau_{\text{pulse}}=4\text{ns}$ ,  $\eta\sim 14\%$ ) and  $160\text{ mW}$  (at  $\tau_{\text{pulse}}=200\text{ns}$ ) at room temperature [1]. Using of several QD planes in the active region of the optically-pumped laser heterostructures enhances the optical confinement factor  $\Gamma$  and increases the quantum efficiency. Simultaneously the increase of the number of QD planes may deteriorate considerably the excitation homogeneity of the active layers, which should lead to increasing the laser threshold. Therefore optimization of the MBE growth of the II-VI QD laser heterostructures and their design is necessary to provide the high  $\Gamma$  factor value, preserving the efficient use of the pumping power.

The Zn(Mg)SSe/ZnSe laser heterostructures were grown by MBE pseudomorphically to GaAs(001) substrate via a GaAs buffer layer. The structures consist of the bottom and top ZnMg<sub>0.12</sub>S<sub>0.16</sub>Se cladding layers with thicknesses of 1300 nm and 10 nm, respectively, the asymmetric superlattice (SL) graded-index waveguide (GIW) [2] with the total thickness of  $\sim 300\text{ nm}$ , and a 2 nm ZnSe cap layer. To realize more equilibrium growth conditions (the higher growth temperature  $T_S\sim 295^\circ\text{C}$ ) the cladding and waveguide layers were grown using only the ZnS and Se effusion cells without an additional Zn cell. The active region of laser heterostructures includes either single, or double, or triple electronically coupled CdSe/ZnSe QD sheets embedded equidistantly in a ZnSe QW of a thickness of 10, 15, and 20 nm, respectively. The ZnSe QW as well as the CdSe QD sheets were grown in a migration enhanced epitaxy (MEE) mode for reduction of the non-equilibrium point defects density in the active region.  $T_S$  was decreased gradually from  $\sim 295$  to  $\sim 280^\circ\text{C}$  during growth of the bottom 5-nm-thick ZnSe QW barrier adjacent to the CdSe QD sheets and increased back to  $295^\circ\text{C}$  on the top one. The MEE growth of CdSe QDs (nominal thickness of  $\sim 2.8\text{ ML}$ ) proceeded with long interruptions after the Se deposition pulses, resulting both in the improved uniformity of the QD array and the increase in their integral luminescence intensity [3].

Structural, lasing and internal laser characteristics of the structures are presented. The internal quantum efficiency and internal losses for the structures with single and triple QD planes are  $\eta_i \sim 76.3\%$ ,  $\alpha_i \sim 3.9\text{ cm}^{-1}$  and  $\eta_i \sim 71.8\%$ ,  $\alpha_i \sim 4.6\text{ cm}^{-1}$  respectively. These parameters demonstrate the relatively high level of excitation homogeneity. However the triple-QD-planes structure exhibited the twice higher characteristic gain ( $\Gamma G_0 \sim 155\text{ cm}^{-1}$ ), but also higher  $I_{\text{th}}$ . The work at the Ioffe Institute was supported by RSF Project #14-22-00107.

[1] S.V. Ivanov, S.V. Sorokin et al., 16 Int. Conf. "Laser Optics 2014", St. Petersburg, Russia, (2014).

[2] I.V. Sedova, E.V. Lutsenko, S.V. Gronin et al., Appl. Phys. Lett. **98**, 171103 (2011).

[3] I.V. Sedova, S.V. Sorokin, A.A. Sitnikova et al., Inst. Phys. Conf. Ser. **174**, Section 3, 161 (2003).

## INOVATIVE APPROACH TO THE LASER MECHANOLUMINESCENCE IN II-VI COMPOUNDS

Manas Sahu

Dept. of Physics of Sound, Indira Kala Sangit Vishwavidyalaya Khairagarh (C.G.) India  
manas\_sahu25@rediffmail.com

### ABSTRACT

When a II-VI compounds exposed to laser pulse they will produce a shock-wave in the crystal and consequently the deformation of crystal takes place. For the laser-pulse of short duration the change in number of electrons in the conduction band and shallow traps finally we obtain the maximum intensity and corresponding time. The decay time of ML will be equal to the life time of electrons in the shallow traps. The ratio  $I_{m2}/I_{m1}$  depend on the probability of transfer of electrons from the conduction band to shallow traps and on the ratio of pinning time of dislocation and life time of electrons in the shallow traps. By using laser pulse and an optical fiber the ML may be observed owing to the movement of single dislocation in II-VI compounds.

### INTRODUCTION

Luminescence induced during mechanical deformation of solids is known as mechanoluminescence (ML). ML links mechanical spectroscopic, electrical structural and other properties of solid. A large number of organic and inorganic solids exhibits the phenomenon of ML can excited by grinding, rubbing, cutting cleaving, compressing or by impulsive deformation of solids [1-6]. We have been interested whether ML could be made to occur using a high energy laser pulses as the stress inducing agent [7]. The present paper reports the theory of laser ML in II-VI semiconductors. In analogy with the laser thermo luminescence the ML caused by the deformation owing to laser pulses may be called as laser ML. The others materials like elemental and III-V semiconductors exhibit ML, during their fracture, which is not related to the movement of dislocations hence laser ML in this semiconductors may be observed during only when intense laser shocks pulses instead of laser will create crakes in this semiconductor as such theory of laser ML in these semiconductors may be quite different from that of II-VI semiconductors whereby intense ML is observed during the movement of dislocations in these semiconductors.

### THEORY

An analysis of the possible ML mechanisms has shown that the interacting between charged dislocations and activator centers leads to activator ionization. Ionization may occur by tunneling of electrons from the impurity level of the conduction band under the operation of strong electric field close to a charged dislocation [8-11].

Supposing a II-VI semiconductor like ZnS is exposed to an infrared laser pulse whose intensity is give by  $I - I_0 \exp(-\delta t)$ , where  $I_0$  is the intensity at  $t = 0$  and  $\delta$  is a factor inversely related to the pulse duration of laser. It is known that the laser pulse produces a shock-wave in the crystal and consequently the deformation of crystal takes place [12-14]. For a laser pulse of short duration and low pulse energy, the local heating will not be significant and consequently the intensity of black body radiation may be assumed to be negligible as compared to that of the laser ML produced in the bulk of crystal. It is to be noted II-VI compounds exhibit ML even during their plastic deformation.

## Fabrication of the fully hybrid microcavities based on Zn(S)Se

Kozlovsky V.<sup>1</sup>, Krivobok V.<sup>1\*</sup>, Nikolaev S.<sup>1</sup>, Onishchenko E.<sup>1</sup>, Pruchkina A.<sup>1</sup>, Kuznetsov P.<sup>2</sup>, Jitov V.<sup>2</sup>

<sup>1</sup>Lebedev Physical Institute, Moscow, Russia

<sup>2</sup>Institute of Radioengineering and Electronics, Fryazino, Russia

\*krivobok@lebedev.ru

Because of a relatively high Rabi splitting and an exciton binding energy thin ZnSe epilayer is a promising material for the polariton “laser” operating at room temperature [1]. For its implementation one needs to explore a microcavity with high Q-factor of ~1000. For GaAs-related microcavity, the high Q-factor may be achieved by using distributed bragg reflection (DBR) AlAs/GaAs mirrors grown along with an active epilayer placed between these DBR mirrors in a single growth run. It is more difficult to grow high reflective DBR mirrors on the basis of ZnSe-related compounds [1]. Therefore a use of dielectric DBR mirrors is an alternative way to achieve the high Q-factor with Zn(S)Se microcavity.

Such a microcavity may be prepared by the following manner. First, a Zn(S)Se epilayer or ZnSe/ZnMgSSe QW structure is grown on GaAs substrate. Then the first dielectric DBR mirror based on quarter-wave alternative SiO<sub>2</sub>-Ta<sub>2</sub>O<sub>5</sub> layers is coated on the epilayer. The structure is glued to a sapphire substrate by the first DBR mirror. The GaAs substrate is removed by grinding and chemical etching. The second dielectric DBR mirror is coated on the free surface. Similar technology was successfully used for e-beam pumped laser [2]. But the total thickness of the heterostructure transferred from GaAs substrate to the sapphire one was several microns in this case. It is much thicker than the emission wavelength while the thickness of the polariton microcavity should be comparable with the wavelength.

Therefore some problems may occur in the case of using such a technique of the polariton microcavity fabrication. It is naturally to assume that growth of the Zn(S)Se film of a subcritical thickness on GaAs substrates should provide the necessary surface quality in two-dimensional growth conditions. Nevertheless, many authors [3-6] have observed hillocks on the surface of ZnSe epitaxial layers grown on GaAs substrates, their density exceeded 10<sup>8</sup> cm<sup>-2</sup>. The formation of such hillocks may considerably decrease the Q-factor. Other problem may be connected with a formation of additional defects within the Zn(S)Se epilayer during the microcavity fabrication process.

In this work we study a mechanism of hillock formation and ways of their removing. We have found that the hillocks may be efficiently removed by annealing at T = 260 °C (e.g., in H<sub>2</sub> atmosphere) before mirror coating. Also we analyzed the spectral position of free excitons X<sub>hh</sub>, X<sub>lh</sub> and exciton-impurity complexes depending on the value of intrinsic strain of MOVPE-grown isomorphous ZnSSe/GaAs epilayers. The results obtained were used for strain monitoring in the structures after coating mirrors, gluing and removing GaAs processes. We found that proposed technology does not worsen the epilayer quality. The cavity mode FWHM in a spectral range 440-450 nm was as small as 0.8 nm that corresponds to Q = 560. The results of exciton-phonon coupling studies in the hybrid Zn(S)Se microcavity will be presented also.

- [1] K. Sebald et al, Appl. Phys. Lett. 100, 161104 (2012).
- [2] Bondarev V.Y. et al, Quantum Electronics, 34, 919 (2004).
- [3] X. B. Zhang and S. K. Hark, Appl. Phys. Lett., 74, No. 25, 3857, (1999).
- [4] M. Lopez-Lopez, A. Guillen-Cervantes et al, J. of Crystal Growth, 193, 528 (1998).
- [5] J. B. Smathers and E. Kneidler, Appl. Phys. Lett., 72, 10, 1238, (1998).
- [6] X. B. Zhang, K.L. Ha, S.K. Hark J. of Crystal Growth, 223, 528, (2001).

## Optical properties of diluted II-VI magnetic semiconductor nanostructures

Bingsuo ZOU\*, Ruibin Liu, Lijie Shi, Yongyou Zhang

Beijing Key lab of nanophotonics and ultrafine optoelectronic systems, Beijing Institute of Technology, Beijing 100081, China

\*E-mail: zoubs@bit.edu.cn

Optical properties of diluted magnetic semiconductor (DMS) are not well understood so far, especially relationship to their ferromagnetism. Here we prepared Mn ion doped ZnO, CdS and ZnSe nanostructures by CVD method, studied their optical properties via microphotoluminescence techniques, found many very interesting properties, which are all related to the exciton magnetic polaron (EMP), itinerant or partially itinerant, their energy levels are agree well with the AB initio calculations.

In ZnO:Mn nanowires, the EMP can show up with free exciton together for very diluted doping (<0.001%), this EMP can form condensate to produce single mode lasing line at fs pulse excitation along with the disappearing of free excitons, which indicate a condensation of EMP. With a little bit large amount of Mn doping, the nanowire show EMP lasing mode with background at fs laser pulse excitation, but at even high power, some electron-hole plasma induced lasing modes could be observed due to the carrier effect. The time-delayed photoluminescence by ns laser pulse are also studied, only free EMP and localized EMP(d-d transition) show up in the emission spectra, we gave the clear assignments for all the d-d transitions of Mn in ZnO, which have been argued for a long time. It is more interesting that these d-d transitions exhibit clear enhanced coherent relaxation behaviors with increasing excitation power, like that by free excitons, even couple with LO phonons, behave a collective spin-dependent coherent radiation, which may be used for quantum modulation applications. We also observed the Mn-O-Mn cluster peak in the long wavelength range, which may be related to the ferromagnetic properties.

In CdS:Mn nanowires, we found many peaks longer than the single Mn ion emission band (575nm) when increasing the Mn concentration, we used a simple Hydrogen-like cloud theoretical model to describe them well, in this model, the Mn-S-Mn-S aggregate with variable Mn ion number and their ferromagnetic coupling are considered. The SQUID detection proved the ferromagnetic behavior of the aggregate, and MFM imaging indicated its cluster nature in a microbelt or nanowire. Ab initio calculation results also support our assignments. The aggregation of Mn ion in II-VI semiconductor microstructures can produce ferromagnetic and PL emission at the same time.

[1] Liu Ruibin, Shi Lijie, Zou Bingsuo\*, Magnetic Exciton Relaxation and Spin-Spin Interaction by the Time-Delayed Photoluminescence Spectra of ZnO:Mn Nanowires, ACS APPLIED MATERIALS & INTERFACES, 6, 10353-10366 (2014)

[2] Kamran Muhammad Arshad, Liu Ruibin, Shi Li-Jie, Li Zi-An, Marzi Thomas, Schoeppner Christian, Farle Michael, Zou, Bingsuo\*, Tunable emission properties by ferromagnetic coupling Mn(II) aggregates in Mn-doped CdS microbelts/nanowires, NANOTECHNOLOGY, 25(38),385201(2014)

## Exciton Spin Hall Effect in Quantum Wells

V.Kochereshko<sup>1,2</sup>, V.Kats<sup>1,2</sup>, A.Platonov<sup>1</sup>, L.Golub<sup>1</sup>, A-V.Tsakaev<sup>2</sup>  
*Ioffe Physical Technical Institute 194021, Saint Petersburg, Russia*  
*Saint Petersburg State University, Saint Petersburg, Russia*

We report on theoretical and experimental study of Exciton Spin Hall effect in structures with symmetric and asymmetric quantum well based on ZnSe and GaAs semiconductors. From the experimentally obtained spectra, values of linear in the wave vector contributions into the exciton dispersion through the Dresselhaus and Rashba mechanisms have been determined. Structures with a single 8 nm width symmetric quantum well ZnSe/ZnMgSSe and asymmetric 10 nm quantum well based on GaAs/AlGaAs grown by MBE in the [001] direction were studied experimentally.

Reflectivity spectra were measured at oblique incidence at the angle of  $45^\circ$ . When the incident light was linearly polarized in  $S$  polarization and  $S$  component was detected the reflectivity spectrum contained two resonances: the excitons with heavy hole and with light hole. The amplitude of the reflection line for the heavy hole exciton, as expected, was much larger than the amplitude of the light hole exciton.

In crossed polarizers, when the incident light was  $S$  polarized and the reflected light was detected in  $P$  polarization, or when the incident light was in  $P$  polarization, and reflected light was detected in  $S$  polarization the signal was expected to be absent. However, in the experiment we observed a conversion of the polarizations from  $P$  into  $S$  and vice versa.

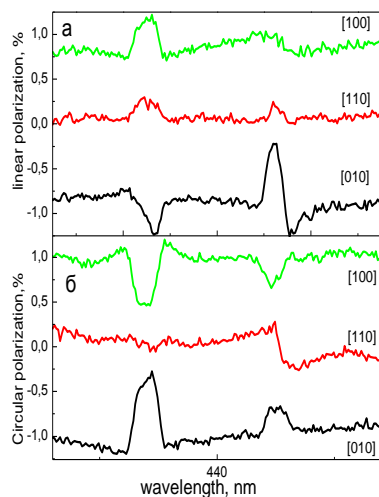


Figure 1 shows the spectrum of the reflected signal in the  $S$  polarization when incident light was in  $P$  polarization (Figure 1a) and when we analyze circularly polarized components of the reflected light (Figure 1b). The amplitude of the line of the light hole exciton in these spectra is considerably higher than the amplitude of the heavy hole exciton line. The figure also shows that when the direction of the wave vector  $K$  is rotated from [100] to [010] crystal direction the signal changes its sign and becomes zero for the [110] direction. The residual signal observed at the heavy line of the exciton may be associated with a weak interface birefringence existing in these structures. [1].

The observed phenomenon is explained by the influence of the linear terms in the exciton wave vector in the exciton dispersion. For symmetric structures the linear in  $K$  terms emerge due to the Dresselhaus contribution. In an asymmetric structure we observed mutual effect from Dresselhaus and Rashba contributions [2]. The observed phenomenon is an analog of Spin Hall effect for electrons and optical spin Hall effect in microcavities [3].

[1] A.V.Platonov, V.P.Kochereshko, E.L.Ivchenko, et al. *Phys. Rev. Lett.* **83**, 3546, (1999)

[2] N.S.Averkiev, L.E.Golub, A.S.Gurevich, et al. *Phys. Rev. B* **74**, 033305 (2006)

[3] Alexey Kavokin, Guillaume Malpuech, and Mikhail Glazov *Phys. Rev. Lett.* **95**, 136601 (2005)

## The digital filtration preprocessing of variable magnetic field Hall data before mobility spectrum analysis for p-MCT films

A.V. Trifanov<sup>1,2</sup>, D.Yu. Protasov<sup>2</sup>, V.Ya. Kostyuchenko<sup>3</sup>, N.N. Mikhailov<sup>2</sup>, S.A. Dvoretzky<sup>2</sup>

<sup>1</sup>*Siberian State University of Geosystems and Technology, 10 Plakhotnogo Str., Novosibirsk, 630108, Russia*

<sup>2</sup>*Rzhanov Institute of Semiconductor Physics SB RAS, Lavrentiev Prospect, 13, Novosibirsk, 630090, Russia*

<sup>3</sup>*Novosibirsk State Technical University, 20 Prospekt K. Marksa, Novosibirsk, 630073, Russia*

Currently for determination of density and mobility of charge carriers at mixed conductivity regime, various methods based on well-known mobility spectrum analysis method [1] are widely used. But these methods have a strong sensitivity to errors in initial experimental data, which are magnetic field dependences of Hall Effect and magnetoresistance. Usually for elimination of parasitic signal due to contacts nonequipotentiality in Hall bar or due such effects as Seebeck and Nernst-Ettingshausen, the averaging on magnetic and electric fields are applied. Unfortunately, for random uncertainty of Hall voltage or magnetoresistance the averaging has not such efficiency.

Most part of modern Hall measurement systems are computer-aided, therefore these systems have possibility to collect a large massive of experimental data. It is allows accepting to them digital methods of data processing. If magnetic field at Hall measurements changes slowly (about 1 T/min), then the valid signal have a smooth time dependency and corresponding to them spectra are located in low-frequency region. In contrast to this, the noise is similar to small oscillation with short period and its spectrum is located in high-frequency region. In this work the weighting digital-data low-pass filter for noise suppression was realized with using of Blakman window function.

The mobility spectrums for MBE p-Hg<sub>0.22</sub>Cd<sub>0.78</sub>Te films at 77 K without and with digital filtration of variable field Hall data are shown on Fig. 1a and 1b, respectively.

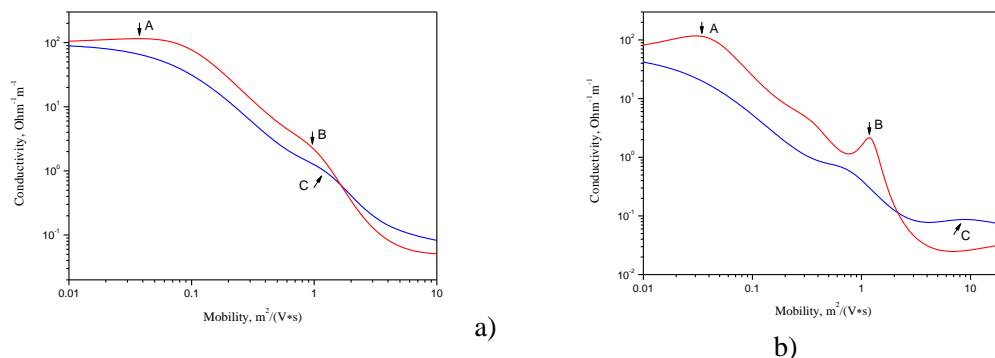


Fig. 1. The mobility spectrum for (a) unfiltered and (b) filtered variable field Hall data: red color – holes part, blue – electron part.

As one can see from Fig.1, after digital filtration the peaks A and B from heavy and light holes became more pronounced that as a result increases the accuracy of determination of their parameters. The peak C one correspond to two-dimensional electrons localized in layer near substrate. After digital filtration it locates to high-mobility region and very well correlated to mobility of minor electrons, determined by magnetoconductivity method [2].

Influence of digital filter parameters on an error of charge carriers density and mobility determination is discussed.

1. W.A. Beck, J.R. Anderson, J. Appl. Phys. **62**(2), 541 (1987)

2. V.S. Varavin, S.A. Dvoretzki, V.Ya. Kostyuchenko, V.N. Ovsyuk, D.Yu. Protasov, Semiconductors, **38**, N 5, 514 (2004)

## MCT Surface Passivation by Atomic Layer Deposition of Thin Al<sub>2</sub>O<sub>3</sub> Films

G.Yu. Sidorov\*, V.V. Vasilyev, I.V. Sabinina,  
 A.P. Kovchavtsev, A.E. Nastovjak, and A.V. Tsarenko  
 Institute of Semiconductor Physics SB RAS, Novosibirsk, Russian Federation  
 \*e-mail: [george@isp.nsc.ru](mailto:george@isp.nsc.ru)

Surface passivation of HgCdTe epilayers is an important process of focal plane arrays production. Two methods of p-n junctions passivation are used. The first method involves creation of a variband layer with increasing bandgap on top of the photosensitive layer which results in suppression of the generation-recombination currents on the surface of the semiconductor. Second method is creation of the protective wide-gap semiconductor or dielectric film on top of the semiconductor layer. Using such films provides additional reduction of leakage currents on the surface of the p-n junction and protect the surface of the variable-gap layer during photolithographic processes used in IR FPA production.

We have investigated the passivation properties of Al<sub>2</sub>O<sub>3</sub> films (~80 nm) deposited by atomic layer deposition (ALD) at low temperatures (120°C) using Al(CH<sub>3</sub>)<sub>3</sub> (TMA) and remote oxygen plasma process. MOS structures consisting of MBE-grown p and n-type Hg<sub>1-x</sub>Cd<sub>x</sub>Te (x~0.22)/Al<sub>2</sub>O<sub>3</sub>/In were studied. The variband layer on the surface of CMT had x varying from 0.22 to 0.45 and a thickness of about 0.4 microns. On some MOS structures the variband layer was removed prior to Al<sub>2</sub>O<sub>3</sub> film deposition. Temperature (77-300K) and frequency (1kHz-1MHz) dependencies of C-V characteristics were measured.

MOS structure with p-Hg<sub>1-x</sub>Cd<sub>x</sub>Te without variband layer. The relative permittivity was derived from the capacitance value in hole enhancement mode and is estimated as  $\epsilon_i \approx 7$ . At zero bias MOS structure was in the depletion mode and the value of the built-in charge was estimated as  $\approx +2.5 \cdot 10^{-8} \text{ C/cm}^2$ . C-V curve at 1 MHz frequency at T=77 K has a typical high frequency form. The trapped charge value in the aluminum oxide film was calculated using the C-V curves hysteresis in voltage range of  $\pm 0.5 \text{ V}$  and was estimated as  $\approx +3 \cdot 10^{-9} \text{ C/cm}^2$ . With increase of the bias sweep up to  $\pm 25 \text{ V}$  the trapped charge value increases up to  $\approx +2.2 \cdot 10^{-7} \text{ C/cm}^2$ . The frequency and temperature dependences of C-V characteristics is consistent with theoretical calculations which were carried out using the drift-diffusion model. In this model the self-consistent system of Poisson and continuity equations for electrons and holes is being solved. Influence of surface states was not taken into account.

MOS structure with p-Hg<sub>1-x</sub>Cd<sub>x</sub>Te with variband layer. The behavior of the frequency and temperature dependences of the C-V curves was similar to the previous case. Experimental C-V are offset from the theoretical curves and the corresponding charge in the oxide value is  $+8.2 \cdot 10^{-8} \text{ C/cm}^2$ . The main difference is an extended low-frequency voltage minimum on C-V curves which can't be explained with the theoretical model used.

MOS structure on samples n-Hg<sub>1-x</sub>Cd<sub>x</sub>Te without variband layer. No built-in charge in the dielectric was found. Unlike the previous cases C-V curve at 1 MHz had a form of medium-frequency curves instead of a typical high-frequency form with a minimum and an increase of capacitance in inversion. With decrease of the frequency to 10 kHz the C-V curves transformed into typical low-frequency form. Theoretical calculations of frequency and temperature dependences correlate with the experimental data.

MOS structure on samples n-Hg<sub>1-x</sub>Cd<sub>x</sub>Te with variband layer. Experimental C-V curves were "stretched" vertically compared to theoretical calculation and had a bigger hysteresis, which indicates an intense trapping of the charge in the dielectric film. There probably is a Fermi-level pinning effect on surface traps. In the inversion region at a frequency of 1 MHz the C-V curve had a medium-frequency form and with frequency decrease it transformed into a low-frequency form.

## Optical properties of single wurtzite/zinc-blende ZnSe nanowires grown at low temperature

**V. Zannier<sup>1,2\*</sup>, T. Cremel<sup>3,4\*</sup>, A. Artioli<sup>3,5</sup>, D. Ferrand<sup>3,5</sup>, K. Kheng<sup>3,4</sup>, V. Grillo<sup>6,7</sup> and S. Rubini<sup>1</sup>**

<sup>1</sup>*IOM-CNR Laboratorio TASC, S. S. 14, Km. 163.5, I-34149 Trieste, Italy*

<sup>2</sup>*Department of Physics, University of Trieste, Via Valerio 2, I-34127 Trieste, Italy*

<sup>3</sup>*Univ. Grenoble Alpes, F-38000 Grenoble, France*

<sup>4</sup>*CEA, INAC-SP2M, F-38000 Grenoble, France*

<sup>5</sup>*CNRS, Institut Néel, F-38000 Grenoble, France*

<sup>6</sup>*IMEM-CNR, Parco Area delle Scienze 37/A, I-43010 Parma, Italy*

<sup>7</sup>*S3 NANO-CNR, Via Campi 213/A, I-41125 Modena, Italy*

\*[valentina.zannier@nano.cnr.it](mailto:valentina.zannier@nano.cnr.it) and [thibault.cremel@cea.fr](mailto:thibault.cremel@cea.fr)

We have grown ZnSe nanowires (NWs) at low temperature (300°C) on a GaAs(111)B substrate by molecular beam epitaxy [1]. Transmission electron microscopy (TEM) studies show that the ZnSe(111)B NW structure is mainly WZ and alternations of wurtzite (WZ) / zinc-blende (ZB) phases can be observed. This polytypism has been studied by TEM, micro-photoluminescence and cathodoluminescence to correlate the NWs crystal structure to their optical properties. A dominant intense near-band-edge emission as well as the WZ ZnSe free exciton line are observed. The NW emission displays linear polarization perpendicular to the nanowires axis, in contrast with the usually observed light polarization along the axis [2]; this effect is explained by the selection rules in WZ structure. A type II band alignment between zinc-blende and wurtzite ZnSe has been deduced from decay-time measurements. From these optical measurements, we deduce a value for the ZB/WZ ZnSe conduction and valence band offsets.

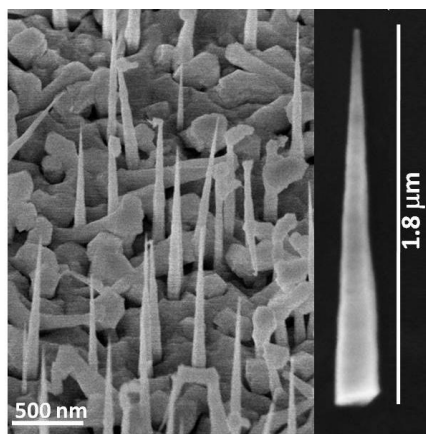


Figure 1. Tilted-view SEM image (45°) of ZnSe NWs grown at 300°C on a GaAs(111)B substrate.

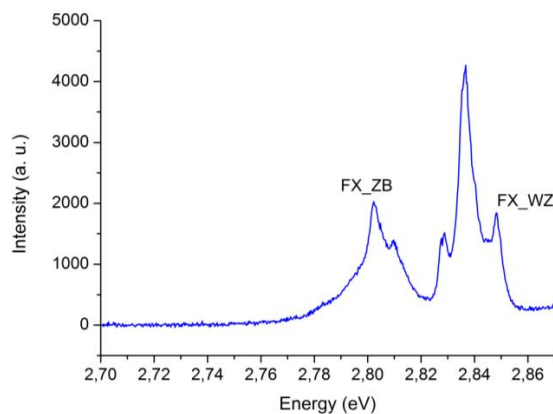


Figure 2. Photoluminescence spectrum of a single ZB/WZ ZnSe NW acquired at 5K with a 405nm laser excitation of 300 μW.

- [1] V. Zannier, F. Martelli, V. Grillo, J. R. Plaisier, A. Lausi, and S. Rubini, *Physica Status Solidi - Rapid Research Letters* **8**, 182 (2014).  
 [2] J. Wang, M. S. Gudixsen, X. Duan, Y. Cui, and C. M. Lieber, *Science* **293**, 1455 (2001).

## Role of the electron-phonon interaction in the temperature dependence of the phonon mode frequency in the II-VI compound alloys

J. Polit<sup>1</sup>, M. Woźny,<sup>1</sup> J. Cebulski,<sup>1</sup> A. Marcelli,<sup>2</sup> M. Piccinini<sup>2</sup> and E.M. Sheregii<sup>1</sup>

<sup>1</sup>Centre for Microelectronics and Nanotechnology, University of Rzeszów, S. Pigonia 1, 35-959 Rzeszów, Poland

<sup>2</sup>INFN LNF, Via E. Fermi, 44, I-00040 Frascati (RM), Italy

\*sheregii@ur.edu.pl

The cubic II-VI systems HgTe, CdTe and ZnTe are extremely interesting technologically materials with many applications such as infrared as well as quantum electronics devices. They belong to a large set of artificial nanostructured materials which exhibit new properties such as those shown by topologically insulators or massless fermions layers with the Dirac points which properties could be astonishing from application point of view. The phonon states in such systems are of particular interest because of unexpected singularity in the temperature dependence of the phonon frequency<sup>1,2</sup>. We present an experimental investigation of the temperature dependence of the phonon mode frequencies for Hg-based II-VI semiconductor alloys. In the case of the ternary Hg<sub>0.9</sub>Zn<sub>0.1</sub>Te alloy was shown a discontinuity in the temperature dependence of the HgTe-like T<sub>0</sub>-mode and of the ZnTe-like T<sub>1</sub>-mode similarly to the Hg<sub>0.85</sub>Cd<sub>0.15</sub>Te system<sup>1</sup>. A generalization of the theoretical temperature shift equation of the phonon mode frequency is derived that includes both the anharmonic contribution and the electron-phonon (e-p) interaction which in this case is returnable - the electron subsystem effect on the phonon one. Data show that our equation satisfactorily describes the temperature shift of both Hg<sub>0.85</sub>Cd<sub>0.15</sub>Te and Hg<sub>0.90</sub>Zn<sub>0.10</sub>Te containing Dirac point ( $E_g \equiv \Gamma_6 - \Gamma_8 = 0$ ) although one of the two constants describing the anharmonic shift of the HgTe-like mode should be positive what is abnormal too<sup>3</sup>. In the case of the Hg<sub>0.80</sub>Cd<sub>0.20</sub>Te and Hg<sub>0.763</sub>Zn<sub>0.237</sub>Te semiconductor alloys the role of the returnable e-p contribution is negligible but a positive temperature shift for the HgTe-like modes occurs. This result does not allow explaining the positive temperature shift of these modes merely by the contribution of the e-p interaction. Indeed, the relativistic contribution to the chemical bonds induces an abnormal temperature shift of the electron states in Hg-based semiconductors - the effect is expected since the Hg d spin-orbit split contribution may lead to an abnormal temperature shift of HgTe-like modes.

[1] E.M. Sheregii, J. Cebulski, A. Marcelli, M. Piccinini, *Phys. Rev. Lett.*, **102**, 045504, (2009)

[2] J. Polit, E.M. Sheregii, J. Cebulski, A. Kisiel, A. Marcelli, B. Robouch, A. Micielski, *Phys. Rev. B* **82**, 014306-1-12 (2010)

[3] M. Wozny, J. Cebulski, A. Marcelli, M. Piccinini, and E. M. Sheregii, *J. Appl. Phys.*, **117**, 025702 (2015)

## Polariton Lasing and Phase Diagram of a ZnO Microcavity grown on a Patterned Silicon Substrate

O. Jamadi<sup>1,2\*</sup>, E. Mallet<sup>1,2</sup>, F. Réveret<sup>1,2</sup>, F. Médard<sup>1,2</sup>, P. Disseix<sup>1,2</sup>, M. Mihailovic<sup>1,2</sup>, D. Solnyshkov<sup>1,2</sup>, G. Malpuech<sup>1,2</sup>, J. Leymarie<sup>1,2</sup>, S. Bouchoule<sup>3</sup>, X. Lafosse<sup>3</sup>, G. Gommé<sup>4</sup>, F. Li<sup>4</sup>, M.J. Rashid<sup>4</sup>, J. Zuniga-Perez<sup>4</sup>, and F. Semond<sup>4</sup>

<sup>1</sup>Clermont Université, Institut Pascal (IP), BP 10448, F-63000 Clermont-Ferrand, France

<sup>2</sup>CNRS, UMR 6602, IP, F-63171 Aubière, France

<sup>3</sup>LPN-CNRS, route de Nozay, F-91460 Marcoussis, France

<sup>4</sup>CRHEA-CNRS, rue B. Grégory, Sophia Antipolis, F-06560 Valbonne, France

\*Author for correspondence: omar.jamadi@gmail.com

Organic as well as wide bandgap inorganic semiconductors (GaN and ZnO, in particular) appear as the best alternative to obtain polariton lasing at room temperature. This coherent emission without population inversion was recently observed in bulk or multiple quantum well microcavities based on GaN [1-2] and ZnO [3]. We present here polariton lasing in a ZnO bulk microcavity grown by molecular beam epitaxy on a patterned Si substrate. A 30-pair AlN/AlGaIn bottom distributed Bragg reflector (DBR) was grown without cracks thanks to the use of a pre-patterned Si substrate, allowing for an efficient strain relaxation. After the subsequent growth of the ZnO active region, the cavity was completed by a top dielectric HfO<sub>2</sub>/SiO<sub>2</sub> DBR. The microcavity exhibits photonic properties at the state-of-the-art [4]: an average quality factor larger than 1000 (with local values as high as 3500) and a low photonic disorder. The Rabi splitting of this microcavity is evaluated to be equal to 160 meV. The combination of a high Rabi splitting and an intentionally weak thickness gradient in the active layer across the wafer, has allowed us to evidence polariton lasing in a large exciton-cavity photon detuning range.

In this work we will present the laser threshold as a function of the detuning for temperatures going from 5 K up to 300 K [Fig. 1(a)]; this ensemble of data, known as the phase diagram, will be compared to numerical simulations [Fig. 1(b)]. The analysis of these results highlight the importance of polariton-phonon interactions on polariton relaxation within a ZnO microcavity. Thanks to the phase diagram of a GaN bulk microcavity, elaborated between similar DBRs (on patterned Si substrate) and therefore presenting similar photonic properties, we will objectively compare polariton lasing in these two wide bandgap semiconductors.

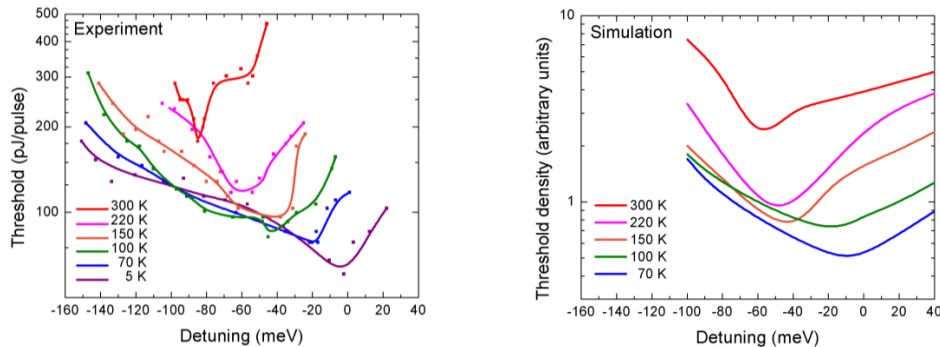


Fig. 1. (a) Detuning dependence of the polariton lasing threshold under femto- (5 K-220 K) and picoseconds excitation (300 K). (b) Polariton condensation threshold density calculated within the semi-classical Boltzmann equation.

- [1] S. Christopoulos et al., Phys. Rev. Lett., **98**, 126405 (2007)  
 [2] G. Christmann et al., App. Phys. Lett., **93**, 051102 (2008)  
 [3] F. Li et al., Phys. Rev. Lett., **110**, 196406 (2013)  
 [4] J. Zuniga-Perez et al., Appl. Phys. Lett., **104**, 241113 (2014)

## Study of ZnO exciton-polariton properties by linear and non-linear spectroscopies

E. Mallet<sup>1,2</sup>, O. Jamadi<sup>1,2</sup>, F. Réveret<sup>1,2\*</sup>, P. Disseix<sup>1,2</sup>, F. Médard<sup>1,2</sup>, M. Mihailovic<sup>1,2</sup>, T.V. Shubina<sup>3</sup>, J. Leymarie<sup>1,2</sup>, S. Bouchoule,<sup>4</sup> X. Lafosse<sup>4</sup>, G. Gommé<sup>5</sup>, F. Li<sup>5</sup>, M.J. Rashid<sup>5</sup>, J. Zuniga-Perez<sup>5</sup> and F. Semond<sup>5</sup>

<sup>1</sup>Université Clermont Auvergne, Institut Pascal (IP), BP 80026, F-63000 CLERMONT-FERRAND, France

<sup>2</sup>CNRS, UMR 6602, F-63171 Aubière, France

<sup>3</sup>Ioffe Physical-Technical Institute of RAS, St. Petersburg 194021, Russia

<sup>4</sup>LPN-CNRS, route de Nozay, F-91460 Marcoussis, France

<sup>5</sup>CRHEA-CNRS, rue B. Grégory, Sophia Antipolis, F-06560 Valbonne, France

\*Author for correspondence: francois.reveret@univ-bpclermont.fr

ZnO is a wide bandgap semiconductor emitting in the near UV region and for several decades its optical properties have been intensively investigated. However some of its fundamental characteristics, such as the origin of the excitonic broadening at low temperature or the exciton-phonon interaction, differ from that of another wide bandgap semiconductor, GaN. These differences have been highlighted recently by a thorough spectroscopic study combining linear and non-linear measurements on high quality samples [1]. In bulk ZnO, the dissymmetry between the homogeneous broadenings of A and B excitons observed through spectrally-resolved degenerate four-wave mixing (Sr-DFWM) can be explained mainly through the exciton-impurity scattering (figure 1a). Concerning bulk GaN, the homogeneous damping induced by exciton-impurity interaction is weak compared to the inhomogeneous one, which is due to strain fluctuations and dominates at low temperature. The accurate determination of excitonic parameters was obtained from the combination of continuous-wave reflectivity, autocorrelation of reflectivity, photoluminescence and degenerate four-wave mixing. Moreover, the comparison between GaN and ZnO leads to a better understanding of the various interaction processes (e.g. exciton-impurities scattering, exciton-phonon interactions ...), which could play an important role on polaritonic device operation. To go further insight into the relaxation processes of polaritons, a ZnO-based microcavity is investigated by degenerate four wave mixing experiments. In this optical resonator, the confined photon strongly interacts with ZnO excitons giving rise to polaritons, quasi particles sharing properties with both, excitons and cavity photons [2]. The excitonic weight of the polariton, i.e. the polaritonic trap depth in reciprocal space, can be easily tuned thanks to an intentional thickness gradient of the active layer across the wafer. First measurements will be presented and the influence of the polaritonic trap will be discussed.

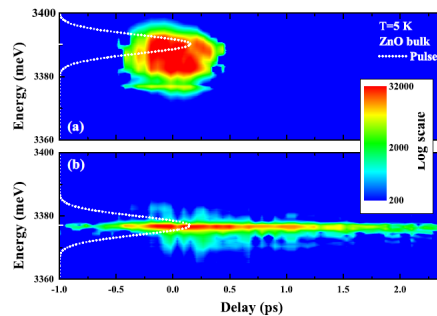


Figure 1: Sr-DFWM spectra of bulk ZnO recorded at 5 K with a pulse energy centered respectively on A and B excitonic resonances. The dephasing time is larger for the A transition. The temporal resolution is 0.06 ps.

[1] E. Mallet *et al.*, Phys. Rev. B **87**, 161202(R) (2013), E. Mallet *et al.*, Phys. Rev. B **90**, 045204 (2014)

[2] J. Zuniga-Perez *et al.*, Appl. Phys. Lett. **104** (2014) 241113

## Electric Field Induced Reversible Photoluminescence Quenching in ZnO Films

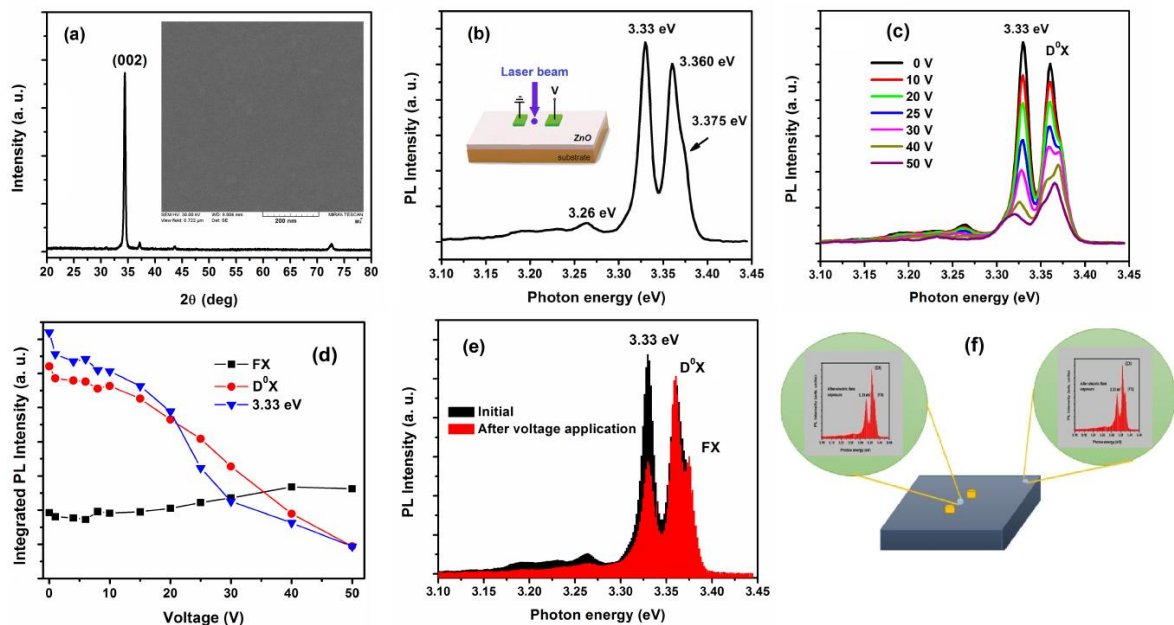
Vadim Sh.Yalishev<sup>1\*</sup>, Shavkat U. Yuldashev<sup>1</sup>, Bae Ho Park<sup>2</sup>, and Tae Won Kang<sup>1\*</sup>

<sup>1</sup>Quantum-Functional Semiconductor Research Center, Dongguk University, 3-26 Pil-dong, Chung-gu, Seoul, South Korea

<sup>2</sup>Division of Quantum Phases & Devices, School of Physics, Konkuk University, 1 Hwayang-dong, Gwangjin-gu, Seoul, South Korea

\*E-mail: yalvad@yahoo.com; twkang@dongguk.edu

PL measurement under the electric field is a useful technique in understanding optical and electronic properties of the material, both fundamental properties and defects. In this work, we studied the effect of voltage application on excitonic emissions in ZnO films at low temperature. Intensity of bound exciton lines decreased when samples were biased. After removing of bias, photoluminescence intensity of the bound exciton at 3.33 eV did not return to its initial state, and this change in the spectrum was observed over the entire film, remaining for a long time. Besides the photoluminescence intensity, thermal activation energy of the 3.33 eV emission line and resistance of the film have been also changed. The value of the activation energy has become well fit with the exciton binding energy in contrast to the unsuitable small value usually observed for this 3.33 eV emission. All changes can be returned to the initial state by application of voltage with opposite polarity. Modification of a surface charge distribution is proposed as a model for observed effects.



## Electrical Characteristic of ZnO Thin Films Grown on Different p-Si Substrate Elaborated by Sol-Gel Spin-Coating Method

W. Chebil<sup>1</sup>, A. Fouzri<sup>1,2,\*</sup>, A. Fargi<sup>3</sup>, B. Azeza<sup>4</sup> and V. Sallet<sup>5</sup>

<sup>1</sup>Laboratoire Physico-chimie des Matériaux ; Unité de Service Commun de Recherche « High resolution X-ray diffractometer », Département de Physique, Université de Monastir, Faculté des Sciences de Monastir, Avenue de l'Environnement, 5019 Monastir, Tunisia.

<sup>2</sup>Institut Supérieur des Sciences Appliquées et de Technologie de Sousse, Université de Sousse, Tunisia.

<sup>3</sup>Laboratoire de Microélectronique et Instrumentation, Faculté des Sciences de Monastir, Université de Monastir, Avenue de l'environnement 5019, Monastir, Tunisia.

<sup>4</sup>Laboratoire Micro-Optoélectroniques et Nanostructures, Faculté des Sciences de Monastir, Université de Monastir, Avenue de l'environnement 5019, Monastir, Tunisia.

<sup>5</sup>Groupe d'Etude de la Matière Condensée, Centre National de la Recherche Scientifique/Université de Versailles Saint Quentin en Yvelines 78035 Versailles, France.

\*Corresponding author: [Fouzri.Afif@gmail.com](mailto:Fouzri.Afif@gmail.com)

Nanostructured ZnO is an important material for many high technological applications including diodes, solar cells, sensors, transparent conducting films, and photovoltaic devices. Efforts have been devoted by some researchers to produce p-type ZnO thin films in order to fully utilize the potential of ZnO. But the difficulty in producing stable and high quality p-type doping of ZnO has led researchers to grow n-ZnO on different p-type substrates to ensure the usability of ZnO thin films in different photonic and optoelectronic devices. Different heterojunction devices such as n-ZnO/p-Si, p-SrCu<sub>2</sub>O<sub>2</sub>/n-ZnO, p-ZnRh<sub>2</sub>O<sub>4</sub>/n-ZnO and p-NiO/n-ZnO have been reported in past [1-2]. Among these, n-ZnO/p-Si heterojunction is a suitable choice due its several advantages such as high quality and large area p-type substrates available at low cost.

In this study, the ZnO thin films are deposited by sol-gel spin coating technique on p-type crystalline silicon (Si) with [100] orientation, etched silicon and porous Silicon. The properties of ZnO thin films grown on each sample have been characterized by X-ray diffraction (XRD), scanning electron microscopy (SEM) and current-voltage measurement (I-V). The structural analyses showed that the obtained thin films were polycrystalline with a hexagonal wurtzite structure and preferentially oriented along the c-axis direction. Morphological study revealed the presence of rounded and faceted grains irregularly distributed on the surface of all samples. The I-V characteristics for all sample exhibit successful diode formation. The heterojunction parameters were evaluated from the (I-V) under dark and illumination at room temperature. The ideality factor barrier height and series resistance are determined by using Norde's and Cheung's methods. Best electrical properties are obtained for the ZnO layer deposited on porous silicon.

[1] J.D. Lee, C.Y. Park, H.S. Kim, J.J. Lee, Y.G. Choo, J. Phys. D: Appl. Phys. **43**, 365403 (2010).

[2] H. Ohta, M. Kamiya, T. Kamiya, M. Hirano, H. Hosono, Thin Solid Films, **445**, 317 (2003).

## Electrical properties of the V-defects of epitaxial HgCdTe

V. A. Novikov<sup>1</sup>, D. V. Grigoryev<sup>1</sup>, D. A. Bezrodnyy<sup>1</sup>, A. V. Voitsekhovskii<sup>1</sup>, S. A. Dvoretiskii<sup>2</sup>, N.N. Mikhailov<sup>2</sup>, M.V. Yakushev<sup>2</sup>

<sup>1</sup>Tomsk State University, 634050, 36, Lenina Avenue, Tomsk, Russia

<sup>2</sup>Institute of Semiconductor Physics, Siberian Branch, Russian Academy of Sciences, 630090, 13, pr. Lavrentieva, Novosibirsk, Russia

Heteroepitaxial layers of HgCdTe grown by means of molecular beam epitaxy on GaAs (3 1 0) substrates contain macroscopic V-defects. These defects represent the inclusions of the polycrystalline phase with the component composition different from that of the bulk material. The presence of a large number of interfaces and the local variation of the component concentration lead to significant changes of the electrophysical properties of the V-defect. For this reason the analysis of the local distribution of the electrical characteristics of HgCdTe in a V-defect region plays a significant role for the process of manufacturing both the epitaxial structures themselves and the prefabricated devices based on such structures.

Using the scanning probe microscopy (SPM) one can obtain the distribution of the surface potential, capacitive contrast and the current strength along the surface of an epitaxial film and a V-defect with the resolution of not less than 50 nm in the plane of scan (fig. 1). The joint analysis of the obtained SPM data on the electrical properties of individual crystalline grains shows that there exists an additional electric field on the periphery of the grains. This field results in the formation of the potential barriers that prevent the exchange of charge carriers between the adjacent crystalline grains and the epitaxial film as it can be seen from fig. 1d.

The analysis of the current strength distribution versus the value of the bias applied to the needle-point shows that at a temperature of 300K the electroconductive area of a V-defect increases in good agreement with the linear law and reaches 60% at a voltage of -10V on the needle-point.

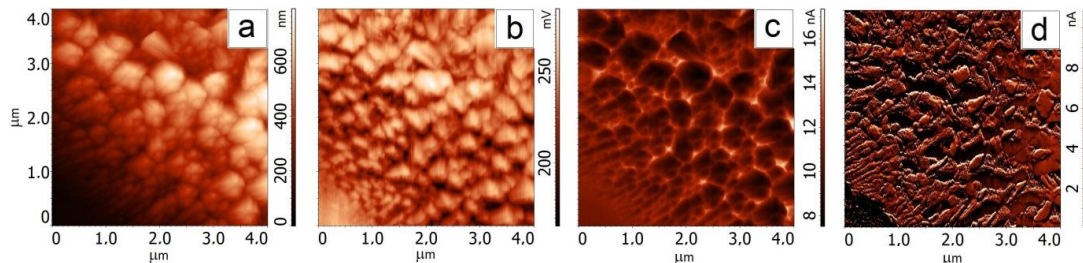


Fig. 1. SPM image of aHgCdTe V-defect a) surface morphology; b) distribution of the contact potential difference; c) capacitive contrast; d) spreading resistance

As it was demonstrated the use of the scanning probe microscopy allows one to obtain a high-precision spatial distribution of the material electrical properties. The analysis of the surface potential showed that the measured value is different for individual crystalline grains indicating that there are variations of the molar concentrations of Cd and Hg. The analysis of the capacitive contrast and the current strength distribution showed that there is an additional electric barrier along the periphery of the crystalline grains that form V-defects.

## Optical properties of II-VI-based Bragg-polariton samples

K. Sebald<sup>1</sup>, SK. S. Rahman<sup>1</sup>, M. Cornelius<sup>1</sup>, J. Gutowski<sup>1</sup>, T. Klein<sup>2</sup>, S. Klembt<sup>2\*</sup>, D. Hommel<sup>2\*\*</sup>

<sup>1</sup>Semiconductor Optics, <sup>2</sup>Semiconductor Epitaxy, Institute of Solid State Physics, University of Bremen, Germany

The strong light-matter interaction has attracted much interest in the last decade because of the possibility to create optoelectronic devices whose operation is based on the properties of cavity-exciton polaritons. In recent years, Bragg polaritons have been discussed as a new tool for tailoring light-matter coupling. Bragg-polariton structures can be created by the incorporation of quantum wells (QWs) with their excitonic resonances periodically in a photonic crystal structure like a distributed Bragg reflector (DBR). In this case, the light-matter interaction occurs between the QW excitons and the Bragg-mirror modes resulting in the creation of Bragg-polaritons. The advantage of this sample type is the high number of QWs which can be positioned at the field maximum of the Bragg mode. This is in contrast to the microcavity (MC) concept where the QWs are positioned at the cavity field maximum. In order to increase the Rabi splitting energy in such MCs, more QWs have to be used resulting in a thicker cavity. This hampers the increase of the Rabi splitting energy because of additional absorption losses and a larger mode volume. The strong light-matter coupling regime in a Bragg-polariton sample is indicated, as for a MC, by an anticrossing of the excitonic resonance and the photonic mode. This effect was already reported for CdTe and ZnO QWs in a MC, with Rabi splitting energies of 7.5 meV and 30 meV, respectively [1,2]. Bragg-polariton samples with InGaAs QWs show a Rabi splitting energy of 9.3 meV [3]. In this contribution we report on the optical properties of a Bragg-polariton sample grown by MBE. Three ZnSe QWs are embedded in the center of the high-index material made of ZnMgSSe with a total thickness of  $3\lambda/4$ , while the low-index material consists of a superlattice of MgS and ZnCdSe with a total thickness of  $\lambda/4$ . Eight of these Bragg-polariton layers are grown on four plain DBR layers. Micro-reflectivity measurements were performed and the experimental findings are compared to calculations. The energy position of the excitonic resonance was tuned relative to the Bragg-mode by changing the sample temperature. Further, a thickness gradient of the DBR layers over the sample also allows to tune the Bragg-mode resonance relative to the exciton energy. In both cases an anticrossing of the Bragg-polariton branches can be observed. The energy splitting between the upper and lower Bragg-polariton branch is in the order of 60 meV when the uncoupled exciton and Bragg-mode are at resonance at  $T=150$  K. The Bragg-mode tuning relative to the excitonic resonances was performed at a different sample piece which shows a smaller splitting energy of about 40 meV. In both cases a contribution of the middle polariton branch can be identified. The experimental findings are in good agreement with calculations based on the vectorial transfer matrix method and on an oscillator model taking into account the oscillator strengths of the excitons as found in literature. The deduced splitting energy is considerably larger than the Rabi splitting energy of 19 meV found by us in a comparable sample with three ZnSe QWs embedded in a Fabry-Pérot MC [4]. Hence, these results, showing strong coupling in a ZnSe-based Bragg-polariton sample, are promising with respect to the realization of polariton based devices operating near room temperature.

[1] M. Richard, et al., Appl. Phys. Lett. **86**, 071916 (2005).

[2] S. Faure, et al., Appl. Phys. Lett. **95**, 121102 (2009).

[3] A. Askitopoulos, et al., Phys. Rev. Lett. **106**, 076401 (2011).

[4] K. Sebald, et al., Appl. Phys. Lett. **100**, 161104 (2012).

Current affiliation: \*Institute Néel, CNRS/UJF Grenoble, France; \*\*Institute of Experimental Physics, University of Wrocław and Wrocław Research Center EIT, Poland

## Study on the contact resistivity of Au contacts to (Cd, Mn)Te crystals

Linjun Wang, Jijun Zhang\*, Min Shen, Jiahua Min, Xiaoyan Liang, Lin Wang, and Wenqi Wu

<sup>1</sup>School of Materials science and engineering, Shanghai University, Shanghai, PR China  
\*zhangjijun222@shu.edu.cn

Recently, (Cd, Mn)Te is demonstrated to be a good candidate to compete with (Cd, Zn)Te in room-temperature x-ray and  $\gamma$ -ray nuclear detector applications. The potential use of (Cd, Mn)Te for room-temperature radiation detector was first reported by Burger et al. in 1999 [1]. Then large improvement has been achieved in the crystal growth of (Cd, Mn)Te single crystal for detector applications [2]. The performance of (Cd, Mn)Te detector depends not only on the quality of (Cd, Mn)Te wafer material, but also on the metal to (Cd, Mn)Te contact properties [3]. Ohmic contacts between metal and (Cd, Mn)Te crystal are extremely important for both the electrical properties and performances of (Cd, Mn)Te detector. Low contact resistance share less voltage and is advantage in collecting carriers with low barrier height, which are in favor of improving the energy resolution of (Cd, Mn)Te detector [3].

In this work, the Ohmic characteristics of Au/(Cd, Mn)Te contact were investigated by Monocycle Transmission Line Model (MTLM). The Au contacts on (Cd, Mn)Te wafers were deposited with the electroless AuCl<sub>3</sub> technique. The influence of surface polishing and annealing on the contact resistivity ( $\rho_c$ ) of Au/(Cd, Mn)Te were analyzed. The (Cd, Mn)Te wafers were prepared by various surface treatments, such as, Chemical Polishing (CP), Chemical-Mechanical Polishing (CMP) and Chemical Mechanical Polishing followed Chemical Polishing (CMP+CP). The  $\rho_c$  values of Au/(Cd, Mn)Te on the CP, CMP and CMP+CP were 544.5  $\Omega\cdot\text{cm}^2$ , 89.0  $\Omega\cdot\text{cm}^2$  and 15.0  $\Omega\cdot\text{cm}^2$ , respectively. The surface morphology and composition of (Cd, Mn)Te wafers were characterized by AFM and XPS, which revealed that the surface roughness and Te-rich state had great effect on the contact resistivity of Au/(Cd, Mn)Te. After annealing at 150 °C for 1 h, the  $\rho_c$  values of the Au/(Cd, Mn)Te contact were decreased to 313.6  $\Omega\cdot\text{cm}^2$ , 30.2  $\Omega\cdot\text{cm}^2$  and 3.9  $\Omega\cdot\text{cm}^2$ , respectively. The results show that the high quality ohmic contact can be achieved by improving the surface treatment and annealing process of Au/(Cd, Mn)Te contact.

- [1] A. Burger, K. Chattopadhyay, H. Chen, D. Shi, S. H. Morgan, W. E. Collins, Fabrication and evaluation of cadmium manganese telluride gamma ray detectors, *J. Cryst. Growth* 872 (1) (1999) 198-199.
- [2] R. Rafiei, M. I. Reinhard, K. Kim, D. A. Prokopovich, D. Boardman, A. Sarbutt, G. C. Watt, A. E. Bolotnikov, L. J. Bignell, R. B. James, High-Purity CdMnTe Radiation Detectors: A High-Resolution Spectroscopic Evaluation, *IEEE Trans. Nucl. Sci.* 60 (2) (2013) 1450-1456.
- [3] Witkowska-Baran, M, Mycielski, A, Kochanowska, D, Szadkowski, A. J., Jakiela, R, Witkowska, B, Kaliszek, W, Domagala, J, Lusakowska. E, Domukhovski. V, Contacts for High-Resistivity (Cd,Mn)Te Crystals, *IEEE Trans. Nucl. Sci.* 58 (1) (2011) 347-353.

## Light Emitting Properties Dependent on Nitride Stoichiometry of Si-rich-SiN<sub>x</sub> Films Grown by PECVD

T.V. Torchynska<sup>1</sup>, J.L. Casas Espinola<sup>1</sup>, J. A. Bentosa Gutiérrez<sup>1</sup>,  
L. Khomenkova<sup>2</sup> and A. Slaoui<sup>3</sup>

<sup>1</sup>National Polytechnic Institute, Mexico DF, Mexico

<sup>2</sup>V. Lashkaryov Institute of Semiconductor Physics at NASU, Ukraine

<sup>3</sup>ICube, 23 rue du Loess, BP 20 CR, 67037 Strasbourg Cedex 2, France

[\\*torch@esfm.ipn.mx](mailto:*torch@esfm.ipn.mx)

Bandgap engineering of Si-based materials through the control of the distribution of Si nanocrystals (Si-NCs) offered future applications of Si-based nanostructured materials in optoelectronics as low-cost, miniaturized, and CMOS-compatible, light-emitting, solar cell and photovoltaic devices. Present work deals with the Si-rich silicon nitride films were grown by PECVD technique on silicon substrates. The film stoichiometry was controlled via variation of NH<sub>3</sub>/SiH<sub>4</sub> ratio from R=0.45 up to 1.0. Thermal treatment was performed at 1100°C for 30 min in nitrogen flow to form Si-NCs. To control structural and light emitting properties of the films Raman scattering, X-ray diffraction (XRD), Transmission electron microscopy (TEM), Atomic force microscope (AFM) and photoluminescence (PL) methods were used. The evolutions of PL spectra with the temperature of measurements from 20 to 300 K, as well as with the change of the excitation light quanta and excitation power densities, were studied aiming the determination of the types of optical transitions.

The PL spectra were found to be complex and the shape and magnitude of PL spectra depends on silicon nitride stoichiometry. The increase of gas ratio from R=0.63 to R=1 results in the shift of PL peak position from 1.6 eV up to 2.7 eV. Analysis of the temperature dependence of PL spectra revealed the presence of several PL components with the maxima at 2.9-3.0 eV, 2.5-2.7 eV, 1.9-2.2 eV and 1.8-1.9 eV. The peak position of the former three PL components unchanged with the decrease of temperature of the measurements. This allows describing all these components to the defects of silicon nitride host. At the same time, PL band peaked at 1.8-1.9 eV showed high-energy shift with sample cooling and can be ascribed to the exciton recombination inside Si-ncs. The presence of these latter was confirmed by Raman scattering spectra and TEM images. The nature of light emitting defects in silicon nitride, the mechanism of photoluminescence and the way for the optimization of optical properties are discussed.

# The stochastic model for ternary and quaternary alloys: Application of the Bernoulli relation to the phonon spectra of mixed crystals

Polit Jacek <sup>1, @</sup>, Michał Marchewka, Mariusz Wozny, Andrzej Kisiel, Benjamin Robouch, Eugeniusz Sheregii, Marcelli Claudio, <sup>@</sup>  
<sup>1</sup> : Centre for Microelectronics and Nanotechnology, (CMiN) - [Website](#)  
*Pigonia 1, 35-959 Rzeszow - Poland*

**Abstract:** To understand and interpret the experimental data on the phonon spectra of the solid solutions it is necessary to describe mathematically the non-regular distribution of atoms in its lattices. It occurs that such description is possible in case of the strongly chaotically (stochastically) homogenous distribution what require a very great number of atoms and a very carefully mixed alloys. These conditions are fulfilled generally in case of the high quality homogenous semiconductor solid solutions of the III-V and II-VI semiconductor compounds. In this case we can use the Bernoulli relation describing a probability to occur a one from  $n$  equivalent events what can be apply to the probability to find one from  $n$  configurations in the solid solution lattice. The results described in this paper for ternary HgCdTe and GaAsP as well as quaternary HgZnCdTe can give affirmative answer on the question: whether geometry of chaos e.g. the Bernoulli relation is enough to describe the observed phonon spectra.

**Keywords:** Chaotic modeling, Phonon spectra, Solid solutions, Chaotic simulation.

**Poster Session 3 - ThP**  
**Theory and band structure**

## Hall Effect and Negative Energy Gap in HgTe/CdTe Superlattice with Thick Quantum Wells

Nafidi A<sup>1\*</sup>, Boutramane A<sup>1</sup>, Barkissy D<sup>1</sup>, Charifi H<sup>1</sup>, El Gouti T<sup>1</sup>, Saba A<sup>1</sup>, Marí Soucase B<sup>2</sup>

<sup>1</sup> LCMP Nano Re, University Ibn Zohr, Faculty of sciences, Agadir Morocco.

<sup>2</sup> Laboratory of Optoelectronics, Universitat Politècnica de València, Spain

\*nafidi21@yahoo.fr

We report here manifestation of negative energy gap, resonant state and transition semiconductor-semimetal induced by temperature in transport properties and bands structure in HgTe ( $d_1=40$  nm)/CdTe ( $d_2=15$  nm) superlattice (SL) grown by MBE. Calculations of the spectres of energy  $E(d_2)$ ,  $E(k_z)$  and  $E(k_p)$ , respectively, in the direction of growth and in plane of the superlattice; were performed in the envelope function formalism. The energy  $E(d_2, \Gamma, 77$  K), shown that when  $d_2$  increase the gap  $E_g$  decrease to zero at the transition semiconductor to semimetal (SC-SM) conductivity behaviour (at  $d_2=11,5$  nm) and become negative accusing a semi metallic conduction. Whereas the band gap  $E_g(T)$  increases from  $-4.1$  meV at  $4.2$  K, to  $0$  at  $148$  K with a transition (SM-SC) and to  $6.06$  meV at  $300$  K. At  $4.2$  K, the sample exhibits n type conductivity with a Hall mobility of  $1600$  cm<sup>2</sup>/Vs, increase with the temperature and reach a maximum of  $8000$  cm<sup>2</sup>/Vs at  $T=148$  K of the transition (SM-SC) and decreases in the intrinsic regime. The weak-field Hall coefficient present a small maximum at about  $31$  K attributed to the presence of an acceptor resonant state. In intrinsic regime,  $R_H T^{3/2}$  indicates a gap  $E_g=5,3$ meV in agreement with calculated  $E_g(\Gamma, 300$  K)=  $E_1$ - $HH_1=6$  meV.. The formalism used here predicts that this sample is a narrow gap semimetallic, two-dimensional and far-infrared detector

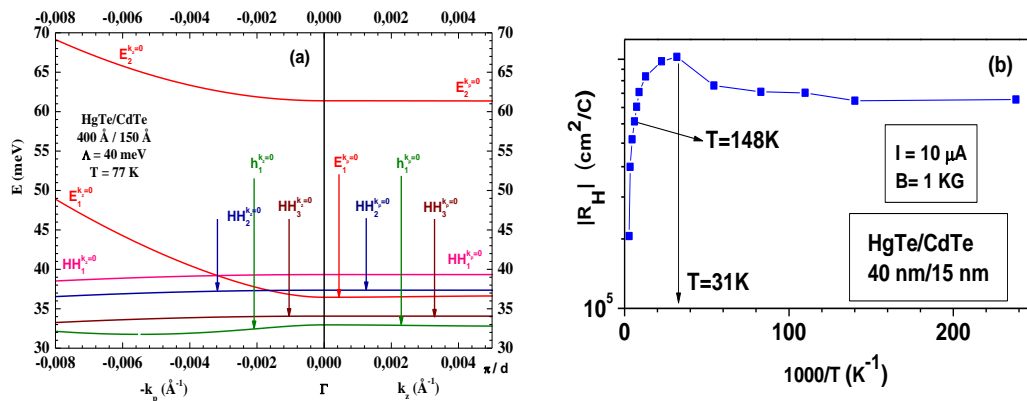


**Fig.. (a)** Calculated bands along the wave vector  $k_z$  in the right and in plane  $k_p(k_x, k_y)$  for  $k_z=0$  in the left at  $77$  K (b) Temperature dependence of weak-field Hall coefficient in the investigated HgTe/CdTe superlattice.

- [1] L. Esaki, R. Tsu, IBM J. Res. Development (1970) 61. G. Bastard, Phys. Rev. B 25 (1982) 7584.
- [2] M. Braigue, A. Nafidi et al, AIP Conference Proceedings 1416, New York: American Institute of Physics (2011) 68-71.
- [3] M. Braigue, A. Nafidi, A. Idbaha, et al, Journal of Low Temperature Physics, Volume 171, Issue 5-6, (2013), 808-817

Figures

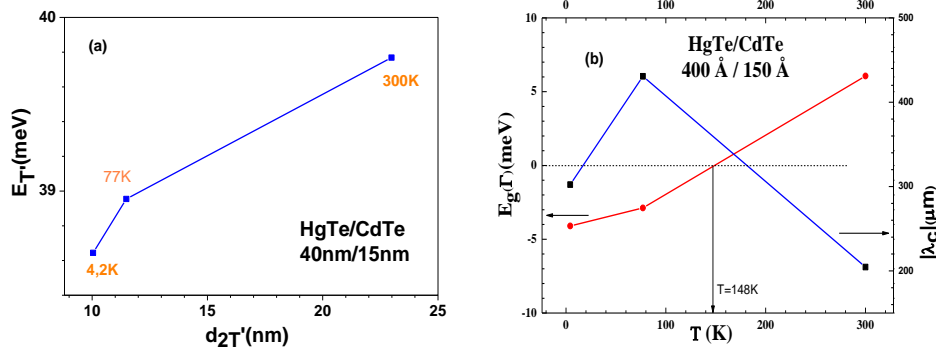


Fig.1. (a) Temperature dependence of the coordinates of the transition dot  $T'$  ( $E_T$ ,  $d_{2T'}$ ) at the center  $\Gamma$  and (b) Temperature dependence of the band gap  $E_g$  ( $\Gamma$ ) and cut-off wavelength  $\lambda_c$ , at the center  $\Gamma$  in the investigated HgTe/CdTe superlattice

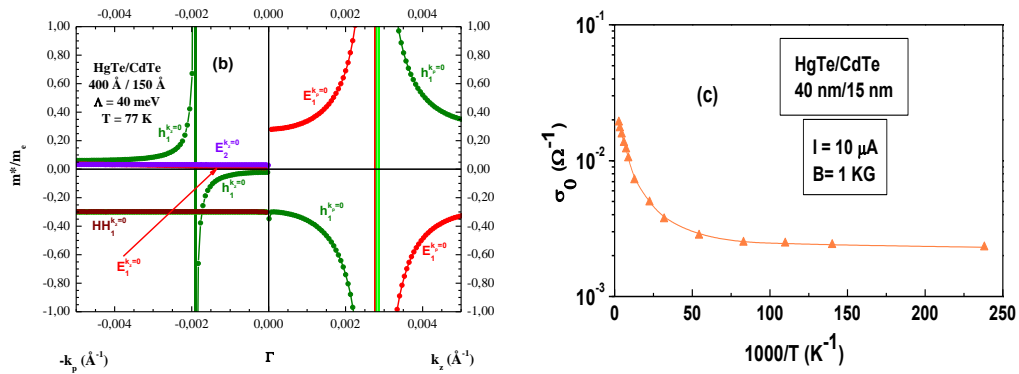


Fig.2. (a) Calculated bands along the wave vector  $k_z$  in the right and in plane  $k_p$  ( $k_x, k_y$ ) for  $k_z=0$  in the left at 77 K, (b) Temperature dependence of the conductivity in the investigated HgTe/CdTe superlattice

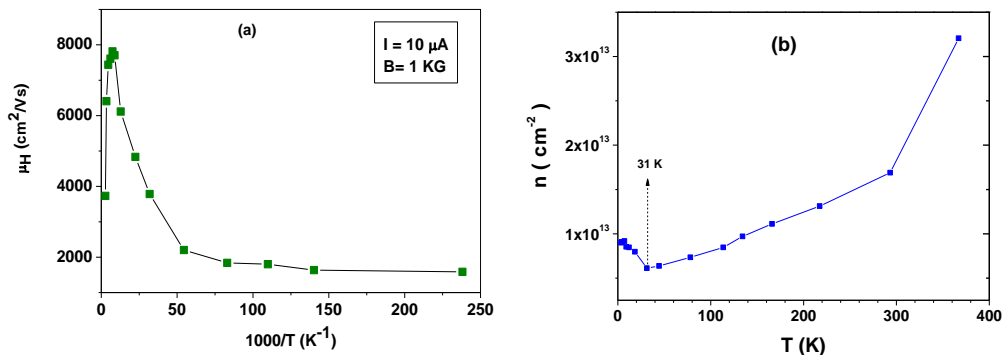


Fig. 3. Temperature dependence (a) of the Hall mobility, (b) of the electrons concentration in the investigated HgTe/CdTe superlattice.

## Electronic Structure, Effective Mass and Magneto-Transport Properties in HgTe-CdTe Superlattice with Large Quantum Well Thickness

Nafidi A<sup>1\*</sup>, Barkissy D<sup>1</sup>, Boutramane A<sup>1</sup>, Hannour A<sup>1</sup>, Elanique A<sup>1</sup>, Massaq M<sup>1</sup>. and Marí Soucase B<sup>2</sup>

<sup>1</sup> LCMP Nano Re, University Ibn Zohr, Faculty of sciences, Agadir Morocco.

<sup>2</sup> Laboratory of Optoelectronics, Universitat Politècnica of València, Spain

\*nafidi21@yahoo.fr

We have carried out the bands structures, effective masses and magneto-transport results in HgTe ( $d_1=40$  nm) / CdTe ( $d_2=15$  nm) superlattice (SL). Bands structures  $E(d_2)$ ,  $E(k_z)$  and  $E(k_p)$ , respectively, in the direction of growth and in plane of the superlattice; were performed in the envelope function formalism. The energy  $E(d_2, \Gamma, 4.2$  K), shown that when  $d_2$  increase the band gap  $E_g$  decrease to zero at the transition semiconductor to semimetal conductivity behaviour (at the dot  $T'$  ( $d_{2T'}=10$  nm,  $E_{T'}=38$  meV)) and become negative accusing a semimetallic conduction. For each  $d_2$ , the gap  $E_g(\Gamma)$  increases when  $d_1/d_2$  decreases (id the quantum well thickness). The cutoff wavelength  $|\lambda_c|$  diverge at  $T'$  with  $d_2=5,4$  nm, 10 nm, 15 nm, . . . respectively for  $d_1/d_2=4.09, 2.67, 1.87, . . .$ . The angular transverse magnetoresistance  $\rho/\rho_0(B)$  follows the two-dimensional (2D) dependence. A reversal of the sign of the Hall coefficient at 4.2 K occurs at about 3.2 T. It may be inferred to the existence of, at least, two types of carriers which suggests a semimetallic conduction. The Boltzmann equation of Hall constant  $R_H(B)$  lead to an electron mobility  $\mu_n=6700$  cm<sup>2</sup>/Vs and a concentration  $n=6.2 \cdot 10^{11}$  cm<sup>-2</sup> (with  $\mu_n/\mu_p=15$  and  $p/n=42$ ). At low temperatures the sample exhibits n type conductivity. After 3.2 T the mobility is assumed by the holes conduction. Our study reveals that this sample is a narrow gap semimetallic, two-dimensional and far-infrared detector ( $204 \mu\text{m} < \lambda_c < 430 \mu\text{m}$ ).

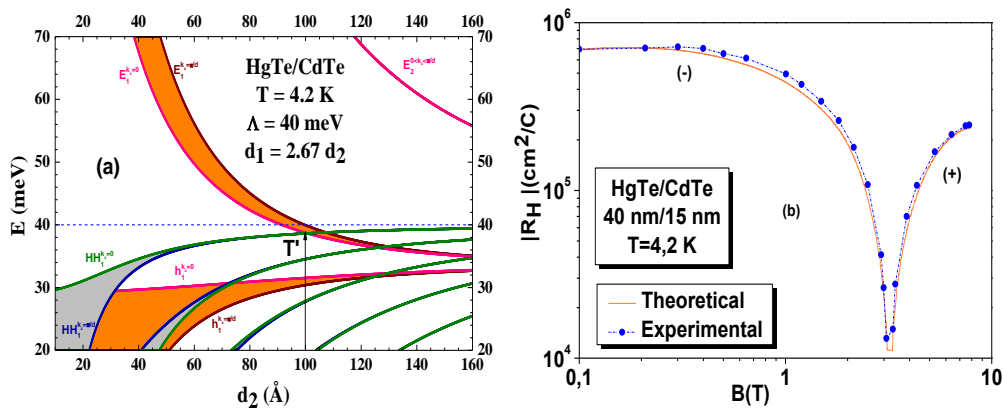


**Fig.** (a) Bands Structure calculated at 4,2 K at the center  $\Gamma$  ( $k_z=0$ ) and the limit ( $k_z= \pi/d$ ) of the first Brillouin zone as a function of layer thickness for HgTe/CdTe superlattice  $T'$  is the dot of the transition semiconductor-semimetal; (b) Magnetic field dependence of the Hall coefficient at 4.2K.

- [1] G. Bastard, Phys. Rev. B 25 (1982) 7584. L. Esaki, R. Tsu, IBM J. Res. Development, 61, (1970).
- [2] M. Braigue, A. Nafidi, et al, J Supercond. Nov. Magn. 25, 2611, (2012).
- [3] A. Nafidi, "Correlation Between Band Structure and Magneto- Transport Properties..."; in the book "Optoelectronic-Advanced Materials and Devices", book editor: Sergei Pyshkin, InTech, (2013) <http://dx.doi.org/10.5772/52101>.

## Figures

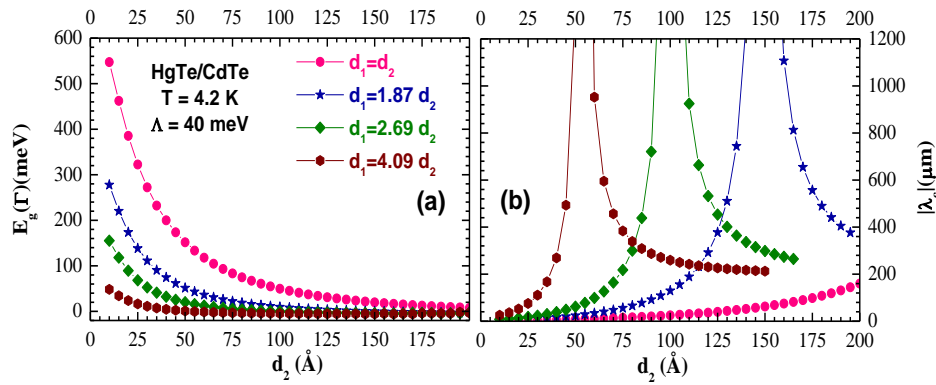


**Fig. 1.** (a)  $E_g$  (eV) and (b)  $|\lambda_c|$  as function of  $d_2$  for various  $d_1/d_2$  at 4.2 K in HgTe/CdTe superlattice.

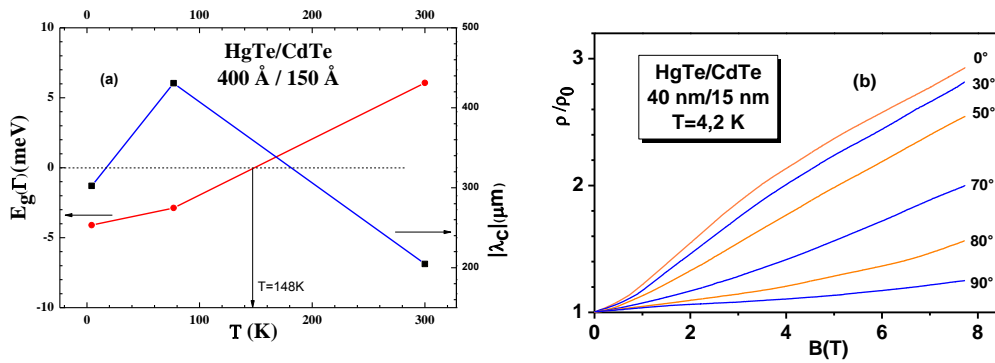


**Fig. 2.** (a) Temperature dependence of the band gap  $E_g$  and cut-off wavelength  $\lambda_c$  at the center  $\Gamma$  of the first Brillouin zone; (b) Variation of the magnetoresistance of the sample with various angles between the magnetic field and the normal to the HgTe/CdTe

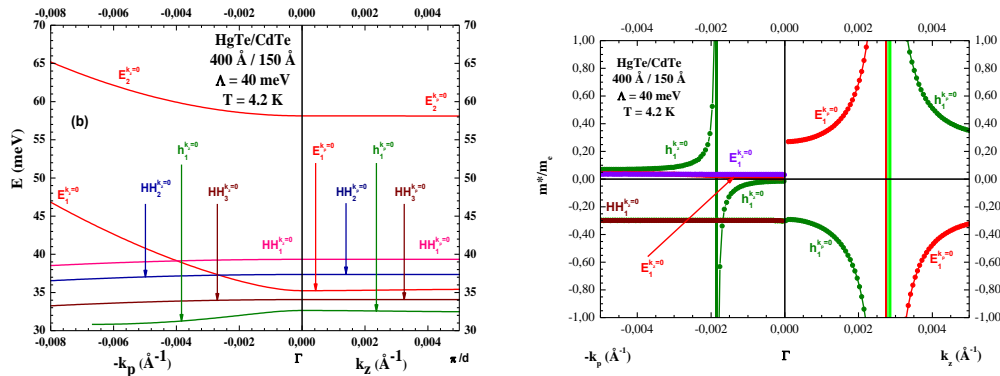


**Figure 3:** (a) Calculated bands along the wave vector  $k_z$  in the right and in plane  $k_p(k_x, k_y)$  for  $k_z=0$  in the left, of the HgTe/CdTe superlattice at 4.2 K. (b) Calculated relative effective mass bands along the wave vector  $k_z$  and in plane  $k_p$  of the HgTe/CdTe superlattice at 4.2 K.

## Donor impurity states in $\text{Ga}_x\text{In}_{1-x}\text{As}_y\text{P}_{1-y}$ stepped quantum well with magnetic field

Hailong Wang<sup>1\*</sup>, Xin Yin<sup>1</sup>, Qian Gong<sup>2</sup>, Shumin Wang<sup>2</sup>

<sup>1</sup>College of Physics and Engineering, Qufu Normal University, Qufu 273165, China

<sup>2</sup>State Key Laboratory of Functional Materials for Informatics, Shanghai Institute of Microsystem and Information Technology, Chinese Academy of Sciences, Shanghai 200050, China

\* H. Wang, e-mail: hlwang@mail.qfnu.edu.cn

The understanding of the electronic properties of impurities in quantum wells (QWs) is important because the transport properties of devices made from these materials are strongly affected by the presence of shallow impurities. Impurity states play a very important role in the semiconductor optoelectronic devices. Research on the electronic structure properties of QWs under the external magnetic field can provide useful information on the potential application of semiconductor QWs. In the previous, we have calculated the electronic structure properties of quantum dots (QDs) and quantum-well wires (QWWs) in the framework of effective-mass envelope-function theory using the plane wave basis [1-3].

Here, we calculate the effects of the magnetic field on the binding energy of the hydrogenic impurities in  $\text{Ga}_x\text{In}_{1-x}\text{As}_y\text{P}_{1-y}$  stepped quantum well by variational method within the framework of effective mass approximation. The binding energy of hydrogenic impurity, with different stepped well widths, as a function of the impurity positions and as a function of the magnetic field are given. When the donor impurities are located in the stepped quantum well center, the impurity binding energy reaches its maximum with the smaller stepped well width and larger magnetic field. With the influence of magnetic field, the binding energy of a hydrogenic impurity increases significantly. We hope that our calculation results are helpful for further investigations of the physics and device applications of  $\text{Ga}_x\text{In}_{1-x}\text{As}_y\text{P}_{1-y}$  stepped quantum well.

### Acknowledgements

This work is supported by the National Natural Science Foundation of China (Grant No. 61176065), Shandong Province Natural Science Foundation (Grant No. ZR2014FM011) and the Open Project of State Key Laboratory of Functional Materials for Informatics (Grant No. SKL201307).

[1] H.L. Wang, L.M. Jiang, Q. Gong and S. L. Feng, *Physica B* **405**, 3818 (2010).

[2] H.T. Wu, H.L. Wang, L.M. Jiang, Q. Gong and S. L. Feng, *Physica B* **404**, 122 (2009)

[3] L.M. Jiang, H.L. Wang, H.T. Wu, Q. Gong and S. L. Feng, *J. Appl. Phys.* **105**, 053710 (2009).

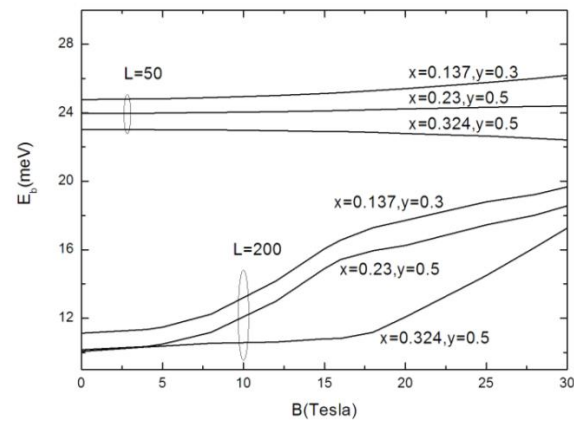


Fig.1 Variation of the impurity binding energy  $E_b$  as a function of the magnetic field  $B$ , for both different Ga, As concentrations and well widths in the  $\text{InP}/\text{Ga}_{0.419}\text{In}_{0.581}\text{As}_{0.9}\text{P}_{0.1}/\text{Ga}_x\text{In}_{1-x}\text{As}_y\text{P}_{1-y}/\text{InP}$  stepped quantum well.

## Atomistic Modeling of ZnSe: A Molecular Dynamics Study

José Pedro Rino

Department of Physics, Universidade Federal de São Carlos, São Carlos, Brasil)

djpr@df.ufscar.br

An effective many-body interatomic potential is proposed for Zinc Selenide, which takes into account two- and three-body interactions. Such a potential is used in molecular dynamics simulation to describe the energetic of the zinc-blende, wurtzite and rock salt structures of ZnSe. The two-body term of the effective interatomic potential consists of steric repulsion due to atomic sizes, Coulomb interactions due to charge transfer, charge-induced dipole and van der Waals attractions. The three-body term has the role of describing the covalent character of the material, and it considers both Zn-Se-Zn and Se-Zn-Se interactions, which are angle dependent. Molecular dynamics calculations with the proposed interaction potential correctly reproduce reported behaviors, namely, cohesive energy, bulk modulus,  $C_{11}$  elastic constant at room temperature [1] and the vibrational density of states [2] of the zinc-blende structure. Figure 1 shows the energy per particle as a function of volume per particle for zinc-blende, wurtzite and rock salt structures. As it can be seen, the wurtzite structure is less stable than the zinc-blende one (differing by 0.0085 meV). Based on the common tangent between the zinc-blende and the rock salt phases, we can estimate the pressure for structural transformation in 9.9 GPa, which is in agreement with experimental results [3]. Cooling from the liquid amorphous or re-crystallized material can also be obtained, as it is displayed in Figure 2.

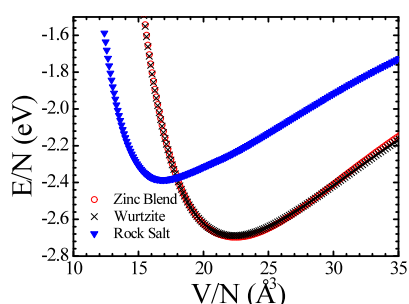


Figure 1: Energy per particle as a function of volume per particle for wurtzite, zinc-blende and rock salt structures.

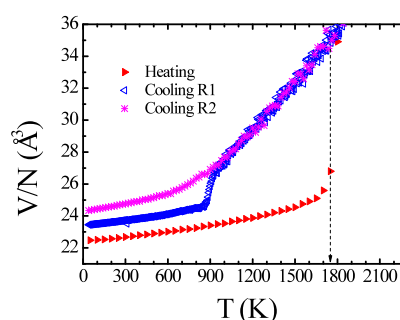


Figure 2: Volume per particle as a function of temperature. Different cooling rate can re-crystallize the original structure.

- [1] W. A. Harrison, *Electronic Structure and the Properties of Solids: The Physics of the Chemical Bond*, Freeman, San Francisco, (1980).
- [2] H. Bliz and W. Kress, *Phonon Dispersion Relations in Insulators*, Springer Verlag, New York (1979).
- [3] A. Mujica, A. Rubio, A. Munoz, and R.J. Needs, *Rev. Mod. Phys.* **75**, 863 (2003), and references there in.

## Electron-phonon interaction in anisotropic II-VI quantum wells

A.Yu. Maslov\*, O.V. Proshina  
 Ioffe Institute, Saint-Petersburg, Russia  
 \*maslov.ton@mail.ioffe.ru

Many of the II-VI compounds allow the coexistence of several crystalline modifications. Heterojunctions between the compounds of cubic and hexagonal symmetry there are quite often. This fact should be taken into account in the study of electron and phonon properties of quantum wells.

In this work the theoretical study of the features of optical phonon spectrum and electron-phonon interaction is performed for heterostructures where the symmetries of quantum well and barrier materials are different. The various orientations of optical axis respect to the quantum well plane are examined in hexagonal structures. Earlier we have shown that in heterostructures of cubic symmetry the interaction of electrons with interface optical phonons plays a decisive role [1]. It is the interaction with the interface optical phonons defines the effective parameter of electron-phonon interaction. This parameter is required to describe the relaxation of carriers in the quantum well and the appearance of polaron mass of charge carriers. In heterostructures under study the spectrum of interface phonons and parameters of the electron-phonon interaction are determined by the dielectric anisotropy of hexagonal structure. Particularly for quantum well based on hexagonal symmetry material with barriers of cubic symmetry the spectrum of the symmetric mode of interface optical phonons is given by:

$$\varepsilon^{(b)}(\omega) = -\varepsilon_{\parallel}^{(w)}(\omega) \sqrt{\frac{\varepsilon_{\perp}^{(w)}(\omega)}{\varepsilon_{\parallel}^{(w)}(\omega)}} \operatorname{th} \left( \sqrt{\frac{\varepsilon_{\perp}^{(w)}(\omega)}{\varepsilon_{\parallel}^{(w)}(\omega)}} \frac{qL}{2} \right), \quad (1)$$

where  $\varepsilon^{(b)}(\omega)$  is the barrier dielectric function,  $\varepsilon_{\parallel}^{(w)}(\omega)$  and  $\varepsilon_{\perp}^{(w)}(\omega)$  are the dielectric functions of hexagonal material of quantum well in the directions parallel and perpendicular to the optical axis, respectively;  $L$  is the quantum well width. When  $\varepsilon_{\parallel}^{(w)}(\omega) = \varepsilon_{\perp}^{(w)}(\omega)$ , the equation (1) coincides with the known result for interface phonon spectrum in the structure of cubic symmetry [2]. With various frequency dependences of the dielectric functions  $\varepsilon_{\parallel}^{(w)}(\omega)$  and  $\varepsilon_{\perp}^{(w)}(\omega)$  in the region of small wave numbers the interface phonons behave in quadratic dispersion law that differs from the problem with quantum well of cubic symmetry. At strong distinction of optical phonon frequencies from the expressions for  $\varepsilon_{\parallel}^{(w)}(\omega)$  and  $\varepsilon_{\perp}^{(w)}(\omega)$  the additional branches of optical phonons may arise in the structure. These branches are absent in the quantum well material and on separate hetero-interface.

Account of all phonon branches of the spectrum allows us to describe the experimental data on effective mass value change for *ZnO-ZnMgO* quantum well [3].

This work was partially supported by the President program of Leading Scientific Schools (project no. 5062.2014.2).

[1] A.Yu. Maslov, O.V. Proshina, *Phys. Stat. Sol. C* **7**, 1609-1611 (2010); *Semiconductors*, in print, (2015).

[2] M. Mori, T. Ando, *Phys. Rev. B* **40**, 6175-6188 (1989).

[3] Y. Imanaka, T. Takamasu, H. Tampo, H. Shibata, and S. Niki, *Phys. Stat. Sol. C* **7**, 1599-1601 (2010).

## Full potential calculation of structural, electronic and thermodynamic properties of $\text{Zn}_{1-x}\text{Ca}_x\text{S}$ ternary alloy

S Labidi<sup>1</sup> and M. Labidi<sup>2</sup>

<sup>1</sup> Laboratoire des Nanomatériaux, Corrosion et Traitements de Surfaces, Département de Physique, Faculté des Sciences, Université Badji Mokhtar, BP 12, 23000 Annaba, Algerie

<sup>2</sup>Ecole Préparatoire aux Sciences et Techniques, B.P.218 Annaba 23000 Cité safsaf  
labidisalima@yahoo.fr

The ground-state properties of  $\text{Zn}_{1-x}\text{Ca}_x\text{S}$  mixed crystals in the Zinc-blende structure were investigated using an accurate first principles total-energy calculations based on the full-potential augmented plane-wave (FP-LAPW) method within the density functional theory (DFT) in the local density approximation (LDA), and two developed refinements, namely the generalized gradient approximation (GGA) of Perdew et al. for the structural properties and Engel-Vosko for the band gap calculations. Quantities such as, equilibrium lattice constants, bulk modulus, band gap and effective mass were calculated as a function of calcium molar fraction  $x$ . These parameters were found to depend non-linearly on alloy composition  $x$ . The microscopic origins of the gap bowing were explained using the approach of Zunger and co-workers. On the other hand, the thermodynamic stability of this alloy was investigated by calculating the excess enthalpy of mixing  $\Delta H_m$  as well as the phase diagram.

[1] S. labidi M. Boudjendlia, M. labidi and R. Bensalem, Chin. J. Phys. **52**, 1081 (2014)

[2] S. Labidi, M. Labidi, H. Meradji, S. Ghemid, F. El Haj Hassan, Comput. Mater. Sci.50, 1077-1082 (2011)

## Structural, electronic and thermodynamic properties of $\text{Sr}_x\text{Ca}_{1-x}\text{S}$ : A first-principles study

M. Labidi<sup>1</sup>, S. Labidi<sup>2</sup>, M. Boudjendlia<sup>2</sup>, J. Zeroual<sup>2</sup> and R. Bensalem<sup>2</sup>

<sup>1</sup>Ecole Préparatoire aux Sciences et Techniques, B.P.218 Annaba 23000 Cité safsaf

<sup>2</sup>Laboratoire des Nanomatériaux, Corrosion et Traitements de Surfaces, Département de Physique, Faculté des Sciences, Université Badji Mokhtar, BP 12, 23000 Annaba, Algeria

[Labidimalika4@yahoo.fr](mailto:Labidimalika4@yahoo.fr)

First principles calculations have been performed within the framework of density functional theory to investigate the structural, electronic and thermodynamic properties of  $\text{Sr}_x\text{Ca}_{1-x}\text{S}$  ternary alloys. The exchange-correlation potential for structural properties was calculated by the standard local density approximation (LDA) and GGA (PBE), a more accurate nonempirical density functional generalized gradient approximation (GGA), as proposed by Wu and Cohen [Phys. Rev. B **73**, 235116 (2006)], while for electronic properties, the Engel and Vosko GGA (EVGGA) and the modified Becke-Johnson (MBJ) schemes were also applied. Deviation of the lattice constants from Vegard's law and bulk modulus from linear concentration dependence (LCD) were observed for the ternary alloys. The MBJ band gaps values agree well with the available experimental results. In addition the thermodynamic stability of the alloys was investigated by calculating the critical temperatures of alloys.

[1] S. labidi M. Boudjendlia, M. labidi and R. Bensalem, Chin. J. Phys. **52**, 1081 (2014)

[2] S. labidi, H. Meradji, S. Ghemid, M. Labidi and F. El Haj Hassan, J. Phys.: Condens. Matter **20**, 445213 (2008)

## Shape and DMS Doping Effects on the Current and Efficiency of II-VI Quantum Dots Based Solar Cells.

Augusto M. Alcalde<sup>1</sup>, Silvio J. Prado<sup>2</sup>

<sup>1</sup>Instituto de Física, Universidade Federal de Uberlândia, MG, Brazil

<sup>2</sup>Faculdade de Ciências Integradas do Pontal, Universidade Federal de Uberlândia, MG, Brazil

\*alcalde@fafis.ufu.br

In this work we show calculation of efficiency and photocurrent of solar cells based on II-VI quantum dots. We focus our attention on the effects of the quantum dot shape over the optical properties as optical absorption and photocurrent. In the theoretical framework of the k.p multiband calculation, we show how the quantum shape produces drastic changes on the optical selection rules. To illustrate the quantum dot size and shape effects on the relevant properties of solar cells, we consider spherical, semi-spherical and cylindrical quantum dots.

We also explore the effect of Mn ion doping in the dilute regime (DMS) on the relevant optical properties. As we previously report [1,2], the interplay of quantum dot geometry and Mn concentration can modulate significantly the optical absorption. Theoretical findings regarding both broken symmetry and Mn concentration were studied by contrasting two different systems: CdTe/CdMnTe in core-shell configuration, and HgMnTe/CdMnTe, and changing the confinement geometry, dot size, and magnetic doping concentration.

- [1] S. J. Prado, L. Villegas-Lelovsky, A. M. Alcalde, V. López-Richard and G. E. Marques. *Nanoscale Research Letters* **7**, 374, (2012)
- [2] S. J. Prado, V. López-Richard, A. M. Alcalde, G. E. Marques and C. Trallero-Giner, *Applied Physics Letters* **88**, 1-3, (2006).

**Poster Session 3 - ThP**

**Solar cells**

## Preparation and characterization of chemically spray deposited MoO<sub>3</sub> thin films and their application as buffer layers in CuPc/C<sub>60</sub> based solar cells

Y. Mouchaal<sup>1,2\*</sup>, G. Cabailh<sup>2</sup>, A. Khelil<sup>1</sup>

<sup>1</sup>Laboratoire de Physique des Couches Minces et Matériaux pour l'Electronique, Université d'Oran, Oran, Algeria

<sup>2</sup>Institut des Nanosciences de Paris, UPMC – Université Paris 06, Paris, France

\* mouchaal@insp.jussieu.fr

Organic photovoltaic (OPV) cells based on a small molecular planar hetero-junction have attracted much attention since Tang reported the first efficient device in 1986 [1]. Under illumination, the charges are generated in the active layer as a result of photo-excitation, and are subsequently collected at the electrodes. Indium tin oxide (ITO) is used as the transparent hole collecting anode and a low work function metal is used as the electron collecting cathode.

We show in the present work that using an ITO surface coated with a MoO<sub>3</sub> buffer layer as the anode results in enhanced device performance [2]. XDR and AFM techniques were used to characterize the morphology of the deposits. The films with optimum thickness (4 nm after optimization) are amorphous. The organic solar cells structures used in this study after optimization were: ITO/MoO<sub>3</sub> (4 nm)/CuPc (35 nm)/C<sub>60</sub>/BCP/Al. The multi-layer hetero-junction structure has indium tin oxide (ITO) as the bottom anode. We investigate the hole barrier present at the ITO/organic interface which can eventually be systematically avoided by insertion of thin MoO<sub>3</sub> layer between ITO and the organic electron donor material [3].

After electrical characterizations of the manufactured solar cells performed with an automated I–V tester, in the dark and under sun global AM 1.5 simulated illumination we confirm that spray deposited MoO<sub>3</sub> thin films (4 nm thick) can be used as buffer layers at the anode/organic interface material. These MoO<sub>3</sub> buffer layers allow improving the efficiency by 50% within the solar cells reaching 1,7 %.

[1] C. W. Tang, *App. Phys. Letters*, **48**, 183, (1986).

[2] L. S. Roman, M. Berggren, and O. Inganäs, *Appl. Phys. Lett.* **75**, 3557, (1999).

[3] F. Deschler, D. Riedel, B. Ecker, E. Hauff, E. D. Como, and R. C. I. MacKenzi, *Chem. Phys.* **15**, 764, (2013).

## Application of CdZnS/ZnS Nanocrystals as a Down-converter on the Front Surface of Photovoltaic Cells

Joon-Suh Park<sup>1</sup>, Il Ki Han<sup>1</sup>, Young I. Jhon<sup>2</sup>, Young Min Jhon<sup>2</sup>, Soo Jin Lee<sup>1,3</sup>,  
and Woon Jo Cho<sup>1,\*</sup>

<sup>1</sup>Nano-photonics Research Center and <sup>2</sup>Sensor System Research Center,  
Korea Institute of Science and Technology, Hwarangno 14-gil 5, Seongbuk-gu,  
Seoul, 136-791, Republic of Korea

<sup>3</sup>Department of Nuclear Medicine, National Cancer Center, 323 Ilsan-ro,  
Ilsandong-gu, Goyang-si Gyeonggi-do, 410-769, Republic of Korea

\*wooncho@kist.re.kr

A luminescent converter, called a down-converter, could convert high-energy photons into two or more lower-energy photons. And hence it might result in a more efficient device when it is placed on the front surface of a conventional solar cell [1].

For quantum dots, one of the luminescent nanocrystals, to be used as the down-converter of photovoltaic cells, the bandgap of the nanocrystals should be tuned so as to take energy over an UV to blue range of the solar spectrum. As for silicon-based solar cells, the solar energy over a range 300 nm to 400 nm generates less number of excitons and hence less electricity since a spectral response of the device is not strong enough in the range of UV to blue range.

We have applied ZnCdS nanocrystals as the down-converter. ZnCdS/ZnS quantum dots were synthesized in house, mostly according to a reported route [2]. The room temperature photoluminescence of the prepared nanocrystals were ranged 450 nm to 460 nm. The peaks of a photoluminescence excitation were located at 360 nm, 400 nm and 440 nm. The prepared nanocrystals were coated on a heterojunction with intrinsic thin layer (HIT) solar cells. The relative efficiency of HIT cells increased by about 2 % by coating ZnCdS/ZnS quantum dots on the front side. Some engineering parameters will be discussed about the down-converters for the photovoltaic cells.

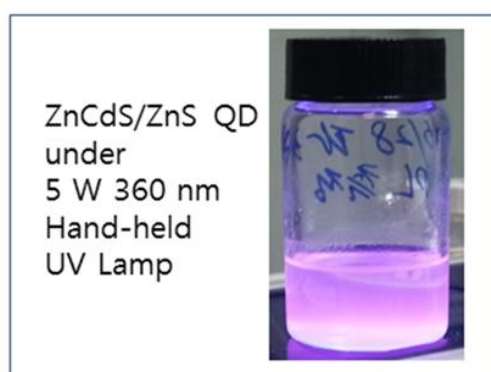


Fig. 1 Camera image of colloidal ZnCdS/ZnS nanoparticles in solvent

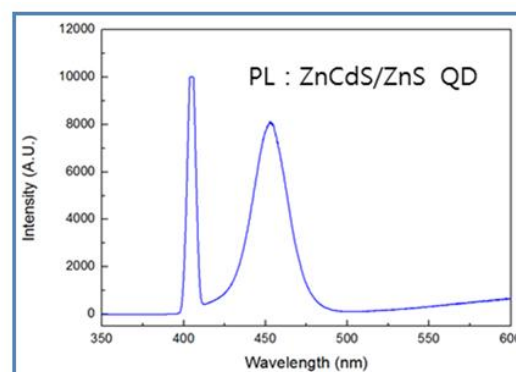


Fig. 2 Room temperature PL spectra of ZnCdS/ZnS nanoparticles (peak : 450 nm)

- [1] T. Trupke, M. A. Green, and P. Würfel, *Journal of Applied Physics*, **92**, 1668, (2002).  
[2] Wan Ki Bae, Min Ki Nam, Kookheon Char, and Seonghoon Lee, *Chem. Mater.*, **20**, 5307, (2008).

## Monocrystalline ZnTe/CdTe/MgCdTe Double-Heterostructure Solar Cells Grown on InSb Substrates

Jacob Becker<sup>1,2</sup>, Ying-Shen Kuo<sup>1,2</sup>, Shi Liu<sup>1,2</sup>, Yuan Zhao<sup>1,2</sup>, Xin-Hao Zhao<sup>1,3</sup>, Peng-Yu Su<sup>4</sup>, Ishwara Bhat<sup>4</sup>, and Yong-Hang Zhang<sup>1,2\*</sup>

<sup>1</sup>Center for Photonics Innovation, Arizona State University, Tempe, AZ 85287

<sup>2</sup>School of Electrical, Computer and Energy Engineering, Arizona State University, Tempe, AZ 85287

<sup>3</sup>School for Engineering of Matter, Transport and Energy, Arizona State University, Tempe, AZ 85287

<sup>4</sup>Department of Electrical, Computer, and Systems Engineering, Rensselaer Polytechnic Institute, Troy, NY 12180

\*Corresponding author, E-mail: yhzhang@asu.edu

CdTe is one of the most promising semiconductor candidates for efficient and low-cost thin-film solar cells due to its nearly ideal bandgap (1.5 eV) and large absorption coefficient. Polycrystalline CdS/CdTe solar cells have achieved a record efficiency of 21.0 % demonstrated by First Solar [1], while monocrystalline CdTe has only reached an efficiency of 13.4 % [2]; however, both are far from the detailed balanced limit of 32.1 %. The monocrystalline CdTe solar cell is expected to reach an even higher efficiency than the current record. Recently, high-quality monocrystalline MgCdTe/CdTe/MgCdTe double heterostructures grown on lattice-matched InSb (001) substrates by molecular beam epitaxy (MBE) have been demonstrated with record-long minority carrier lifetimes up to 2.6  $\mu$ s for various structures [3-4]. This abstract reports the demonstration of monocrystalline single-junction CdTe solar cells grown on InSb substrates.

Monocrystalline p-ZnTe/p-CdTe/n-CdTe/n-MgCdTe double-heterostructure (DH) solar cells are designed, and demonstrated with a maximum efficiency of 10.67 %, an open-circuit voltage ( $V_{OC}$ ) of 746 mV, a short-circuit current density ( $J_{SC}$ ) of 21.22 mA/cm<sup>2</sup> and a fill factor (FF) of 67.4 %. The low efficiency is mainly due to the combination of the low  $V_{OC}$  and small FF, which are attributed to high interface recombination velocity at the ZnTe/CdTe interface, and p-CdTe/n-CdTe regrowth interface.

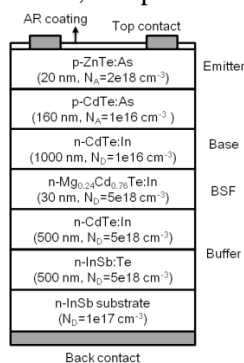


Fig. 1 Schematic layer structure of the ZnTe/CdTe/MgCdTe DH solar cell

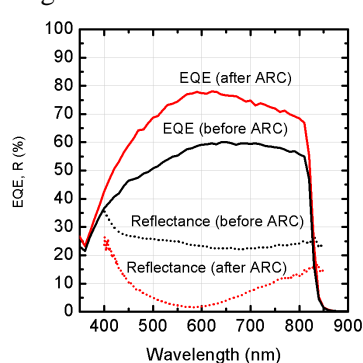


Fig. 2 Measured EQE and reflectance of the ZnTe/CdTe/MgCdTe DH solar cell before/after the AR coating

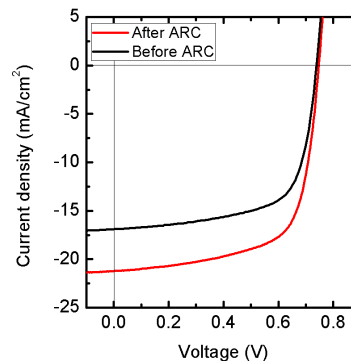


Fig. 3 J-V characteristic of the device measured under AM 1.5G illumination at room temperature

- [1] First Solar Press Release, 5 August 2014, (accessed at <http://investor.firstsolar.com> on 5 September 2014).
- [2] T. Nakazawa, K. Takamizawa, and K. Ito, Applied Physics Letters. 50, 279 (1987).
- [3] X.-H. Zhao, M. J. DiNezza, S. Liu, S. Lin, Y. Zhao, and Y.-H. Zhang, Journal of Vacuum Science and Technology B, vol. 32, p. 040601 (2014).
- [4] S. Liu, X.-H. Zhao, C. Campbell, M. Lassise, Y. Zhao, and Y.-H. Zhang, submitted to 17th International Conference of II-VI Compounds and Related Materials, Paris, September 2015.

Material	Polycrystalline Record	Monocrystalline Record	Detailed Balance
	Efficiency	Efficiency	Limit
CdTe	21.0 %	13.4 %	32.1 %
GaAs	18.4 %	28.8 %	33.2 %

Table.1 Record efficiencies and detailed balance limits of GaAs and CdTe single-junction solar cells. By comparing these values with single-junction monocrystalline and polycrystalline GaAs solar cells, which have record efficiencies of 28.8 % and 18.4 %, respectively, intuitively the monocrystalline CdTe solar cell should be able to achieve an efficiency much closer to the Shockley-Queisser limit than the current record of 21.0%.

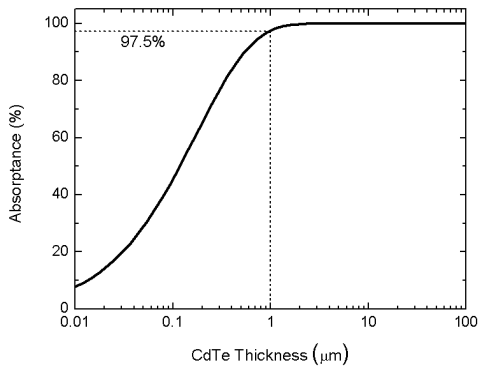


Fig. 4 Absorbance as a function of CdTe layer thickness for the AM1.5G spectrum. The CdTe base layer thickness is designed to be 1 μm to attain a 97.5 % absorbance, which is defined as the ratio of the absorbed photon flux to the total solar photon flux for energies above the bandgap. X-Ray Diffraction results also show that 1 μm of CdTe is coherently strained on InSb.

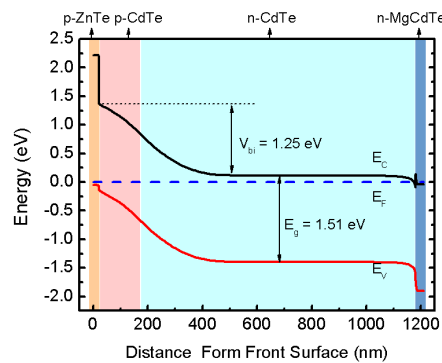


Fig. 5 Schematic band edge diagram of the ZnTe/CdTe/MgCdTe DH. The calculated built-in voltage is 1.25 eV. The interface of ZnTe/CdTe is a type-II alignment and lattice mismatched, which is responsible for the low open circuit voltage due to non-radiative recombination.

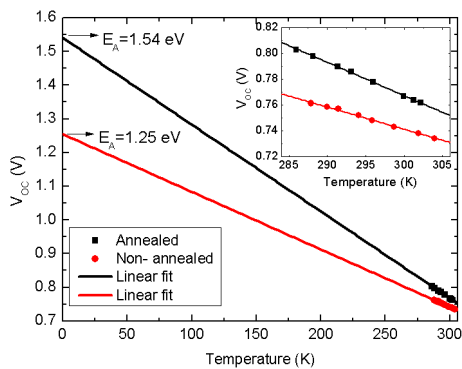


Fig. 6  $V_{OC}$  vs. temperature of the ZnTe/CdTe/MgCdTe DH solar cells measured under AM1.5G one sun illumination. The activation energies of 1.25 eV and 1.54 eV for the non-annealed and annealed device can be obtained. Annealing reduces the interface misfit dislocations and results in  $E_A \sim E_g$ , which implies SRH recombination dominates. The non-annealed devices show lower  $V_{OC}$  at room temperature and  $E_A < E_g$ , indicating that the  $V_{OC}$  is mainly affected by a different mechanism, such as interface recombination.

## Highly Cr-doped ZnS for intermediate band solar cells

M. Nematollahi<sup>1\*</sup>, X. Yang<sup>1</sup>, E. Seim<sup>1</sup>, P. E. Vullum<sup>1,2</sup>, R. Holmestad<sup>1</sup>,  
U. J. Gibson<sup>1</sup>, and T. W. Reenaas<sup>1</sup>,

<sup>1</sup> Department of Physics, Norwegian University of Science and Technology (NTNU), Norway

<sup>2</sup> SINTEF Materials and Chemistry, Trondheim, Norway

\*m.nematollahi@ntnu.no

Chromium doped zinc sulfide (ZnS:Cr) has been proposed as an intermediate band (IB) material based on density functional theory studies [1]. Realization of an IB solar cell (IBSC) can potentially enhance the efficiency by about 50% compared to a single junction solar cell [2]. Dilute ZnS:Cr has been used as laser material for tunable near- and mid-infrared lasers [3], but for IBSCs a high Cr content is required to have a high absorption coefficient and to suppress non-radiative recombination [4]. One of the main challenges in fabrication of materials with high density of deep-level dopants is degradation of crystal structure and electronic properties [5]. Therefore, a better understanding of the structural properties of such materials would be beneficial for the progress of IBSC development. Here, we have studied compositional and structural properties of undoped and ZnS:Cr films in details.

The films were grown on p-Si(100) substrates by pulsed laser deposition under various growth conditions. The Cr content in the films varied between 2.0 to 5.0 at% reproducibly, by varying the laser fluence (1.0 – 7.8 J/cm<sup>2</sup>). Energy dispersive X-ray spectroscopy showed that Cr is relatively uniformly distributed in the films, but with some local variations. A local increase in Cr content corresponded to a decrease in Zn content, with constant S content. This result suggests that most Cr atoms substitute Zn atoms, and this is verified by X-ray photoelectron spectroscopy where Cr<sup>2+</sup> was found to be the dominant valence state. It has been reported that Cr<sup>2+</sup> substitutes Zn<sup>2+</sup> in ZnS:Cr when the Cr content is below 0.8 at.%, but some Cr<sup>+</sup> is also present for higher Cr content [3, 6]. In our films, we observe that when the Cr content is above 2.0 at% Cr<sup>0</sup> and Cr<sup>3+</sup> are always present.

The structural properties were studied by X-ray diffraction (XRD), and we found that the films were highly textured and the crystal structure was a mix of zinc blende (ZB) and wurtzite (W). With increasing Cr content, the W/ZB ratio increases. Selected films (Cr ~ 4% and 4.5%) were also studied by scanning and transmission electron microscopy (S/TEM), and it was confirmed that the films with highest Cr content are hexagonal (W) with [001] as the primary growth direction. The presence of stacking faults was also confirmed by XRD and TEM.

We have also fabricated ZnO:Al/ZnS:Cr(ZnS)/Si solar cells, and the devices with ZnS:Cr shows 26 times higher efficiency compared to the devices with ZnS [7]. However, the efficiency is still low (~ 2%).

- [1] Tablero, C., J. Appl. Phys. **108**, 093114-7 (2010).
- [2] Luque, A. and A. Martí, Phys. Rev. Lett. **78**, 5014 (1997).
- [3] Vlasenko, N.A., et al., Ann. Phys-Berlin **525**, 889-905 (2013).
- [4] Luque, A., et al. Physica B **382**, 320-327 (2006).
- [5] Ramiro, I., et al., IEEE J. Photovolt. **4**, 736-748 (2014).
- [6] Vlasenko, N., et al. Quantum Electronics & Optoelectronics (SPQEO) **8**, 25-29 (2005).
- [7] Nematollahi, M., et al. 6th World Conference on Photovoltaic Energy Conversion, Kyoto, Japan (2014).

## Photoresponse Enhancement of Cu<sub>2</sub>O Solar Cell with Sulfur-doped ZnO Buffer Layer to Mediate the Interfacial Band Alignment

Wenzhe Niu, [Liping Zhu\\*](mailto:zlp1@zju.edu.cn)

State Key Laboratory of Silicon Materials, School of Materials Science and Engineering,  
Zhejiang University, Hangzhou 310027, People's Republic of China

E-mail: [zlp1@zju.edu.cn](mailto:zlp1@zju.edu.cn)

It is promising that the efficiency of cuprous oxide (Cu<sub>2</sub>O) based heterojunction solar cell can be improved by inserting a buffer layer to mediate the energy alignment at the interface. In this work, a sulfur-doped ZnO (ZnOS) buffer layer with properly tuned band alignment was introduced to the Cu<sub>2</sub>O/AZO heterojunction solar cells to form an interface-recombination barrier, which enhanced the open-circuit voltage extremely. The mechanism of buffer layer was investigated, which reveals the increase of conduct band edge of ZnOS buffer layer, thereby mitigating the interfacial recombination. This work shed light on the optimization of the interfacial band alignment of heterojunction solar cell, improving the photoresponse property.

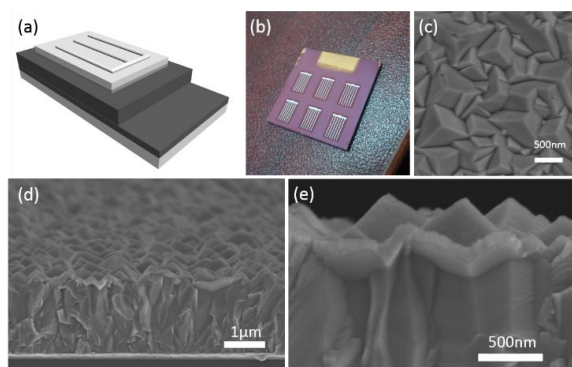


**Fig. 1** (a) Schematic illustration of the device structure. From top to bottom are Al, AZO, ZnO or ZnOS, Cu<sub>2</sub>O, Au, silica orderly. (b) The photograph of the fabricated solar cell. (c) The surface morphology of the as-grown Cu<sub>2</sub>O layer. (d) The cross-section SEM image of the solar cell. (e) Magnified SEM image near the heterojunction interface.

## Performance of $p^+$ -ZnTe/ $p$ -ZnTe:O/ $n^+$ -GaAs Intermediate Band Solar Cells Grown by Pulsed Laser Deposition

Kyoung Su Lee, Gyujin Oh, and Eun Kyu Kim\*

*Department of Physics, Hanyang University, Seoul 133-791, Korea*

\*E-mail: [ek-kim@hanyang.ac.kr](mailto:ek-kim@hanyang.ac.kr)

Low-cost, high efficiency solar cells are tremendous interests for the realization of a renewable and clean energy source. ZnTe based solar cells have a possibility of high efficiency with formation of an intermediated energy band structure by impurity doping.[1,2] In this work, the  $p^+$ ZnTe/ $p$ -ZnTe:O/ $n^+$ GaAs structures were fabricated by pulsed laser deposition (PLD) technique. A pulsed (10 Hz) Nd:YAG laser operating at a wavelength of 266 nm was used to produce a plasma plume ablated from ZnTe target, whose density of laser energy was  $4.5 \text{ J/cm}^2$ . The base pressure of PLD chamber was kept at a pressure of approximately  $4 \times 10^{-7}$  Torr. During deposition of ZnTe film,  $\text{N}_2$  and  $\text{O}_2$  gases were introduced from 30 to 70 mTorr. The  $p^+$ -ZnTe and  $p$ -ZnTe:O thin films were grown at temperature of  $250 \text{ }^\circ\text{C}$  on  $n^+$ -GaAs substrates. For fabricating  $p^+$ -ZnTe/ $p$ -ZnTe:O/ $n^+$ GaAs solar cells, Au metal grids were depositing on the ZnTe film by thermal evaporation method. Figure 1 shows the schematic diagram of completed device. The current-voltage characteristics of these devices were measured by using HP 4156A semiconductor parameter analyzer. Finally, the solar cell performance was characterized by using an Air Mass 1.5 Global (AM 1.5 G) solar simulator with an irradiation intensity of  $100 \text{ mW cm}^{-2}$ .

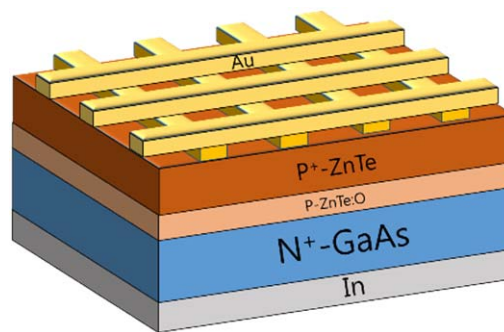


Figure 1. Schematic diagram of  $p^+$ -ZnTe/ $p$ -ZnTe:O/ $n^+$ -GaAs intermediated solar cell.

[1] S. W. Pak, J. Suh, D. U. Lee, and E. K. Kim, Jpn. J. of Appl. Phys. **51**, 01AD04 (2012).

[2] D. U. Lee, S. P. Kim, K. S. Lee, S. W. Pak and E. K. Kim, Appl. Phys. Lett. **103**, 263901 (2013).

## Effect of electron correlations on the exciton dynamics of CdTe(Se)/CdTe(Se) core/shell for MEG solar cells

Stanko Tomić\*, Edward Tyrrell and Jacek Miloszewski  
Joule Physics Laboratory, University of Salford, Manchester M5 4WT, UK  
\*E-mail: s.tomic@salford.ac.uk

The efficiency of multi-exiton generation (MEG) in colloidal QDs is determined by the competition between MEG and other hot electron-cooling processes. These have characteristic times of  $t(\text{MEG}) \sim t(\text{cooling}) \sim 1$  ps in the colloidal QDs studied to date but for high efficiency  $t(\text{cool}) \gg t(\text{MEG})$  is required [1,2]. The core/shell QDs with type II band alignment offers extra degree of freedom in mediating both the optical dipoles and the Coulomb interaction between charges in such structures. To assess faithfully the effect of electron correlations on the radiative and Auger related times, a theoretical methodology was established, based on an multi-band  $\mathbf{k}, \mathbf{p}$  Hamiltonian, with correct  $C_{2v}$  atomistic symmetry of the zinc-blend material [3]. Excitonic states were found using the full Configuration interaction method, that includes explicitly the effects of Coulomb interaction, exact exchange and correlations between many-electron configurations. Relevant parameters as well as dielectric constants of CdSe and CdTe at the transition energies are predicted using ab initio time-dependent density functional theory [4]. We map the  $1S(e)nS(h)$  ( $n = 1, 2, 3$ ) exciton correlation energy relative to the strong confinement approximation as a function of core radius and shell thickness for uniform and non-uniform spatial dielectric constants. The type-II confinement potentials mean that dielectric confinement has a large effect on the wave functions and exciton energies in such heterostructures, mainly increasing the correlation energy for QDs in which the corresponding single-particle hole is delocalized [5]. We also find that correlation leads to large changes in the momentum matrix element, particularly for the lowest CdSe/CdTe QD exciton in which it is increased up to a factor of  $\sim 8$  in the presence of dielectric confinement. Overall dielectric confinement affected the exciton properties in CdSe/CdTe QDs more than the inverse heterostructures due to the band alignment, which encourages holes to localize in the shell. Using the correlated excitonic energies and correlated optical dipoles we have predicted that the radiative times increase only for one order of magnitude (from  $\sim 20$  ns to  $\sim 150$  ns) by changing the QD shell thicknesses from 0 to 2 nm. Those results are in excellent agreement with experimentally measured radiative time on similar type II QD structures [2,6]. However in the same range of shell thicknesses change, the non-radiative Auger electron cooling times increase for three orders of magnitude (from  $\sim 1$  ps to  $\sim 1$  ns). Such dramatic slow down of the Auger electron cooling could be of the potential benefit for increased MEG efficiency.

- [1] A. Pandey, P. Guyot-Sionnest, *Science* **322** (5903), 929 (2008)
- [2] Z. Deutsch, A. Avidan, I. Pinkas and D. Oron, *Phys. Chem. Chem. Phys.* **13**, 3210 (2011)
- [3] S Tomić and N Vukmirović *J. Appl Phys* **110**, 053710 (2011)
- [4] L. Bernasconi, S. Tomić et al, *Phys Rev B* **83**, 195325 (2011)
- [5] E. Tyrrell and S. Tomić, submitted to *J. Phys. Chem. C*
- [6] K. Gong, Y. Zeng, D. F. Kelley, *J. Phys. Chem. C* **117**, 20268 (2013)

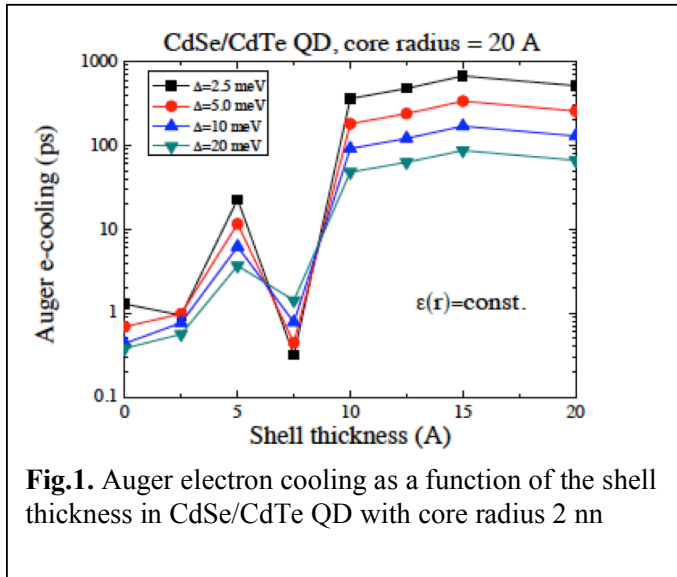


**Fig.1.** Auger electron cooling as a function of the shell thickness in CdSe/CdTe QD with core radius 2 nm

## Issues with Application of CBD CdS in CdS/i-ZnO/ZnO:Al Window Layer

Natalia Maticiuc<sup>1\*</sup>, Tamara Potlog<sup>2</sup>, and Jaan Hiie<sup>1</sup>

<sup>1</sup>Department of Materials Science, Tallinn University of Technology, Tallinn, Estonia

<sup>2</sup>Faculty of Physics, Moldova State University, Chişinău, Moldova

\*nataliamaticiuc@yahoo.com

CdS thin film is one of the most studied II-VI semiconductors applied in thin film solar cell technology. Chemical bath deposition (CBD) is widely applied for CdS deposition due to technological feasibility and conformal coverage. Either it is used in substrate CIGS solar cell or superstrate CdTe solar cell, CdS film is subjected to thermal treatments during deposition of i-ZnO/ZnO:Al front contact by sputtering or during CdTe deposition and CdCl<sub>2</sub> treatment processes. In both cases the changes of CdS properties have a strong influence on the final parameters of the device. However, there is lack of a commonly accepted understanding of physico-chemical nature of the processes taking place in the thermal annealing and resulting in changes of structural, optical, and electrical properties of CdS. In this sense we made a systematic research of CBD CdS annealing in a wide range of temperatures, durations and atmospheres.

Kinetics of thermal annealing indicates to the reproducible increase in electron concentration for low temperature region (200 – 300 °C), independent on the duration of the process (Fig. 1). The changes in the electron concentration of CdS were explained by decomposition of hydroxide group, incorporated on sulfur site (OH)<sub>S</sub> in the deposition process.



The presence of hydroxide in CBD CdS has been confirmed by XPS and FTIR analyses [1, 2].

Incorporation of (OH)<sub>S</sub> into CdS results in stressed crystalline lattice with (111) XRD peak between hexagonal and cubic modifications. Evaporation of water results in destruction of CdS crystallites, whereas transition from (OH)<sub>S</sub> substitution to O<sub>S</sub> in the sulfur sub-lattice is accompanied by the shrinking of the lattice and narrowing of the band gap. At higher annealing temperatures >400 °C the bulk values of lattice constant and band gap for pure CdS restore due to the out-diffusion of oxygen and Cd [3].

Several experimental data suggested that in the sputtering process of i-ZnO and ZnO:Al the substrate temperature increases up to 200 °C. We found that during the sputtering of the ZnO layers the sheet resistance of as deposited CBD CdS film decreased by three orders of magnitude corresponding to 10<sup>19</sup> cm<sup>-3</sup> electron concentration. This creates then <sup>+/n</sup> concentration type reverse junction between low resistance CdS and high resistance i-ZnO and decreases the efficiency of solar cell.

Our studies on the impact of various annealing atmospheres allow us to manage the electron concentration in the CdS films.

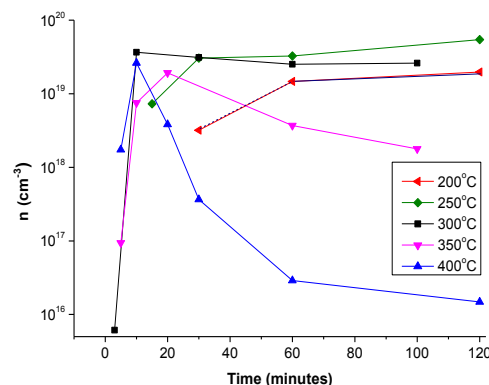


Fig. 1. Electron concentration of CBD CdS films annealed in H<sub>2</sub> at various temperatures vs. time.

[1] W.J. Danaher, L.E. Lyons, G.C. Morris, Sol. Energy Mater. **12**(2), 137, (1985).

[2] D.W. Niles, G. Herdt, M. Al-Jassim, J. Appl. Phys. **81**(4), 1978, (1997).

[3] N. Maticiuc, J. Hiie, V. Mikli, T. Potlog, V. Valdna, Mater. Sci. Semicond. Process. **26**, 169, (2014).